Journal of Toxicology

State of the Science: Biologically Based Modeling in Risk Assessment

Guest Editors: Jane C. Caldwell, Kannan Krishnan, and Marina V. Evans

State of the Science: Biologically Based Modeling in Risk Assessment

Journal of Toxicology

State of the Science: Biologically Based Modeling in Risk Assessment

Guest Editors: Jane C. Caldwell, Kannan Krishnan, and Marina V. Evans

Editorial Board

Contents

Hindawi Publishing Corporation
Journal of Toxicology
Volume 2012, Article ID 758182, 2 pages
doi:10.1155/2012/758182

Editorial

State of the Science: Biologically Based Modeling in Risk Assessment

Jane C. Caldwell,[1] Kannan Krishnan,[2] and Marina V. Evans[3]

[1] *National Center for Environmental Assessment, Office of Research and Development, US Environmental Protection Agency, Washington, DC 20460, USA*
[2] *Department of Occupational and Environmental Health, Faculty of Medicine, Université de Montréal, Montreal, QC, Canada H3T 1A8*
[3] *National Health and Environmental Effects Research Laboratory, Office of Research and Development, US Environmental Protection Agency, Research Triangle Park, NC 27711, USA*

Correspondence should be addressed to Jane C. Caldwell, caldwell.jane@epa.gov

Received 4 October 2012; Accepted 4 October 2012

The health risk assessment from exposure to a particular agent is preferred when the assessment is based on a relevant measure of internal dose (e.g., maximal concentration of an active metabolite in target tissue) rather than simply the administered dose or exposure concentration. To obtain such measurements, the relevant biology, physicochemical properties, and biochemical mechanisms of a specific agent are used to construct biologically based models that can be used to predict its uptake, disposition, target tissue dose, and ensuing tissue responses in test animals and humans. The focus of this special issue is the state of the science underlying the development and application of a specific type of biologically based model (i.e., physiologically based pharmacokinetic or (PBPK) models) in risk assessment. The fourteen papers presented herein address critical issues and advances relating to their use in current risk assessment approaches with a focus on their use in emerging toxicology paradigms as well.

The first paper in this issue (J. C. Caldwell et al.) presents an overview that (1) briefly introduces the papers contained in this special issue; (2) provides context for how they inform best modeling practices and state-of-the-art risk assessment applications of PBPK models; (3) discusses limitations and bridges of modeling approaches for future applications and how papers within the issue fit into that emerging science. Specifically, novel approaches for estimation/characterization of metabolic parameters for PBPK models are examined in two articles (i.e., W. S. Cuello et al. and T. Peyret and K. Krishnan) with application of PBPK models for determination of exposure and interpretation of biomarker data examined in three articles (i.e., R. A. Becker et al., C. Lu and Andres, and K. McNally et al.). The special issue contains several case studies that illustrate the development and/or use of quantitative models to address specific needs of risk assessment of selected chemicals (i.e., H. Mielke and U. Gundert-Remy, M. D. Taylor et al., D. C. Dorman et al., and C. Huynh-Delerme et al.) and chemical mixtures (N. C. Y. Wang et al. and A. F. Sasso et al.). The impact of human population subgroup variability on the magnitude of uncertainty factor developed as part of risk assessment of volatile organic chemicals is also described (i.e., M. Valcke et al.). A broader perspective on the use of PBPK models for addressing contemporary issues in risk assessment is presented along with a progress report on the development of a PBPK "tool-box" for more general applications (i.e., M. Mumtaz et al.).

In summary, the collection of papers by leading experts in this field that comprise this special issue provides insight and tools for a wide spectrum of risk assessment applications. These papers can be used for (1) facilitation of the screening and prioritization of chemicals, (2) linkage of exposure to internal dose, (3) analysis of mechanistic information and prediction of risk to chemical mixtures, and (4) provision of computational techniques and tools to address uncertainty and variability questions related to identification and prediction of responses and pharmacokinetics in potentially

sensitive subpopulations. We hope that this "snapshot" of the current state of the science, best practices, and challenges for application of these tools in emerging risk assessment approaches and data will be of tremendous interest to the regulatory and scientific communities internationally. This information can build a foundation for use of these predictive models for a variety of applications and for future reduction of uncertainty in those predictions.

Disclaimer

The views expressed in this editorial are those of the guest editors and do not necessarily reflect the views or policies of the US Environmental Protection Agency.

Acknowledgment

Such an effort not only involves a great many authors but also reviewers. The authors would like to thank each for their cooperation, diligence, and timely contributions. They would also like to thank the Hindawi Press Editorial staff, Nehal Salama and Lydia Samir, for their cooperation, patience, and hard work from the conception and compilation phases through the editing and publication of this special issue.

Jane C. Caldwell
Kannan Krishnan
Marina V. Evans

Hindawi Publishing Corporation
Journal of Toxicology
Volume 2012, Article ID 852384, 10 pages
doi:10.1155/2012/852384

Review Article

Cutting Edge PBPK Models and Analyses: Providing the Basis for Future Modeling Efforts and Bridges to Emerging Toxicology Paradigms

Jane C. Caldwell,[1] Marina V. Evans,[2] and Kannan Krishnan[3]

[1] *National Center for Environmental Assessment Office of Research and Development, U.S. Environmental Protection Agency, 1200 Pennsylvania Avenue, Washington, DC 20460, USA*
[2] *National Health and Environmental Effects Research Laboratory, Office of Research and Development, U.S. Environmental Protection Agency, Research Triangle Park, NC 27711, USA*
[3] *Department of Occupational and Environmental Health, Université de Montréal, Montreal, QC, Canada H3C 3J7*

Correspondence should be addressed to Jane C. Caldwell, caldwell.jane@epa.gov

Received 9 April 2012; Accepted 21 June 2012

Academic Editor: Jack Ng

Physiologically based Pharmacokinetic (PBPK) models are used for predictions of internal or target dose from environmental and pharmacologic chemical exposures. Their use in human risk assessment is dependent on the nature of databases (animal or human) used to develop and test them, and includes extrapolations across species, experimental paradigms, and determination of variability of response within human populations. Integration of state-of-the science PBPK modeling with emerging computational toxicology models is critical for extrapolation between *in vitro* exposures, *in vivo* physiologic exposure, whole organism responses, and long-term health outcomes. This special issue contains papers that can provide the basis for future modeling efforts and provide bridges to emerging toxicology paradigms. In this overview paper, we present an overview of the field and introduction for these papers that includes discussions of model development, best practices, risk-assessment applications of PBPK models, and limitations and bridges of modeling approaches for future applications. Specifically, issues addressed include: (a) increased understanding of human variability of pharmacokinetics and pharmacodynamics in the population, (b) exploration of mode of action hypotheses (MOA), (c) application of biological modeling in the risk assessment of individual chemicals and chemical mixtures, and (d) identification and discussion of uncertainties in the modeling process.

1. Introduction: PBPK Modeling

After exposure of environmental pollutants or pharmaceuticals to humans, experimental animals and, where relevant, cellular systems, potential adverse effects are dependent on an agent's toxicokinetic information (absorption, distribution, metabolism, and elimination (ADME). Physiologically based pharmacokinetic (PBPK) models are a class of biological models that utilize this information to translate external exposures into an internal (target) dose in the body. PBPK models are not only often used to predict toxicologically relevant internal doses, but also to account for any nonlinearities between internal and external applied dose or exposure. Traditionally, these models have been used for performing extrapolations between different routes of exposure and between different species; they use species specific anatomical, physiological, chemical-specific, and biochemical parameters [1, 2]. However, parameters may vary between species and chemicals of interest (e.g., solubility and metabolic transformation rates within tissues of the body) and the accuracy of any PBPK model dependent on the accuracy of its parameter information [3]. Not only are metabolic parameters species-specific, but in many cases considerable parameter variability exists between individuals within populations. The impact of parameter variability on predictions of toxicologically relevant doses can be estimated

through PBPK model configuration changes. Although thought to be greater in humans than in the test animals often used to test toxicity, the impact of variability within species can be estimated by sensitivity and uncertainty analyses of PBPK models.

PBPK models describe the mass balance of materials within and between various tissue compartments. In terms of model structure, if the transfer of substances across the capillary and cellular membrane is very rapid compared to the perfusion rate of the tissue, then the three compartments can be collapsed into one homogeneous compartment depicting the whole organ. In these cases, the model is called a "flow-limited" model, and the ratio of concentration between the blood and the organ (partition coefficient) is governed by the solubilities in each tissue and metabolic processes within the organ [3]. Therefore, the disposition of a chemical throughout the body is governed by partitioning between organs and blood, partitioning between blood and air, blood flows to organs, ventilation rates, absorption rates, metabolic rates, and elimination rates [3].

Toxicological applications for PBPK modeling have been increasing over the last 30 years. The many applications and role of this science include determining: (a) environmental exposure from sampling of parent and/or metabolite(s) in tissue and biological fluids, (b) target organ or system concentrations of parent and/or metabolite(s) from exposure, (c) the appropriate dose metric from mode of action (MOA) information, and (d) the use of PBPK modeling to test hypothesis regarding the effects of metabolic variation. When human data (e.g., pharmacokinetic and exposure) are available, PBPK models can be used directly to transform external exposure estimates into internal doses. When experimental animal data are only available, extrapolation uncertainty can be reduced by the use of an appropriate PBPK model. However, this reduction in one type of uncertainty may be outweighed by the introduction of other types of uncertainty associated with the structure and assumptions inherent in the modeling. Such uncertainty includes the limitations of describing the scope and nature of variability of pharmacokinetics and pharmacodynamics of an agent within the human population. Human variability could be due to differences among individual adults, across genders, or between life stages. In support of human health assessments, a key expectation of future PBPK modeling efforts increased ability to accommodate increases in knowledge of population variability in a number of areas, such as target organ structure, types and numbers of cells at risk to toxicant exposure, age- and gender-specific differences, and human activity patterns. In this way, mechanistic and mode of action (MOA) explanations can be linked to quantified measures of exposure.

The cover of this special issue (i.e., shown below in Figure 1) illustrates key extrapolations made between the cellular *in vitro* responses from single cells to risk of health effects in humans. These steps include (1) interpretation of *in vitro* cellular signals within a complex network of signaling pathways at the cellular level (i.e., the pathway shown is for NFκB which is relatively complex and context dependent on its action [4]), (2) construction of a validated PBPK model (i.e., the recently published PBPK model for trichloroethylene which represents a complex and state of the art effort), and (3) extrapolation of internal dose and response of a target organ or system in DaVinci's "ideal man." While such a prediction to the ideal or "average" individual is often the reported result, such predictions are not representative of sensitive subpopulations that are epigenetically and genetically diverse, and more liable to express an endpoint of concern resulting from concurrent exposures, gender, age, and stage of development. The goals of this editorial overview are threefold: (1) to highlight the principles of best practices in PBPK models intended for risk assessment application, (2) to provide a perspective on the articles in the special issue, and (3) to present our viewpoints of what represents the cutting edge of science in this field and what specific research needs and approaches may be useful in making progress towards future applications.

2. Best Practices

Computational models of toxicological processes are developed based on hypothetical or proven interrelationships among critical processes and parameters. However, before they can be used confidently in risk assessments or other applications, it is essential that the model structure, parameters, and performance are evaluated systematically. Even though the terms—model validation and model evaluation—are used interchangeably or preferentially, they refer to whether a model with a given set of input parameters can reasonably reproduce the system behavior for a defined set of conditions, and whether the key determinants of the system behavior have been adequately captured by the model [5]. Often, the developers of the model and those who apply the model have different views and expectations in regard to model validation.

An important aspect in assessing the performance of a PBPK model is how well it fits several data sets. It is important to be able to understand and characterize the strengths, limitations, and relevance of the data to the endpoint(s) of concern, and to choose measured endpoints for comparison with predicted results. The accuracy and precision of the methods used in each study used to provide that data and the apparent reproducibility of results must be examined so that such judgments can be made. Variation of results reported from differing studies may reflect human variability of response, the effects of differing exposure protocols, or differences in the accuracy or precision of measured values in each study [3].

Even though there has been extensive focus on a model's ability to provide predictions that match closely with some limited data, the more relevant goal should be to characterize the level of confidence in the model's fit for a specific purpose or end-use. Accordingly, there is increasing emphasis on evaluating a model rather than validating a model (e.g., [6]). If a model has been developed for a specific purpose (e.g., a particular risk assessment application), then relevant aspects of the model should be evaluated in context. In this regard, the International Program on Chemical Safety (IPCS) of the World Health Organization (WHO) has recently published

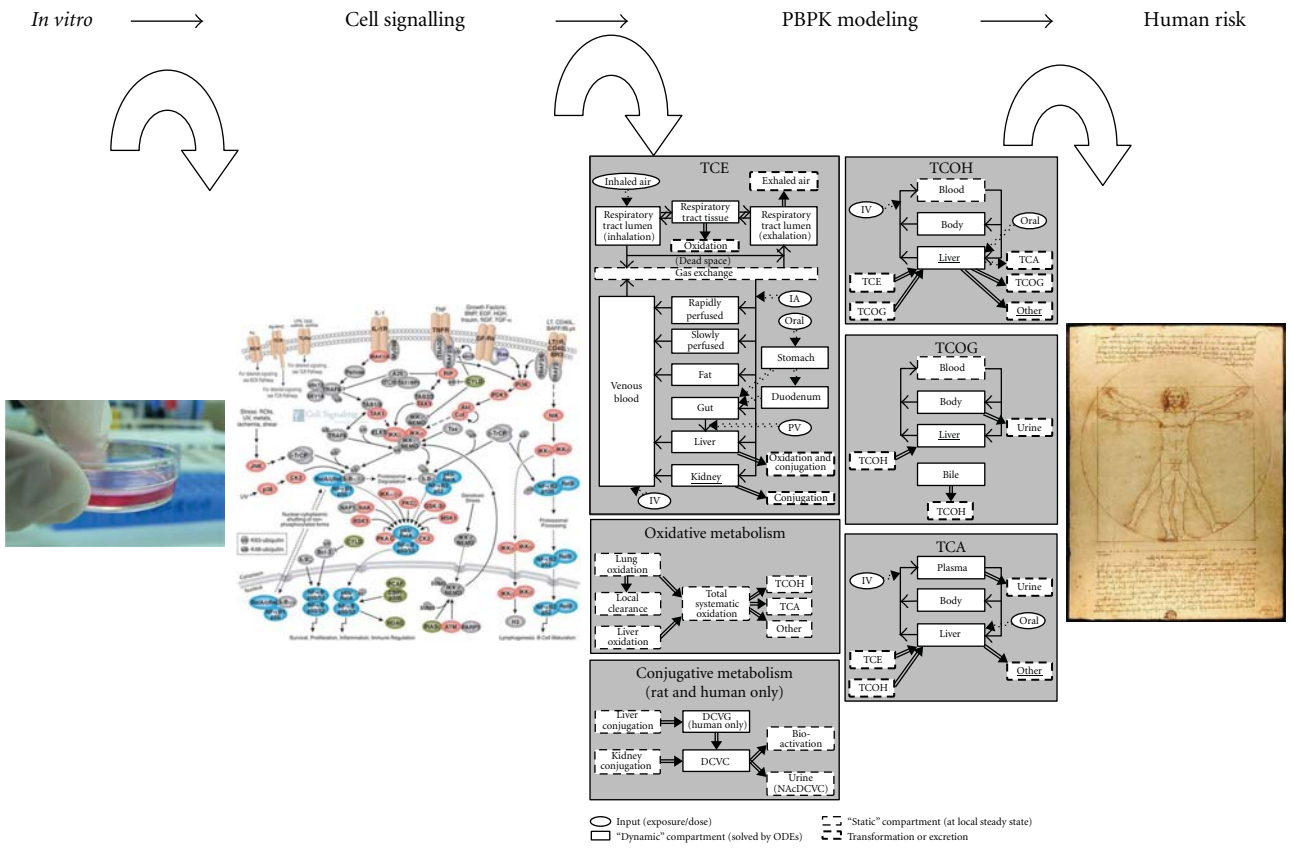

Figure 1: This figure represents, in simplistic fashion, major extrapolations between data that has been derived from *in vitro* isolated cell systems to interpretations of that data for cell-signaling pathways, the extrapolation of cell signaling results in regard to PBPK models that assign appropriate dose metrics and target organ concentrations, and finally the prediction of human risk from resulting models for a particular xenobiotic exposure.

guidelines for characterization and purpose-specific evaluation of PBPK models [7]. A detailed description of the PBPK model evaluation process for use in risk assessment is also described in a recent publication [8]. Accordingly, if the model is to be used for conducting interspecies extrapolation for the oral route based on a particular dose metric (e.g., AUC), then the evaluation should focus on the ability of the model to provide the relevant simulations, and not on generically "validating" the model for all possible applications. Thus, the level of confidence in the use of a PBPK model for a defined and specific purpose in a risk assessment (e.g., prediction of a dose metric for conducting rat to human extrapolation) can be established on the basis of the following [7]: In this context, the following key aspects/questions are evaluated [7].

(i) Do the model structure and parameters have a reasonable biological basis?

(ii) How well does the PBPK model reproduce the chemical-specific pharmacokinetic data under various experimental or exposure conditions?

(iii) How reliable is the PBPK model with regard to its predictions of dose metrics relevant to risk assessment? In this regard, it is important to evaluate the level of sensitivity of the predictions to the model parameters and the level of uncertainty of the parameter values. Emphasis is placed on sensitivity and uncertainty sensitivity analyses so as to identify the following:

(a) the model parameters that most strongly influence the dose metrics associated with human risk assessment conditions (e.g. exposure pathways, relevant exposure conditions such as acute or chronic), and

(b) the model parameters that have the most influence on the dose metrics associated with the study or studies from which the critical endpoints are derived (i.e. toxicity, epidemiological, and clinical studies).

Documentation of model development is not only essential for evaluation of the key aspects of the model that appear to function appropriately, but also for those that did not during the development process. The following general principles constitute the current state of best practice in PBPK modeling [7–10]. (1) The model should be capable of simulating all potentially useful dose metrics for the exposure routes, lifestages, and doses in the species of relevance to

an assessment; (2) the structure of the PBPK model should contain the target organ (or a surrogate tissue) as well as compartments representing tissues of unique physiological and biochemical relevance to the pharmacokinetics of the chemical; (3) the equations chosen to describe ADME should be scientifically supported; (4) the tissue volumes, flow rates, ventilation: perfusion ratios used in the model should be within physiological limits, the sum total of the tissue volumes should not exceed the body weight, and the sum total of tissue blood flow rates should equal cardiac output; (5) partition coefficients for the model should be obtained using *in vitro* methods, *in vivo* data obtained at steady-state, or theoretical algorithms within their boundary of valid application; (6) biochemical parameters for the model should be estimated from *in vivo* data or on basis of adequate scaling of *in vitro* data; (7) solutions to the differential equations in a PBPK model need not to be evaluated if a highly reputable commercial or open source simulation software has been used although an appropriate algorithm should have been selected; (8) the appropriateness of the integration algorithm and integration intervals should be justified, particularly when a new software tool or a custom-made program is used for modeling; (9) evaluation of the model structure and parameters should be conducted to ensure that the model adequately predicts the pharmacokinetic behavior (i.e., bumps and valleys in the concentration versus time plot) of the chemical and that the parameters (point estimates, range of values, or distributions) consistently describe available data; (10) sensitivity, uncertainty, and variability analyses should be conducted using acceptable statistical methods.

3. State-of-the Art Application of PBPK Modeling in Risk Assessments

While the toxicological profiles and IRIS values produced by EPA are not complete risk assessments, they provide information on a chemical's potential for causing adverse health effects along with information about the relationship between the dose of the substance and the biological response. When this information is combined with information about exposure, these values are used internationally to characterize the public health risks of chemical substances [11]. PBPK models have been developed for several high profile chemicals that are the subject of EPA IRIS assessments. Recent state-of-the-art analyses have used PBPK models and human and rodent data sets for such applications to high impact and complex risk assessments. They form a bridge for future development of PBPK model applications to even more complex data sets.

Dichloromethane (methylene chloride or DCM) has been modeled to have two pathways of metabolism (i.e., oxidative and GSH conjugation pathway) with the GSH pathway assumed to be responsible for its carcinogenicity [12, 13]. Alternatively for one of the most important P450 isozymes (CYP2E1) in the toxicology of environmental exposures, new PBPK models and a reexamination of *in vitro* and *in vivo* data show that DCM metabolism can primarily occur through this enzyme via the oxidative pathway, but with two sites for DCM metabolism [14, 15]. Trichloroethylene (TCE) is a widespread environmental contaminant with complex metabolism that also involves the same two pathways [16]. Both pathways of metabolism are a crucial component of its toxicity, particularly in liver (via the oxidative pathway) and kidney (via the GSH pathway). A state-of-the-art PBPK model for TCE with detailed lung compartments, extensive rodent and human datasets, and Bayesian analyses have been used to (1) characterize uncertainty and variability in these metabolic pathways, and (2) to describe the complex mixture of internal exposures of metabolites linked to TCE's MOA in several target organs that includes predictions of GSH conjugation and bioactivation in the kidney [16–18].

While metabolism is usually limited by the blood flow into the liver of the parent compound (i.e., flow-limited), in the case of methyl tertiary butyl ether (MTBE) metabolism is limited by the ability of the enzyme to metabolize the parent compound (i.e., enzyme-limited) [3]. In this case, human microsomal data in combination with an updated PBPK model may be used to (1) predict human variability for dose metrics potentially associated with human response, and (2) to test hypothetical scenarios representative of the range of human metabolism of MTBE [3]. This example illustrates the use of microsomal metabolism differences in conjunction with PBPK models as a more robust tool than microsomal metabolism differences alone to predict differences in risk.

Evans and Caldwell [14] brought forth that the use of two binding sites for CYP2E1 has the potential not only to account for the broad range of chemicals that it is able to metabolize, but also inferences regarding PBPK modeling and the use of chamber data to discern pharmacokinetics and MOA. The two-binding-site work by Evans and Caldwell [14] was commented on a letter to the editor authored by Anders et al., [19] followed by a response by Evans and Caldwell [15]. In this Special issue Cuello et al. use a similar approach to analyze inhalation chamber data, metabolism data (CYP2E1 and GSH conjugation), and a PBPK model to examine the plausibility of whether two sites on the same enzyme or two separate enzymes can account for *in vivo* metabolic clearance profiles of bromochloromethane, a brominated disinfection byproduct. For both metabolic hypotheses, sensitivity analyses of *in vivo* experimental data are used to evaluate model parameter impacts on predicted outcomes, and to guide the design of future experiments needed to fully address the metabolic mechanisms involved for this specific chemical.

As the available database and PBPK models for a particular chemical can be complex, another layer of complexity can be added from the existence of internal and external metabolite exposure (e.g., TCE and its metabolites) or coexposures to similar compounds. In this special issue, Sasso et al. present a lipid-based PBPK model for the analysis of a mixture of six polychlorinated biphenyls (PCBs) in rats. Population Bayesian analysis was applied that incorporated an internal exposure-response model linking enzyme induction and metabolic rate. The PBPK model was specialized to simulate concentrations of highly lipophilic compounds in tissue lipids without the need for partition coefficients. In addition, a hierarchical treatment of

population metabolic parameters and a CYP450 induction model were incorporated, and Markov-Chain Monte Carlo simulation applied. For all dose levels and dose profiles, the model predicted PCB concentrations in multiple tissues. This specific computational technique provides an alternate approach for analysis of compounds for which partition coefficients are not experimentally available (e.g., as is the case for most nonvolatile compounds).

After exposure, a chemical's MOA and background metabolite exposure affects the selection of an appropriate dose metric for modeling internal concentrations in target organs or systems. Along with differences in pharmacokinetic parameters, there is variability in response to a particular dose metric concentration within the human population due to a number of factors that include developmental status and age at exposure (i.e. children versus adults). The differences in pharmacokinetic parameters and development of PBPK models between potential sensitive human subpopulations and/or life stages are the subject of several papers in this Special issue.

In 2008, Health Canada concluded that (1) while recent developments in PBPK modeling of manganese were important and informative, the science was not appropriate at that point in time for establishing a health-based reference concentration for inhaled manganese, and (2) a validated, peer-reviewed human inhalation PBPK model for manganese parameterized for the various subgroups of concern was needed [20]. These subgroups include neonates, iron-deficient individuals, and others with certain medical conditions such as cholestatic liver disease [21, 22]. In this special issue, Dorman et al. present a review of the topic as it relates to generation of pharmacokinetic information on the inorganic manganese combustion products of the organometallic fuel additive methylcyclopentadienyl manganese tricarbonyl (MMT) in compliance with the test rule under the US Clean Air Act. The Alternative Tier 2 testing program for MMT is described with emphasis on the development of pharmacokinetic data and generation of PBPK models for manganese. In the companion paper, Taylor et al. review (1) the development of PBPK models for experimental animals and human at various stages of development, (2) relevant risk assessment applications of the models, and (3) model predictions of manganese tissue concentrations for individuals with altered physiology due to life stage or condition including age (e.g., fetal, neonatal), pregnancy status, liver disease, or chronic inhalation exposure to manganese. Applications of such model predictions include the development of uncertainty factors for use in risk assessments that take into account these populations.

The impact of variability in human whole and subpopulations on uncertainty factors was also examined by Valcke et al. in this special issue; human kinetic adjustment factors (HKAF) were discussed for inhaled volatile organic chemicals (VOCs). Population distributions (i.e., for adults, elderly, children, neonates and pregnant women) of blood concentrations and rates of metabolism were generated by Monte Carlo simulations to a steady-state algorithm for Benzene and 1,4-dioxane (1,4-D) exposure. For these specific blood-flow-limited volatiles, blood concentration-based HKAFs were the most affected in distinct subpopulations (i.e, blood concentration having a greater effect than rates of metabolism).

For one of the three case studies presented for PBPK model applications in risk assessment, the specific effects of age are also reported by Mielke and Gundert-Remy in this special issue. In the first case study, lower enzyme expression levels in newborn infants are used to estimate bisphenol A (BPA) blood levels near the TDI for the oral exposure as calculated by the European Food Safety Authority (EFSA). In another case study, adult risk is reported from dermal exposures to BPA. Finally, after dermal exposure to coumarin via cosmetic products, PBPK modeling was used to identify liver peak concentration (the dose metric used for liver toxicity). Dermal and oral exposure pathways were compared. In these cases PBPK modeling was useful to support risk assessments.

When linked with biomarker data, the reconstruction of exposure dose using PBPK modeling has been offered as a valuable tool. However, as noted by McNally et al. in this special issue, due to the lack of exposure and kinetic data, the correlation of biomarker levels with exposure concentrations leads to difficulty in utilizing biomonitoring data for biological guidance values. McNally et al., use exposure reconstruction (i.e., reverse dosimetry), PBPK modeling, global sensitivity analysis, Bayesian inference, and Markov chain Monte Carlo simulation to obtain a population estimate of inhalation exposure to *m*-xylene. The importance of model structure and dimensionality is also examined with respect to its ability to reconstruct exposure.

The example of chlorpyrifos illustrates the need to take into account differences in susceptibility and the need to understand background exposures of its metabolites in children to reconstruct exposure through PBPK modeling. The PBPK model of Lu et al. [23] had limited success in predicting exposure from urine measurements due to the combination of different sources of exposure. However, the PBPK model for chlorpyrifos was a valuable tool when describing urine in children having ingested specific known amounts of chlorpyrifos. Using urinary biomarker data as the input, Lu et al. report in this special issue the development of a simplified pharmacokinetic model (SPK) for estimation of absorbed doses of chlorpyrifos. Of note, the dose estimates using the SPK model for individual children were significantly higher than those from the conventional PBPK modeling using aggregate environmental measurements of chlorpyrifos as the inputs.

As demonstrated by the work of Lu et al., simplifications of PBPK models are being developed, but the types of data used to support such efforts are not always available. There is a need for simplified modeling approaches that are still valid for use in risk assessment. While all risk assessments involve uncertainty related to extrapolations from study data to human risk from environmental or pharmaceutical exposures, PBPK models themselves contain two types of uncertainty [3]. Model uncertainty refers to the lack of knowledge needed to determine whether the scientific theory on which a model is based is correct (e.g., alternative choices for model structure, dose metrics, extrapolation approaches, and the appropriateness of surrogate data as

in inferences about children from adult data). Parameter uncertainty refers to lack of knowledge about the values of a model's parameters which leads to a distribution of values for each parameter; this uncertainty includes random measurement errors, systematic measurement errors, the use of surrogate data instead of direct measurements, misclassification of exposure status, random sample errors, and the use of an unrepresentative sample. Simplified PBPK model development will need to be specific enough for the types of compounds and scenarios modeled to address both of these types of uncertainty.

For use in site-specific health assessments, Mumtaz et al. (this special issue) report progress on the ATSDR's initiative to develop a PBPK tool box. This tool is designed to contain a series of published models coded in Berkeley Madonna. Ongoing efforts focus on producing a Web linkage to a PBPK database and models that can be accessed for use in assessment activities. In addition, Mumtaz et al. present examples of PBPK model applications that led to (1) derivation of minimal risk levels (MRLs), (2) risk assessment of mixtures, (3) assessment of occupational exposures, (4) site specific assessment, and (5) interpretation of human biomonitoring data.

Finally, in another current application of PBPK models, data from a single patient are used for a clinical case study. In this special issue, the brief communication of Huynh-Delerme et al. is a good example of this type of practical application of PBPK modeling. Potential ethanol exposure was predicted from inhalation or dermal uptake after repeated use of an ethanol-based hand sanitizer. The study investigated whether blood concentrations could be correlated with the incidence of acute pancreatitis in a single patient potentially exposed in the classroom. Thus, this example illustrates another way of applying PBPK models in characterizing the association between health effects and chemical exposures in humans.

4. Bridges and Limitations for Future Applications

Extrapolation between rodents and humans of the pharmacokinetic behavior of an agent, using only differences in a power of the body weight, inherently assumes that metabolic clearance is scaled consistently across species. However, this assumption does not hold for all dose metrics and enzyme systems [7], and issues arise as to how appropriately scale across species. Extrapolation based on appropriate dose metrics simulated with PBPK models for the test and target species is the preferred approach [7, 24].

Most PBPK models have been developed and tested with experimental animal data and used for extrapolation purposes. Increasingly, this type of data is less available and *in vitro* data or high throughput data from gene expression microarrays are being developed as replacements for animal testing [25, 26]. Although in place for about 10 years, microarray data is no longer the cutting edge with RNA sequencing taking its place for exploration of what types of responses and genetic predispositions lead to cancer and noncancer outcomes. Cell-signaling and gene expression data must in turn be processed through complex informatics approaches to identify pathways and relationships that can further be understood in a physiological context [27, 28]. For relevant dose metrics, PBPK model predictions provide the bridge between concentrations associated with specific cellular responses *in vitro* for a particular paradigm, and the extrapolation to concentrations at the target system or organ in the whole organism. However, all modeling should have phenotypic anchoring in physiology, toxicology, and sound modeling and mathematics to test and understand the models.

The PBPK modeling approach has also been applied to conducting *in vitro* to *in vivo* extrapolations of equivalent doses on the basis of appropriate dose metrics [29–32]. Whole-body PBPK models have been developed for extrapolating the *in vitro* concentration-response curve to *in vivo* dose response [33]. In the context of the next generation toxicity testing initiatives, more recent development in terms of cellular-level PBPK models (e.g., [34]), and biologically based algorithms to predict partitioning into cells, interstitial fluids, and vascular compartments (e.g., [35, 36]) are likely to facilitate more elegant implementation of the *in vitro* to *in vivo* paradigms.

Such biologically based mechanistic algorithms have been developed for the determination of partition coefficients (PCs) that represent the equilibrium ratio of chemical concentration and are, in turn, key input parameters of PBPK models (e.g., blood : air, tissue : blood). The composition of cells, interstitial fluid, and vascular components along with the physiochemical characteristics of chemicals are used in these algorithms to help predict PCs of new chemicals based on QSARs; the algorithms can then be used to help characterize human variability. Initially based on chemical solubility in water and lipid (i.e., from n-octanol : water PCs or vegetable : water PCs ($P_{o:w}$)), first generation efforts focused on prediction of tissue : blood PCs of VOCs, for which macromolecular binding in tissue and blood is negligible [37, 38]. These algorithms were also used to estimate preliminary PCs (e.g., tissue : air, blood : air, tissue : blood) for nonionized and low molecular weight organic chemicals with (1) negligible protein binding (or assumed to be negligible) and (2) one or more CH_3, CH_2, CH, C, C=C, H, Cl, Br, F, benzene ring, or H in benzene ring fragments.

On the basis of the solubility and binding processes that are relevant to both ionic and nonionic forms and found in both intracellular and extracellular matrices, the second-generation algorithms not only predicted PCs, but also distribution coefficients (i.e., the sum of ionized and non-ionized forms of chemical in both matrices) [39, 40]. Most recently, Schmitt [35] and Peyret et al. [41] integrated existing algorithms within a single equation for the prediction of distribution coefficients for drugs and environmental chemicals, respectively. Ionization, lipid solubility, water solubility, and tissue binding characteristics (i.e., binding to tissue proteins, acid phospholipids, plasma proteins and hemoglobin) were used in these integrated algorithms to facilitate the prediction of the PCs. When only chemical solubility in lipids and water determine partitioning, all

existing algorithms give the same prediction as that of the first-generation algorithm of Poulin and Krishnan [37]; however, when binding to various components is significant then second generation algorithms have been used as reported for the development of PBPK models for pharmaceuticals [42]. However, despite the availability of algorithms and QSARs for predicting partition coefficients of organic chemicals, the availability of metabolism rates for PBPK model development remains a major limiting factor. Very limited research has been conducted for predicting maximal velocity ($V_{\max}$) and Michaelis affinity constant (K_m) for hepatic and extrahepatic metabolism of chemicals (reviewed in [36]). Even though a molecular structure-based QSAR for hepatic clearance has been developed for integration within PBPK models of VOCs, there has not been any attempt to develop global QSARs or quantitative property-property relationships (QPPRs) for wider applicability and integration within PBPK models.

In this special issue, Peyret and Krishnan used QPPR relationship to predict intrinsic clearance ($V_{\max}/K_m$) for volatile organic chemicals. Estimates of intrinsic clearance were then used to parameterize a PBPK model for predicting a blood concentration time course for a series of chemicals. This approach presented in this paper is an initial attempt to develop global QPPRs for estimating intrinsic clearance for incorporation within PBPK models. The approach allows for generation of pharmacokinetic profiles that are consistent with the level of uncertainty in model predictions of intrinsic clearance. It is important to note the limitations of such estimates in order to provide transparency in the risk assessment context, but also to aid in the design of future studies for reduction of uncertainty.

Human liver tissues, hepatocytes, and microsomes continue to represent useful systems to explore individual differences in metabolism of xenobiotics. However, alone these data are not adequate to predict differences in human responses [43]. Under circumstances where rate of metabolism and not blood flow determines *in vivo* intrinsic clearance [3], variability of metabolism extrapolated from human microsomal data can be informative when coupled with an appropriate PBPK model. However, there is uncertainty with procedures extrapolating metabolic values from *in vitro* systems, especially for enzymes that are membrane bound. Recently, a computational approach for the accurate estimation of metabolic clearance for membrane bound compounds (such as P450s) has been developed to address the complexity of these issues [44].

Given the desire to reduce the use of extensive animals testing, there is great interest in extrapolation of *in vitro* toxicity data (human and rodent systems) with PBPK models to calculate human equivalent doses for a given concentration *in vitro*. The corresponding NOAEC or AC_{50}% (i.e., the concentration at 50% some specified maximal activity) could therefore be calculated using full-blown PBPK models or steady-state algorithms. The feasibility of using steady-state algorithms and *in vitro* screens to conduct *in vitro-in vivo* extrapolation for hazard ranking development has been reported [45, 46]. However, the adequacy of these approaches with regard to their assumption of 100% oral bioavailability and attainment of steady state during oral exposures needs to be further evaluated as a function of the information on chemical-specific dose metrics and MOA.

Although PBPK models and steady-state algorithms are designed to predict tissue and/or blood concentrations, further steps are needed to predict effects from internal doses. After estimation of internal dose from an external dose via PBPK modeling, biologically based dose-response (BBDR) models use internal dose estimates to predict response or toxicity through, for example, statistical correlations. Such BBDR models have been proposed as a computational tool for estimation of human risk. In general, there are a larger number of published PBPK models than BBDR models. The development of BBDR models is usually dependent on prior development of PBPK models; the added complexity and MOA information needed for BBDR model development may also hinder such model development. A BBDR model must also specify dosimetric and effect relationships across different species and exposure types in order to be considered successful, but such modeling does offer a unique opportunity to incorporate MOA information into one framework [47]. However, in addition to the uncertainty in both PBPK and BBDR models themselves, there is inherent uncertainty in the linkage of both components.

One of the major areas of BBDR development has been the quantification of cancer data through the use of two-stage clonal expansion models [48]. Although these BBDR models are biologically defensible, one of their inherent limitations is associated with the uncertainty of extrapolation from high doses (experimental data) to low doses (environmental exposure), as discussed by Crump et al. [49]. The technological problem becomes one of quantification of effect at low doses, where the noise in the data can overshadow the toxicological effect being measured. Hence, the advantage introduced by the addition of mechanistic steps into the model can be negated by both the inability to describe the dose response curve at low concentrations and to quantify the uncertainty introduced by the extrapolation process itself. These aspects of the process are not necessarily dependent on the biological mechanism used to describe the relationship.

BBDR model development can be used to investigate potential MOAs or the ability to identify data gaps. For a series of chemicals having a common MOA, a generalized BBDR model would be expected to explain relevant data for all chemicals. However, a recent application of BBDR modeling using a common liver MOA of action for several chemicals was successful in fitting the data for the individual chemicals but was not able to provide a generalized BBDR model common to all chemicals [50]. These authors indicated that, specifically for chloroform, the model may have oversimplified events leading to cancer. Although additional data may be helpful in establishing these details, the impact of uncertainty in the MOA should be addressed alongside BBDR model development [49].

Environmental exposures to contaminants do not occur in isolation but as mixtures. The health effects associated with mixture exposures are a result of not only the toxicity of each component, but also the interactions among the components. Even though the hazard characterization of

individual specific chemicals has been the primary focus of numerous agencies (e.g., EPA and IARC), site-specific risk assessments are often for exposure to multiple chemicals. PBPK modeling approaches are continually being developed for mixtures. In this special issue, several papers addressed this subject (Sasso et al., Wang et al., and Becker et al.). Sasso et al. developed a PBPK model for a mixture of polychlorinated biphenyls. Complex total petroleum hydrocarbon (TPH) mixtures and their associated risks to human health were assessed by Wang et al. utilizing *in silico* or computational toxicological modeling approaches (i.e., comparative molecular field analysis and hierarchical clustering) in conjunction with established mixture risk assessment methods. Wang et al.'s *in silico* approach was compared to expert-driven judgment of fractionation of TPHs and their associated potential. The continued development of modeling approaches for complex mixtures is expected to both provide consistency in the appropriate grouping of chemicals in mixture analyses, and to predict the contribution of the individual chemicals to the overall toxicity.

On a broader scale, Becker et al. note that the evaluation of a large number of chemicals in commerce for potential human health risk has become a focus of attention in North America and Europe. Using translation from an external dose to a biomarker concentration framework, Becker et al. describe approaches for development of screening-level exposure guidance values. Specifically, applications of tools and concepts are discussed that include the threshold of toxicologic concern (TTC), biomonitoring equivalents (BEs), and generic toxicokinetic and physiologically based toxicokinetic models.

5. Summary and Conclusions

Along with traditional uses of route-to-route and species-to-species extrapolations, PBPK models are being developed and tested for MOA applications and, based on biological sampling of metabolites and parent compounds in human tissue, reconstruction of exposure from model predictions. Increasingly sophisticated mathematical approaches and analyses are also being used to examine variability in pharmacokinetics. With less animal data available for model inputs, current efforts for screening and future efforts for new toxicology tests to replace animal testing are focusing on approaches based on either simplified models suitable for application to *in vitro* information or less-extensive animal data. In addition to *in vitro* to *in vivo* extrapolation, PBPK modeling applications continue to be developed as risk assessment tools for mixtures risk assessments, and developed for mechanism-based predictions that allow for linkage between internal dose-derived predictions (i.e. from PBPK models) and dose response (i.e. from BBDR models). In summary, as exemplified by the papers in this special issue, PBPK modeling provides tools for a wide spectrum of risk assessment applications that include (1) facilitation of the screening and prioritization of chemicals, (2) linkage of exposure to internal dose, (3) use in analysis of mechanistic information and prediction of risk to chemical mixtures, and (4) provision of computational techniques and tools to address uncertainty and variability questions related to identification and prediction of responses and pharmacokinetics in potentially sensitive subpopulations.

Abbreviations

1,4-D:	1,4-dioxane
ADME:	Absorption, distribution, metabolism, and elimination
BEs:	Biomonitoring equivalents
BPA:	Bisphenol A
CYP:	Cytochrome P450
DCM:	Dichloromethane
EFSA:	European Food Safety Authority
EPA:	Environmental Protection Agency
HKAF:	Human kinetic adjustment factor
IARC:	International Agency for Research on Cancer
IPCS:	International Program on Chemical Safety
IRIS:	Integrated Risk Information System
MMT:	Methylcyclopentadienyl manganese tricarbonyl
MTBE:	Methyl tertiary butyl ether
MOA:	Mode of action
NFκB:	Nuclear factor kappa-light-chain-enhancer of activated B cells
OECD:	Organization for Economic Co-operation and Development
PBPK:	Physiologically based pharmacokinetic
QSAR:	Quantitative structure-activity relationship
RT-PCR:	Real-time polymerase chain reaction
TDI:	Tolerated daily intake
TPH:	Total petroleum hydrocarbon
TTC:	Threshold of toxicologic concern
VOCs:	Volatile organic chemicals
WHO:	World Health Organization.

Disclaimer

The views expressed in this paper are those of the authors and do not necessarily reflect the views or policies of the U.S. Environmental Protection Agency.

Conflict of Interests

The authors declare no competing financial interests.

Disclosure

The authors declare no competing financial interests. This paper is part of a Journal of Toxicology special issue on "State of the Science: Biologically Based Modeling in Risk Assessment." J. C. Caldwell served as lead guest editor and M. V. Evans and K. Krishnan as guest editors of the special issue.

References

[1] M. Reddy, H. J. Clewell, M. E. Andersen, and R. S. H. Yang, *Physiologically-Based Pharmacokinetic Modeling: Science and Applications*, Wiley Inter-Science, 2005.

[2] K. Krishnan, G. D. Loizou, M. Spendiff, J. C. Lipscomb, and M. E. Andersen, "PBPK modeling: a primer," in *Quantitative Modeloint in Toxicology*, K. Krishnan and M. E. Andersen, Eds., pp. P21–P58, John Wiley & Sons, Chichester, UK, 2010.

[3] J. N. Blancato, M. V. Evans, F. R. Power, and J. C. Caldwell, "Development and use of PBPK modeling and the impact of metabolism on variability in dose metrics for the risk assessment of methyl tertiary butyl ether (MTBE)," *Journal of Environmental Protection*, vol. 1, pp. 29–51, 2008.

[4] J. D. Scheff, S. E. Calvano, S. F. Lowry, and I. P. Androulakis, "Modeling the influence of circadian rhythms on the acute inflammatory response," *Journal of Theoretical Biology*, vol. 264, no. 3, pp. 1068–1076, 2010.

[5] K. Krishnan and M. E. Andersen, "Physiologically-based pharmacokinetic and toxicokinetic modeling," in *Principles and Methods in Toxicology*, A. Wallace Hayes, Ed., pp. 232–291, Taylor and Francis, New York, NY, USA, 2007.

[6] H. A. Barton, W. A. Chiu, R. W. Setzer et al., "Characterizing uncertainty and variability in physiologically-based pharmacokinetic (PBPK) models: state of the science and needs for research and implementation," *Toxicological Sciences*, vol. 99, no. 2, pp. 395–402, 2007.

[7] World Health Organization (WHO), *Characterization and Application of Physiologically Based Pharmacokinetic Models in Risk Assessment*, World Health Organization, International Programme on Chemical Safety, Geneva, Switzerland, 2010.

[8] E. D. McLanahan, H. El-Masri, L. M. Sweeney et al., "Physiologically based pharmacokinetic model use in risk assessment—why being published is not enough," *Toxicological Sciences*, vol. 126, no. 1, pp. 5–15, 2012.

[9] U.S. EPA, "Approaches for the application of physiologically based pharmacokinetic (PBPK) models and supporting data in risk assessment," Final Report EPA/600/R-05/043A, US Environmental Protection Agency, Washington, DC, USA, 2006.

[10] W. A. Chiu, H. A. Barton, R. S. DeWoskin et al., "Evaluation of physiologically based pharmacokinetic models for use in risk assessment," *Journal of Applied Toxicology*, vol. 27, no. 3, pp. 218–237, 2007.

[11] P. Anastas, Written testimony by EPA's Assistant Administrator for Research and Development for hearing on EPA's Integrated Risk Information System before the U.S. House of Representatives, Committee on Energy and Commerce, Subcommittee on Environment and Economy, 2011, http://republicans.energycommerce.house.gov/Media/file/Hearings/Environment/100611/Anastas.pdf.

[12] M. L. Gargas, M. E. Andersen, and H. J. Clewell III, "A physiologically based simulation approach for determining metabolic constants from gas uptake data," *Toxicology and Applied Pharmacology*, vol. 86, no. 3, pp. 341–352, 1986.

[13] M. E. Andersen, H. J. Clewell III, M. L. Gargas, F. A. Smith, and R. H. Reitz, "Physiologically based pharmacokinetics and the risk assessment process for methylene chloride," *Toxicology and Applied Pharmacology*, vol. 87, no. 2, pp. 185–205, 1987.

[14] M. V. Evans and J. C. Caldwell, "Evaluation of two different metabolic hypotheses for dichloromethane toxicity using physiologically based pharmacokinetic modeling for in vivo inhalation gas uptake data exposure in female B6C3F1 mice," *Toxicology and Applied Pharmacology*, vol. 244, no. 3, pp. 280–290, 2010.

[15] M. V. Evans and J. C. Caldwell, "Response to letter to the Editor by Anders et al," *Toxicology and Applied Pharmacology*, vol. 248, no. 1, pp. 65–67, 2010.

[16] U.S. EPA, "Toxicological review of trichloroethylene," CAS 79-01-6, In Support of Summary Information on the Integrated Risk Information System (IRIS), 2011.

[17] W. A. Chiu, M. S. Okino, and M. V. Evans, "Characterizing uncertainty and population variability in the toxicokinetics of trichloroethylene and metabolites in mice, rats, and humans using an updated database, physiologically based pharmacokinetic (PBPK) model, and Bayesian approach," *Toxicology and Applied Pharmacology*, vol. 241, no. 1, pp. 36–60, 2009.

[18] M. V. Evans, W. A. Chiu, M. S. Okino, and J. C. Caldwell, "Development of an updated PBPK model for trichloroethylene and metabolites in mice, and its application to discern the role of oxidative metabolism in TCE-induced hepatomegaly," *Toxicology and Applied Pharmacology*, vol. 236, no. 3, pp. 329–340, 2009.

[19] M. W. Anders, M. E. Andersen, H. J. Clewell III, M. L. Gargas, F. P. Guengerich, and R. H. Reitz, "Evaluation of two different metabolic hypotheses for dichloromethane toxicity using physiologically based pharmacokinetic modeling of in vivo gas uptake data exposure in female B6C3F1 mice," *Toxicology and Applied Pharmacology*, vol. 248, no. 1, pp. 63–64, 2010.

[20] Health Canada, "Human health risk assessment for inhaled manganese—Results of public comments: major comments and responses, 2008," http://www.hc-sc.gc.ca/ewh-semt/consult/-2008/manganese/result-eng.php.

[21] OEHHA and California EPA, Reference exposure levels for acrolein, acetaldehyde, arsenic, mercury, manganese, and formaldehyde, 2008, http://oehha.ca.gov/air/hot_spots/2008/AppendixD1_final.pdf.

[22] ATSDR, "Toxicological profile for manganese," draft for public comments period ended on February 26, 2009, 2008, http://www.atsdr.cdc.gov/toxprofiles/tp.asp?id=102&tid=23.

[23] C. Lu, C. M. Holbrook, and L. M. Andres, "The implications of using a physiologically based pharmacokinetic (PBPK) model for pesticide risk assessment," *Environmental Health Perspectives*, vol. 118, no. 1, pp. 125–130, 2010.

[24] C. M. Thompson, B. Sonawane, H. A. Barton et al., "Approaches for applications of physiologically based pharmacokinetic models in risk assessment," *Journal of Toxicology and Environmental Health B*, vol. 11, no. 7, pp. 519–547, 2008.

[25] R. S. Judson, H. M. Mortensen, I. Shah, T. B. Knudsen, and F. Elloumi, "Using pathway modules as targets for assay development in xenobiotic screening," *Molecular BioSystems*, vol. 8, no. 2, pp. 531–542, 2012.

[26] N. C. Kleinstreuer, R. S. Judson, D. M. Reif et al., "Environmental impact on vascular development predicted by high-throughput screening," *Environmental Health Perspectives*, vol. 119, no. 11, pp. 1596–1603, 2011.

[27] A. A. Margolin and A. Califano, "Theory and limitations of genetic network inference from microarray data," *Annals of the New York Academy of Sciences*, vol. 1115, pp. 51–72, 2007.

[28] J. Imura, K. Kashima, M. Kusano, and T. Morohoshi, "Peicewise affine systems approach to control of biological networks," *Philosophical Transactions A*, vol. 368, no. 1930, pp. 4977–4993, 2010.

[29] J. DeJongh, A. Forsby, J. B. Houston, M. Beckman, R. Combes, and B. J. Blaauboer, "An integrated approach to the prediction of systemic toxicity using computer-based biokinetic models and biological in vitro test methods: overview of a prevalidation study based on the ECITTS," *Toxicology in Vitro*, vol. 13, no. 4-5, pp. 549–554, 1999.

[30] B. J. Blaauboer, "The integration of data on physico-chemical properties, in vitro-derived toxicity data and physiologically based kinetic and dynamic as modelling a tool in hazard and risk assessment. A commentary," *Toxicology Letters*, vol. 138, no. 1-2, pp. 161–171, 2003.

[31] B. J. Blaauboer and M. E. Andersen, "The need for a new toxicity testing and risk analysis paradigm to implement REACH or any other large scale testing initiative," *Archives of Toxicology*, vol. 81, no. 5, pp. 385–387, 2007.

[32] A. Forsby and B. Blaauboer, "Integration of in vitro neurotoxicity data with biokinetic modelling for the estimation of in vivo neurotoxicity," *Human and Experimental Toxicology*, vol. 26, no. 4, pp. 333–338, 2007.

[33] J. Louisse, E. de Jong, J. J. M. van de Sandt et al., "The use of in vitro toxicity data and physiologically based kinetic modeling to predict dose-response curves for in vivo developmental toxicity of glycol ethers in rat and man," *Toxicological Sciences*, vol. 118, no. 2, pp. 470–484, 2010.

[34] A. N. Edginton, G. Ahr, S. Willmann, and H. Stass, "Defining the role of macrophages in local moxifloxacin tissue concentrations using biopsy data and Whole-body physiologically based pharmacokinetic modelling," *Clinical Pharmacokinetics*, vol. 48, no. 3, pp. 181–187, 2009.

[35] W. Schmitt, "General approach for the calculation of tissue to plasma partition coefficients," *Toxicology in Vitro*, vol. 22, no. 2, pp. 457–467, 2008.

[36] T. Peyret and K. Krishnan, "QSARs for PBPK modelling of environmental contaminants," *SAR and QSAR in Environmental Research*, vol. 22, no. 1-2, pp. 129–169, 2011.

[37] P. Poulin and K. Krishnan, "A biologically-based algorithm for predicting human tissue: blood partition coefficients of organic chemicals," *Human and Experimental Toxicology*, vol. 14, no. 3, pp. 273–280, 1995.

[38] P. Poulin and K. Krishnan, "Molecular structure-based prediction of the partition coefficients of organic chemicals for physiological pharmacokinetic models," *Toxicology Methods*, vol. 6, no. 3, pp. 117–137, 1996.

[39] T. Rodgers, D. Leahy, and M. Rowland, "Tissue distribution of basic drugs: accounting for enantiomeric, compound and regional differences amongst β-blocking drugs in rat," *Journal of Pharmaceutical Sciences*, vol. 94, no. 6, pp. 1237–1248, 2005.

[40] T. Rodgers and M. Rowland, "Physiologically based pharmacokinetic modelling 2: predicting the tissue distribution of acids, very weak bases, neutrals and zwitterions," *Journal of Pharmaceutical Sciences*, vol. 95, no. 6, pp. 1238–1257, 2006.

[41] T. Peyret, P. Poulin, and K. Krishnan, "A unified algorithm for predicting partition coefficients for PBPK modeling of drugs and environmental chemicals," *Toxicology and Applied Pharmacology*, vol. 249, no. 3, pp. 197–207, 2010.

[42] M. D. Thompson and D. A. Beard, "Physiologically based pharmacokinetic tissue compartment model selection in drug development and risk assessment," *Journal of Pharmaceutical Sciences*, vol. 101, no. 1, pp. 424–435, 2012.

[43] J. C. Lipscomb, J. W. Fisher, P. D. Confer, and J. Z. Byczkowski, "In vitro to in vivo extrapolation for trichloroethylene metabolism in humans," *Toxicology and Applied Pharmacology*, vol. 152, no. 2, pp. 376–387, 1998.

[44] P. Poulin, J. R. Kenny, C. E. Hop, and S. Haddad, "In vitro-in vivo extrapolation of clearance: modeling hepatic metabolic clearance of highly bound drugs and comparative assessment with existing calculation methods," *Journal of Pharmaceutical Sciences*, vol. 101, no. 2, pp. 838–851, 2012.

[45] D. M. Rotroff, B. A. Wetmore, D. J. Dix et al., "Incorporating human dosimetry and exposure into high-throughput in vitro toxicity screening," *Toxicological Sciences*, vol. 117, no. 2, pp. 348–358, 2010.

[46] B. A. Wetmore, J. F. Wambaugh, S. S. Ferguson et al., "Integration of dosimetry, exposure, and high-throughput screening data in chemical toxicity assessment," *Toxicological Sciences*, vol. 125, no. 1, pp. 157–174, 2012.

[47] H. J. Clewell and M. E. Andersen, "Applying mode-of-action and pharmacokinetic considerations in contemporary cancer risk assessments: an example with trichloroethylene," *Critical Reviews in Toxicology*, vol. 34, no. 5, pp. 385–445, 2004.

[48] S. H. Moolgavkar, "Biologically motivated two-stage model for cancer risk assessment," *Toxicology Letters*, vol. 43, no. 1–3, pp. 139–150, 1988.

[49] K. S. Crump, C. Chen, W. A. Chiu et al., "What role for biologically based dose-response models in estimating low-dose risk?" *Environmental Health Perspectives*, vol. 118, no. 5, pp. 585–588, 2010.

[50] N. S. Luke, R. Sams, M. J. DeVito, R. B. Conolly, and H. A. El-Masri, "Development of a quantitative model incorporating key events in a hepatotoxic mode of action to predict tumor incidence," *Toxicological Sciences*, vol. 115, no. 1, pp. 253–266, 2010.

Hindawi Publishing Corporation
Journal of Toxicology
Volume 2012, Article ID 629781, 14 pages
doi:10.1155/2012/629781

Research Article

Physiologically Based Pharmacokinetic (PBPK) Modeling of Metabolic Pathways of Bromochloromethane in Rats

W. S. Cuello,[1] T. A. T. Janes,[1] J. M. Jessee,[1] M. A. Venecek,[1] M. E. Sawyer,[2] C. R. Eklund,[3] and M. V. Evans[3]

[1] *Research Experience for Undergraduate participant, Department of Mathematics, North Carolina State University, Raleigh, NC 27695, USA*
[2] *Department of Mathematics, North Carolina State University, Raleigh, NC 27695, USA*
[3] *National Health and Environmental Effects Research Laboratory, US Environmental Protection Agency, Office of Research and Development, Research Triangle Park, NC 27709, USA*

Correspondence should be addressed to M. V. Evans, evans.marina@epa.gov

Received 18 January 2012; Revised 27 March 2012; Accepted 30 March 2012

Academic Editor: Kannan Krishnan

Bromochloromethane (BCM) is a volatile compound and a by-product of disinfection of water by chlorination. Physiologically based pharmacokinetic (PBPK) models are used in risk assessment applications. An updated PBPK model for BCM is generated and applied to hypotheses testing calibrated using vapor uptake data. The two different metabolic hypotheses examined are (1) a two-pathway model using both CYP2E1 and glutathione transferase enzymes and (2) a two-binding site model where metabolism can occur on one enzyme, CYP2E1. Our computer simulations show that both hypotheses describe the experimental data in a similar manner. The two pathway results were comparable to previously reported values ($V_{\max} = 3.8$ mg/hour, $K_m = 0.35$ mg/liter, and $k_{GST} = 4.7$/hour). The two binding site results were $V_{\max_1} = 3.7$ mg/hour, $K_{m_1} = 0.3$ mg/hour, $CL_2 = 0.047$ liter/hour. In addition, we explore the sensitivity of different parameters for each model using our obtained optimized values.

1. Introduction

Bromochloromethane (BCM, CH_2BrCl, CAS number 83847-49-8) is a volatile solvent historically used in portable fire extinguishers. BCM was gradually replaced by halons in the 1970s and banned in 2002 due to its ozone depletion potential. However, BCM is still used as an intermediate in the production of other solvents [1] and is rapidly absorbed via inhalation due to its volatility [2]. Similar to other halomethanes, there is a suggestion of hepato- and nephro-toxicity due to prolonged exposure [2]. Another potential source of exposure for BCM is through oral ingestion via water, since BCM is considered a water disinfection byproduct [3], and is listed within the U.S.A EPA's Candidate Contaminant List (CCL). Additional research on brominated disinfection by-products (DBPs) has been proposed because there is evidence that brominated species can be more potent than chlorinated compounds [4]. The occurrence of brominated disinfection by-products (e.g., bromochloromethane) is an added consideration for coastal areas due to potential bromine intrusion from seawater and subsequent transformation of chlorinated by-products into brominated species [5]. Given the potential health impact of brominated chemicals, we chose to study BCM in consideration of both increased potential for exposure near coastline utilities, and on the basis of a deficiency and availability of published data. Based on a recent PubMed search, the published literature for BCM is much less than that of the well-studied bromodichloromethane (BDCM, $CHBrCl_2$, CAS number 75-27-4), another structurally related DBP.

Physiologically based pharmacokinetic (PBPK) models are computational tools that are increasingly used to address risk assessment issues, particularly in quantifying the relationship between measures of external exposure and internal dose [6]. PBPK models are sets of equations representing the flow of blood and toxicant into and out of organs and body tissues. Unlike classical pharmacokinetic models,

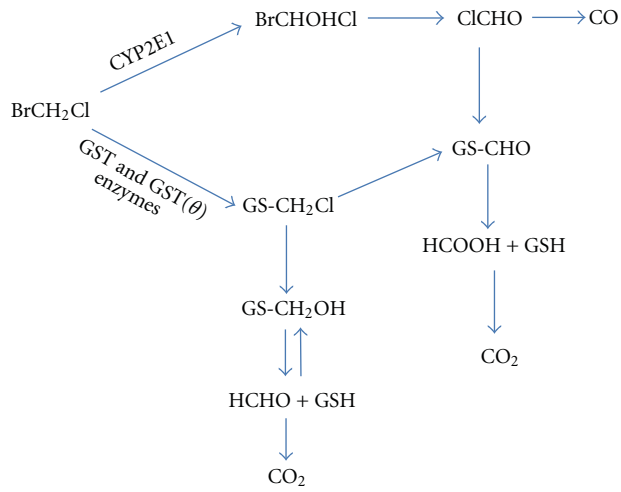

Figure 1: Schematic representation of BCM metabolism, adapted from [13].

PBPK models include species-specific physiological, chemical, and biochemical parameters, allowing for extrapolation to humans [7]. The interaction between modelers and biologists is crucial in determining the final representation of organs to ensure inclusion of target organs, special physicochemical properties and toxicity. An accurate mathematical description of biological processes (i.e., an accurate model) requires synthesis of mathematics, modeling, and systems biology. The expectation of such an approach is that an integrated modeling effort and its application to quantification of health risk assessment would increase our confidence in the simulated results.

For volatile halogenated methanes, metabolism is an important component studied to provide explanations of how toxicity occurs. The complex kinetics suggested for dihalomethane metabolism (e.g., BCM) consists of two components: a saturable Michaelis-Menten hyperbola superimposed with a linear pathway [9]. This linear pathway does not appear to saturate and shows a continued proportional increase at higher exposure concentrations. At lower concentrations, the contribution of this linear pathway is smaller than that of the saturable component. The question becomes what are the physiological counterparts of these two different metabolism components? What enzymes may exhibit such different characteristics? Previous PBPK modeling work with dichloromethane (DCM, CH_2Cl_2, CAS number 75-09-2) led to the hypothesis that two different enzymes are involved in its metabolism: CYP2E1, a P450 isoenzyme, and GST (GSH S-transferase). The early PBPK modeling work was followed by experiments showing that the GST pathway, although numerically small, was an important pathway toxicologically. Based on experimental evidence, the GST pathway is believed to be responsible for the carcinogenicity of these compounds [15]. The early PBPK modeling paved the way for establishing a two-pathway hypothesis which includes both P450 and glutathione transferase (GST) enzymes [9]. Based on these concepts, the proposed metabolic scheme for bromochloromethane is shown in (Figure 1). Specifically for BCM, the two-pathway hypothesis was first suggested by PBPK modeling followed by experimental confirmation of adduct formation from the GST pathway in bacterial assays [16]. Using an *in vitro* Salmonella assay, BCM was confirmed to be mutagenic in the presence of cytosol (GST containing fraction) relative to other structurally related halomethanes [17]. Based on structural similarity with other brominated ethanes (i.e., 1,2-dibromoethane), where plasma bromide was used to track metabolism, the existence of a small but relevant GST pathway is to be expected for BCM [18]. However, we were not able to find *in vivo* studies that can be used to quantify the linear pathway for BCM, other than suggestions that *in vivo* data is lacking [13].

Other than having two different enzymes describe the complex kinetics, is there another plausible explanation for the linear kinetics exhibited by the *in vivo* closed chamber data? If so, can PBPK modeling be used to explain the additional linear kinetics? In recent years, the realization has been made that several P450s may exhibit atypical kinetics, that is, complex kinetics that cannot be explained by the single saturable Michaelis-Menten kinetics [19]. In an attempt to better describe these increased complexities, biochemical models with two sites have been developed to describe the linear kinetics exhibited at higher concentrations [20]. These complex biochemical models have an additional binding site, which is simultaneously available to the substrate (Figure 2). Once binding to the second site occurs, a conformational change takes place that modifies the metabolism of the first site. We propose that a PBPK model for BCM can be constructed to show the plausibility of a second site model. At this point in time, we are not suggesting that one kinetic model is more realistic than the other, but are investigating the possibility of alternative pathways based on atypical kinetics and its implications for metabolism. Interestingly, one potential way to distinguish between the two mechanism is by the type of metabolites excreted. With two-sites in a single enzyme, the metabolites produced would probably be reactive products of CYP2E1 oxidation. In contrast, a two-pathway mechanisms would have glutathione containing metabolites during excretion.

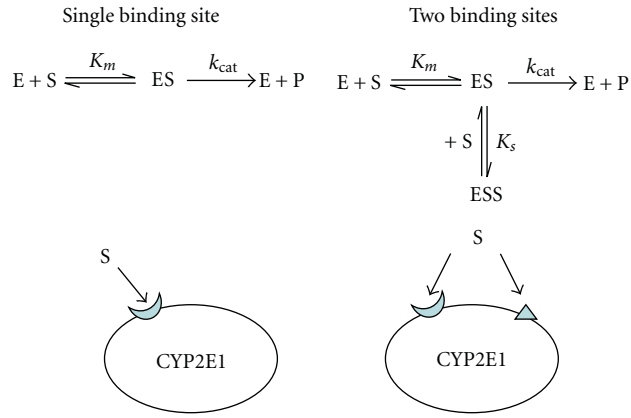

Figure 2: Comparison of single-sited and two-sited kinetics, adapted from [14].

When testing a new hypothesis using PBPK model simulations, one possible question becomes how to rank the importance of relative metabolic parameters. We believe that this question is particularly relevant when trying to distinguish between metabolic constants that are numerically small. Sensitivity analysis is a mathematical tool that allows determination of how the change in one parameter affects model predictions. When conducting sensitivity analysis, the model is run repeatedly to determine how changes in parameter values relate to changes in a prediction. Although optimization is performed before sensitivity analysis, modeling behavior insights come from the sequential sensitivity analysis. The sensitivity analysis results will also be dependent on the values obtained from the optimization. Both techniques are combined since the first is needed to find the "correct" parameter values, while sensitivity analysis looks for impact across parameters. In the present work, both techniques were used to identify potential issues with metabolic parameter quantification. Once the optimization is performed, sensitivity analysis can determine if a unique set of values exist for the optimized results. In general, sensitivity analysis has been used in combination with PBPK modeling to estimate the relative ranking of different model parameters [21], sometimes including the interaction between parameters [22]. Local sensitivity analysis is the simplest form of sensitivity analysis, which allows for estimation of the impact of each parameter individually. One potential analogy is that this type of sensitivity analysis is similar to a worst-case scenario estimate for the variability of each parameter. In addition to ease of implementation, another advantage of this analysis is its ability to sort potential identifiability issues, or to state whether the optimization provides unique estimates for the resulting values obtained for the different modeling hypotheses.

In summary, the goals of this study were (1) to use PBPK modeling in combination with BCM closed chamber data to test two potential metabolic hypotheses: a two-pathway enzyme combination of CYP2E1 and GST and a one enzyme mechanism consisting of two binding sites for CYP2E1; (2) to make use of sensitivity analysis to identify important model parameters; (3) to compare the fits across different metabolic hypotheses and suggest future experiments that lead to increased confidence in our simulations.

2. Methods

2.1. PBPK Models

2.1.1. Closed Chamber Data. Inhalation closed chamber data for BCM in rats were obtained from the published literature [9] digitized using UN-SCAN-IT 6.0 (Silk Scientific, Orem, UT, USA). Inhalation closed chamber data were collected from a sealed system, allowing for quantification of metabolism. A BCM bolus was injected into the chamber at time zero. After equilibrium between the rat and air inside the chamber, BCM decreased with time as it was distributed into tissues and metabolized by the rodent. A PBPK model was then constructed to describe the decline in air chamber concentration. The metabolic parameters were calculated using optimization techniques in combination with the inhalation data. Different metabolic hypotheses were investigated by using a PBPK model with the closed chamber-derived metabolic parameters to predict metabolism.

2.1.2. Core Model. A flow-limited PBPK model based on the structure described by Ramsey and Andersen [23] was used to describe BCM metabolism (Figure 3). A seven-compartment model (lung, blood, adipose, rapidly perfused tissue, slowly perfused tissue, liver, and kidney) was developed for BCM, with the assumption that metabolism occurred via the same enzymes in liver and kidney. All physiological parameters were obtained from the literature as shown in Table 1 . Differential equations based on mass conservation principles were derived for each organ. Lung and blood compartments use a steady state assumption, simplifying the overall solutions for the model. Tissue to blood partition coefficients were calculated using experimentally-derived BCM coefficients from Gargas et al., 1986 [9] (described in the appendix). After derivation, all equations were coded into MatLab (MathWorks, version 7.11.0.584) using the equation solver *ode15s*.

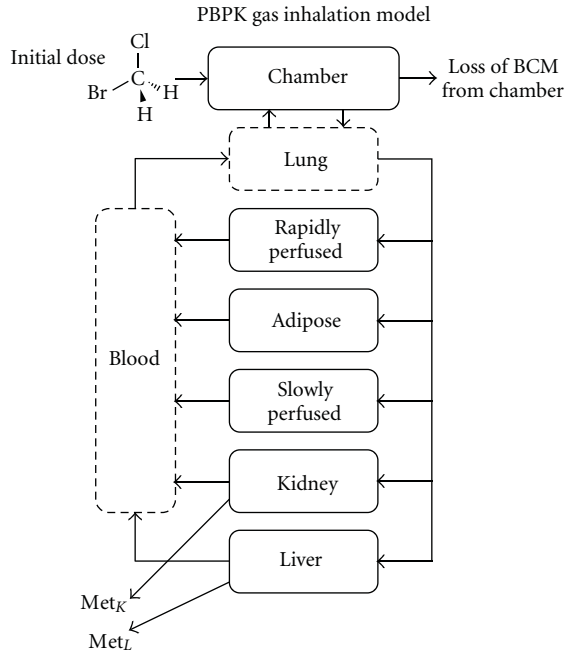

Figure 3: Schematic representation of PBPK model used for BCM.

Table 1: Parameters for adult Fisher 344 rats and corresponding significance in the PBPK model. (Note: partition coefficients are unitless [8].)

Parameter		Significance	Value	Source
Miscellaneous	BW	Body weight	0.25 kg	[9]
	QCC	Cardiac output	15 L/hr/kg$^{0.75}$	[10–12]
	loss	Chamber loss rate	0.025 (1/hr)	[9]
	N	Number of rats	3	[9]
	V_{cha}	Chamber volume	9 (L)	[9]
Flow rates (L/hr)	QV	Ventilation/perfusion rate	1.7	[12]
	q_1	Rapidly perfused blood flow rate	$QV - \sum q_i$	$\sum q_i$ is the sum of other compartments
	q_2	Blood flow fraction to adipose	0.082	[11]
	q_3	Blood flow fraction to slowly perfused	0.257	Muscle+bone+skin values from [11]
	q_4	Blood flow fraction to kidney	0.138	[11]
	q_5	Blood flow fraction to liver	0.242	[11]
Partition coefficient	P_{art}	Blood/air	41.5	[9]
	P_{liv}	Liver/blood	0.7	[9]
	P_{rap}	Rapidly perfused/blood	0.7	Assumed to be same as liver
	P_{kid}	Kidney/blood	0.7	Assumed to be same as liver
	P_{slow}	Slowly perfused/blood	0.267	Muscle [9]
	P_{adi}	Adipose/blood	7.8	[9]
Volume (L)	V_{slow}	Volume fraction for slowly perfused	0.674	[11]
	V_{liv}	Volume fraction for liver	0.044	[11]
	V_{kidney}	Volume fraction for kidney	0.0075	[11]
	V_{adi}	Volume fraction for adipose	0.112	[11]
	V_{rap}	Rapidly perfused	$0.91 - \sum V_i$	Total vol. — sum of all other compartments. Blood is 9% of BW

2.1.3. Metabolic Hypotheses Testing. The current work tested two different metabolic hypotheses using the same basic PBPK model structure, varying only the equations for liver and kidney metabolism. Previously, Gargas et al. [9] evaluated typical Michaelis-Menten kinetics, with metabolism described by a single CYP2E1 binding site. The results of their simulations demonstrated that the addition of a linear term was necessary to describe the closed chamber data. Thus, a two-pathway model with two different enzymes, CYP2E1 exhibiting Michaelis-Menten kinetics and GST exhibiting linear kinetics, provided much better fits to the data than the model that incorporated only Michaelis-Menten kinetics [9]. Here, the two-pathway model (Michaelis-Menten and GST) described by [9] is compared to the two-binding site model described by Evans and Caldwell [24]. In the two-binding site model, a modified Michaelis-Menten equation that includes two binding sites for CYP2E1 is used to describe BCM metabolism.

2.1.4. Two-Pathway Kinetics. The two-pathway description uses Michaelis-Menten kinetics in addition to a linear term to account for GST metabolism. The equations listed below represent the additional metabolic term in both the liver (Met_l) and the kidney (Met_k). Liver is set to account for 94.8% of total body metabolism and the kidney 5.2% based on [25]:

$$\begin{aligned} Met_l &= 0.948\left(\frac{V_{\max}[\mathrm{C_{liv}}]}{K_m + [\mathrm{C_{liv}}]} + k_{\mathrm{GST}}[C_{\mathrm{liv}}]V_{\mathrm{liv}}\right), \\ Met_k &= 0.052\left(\frac{V_{\max}[\mathrm{C_{kid}}]}{K_m + [\mathrm{C_{kid}}]} + k_{\mathrm{GST}}[C_{\mathrm{kid}}]V_{\mathrm{kid}}\right), \end{aligned} \tag{1}$$

where (i) $V_{\max}$: maximum velocity of the reaction, mg/hour, (ii) K_m: affinity constant, mg/liter, (iii) k_{GST}: proportionality constant for linear pathway metabolized by glutathione transferase, /hour.

2.1.5. Two-Binding Site Kinetics. Linear kinetics at higher concentrations can also be described using a dual binding site, as demonstrated for dichloromethane using closed chamber data [24]. In this case, CYP2E1 undergoes a structural change in which two separate binding sites are simultaneously available to BCM, and metabolism is achieved with one enzyme. For the dual binding site equation, the squared concentration term becomes asymptotically linear at higher exposure concentrations. This squared term is not present in the typical Michaelis-Menten equation and will lead to a different rate of ascent to the asymptote. The modified Michaelis-Menten equation reflecting two binding sites in one enzyme [20] becomes

$$\begin{aligned} Met_l &= 0.948\left(\frac{V_{\max_1}[\mathrm{C_{liv}}] + \mathrm{CL_2}[C_{\mathrm{liv}}]^2}{K_{m_1} + [\mathrm{C_{liv}}]}\right), \\ Met_k &= 0.052\left(\frac{V_{\max_1}[\mathrm{C_{kid}}] + \mathrm{CL_2}[C_{\mathrm{kid}}]^2}{K_{m_1} + [\mathrm{C_{kid}}]}\right), \end{aligned} \tag{2}$$

where (i) $V_{\max_1}$: maximum metabolic rate for the first binding site, mg/hour. The second binding site is accounted for by $\mathrm{CL_2}$, (ii) K_{m_1}: affinity constant for the first binding site, mg/liter, (iii) $\mathrm{CL_2}$: clearance constant consisting of the ratio of the maximum metabolic rate and the affinity constant, $V_{\max_2}/K_{m_2}$, for second binding site, liter/hour.

2.2. Comparison of the Different Metabolic Models. A total of six metabolic parameters were optimized using five closed chamber data sets, each having a different starting concentration. Optimizations were performed using the natural log of the data with MatLab's *fminsearch* function (MathWorks, version 7.11.0.584). For the two-pathway model, three parameters were optimized using the digitized data: $V_{\max}$, K_m, and k_{GST}. For the two-binding site model, three parameters were optimized using the digitized data: $V_{\max_1}$, K_{m_1}, and $\mathrm{CL_2}$. The function *fminsearch*, available in the standard MatLab package, tries to minimize a "cost" as the minimum difference between data and simulation. The best overall fit minimized by *fminsearch* includes the entire data range (200–4000 ppm).

2.3. Physiological Value Selection. The physiological values to be used in the PBPK model have been updated from those used in the original simulations of the data in 1986. As an example, cardiac output values for F344 rats are now available [11]. The range of normalized cardiac output values for F344 rats values (QCC) is between 10–20 liters/hour/kg$^{0.75}$, due to dependence of cardiac output on age. We decided to use the mean value of 15 liters/hour/kg$^{0.75}$, since a 225 g rat is considered adult [10]. The ventilation rate for rats was calculated using the ventilation perfusion ratio, which varies between 1–4 fold due to differences in measurement methodology [22, Table 31]. Since the mean value of 15 liters/hour/kg$^{0.75}$ matched the values used in the benzene PBPK model dated from approximately the same time period as the Gargas dataset, we used the same ventilation perfusion rate as in Medinsky et al. [12] for consistency. The F344-specific tissue perfusion and volume values were adopted from [11].

2.4. Sensitivity Analysis. Sensitivity coefficients were calculated with partial derivatives for each variable of interest with respect to the model parameter being specified in the model. Sensitivity coefficients were then normalized by both the variable and model parameter. The resulting time course for each sensitivity coefficient was plotted. Sensitivity coefficients were calculated using Automated Differentiation written by Martin Fink and available at MatlabCentral (http://www.mathworks.com/matlabcentral/). Another Matlab function written by Adam Attarian (*tssolve* NC State University, Raleigh, NC, USA) was used to organize the partial derivatives and for the final plots. A three-dimensional surface was generated to show variation in sensitivity coefficients with time, and variability within the metabolic parameter. These tests were performed to check stability of the sensitivity coefficients when introducing variability around the optimized estimates.

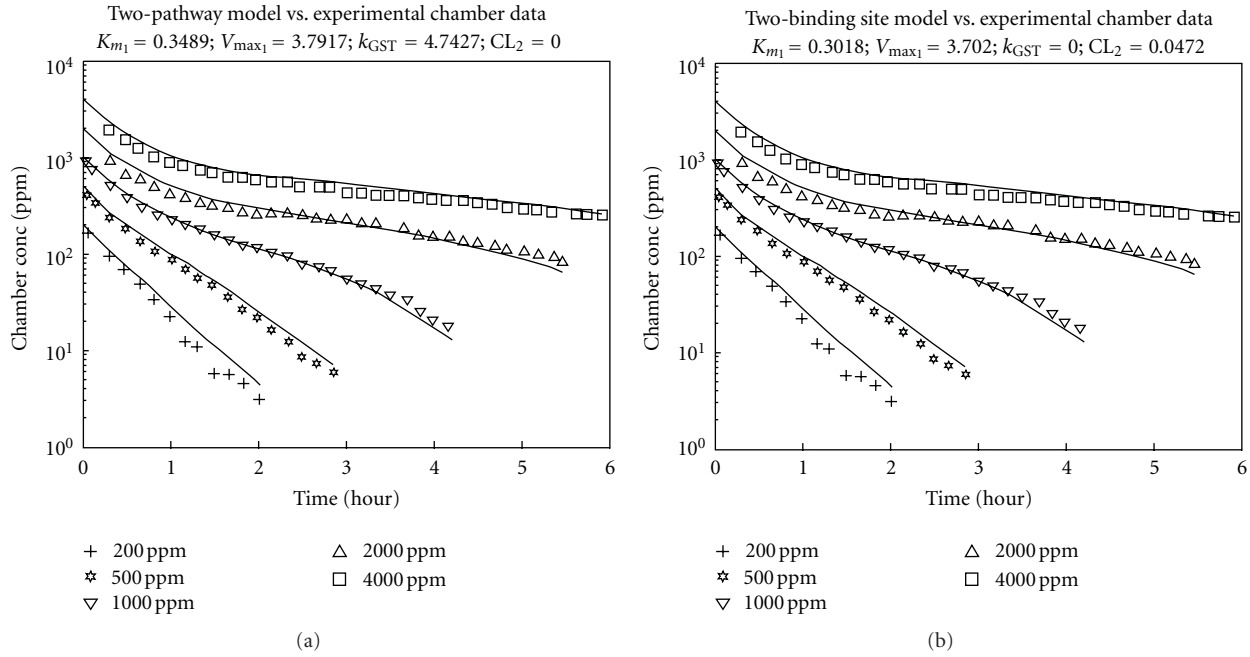

Figure 4: PBPK modeling results using two different metabolic hypotheses. (a) shows results for the two-pathway model. (b) shows results for the two-binding site model.

Table 2: Optimized parameter results.

Two-pathway model		Two-binding site model	
V_{max}	3.8 mg/hour	V_{max_1}	3.7 mg/hour
K_m	0.35 mg/liter	K_{m_1}	0.3 mg/liter
k_{GST}	4.5/hour	CL_2	0.047 liter/hour

3. Results

The optimization results are shown in Table 2. For all concentrations studied, the two-pathway and two-binding site models gave very similar descriptions of the closed chamber data (Figure 4). Both the V_{max} and K_m values are similar for the two-pathway and two-binding models. The two-pathway parameter values were as follows:

$$\begin{aligned} V_{max} &= 3.8\,\text{mg/hour}, \\ K_m &= 0.35\,\text{mg/liter}, \\ k_{GST} &= 4.7/\text{hour}. \end{aligned} \tag{3}$$

The two-binding site hypothesis uses Michaelis-Menten parameters V_{max_1} and K_{m_1} to describe the first site, and clearance CL_2, defined to be the ratio of V_{max_2} and K_{m_2}, for the second site. The two-binding site results were as follows:

$$\begin{aligned} V_{max_1} &= 3.7\,\text{mg/hour}, \\ K_{m_1} &= 0.3\,\text{mg/liter}, \\ CL_2 &= 0.047\ \text{liters/hour}. \end{aligned} \tag{4}$$

When comparing the values for both metabolic hypotheses, Michaelis-Menten results for the two-binding site hypothesis are very similar to the Michaelis-Menten values for the two-pathway hypothesis. The V_{max} and K_m values are similar for the two pathway and two-binding models. Based on these results, both metabolic hypotheses are considered equally plausible.

Normalized sensitivity coefficients for all model parameters were calculated after optimization results were obtained. The majority of resulting sensitivity coefficients were not shown, since we are focusing on metabolic parameters: V_{max}, K_m, k_{GST}, or CL_2. The authors performed sensitivity analysis using 500 ppm as the initial concentration. Each sensitivity figure consists of two panels. The first panel presents sensitivity coefficients calculated for the impact of air chamber concentration on the simulated value of V_{max} and the second panel presents sensitivity coefficients for liver concentration of BCM. Figure 5 presents sensitivity results for the two-pathway model. The sensitivity coefficients for V_{max} have the highest values. The V_{max} sensitivity coefficients for liver concentration are larger than those obtained using chamber air as the experimental variable. Figure 6 presents sensitivity results for the two-binding site model. The sensitivity coefficients for V_{max} also have the highest values, particularly when comparing liver coefficients versus chamber air coefficients. For both model hypotheses, peak V_{max} sensitivity occurs within the first two hours.

A three-dimensional plot of liver sensitivity coefficients for the two-pathway model is presented in Figure 7. The third dimension represents variability in V_{max} generated by repeating sensitivity analysis simulations that vary V_{max} between 2.5–4.5 mg/hour (to include the mean value 3.8 mg/hour). Based on the value of V_{max}, there is a peak in sensitivity to V_{max} occurring within the first 3 hours. The chamber air

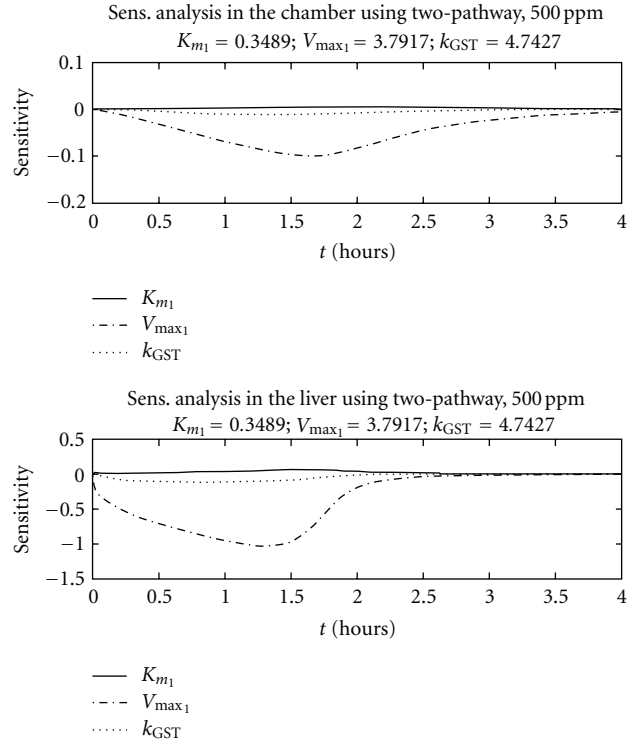

Figure 5: Sensitivity coefficients for the two-pathway model at 500 ppm. Each concentration includes the analysis using air and liver concentrations.

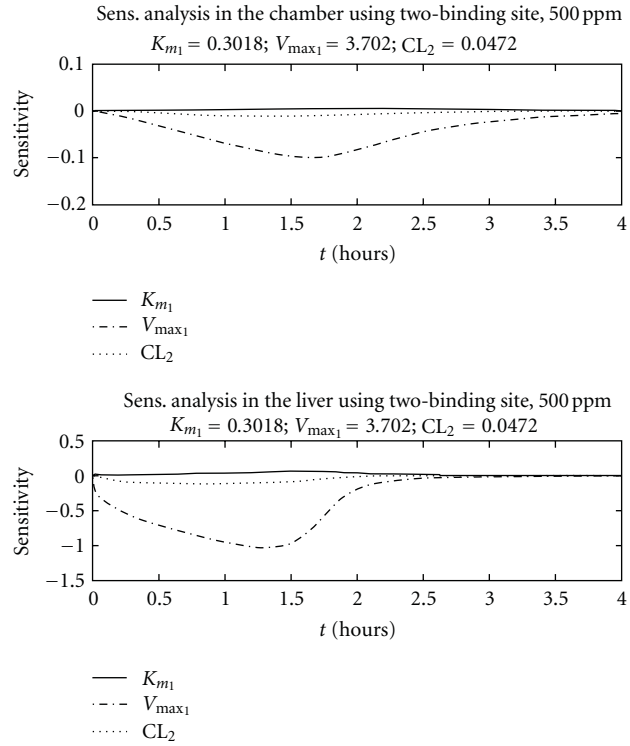

Figure 6: Sensitivity coefficients for the two-binding site model at 500 ppm. Each concentration includes the analysis using air and liver concentrations.

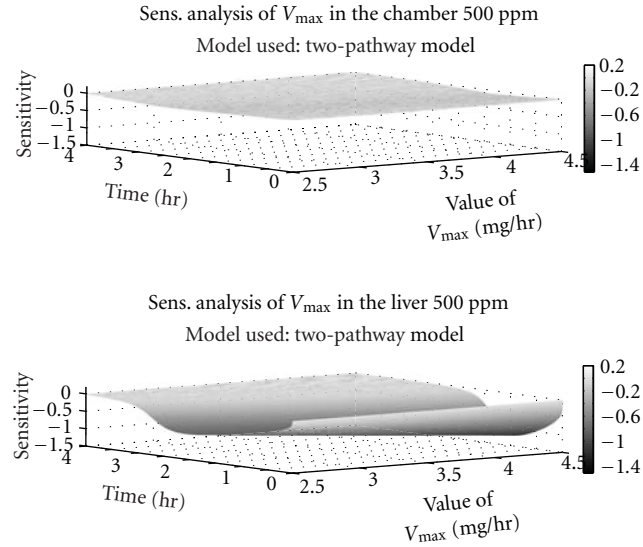

Figure 7: Three-dimensional sensitivity analysis plot for the two-pathway model at 500 ppm.

concentration plot shows a much shallower surface, with no obvious peaks in sensitivity towards V_{max} shown.

4. Discussion

Risk assessments for volatile chemicals have used PBPK models to account for differences across routes and extrapolate from rodent experiments to human populations [26, 27]. The use of a PBPK model allows for the integration of physiological, chemical, and biochemical information with different kinetic hypotheses. Closed chamber inhalation data are a measure of total rate of metabolism represented by the decrease in the concentration of the volatile chemical inside the chamber after a bolus injection. One application of closed chamber inhalation data in combination with PBPK modeling has been the suggestion of metabolic hypotheses leading to effects in a target organ, particularly for halomethanes [9, 28]. In this context, PBPK models have been proposed as useful computational tools for risk assessments.

PBPK models have played a decisive role in the suggestion of an *in vivo* role for the GST pathway (two-pathway model) and its contribution to toxicity for halogenated compounds [15, 28]. In the case of DCM, the GSH conjugation pathway has a small proportionality constant (~0.01/hour [24]), while the GST pathway for BCM is larger (~5.3/hour [9]). Following the inclusion of a linear pathway in the PBPK model for halogens, *in vitro* work in bacterial systems provided the first evidence that GST was the enzyme associated with the additional linear pathway. *In vitro* work also suggested that as the number of bromines included in the compound increased, the resulting genotoxicity was larger. For example, Thier et al. [16] demonstrated that the genotoxicity of CH_2Cl_2 (DCM) was less than that of CH_2ClBr (BCM), which was less than that of CH_2Br_2 (dibromomethane) toxicity. Prior to these experiments, there was no experimental evidence that dihalomethanes such as BCM were metabolized via a GST pathway. The only suggestion for the existence of this second pathway came from PBPK modeling and closed chamber data.

The current PBPK model making use of a two-pathway mechanism gives a similar k_{GST} value to that of previous models (Table 2 versus [9, 29, 30]). (It is important to note that both PBPK models in [29, 30] were based on [9]. In addition, the V_{max} and K_m values are slightly different when compared to [9]: 2.57 mg/hour and 0.3 mg/liter, resp.). We attribute the difference in optimized values to differences in physiological constants used in our model. The current PBPK model made use of F344 specific values [11], which correlates to the strain used in the closed chamber experiments. It is important to note that the F344 physiological values were not available at the time when the first BCM model was published (1986). The largest differences in volume or flow for the compartments used in the two different BCM PBPK models probably lie in the lumped compartments, namely, the rapidly and slowly perfused compartments.

To our knowledge, there is no previous PBPK work that makes use of a two-binding site mechanism for BCM, making a comparison of our linear CL_2 constant with previous models not possible. An important realization of this PBPK modeling effort is that both metabolic hypotheses appeared equally plausible. In order to help convince ourselves that this was the case, the available BCM *in vivo* literature was studied. Early *in vivo* experiments with halomethanes confirmed the enzymatic role for GST for other iodinated or brominated compounds but not for BCM [31]. This paper refers to earlier work and states that specifically for BCM, a BCM-GST reaction is not present in measurable amounts. This early indication concludes that GST is not involved as a major component of BCM metabolism. Another indication that the GST pathway is very small *in vivo* comes from the vapor uptake experiments, where treatment with pyrazole almost completely suppressed BCM metabolism as shown

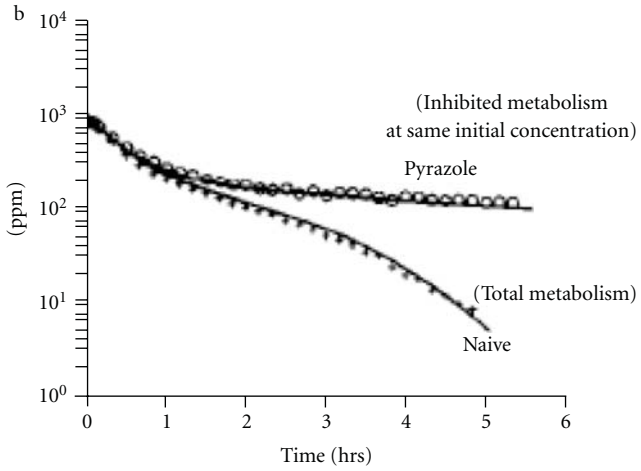

Figure 8: BCM vapor uptake with pyrazole treatment [9].

in Figure 8, from [9]. Since CYP2E1 has been shown to be the major P450 contributing to its oxidative metabolism [32], the *in vivo* metabolic decrease observed at this high concentration argues for the predominance of CYP2E1 over other P450s. In addition, the *in vitro* kinetic values reported by [16] also suggest a small kinetic constant when compared to ethylene dibromide or dibromomethane. The ability to numerically estimate metabolic constants for the linear pathway using sensitivity analysis will be discussed later.

Several P450s (2A1, 2B1, and 2E1) have shown atypical kinetics, explained by allosteric mechanisms making use of a second site at least *in vitro* [33]. Li et al. [33] performed simulations to confirm the relative small size of CYP2E1's active site, stating that for this enzyme the reaction proceeds by the cooperative binding of two substrates simultaneously to form a ternary complex. The substrate that binds in the active site is usually called active substrate, while the other one that binds in the effector site, and that controls the oxidation of the active substrate is called effector substrate [33].

Effector substrates are becoming increasingly studied to offer potential explanations for drug-to-drug interactions. CYP2E1 specifically plays a diverse role in physiology, toxicity, and metabolism. For example, CYP2E1 is a P450 isoform with an important role in glycogenesis, and its physiological role is increasingly being recognized [34]. At present, this isoform is known to metabolize about 70 different compounds of varying size, including alcohols, ketones, nitrosamines, anesthetics, and even long-chain fatty acids. One of the questions recently resolved by studying human CYP2E1 structure is based on addressing how is it possible for this enzyme, with a small active site, to metabolize substrates ranging in a wide number of sizes (including fatty acids). In fact, it is the suggestion of a channel structure available as a second site, and in proximity to the active site, that becomes a solution to help explain CYP2E1's flexibility to accommodate different sized substrates [35]. Although BCM is a small molecule, probably able to fit in the active site, the existence of a second site does describe linear kinetics at higher exposure concentrations. The second site model thus became a candidate for inclusion in a PBPK model calibrated using *in vivo* data for BCM. Since the second binding site in CYP2E1 is involved in fatty acid metabolism, we propose that BCM binding to this second site may impair fatty acid metabolism and may indirectly prevent normal metabolism of larger molecules that may be already impaired in chronic illnesses such as diabetes. This proposed effect is hypothesized to occur in addition to the glutathione-based toxicity based on a two-pathway hypothesis.

When using optimization to estimate metabolic model parameters, correlation can be an important issue that may impact the ability to estimate unique values for the parameters. Basic algebra reminds us that a system of equations can be uniquely solved when the number of parameters is equal to the number of equations, assuming that the estimates are independent of each other. In general, the unique estimation of K_m will depend on having an independent estimate for $V_{\max}$. Since K_m is interrelated to $V_{\max}$, experiments with multiple concentrations are needed, and the concentrations used must be high enough that metabolic saturation is reached.

One of the applications of local sensitivity analysis is to help illustrate the existence of these potential correlations between parameters because this affects the ability to solve for unique estimates. For more complex metabolic models, the relationship between metabolic parameters may not be obvious. Sensitivity analysis theory states that parameters are uniquely identifiable when the sensitivity coefficients cannot add to zero [36]. For example, if all sensitivity coefficients examined are positive, then their sum cannot be equal to zero. Using this reasoning, these authors examined the time course plots for 500 ppm and the sensitivity coefficients for both metabolic hypotheses. The sensitivity coefficients can be estimated for the different variables included in the model, allowing the analysis to suggest improvements in the experimental design. For this reason, liver concentration was selected as a possible experimental variable. When compared with chamber concentration, liver concentration resulted in increased sensitivity towards $V_{\max}$. Since sensitivity coefficients for other metabolic parameters were nearly zero, $V_{\max}$ is uniquely identifiable when using closed chamber experiments. At higher concentrations, the sensitivity coefficients for both k_{GST} or CL_2 increase with exposure time (results not shown). This current sensitivity analysis corroborates the importance of these two additional parameters at higher concentrations.

We utilized a method using local sensitivity analysis as an initial step to help determine identifiability issues. When unique identifiability is guaranteed, the ability to have one unique solution is also guaranteed. Therefore, local sensitivity analysis can be seen as a first step towards increasing our confidence in the parameters obtained as a solution. The results of our sensitivity analysis suggest that measuring liver concentration would provide improved estimates for $V_{\max}$ at intermediate concentrations and improved estimates for the linear constants k_{GST} or CL_2 at high concentrations. To combat uncertainty in the estimates for $V_{\max}$ and other metabolic parameters, we implemented a novel

approach by estimating the three-dimensional surface for the sensitivity coefficient changing with time, and including variability in the metabolic estimate of concern. If future experiments include liver concentration measurements, our three-dimensional analysis at 500 ppm suggests that peak information on V_{max} occurs before 2 hours, suggesting that experiment duration can be shortened by several hours. The application of PBPK modeling and three-dimensional sensitivity analyses can be helpful to design future experiments aimed at refining metabolic estimates.

The combination of optimization and sensitivity analysis presented in this paper also leads to different suggestions for future experimental design. *In vivo* experiments using the vapor uptake approach take advantage of a noninvasive approach to estimate V_{max} and K_m by using air chamber concentration. However, the current sensitivity analysis suggests an increased advantage to using *in vitro* approaches to estimate metabolic parameters. The sensitivity analysis performed consistently indicates that liver tissue measurements increase our ability to estimate V_{max} and k_{GST} for the two-pathway hypothesis. The same sensitivity analysis tools also indicate that our ability to estimate V_{max_1} and CL_2 for two-binding site hypothesis is similar to that for the two-pathway hypothesis. The sensitivity analysis for liver tissue concentration also suggests a peak or maximum ability to estimate V_{max} for an experiment taking 2 hours (instead of 6). Future experiments can include the possible combination of *in vivo* and *in vitro* vapor uptake techniques performed using intermediate concentrations just above and below metabolic saturation (500 ppm in this case).

Future *in vivo* research is needed to answer definitely the question as to whether BCM's atypical metabolism can be described by a two different enzymes or by one enzyme with multiple binding sites. In this paper, we have used PBPK modeling to demonstrate the plausibility of both mechanisms in describing a linear kinetic pathway at higher concentrations. In order to determine if two separate enzymes are involved, a pharmacological agent can be used to deplete the GST pathway to determine if metabolism can proceed without GSH conjugation. As an example, such experiments have been performed for dichloromethane, using phorone as an pharmacological agent leading to GSH depletion [37]. These experiments were performed *in vitro*, using microsomes harvested from the GSH-depleted animals and used with vial equilibration techniques (to determine total changes in amount metabolized *in vitro*). Based on their results, the GST pathway was a small quantitative component of the total amount metabolized. Based on calculations provided by the current PBPK model, the GST pathway is expected to be less than 5% of the total amount metabolized. This small percent of amount metabolized difference is what is being described as either GST- or CYP2E1-dependent. In order to experimentally measure the difference in GST-mediated metabolism, a pharmacological agent such as phorone could be used for the next series of closed-chamber experiments and compared to BCM exposure without the phorone exposure. The difference between the two experiments would provide the actual difference in total metabolism observed between the two pathways.

As stated before, closed chamber inhalation experiments quantify changes in total chemical disappearance; thus, additional experiments are necessary to identify the actual P450 isoform involved in BCM metabolism. The confirmation of CYP2E1 as being the major P450 involved for *in vivo* BCM metabolism was obtained by using different P450 specific inhibitors and inducers to examine differences in CO production [32]. The use of inhibitors has become an important experimental tool to discern kinetic mechanisms involved in metabolism of different P450 isoforms. Pyrazole (CAS number 288-13-1), and its derivatives have been, used as CYP2E1 inhibitors by measuring total metabolic disappearance in microsomal fractions [38]. Recently, a structurally analog of pyrazole, 4-methylpyrazole or (4-MP), has been used to describe its CYP2E1 inhibition properties using a second-site kinetic mechanism [14]. These authors explained the inhibitory mechanism for 4-MP by adding a second-site to fit the experimental results using pNP (4-nitrophenol, CAS number 100-02-7) oxidation as a marker for CYP2E1 activity [39]. Future *in vivo* closed chamber experiments can make use of the *in vitro* paradigm used by [14] in that increasing pyrazole concentrations can be used to distinguish between the single-site or double-site models. These proposed experiments would add a dose response element to the single dose pyrazole inhibition experiments already performed by [9] as shown in Figure 8. A PBPK model can then be used to describe the resulting pyrazole inhibition as either containing a single or double site enzyme.

In summary, a combination of closed chamber data and PBPK modeling was used to examine different metabolic descriptions for BCM. The standard two-pathway description was compared to a two-binding site model within the same enzyme. Metabolic parameters for the different descriptions were optimized using the gas uptake data for BCM. Different metabolic parameters have different concentration ranges that determine their ability to be measured, and sensitivity analysis was used to demonstrate identifiability relationships between parameters. The benefits of these computational tools towards improved health risk assessments rely on their ability to accurately describe metabolic hypotheses.

5. MatLab Codes

There are three distinct sections to the code used to generate the results found in this paper. These sections are Data Transformations and Initialization, Compartmental Models, and Sensitivity Analysis. In addition to the brief descriptions below, each function has an extensive help section at the top of each *m* file. Note that the names of the functions are italicized for clarity.

5.1. Data Transformations and Initialization. Almost all of the codes used for modeling require access to physiological parameters and the data set; the script file *params* writes these parameters into the working directory as well as converts the

original data (in parts per million) to a form usable by the model (in mg/liter). Note that *params* is called before any other function as it generates a. *mat* file containing relevant parameters called by the other functions in the model.

5.2. Compartmental Models. The heart of the compartmental model is *ode15s*, a stiff ordinary differential equation (ODE) solver part of the standard MatLab package. There are several functions that build upon the output from the ODE solver. The main file, *BCMmain*, allows the user to choose to optimize for the metabolic parameters or to use the inputted values to plot the original data concentrations (in ppm) versus the model curves on a logarithmic scale.

BCMmain, when used strictly as a plotting tool, is self-contained (aside from calling the file generated by *params* and the ODE solver). In addition to a plot output, *BCMmain* also outputs a string containing the absolute root mean square error (rmse) and the relative rmse for the fit of each model at each concentration. The absolute error is calculated by comparing the two-norm of the vector containing the difference between the model predictions and the given data divided by the number of elements in the vector. The relative rmse error is given by the absolute error at each concentration divided by the initial concentration. This gives a sense of the percent error in the model.

When choosing to optimize for metabolic parameters, *BCMmain* calls on the function *optthis*, which uses a combination of *fminsearch* and a least-squares method to optimize for the parameters. The function *fminsearch*, available in the standard MatLab package, tries to minimize a "cost"; we define this cost to be the sum of the difference (obtained by linear-least squares) between the model predictions and data at each concentration. The equations for the PBPK model are contained in the file *pbpk*, which is called upon by the ODE solver and the curve-fitting functions. The output of *optthis* is the vector of metabolic parameters that yields the best fit (after a specified number of iterations) used to plot the model in *BCMmain*.

5.3. Sensitivity Analysis. There are two main functions used for the sensitivity analysis aspect of the code. The first function, *plot2dsens* takes in user-specified parameters and plots the sensitivity of these parameters in the chamber and the liver compartments. We choose these compartments due to their importance in obtaining data from the chamber as a noninvasive way; however data obtained from the liver may yield more insight. A second function, *plot3dsens*, and its associated helper function *modelchoice*, are designed to give a three-dimensional plot that shows the sensitivity of one parameter with respect to time as it varies over a user-input range in each compartment of interest. This analysis divides up the range of the parameter of interest into a user-specified number of subintervals and calculates the sensitivity of the parameter using the subinterval value as the parameter value in the same sense as the two-dimensional model. The sensitivity plots are then spliced together into a three-dimensional plot.

Both sensitivity functions require the use of *tssolve*, created by Adam Attarian (North Carolina State University, http://www4.ncsu.edu/~arattari/), which in turn requires Martin Fink's *myAD* package. Both functions are available from the MathWorks website (http://www.mathworks.com).

5.4. Code Evaluation. One of the questions addressed in the present work is how to validate new code that is generated to study a chemical, such as the case for BCM. These authors approached this question on several fronts. First, a search was made for existing code using a similar chemical to BCM. The previously published DCM model [24] was selected for a comparison with BCM. The DCM code was converted to model BCM by changing chemical-specific parameters to reflect those of BCM. The simulations were performed using the BCM/DCM version. Results of these simulations were then compared with the newly created BCM code and found to be identical. Once the new BCM code was verified to be correct, the second step was to optimize for the parameters describing two-pathway kinetics and determine their similarity with previously published values (see Results). This additional step ensures that the new PBPK model description accurately depicts BCM metabolism.

Appendix

The differential equations used to describe each compartment in the PBPK model were developed using the law of conservation of mass: the amount of BCM flowing into each compartment must equal the amount of BCM leaving the compartment, whether it is through blood flow or ventilation, or through loss by metabolism or condensation. The following abbreviations can be found in Table 1:

$$\begin{aligned}\frac{dA_{\text{ven}}}{dt} &= q_1 C_{\text{rap}} + q_2 C_{\text{adi}} + q_3 C_{\text{slow}} \\ &\quad + q_4 C_{\text{kid}} + q_5 C_{\text{liv}} \\ &\quad - QCC \cdot C_{\text{ven}},\end{aligned} \tag{A.1}$$

$$\Longrightarrow C_{\text{ven}} = \frac{q_1 C_{\text{rap}} + q_2 C_{\text{adi}} + q_3 C_{\text{slow}} + q_4 C_{\text{kid}} + q_5 C_{\text{liv}}}{QCC}, \tag{A.2}$$

$$\begin{aligned}\frac{dA_{\text{lung}}}{dt} &= QCC \cdot C_{\text{ven}} + QV \cdot C_{\text{inh}}, \\ &\quad - C_{\text{art}}\left(QCC + \left(\frac{QV}{P_{\text{Bld}}}\right)\right),\end{aligned} \tag{A.3}$$

$$\Longrightarrow C_{\text{art}} = \frac{QCC \cdot C_{\text{ven}} + QV \cdot C_{\text{inh}}}{QCC + QV/P_{\text{Bld}}}, \tag{A.4}$$

$$C_{\text{exh}} = \frac{C_{\text{art}}}{P_{\text{Bld}}}, \tag{A.5}$$

$$\frac{dA_{\text{inh}}}{dt} = N \cdot QV \cdot (C_{\text{exh}} - C_{\text{inh}}) - \text{loss} \cdot A_{\text{inh}}, \tag{A.6}$$

$$\frac{dA_{\text{rap}}}{dt} = q_1 \cdot \left(C_{\text{art}} - C_{\text{rap}}\right), \tag{A.7}$$

$$\frac{dA_{\text{adi}}}{dt} = q_2 \cdot (C_{\text{art}} - C_{\text{adi}}), \tag{A.8}$$

$$\frac{dA_{\text{slow}}}{dt} = q_3 \cdot (C_{\text{art}} - C_{\text{slow}}), \tag{A.9}$$

$$\frac{dA_{\text{kid}}}{dt} = q_4 \cdot (C_{\text{art}} - C_{\text{kid}}) - Met_K, \tag{A.10}$$

$$\frac{dA_{\text{liv}}}{dt} = q_5 \cdot (C_{\text{art}} - C_{\text{liv}}) - Met_L. \tag{A.11}$$

For (A.1)–(A.11), we denote the venous concentration of BCM leaving a specific compartment comp as $C_{\text{comp}} = A_{\text{comp}}/(V_{\text{comp}} \cdot P_{\text{comp}})$, where A_{comp} is the amount of BCM in the compartment, V_{comp} is the volume of the compartment, and P_{comp} is the partition coefficient for the compartment. Note there is no associated partition coefficient for the chamber, thus the concentration in the chamber is denoted by $C_{\text{inh}} = A_{\text{inh}}/V_{\text{cha}}$. Partition coefficients (given in Table 1) describe the measure of the differential solubility of BCM as the chemical passes between two different phases; this unitless ratio accounts for the amount of BCM absorbed by compartmental tissue as it passes from the compartment back into the bloodstream. Previous studies have determined the tissue/air and blood/air partition coefficients for BCM [9]. To determine the tissue/blood partition coefficient for each compartment, (A.12) is used:

$$P_{\text{organ}} = \text{tissue} : \text{blood} = \frac{\text{tissue} : \text{air}}{\text{blood} : \text{air}}. \tag{A.12}$$

Several assumptions were made for the construction of each equation in the system: Initially, a differential equation, (A.1), was created to represent the amount of BCM in the venous compartment. However, simulations in MatLab demonstrated that the amount of BCM in the venous compartment approached equilibrium very quickly with respect to the length of the experiment. This allowed us to set (A.1) equal to zero to obtain an algebraic expression for the concentration of BCM in the venous compartment with respect to the concentration of BCM in the other compartments. A similar technique was used with the lung compartment (A.3), obtaining an algebraic expression for the concentration of BCM in the arterial compartment.

List of Abbreviations

Chemicals

4-MP: 4-methylpyrazole
BCM: Bromochloromethane
BDCM: Bromodichloromethane
DBP: Disinfection by-products
DCM: Dichloromethane
GST: Glutathione transferase
PBPK: Physiologically-based pharmacokinetic model
CCL: Candidate Contaminant List, Office of Water, US EPA.

Equation Variables

$V_{\max}$: Maximum metabolic rate, mg/hour
$V_{\max_i}$: Maximum metabolic rate for binding site i in two-binding site hypothesis, mg/hour
K_m: Affinity constant, mg/liter
K_{m_i}: Affinity constant for binding site i in two-binding site hypothesis, mg/liter
k_{GST}: Proportionality constant for linear pathway metabolized by GST, /hour
CL_2: clearance constant consisting of the ratio of the maximum metabolic rate and the affinity constant, $V_{\max_2}/K_{m_2}$, for second binding site, liter/hour
$A_{\text{compartment}}$: Amount of BCM in compartment
$P_{\text{compartment}}$: Partition coefficient for compartment
$V_{\text{compartment}}$: Volume of compartment, liters
$C_{\text{compartment}}$: Concentration of BCM in compartment, given by $C_{\text{comp}} = A_{\text{comp}}/(V_{\text{comp}} \cdot P_{\text{comp}})$.

Disclaimer

This paper has been reviewed by the US Environmental Protection Agency and approved for publication. The views expressed in this paper are those of the authors and do not necessarily reflect the views or policies of the U S Environmental Protection Agency.

Acknowledgments

The authors would like to thank North Carolina State University and the US EPA for making this work possible. The following reviewers from the US EPA provided insightful comments: Drs. William Lefew, Rogelio Tornero-Velez, and Jane Ellen Simmons. Also a special thanks to the support from the NSF and NSA funding offices. The Research Experience for Undergraduates (REU) work was possible due to NSF Grant numbers DMS-0636568, DMS-0552571 and DMS-1063010 and NSA Grant number H9823-10-1-0252.

References

[1] U.S. EPA, "Bromochloromethane testing rationale," Tech. Rep. CAS 74-97-5 (NTIS 201-16826A), U.S. Environmental Protection Agency, Washington, DC, USA, 2009.

[2] U.S. EPA, "Health and environmental effects document for bromochloromethane," Tech. Rep. EPA/600/8-91/016 (NTSI PB91213702), U.S. Environmental Protection Agency, Washington, DC, USA, 1990.

[3] U.S. EPA, "The occurrence of disinfection by-products (dbps) of health concern in drinking water: results of a nationwide dbp occurrence study," Tech. Rep. EPA/600/R-02/068, U.S. Environmental Protection Agency, Washington, DC, USA, 2002.

[4] S. D. Richardson, M. J. Plewa, E. D. Wagner, R. Schoeny, and D. M. DeMarini, "Occurrence, genotoxicity, and carcinogenicity of regulated and emerging disinfection by-products in

drinking water: a review and roadmap for research," *Mutation Research*, vol. 636, no. 1–3, pp. 178–242, 2007.

[5] Y. Y. Wei, Y. Liu, R. H. Dai et al., "Trihalomethanes and haloacetic acid species from the chlorination of algal organic matter and bromide," *Water Science and Technology*, vol. 63, no. 6, pp. 1111–1120, 2011.

[6] C. M. Thompson, B. Sonawane, H. A. Barton et al., "Approaches for applications of physiologically based pharmacokinetic models in risk assessment," *Journal of Toxicology and Environmental Health B*, vol. 11, no. 7, pp. 519–547, 2008.

[7] A. N. Edginton and G. Joshi, "Have physiologically-based pharmacokinetic models delivered?" *Expert Opinion on Drug Metabolism and Toxicology*, vol. 7, no. 8, pp. 929–934, 2011.

[8] M. L. Gargas and M. E. Andersen, "Determining kinetic constants of chlorinated ethane metabolism in the rat from rates of exhalation," *Toxicology and Applied Pharmacology*, vol. 99, no. 2, pp. 344–353, 1989.

[9] M. L. Gargas, M. E. Andersen, and H. J. Clewell, "A physiologically based simulation approach for determining metabolic constants from gas uptake data," *Toxicology and Applied Pharmacology*, vol. 86, no. 3, pp. 341–352, 1986.

[10] R. P. Brown, M. D. Delp, S. L. Lindstedt, L. R. Rhomberg, and R. P. Beliles, "Physiological parameter values for physiologically based pharmacokinetic models," *Toxicology and Industrial Health*, vol. 13, no. 4, pp. 407–484, 1997.

[11] M. D. Delp, M. V. Evans, and C. Duan, "Effects of aging on cardiac output, regional blood flow, and body composition in Fischer-344 rats," *Journal of Applied Physiology*, vol. 85, no. 5, pp. 1813–1822, 1998.

[12] M. A. Medinsky, P. J. Sabourin, R. F. Henderson, G. Lucier, and L. S. Birnbaum, "Differences in the pathways for metabolism of benzene in rats and mice simulated by a physiological model," *Environmental Health Perspectives*, vol. 82, pp. 43–49, 1989.

[13] HSE, *Bromochloromethane Risk Assessment Document*, Health and Safety Executive Books, Suffolk, UK, 2000.

[14] S. L. Collom, R. M. Laddusaw, A. M. Burch, P. Kuzmic, M. D. Perry, and G. P. Miller, "CYP2E1 substrate inhibition: mechanistic interpretation through an effector site for monocyclic compounds," *Journal of Biological Chemistry*, vol. 283, no. 6, pp. 3487–3496, 2008.

[15] M. W. Anders, "Chemical toxicology of reactive intermediates formed by the glutathione-dependent bioactivation of halogen-containing compounds," *Chemical Research in Toxicology*, vol. 21, no. 1, pp. 145–159, 2008.

[16] R. Thier, J. B. Taylor, S. E. Pemble et al., "Expression of mammalian glutathione S-transferase 5-5 in Salmonella typhimurium TA1535 leads to base-pair mutations upon exposure to dihalomethanes," *Proceedings of the National Academy of Sciences of the United States of America*, vol. 90, no. 18, pp. 8576–8580, 1993.

[17] B. Kundu, S. D. Richardson, C. A. Granville et al., "Comparative mutagenicity of halomethanes and halonitromethanes in Salmonella TA100: structure-activity analysis and mutation spectra," *Mutation Research*, vol. 554, no. 1-2, pp. 335–350, 2004.

[18] R. D. White, A. J. Gandolfi, G. T. Bowden, and I. G. Sipes, "Deuterium isotope effect on the metabolism and toxicity of 1,2-dibromoethane," *Toxicology and Applied Pharmacology*, vol. 69, no. 2, pp. 170–178, 1983.

[19] T. S. Tracy, "Atypical cytochrome P450 kinetics: implications for drug discovery," *Drugs in R & D*, vol. 7, no. 6, pp. 349–363, 2006.

[20] K. R. Korzekwa, N. Krishnamachary, M. Shou et al., "Evaluation of atypical cytochrome P450 kinetics with two-substrate models: evidence that multiple substrates can simultaneously bind to cytochrome P450 active sites," *Biochemistry*, vol. 37, pp. 4137–4147, 1998.

[21] M. V. Evans, W. D. Crank, H. M. Yang, and J. E. Simmons, "Applications of sensitivity analysis to a physiologically based pharmacokinetic model for carbon tetrachloride in rats," *Toxicology and Applied Pharmacology*, vol. 128, no. 1, pp. 36–44, 1994.

[22] K. McNally, R. Cotton, and G. D. Loizou, "A workflow for global sensitivity analysis of PBPK models," *Frontiers in Pharmacology*, vol. 2, p. 31, 2011.

[23] J. C. Ramsey and M. E. Andersen, "A physiologically based description of the inhalation pharmacokinetics of styrene in rats and humans," *Toxicology and Applied Pharmacology*, vol. 73, no. 1, pp. 159–175, 1984.

[24] M. V. Evans and J. C. Caldwell, "Evaluation of two different metabolic hypotheses for dichloromethane toxicity using physiologically based pharmacokinetic modeling for in vivo inhalation gas uptake data exposure in female B6C3F1 mice," *Toxicology and Applied Pharmacology*, vol. 244, no. 3, pp. 280–290, 2010.

[25] R. A. Corley, A. L. Mendrala, F. A. Smith et al., "Development of a physiologically based pharmacokinetic model for chloroform," *Toxicology and Applied Pharmacology*, vol. 103, no. 3, pp. 512–527, 1990.

[26] W. A. Chiu, M. S. Okino, and M. V. Evans, "Characterizing uncertainty and population variability in the toxicokinetics of trichloroethylene and metabolites in mice, rats, and humans using an updated database, physiologically based pharmacokinetic (PBPK) model, and Bayesian approach," *Toxicology and Applied Pharmacology*, vol. 241, no. 1, pp. 36–60, 2009.

[27] M. V. Evans, W. A. Chiu, M. S. Okino, and J. C. Caldwell, "Development of an updated PBPK model for trichloroethylene and metabolites in mice, and its application to discern the role of oxidative metabolism in TCE-induced hepatomegaly," *Toxicology and Applied Pharmacology*, vol. 236, no. 3, pp. 329–340, 2009.

[28] M. E. Andersen, H. J. Clewell, M. L. Gargas, F. A. Smith, and R. H. Reitz, "Physiologically based pharmacokinetics and the risk assessment process for methylene chloride," *Toxicology and Applied Pharmacology*, vol. 87, no. 2, pp. 185–205, 1987.

[29] G. W. Jepson and J. N. McDougal, "Physiologically based modeling of nonsteady state dermal absorption of halogenated methanes from an aqueous solution," *Toxicology and Applied Pharmacology*, vol. 144, no. 2, pp. 315–324, 1997.

[30] G. W. Jepson and J. N. McDougal, "Predicting vehicle effects on the dermal absorption of halogenated methanes using physiologically based modeling," *Toxicological Sciences*, vol. 48, no. 2, pp. 180–188, 1999.

[31] M. K. Johnson, "Studies on glutathione S-alkyltransferase of the rat," *Biochemical Journal*, vol. 98, no. 1, pp. 44–56, 1966.

[32] D. Pankow, M. Weise, and P. Hoffmann, "Effect of isoniazid or phenobarbital pretreatment on the metabolism of dihalomethanes to carbon monoxide," *Polish Journal of Occupational Medicine and Environmental Health*, vol. 5, no. 3, pp. 245–250, 1992.

[33] J. Li, D. Q. Wei, J. F. Wang, and Y. X. Li, "A negative cooperativity mechanism of human CYP2E1 inferred from molecular dynamics simulations and free energy calculations," *Journal of Chemical Information and Modeling*, vol. 51, pp. 3217–3225, 2011.

[34] A. Dey and S. M. Kumar, "Cytochrome P450 2E1 and hyperglycemia-induced liver injury," *Cell Biology and Toxicology*, vol. 27, no. 4, pp. 285–310, 2011.

[35] P. R. Porubsky, K. M. Meneely, and E. E. Scott, "Structures of human cytochrome P-450 2E1: insights into the binding of inhibitors and both small molecular weight and fatty acid substrates," *Journal of Biological Chemistry*, vol. 283, no. 48, pp. 33698–33707, 2008.

[36] C. Cobelli and J. J. DiStefano, "Parameter and structural identifiability concepts and ambiguities: a critical review and analysis," *American Journal of Physiology*, vol. 239, no. 1, pp. 7–24, 1980.

[37] C. Kim, R. O. Manning, R. P. Brown, and J. V. Bruckner, "Use of the vial equilibration technique for determination of metabolic rate constants for dichloromethane," *Toxicology and Applied Pharmacology*, vol. 139, no. 2, pp. 243–251, 1996.

[38] D. E. Feierman and A. I. Cederbaum, "Inhibition of microsomal oxidation of ethanol by pyrazole and 4-methylpyrazole in vitro. Increased effectiveness after induction by pyrazole and 4-methylpyrazole," *Biochemical Journal*, vol. 239, no. 3, pp. 671–677, 1986.

[39] D. R. Koop, "Hydroxylation of p-nitrophenol by rabbit ethanol-inducible cytochrome P-450 isozyme 3a," *Molecular Pharmacology*, vol. 29, no. 4, pp. 399–404, 1986.

Hindawi Publishing Corporation
Journal of Toxicology
Volume 2012, Article ID 286079, 22 pages
doi:10.1155/2012/286079

Research Article

Quantitative Property-Property Relationship for Screening-Level Prediction of Intrinsic Clearance of Volatile Organic Chemicals in Rats and Its Integration within PBPK Models to Predict Inhalation Pharmacokinetics in Humans

Thomas Peyret and Kannan Krishnan

Département de Santé Environnementale et Santé au Travail, Université de Montréal, C.P. 6128, Succursale Centre-Ville, Montréal, QC, Canada H3C 3J7

Correspondence should be addressed to Kannan Krishnan, kannan.krishnan@umontreal.ca

Received 31 October 2011; Revised 13 January 2012; Accepted 13 January 2012

Academic Editor: Jane C. Caldwell

The objectives of this study were (i) to develop a screening-level Quantitative property-property relationship (QPPR) for intrinsic clearance (CL_{int}) obtained from *in vivo* animal studies and (ii) to incorporate it with human physiology in a PBPK model for predicting the inhalation pharmacokinetics of VOCs. CL_{int}, calculated as the ratio of the *in vivo* V_{max} (μmol/h/kg bw rat) to the K_m (μM), was obtained for 26 VOCs from the literature. The QPPR model resulting from stepwise linear regression analysis passed the validation step ($R^2 = 0.8$; leave-one-out cross-validation $Q^2 = 0.75$) for CL_{int} normalized to the phospholipid (PL) affinity of the VOCs. The QPPR facilitated the calculation of CL_{int} (L PL/h/kg bw rat) from the input data on log P_{ow}, log blood: water PC and ionization potential. The predictions of the QPPR as lower and upper bounds of the 95% mean confidence intervals (LMCI and UMCI, resp.) were then integrated within a human PBPK model. The ratio of the maximum (using LMCI for CL_{int}) to minimum (using UMCI for CL_{int}) AUC predicted by the QPPR-PBPK model was 1.36 ± 0.4 and ranged from 1.06 (1,1-dichloroethylene) to 2.8 (isoprene). Overall, the integrated QPPR-PBPK modeling method developed in this study is a pragmatic way of characterizing the impact of the lack of knowledge of CL_{int} in predicting human pharmacokinetics of VOCs, as well as the impact of prediction uncertainty of CL_{int} on human pharmacokinetics of VOCs.

1. Introduction

The evolving scientific and regulatory activities in Europe and North America emphasize the need for the development of tools that refine, replace, or reduce the use of animals and human volunteers in pharmacokinetic and toxicity tests [1–3]. The ability to base the toxic responses on the target tissue dose or internal concentration of the toxic moiety of the chemicals is key to the predictive tools reflective of the current state of science. Therefore, physiologically based pharmacokinetic (PBPK) models that are capable of providing *a priori* prediction of the time course of chemicals in blood and tissues is of tremendous interest [4]. PBPK models are mechanistically based mathematical descriptions of the absorption, distribution, metabolism, and excretion of chemicals or pharmaceutical compounds. In PBPK models, the organism is represented as a set of several tissue compartments interconnected by blood flows. In these models, the internal dose measures (e.g., blood or tissue concentrations, amount metabolized) of a chemical are described on the basis of mass-balance differential equations requiring species-specific properties (e.g., alveolar ventilation rate, cardiac output, regional blood flows, and tissue volumes) and chemical-specific input parameters (e.g., partition coefficients and metabolic constants). Although the species-specific values of several physiological parameters are available in the literature [4–6], the partition coefficients (PCs) and metabolic constants need to be determined

experimentally or calculated by using animal-replacement methods for each chemical individually [7]. The values of tissue : blood or tissue : plasma partition coefficients essential for developing PBPK models have been estimated for a wide range of chemicals and chemical classes, including drugs, with the use of tissue composition-based algorithms or QSAR methods (e.g., [8–19]).

Regarding the metabolism parameters (i.e., hepatic clearance, intrinsic clearance, V_{max}, K_m, K_{cat}, free energy of binding, energy of activation, or activation enthalpy), some studies have developed 2-D and 3-D QSARs but with a specific focus on either a single isozyme, a single reaction or a single class of substances [8, 20–38]. None of these past efforts succeeded in predicting both V_{max} and K_m (or CL_{int}) of environmental chemicals for direct incorporation within animal or human PBPK models. Alternatively, few studies utilized the group contribution method of Gao [39–43], to predict metabolic rates for PBPK models. In this method, the chemical is decomposed into different structural fragments or groups, the contributions of which are obtained by regression analysis [39]. Accordingly, these publications demonstrated the feasibility of developing structure-property relationships for the metabolism rates. The group contribution method was successfully used to develop quantitative structure-property relationships (QSPRs) for the tissue : air partition coefficients as well as intrinsic (CL_{int}) and hepatic clearance (CL_h for a group of low-molecular-weight volatile organic chemicals (VOCs) in rats [41, 42]. These QSPR models, in turn, were incorporated within PBPK models to predict reasonably well the blood kinetics of inhaled VOCs in rats. As these QSPRs are species specific, they could not be used to conduct interspecies extrapolations. To overcome this limitation, Béliveau et al. [40] developed biologically based algorithms for PCs and CL_h to conduct rat to human extrapolations of the inhalation toxicokinetics of VOCs. In this study, QSPRs based on the group contribution method were developed for the chemical-specific input parameters of the biological algorithms for PCs (i.e., oil : air, water : air,and blood protein : air) and CL_{int} (intrinsic clearance normalized for cytochrome P450 2E1 content). More recently, QSPRs were developed for the metabolic constants V_{max} (maximum velocity of reaction) and K_m (Michaelis constant) [43] and were further incorporated within a rat PBPK model to predict the toxicokinetics of mixtures of VOCs. Despite the successful use of the group contribution method in QSPR modeling of metabolism rates, their principal limitation relates to the fact that the chemical space they cover is extremely limited (low-molecular-weight VOCs containing one or more of the following fragments: CH_3, CH_2, CH, C, C=C, H, Br, Cl, F, benzene ring, and H on benzene ring). More experimental data on diverse chemicals would be needed to determine the contributions of other molecular fragments, as has been done with P_{ow} (e.g., estimation of the contribution of 130 fragments (i.e., groups) required 1200 measurements of P_{ow}) [44]. To extend the currently available QSPR for CL_{int} to cover more diverse fragments and at the same time respect a reasonable ratio of the number of parameters to the number of observations, extensive experimental data would be required.

Since the critical limitation in the construction of PBPK models for new substances continues to be the metabolism rate, a pragmatic approach—particularly for inhaled VOCs—is to evaluate the maximum and minimum possible blood concentration profiles in exposed individuals. Thus, using a hepatic extraction ratio (E) of 0 and 1 in the PBPK models, Poulin and Krishnan [45] obtained simulations of the physiological limits (i.e., maximal and minimal blood concentration profiles) for inhaled VOCs in humans. Assuming the conceptual PBPK model and the values of its physiological parameters are reliable, the real answer, that is, the actual concentrations and kinetic curve, would be somewhere in between the theoretical limits simulated with these PBPK models [45]. The uncertainty associated with these theoretical bounds can be reduced by developing better estimates of the metabolism constants. This could be done, at a practical level, by developing *in silico* tools that provide a range of plausible values, in lieu of a single accurate point estimate. Such a tool might be of use for the toxicokinetic screening of substances, until the time when the chemical-specific measurements are obtained *in vivo*, *in vitro,* or with a highly precise mechanistic *in silico* method.

Since human exposures to environmental contaminants in most cases do not attain levels that approach or exceed saturation, it is not crucial to predict V_{max} and K_m separately, particularly for simulating kinetics in humans exposed to low atmospheric concentrations of VOCs. Therefore, the availability of *in silico* approaches based on easily available parameters to predict plausible range of CL_{int} would be desirable as a screening-level tool. The objective of this study was therefore to develop a quantitative property-property relationship (QPPR) model of animal data to generate initial estimates (or bounds) of intrinsic clearance of VOCs, for eventual incorporation within a human PBPK model to simulate blood concentration profiles associated with inhalation exposures. In this regard, we focused on evaluating the impact of the uncertainty associated with QPPR predictions of CL_{int} on the blood kinetics of VOCs in humans, relative to that of the uncertainty associated with the total lack of knowledge of the metabolic rate in humans. Furthermore, the reliability of applying the QPPR to predict the area under the blood concentration versus time curve (AUC) of parent chemicals was evaluated, as a function of the sensitivity of the metabolism parameter in the PBPK model and the prediction uncertainty of QPPR model.

2. Methods

A QPPR model for CL_{int} was developed using a calibration set of 26 VOCs. The QPPR predictions were then compared with experimental data for several VOCs and the pharmacokinetics in humans were simulated using integrated QPPR-PBPK models for these 26 VOCs. The predictions of QPPR were evaluated further with an external data set of CL_{int} for 11 VOCs.

2.1. QPPR Modeling for Intrinsic Clearance

2.1.1. Chemicals and Data Sources. The development of a global QPPR model for metabolism was initially undertaken using experimental data on the *in vivo* intrinsic clearance of 26 VOCs in rats, collated and evaluated in previous studies by Béliveau et al. [40, 41] (1,1,1,2-tetrachloroethane; 1,1,2,2-tetrachloroethane; 1,1,2-trichloroethane; 1,1-dichloroethane; 1,1-dichloroethylene; 1,2-dichloroethane; benzene; bromochloromethane; bromodichloromethane; carbon tetrachloride; chloroethane; chloroform; *cis*-1,2-dichloroethylene; dibromomethane; dichloromethane; ethylbenzene; hexachloroethane; isoprene; methyl chloride; *m*-xylene; *n*-hexane; pentachloroethane; styrene; toluene; trichloroethylene; vinyl chloride) [24, 46–53].

Subsequently, the resulting QPPR model was evaluated with experimental *in vivo* data on CL_{int} for 11 additional VOCs in rats (1,1,1-trichloroethane; 1,2,4-trimethylbenzene; bromoform; dibromochloromethane; furan; halothane; *o*-xylene; *trans*-1,2-dichloroethylene; tetrachloroethylene; propylene; ethylene) [46, 48, 54–61]. These 11 chemicals outside the calibration set were also lipophilic, low-molecular-weight VOCs and likely substrates of cytochrome P450 2E1 [32, 62]. Moreover except for halothane and 1,2,4-trimethylbenzene, the chemicals of the evaluation dataset possess values of P_{ow}, ionization potential, and blood : water PC within the range of values for the chemicals in the QPPR calibration set.

2.1.2. Modeling Endpoint. For QPPR modeling, CL_{int} (expressed in units of L blood, CL_{intblood}, or L phospholipids, CL_{intPL}) was used as the endpoint. Initially, CL_{intblood} (L blood/h/kg$^{0.75}$) for all the studied chemicals was computed as allometrically scaled $V_{\max}$ (μmol/h/kg$^{0.75}$)/K_m (μmol/L blood). Since CYPs are located in the endoplasmic reticulum embedded in the phospholipidic bilayer [63], the CL_{intPL} values reflecting chemical affinity for the phospholipids (PL) were subsequently computed. The values of CL_{intPL} (L phospholipid/h/kg$^{0.75}$) were obtained by dividing $V_{\max}$ (μmol/h/kg$^{0.75}$) with K_m expressed as μmol/L PL. The K_m values in μM of PL were obtained by multiplying the values of K_m expressed as μmol/L blood with the chemical-specific phospholipid : blood partition coefficients (P_{plb}) calculated as follows:

$$P_{\text{plb}} = \frac{0.3 \cdot P_{\text{oa}} + 0.7 \cdot P_{\text{wa}}}{P_{\text{ba}}}, \quad (1)$$

where P_{oa} is the *n*-octanol : air PC, P_{wa} the water : air PC, and P_{ba} the blood : air PC.

The above equation computes P_{plb} as the ratio of phospholipid : air to blood : air PCs of the VOCs, based on Poulin and Krishnan [10, 12].

2.1.3. Input Parameters for Transforming the Endpoint. The input parameters required for converting the CL_{int} obtained from the literature were P_{oa}, P_{wa}, and P_{ba}.

(1) P_{oa} and P_{wa}. The *n*-octanol : air PC (P_{oa}), was calculated as the product of the *n*-octanol : water PC (P_{ow}) and P_{wa} (inverse of Henry's law constant at 37.5°C). The values of P_{ow} and P_{wa} were predicted using U.S. EPA's freeware EPISUITE (http://www.epa.gov/opptintr/exposure/pubs/episuite.htm).

(2) P_{ba}. Experimental values were used for rat blood : air [54, 56, 59, 64–68]. The calculated values of P_{plb} for the chemicals used for the development and for the evaluation of the QPPR are reported in Table 1.

2.1.4. Variable Selection. *A priori* list of variables was developed on the basis on mechanistic considerations. The rate and affinity for P450-mediated metabolism would appear to be related to the size, shape, charge, and energy of the substrate; therefore variables that reflect these properties were chosen for the QPPR analysis [21, 23, 27, 28, 32, 69–71]. The descriptors of the size and shape of the molecule were the molecular length, width, depth, volume, surface, and the Kappa 2 index [72], as well as two descriptors used in the work of Lewis et al. [23], namely, the ratio of the molecular length to the molecular width (L/W) and the ratio of the area of the molecule (i.e., length times width) to the square of the depth (a/d^2). The dipole moment and ionization potential (IP) were used as measure of the charge disposition and the energy in the molecule, respectively. The values of all the previously cited descriptors were calculated using commercially available software (Molecular Modeling Pro, Chem SW, Fairfield, CA). Before calculating the molecular descriptors with Molecular Modeling Pro, the 3D molecules were drawn and minimized using the full MM2 (molecular mechanics program) method provided in the software. The dipole moment and the ionization potential were calculated using MOPAC/PM3 program, included in Molecular Modeling Pro.

Hydrophobic descriptors such as $\log P_{\text{ow}}$ (log of the *n*-octanol : water PC) that reflect hydrogen bonding and π-π stacking have already been correlated to the values of metabolic constants [69–71]. In this study, the following physicochemical parameters were chosen to describe the relative solubility and partitioning into diverse biological media: $\log P_{\text{ow}}$, log phospholipid : water PC ($\log P_{\text{plw}}$); log blood : water PC ($\log P_{\text{bw}}$), and log water : air PC ($\log P_{\text{wa}}$). The blood : water and phospholipid : water PCs were obtained by dividing the blood : air and phospholipid : air PCs values by the water : air PC values. The values of P_{ow}, P_{wa}, blood : air, and phospholipid : air PCs were obtained as described for the calculation of P_{plb} (1).

2.1.5. Statistical Analysis. Multilinear regression analysis approach was chosen for the QPPR analysis of CL_{int} because linear regression models are simple, transparent, and easy to reproduce [73]. The regression analysis was performed using SPSS v16 for Windows (SPSS Inc., Chicago, IL). Stepwise regression analysis was performed to select the QPPRs based on the most statistically significant independent variable(s) from an *a priori* list (see Section 2.1.4). The coefficient of determination R^2, the adjusted R^2 (R^2_{adj}; adjusted for number of variables) [73], the standard error of the estimate *s*, and the value and significance of the *F* statistic were calculated. The

Table 1: Partition coefficients used in the human PBPK models.

Chemicals[a]	Partition coefficient (PC)[b]						Reference
	P_{ba}	P_{lb}	P_{rb}	P_{pb}	P_{fb}	P_{plb}	
Benzene	8.19	2.08	2.08	1.26	60.93	4.55	[66]
Bromochloromethane	10.4	2.81	2.81	1.07	31.5	2	[66, 77]
Bromodichloromethane	26.6	1.15	1.15	0.47	19.77	2.48	[78, 79]
Carbon tetrachloride	2.73	5.2	5.2	1.67	131.5	8.57	[66]
Chloroethane	2.69	1.34	1.34	1.2	14.3	4.42	[66]
Chloroform	6.85	3.08	3.08	2.03	29.6	1.93	[66]
Dibromomethane	19.9	3.42	3.42	2.03	39.8	1.78	[66, 77]
Dichloroethane (1,1-)	4.94	2.19	2.19	1.04	33.2	4.27	[66]
Dichloroethane (1,2-)	19.5	1.83	1.83	1.2	17.64	9.25	[66]
Dichloroethylene (1,1-)	0.81	5.46	5.46	2.53	84.69	4.82	[66, 77]
Dichloroethylene (*cis*-1,2)	9.85	1.55	1.55	0.62	23	5.2	[66]
Dichloromethane	9.7	1.46	1.46	0.82	12.4	1.79	[80]
Ethylbenzene	28	2.99	2.15	0.93	55.6	13.2	[67]
Hexachloroethane	52.4	7.04	7.04	1.43	63.4	156	[66]
Hexane (*n*-)	2.13	5.2	5.2	2.9	159	1.89	[47]
Isoprene	0.75	2.57	2.45	1.97	82	11.84	[52]
Methyl chloride	2.48	1.4	1.4	0.39	5.44	3.04	[66]
Pentachloroethane	50.3	5.17	5.17	1.44	81.9	21.7	[66, 77]
Styrene	52	2.7	5.7	1	50	30.2	[50]
Tetrachloroethane (1,1,1,2-)	30.2	2.92	2.92	1.31	71.1	37.3	[66]
Tetrachloroethane (1,1,2,2-)	116	1.69	1.69	0.87	32.47	14.3	[66]
Toluene	15.6	5.36	5.36	1.77	65.4	13.8	[67]
Trichloroethane (1,1,2-)	35.7	2.05	2.05	0.64	40.3	10.1	[66]
Trichloroethylene	8.11	3.35	3.35	1.24	68.3	5.73	[66]
Vinyl chloride	1.16	1.38	1.38	1.81	17.2	4.87	[66]
Xylene (*m*-)	26.4	3.44	3.44	1.59	70.4	15.1	[67]
Bromoform	102.3	2.06	2.06	1.12	40.4	2.44	[78, 79]
Dibromochloromethane	49.2	2.56	2.56	1.13	38.96	1.48	[78, 79]
Dichloroethylene (trans-1,2-)	6.04	1.48	1.48	0.58	24.5	11.7	[66]
Ethylene	0.22	2.05	2.18	2.95	8.73	1.05	[59]
Furan	6.59	0.9	0.9	0.64	9.72	2.75	[56]
Halothane	3.3	2.42	2.42	2.91	44.2	5.82	[58]
Propylene	0.44	1.09	1.2	1.25	11.7	1.52	[54]
Tetrachloroethylene	10.3	5.88	5.88	3.1	119.1	11.1	[57]
Trichloroethane (1,1,1-)	2.53	1.24	3.4	3.4	103.9	21.7	[48]
Trimethylbenzene (1,2,4-)	85	4.4	4.4	2.11	109	19	[61]
Xylene (o-)	34.9	3.09	3.09	1.47	53.8	22.6	[66]

[a] Chemicals in italics were not included in the dataset for the calibration of the model.
[b] P_{ba}: blood : air PC; P_{lb}: liver blood PC; P_{rb} : richly perfused tissues : blood PC; P_{pb}: poorly perfused tissues : blood PC; P_{fb}: fat : blood PC; P_{plb}: phospholipids : blood PC.

normality of the residuals was checked visually on normal probability plots of the standardized residuals (i.e., expected normal cumulative probability versus observed cumulative probability). Leave-one-out cross-validation was conducted and the results were expressed in terms of Q^2, a measure of precision error of the model. The Q^2 was computed as follows [74]:

$$Q^2 = 1 - \frac{\text{PRESS}}{\text{SSY}}, \quad (2)$$

where PRESS is that predicted residual sum of squares and SSY the sum of squares of the response values. The statistical significance ($p < 0.05$) of the regression coefficients was estimated by a t statistic test. Multicollinearity refers to the occurrence of correlation between two independent variables in the multiple linear regression model. Multicollinearity of the variables in the model was assessed by calculating the variance inflation factor (VIF) for all independent variables [75]. The value of VIF was calculated as follows [75]:

$$\mathrm{VIF}_i = \frac{1}{1 - R_i^2}, \tag{3}$$

where VIF_i is the variance inflation factor of the independent variable i in the multilinear regression model and R_i^2 the coefficient of determination of the regression between the independent variable i and the other independent variables in the multilinear regression model.

For each model, the application domain was documented by reporting the ranges of values of the descriptors, the modeled response, and the endpoint.

A QPPR model was considered adequate when: the values of R^2 and R^2_{adj} were ≥ 0.6 [73], the value of Q^2 was ≥ 0.6 [76], and the independent variables were not highly correlated (i.e., VIF < 4) [75].

The predictions of the QPPR model were obtained in terms of lower and upper bounds of the 95% mean confidence intervals (LMCI and UMCI, resp.) in order to represent the uncertainty associated with the mean predicted value. The LMCI and UMCI for the 11 VOCs, not in the QSPR calibration dataset, were obtained by adding them in the SPSS file containing the data used for the QPPR, along with the values of their independent variables only.

2.2. Translation of QPPR Predicted Intrinsic Clearance Values to In Vivo Metabolism Rate and Integration within Human PBPK Models. In the PBPK model, the value of intrinsic clearance was calculated as the product of the QPPR value of CL_{intPL} (L of PL/h/kg$^{0.75}$) and the phospholipid : blood PC (values of P_{plb} in Table 1). The intrinsic clearance (L blood/h/kg$^{0.75}$) was used within the human PBPK models to compute the hepatic clearance.

The rate of metabolism was calculated on the basis of hepatic clearance (i.e., hepatic clearance times the arterial concentration) [4, 40, 41, 45]. For chloroethane, dichloromethane, vinyl chloride, and dibromomethane a first-order constant (1, 2, 1, and 0.7 h^{-1}, resp.) was included in the calculation of the hepatic clearance, CL_h (L/h) [41]:

$$CL_h = Q_L \cdot E, \tag{4}$$

where $E = (CL_{\mathrm{int}} + K_f \cdot V_L)/((CL_{\mathrm{int}} + K_f \cdot V_L) + Q_L)$, Q_L is the blood flow through the liver (L/h), CL_{int} the intrinsic clearance (L blood/h), K_f the first order metabolic constant (h^{-1}), and V_L the liver volume (L).

2.3. PBPK Modeling. The QPPR values of CL_{int} were included in a human PBPK model for inhaled VOCs [50]. Briefly, the PBPK model consisted in four tissue compartments (i.e., liver, fat, richly, and poorly perfused tissues) and a gas exchange lung, which were interconnected by blood flows. The distribution of VOCs into tissue compartments was described as perfusion limited, and the metabolism was limited to liver.

To evaluate the impact of uncertainty on the metabolic rate, for all the chemicals, PBPK simulations were also conducted by setting the value of E to 0.999 (E_{max}) and then to 0.001 (E_{min}), respectively.

The human physiological parameters of the PBPK model (i.e., body weight = 70 kg; cardiac output = 18 L/h/kg$^{0.74}$; alveolar ventilation = 18 L/h/kg$^{0.74}$; tissue compartment volumes, fraction of body weight:liver = 0.026; richly perfused tissues = 0.05; poorly perfused tissues = 0.62; fat = 0.19; perfusion of the tissue compartments, fraction of cardiac output:liver = 0.26; richly perfused tissues = 0.44; poorly perfused tissues = 0.25; fat = 0.05) were obtained from Tardif et al. [67]. Table 1 presents the value of the partition coefficients used in the PBPK model (i.e., blood : air, tissue : blood, and phospholipid : blood PCs). The phospholipid : blood PC was calculated using (1), whereas the blood : air PC and tissue : blood PCs were gathered from the literature [48, 50, 52, 54, 56–59, 61, 66, 67, 77–80].

The PBPK model (differential and algebraic mass-balance equations, physiological parameters, QSPR equations for metabolic constants, and PCs) was written in ACSL (acslX, version 2.5, Aegis Technologies Group, Inc, Huntsville, AL). The model code is included in the supplementary data available online at doi:10.1155/2012/286079. To compare the impact of different (uncertain) scenarios of rate of metabolism on the pharmacokinetics in human, simulations were carried out by setting (i) the value of CL_{int} equal to the lower and upper bound of the QPPR predicted mean 95% confidence interval, or (ii) the liver extraction ratio to 0.001 (no metabolism) and 0.999 (maximum extraction). The 24 h venous blood kinetics corresponding to the four scenarios of metabolism were simulated for an 8 h exposure to 1 ppm of each VOC. The 24 h area under the curve (AUC_{24}) of the venous blood kinetics was also calculated to compare the four scenarios of metabolism simulated with PBPK models. Additionally, the venous blood kinetics of *m*-xylene, toluene, ethylbenzene, dichloromethane, styrene, 1,2,4-trimethylbenzene, and 1,1,1-trichloroethane were compared to experimental data [61, 67, 81–83].

2.4. Analysis of Applicability of the CL_{int} QPPR to PBPK Modeling. The applicability of the QPPR model was evaluated on the basis of the level of uncertainty in the QPPR estimate and the impact (sensitivity) of metabolism on the AUC_{24}. Figure 1 illustrates the role of uncertainty and sensitivity in the reliability of the QPPR-PBPK modeling framework, based on reference [84]. The sensitivity of the metabolism to the AUC was estimated by the ratio of the AUC_{24} obtained with no metabolism (E_{min}) to that obtained with the maximum theoretical metabolism (E_{max}). The sensitivity of AUC_{24} to metabolism was considered to be low, medium, or high if the ratio ($\mathrm{AUC}_{E_{\mathrm{min}}}/\mathrm{AUC}_{E_{\mathrm{max}}}$) was within a factor of 2, within an order of magnitude, or greater. The uncertainty in the QPPR prediction was evaluated by comparing it

Confidence in the QPPR-PBPK model		Impact of metabolism on AUC ($AUC_{E_{min}}/AUC_{E_{max}}$)		
		Low (<2)	Medium (2–10)	High (>10)
QPPR prediction uncertainty (Pred. CL_{intPL}/exp. CL_{intPL})	Low (<2)	High	High	High
	Medium (2–10)	High	Medium	Medium
	High (>10)	High	Medium	Low

Figure 1: Evaluation of the confidence in applying the QPPR for CL_{intPL} in a PBPK model using a sensitivity/uncertainty approach.

to the experimental data. The prediction uncertainty was considered to be low, medium or high if the prediction was within a factor of two, within an order of magnitude and above 10-fold of the experimental data, respectively.

This approach was applied to evaluate the reliability of applying the QPPR within the PBPK model for two situations: (i) for the calibration set of chemicals, for which the uncertainty of the QPPR was evaluated by comparing the predictions of CL_{intPL} with the experimentally derived CL_{intPL} values and (ii) for chemicals in the evaluation dataset, for which the uncertainty in the QPPR prediction was considered to be "high", to replicate the "data poor" situations with new or tested chemicals with unknown experimental CL_{int} values.

3. Results

3.1. QPPR Development. The initial effort to develop a QPPR model for metabolism rate (expressed as $CL_{intblood}$, in units of L blood/hr), based on a stepwise analysis of its relationship to various molecular descriptors and physicochemical properties, was not successful (not shown). Same analysis, repeated for CL_{int} expressed in units of L PL/h (CL_{intPL}), yielded a QPPR that consisted of $\log P_{plw}$, $\log P_{bw}$, and IP (ionization potential, eV) as input parameters. This model satisfied the criteria for an acceptable model in terms of coefficient of determination ($R^2 = 0.802$; $R^2_{adj} = 0.775$), leave-one-out cross validation ($Q^2 = 0.755$), and multicollinearity (VIFs: $\log P_{plw} = 2.42$; $\log P_{bw} = 2.38$; IP = 1.04). The values of the regression coefficients were significant (P value < 0.001 for the constant, $\log P_{plw}$ and $\log P_{bw}$, and 0.007 for IP).

However, as the value of $\log P_{ow}$ can be obtained more readily than $\log P_{plw}$, the regression analysis was repeated by using $\log P_{ow}$, $\log P_{bw}$, and calculated IP, and it yielded the following QPPR:

$$\log CL_{intPL} = 5.63(\pm 1.187) - 1.287(\pm 0.149) \cdot \log P_{ow} + 1.08(\pm 0.233) \cdot \log P_{bw} - 0.328(\pm 0.111) \cdot \text{IP}. \quad (5)$$

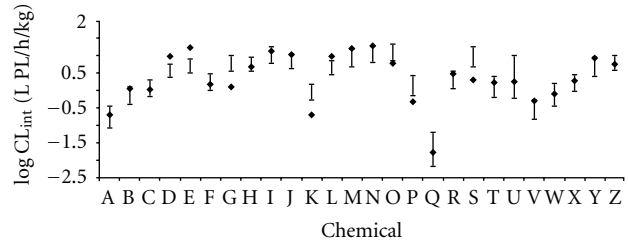

Figure 2: Experimental and predicted values of $\log CL_{int}$ for 26 VOCs. The horizontal bars represent the QPPR predicted LMCI and UMCI, the symbols represent the experimental data. A: 1,1,1,2-tetrachloroethane; B: 1,1,2,2-tetrachloroethane; C: 1,1,2-trichloroethane; D: 1,1-dichloroethane; E: 1,1-dichloroethylene; F: 1,2-dichloroethane; G: 1,2-dichloroethylene (*cis*-); H: benzene; I: bromochloromethane; J: bromodichloromethane; K: carbon tetrachloride; L: chloroethane; M: chloroform; N: dibromomethane; O: dichloromethane; P: ethylbenzene; Q: hexachloroethane; R: isoprene; S: methyl chloride; T: *m*-xylene; U: *n*-hexane; V: pentachloroethane; W: styrene; X: toluene; Y: trichloroethylene; Z: vinyl chloride.

This QPPR model satisfied the criteria for an acceptable model in terms of coefficient of determination ($R^2 = 0.796$; $R^2_{adj} = 0.768$), leave-one-out cross validation ($Q^2 = 0.748$), and multicollinearity (VIFs: $\log P_{ow} = 2.42$; $\log P_{bw} = 2.38$; IP = 1.04). The application domain of the model can be described with [min; max] as follows: $\log P_{ow}$ = [1.09; 4.03]; $\log P_{bw}$ [0.16; 2.49]; calculated ionization potential [9.13;11.28].

The QPPR (5) was subsequently applied to calculate the CL_{intPL} of the VOCs in the calibration set. Table 2 presents the values of the input parameters, along with the experimental data for the 26 VOCs used in QPPR development. Figure 2 illustrates the comparison of the predicted values of CL_{intPL} (LMCI and UMCI) and the experimental data. The uncertainty in the predicted log CL_{intPL} can be characterized by the difference between the UMCI and the LMCI; this value ranged from 0.37 (1,1-dichloroethane) to 1.23 (*n*-hexane) with a mean of 0.54 and a standard deviation of 0.18. The nearest confidence bounds of the predicted log CL_{intPL} were higher than 5-fold of the experimental value (exp.) for three substances (*cis*-1,2-dichloroethylene, LMCI = 0.55 versus exp. = 0.09; styrene, LMCI = −0.45 versus exp. = −0.09; and 1,1,2-trichloroethane, UMCI = 0.46 versus exp. = 0.02). The impact of the imprecision of these QPPR predictions of the metabolic constants on the pharmacokinetics in humans was then evaluated by PBPK modeling.

Figure 3 presents the predictions of the 24 h blood pharmacokinetics following 8 h exposure to 1 ppm of each of the 26 VOCs used in the QPPR analysis. The bold lines represent the simulations obtained using 0 and 1 as the hepatic extraction ratio, whereas the grey area encompassed by thin lines represents the simulation obtained using LMCI and UMCI of predicted CL_{int} in PBPK models. Overall, the envelope of the concentrations predicted using the QPPR predictions reduced the region of uncertainty associated with

Table 2: Input parameters and experimental data of log CL_{intPL}.

Chemical	Input parameters			Log Cl_{intPL}[a] (L_{PL}/h/kg)	Ref V_{max}, K_m
	Log P_{ow}	Log P_{bw}	Ionization potential (eV)		
Benzene	1.99	0.820	9.743	0.667	[53]
Bromochloromethane	1.43	0.642	10.562	1.118	[49]
Bromodichloromethane	1.61	0.717	10.676	1.029	[46]
Carbon tetrachloride	2.44	0.988	10.985	−0.700	[24]
Chloroethane	1.58	0.438	10.410	0.987	[24]
Chloroform	1.52	0.741	10.839	1.192	[24]
Dibromomethane	1.52	0.777	10.587	1.275	[51]
Dichloroethane (1,1-)	1.76	0.624	10.577	0.974	[24]
Dichloroethane (1,2-)	1.83	0.356	10.446	0.163	[24]
Dichloroethylene (1,1-)	2.12	0.922	9.748	1.223	[24]
Dichloroethylene (*cis*-1,2)	1.98	0.752	9.493	0.092	[24]
Dichloromethane	1.34	0.608	10.582	0.777	[24]
Ethylbenzene	3.03	1.386	9.406	−0.334	[49]
Hexachloroethane	4.03	1.315	10.843	−1.767	[24]
Hexane (*n*-)	3.29	2.492	11.276	0.252	[47]
Isoprene	2.58	0.987	9.349	0.472	[52]
Methyl chloride	1.09	0.160	10.473	0.299	[24]
Pentachloroethane	3.11	1.251	10.763	−0.297	[24]
Styrene	2.89	0.889	9.130	−0.088	[50]
Tetrachloroethane (1,1,1,2-)	2.93	0.836	10.728	−0.693	[24]
Tetrachloroethane (1,1,2,2-)	2.19	0.519	10.736	0.051	[24]
Toluene	2.54	0.879	9.442	0.282	[49]
Trichloroethane (1,1,2-)	2.01	0.491	10.689	0.018	[24]
Trichloroethylene	2.47	1.192	9.368	0.916	[24]
Vinyl chloride	1.62	0.433	9.833	0.741	[24]
Xylene (*m*-)	3.09	1.388	9.308	0.218	[48]

[a]: EXP. experimental data (references in Section 2); LMCI and UMCI: lower and upper bound of the 95% mean confidence interval, respectively.

the complete lack of knowledge of hepatic extraction ratio in humans (i.e., ranging from 0 to 1).

The average ratio (± standard deviation) of the PBPK model simulated values of the end-of-exposure blood concentrations (i.e., C_{max}) obtained with E_{min} and E_{max} was 4.19 ± 1.81. The lowest and highest ratios, based on the theoretical bounds of hepatic extraction (i.e., E_{min} and E_{max}), were observed for isoprene (1.63) and 1,1,2,2-tetrachloroethane (8.05), respectively. However, the average ratio (± standard deviation) of the PBPK model simulated values of the end-of-exposure blood concentrations, based on QPPR-generated bounds (LMCI, UMCI), was 1.29 ± 0.27. This ratio was the highest for hexachloroethane (2.39) and the lowest for 1,1-dichloroethylene (1.06).

For the 26 VOCs used in the development of the QPPR, the values of AUC_{24}s for a 1 ppm continuous exposure are reported in Table 3. The ratio of the highest to the lowest AUC predicted with E_{min} and E_{max} was 4.3 ± 1.94 ranging from 1.63 (isoprene) to 8.7 (1,1,2,2-tetrachloroethane). The ratio of the maximum to minimum concentrations predicted using the QPPR metabolism rate was 1.36 ± 0.4 ranging from 1.06 (1,1-dichloroethylene) to 2.8 (isoprene).

Figure 4 illustrates the range of predictions of venous blood pharmacokinetics compared to experimental data [67, 81, 82]. Overall, the predicted envelope of concentrations approximated reasonably the experimental data for dichloromethane, ethylbenzene, styrene, toluene, and *m*-xylene.

3.2. Analysis of Applicability of the CL_{int} QPPR to PBPK Modeling. The reliability of applying the QPPR within the PBPK model was assessed for the 26 VOCs in the calibration dataset (Table 4). The uncertainty of the QPPR prediction was estimated as the ratio of predicted CL_{intPL} to experimental CL_{intPL}. For 3 VOCs (isoprene, 1,1-dichloroethylene, and vinyl chloride) the sensitivity of AUC to CL_{int} was low (ratio of AUCs < 2) whereas uncertainty of the CL_{int} QPPR was low for isoprene and vinyl chloride and medium for 1,1-dichloroethylene. For the other 23 VOCs, the ratio of AUCs was between 2 and 5. For 16 of the later 23 VOCs (benzene; bromochloromethane; bromodichloromethane; chloroform; dibromomethane; 1,2-dichloroethane; hexachloroethane; *n*-hexane; pentachloroethane; styrene;

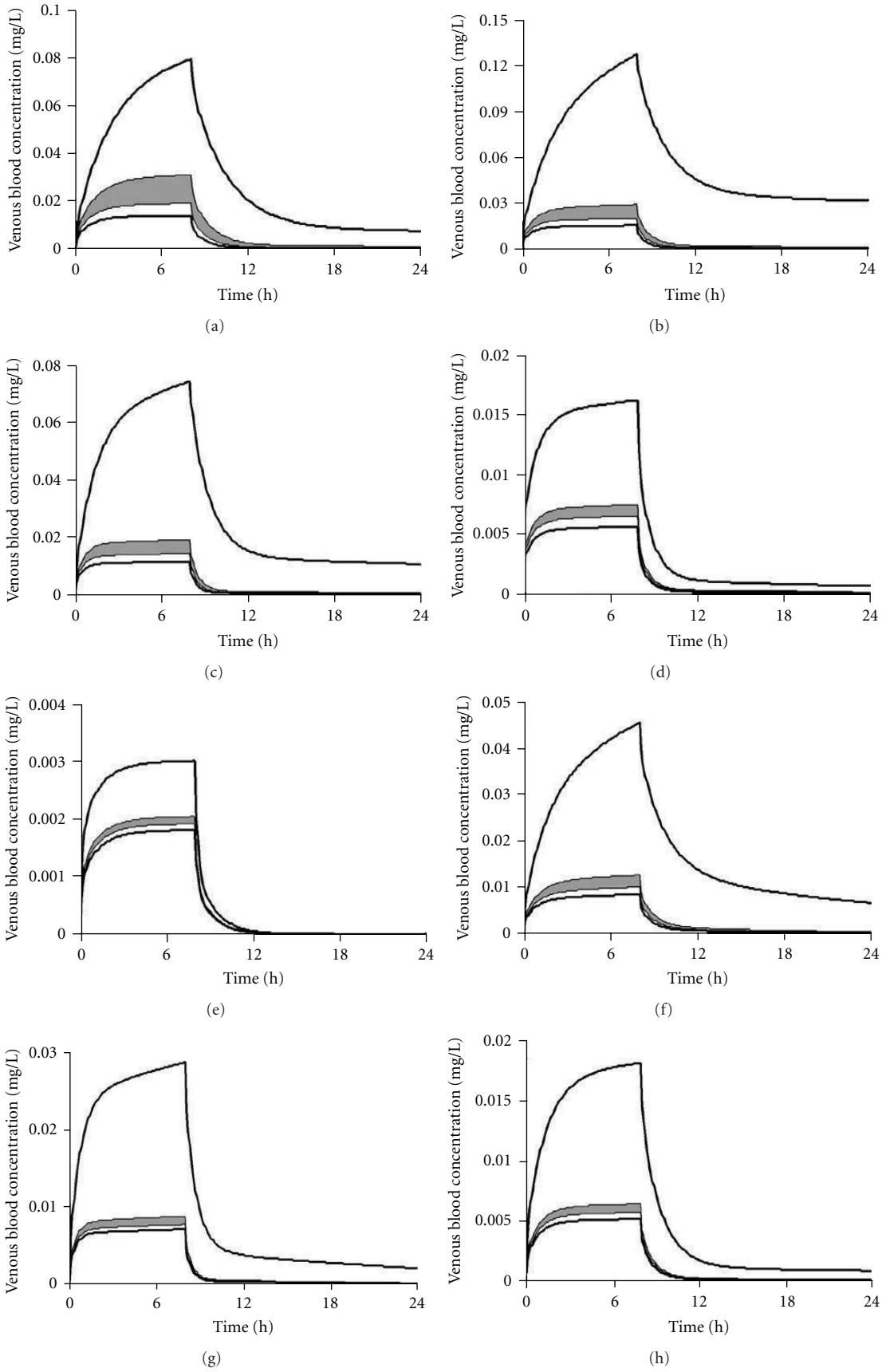

Figure 3: Continued.

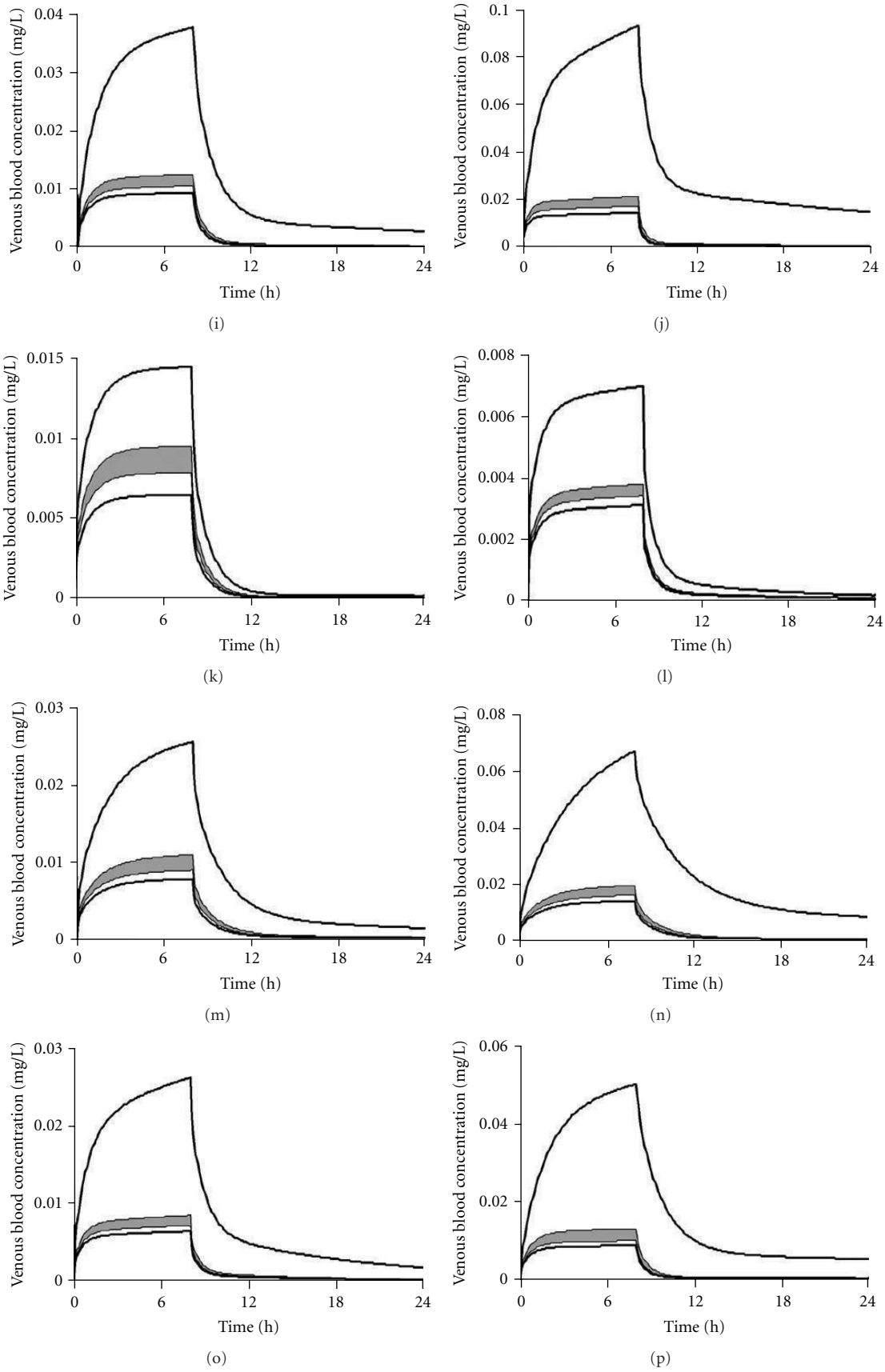

Figure 3: Continued.

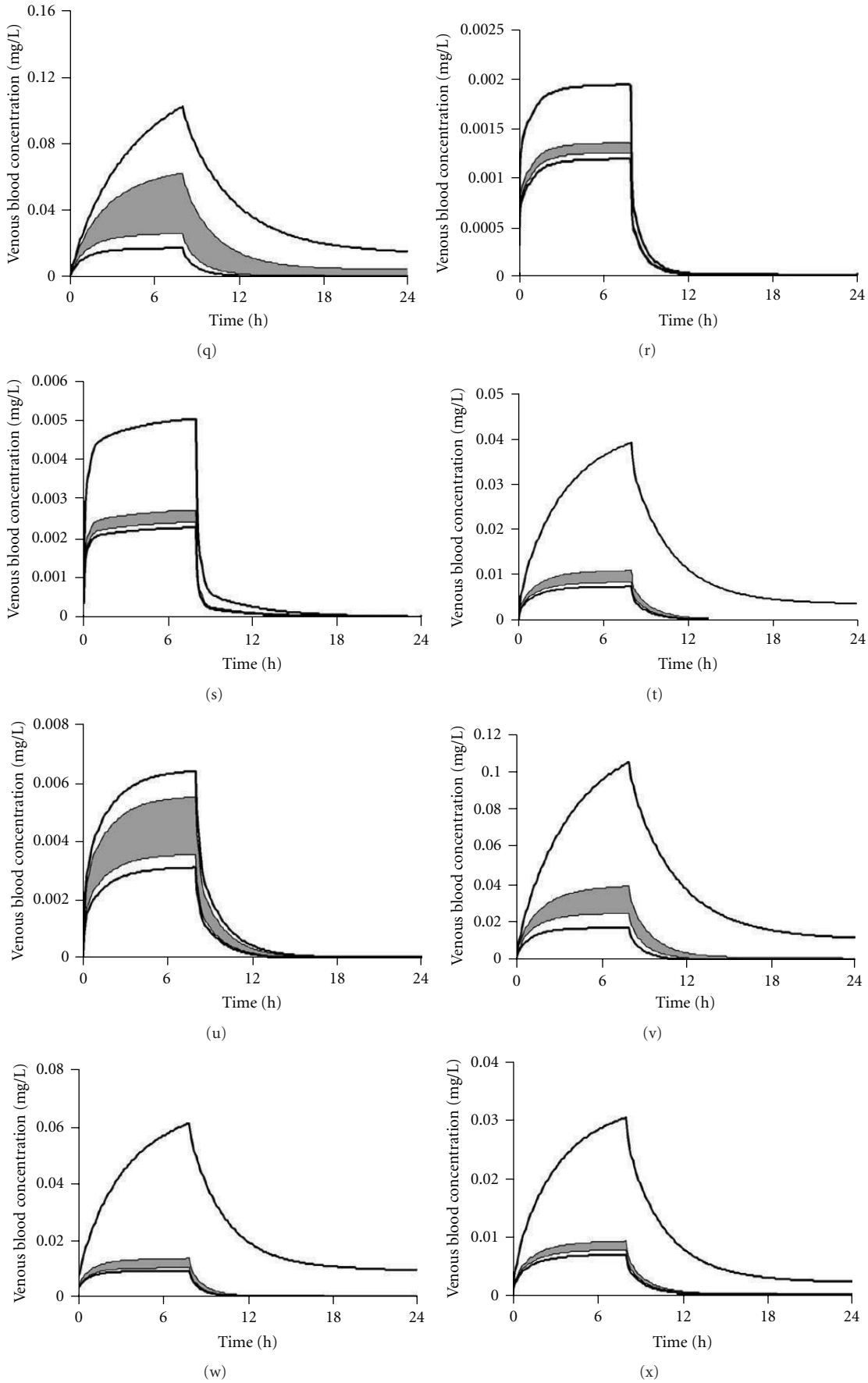

Figure 3: Continued.

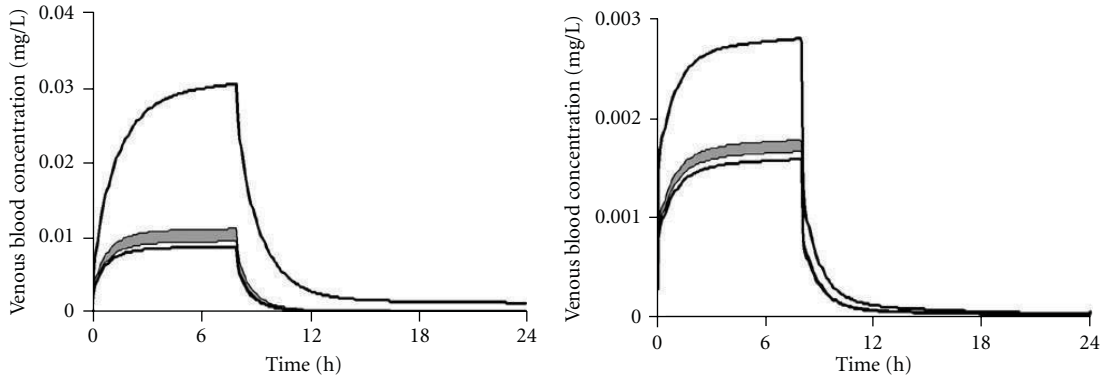

Figure 3: 24 h simulation of the venous blood concentration following inhalation exposure to 1 ppm, 8 h for 26 volatile organic compounds considering maximum and minimum (bold lines) and QPPR-based hepatic extraction (grey area). (a) 1,1,1,2-Tetrachloroethane; (b) 1,1,2,2-tetrachloroethane; (c) 1,1,2-trichloroethane; (d) 1,1-dichloroethane; (e) 1,1-dichloroethylene; (f) 1,2-dichloroethane; (g) 1,2-dichloroethylene (*cis*-); (h) benzene; (i) bromochloromethane; (j) bromodichloromethane; (k) carbon tetrachloride; (l) chloroethane; (m) chloroform; (n) dibromomethane; (o) dichloromethane; (p) ethylbenzene; (q) hexachloroethane; (r) isoprene; (s) methyl chloride; (t) *m*-xylene; (u) *n*-hexane; (v) pentachloroethane; (w) styrene; (x) toluene; (y) trichloroethylene; (z) vinyl chloride.

Table 3: Area under the curve for four metabolic scenarios for the VOCs used in the QPPR development.

Chemicals	24 h Area under the curve (mg/L-h) Metabolic scenario[a]			
	E_{min}	E_{max}	LMCI	UMCI
Benzene	0.437	0.125	0.155	0.138
Bromochloromethane	0.913	0.229	0.305	0.257
Bromodichloromethane	2.380	0.356	0.523	0.422
Carbon tetrachloride	0.34	0.153	0.224	0.186
Chloroethane	0.156	0.069	0.084	0.076
Chloroform	0.599	0.185	0.257	0.211
Dibromomethane	1.659	0.336	0.466	0.384
Dichloroethane (1,1-)	0.391	0.138	0.181	0.158
Dichloroethane (1,2-)	1.142	0.205	0.305	0.241
Dichloroethylene (1,1-)	6.98×10^{-2}	4.22×10^{-2}	4.76×10^{-2}	4.47×10^{-2}
Dichloroethylene (*cis*-1,2)	0.702	0.174	0.214	0.188
Dichloromethane	0.65	0.157	0.206	0.174
Ethylbenzene	1.247	0.216	0.32	0.246
Hexachloroethane	3.071	0.494	1.774	0.738
Hexane (*n*-)	0.15	0.073	0.129	0.084
Isoprene	4.59×10^{-2}	2.81×10^{-2}	0.084	2.95×10^{-2}
Methyl chloride	0.119	0.054	0.064	0.057
Pentachloroethane	2.584	0.418	0.929	0.595
Styrene	1.497	0.222	0.322	0.246
Tetrachloroethane (1,1,1,2-)	1.911	0.337	0.739	0.457
Tetrachloroethane (1,1,2,2-)	3.337	0.384	0.717	0.495
Toluene	0.74	0.168	0.223	0.188
Trichloroethane (1,1,2-)	1.876	0.284	0.474	0.355
Trichloroethylene	0.721	0.209	0.267	0.227
Vinyl chloride	6.68×10^{-2}	3.79×10^{-2}	4.25×10^{-2}	3.98×10^{-2}
Xylene (*m*-)	1.117	0.209	0.308	0.236

[a]: E_{min}: no metabolism; E_{max}: maximum hepatic extraction; LMCI and UMCI: lower and upper bound of the 95% mean confidence interval, respectively.

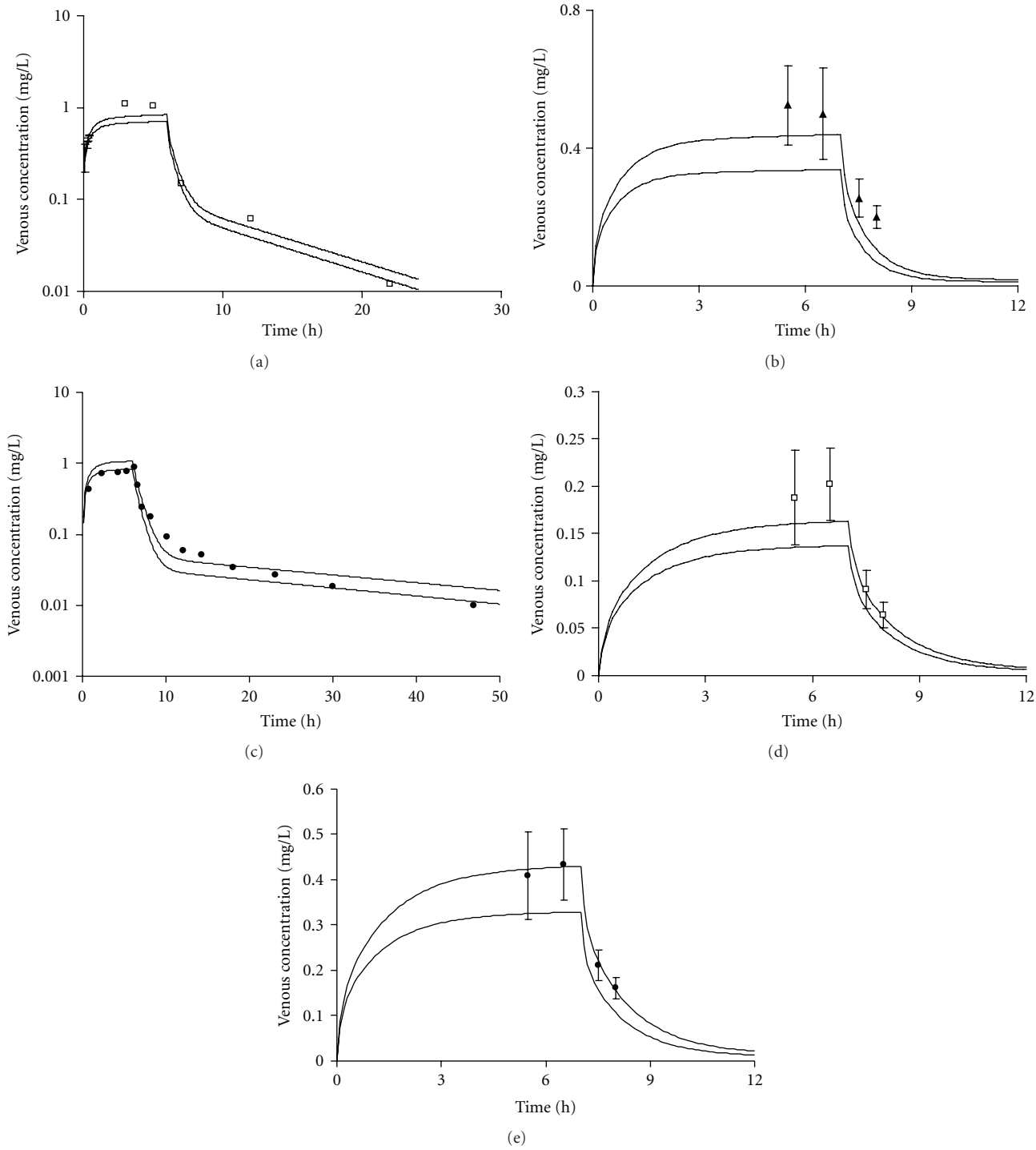

Figure 4: Comparison of PBPK model simulation with experimental data of venous blood concentration following inhalation exposure to (a) 100 ppm, 6 h dichloromethane [77]; (b) 33 ppm, 7 h ethylbenzene [67]; (c) 80 ppm, 6 h styrene [78]; (d) 17 ppm, 7 h toluene [67]; (e) 33 ppm, 7 h *m*-xylene [67]. Bold lines: predicted LMCI and UMCI for CL_{int}.

1,1,1,2-tetrachloroethane; 1,1,2,2-tetrachloroethane; toluene; 1,1,2-trichloroethane; trichloroethylene; *m*-xylene) the prediction uncertainty was low, thus the confidence in using the QPPR in the PBPK model is high for these compounds. The uncertainty was medium for the prediction of CL_{intPL} for 7 VOCs (carbon tetrachloride; chloroethane; 1,1-dichloroethane; *cis*-1,2-dichloroethylene; dichloromethane; ethylbenzene; methyl chloride). Therefore, for these chemicals, the confidence in using the QPPR in an inhalation PBPK model to evaluate the AUC is medium.

Table 4: Reliability analysis of the QPPR for CL_{int} on the PBPK predicted AUC.

		Impact of metabolism on AUC ($AUC_{E_{min}}/AUC_{E_{max}}$)[a]		
		Low (<2)	Medium (2–5)	High (>5)
QPPR prediction uncertainty (Pred./Exp. CL_{intPL})[b]	Low (<2)	Isoprene, vinyl chloride	Benzene; bromochloromethane; bromodichloromethane; chloroform; dibromomethane; 1,2-dichloroethane; hexachloroethane; *n*-hexane; pentachloroethane; styrene; 1,1,1,2-tetrachloroethane; 1,1,2,2-tetrachloroethane; toluene; 1,1,2-trichloroethane; trichloroethylene; *m*-xylene	
	Medium (2–5)	1,1,-Dichloroethylene	Carbon tetrachloride; chloroethane; 1,1-dichloroethane; *cis*-1,2-dichloroethylene; dichloromethane; ethylbenzene; methyl chloride	
	High (>5)			

[a] Calculated as the ratio of the PBPK simulations of 24 h AUC (of venous blood concentration, 1 ppm VOC, 24 h exposure) obtained by setting $E = 0$ (i.e., $CL_{int} = 0$) to that setting $E = 1$ (i.e., $CL_{int} = 1000$).
[b] Calculated as the ratio of the predicted to the experimental values of CL_{intPL}.

Table 5: Input parameters and experimental data on log CL_{int} for VOCs of QPPR evaluation.

Chemical	Input parameters			Log Cl_{intPL}[a] (L$_{PL}$/h/kg)	Ref V_{max}, K_m
	log P_{ow}	log P_{bw}	IP (eV)		
Bromoform	1.79	0.896	10.837	1.006	[46]
Dibromochloromethane	1.70	1.025	10.702	1.108	[46]
Dichloroethylene (*trans*-1,2-)	1.98	0.484	9.512	0.438	[55]
Ethylene	1.27	0.776	10.638	1.208	[59]
Furan	1.36	0.441	9.375	1.773	[56]
Halothane	2.26	0.977	11.039	1.104	[58]
Propylene	1.68	0.995	10.103	1.118	[54]
Tetrachloroethylene	2.97	1.404	9.217	−1.804	[57]
Trichloroethane (1,1,1-)	2.68	0.823	10.751	−2.467	[48]
Trimethylbenzene (1,2,4-)	3.63	1.829	9.084	−0.132	[61]
Xylene (*o*-)	3.09	1.213	9.304	0.163	[60]

[a] Experimental data (references in Section 2).

3.3. QPPR Evaluation. The QPPR model was applied to predict the CL_{intPL} of 11 VOCs that were not in the calibration dataset. Table 5 presents the values of the input parameters along with the experimental data for the 11 VOCs used in QPPR evaluation. Figure 5 illustrates the comparison of the predicted values of CL_{intPL} (LMCI and UMCI) and the experimental data. The average difference (± standard deviation) between the UMCI and the LMCI was 0.57 ± 0.11 ranging from 0.46 (bromoform) to 0.84 (1,2,4-trimethylbenzene). The highest UMCI-LMCI ranges were obtained for furan (0.62), tetrachloroethylene (0.63), and 1,2,4-trimethylbenzene (0.84). The nearest predicted values of UMCI and LMCI on log CL_{intPL} were greater than 5-fold of the experimental data for tetrachloroethylene (LMCI = 0.02 versus exp = −1.8). As in the QPPR development section, the impact of the imprecision on these log CL_{int} predictions on the pharmacokinetics in humans was evaluated by PBPK modeling.

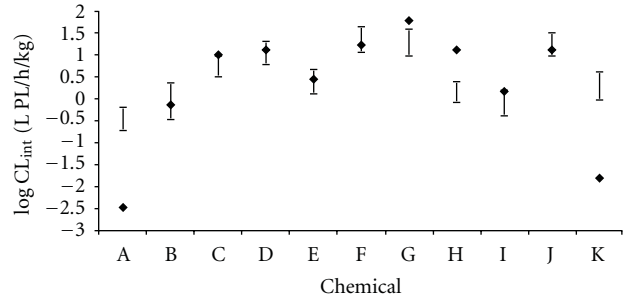

Figure 5: Comparison of the predicted log CL_{int} (LMCI and UMCI) with the experimental data on 11 VOCs. The bars represent the QPPR predictions and the symbols the experimental values. A: 1,1,1-trichloroethane; B: 1,2,4-trimethylbenzene; C: 1,2-dichloroethylene (*trans*-); D: bromoform; E: dibromochloromethane; F: ethylene; G: furan; H: halothane; I: *o*-xylene; J: propylene; K: tetrachloroethylene.

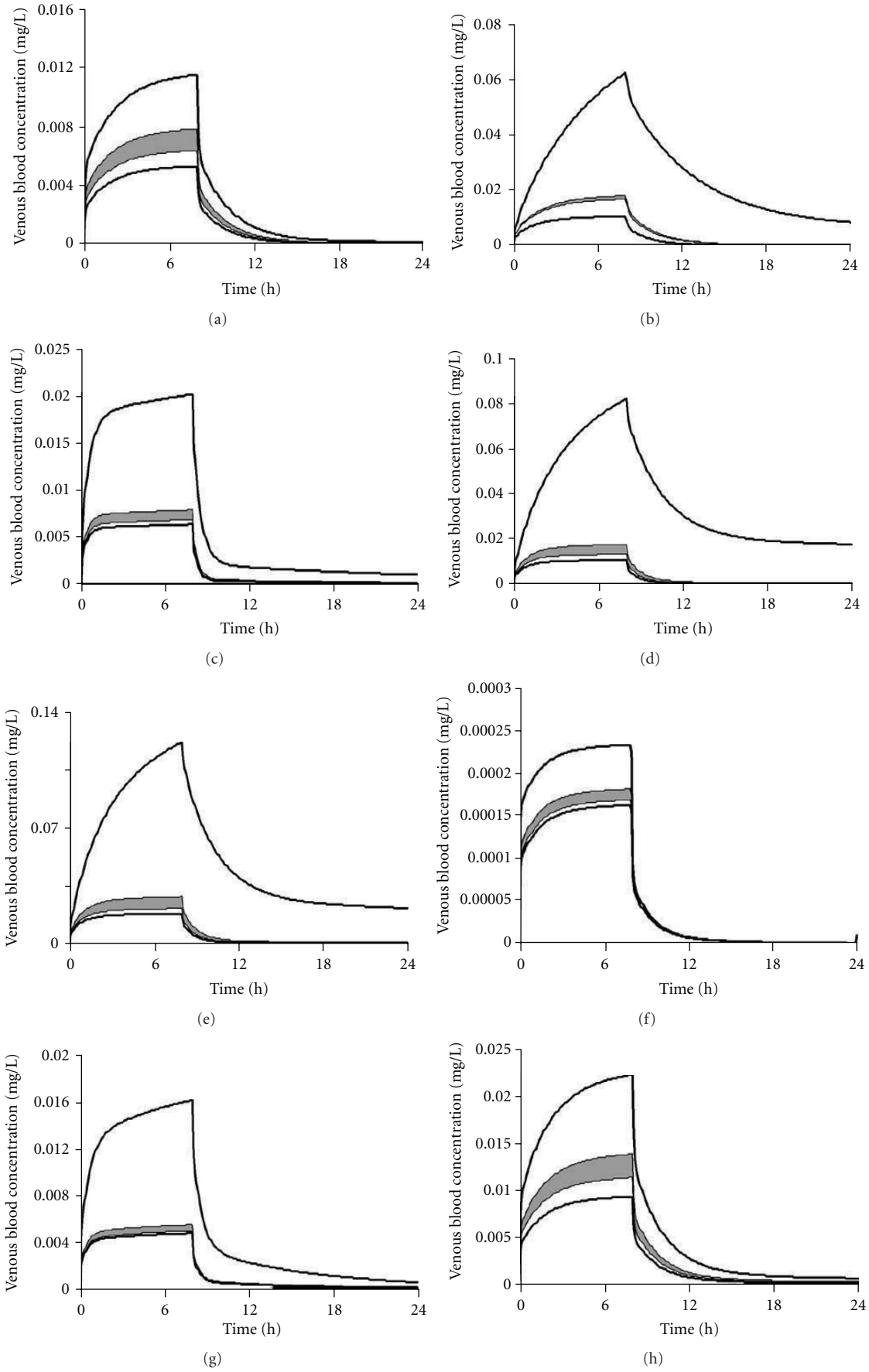

Figure 6: Continued.

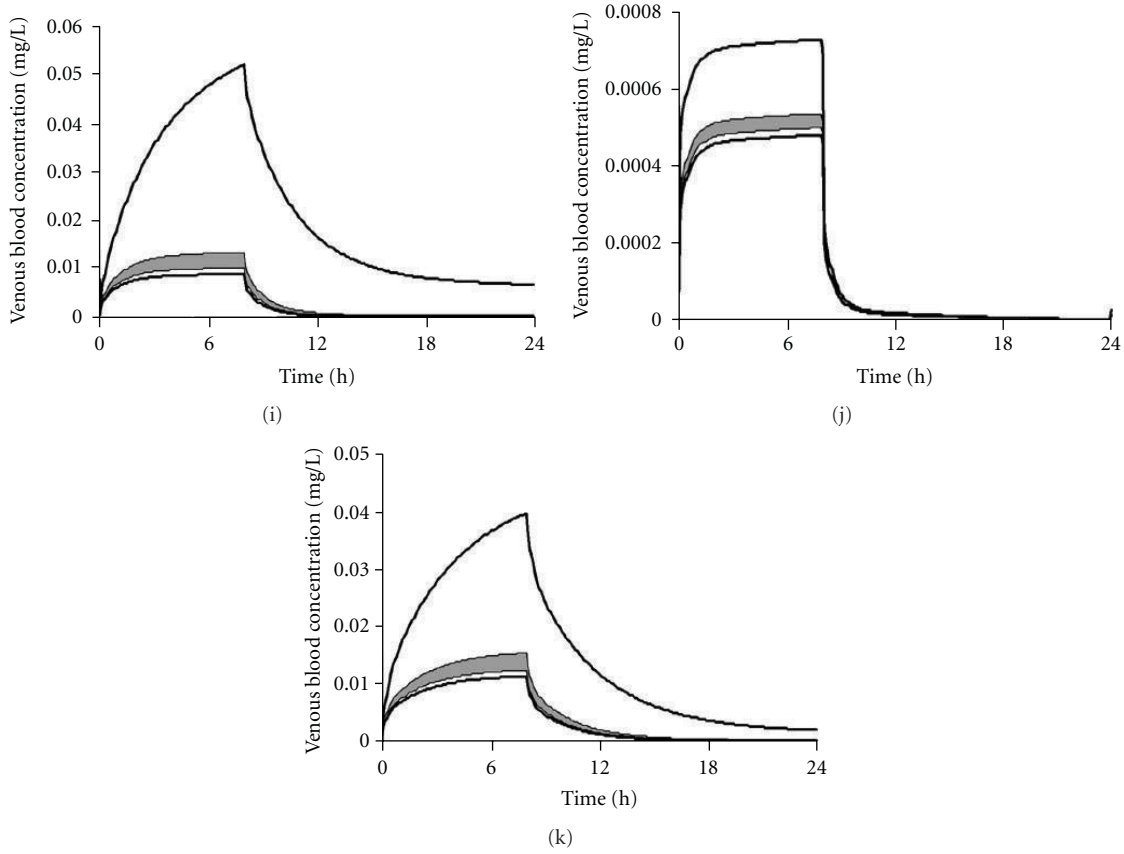

Figure 6: 24 h simulation of the venous blood concentration following inhalation exposure to 1 ppm, 8 h for 11 volatile organic compounds considering maximum and minimum (bold lines) and QPPR-based hepatic extraction (grey area). (a) 1,1,1-Trichloroethane; (b) 1,2,4-trimethylbenzene; (c) 1,2-dichloroethylene (*trans*-); (d) bromoform; (e) dibromochloromethane; (f) ethylene; (g) furan; (h) halothane; (i) *o*-xylene; (j) propylene; (k) tetrachloroethylene.

Figure 6 presents the predictions of the 24 h blood pharmacokinetics following 8 h exposure to 1 ppm of each of the 11 VOCs used in the QPPR evaluation. The bold lines represent the simulations obtained using 0 and 1 as the hepatic extraction ratio, whereas the grey area encompassed by thin lines represents the simulation obtained using LMCI and UMCI of predicted CL_{int} in PBPK models. The reduction of the region of uncertainty associated with the complete lack of knowledge of hepatic extraction ratio in humans (i.e., ranging from 0 to 1) by the envelope of the concentrations predicted using the QPPR predictions was observed for the 11 VOCs.

The mean ratio (± standard deviation) of the PBPK model simulated values of the end-of-exposure blood concentrations obtained with E_{min} and E_{max} was 3.92 ± 2.13 ranging from 1.42 (ethylene) to 7.45 (bromoform). However, the same average ratio (± standard deviation) of PBPK simulated blood concentrations, based on QPPR-generated bounds (LMCI and UMCI) was 1.2 ±0.1, ranging from 1.07 (ethylene) to 1.33 (bromoform).

Table 6 presents the values of the AUC_{24}s (mg/L-h) for the 11 VOCs used in the evaluation of the QPPR. The average ratio of the highest to lowest AUC predicted using E_{min} and E_{max} was 4.08 ± 2.31 (mean ± SD). The lowest and highest ratios, based on the theoretical bounds of hepatic extraction (i.e., $E = 0.001$ or 0.999), were observed for ethylene (1.44) and bromoform (7.96), respectively.

The ratio of the maximum to minimum concentrations predicted using the QPPR metabolism rate was 1.2 ± 0.1, ranging from 1.07 (propylene) to 1.33 (dibromochloromethane).

Figure 7 illustrates the range of predictions for two of the chemicals in the external dataset (1,2,4-trimethylbenzene and 1,1,1-trichloroethane) venous blood pharmacokinetics compared to experimental data [61, 85]. The QPPR-PBPK model-generated "envelope" of concentrations simulated reasonably the experimental data for 1,2,4-trimethylbenzene whereas the blood concentrations of 1,1,1-trichloroethane were underestimated by about 30%.

3.4. Analysis of Applicability of the CL_{int} QPPR to PBPK Modeling. The reliability of applying the QPPR within the PBPK model was assessed for the 11 VOCs in the evaluation dataset, using the framework shown in Figure 1. Considering that the experimental data of CL_{intPL} for new or untested chemicals will be essentially unknown, it is realistic to consider the uncertainty of the QPPR prediction of CL_{intPL} to be high for all chemicals in the evaluation dataset.

Table 6: Area under the curve for four metabolic scenarios, for VOCs in the evaluation dataset.

Chemicals	24 h Area under the curve (mg/L-h) Metabolic scenario[a]			
	E_{min}	E_{max}	LMCI	UMCI
Bromoform	2.122	0.267	0.434	0.328
Dibromochloromethane	3.114	0.45	0.7	0.527
Dichloroethylene (*trans*-1,2-)	0.472	0.149	0.185	0.16
Ethylene	5.87×10^{-3}	4.08×10^{-3}	4.55×10^{-3}	4.23×10^{-3}
Furan	0.388	0.113	0.131	0.118
Halothane	0.523	0.22	0.325	0.266
Propylene	1.76×10^{-2}	1.16×10^{-2}	1.3×10^{-2}	1.21×10^{-2}
Tetrachloroethylene	0.953	0.266	0.363	0.291
Trichloroethane (1,1,1-)	0.271	0.125	0.184	0.15
Trimethylbenzene (1,2,4-)	1.577	0.249	0.425	0.395
Xylene (*o*-)	1.297	0.218	0.325	0.248

[a]: E_{min}: no metabolism; E_{max}: maximum hepatic extraction; LMCI and UMCI: lower and upper bound of the 95% mean confidence interval, respectively.

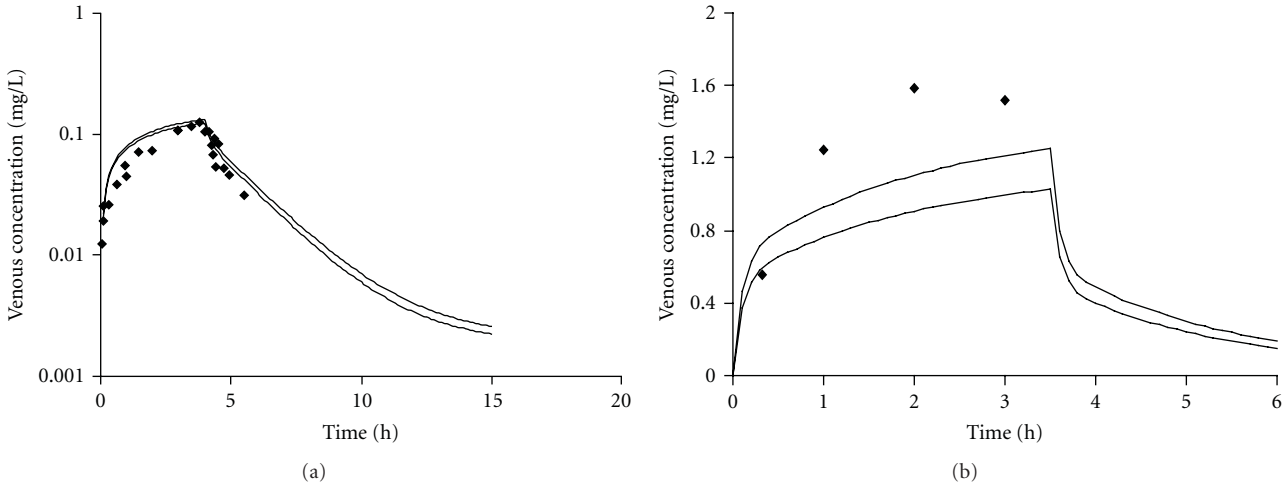

Figure 7: Comparison of PBPK model simulations (bold lines: predicted LMCI and UMCI for CL_{int}) with experimental data of venous blood concentration following inhalation exposure to (a) 8 ppm, 4 h 1,2,4-trimethylbenzene [59] and (b) 175 ppm, 3.5 h 1,1,1-trichloro ethane [85].

The results of the analysis of applicability for the chemicals in the evaluation dataset are reported in Table 7. For 3 VOCs (ethylene; propylene; 1,1,1-trichloroethane) the sensitivity was low (ratio of AUCs < 2) thus the reliability of using their CL_{int} QPPR in the PBPK was considered high. For the other 8 VOCs (bromoform; dibromochloromethane; *trans*-1,2-dichloroethylene; furan; halothane; tetrachloroethylene; 1,2,4-trimethylbenzene; *o*-xylene), the ratio of the maximum to the minimum possible AUCs was between 2 and 5, such that the confidence in using the QPPR in an inhalation PBPK model to evaluate the AUCs is medium for these chemicals.

4. Discussion

SARs, QSAR, QSPRs, and QPPRs have been developed for various toxicological and chemical properties but only very few studies have focused on developing such models to parameterize PBPK models [8, 86]. A limitation in developing PBPK models relates to the availability of the metabolic constants (CL_{int}, V_{max}, and K_m) [8]. Quantitative relationships between structure and metabolism rates have been investigated for a limited number of closely related compounds, even though their applicability to PBPK modeling has not been demonstrated (e.g., QSPR models for K_{cat} and $1/K_m$ [87]). Other works in this area relate to the development of quantum chemical or quantum dynamic methods for prediction of activation energy or enthalpy of activation of P450 mediated reactions [20, 25, 26, 31, 36, 38, 88–91], which have not been used to derive metabolism constants for direct incorporation within rodent or human PBPK models.

The use of the group contribution method to develop QSPRs for integration within PBPK models has been successfully demonstrated, particularly for the inhalation toxicokinetics of VOCs [40–43]. This approach however is limited to VOCs containing one or more of the molecular groups

Table 7: Reliability analysis for the chemicals in the QPPR evaluation dataset.

		Impact of metabolism on AUC ($AUC_{E_{min}}/AUC_{E_{max}}$)[a]		
		Low (<2)	Medium (2–5)	High (>5)
QPPR prediction uncertainty (Pred./Exp. CL_{intPL})[b]	Low (<2)			
	Medium (2–5)			
	High (>5)	Ethylene; propylene; 1,1,1-trichloroethane	Bromoform; dibromochloromethane; *trans*-1,2-dichloroethylene; furan; halothane; tetrachloroethylene; 1,2,4-trimethylbenzene; *o*-xylene	

[a] Calculated as the ratio of the PBPK simulations of 24 h AUC (of venous blood concentration, 1 ppm VOC, 24 h exposure) obtained by setting $E = 0$ (i.e., $CL_{int} = 0$) to that setting $E = 1$ (i.e., $CL_{int} = 1000$).
[b] Calculated as the ratio of the predicted to the experimental values of CL_{intPL}.

or fragments for which the contribution has been evaluated (i.e., CH_3, CH_2, CH, C, C=C, benzene ring, H on benzene ring, and halogens). In order to extend the applicability domain then, it is important to investigate the feasibility of developing QSPRs based on more global, physicochemical properties. In this regard, the present study investigated the development of a QPPR, that used chemical properties rather than chemical structure as input, and it was calibrated to predict CL_{int} expressed in terms of chemical affinity to phospholipids in the endoplasmic reticulum in which CYP enzymes are embedded [63]. This logical transformation of CL_{int} data, reported here for the first time in literature, facilitated the development of more adequate QPPR than the conventional CL_{int} based on blood concentrations. All efforts to develop QPPRs for predicting CL_{int} based on blood concentrations were unsuccessful. The QPPR based chemical affinity to phospholipids–obtained in this study should be regarded as a screening level tool to provide plausible range of metabolism rates in order to facilitate a first-cut evaluation of the blood concentration of inhaled VOCs in humans. The uncertainty associated with this QPPR tool should be evaluated along with the sensitivity of CL_{int} on the dose metrics of the chemical of interest, in the perspective of intended precision. Accordingly, if the dose metric is highly sensitive to CL_{int} and the QPPR predictions of CL_{int} are highly uncertain, then the present tool is of limited use even for screening purposes. In such cases, then *in vivo* or *in vitro* studies can be undertaken to get chemical-specific estimates of CL_{int}.

The QPPR predictions were reasonably in accordance with experimental values for most but not all chemicals in the calibration and evaluation datasets. For some chemicals, the predicted values of log CL_{int} for 1,1,1-trichloroethane (Figure 5(A)) and tetrachloroethylene (Figure 5(K)) exceeded the experimental values by two orders of magnitude. The QSPR for rat hepatic clearance developed by Béliveau and colleagues [41] also overestimated the metabolic rate of these two VOCs. However the PBPK model for 1,1,1-trichlorethane indicated that the AUC of parent chemical in venous blood is not sensitive to V_{max} and K_m [92, 93]. This was demonstrated in Figure 6(a), showing that QPPR-overestimation of CL_{intPL} of 1,1,1-trichloroethane led only to a minimal impact, in terms of the underestimation of the venous blood concentration. In the case of tetrachloroethylene, a poorly metabolized halogenated VOC, the overestimation of the CL_{intPL} led to a 3-fold underestimation of the C_{max} (Figure 6(k)) or a 4-5-fold underestimation of the AUC_{24} (Table 7). If this magnitude of error is not acceptable for screening-level evaluation, then the metabolic rate should be experimentally determined. The combined assessment of the uncertainty/sensitivity of metabolic constants in PBPK models would facilitate the determination of the applicability of the QPPR model, given the level of precision need for an application (Figure 1)

The QPPR developed in this study is a generic tool to provide initial estimates of CL_{int} of VOCs metabolized by hepatic CYP. It does not take into account stereochemistry or other pathway-specific rates and processes, which may be important for some chemicals (e.g., predicted values of CL_{int} are almost identical for 1,1-dichloroethylene and *cis*-1,2-dichloroethylene but experimental values vary by log units of 1.06). Therefore, predictions of CL_{int} based on generic considerations are likely to be inaccurate for specific chemicals but are of limited use in that the estimates (along with the bounds, representing the level of uncertainty) can be integrated with human physiology to provide a first-cut view of the plausible kinetic profiles.

The utility of the QPPR models depends, in part, on the ability to reproducibly calculate the descriptors [74]. Hence, in this study, the descriptors that could be easily calculated and interpreted were chosen and obtained using EPISUITE (for log P_{ow} and P_{wa}) and MMPro (for the ionization potential). However, the blood solubility parameter (i.e., blood : air PC) is additionally required and this can either be obtained experimentally *in vitro* or using other QSARs that account for protein (i.e., haemoglobin and plasma protein) binding in addition to solubility considerations. There are some algorithms and QSARs available in this regard, but

further development is necessary to adequately account for the protein binding phenomena in human blood for various classes of chemicals [8].

The QPPR developed in this study computes CL_{intPL}, which can then be converted to CL_{intblood} for use in PBPK modeling. In an effort to evaluate whether the same input parameters can be used to relate to CL_{intblood}, additional analyses were performed. These yielded the following equation (significant terms only):

$$\log CL_{\text{intblood}} = 5.117 - 0.305 \cdot \log P_{\text{ow}} - 0.324 \cdot \text{IP}. \quad (6)$$

Even though (5) and (6) give almost identical results (one for CL_{intPL} and the other for CL_{intblood}) despite the differing R^2 values (0.796 versus 0.402), it should be noted that (5) was obtained based on statistical analysis of calibration dataset (i.e., modeling) whereas (6) was derived simply by fitting CL_{intblood} to the specific input parameters. Further rearrangements and simplifications of the QPPR, as well as the loss of accuracy associated with such attempts, were not performed in the current study.

The output of the QPPR developed in the present study is $\log CL_{\text{int}}$, which is useful for simulating pharmacokinetics in humans of chemicals at low levels of exposure. CL_{int} is applicable to first-order situations (i.e., when blood levels in humans are much lower than the K_m for metabolizing enzyme) and is derived by dividing the $V_{\max}$ (i.e., the enzyme turn-over) with K_m (representing the affinity of the substrate for the enzyme). The input parameters of the QPPR, namely, $\log P_{\text{ow}}$ and $\log P_{\text{bw}}$, are estimates of the relative solubility in octanol, water, and blood. Then, an interpretation of the model for CL_{int} could be that the binding to the P450 enzyme is a result of hydrophobic interactions [94] which, in turn, can be estimated with parameters reflective of the solubility in *n*-octanol and blood. The solubility in blood is the sum of the solubility in its components (water, phospholipids, neutral lipids, and proteins). Most of the studied VOCs are likely to bind to hemoglobin because of their lipophilicity ($\log P_{\text{ow}}$ value above 1) and low molecular volume [40]. The P_{bw}, thus, is likely an indicator of the binding to proteins, whereas the $\log P_{\text{ow}}$ reflects more the affinity for biotic lipids in the metabolism microenvironment. Similar to $\log P_{\text{ow}}$, the ionization potential has already been correlated with metabolic rates, namely, the $V_{\max}$ and $V_{\max}/k_m$ [23], as this latter parameter could be correlated with the energy needed to break a covalent bond for the oxidation of the substrate.

The QSPR model for CL_{int} developed in this study has a defined theoretical endpoint, is nonambiguous, has a defined domain of application, was analyzed using appropriate goodness-of-fit (R^2) and robustness (Q^2), and has an attempt of mechanistic interpretation. The *in vivo* dataset on 26 VOCs used for the QPPR calibration was chosen because it was previously collated and used in QSPR analyses [40, 41]. These values were taken mainly from the work of Gargas et al. [24]. The QSPR analysis was also attempted with the entire dataset of 37 VOCs (calibration + external dataset) but it did not improve the goodness-of-fit statistics (not shown).

The predicted bounds of the 95% confidence interval of intrinsic clearance were incorporated within a PBPK model to predict the blood toxicokinetics of VOCs. The simulations of blood kinetics were comparable to experimental data for 6 VOCs (toluene, *m*-xylene, ethylbenzene, styrene, dichloromethane,1,2,4-trimethylbenzene, and 1,1,1-trichloroethane, Figures 4 and 7). The simulations obtained in the present study, using lower and upper confidence intervals on the mean predicted CL_{int}, reduced clearly the uncertainty bounds associated with the total lack of knowledge (i.e., E ranging anywhere between 0 and 1). Furthermore, the present study incorporated the QPPR predictions of CL_{int} along with physiological parameters, such that impact on *in vivo* kinetics could be simulated. In effect, in some cases where the uncertainty on CL_{int} predictions was high, it did not translate into a proportionate error on the predictions of kinetics, due to the additional consideration of physiological constraints, and such observations are critical in data-poor situations for designing focused studies to generate chemical-specific data *in vitro* or *in vivo*.

The QPPR developed in this study approximated the experimental rat metabolic constants for the various low-molecular-weight VOCs; and it was used along with the human physiology to generate initial or screening level values of CL_{int} to construct human PBPK models that could be of potential use to interpret data such as measured biomarker levels or for designing kinetic studies to reduce database uncertainty. As shown with some VOCs (e.g., Figure 3: 1,1,1,2-tetrachloroethane, hexachloroethane, and *n*-hexane), the blood concentration profile is extremely influenced by CL_{int}, such that metabolism cannot be neglected in simulating or interpreting human exposure data. And in such cases, the ability to generate at least a range of plausible values of CL_{int}, as done in the present study, would facilitate first in-human simulations of pharmacokinetics of parent chemicals. Integrating information on the impact of metabolism on dose metrics (i.e., AUC) along with prediction uncertainty of the QPPR facilitates the determination of the level of confidence in using this screening level tool. Depending upon the overall confidence in the QPPR application for predicting dose metrics (low, medium, and high) relative to the use purposes, decisions can be made as to the specific studies needed.

Overall, the QPPR developed in the present study allows to predict the CL_{int} of VOCs on the basis of generic molecular descriptors rather than with fragment constants as done previously. The chemical concentration in phospholipids, for the first time, was found to be a dose metric amenable to QPPR analysis. The QPPR was then used to generate range of values of CL_{int}; the level of confidence in these estimates was assessed by considering the impact of CL_{int} on the simulated dose metrics (i.e., AUC of parent chemical in venous blood). For other dose metrics and situations, a more robust QPPR needs to be developed, and such efforts can be based on the methodological developments accomplished in this study. The QPPR-based simulation of pharmacokinetics reduced the range of uncertainty for few substances relative to complete lack of knowledge of the CL_{int}, but it needs to be evaluated/refined with much larger dataset should this screening-level approach be adopted for providing more precise estimates of metabolism rates. Overall, the integrated

QPPR-PBPK model developed in this study is a potentially useful tool for characterizing and reducing the uncertainty associated with the complete lack of knowledge of CL_{int} in predicting human pharmacokinetics of inhaled VOCs.

Acknowledgments

Financial support by Agence Française de Sécurité Sanitaire de l'Environnement et du Travail (AFSSET; EST-2007-85) and Natural Sciences and Engineering Research Council of Canada (NSERC; Discovery grant 138195-2007 RGPIN) is acknowledged.

References

[1] Commission des communautés européennes, *LIVRE BLANC Stratégie pour la future politique dans le domaine des substances chimiques*, 2001.

[2] CEPA, "Loi canadienne sur la protection de l'environnement (1999), Règlement sur les renseignements concernant les substances nouvelles (substances chimiques et polymères)," in *Gazette du Canada partie II*, pp. 1850–2221, Queen's Printer for Canada, Ottawa, Canada, 2005.

[3] United States Environmental Protection Agency, "The U.S. Environmental Protection Agency's strategic plan for evaluating the toxicity of chemicals," Tech. Rep. EPA/100/K-09/001, Office of the Science Advisor, Science Policy Council, Washington, DC, USA, 2009.

[4] K. Krishnan and M. E. Andersen, "Physiologically based pharmacokinetic modeling in toxicology," in *Principles and Methods of Toxicology*, A. W. Hayes, Ed., pp. 231–292, Taylor & Francis, Boca Raton, Fla, USA, 2007.

[5] A. D. Arms and C. C. Travis, "Reference physiological parameters in pharmacokinetic modeling," Tech. Rep. EPA/600/6-88/004, United States Environmental Protection Agency, Washington, DC, USA, 1988.

[6] R. P. Brown, M. D. Delp, S. L. Lindstedt, L. R. Rhomberg, and R. P. Beliles, "Physiological parameter values for physiologically based pharmacokinetic models," *Toxicology and Industrial Health*, vol. 13, no. 4, pp. 407–484, 1997.

[7] M. Béliveau and K. Krishnan, "In Silico approaches for developing physiologically based pharmacokinetic (PBPK) models," in *Alternative Toxicological Methods*, H. Salem and S. A. Katz, Eds., pp. 479–532, CRC Press, Boca Raton, Fla, USA, 2003.

[8] T. Peyret and K. Krishnan, "QSARs for PBPK modelling of environmental contaminants," *SAR and QSAR in Environmental Research*, vol. 22, no. 1-2, pp. 129–169, 2011.

[9] J. DeJongh, H. J. M. Verhaar, and J. L. M. Hermens, "A quantitative property-property relationship (QPPR) approach to estimate in vitro tissue blood partition coefficients of organic chemicals in rats and humans," *Archives of Toxicology*, vol. 72, no. 1, pp. 17–25, 1997.

[10] P. Poulin and K. Krishnan, "An algorithm for predicting tissue: blood partition coefficients of organic chemicals from n-octanol: water partition coefficient data," *Journal of Toxicology and Environmental Health*, vol. 46, no. 1, pp. 117–129, 1995.

[11] P. Poulin and K. Krishnan, "A biologically-based algorithm for predicting human tissue: blood partition coefficients of organic chemicals," *Human and Experimental Toxicology*, vol. 14, no. 3, pp. 273–280, 1995.

[12] P. Poulin and K. Krishnan, "A tissue composition-based algorithm for predicting tissue: air partition coefficients of organic chemicals," *Toxicology and Applied Pharmacology*, vol. 136, no. 1, pp. 126–130, 1996.

[13] P. Poulin and K. Krishnan, "A mechanistic algorithm for predicting blood: air partition coefficients of organic chemicals with the consideration of reversible binding in hemoglobin," *Toxicology and Applied Pharmacology*, vol. 136, no. 1, pp. 131–137, 1996.

[14] P. Poulin and F. P. Theil, "A priori prediction of tissue:plasma partition coefficients of drugs to facilitate the use of physiologically-based pharmacokinetic models in drug discovery," *Journal of Pharmaceutical Sciences*, vol. 89, no. 1, pp. 16–35, 2000.

[15] P. Poulin and F. P. Theil, "Prediction of pharmacokinetics prior to in vivo studies. 1. Mechanism-based prediction of volume of distribution," *Journal of Pharmaceutical Sciences*, vol. 91, no. 1, pp. 129–156, 2002.

[16] T. Rodgers, D. Leahy, and M. Rowland, "Physiologically based pharmacokinetic modeling 1: predicting the tissue distribution of moderate-to-strong bases," *Journal of Pharmaceutical Sciences*, vol. 94, no. 6, pp. 1259–1276, 2005.

[17] T. Rodgers and M. Rowland, "Physiologically based pharmacokinetic modelling 2: predicting the tissue distribution of acids, very weak bases, neutrals and zwitterions," *Journal of Pharmaceutical Sciences*, vol. 95, no. 6, pp. 1238–1257, 2006.

[18] W. Schmitt, "General approach for the calculation of tissue to plasma partition coefficients," *Toxicology in Vitro*, vol. 22, no. 2, pp. 457–467, 2008.

[19] T. Peyret, P. Poulin, and K. Krishnan, "A unified algorithm for predicting partition coefficients for PBPK modeling of drugs and environmental chemicals," *Toxicology and Applied Pharmacology*, vol. 249, no. 3, pp. 197–207, 2010.

[20] P. Rydberg, U. Ryde, and L. Olsen, "Prediction of activation energies for aromatic oxidation by cytochrome P450," *Journal of Physical Chemistry A*, vol. 112, no. 50, pp. 13058–13065, 2008.

[21] D. Zhou, L. Afzelius, S. W. Grimm, T. B. Andersson, R. J. Zauhar, and I. Zamora, "Comparison of methods for the prediction of the metabolic sites for CYP3A4-mediated metabolic reactions," *Drug Metabolism and Disposition*, vol. 34, no. 6, pp. 976–983, 2006.

[22] C. Hansch, S. B. Mekapati, A. Kurup, and R. P. Verma, "QSAR of Cytochrome P450," *Drug Metabolism Reviews*, vol. 36, no. 1, pp. 105–156, 2004.

[23] D. F. V. Lewis, C. Sams, and G. D. Loizou, "A quantitative structure-activity relationship analysis on a series of alkyl benzenes metabolized by human cytochrome P450 2E1," *Journal of Biochemical and Molecular Toxicology*, vol. 17, no. 1, pp. 47–52, 2003.

[24] M. L. Gargas, P. G. Seybold, and M. E. Andersen, "Modeling the tissue solubilities and metabolic rate constant V_{max} of halogenated methanes, ethanes, and ethylenes," *Toxicology Letters*, vol. 43, no. 1–3, pp. 235–256, 1988.

[25] K. R. Korzekwa, J. P. Jones, and J. R. Gillette, "Theoretical studies on cytochrome P-450 mediated hydroxylation: a predictive model for hydrogen atom abstractions," *Journal of the American Chemical Society*, vol. 112, no. 19, pp. 7042–7046, 1990.

[26] H. Yin, M. W. Anders, K. R. Korzekwa et al., "Designing safer chemicals: predicting the rates of metabolism of halogenated alkanes," *Proceedings of the National Academy of Sciences of the*

United States of America, vol. 92, no. 24, pp. 11076–11080, 1995.

[27] C. L. Waller, M. V. Evans, and J. D. Mckinney, "Modeling the cytochrome P450-mediated metabolism of chlorinated volatile organic compounds," *Drug Metabolism and Disposition*, vol. 24, no. 2, pp. 203–210, 1996.

[28] J. Ishizaki, K. Yokogawa, E. Nakashima, and F. Ichimura, "Relationships between the hepatic intrinsic clearance or blood cell-plasma partition coefficient in the rabbit and the lipophilicity of basic drugs," *Journal of Pharmacy and Pharmacology*, vol. 49, no. 8, pp. 768–772, 1997.

[29] D. F. V. Lewis, "Modelling human cytochromes P450 for evaluating drug metabolism: an update," *Drug Metabolism and Drug Interactions*, vol. 16, no. 4, pp. 307–324, 2000.

[30] D. F. V. Lewis, "Quantitative structure-activity relationships (QSARs) within the cytochrome P450 system: QSARs describing substrate binding, inhibition and induction of P450s," *Inflammopharmacology*, vol. 11, no. 1, pp. 43–73, 2003.

[31] J. P. Jones, M. Mysinger, and K. R. Korzekwa, "Computational models for cytochrome P450: a predictive electronic model for aromatic oxidation and hydrogen atom abstraction," *Drug Metabolism and Disposition*, vol. 30, no. 1, pp. 7–12, 2002.

[32] D. F. V. Lewis, "On the recognition of mammalian microsomal cytochrome P450 substrates and their characteristics: towards the prediction of human P450 substrate specificity and metabolism," *Biochemical Pharmacology*, vol. 60, no. 3, pp. 293–306, 2000.

[33] D. F. V. Lewis, S. Modi, and M. Dickins, "Structure-activity relationship for human cytochrome P450 substrates and inhibitors," *Drug Metabolism Reviews*, vol. 34, no. 1-2, pp. 69–82, 2002.

[34] K. V. Balakin, S. Ekins, A. Bugrim et al., "Quantitative structure-metabolism relationship modeling of metabolic N-dealkylation reaction rates," *Drug Metabolism and Disposition*, vol. 32, no. 10, pp. 1111–1120, 2004.

[35] S. Ekins, S. Andreyev, A. Ryabov et al., "Computational prediction of human drug metabolism," *Expert Opinion on Drug Metabolism and Toxicology*, vol. 1, no. 2, pp. 303–324, 2005.

[36] P. N. D'Yachkov, N. V. Kharchevnikova, A. V. Dmitriev, A. V. Kuznetsov, and V. V. Poroikov, "Quantum chemical simulation of cytochrome P450 catalyzed aromatic oxidation: metabolism, toxicity, and biodegradation of benzene derivatives," *International Journal of Quantum Chemistry*, vol. 107, no. 13, pp. 2454–2478, 2007.

[37] G. P. Miller, "Advances in the interpretation and prediction of CYP2E1 metabolism from a biochemical perspective," *Expert Opinion on Drug Metabolism and Toxicology*, vol. 4, no. 8, pp. 1053–1064, 2008.

[38] A. N. Mayeno, J. L. Robinson, R. S. H. Yang, and B. Reisfeld, "Predicting activation enthalpies of cytochrome-P450-mediated hydrogen abstractions. 2. Comparison of semiempirical PM3, SAM1, and AM1 with a density functional theory method," *Journal of Chemical Information and Modeling*, vol. 49, no. 7, pp. 1692–1703, 2009.

[39] C. Gao, R. Goind, and H. H. Tabak, "Application of the group contribution method for predicting the toxicity of organic chemicals," *Environmental Toxicology and Chemistry*, vol. 11, no. 5, pp. 631–636, 1992.

[40] M. Béliveau, J. Lipscomb, R. Tardif, and K. Krishnan, "Quantitative structure-property relationships for interspecies extrapolation of the inhalation pharmacokinetics of organic chemicals," *Chemical Research in Toxicology*, vol. 18, no. 3, pp. 475–485, 2005.

[41] M. Béliveau, R. Tardif, and K. Krishnan, "Quantitative structure-property relationships for physiologically based pharmacokinetic modeling of volatile organic chemicals in rats," *Toxicology and Applied Pharmacology*, vol. 189, no. 3, pp. 221–232, 2003.

[42] E. Kamgang, T. Peyret, and K. Krishnan, "An integrated QSPR-PBPK modelling approach for in vitro-in vivo extrapolation of pharmacokinetics in rats," *SAR and QSAR in Environmental Research*, vol. 19, no. 7-8, pp. 669–680, 2008.

[43] K. Price and K. Krishnan, "An integrated QSAR-PBPK modelling approach for predicting the inhalation toxicokinetics of mixtures of volatile organic chemicals in the rat," *SAR and QSAR in Environmental Research*, vol. 22, no. 1-2, pp. 107–128, 2011.

[44] W. M. Meylan and P. H. Howard, "Atom/fragment contribution method for estimating octanol-water partition coefficients," *Journal of Pharmaceutical Sciences*, vol. 84, no. 1, pp. 83–92, 1995.

[45] P. Poulin and K. Krishnan, "Molecular structure-based prediction of the toxicokinetics of inhaled vapors in humans," *International Journal of Toxicology*, vol. 18, no. 1, pp. 7–18, 1998.

[46] S. Haddad, G. C. Tardif, and R. Tardif, "Development of physiologically based toxicokinetic models for improving the human indoor exposure assessment to water contaminants: trichloroethylene and trihalomethanes," *Journal of Toxicology and Environmental Health A*, vol. 69, no. 23, pp. 2095–2136, 2006.

[47] N. Ali and R. Tardif, "Toxicokinetic modeling of the combined exposure to toluene and n-hexane in rats and humans," *Journal of Occupational Health*, vol. 41, no. 2, pp. 95–103, 1999.

[48] R. Tardif and G. Charest-Tardif, "The importance of measured end-points in demonstrating the occurrence of interactions: a case study with methylchloroform and m-xylene," *Toxicological Sciences*, vol. 49, no. 2, pp. 312–317, 1999.

[49] M. L. Gargas, M. E. Andersen, and H. J. Clewell III, "A physiologically based simulation approach for determining metabolic constants from gas uptake data," *Toxicology and Applied Pharmacology*, vol. 86, no. 3, pp. 341–352, 1986.

[50] J. C. Ramsey and M. E. Andersen, "A physiologically based description of the inhalation pharmacokinetics of styrene in rats and humans," *Toxicology and Applied Pharmacology*, vol. 73, no. 1, pp. 159–175, 1984.

[51] M. L. Gargas, H. J. Clewell III, and M. E. Andersen, "Metabolism of inhaled dihalomethanes in vivo: differentiation of kinetic constants for two independent pathways," *Toxicology and Applied Pharmacology*, vol. 82, no. 2, pp. 211–223, 1986.

[52] J. G. Filser, G. A. Csanády, B. Denk et al., "Toxicokinetics of isoprene in rodents and humans," *Toxicology*, vol. 113, no. 1–3, pp. 278–287, 1996.

[53] S. Haddad, R. Tardif, G. Charest-Tardif, and K. Krishnan, "Physiological modeling of the toxicokinetic interactions in a quaternary mixture of aromatic hydrocarbons," *Toxicology and Applied Pharmacology*, vol. 161, no. 3, pp. 249–257, 1999.

[54] J. G. Filser, R. Schmidbauer, F. Rampf, C. M. Baur, C. Putz, and G. A. Csanady, "Toxicokinetics of inhaled propylene in mouse, rat, and human," *Toxicology and Applied Pharmacology*, vol. 169, no. 1, pp. 40–51, 2000.

[55] M. L. Gargas, H. J. Clewell, and M. E. Andersen, "Gas uptake inhalation techniques and the rates of metabolism of chloromethanes, chloroethanes and chloroethylenes in the rat," *Inhalation Toxicology*, vol. 2, no. 3, pp. 295–319, 1990.

[56] G. L. Kedderis and S. D. Held, "Prediction of furan pharmacokinetics from hepatocyte studies: comparison of bioactivation and hepatic dosimetry in rats, mice, and humans," *Toxicology and Applied Pharmacology*, vol. 140, no. 1, pp. 124–130, 1996.

[57] R. H. Reitz, M. L. Gargas, A. L. Mendrala, and A. M. Schumann, "In vivo and in vitro studies of perchloroethylene metabolism for physiologically based pharmacokinetic modeling in rats, mice, and humans," *Toxicology and Applied Pharmacology*, vol. 136, no. 2, pp. 289–306, 1996.

[58] R. J. Williams, A. Vinegar, J. N. Mcdougal, A. M. Jarabek, and J. W. Fisher, "Rat to human extrapolation of HCFC-123 kinetics deduced from halothane kinetics: a corollary approach to physiologically based pharmacokinetic modeling," *Fundamental and Applied Toxicology*, vol. 30, no. 1, pp. 55–66, 1996.

[59] G. A. Csanády, B. Denk, C. Pütz et al., "A physiological toxicokinetic model for exogenous and endogenous ethylene and ethylene oxide in rat, mouse, and human: formation of 2-hydroxyethyl adducts with hemoglobin and DNA," *Toxicology and Applied Pharmacology*, vol. 165, no. 1, pp. 1–26, 2000.

[60] J. E. Dennison, M. E. Andersen, and R. S. H. Yang, "Characterization of the pharmacokinetics of gasoline using PBPK modeling with a complex mixtures chemical lumping approach," *Inhalation Toxicology*, vol. 15, no. 10, pp. 961–986, 2003.

[61] A. M. Hissink, J. Krüse, B. M. Kulig et al., "Model studies for evaluating the neurobehavioral effects of complex hydrocarbon solvents. III. PBPK modeling of white spirit constituents as a tool for integrating animal and human test data," *NeuroToxicology*, vol. 28, no. 4, pp. 751–760, 2007.

[62] D. F. V. Lewis, *Guide to Cytochromes P450: Structure and Function*, Taylor & Francis, London, UK, 2001.

[63] A. I. Archakov and G. I. Bachmanova, Eds., *Cytochrome P-450 and Active Oxygen*, Taylor & Francis, London, UK, 1990.

[64] Z. Fang, J. Sonner, M. J. Laster et al., "Anesthetic and convulsant properties of aromatic compounds and cycloalkanes: implications for mechanisms of narcosis," *Anesthesia and Analgesia*, vol. 83, no. 5, pp. 1097–1104, 1996.

[65] P. D. Lilly, M. E. Andersen, T. M. Ross, and R. A. Pegram, "Physiologically based estimation of in vivo rates of bromodichloromethane metabolism," *Toxicology*, vol. 124, no. 2, pp. 141–152, 1997.

[66] M. L. Gargas, R. J. Burgess, D. E. Voisard, G. H. Cason, and M. E. Andersen, "Partition coefficients of low-molecular-weight volatile chemicals in various liquids and tissues," *Toxicology and Applied Pharmacology*, vol. 98, no. 1, pp. 87–99, 1989.

[67] R. Tardif, G. Charest-Tardif, J. Brodeur, and K. Krishnan, "Physiologically based pharmacokinetic modeling of a ternary mixture of alkyl benzenes in rats and humans," *Toxicology and Applied Pharmacology*, vol. 144, no. 1, pp. 120–134, 1997.

[68] M. Béliveau and K. Krishnan, "Estimation of rat blood: air partition coefficients of volatile organic chemicals using reconstituted mixtures of blood components," *Toxicology Letters*, vol. 116, no. 3, pp. 183–188, 2000.

[69] C. Hansch and L. Zhang, "Quantitative structure-activity relationships of cytochrome P-450," *Drug Metabolism Reviews*, vol. 25, no. 1-2, pp. 1–48, 1993.

[70] D. F. V. Lewis and M. Dickins, "Baseline lipophilicity relationships in human cytochromes P450 associated with drug metabolism," *Drug Metabolism Reviews*, vol. 35, no. 1, pp. 1–18, 2003.

[71] D. F. V. Lewis and Y. Ito, "Human P450s involved in drug metabolism and the use of structural modelling for understanding substrate selectivity and binding affinity," *Xenobiotica*, vol. 39, no. 8, pp. 625–635, 2009.

[72] L. B. Kier, "A shape index from molecular graphs," *Quantitative Structure-Activity Relationships*, vol. 4, no. 3, pp. 109–116, 1985.

[73] Organisation for Economic Co-operation and Development, "Guidance document on the validation of (quantitative) structure-activity relationship [(Q)SAR] models," Tech. Rep., OECD-OCDE, Paris, France, 2007, OECD Environment Health and Safety Publications, Editor.

[74] P. Gramatica, "Principles of QSAR models validation: Internal and external," *QSAR and Combinatorial Science*, vol. 26, no. 5, pp. 694–701, 2007.

[75] S. A. Glantz and B. K. Slinker, *Primer of Applied Regression and Analysis of Variance*, McGraw-Hill, New York, NY, USA, 2nd edition, 2001.

[76] S. Wold, "Validation of QSARs," *Quantitative Structure Activity Relashionship*, vol. 10, pp. 191–193, 1991.

[77] C. J. W. Meulenberg and H. P. M. Vijverberg, "Empirical relations predicting human and rat tissue: air partition coefficients of volatile organic compounds," *Toxicology and Applied Pharmacology*, vol. 165, no. 3, pp. 206–216, 2000.

[78] S. Batterman, L. Zhang, S. Wang, and A. Franzblau, "Partition coefficients for the trihalomethanes among blood, urine, water, milk and air," *Science of the Total Environment*, vol. 284, no. 1–3, pp. 237–247, 2002.

[79] L. M. da Silva, G. Charest-Tardif, K. Krishnan, and R. Tardif, "Influence of oral administration of a quaternary mixture of trihalomethanes on their blood kinetics in the rat," *Toxicology Letters*, vol. 106, no. 1, pp. 49–57, 1999.

[80] M. E. Andersen, H. J. Clewell, M. L. Gargas, F. A. Smith, and R. H. Reitz, "Physiologically based pharmacokinetics and the risk assessment process for methylene chloride," *Toxicology and Applied Pharmacology*, vol. 87, no. 2, pp. 185–205, 1987.

[81] J. C. Ramsey, J. D. Young, R. J. Karbowski, M. B. Chenoweth, L. P. McCarty, and W. H. Braun, "Pharmacokinetics of inhaled styrene in human volunteers," *Toxicology and Applied Pharmacology*, vol. 53, no. 1, pp. 54–63, 1980.

[82] M. E. Andersen, H. J. Clewell, M. L. Gargas et al., "Physiologically based pharmacokinetic modeling with dichloromethane, its metabolite, carbon monoxide, and blood carboxyhemoglobin in rats and humans," *Toxicology and Applied Pharmacology*, vol. 108, no. 1, pp. 14–27, 1991.

[83] T. M. Cahill, I. Cousins, and D. Mackay, "Development and application of a generalized physiologically based pharmacokinetic model for multiple environmental contaminants," *Environmental Toxicology and Chemistry*, vol. 22, no. 1, pp. 26–34, 2003.

[84] International Programme on Chemical Safety, *Characterization and Application of Physiologically Based Pharmacokinetic Models in Risk Assessment*, International Programme on Chemical Safety, 2010.

[85] C. J. MacKay, L. Campbell, A. M. Samuel et al., "Behavioral changes during exposure to 1,1,1-trichloroethane: time-course and relationship to blood solvent levels," *American Journal of Industrial Medicine*, vol. 11, no. 2, pp. 223–239, 1987.

[86] M. T. D. Cronin and D. Livingstone, *Predicting Chemical Toxicity and Fate*, CRC Press, Boca Raton, Fla, USA, 2004.

[87] H. Gao and C. Hansch, "QSAR of P450 oxidation: on the value of comparing kcat and km with kcat/km," *Drug Metabolism Reviews*, vol. 28, no. 4, pp. 513–526, 1996.

[88] J. P. Jones, K. R. Korzekwa, F. J. Eric, and R. W. Michael, "Predicting the rates and regioselectivity of reactions mediated by the P450 superfamily," in *Methods in Enzymology*, pp. 326–335, Academic Press, New York, NY, USA, 1996.

[89] D. L. Harris, J.-Y. Park, L. Gruenke, and L. Waskell, "Theoretical study of the ligand-CYP2B4 complexes: effect of structure on binding free energies and heme spin state," *Proteins*, vol. 55, no. 4, pp. 895–914, 2004.

[90] L. Olsen, P. Rydberg, T. H. Rod, and U. Ryde, "Prediction of activation energies for hydrogen abstraction by cytochrome P450," *Journal of Medicinal Chemistry*, vol. 49, no. 22, pp. 6489–6499, 2006.

[91] D. N. Kim, K. H. Cho, W. S. Oh et al., "EaMEAD: activation energy prediction of cytochrome p450 mediated metabolism with effective atomic descriptors," *Journal of Chemical Information and Modeling*, vol. 49, no. 7, pp. 1643–1654, 2009.

[92] Y. Lu, S. Rieth, M. Lohitnavy et al., "Application of PBPK modeling in support of the derivation of toxicity reference values for 1-trichloroethane," *Regulatory Toxicology and Pharmacology*, vol. 50, no. 2, pp. 249–260, 2008.

[93] R. H. Reitz, J. N. McDougal, M. W. Himmelstein, R. J. Nolan, and A. M. Schumann, "Physiologically based pharmacokinetic modeling with methylchloroform: implications for interspecies, high dose/low dose, and dose route extrapolations," *Toxicology and Applied Pharmacology*, vol. 95, no. 2, pp. 185–199, 1988.

[94] M. H. Wang, D. Wade, L. Chen, S. White, and C. S. Yang, "Probing the active sites of rat and human cytochrome P450 2E1 with alcohols and carboxylic acids," *Archives of Biochemistry and Biophysics*, vol. 317, no. 1, pp. 299–304, 1995.

Hindawi Publishing Corporation
Journal of Toxicology
Volume 2012, Article ID 359471, 11 pages
doi:10.1155/2012/359471

Review Article

Physiologically Based Toxicokinetic Modelling as a Tool to Support Risk Assessment: Three Case Studies

Hans Mielke[1] and Ursula Gundert-Remy[1,2]

[1] *Federal Institute for Risk Assessment, Max Dohrn Strasse 8-10, 10589 Berlin, Germany*
[2] *Institute for Clinical Pharmacology and Toxicology, Charité-Universitätsmedizin Berlin, Charitéplatz 1, 10117 Berlin, Germany*

Correspondence should be addressed to Hans Mielke, hans.mielke@bfr.bund.de

Received 10 October 2011; Revised 28 January 2012; Accepted 16 February 2012

Academic Editor: Jane C. Caldwell

In this contribution we present three case studies of physiologically based toxicokinetic (PBTK) modelling in regulatory risk assessment. (1) Age-dependent lower enzyme expression in the newborn leads to bisphenol A (BPA) blood levels which are near the levels of the tolerated daily intake (TDI) at the oral exposure as calculated by EFSA. (2) Dermal exposure of BPA by receipts, car park tickets, and so forth, contribute to the exposure towards BPA. However, at the present levels of dermal exposure there is no risk for the adult. (3) Dermal exposure towards coumarin via cosmetic products leads to external exposures of two-fold the TDI. PBTK modeling helped to identify liver peak concentration as the metric for liver toxicity. After dermal exposure of twice the TDI, the liver peak concentration was lower than that present after oral exposure with the TDI dose. In the presented cases, PBTK modeling was useful to reach scientifically sound regulatory decisions.

1. Introduction

Physiologically based pharmaco-/toxico-kinetic (PBPK/PBTK) modelling has a long history. The principle has been introduced by Teorell as early as 1937 [1], but uptake and further development has been slow. Beginning in the 60s, pharmacokinetics became a constituent part in drug development. In drug development a data-rich situation is given, and studies in human beings can be performed without ethical constraints. Hence, the kinetic paradigm developed under those conditions was a top down approach, where the structure of the kinetic model using compartmen-tal models was determined by the statistically best fit to the data [2]. The kinetic parameters were estimated out of the data. Without further information the parameters are hard to interpret in a physiological context. Physiologically based pharmacokinetic models have not been used in drug kinetics to a great extent with the exception of modelling the fate of anaesthetic drugs, where it has always been an interesting approach [3, 4]. However, in the past twenty years there is growing interest in this approach as a technique to support defining the dose which is intended to be given in the first studies in humans based on preclinical in vitro and in vivo animal study results, the so-called first dose in man [5]. Similarly in toxicology, interest is growing to apply this approach to be used in risk assessment and recently an internationally agreed document has been published on the topic [6]. Here, the typical situation for a chemical is characterized by existence of data in animal species but only few, if any experimental data in humans. For risk assessment or setting limit values (e.g., tolerated daily intake (TDI), accepted daily intake (ADI), occupational exposure limit (OEL)) the animal data have to be extrapolated to the human physiology and in addition, also to the physiology of the whole population including special subgroups. Typically, default factors have been used. A factor of ten is seen to be appropriate for the species difference between animal and man (4 for toxicokinetic differences, 2.5 for toxicodynamic differences) and a second factor of ten is applied for the interspecies differences in the human population (3.2 for toxicokinetic differences; 3.2 for toxicodynamic differences). PBTK modelling may help to derive chemical-specific assessment factors at least for the kinetic portion of the chemical-specific assessment factors [7]. On the other hand,

PBTK modelling may also help to better understand the mode of action by identifying which kinetic metric is really related to the toxic effect, which is to be assessed [6].

In this contribution we present three case studies, where we used PBTK modelling in order to perform a targeted risk assessment. In two cases the uncertainty surrounding the use of default values has been reduced. In one other case, the PBTK modelling supported an outcome of the assessment which is different from the default approach and also helped to identify the relevant toxicokinetic metric, thus offering some insight into the mode of action.

The modelling procedures of the examples have already been published in detail. The aim of this paper is to show how to embed PBTK modelling into a regulatory decision making process.

2. Regulatory Problem, Methods, and Results: Case Studies

2.1. Case Study. Bisphenol A: Exposure in Newborns [8]

2.1.1. Regulatory Context. Bisphenol A (BPA) is a chemical used for the production of epoxy resins and polycarbonate plastics [9, 10]. Food in contact with plastic materials is one source of human exposure. Feeding bottles from plastic materials containing BPA have been identified to be a major source for exposure to infants, including neonates, whereby the oral intake by bottle fed infants was estimated to be 11 μg/kg/day (worst-case estimate), several fold higher than the oral exposure of adults by the European Food Safety Agency (EFSA) [10]. The TDI (tolerated daily intake) is 50 μg/kg/day derived from animal data [10]. It should be mentioned that there is ongoing controversy about the TDI being 50 μg/kg/d as derived by EFSA and other regulatory agencies. There are studies showing effects of BPA below 50 μg/kg/d, and some scientists are with the opinion that these studies should be used as the basis to derive the TDI [11]. We nevertheless used the regulatory TDI of 50 μg/kg/d for our modelling purposes. By definition the TDI is not thought to be relevant for children below the age of 3 months. There is, however, no health-based limit value for infants of this age available. Therefore, we used this value for risk assessment. Although EFSA raised no concern for newborns it remained open whether the impairment of glucuronidation in the newborn with a capacity of less than 10% of the adult [12] may result in increased internal exposure. It should be noted that glucuronidation accounts to 85–95.5% of the metabolic clearance in adults [13, 14].

2.1.2. Why PBTK Modelling? The exposure for the bottle-fed neonate is at 1/5 of the TDI which has to be considered in conjunction with the glucuronidation capacity of less that 10% of the normal value [12]. It is highly uncertain to which extent a minor pathway (sulfation) contributing 15–7.5% to the metabolic elimination in the adult [13, 14] may compensate for the impaired metabolic capacity of the predominant pathway (glucuronidation). In order to reduce the uncertainty, we modelled the internal exposure by a human model for children of different ages including newborns and for adults in which we implemented both metabolic pathways, and we compared the internal concentrations of children at different ages and the adult with the exposure by a dose at the TDI.

2.1.3. What Has Been Done? Starting from a PBTK model containing physiological data at different ages [15], we modified the input into the model from inhalation exposure to oral exposure. The only elimination was by metabolism. Glucuronidation was parametrized using published in vitro data on V_{max} and K_m in hepatocytes of adult humans [16] according to the formula given in [17]. Sulfation was modelled according to the relative contribution to the metabolic clearance [13]. For the newborns and infants, we searched after information on the expression of the respective enzymes in different ages and used this information to adjust the metabolic parameters. BPA undergoes glucuronidation by the UDP-glucuronyltransferase UTG2B15 in man [18]. As age-dependent expression of this enzyme is not available we used data on UTG2B7 which is from the same UTG family and has a high degree of homology with UTG2B15 [12]. The sulfation of BPA is mediated by SULT 1A1 which is expressed already in utero at high levels similar to the adult levels [19]. Ginsberg and Rice [20] claimed that tissue BPA concentrations may be higher due to deconjugation of the metabolites in tissues. We calculated that given the low partition coefficient of the polar conjugated metabolites, less than 10% of the concentration of the conjugated metabolites will enter the tissues. Nishikawa et al. [21] demonstrated that deglucuronidation is taking place, however, only to the small extent of 4.4% in the fetus as calculated by Hengstler et al. [22]. Thus, we are with the opinion that even if assuming deconjugation of metabolites in tissues, this process can be omitted from the model because it does not increase the concentration by more than about 5%.

We modelled the concentration of the parent chemical BPA in blood at a dose of 11 μg/kg/day for newborn (exposure assessment by [10]) and compared the steady state concentration in blood of this dose with the steady state concentration in blood in an adult, given the identical dose of 11 μg/kg/day. In the newborn, the concentration in blood was 3.3 fold higher as compared to the adult (Table 1). The steady state concentration in blood in the newborn of the realistic worst case exposure scenario did not exceed the adult steady state concentration in blood at a dose of 50 μg/kg/day which is the tolerated daily intake (TDI). However, it was only 26.2% below this value (Table 1(a)). We also modelled urinary excretion of the metabolites and determined the relative contribution of the glucuronidation versus the sulfation pathway. Table 1(b) shows that in the newborn the sulfation pathway is predominant and that with increasing age (and maturation of the glucuronide pathway [12]) excretion by sulfation pathway decreases and glucuronidation becomes the predominant pathway.

2.1.4. Sources of Uncertainty. Our model has several limitations. We scaled V_{max} from in vitro the in vivo situation using a published formula which is the result of a consensus [17]. Partition coefficients were taken from experimental

Table 1: BPA steady state concentration in blood after oral exposure by 11 μg/kg/day in bottle fed newborns. The steady state concentration (SSC) is compared to a steady state concentration in an adult exposed to 11 μg/kg/day and to the 50 μg/kg/day on the oral route. It can be seen that the steady state concentration in the newborn is three-fold higher than in the adult due to the fact that the metabolism of BPA by glucuronidation is impaired in the newborn. However, the SSC in the newborn does not exceed the SSC of an oral dose of 50 μg/kg/d. The oral dose of 50 μg/kg/d equals the tolerated daily intake derived from animal studies. It is thought to be a level without adversely influencing the health calculated for the population older than 3 months. The SSC of 50 μg/kg/d has been simulated with the model parameters of an adult. Relative contribution of the two pathways in the metabolism of BPA in relation to age (and related to age extent of impaired glucuronide conjugation). 85% of a dose of BPA is metabolized to the glucuronide conjugate to and the remaining 15% to the sulfate conjugate in the adult. The enzyme which mediates the conjugation to BPA-glucuronide (uridine diphosphate-glucuronosyltransferase 2B15, UTG 2B15) is expressed at birth to only 10% of the adult level. The expression levels reach adult levels by the age of 1.5 years. The relative percentage of the glucuronidation pathway depends on the expression level of UTG 2B15. In the newborn only 36% of the absorbed dose is metabolized via glucuronidation, whereas 64% of the absorbed dose is sulfated.

(a)

	Oral exposure (μg/kg/day)	Steady state concentration (SSC) (ng/mL)	Percentage of TDI SSC	SSC newborn/SSC adult at 11 μg/kg/day
Newborn (bottle-fed)	11 (EFSA, 2006)	0.096	73.8	3.3
Adult	11 (hypothetical)	0.029	22.3	—
Adult	50 (TDI)	0.13	100	—

(b)

	Sulfate conjugate (percentage of the absorbed dose)	Glucuronide conjugate (percentage of the absorbed dose)
Newborn	64%	36%
3 months	31%	69%
6 months	18%	82%
1.5 year	15%	85%
Adult	15%	85%

data in rats because data in humans were not available. The rate of absorption was estimated using the time course of urinary excretion of the conjugated metabolite which is an imprecise estimate. Finally, we assumed perfusion-limited distribution into the tissues. Concerning the age-dependent expression of UTG 2B15, we assumed that the expression pattern is the same as UTG 2B7. The data needed for validation of the model are not at hand as in experimental studies with known exposure the parent compound BPA was below the level of detection (overview in [22]). The remaining uncertainty is given by the unknown ontogeny of UTG2B15 and by the imprecise estimate of the rate of absorption. However, the simulation results were not contradictory to published simulation results, where parameter estimation has been performed differently [22]. Therefore, we do have some confidence in the results (Figure 1).

2.1.5. Conclusion. The PBTK modelling results confirmed the risk assessment which has been performed on rather qualitative estimates than on quantification. However, because internal exposure expressed as the concentration in blood has been simulated for the external exposure at 11 μg/kg/d in the newborn and for the exposure at the TDI for an adult, it can be seen that the oral exposure with 11 μg/kg/day exhausted the TDI to 74%. Hence, it can be stated that, at oral exposure as calculated by EFSA [10], no risk is present unless exposures not accounted for so far, for example, by dermal route at high doses, would become known. As far as it is known today, there is no dermal exposure in the newborn and infant whereas dermal exposure in the adult has been found (see case study no. 2).

It is a belief that one pathway of elimination can "compensate" for a second pathway when impaired [23]. However, as shown here, although in the newborn the sulfation exceeds glucuronidation, the increased percentage eliminated via the sulfate pathway does not fully "compensate" for the impaired glucuronidation pathway which is indicated by the difference in blood levels between newborns and adults (Table 1(a)). This finding is of general importance for risk assessment in newborns and other populations at risk with impaired metabolic and renal elimination function.

2.2. Case Study. Bisphenol A: Dermal Exposure [24]

2.2.1. Regulatory Context. The oral route of exposure has been assumed to be the main source of exposure in consumer risk assessment of BPA [22, 24]. However, in the past several authors reported blood concentrations of BPA which were far higher than could be explained by the estimated exposure on the oral route up to now [25, 26] (citing the authors with the lowest and the highest concentrations in blood). Concerns have always been raised that the present risk assessment considering only the oral route of exposure is overlooking exposures by other routes which have to be considered to assess the true risk from BPA exposures. In 2010, several reports have been published reporting that BPA

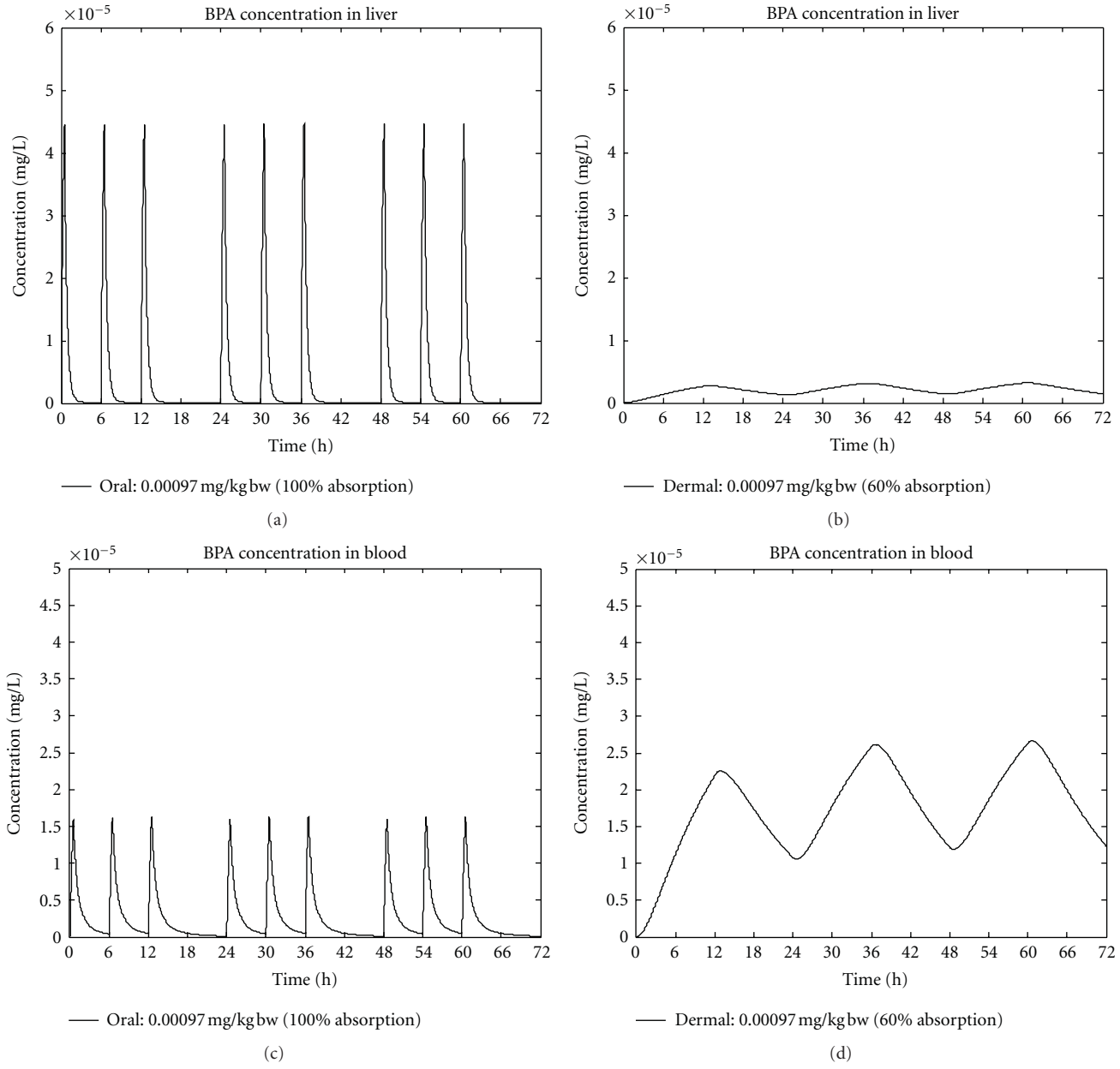

Figure 1: BPA: simulation results oral versus dermal route. Humans are exposed towards BPA on the oral and on the dermal routes.

is present in thermal printing papers and products made from thermal printing paper such as receipts, car park tickets, queue tickets, ATM receipts, lottery slips, and plane, train, and bus tickets in the percentage range (0.8–3.2%) [27–29]. Furthermore, BPA is taken up on the surface of the fingers when BPA-containing paper is touched, and it is getting into the skin [27]. In [27], a daily dermal exposure of 71 μg/day is estimated for the consumer, corresponding to roughly 1 μg BPA/kg/day on this route.

The question is whether the additional external dermal exposure which is in the range of the external oral exposure would explain the high blood concentrations which in turn would raise concern. The TDI of 50 μg/kg/day for BPA is derived from an oral study, the target organ being the liver. In the standard risk assessment the procedure is to correct the external dermal dose for the percentage of dermal absorption relative to the oral absorption. This corrected dose is then added to the oral dose. If the sum is below the TDI, no concern will be raised. As dermal exposure is a newly detected route of exposure, we applied a reverse reference scenario and estimated the dermal exposure doses necessary to yield the reported blood concentrations adding to the maximum external oral exposure estimated by FAO/WHO [30]. We did this in order to clarify whether the exposure

by the dermal route can explain the high concentrations measured by some authors in blood, and whether this constitutes a concern (Table 2(b)).

2.2.2. Why PBTK Modelling? The described approach for route-to-route extrapolation is in line with the standard procedure for risk assessment. However, there are two questions. First, as the liver is the target tissue, to what extent is the liver exposed by the dermal route. Second question was to which extent is the exposure of organs other than the liver increased by dermal exposure. Given the fact that BPA has a high first pass in the liver, it is anticipated that the route of exposure is an important determinant for the concentration in organs other than the liver. A PBTK analysis was the way to tackle the problem.

2.2.3. What Has Been Done?

(1) *Dermal Modelling: Risk Assessment.* We simulated the BPA concentration time profile in blood, liver, and kidney using a PBTK human model with oral route of exposure already published [8] (see above) and added a dermal pathway of exposure. The concentration time profile in kidney was simulated because minimal-to-mild nephropathy was related to doses above 50 mg/kg/day given orally in a study [31]. The extent of dermal absorption of BPA has been reported by several authors with varying values, that is, 10% [9], 13% [32], 46% [33], and 60% [27]. Based on the data of [27], we assumed that dermal absorption could be described by a diffusion process of first order and estimated a half-life of 8 hours, whereas oral absorption half-life was assumed to be 15 min as in the study of [34] the maximum concentration in the urine occurred at roughly 1 h. We performed the simulations assuming that the extent of absorption is 10%, 13%, 46%, or 60%. Here, we report only the results obtained with 60% dermal absorption. We compared the output of simulations of a dermal dose of 71 μg (0.97 μg/kg/day), given as a single dose, of an identical oral dose of 0.97 μg/kg/day, given in three equal portions, an oral dose of 4.2 μg/kg/d (FAO/WHO estimate [30]), given in three equal portions, and of 50 μg/kg/day (the TDI), given in three equal portions. The results showed that dermal exposure leads to lower peak concentration in the target organ liver and to higher peak concentrations in blood and kidney as compared to the oral exposure. The AUC in blood and kidney is higher after dermal exposure as compared to dosing on the oral route. AUC in the liver is determined by the extent of absorption (Table 2(a)). With the dose of 50 μg/kg/day (TDI level) by the oral route AUC in the liver is 96 fold higher. C_{max} in the liver depends on the extent of absorption, the proportion of cardiac output which is going through the liver (22.5%) and also from the absorption half-life with slow absorption leading to low peak concentrations in the liver and fast absorption leading to high peak concentrations in the liver. C_{max} in the liver was 700 fold higher after 50 μg/kg/day (TDI level) on the oral route than after 0.97 μg/kg/day by the dermal route.

(2) *Assessment of Dermal Exposure Necessary to Yield Reported Concentrations in Blood.* In addition, in order to clarify whether blood concentrations as measured by several authors were in the range of exposures measured so far we finally calculated the dermal dose, which its intake would be necessary to reach the reported concentrations of 0.33 ng/mL [25] and 5.9 ng/mL [26] when combined with the maximum oral intake of 4.2 μg/kg/day as estimated by [30]. As can be seen in Table 1(b), the dermal doses of 9.4 μg/kg/day and of 211.8 μg/kg/day are necessary to yield concentration of 0.33 ng/mL and of 5.9 ng/mL from combined oral (as estimated by [18]) and dermal exposure, respectively.

The modeling results are in line with the physiology of dermal versus oral absorption. When absorbed through the skin, BPA first enters the venous blood. The venous blood is drained into the upper main vein, passing the right ventricle and the lungs and entering the left atrium and left ventricle. By this process the amount absorbed is mixed in the bloodstream coming from other organs. From the left ventricle, BPA is distributed via arterial blood throughout the body. In contrast, after oral administration BPA is directly delivered to the liver via the portal vein after passing through the intestinal wall. Taking all aspects together, after absorption through the skin the blood in the portal vein has a lower concentration as compared to the oral route because of the physiology. Furthermore, dermal absorption of BPA is much slower than the oral absorption which is the general rule. Thus, C_{max} in the liver is several fold lower after dermal as compared to the oral administration.

2.2.4. Source of Uncertainty. Our model has the limitations as mentioned for the BPA model above. In addition, the parameter for the rate and extent of dermal absorption as taken from the publication of Biedermann et al. [27] are approximations. The data needed to resolve this uncertainty are not easily obtained as an experimental in vivo study in humans would be necessary to be performed. Given the level of detection, we do not expect that this data need will be solved in the near future. Even in the most recent study [35] BPA concentrations were below the detection limit of 1.3 nM as analysed by CDC. Therefore, this very important point is a remaining source of uncertainty. Nevertheless, as we made worst-case assumptions the simulation results are of value to inform risk assessment.

2.2.5. Conclusion. For the risk assessment, concerning liver toxicity we cannot determine what the relevant metric is. There are no data which would allow deciding whether toxicity is related to AUC or to C_{max}.

For regulatory decision making, the PBTK modelling and simulation results were helpful to identify a relevant route of exposure for the consumer which results in higher blood concentration than after the identical dose on the oral route. From the modeling results we can decide that the worst-case exposure estimate for consumers on the dermal route is safe.

Even if higher blood concentration of a dose given by the dermal route is taken into consideration, the doses to reach the concentrations reported by most of the authors in

Table 2: BPA: Simulation results comparing of oral and dermal exposure. Results are given as C_{max} (pg/g) and AUC (pg/g × h) in blood, liver, and kidney after dermal (extent of absorption 60% of the dose), and oral (extent of absorption 90% of the dose) administration. The external oral doses are identical with the external dermal dose (0.97 μg/kg/d), a dose estimated by FAO/WHO (4.2 μg/kg/d) as the upper level estimate and a dose at the tolerated daily intake (TDI) (50 μg/kg/d). BPA undergoes first pass in the liver. The first pass in the liver produces a lower concentration in the systemic circulation (C_{max} and AUC in blood) compared to values after the dermal administration despite identical doses and a lower extent of absorption through skin as compared to the oral absorption. In contrast, C_{max} and AUC in the liver are higher after oral as compared to the dermal exposure. Dermal dose (μg/kg/d) of BPA which corresponds to the concentration difference between blood concentrations published by Sajiki et al., 1999 [25] and by Padmanabhan et al., 2008 [26] and the estimated oral dose by FAO/WHO, 2010. The blood concentration of BPA in a person who has ingested BPA at the upper level of oral exposure (4.2 μg/kg/d) as calculated by FAO/WHO is 70.6 pg/mL. Sajiki et al., 1999 [25] has measured a mean blood concentration of 330 pg/mL and Padmanabhan et al., 2008 [26], a mean blood concentration of 5900 pg/mL. We calculated the difference of the blood concentrations measured by Sajiki et al. and by Padmanabhan et al. [25, 26] and the modelled blood concentration caused by an oral dose of 4.2 μg/kg/d. We then modelled the dermal dose which would be necessary to produce the concentration corresponding to the difference between measured and modelled concentration. It can be seen that this dose (9.4 and 211.8 μg/kg/d, resp.) is 10 to 200 fold higher than the experimentally measured dose of 0.97 μg/kg/d [27].

(a)

Route of administration	Dose (μg/kg/d)	Extent of absorption (percentage of dose)	Absorption half-life (hrs)	Blood*		Liver		Kidney	
				C_{max} (pg/g)	AUC (pg/g × h)	C_{max} (pg/g)	AUC (pg/g × h)	C_{max} (pg/g)	AUC (pg/g × h)
Dermal	0.97**	60	8	26.7	416.7	3.2	50.3	36.1	563.3
oral	0.97**	90	0.25	16.3	64.0	44.7	93.3	22.0	86.3
	4.2**	90	0.25	70.6	277.1	193.5	403.9	95.3	373.7
	50 (TDI)**	90	0.25	841.0	3293.3	2300	4800	1140	4433

* Blood concentration in the systemic circulation, not in the portal vein. In case of the oral route of administration, concentration in the portal vein is higher than concentration in the systemic circulation.
** Dermal dose given at once, whereas the oral doses are given in three divided portions.

(b)

Blood concentration (mean; pg/mL)	Blood concentration of the oral dose of 4.2 μg/kg/d (pg/mL)	Difference of the concentrations (pg/mL)	Dermal dose corresponding to the concentration difference (μg/kg/d)
330 [25]	70.6	259.4	9.4
5900 [26]	70.6	5,829.4	211.8

the literature are orders of magnitude higher than estimated, based on measurements. In this respect it should be noted that all studies in which high blood concentrations measured were uncontrolled, in particular uncontrolled in terms of the material of collecting blood, previous treatment of patients (e.g., intensive care or Cesarean section). It has been demonstrated that in intensive care the exposure towards BPA can be extremely high [36]. Hence, the high BPA concentrations measured by some authors might be explained by exposure via the intravenous route (medical devices) or by contamination when taking blood. Hence, we are with the opinion that the credibility of measured concentrations by [25, 26] is highly uncertain.

2.3. Case Study. Coumarin: Dermal Exposure [37]

2.3.1. Regulatory Context. Coumarin risk assessment has been performed because coumarin exposure by the oral route became a matter of concern. In addition to the oral route, humans may be exposed to coumarin by the dermal route because coumarin is used in several cosmetic products. In 2004 in an EFSA report, the risk from oral exposure by coumarin has been assessed. In this report, exposure to coumarin from cosmetic products has been mentioned being twice as high as the exposure via food [38]. Two German surveys provided detailed information on the contents of coumarin in cosmetic products [39, 40]. In the EU, there are generally agreed procedures [41–45] on how to calculate external exposure via cosmetic products based on the contents of cosmetics using default assumption on the use pattern and use frequency. Using the German data and the EU-procedures, the German Federal Institute for Risk Assessment (BfR) calculated the external coumarin exposure for a consumer by the dermal route by cosmetic products. A correction factor for skin absorption was introduced based on experimental data for route-to-route extrapolation [46, 47]. Under the assumption of a worst-case scenario the exposure level was 0.14 mg/kg bw/day which exceeds the TDI of coumarin at the level of 0.1 mg/kg bw/day and raised concern [48]. It has to be mentioned that the TDI was derived from oral studies, and that the target organ was the liver showing dose-dependent signs of toxicity.

2.3.2. Why PBTK Modelling? The risk assessment procedure is in line with the standard approach for route-to-route extrapolation. In the case of coumarin, however, the question was whether it is appropriate to use an oral TDI as a limit

value to assess the risk resulting from dermal exposure or whether specific considerations apply for a substance with high first-pass elimination via hepatic metabolism such as coumarin. As there was some uncertainty concerning this question the risk assessment required further verification and substantiation. The way to solve the problem has been to perform a PBTK analysis in which it turned out that the crucial point was to identify the relevant dose metric for the toxicological endpoint which is liver toxicity.

2.3.3. What Has Been Done?

(1) *PBTK Modelling of the Target Concentrations in Humans.* In humans, the kinetics of the parent compound coumarin has been studied following oral or intravenous administration of the compound [49–52]. Furthermore, in vivo and in vitro results on dermal absorption were available [44, 45]. Metabolism of coumarin was studied in in vitro experiments, and human K_m and V_{max} values have been published [53]. The available data did allow us to use them for a human PBTK model with oral and dermal route of exposure.In the human model, we modelled absorption of 100% [50] and similar absorption half-lives (20 min for the oral and 30 min for the dermal absorption) in accordance with experimental results [46, 47, 50]. The dermal exposure to coumarin at a level of 0.1 mg/kg bw (i.e., oral TDI) resulted in a lower simulated peak concentration in the liver ($C_{max\text{-}hep}$ = 1.2 μg/kg liver) compared to the situation when the identical dose was given by the oral route ($C_{max\text{-}hep}$ = 3.6 μg/kg liver). The difference between oral $C_{max\text{-}hep}$ and dermal $C_{max\text{-}hep}$ increases when the rate of dermal absorption decreases. For example, in particular circumstances depending on the cosmetic preparation, as has experimentally been shown, the dermal absorption half-life is 960 min. With an extent of absorption of 100% through the skin, and this absorption half-life the peak concentration in the liver is 0.06 μg/kg liver. The AUC in the liver in all cases (oral and dermal) is the same (see Table 3).

The route-dependent difference of AUC in blood is explained by the fact that after oral administration the absorbed dose is undergoing first pass in the liver before entering the systemic circulation, whereas after dermal exposure the absorbed dose is undergoing first pass in the skin to a negligible extent (which we did not include into our model) before entering the systemic circulation. Hence, in this case, the systemic availability, also called bioavailability, is different from the extent of absorption. The same explanation holds true for the difference in C_{max} in blood.The question was whether differing C_{max} values in the liver depending on the route of administration are relevant for the risk assessment.

(2) *PBTK Modelling of Rat Data.* We identified 11 oral rat studies in the literature with information on doses and duration of the study and also information on feeding the doses (dietary or gavage). The information on dose (between 2.3 mg/kg/day and 535 mg/kg/day) and duration of exposure (between 4 weeks and 104 weeks) was used in a rat PBTK model to simulate concentration-time profiles in blood and in the liver. Rat metabolism data (K_m and V_{max}) were available from published source [53]. The resulting 31 values for the C_{max} in the liver and AUC in the liver ranged from 0.6 to 197.1 μg/g and from 529 to 590 227 μg/g $\times$ h.

(3) *Assessing the Relationship between Liver Toxicity and C_{max} Versus AUC in the Liver.* In the 11 studies we identified 31 hepatotoxic responses described as the main toxicological endpoint. In each study the severity of the hepatotoxicity increased with increasing dose. We used the description of the hepatotoxic effect to grade the response into a five-point grading scale in which zero is no effect, and four is massive liver toxicity.

In order to solve the question whether the relevant toxicokinetic metric is C_{max} or AUC in the target organ liver, we combined graded hepatic toxicity responses with C_{max}- and AUC-values in the liver as resulting from PBTK simulations in a rat model.

We performed a graphical analysis to identify whether liver toxicity was related to AUC_{hep} or to $C_{max\text{-}hep}$. The analysis revealed that the severity grade of hepatotoxicity increases systematically with increasing $C_{max\text{-}hep}$, whereas for AUC_{hep} no systematic increase of the severity grade with increasing AUC_{hep} could be seen (Figures 2(a) and 2(b)).

2.3.4. Source of Uncertainty. Our model has the following limitations. We scaled V_{max} from in vitro to in vivo situation using a published formula which is the result of a consensus [17]. Partition coefficients were calculated values and not experimentally obtained [5]. Although the rate and extent of absorption by the oral route and by the dermal route were taken from experimental data in humans, the data on the dermal route was estimated using the time course of urinary excretion of the conjugated metabolite which is an imprecise estimate. Finally, we assumed, perfusion limited distribution into the tissues which determines the time course in the tissue of interest, that is, the liver. The data needed to resolve this uncertainty are not easily obtained as an experimental in vivo study in humans would be necessary to be performed, in which the parent compound has to be measured. Therefore, there is remaining uncertainty. Nevertheless, when we compared the simulated oral data with the published experimental data in humans the simulation predicted the time course fairly well [37].

2.3.5. Conclusion. The findings indicate that in rats coumarin-mediated liver toxicity is related to the peak liver concentration rather than to AUC in the liver. Hence, standard procedures for route-to-route extrapolation are not appropriate as they can only adjust for the amount entering the body and not for the peak concentration in the relevant organ. In conclusion, the PBTK modelling resulted in a different outcome of the risk assessment compared to the conventional approach based on external exposure or dose. As the peak concentration in the liver after dermal exposure is below the peak liver concentration resulting from oral exposure with a dose corresponding to the TDI, and

Table 3: Comparison of the peak concentrations and AUC in blood and liver after oral and dermal exposure towards coumarin. C_{max} and AUC of coumarin were modelled in liver and in blood after 0.1 mg/kg by the oral route (extent of absorption 100%; half-life of absorption 20 min) and dermal route (extent of absorption 100%; half-life of absorption 30 min and 960 min dependent on the cosmetic preparation). It can be seen that the AUC in the liver is identical because the amount absorbed and reaching the liver is the same. However, because of differences in the absorption half-life C_{max} in the liver differs. In blood, AUC is different due to first pass in the liver. Even if the extent of absorption is identical the amount of coumarin reaching the systemic circulation after oral exposure is lower than after dermal exposure. C_{max} in blood depends on the rate of absorption, expressed as half-life. If half-life of dermal absorption is similar to the oral absorption (30 min versus 20 min), C_{max} is higher after dermal exposure (due to first pass in the liver after oral exposure and no first pass in the skin). If half-life of dermal absorption is prolonged as compared to the oral half-life of absorption (960 min versus 20 min). C_{max} is lower. Thus, it is not only the extent but also the rate of absorption, which matters in comparing oral and dermal exposure.

Dose (mg/kg)	Route of administration	Dose fraction which is absorbed	Absorption half-life (min)	C_{max} liver (μg/kg)	AUC liver (μg/kg × h)	C_{max} blood (μg/kg)	AUC blood (μg/kg × h)
0.1	Oral	1.0	20	3.6	1.8	3.1	32
0.1	Dermal	1.0	30	1.2	1.8	51	77
0.1	Dermal	1.0	960	0.06	1.8	2.7	77

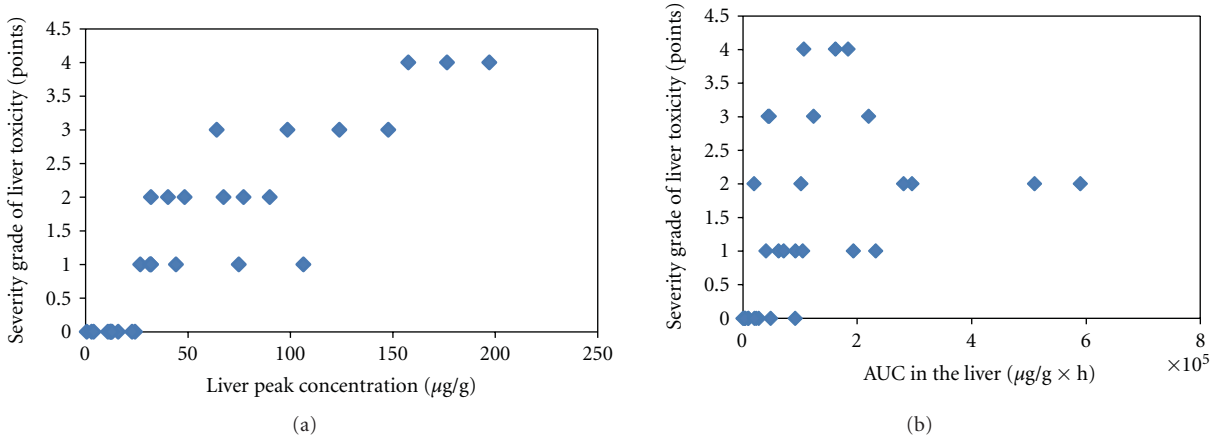

Figure 2: Exploration of which toxicokinetic metric is toxicodynamically relevant. Severity grade of liver toxicity (points) in relation to (a) the peak concentration in the liver (μg/g liver tissue) for coumarin in rat. (b) AUC in the liver (μg/g × h) for coumarin in rat. A toxicokinetic model has been constructed for the rat, and C_{max} and AUC were simulated with doses and duration of exposure taken from published studies ($n = 11$). The toxicological endpoint in the studies was liver toxicity the degree of which differed, and we graded the toxicity in a scale from 0 to 4. C_{max} in the liver (liver peak concentration) was better correlated to liver toxicity than AUC in the liver indicating that it C_{max} in the liver is the toxicologically relevant toxicokinetic metric.

peak concentration is the relevant metric, it can be stated that there is no health concern by the current exposure by cosmetic products.

As a general comment, it can be concluded that in route-to-route extrapolation for chemicals with high first-pass elimination via hepatic metabolism special attention has to be given not to underestimate the possible risk in organs other than the liver as tissue exposure (AUC) can be higher. PBTK Can help to estimate critical dose metrics (e.g., AUC and C_{max}) for various tissues within the body as a function of exposure route and intensity. While the example for coumarin shows that dermal exposures lead to lower C_{max} of parent compound in liver as compared to an oral exposure, for compounds that have toxicities related to AUC in the liver or other target organs, dermal may lead to higher critical dose metrics. PBPK modelling helps risk assessors address these important toxicology and risk assessment issues.

3. General Conclusion

Risk assessment of chemicals in general and also targeted risk assessments are demanding processes. In particular, for targeted risk assessment in a regulatory environment questions have to be definitively answered. Risk assessment needs several extrapolation steps which are based on assumptions which are inherently surrounded with uncertainty. Often default assumptions have to be applied because of lack of data. However, even in cases where more data is available the preferred regulatory procedure is to apply default assumptions. In the last decade, PBTK modelling has been advocated as a means to support risk assessment and to reduce the uncertainty [6]. There is increasing awareness in regulatory decision making on the usefulness of this approach. The following examples show that BPPK modelling has found regulatory acceptance in the interspecies

extrapolation from animal to man, namely, vinyl acetate, 2-butoxyethanol, propylene methyl glycol (EU Existing Chemicals Program), formaldehyde, 2-butoxyethanol (UK Health and Safety Executive), tetrachloroethylene, styrene, diethylhexlyphthalate (Health Canada), dichloromethane, ethylene glycol monobutyl ether, and vinyl chloride (US EPA (IRIS)) [54]. Cadmium is one example where human variability has been quantified, and a chemical specific factor was used instead of the default factor [54]. The cases we present in this contribution deal with scenarios, where modelling was done in human models. In the first case, the purpose was to quantify intraspecies variability for a substance, where two metabolic pathways with different maturation states in the newborn are present. In cases two and three, we elucidated the pitfalls of the conventional approach for oral to dermal extrapolation for substances with high first-pass elimination via hepatic metabolism. The three case studies demonstrate that the extrapolation using conventional approaches may lead to regulatory decisions which bear the possibility to overlook problems or to overstate the risk. In the three cases, PBTK modelling helped inform risk assessment. The answers to the questions require a physiologically appropriate structural model, knowledge on the physiological changes by life stages, and kinetics of absorption by various routes of exposure. By using modelling approaches the uncertainty is reduced. In this contribution we do not deal with uncertainty and variability in PBTK models as addressed by others for example, [55, 56]. However, we applied the lessons learned [54], and we hope that the case studies are convincing for regulators, the public, and also for scientists.

References

[1] T. Teorell, "Kinetics of distribution of substances administered to body," *Archives Internationales de Pharmacodynamie et de Therapie*, vol. 57, pp. 205–240, 1937.

[2] S. G. Dahl, L. Aarons, U. Gundert-Remy et al., "Incorporating physiological and biochemical mechanisms into pharmacokinetic-pharmacodynamic models: a conceptual framework," *Basic and Clinical Pharmacology and Toxicology*, vol. 106, no. 1, pp. 2–12, 2010.

[3] W. W. Mapleton, "Chest gas-exchange theory using an electrical analogue," *Journal of Applied Physiology*, vol. 19, pp. 1193–1199, 1964.

[4] M. N. Ashman, W. B. Blesser, and R. M. Epstein, "A nonlinear model for the uptake and distribution of halothane in man," *Anesthesiology*, vol. 33, no. 4, pp. 419–429, 1970.

[5] P. Poulin and F. P. Theil, "Prediction of pharmacokinetics prior to in vivo studies—II. Generic physiologically based pharmacokinetic models of drug disposition," *Journal of Pharmaceutical Sciences*, vol. 91, no. 5, pp. 1358–1370, 2002.

[6] IPCS/WHO, "Characterization and Application of Physiologically Based Pharmacokinetic models in Risk Assessment," 2010.

[7] IPCS/WHO, "Chemical specific adjustment factors for interspecies differences and intraspecies variability: guidance document for use of data in dose/concentration response assessment," 2005.

[8] H. Mielke and U. Gundert-Remy, "Bisphenol A levels in blood depend on age and exposure," *Toxicology Letters*, vol. 190, no. 1, pp. 32–40, 2009.

[9] European Union (EU), "Risk Assessment Report 4,4′-isopropylidenediphenol (bisphenol-A) CAS No: 80-05-7 EINECS No: 201-245-8 Series," 3rd Priority List Volume 37, Office for Official Publications of the European Communities, 2003.

[10] EFSA (European Food Safety Authority), "Opinion of the Scientific Panel on Food Additives, Flavourings, Processing Aids and Materials in Contact with Food (AFC) related to 2,2-bis(4-hydroxyphenyl)propane; Question number EFSA-Q-2005-100," 2011, http://www.efsa.europa.eu/en/efsajournal/pub/428.htm.

[11] F. S. vom Saal and C. Hughes, "An extensive new literature concerning low-dose effects of bisphenol A shows the need for a new risk assessment," *Environmental Health Perspectives*, vol. 113, no. 8, pp. 926–933, 2005.

[12] M. J. Zaya, R. N. Hines, and J. C. Stevens, "Epirubicin glucuronidation and UGT2B7 developmental expression," *Drug Metabolism and Disposition*, vol. 34, no. 12, pp. 2097–2101, 2006.

[13] X. Ye, Z. Kuklenyik, L. L. Needham, and A. M. Calafat, "Quantification of urinary conjugates of bisphenol A, 2,5-dichlorophenol, and 2-hydroxy-4-methoxybenzophenone in humans by online solid phase extraction-high performance liquid chromatography-tandem mass spectrometry," *Analytical and Bioanalytical Chemistry*, vol. 383, no. 4, pp. 638–644, 2005.

[14] H. Kurebayashi, K. Okudaira, and Y. Ohno, "Species difference of metabolic clearance of bisphenol A using cryopreserved hepatocytes from rats, monkeys and humans," *Toxicology Letters*, vol. 198, no. 2, pp. 210–215, 2010.

[15] K. Abraham, H. Mielke, W. Huisinga, and U. Gundert-Remy, "Elevated internal exposure of children in simulated acute inhalation of volatile organic compounds: effects of concentration and duration," *Archives of Toxicology*, vol. 79, no. 2, pp. 63–73, 2005.

[16] R. K. Kuester and I. G. Sipes, "Prediction of metabolic clearance of bisphenol A (4,4′-dihydroxy-2,2- diphenylpropane) using cryopreserved human hepatocytes," *Drug Metabolism and Disposition*, vol. 35, no. 10, pp. 1910–1915, 2007.

[17] Z. E. Barter, M. K. Bayliss, P. H. Beaune et al., "Scaling factors for the extrapolation of in vivo metabolic drug clearance from in vitro data: reaching a consensus on values of human microsomal protein and hepatocellularity per gram of liver," *Current Drug Metabolism*, vol. 8, no. 1, pp. 33–45, 2007.

[18] N. Hanioka, T. Naito, and S. Narimatsu, "Human UDP-glucuronosyltransferase isoforms involved in bisphenol A glucuronidation," *Chemosphere*, vol. 74, no. 1, pp. 33–36, 2008.

[19] Z. Duanmu, A. Weckle, S. B. Koukouritaki et al., "Developmental expression of aryl, estrogen, and hydroxysteroid sulfotransferases in pre- and postnatal human liver," *Journal of Pharmacology and Experimental Therapeutics*, vol. 316, no. 3, pp. 1310–1317, 2006.

[20] G. Ginsberg and D. C. Rice, "Does rapid metabolism ensure negligible risk from bisphenol A?" *Environmental Health Perspectives*, vol. 117, no. 11, pp. 1639–1643, 2009.

[21] M. Nishikawa, H. Iwano, R. Yanagisawa, N. Koike, H. Inoue, and H. Yokota, "Placental transfer of conjugated bisphenol A and subsequent reactivation in the rat fetus," *Environmental Health Perspectives*, vol. 118, no. 9, pp. 1196–1203, 2010.

[22] J. G. Hengstler, H. Foth, T. Gebel et al., "Cutting edge topics of the current controversy on BPA," *Critical Reviews in Toxicology*, vol. 41, pp. 263–291, 2011.
[23] "EFSA toxicokinetics of bisphenol A," *The EFSA Journal*, vol. 759, pp. 1–10, 2008.
[24] H. Mielke, F. Partosch, and U. Gundert-Remy, "The contribution of dermal exposure to the internal exposure of bisphenol A in man," *Toxicology Letters*, vol. 204, no. 2-3, pp. 190–198, 2011.
[25] J. Sajiki, K. Takahashi, and J. Yonekubo, "Sensitive method for the determination of bisphenol-A in serum using two systems of high-performance liquid chromatography," *Journal of Chromatography B*, vol. 736, no. 1-2, pp. 255–261, 1999.
[26] V. Padmanabhan, K. Siefert, S. Ransom et al., "Maternal bisphenol-A levels at delivery: a looming problem?" *Journal of Perinatology*, vol. 28, no. 4, pp. 258–263, 2008.
[27] S. Biedermann, P. Tschudin, and K. Grob, "Transfer of bisphenol A from thermal printer paper to the skin," *Analytical and Bioanalytical Chemistry*, vol. 398, no. 1, pp. 571–576, 2010.
[28] T. Mendum, E. Stoler, H. van Benschoten, and J. C. Warner, "Concentration of bisphenol A in thermal paper," *Green Chemistry Letters and Reviews*, vol. 4, no. 1, pp. 81–86, 2011.
[29] T. Östberg and E. Noaksson, "Bisfenol A in svenska kvitton," Analysresultat. Institutet för tillämoa grön kemi. Jämtlands läns Landsting, 2010.
[30] FAO/WHO Joint FAO/WHO, "Expert Meeting to Review Toxicological and Health Aspects of Bisphenol A," Summary Report, 2010.
[31] R. W. Tyl, C. B. Myers, M. C. Marr et al., "Three-generation reproductive toxicity study of dietary bisphenol A in CD Sprague-Dawley rats," *Toxicological Sciences*, vol. 68, no. 1, pp. 121–146, 2002.
[32] T. J. Mørck, G. Sorda, N. Bechi et al., "Placental transport and in vitro effects of Bisphenol A," *Reproductive Toxicology*, vol. 30, no. 1, pp. 131–137, 2010.
[33] D. Zalko, C. Jacques, H. Duplan, S. Bruel, and E. Perdu, "Viable skin efficiently absorbs and metabolizes bisphenol A," *Chemosphere*, vol. 82, no. 3, pp. 424–430, 2011.
[34] T. Tsukioka, J. Terasawa, S. Sato, Y. Hatayama, T. Makino, and H. Nakazawa, "Development of analytical method for determining trace amounts of BPA in urine samples and estimation of exposure to BPA," *Journal of Environmental Chemistry*, vol. 14, pp. 57–63, 2004.
[35] J. G. Teeguarden, A. M. Calafat, X. Ye et al., "Twenty-four hour human urine and serum profiles of bisphenol A during high-dietary exposure," *Toxicological Sciences*, vol. 123, no. 1, pp. 48–57, 2011.
[36] A. M. Calafat, J. Weuve, X. Ye et al., "Exposure to bisphenol A and other phenols in neonatal intensive care unit premature infants," *Environmental Health Perspectives*, vol. 117, no. 4, pp. 639–644, 2009.
[37] H. Mielke, K. Abraham, M. Götz et al., "Physiologically based toxicokinetic modelling as a tool to assess target organ toxicity in route-to-route extrapolation—the case of coumarin," *Toxicology Letters*, vol. 202, no. 2, pp. 100–110, 2011.
[38] EFSA (European Food Safety Authority), "Opinion of the scientific panel on food additives, flavourings, processing aids and materials in contact with food (AFC) on a request from the commission related to Coumarin," *The EFSA Journal*, vol. 104, pp. 1–136, 2004.
[39] W. Umbach, *Kosmetik von Kopf bis Fuss*, Wiley-VCH, Weinheim, Germany, 3rd edition, 2004.
[40] "Inspectorate of the German States," Internal Report, 2005.
[41] Scientific Committee on Cosmetic Products and Non-Food Products intended for Consumers (SCCNFP), "Opinion concerning 6-Acetyl-1,1,2,4,4,7-Hexamethyltetryltetralin (AHTN) SCCNFP/0609/02," 2002.
[42] Scientific Committee on Cosmetic Products and Non-Food Products intended for Consumers (SCCNFP), "Opinion concerning Hexahydrohexamethyl-cyclopenta (γ)-2-benzopyran (HHCB) SCCNFP/0610/02," 2002.
[43] Scientific Committee on Cosmetic Products and Non-Food Products intended for Consumers (SCCNFP), "Note for Guidance for testing of cosmetic ingredients and their safety evaluation," 5th revision, 2003.
[44] Scientific Committee on Cosmetic Products and Non-Food Products intended for Consumers (SCCNFP), 2004, "Opinion concerning musk xylene and musk keton, SCCNFP/0817/04. Scientific Committee on Consumer Products (SCCP). Note for Guidance for testing of cosmetic ingredients and their safety evaluation," 6th revision, 2006.
[45] Scientific Committee on Food (SCF), Opinion on coumarin (a constituent of natural flavouring source materials limited by Annex II of flavourings directive 88/388/EEC), expressed on 16 December 1994. Reports of the Scientific Committee on Food (36th series). European Commission, Directorate General Industry. Luxembourg, 1997.
[46] S. A. J. Beckley-Kartey, S. A. M. Hotchkiss, and M. Capel, "Comparative in vitro skin absorption and metabolism of coumarin (1,2-benzopyrone) in human, rat, and mouse," *Toxicology and Applied Pharmacology*, vol. 145, no. 1, pp. 34–42, 1997.
[47] R. A. Ford, D. R. Hawkins, B. C. Mayo, and A. M. Api, "The in vivo dermal absorption and metabolism of [4-^{14}C]coumarin by rats and by human volunteers under simulated conditions of use in fragrances," *Food and Chemical Toxicology*, vol. 39, no. 2, pp. 153–162, 2001.
[48] BfR (Bundesinstitut fuer Risikobewertung). Kosmetika können wesentlich zur Gesamtaufnahme von Cumarin beitragen. (BfR Nr. 049/2007), 2007, http://www.bfr.bund.de/cm/206/kosmetika_koennen_wesentlich_zur_gesamtaufnahme_von_cumarin_beitragen.pdf.
[49] W. A. Ritschel, K. A. Hoffmann, H. S. Tan, and P. R. Sanders, "Pharmacokinetics of coumarin upon i.v. administration in man," *Drug Research*, vol. 26, no. 7, pp. 1382–1387, 1976.
[50] W. A. Ritschel, M. E. Brady, and H. S.I. Tan, "Pharmacokinetics of coumarin and its 7-hydroxy-metabolites upon intravenous and peroral administration of coumarin in man," *European Journal of Clinical Pharmacology*, vol. 12, no. 6, pp. 457–461, 1977.
[51] W. A. Ritschel, M. E. Brady, and H. S. I. Tan, "First-pass effect of coumarin in man," *International Journal of Clinical Pharmacology Therapy and Toxicology*, vol. 17, no. 3, pp. 99–103, 1979.
[52] W. A. Ritschel and S. A. Hussain, "Transdermal absorption and topical availability of coumarin," *Methods & Findings in Experimental & Clinical Pharmacology*, vol. 10, pp. 165–169, 1988.
[53] I. M. C. M. Rietjens, M. G. Boersma, M. Zaleska, and A. Punt, "Differences in simulated liver concentrations of toxic coumarin metabolites in rats and different human populations evaluated through physiologically based biokinetic (PBBK) modeling," *Toxicology in Vitro*, vol. 22, no. 8, pp. 1890–1901, 2008.
[54] G. Loizou, M. Spendiff, H. A. Barton et al., "Development of good modelling practice for physiologically based pharmacokinetic models for use in risk assessment: the first steps,"

Regulatory Toxicology and Pharmacology, vol. 50, no. 3, pp. 400–411, 2008.

[55] H. A. Barton, W. A. Chiu, R. Woodrow Setzer et al., "Characterizing uncertainty and variability in physiologically based pharmacokinetic models: state of the science and needs for research and implementation," *Toxicological Sciences*, vol. 99, no. 2, pp. 395–402, 2007.

[56] A. Y. Weiße and W. Huisinga, "Error-controlled global sensitivity analysis of ordinary differential equations," *Journal of Computational Physics*, vol. 230, no. 17, pp. 6824–6842, 2011.

Hindawi Publishing Corporation
Journal of Toxicology
Volume 2012, Article ID 791431, 17 pages
doi:10.1155/2012/791431

Research Article

Update on a Pharmacokinetic-Centric Alternative Tier II Program for MMT—Part II: Physiologically Based Pharmacokinetic Modeling and Manganese Risk Assessment

Michael D. Taylor,[1] Harvey J. Clewell III,[2] Melvin E. Andersen,[2] Jeffry D. Schroeter,[2] Miyoung Yoon,[2] Athena M. Keene,[1] and David C. Dorman[3]

[1] *Health, Safety, Environment, and Security, Afton Chemical Corp., Richmond, VA 23219, USA*
[2] *Institute for Chemical Safety Sciences, The Hamner Institutes for Health Sciences, Research Triangle Park, NC 27709, USA*
[3] *College of Veterinary Medicine, North Carolina State University, Raleigh, NC 27606, USA*

Correspondence should be addressed to Michael D. Taylor, mike.taylor@aftonchemical.com

Received 22 October 2011; Accepted 25 January 2012

Academic Editor: Kannan Krishnan

Recently, a variety of physiologically based pharmacokinetic (PBPK) models have been developed for the essential element manganese. This paper reviews the development of PBPK models (e.g., adult, pregnant, lactating, and neonatal rats, nonhuman primates, and adult, pregnant, lactating, and neonatal humans) and relevant risk assessment applications. Each PBPK model incorporates critical features including dose-dependent saturable tissue capacities and asymmetrical diffusional flux of manganese into brain and other tissues. Varied influx and efflux diffusion rate and binding constants for different brain regions account for the differential increases in regional brain manganese concentrations observed experimentally. We also present novel PBPK simulations to predict manganese tissue concentrations in fetal, neonatal, pregnant, or aged individuals, as well as individuals with liver disease or chronic manganese inhalation. The results of these simulations could help guide risk assessors in the application of uncertainty factors as they establish exposure guidelines for the general public or workers.

1. Introduction

As an essential element, manganese (Mn) is required for normal function of the central nervous system (CNS) and other tissues [1]. As with all other metals, manganese toxicity can occur with excessive exposure. A variety of clinical effects are associated with manganese toxicity, including manganism, a parkinsonian movement disorder that primarily affects dopaminergic and γ-aminobutyric acid- (GABA-) containing mid-brain structures that control motor functions [2]. More subtle effects can also occur. For example, workers exposed chronically to manganese can develop changes in visual reaction time, hand steadiness, and eye-hand coordination [3]. These neurotoxic syndromes develop when either manganese intake is excessive (e.g., following high-dose oral, inhalation, or parenteral manganese exposure) or when hepatobiliary clearance of this metal is impaired. This observation suggests that the dose of manganese delivered to target regions within the CNS is the primary determinant for manganese neurotoxicity.

The U.S. Environmental Protection Agency's (USEPA) list of hazardous air pollutants includes manganese compounds. The USEPA and health agencies in other countries have raised concerns that chronic inhalation of low levels of manganese in ambient air may pose a risk to public health due to the possible accumulation of manganese in target tissues [4]. These concerns prompted the USEPA to call for a series of pharmacokinetic studies, as well as the development of physiologically based pharmacokinetic (PBPK) models for manganese as part of the testing requirements

for the organometallic fuel additive methylcyclopentadienyl manganese tricarbonyl (MMT®, a registered trademark of Afton Chemical Corporation) [5]. Part I of this two part series discussed the development of the USEPA's Alternative Tier II testing program for MMT that collected critical pharmacokinetic data for manganese in rodents and nonhuman primates [5]. All test reports and correspondence related to the Alternative Tier 2 Testing for MMT can be found in the Federal Docket Management System (FDMS) at http://www.regulations.gov/ identified by docket number EPA-HQ-OAR-2004-0074.

One objective of the MMT Alternative Tier 2 program was to generate data to support the development of PBPK models for manganese [5, 6]. Development of these models represents an effort that spans more than a decade. Key pharmacokinetic data needed to support PBPK model development and a paradigm for a tissue-dose-based health risk assessment for manganese were initially described by Andersen and coworkers [7] in 1999 and helped guide future studies. Numerous animal experiments have subsequently addressed many of the data gaps raised by Andersen and coworkers [7] (reviewed in [5, 6, 8]). This manuscript describes the development of a series of PBPK models for manganese. Moreover, we provide a framework for their application to risk assessment.

2. Manganese PBPK Models: Development and Status

The development of the PBPK models proceeded in a stepwise, iterative fashion with increasing model complexity being added at each step. Table 1 provides an overview of the initial "first generation" models developed for this research program. The earliest dosimetry models were adapted from pharmacokinetic models developed for zinc, copper, and other essential metals that focused on dietary intake and deficiency. Features of these models that were deemed important for manganese include features of these models that were deemed important for manganese include the ability to describe homeostatic control of an essential element under normal and deficient dietary conditions, and the use of compartmental and linear exchange rates to distribute the essential element into tissues and cellular compartments. The earliest manganese models were used to quantitatively test assumptions regarding the movement of manganese from the rodent gastrointestinal tract (GIT) and liver [9] and to ascertain the degree to which systemic and orally derived manganese are handled similarly in the liver [10]. The resulting pharmacokinetic models accurately described the decreased gastrointestinal (GI) manganese uptake and increased hepatobiliary elimination that is seen with rising levels of manganese in the diet.

Early efforts also developed an initial framework for a multicompartment PBPK model. These models evaluated the kinetic behaviors of manganese in the brain, liver, and respiratory tract during and after manganese inhalation [12, 13]. Several model structures were considered during this developmental phase (Table 1). Ultimately, manganese kinetics were best described using a model that included dose-dependent saturable tissue binding as well as free and bound manganese [13]. In this context, bound manganese was confined to tissues and reflected basal manganese concentrations. Free manganese circulates in the blood and increasing concentrations resulted during manganese inhalation. Free manganese was rapidly cleared following exposure, thereby returning tissue manganese concentrations to their original basal levels. This rise of free brain manganese concentration was described with diffusion rate constants (k_{in} and k_{out}). Peak tissue manganese concentrations were constrained by the tissue maximal binding capacity (B_{max}). Importantly, dose dependencies predicted by the Nong model [13] were consistent with the total manganese tissue levels measured in rats following manganese inhalation. The model also replicated the rapid increases in tissue manganese concentrations seen at the highest inhaled manganese concentrations, as well as the rapid return to baseline after exposure ceased. The model developed by Nong and coworkers [13] for the adult rat incorporated these and other features and was used as the basis for all subsequent "second generation" animal PBPK models (Table 2).

Starting in 2009, the focus of the modeling effort began to shift to the development of more complete PBPK models for animals (Table 2). These models retained many of the features found in the Nong model [13], including dose-dependent saturable tissue capacities and asymmetrical diffusional flux of manganese into various tissue compartments. The second generation models also used airway deposition models based on particulate aerodynamics to describe manganese delivery to the respiratory tract [17]. Descriptions of the upper airways were broadened to include descriptions of the nasal cavity and olfactory epithelium using data published by Schroeter et al. [18]. Regarding the CNS, separate compartments for the olfactory bulb, striatum, pituitary gland, and cerebellum were developed. Specific influx and efflux diffusion rate constants (k_{in}, k_{out}) and binding constants (B_{max}, k_a, k_d) for different brain regions were used to account for the differential increases in regional brain manganese concentrations seen under various experimental conditions. These modifications led to the publication of the revised adult rat model depicted in Figure 1 [14]. Additional models were subsequently developed to describe lactational [15] and gestational [16] transfer of manganese in rats. In all cases, model output was compared to inhalation data obtained under this test program and that from the available literature.

In 2009, Nong and coworkers also described the development of a PBPK model for nonhuman primates from the revised adult rat model [14]. The monkey PBPK model was viewed as a critical step in the evolution of appropriate human models (Figure 2). One goal of the modeling effort was to retain as many features present in the rat model as possible. Body weight, tissue volumes, olfactory and respiratory tissues surface areas, ventilation rates, blood flows, and certain other model parameters were adjusted to describe monkey physiology while others (biliary clearance and brain diffusional fluxes) were allometrically scaled based on body

Table 1: Overview of initial "first generation" pharmacokinetic models developed for manganese.

Model goal(s)	Brief model description	Route(s) of exposure‡ and species	Mn pharmacokinetic data set(s) used in model development	Reference
Describe dose dependent gastrointestinal uptake and biliary elimination of Mn	Two-compartment distribution model that described Mn movement between the intestinal lumen and the liver using simple rate constants (k_{in} and k_{out}).	Mn: O, INH ^{54}Mn: IV Rodent	Tracer studies evaluating ^{54}Mn whole-body elimination kinetics including a dietary Mn balance study, two biliary elimination studies, and one acute and one chronic study.	[9]
Develop quantitative descriptions of Mn delivered to the liver from the systemic circulation.	Gut lumen, liver blood, systemic blood, and a tissue compartments. Model parameters described gut uptake, ^{54}Mn tracer kinetics, and hepatic extraction of Mn from oral and systemic pools.	Mn: O, INH ^{54}Mn: IV Rodent	Animals exposed to either inhaled or dietary Mn. These studies also evaluated ^{54}Mn whole-body elimination kinetics.	[10]
Describe the olfactory transport of Mn.	Compartments included: blood, olfactory epithelium, olfactory bulb, olfactory tract and tubercle, and striatum. Each compartment included a free and bound fraction.	^{54}Mn: INH Rat	Rats exposed (90 min) nose-only to either exposure to $^{54}MnCl_2$ or $^{54}MnHPO_4$.	[11]
Develop the basic structure of a multiroute PBPK model for Mn.	Blood, brain, respiratory tract (nasal and lung), liver, kidneys, bone, and muscle (rest of body) compartments consisting of a "shallow" tissue pool in rapid equilibration with blood and a "deep" tissue store, connected to the shallow pool by transfer rate constants [1].	^{54}Mn: IP, INH Rodent	Rodent tracer studies describing ^{54}Mn distribution to various tissues and ^{54}Mn elimination kinetics.	[12]
Develop a multiroute Mn PBPK model for adult rats.	Same compartments as above [4]. Model A used simple rate constants [1] to describe inter-compartmental movement of Mn. Model B had tissue binding kinetics described by dissociation and association constants (k_d and k_a), and maximum concentration of binding capacity (B_{max}).	Mn: O, INH ^{54}Mn: IV Rat	Rats fed on diets containing 2 to 100 ppm Mn, Rats fed a diet containing 125 ppm Mn and exposed via inhalation at 0.0 to 3.00 mg Mn/m^3 each day for 14 d. Rats exposed to 0.1 or 0.5 mg Mn/m^3 for 6 h/d, 5 d/wk over a 90-day period.	[13]

‡O: oral; IP: intraperitoneal; IV: intravenous; INH: inhalation. Where applicable, Mn tracer form and route of exposure have also been provided.

Table 2: Overview of "second generation" PBPK models developed for manganese.

Model goal(s)	Brief model description	Route(s) of exposure[‡] and species	Mn pharmacokinetic data set(s) used in model development	Reference
Develop a multiroute Mn PBPK model for adult rats and monkeys.	Blood, brain (striatum, pituitary gland, olfactory bulb, and cerebellum), respiratory tract (olfactory mucosa and lung epithelium), liver, kidneys, bone, and "rest of body" compartments. Saturable Mn binding in all tissues, preferential accumulation of Mn in several brain regions. Deposition of Mn within the respiratory tract and olfactory uptake and "nose-to-brain" Mn transport were based in part on additional models describing regional particle deposition within the respiratory tract.	Mn: O, INH Rat Rhesus monkey	Rat 14- and 90-day inhalation studies. In monkeys, model parameters were first calibrated using steady-state tissue Mn concentrations from rhesus monkeys fed a diet containing 133 ppm Mn. The model was then applied to simulate 65 exposure days of weekly (6 h/day; 5 days/week) inhalation exposures to soluble $MnSO_4$ at 0.03 to 1.5 mg Mn/m^3.	[14]
Develop a PBPK model for lactating dam and neonates.	Same compartments for the dam and pups as above [6] except for excluding pituitary gland and including mammary gland (dam only). Saturable binding and other model features similar to above [6]. Dietary (e.g., transfer of free Mn in milk) and inhalation inputs to pups.	Mn: O, INH Rat	Dams and their offspring were exposed to air or $MnSO_4$ (0.05, 0.5, or 1 mg Mn/m^3) for 6 h/day, 7 days/week starting 28 days prior to breeding through postnatal day 18.	[15]
Develop a PBPK model that could predict fetal Mn dose and Mn disposition in the dam and fetus following maternal Mn exposure.	Same compartments for the dam as above [6] except for excluding the pituitary gland and including the placenta. Fetal model included blood, brain, lung, bone, liver, and "rest of body" compartments. Saturable binding and other model features similar to above [6]. Placental transfer to fetus.	Mn: O, INH Rat	Dams fed a 10-ppm Mn diet were exposed to air or $MnSO_4$ (0.05, 0.5, or 1 mg Mn/m^3) for 6 h/day, 7 days/week starting 28 days prior to breeding through gestation day 20.	[16]

[‡]O: oral; INH: inhalation.

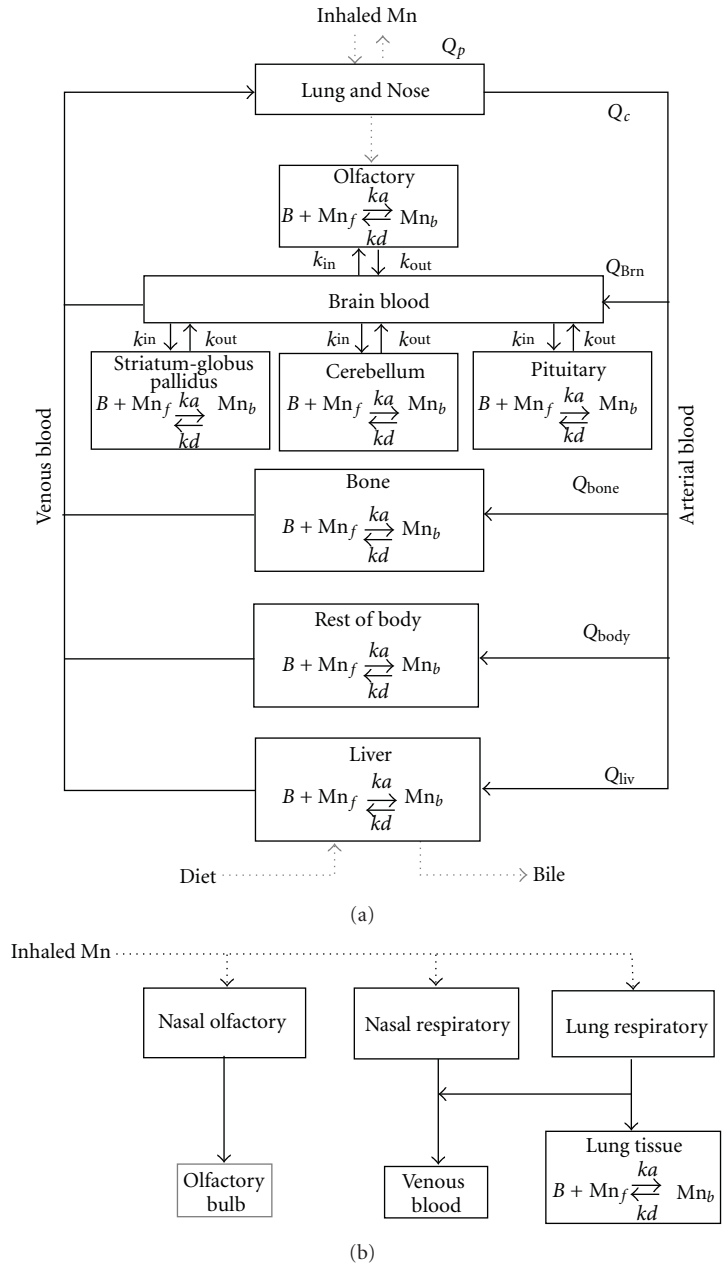

Figure 1: The PBPK model structure developed by Nong and coworkers [14] describing tissue manganese kinetics in adult rats. The overall PBPK model structure is shown in (a); an expanded view of the respiratory tract modeling is shown in (b). Inhaled manganese is absorbed through deposition of particles on the nasal and lung epithelium. Most of the manganese deposited in the nasal cavity is absorbed into the systemic blood while a small fraction undergoes direct delivery to the olfactory bulb. Every tissue has a binding capacity, $B_{\max}$, with affinity defined by association and dissociation rate constants (k_a, k_d). Free manganese moves in the blood throughout the body and is stored in each tissue as bound manganese. Influx and efflux diffusion rate constants (k_{in}, k_{out}) allow for differential increases in manganese levels for different tissues. Q_p, Q_c, Q_{tissue} refer to pulmonary ventilation, cardiac output, and tissue blood flows. Reprinted from [14] (with permission).

weight. Tissue-specific binding capacities were scaled to their respective tissue volumes while tissue-binding rate constants (k_a and k_d) were nearly constant from rat to monkeys. Dietary uptake and basal biliary excretion rates were also adjusted to fit measured background tissue manganese concentrations.

The final steps in the modeling program were to develop PBPK models for humans (Table 3). The starting point for this effort was the monkey PBPK model developed by Nong et al. [14] with appropriate changes in physiological descriptions, allometric scaling of biliary clearance and brain diffusional fluxes to body weight, and small changes in tissue

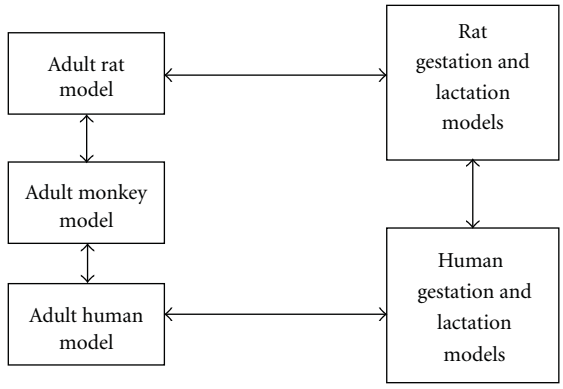

Figure 2: Parallelogram approach for developing Mn PBPK models for adult humans, as well as gestation and lactation.

binding rate constants (k_a and k_d). A significant change in the model involved the use of a more physiological description of the GIT to address an apparent delay in GI absorption evident in tracer Mn studies in primates [19] and the differential enterocyte turnover rates across lifestages [20]. Schroeter and coworkers [19] included a series of gut compartments (e.g., GI lumen and epithelium) to better describe the absorption of ingested manganese and storage of this metal. The epithelial linings of the small and large intestine have a high cellular turnover and contain rapidly proliferating cells (enterocytes) which replace those that are shed into the lumen. Enterocytes are an important site for metal uptake and ultimately excretion through the sloughing of these cells. In our model, manganese transfer from the upper GIT epithelium to the lower GIT resulted from sloughing of enterocytes from the epithelial layer. The manganese found in shed enterocytes was ultimately excreted into feces without entering the systemic circulation. This allowed for the differential rates of enterocyte sloughing found in different life stages to be accounted for [19, 20]. The fraction of manganese absorbed by the GIT (F_{dietup}) and the biliary excretion rate constant (k_{bileC}) were calibrated based on steady-state tissue concentrations and ^{54}Mn tracer studies. Induction of biliary elimination of manganese was also included in the model. These changes in model structure were sufficient to capture the observed dose-dependent changes in manganese absorption by the GIT and biliary excretion by the hepatobiliary system. Schroeter and coworkers [19] used a step-wise approach to model development by first developing a revised monkey PBPK model, followed by an adult human model, which was validated by the available human Mn tracer data [19]. The final step in the modeling efforts culminated in the development of a model that described gestational and lactational transfer of manganese in humans [20].

3. PBPK Models in Manganese Risk Assessment: Why Tissue Dose Matters

As an essential metal, manganese is found in all mammalian tissues. Several homeostatic mechanisms have evolved to tightly regulate these tissue manganese concentrations within a normal range of values. For most tissues, normal manganese concentrations in humans range from 0.15 to 4 μg Mn/g of wet tissue [1]. As noted earlier, manganese neurotoxicity occurs when manganese intake exceeds elimination, resulting in manganese accumulation in brain regions including the globus pallidus, which is particularly sensitive to manganese accumulation during overexposure. Although manganese neurotoxicity is sensitive to exposure dose, it is relatively insensitive to route of exposure, as similar neurological responses have been linked to prolonged high-dose manganese inhalation, drinking water ingestion, long-term total parenteral nutrition (TPN), or impaired manganese clearance because of hepatobiliary dysfunction [24]. Because of the ubiquitous nature of manganese and the role of dietary manganese in establishing steady-state tissue concentrations, risk assessments of inhaled manganese should consider the essentiality of manganese from diet to establish the tissue concentrations that will be altered with increasing levels of inhaled or ingested manganese. Therefore, to understand the risk to humans from excessive manganese exposure, it is important to determine the exposure conditions that result in manganese concentrations in the brain that are increased significantly compared with brain manganese concentrations arising from normal dietary intake [7]. Pharmacokinetic models can be used to help establish safe exposure levels by predicting exposure conditions that lead to toxicologically significant increases in tissue manganese.

4. Application of PBPK Models in Human Health Risk Assessment

One of the first attempts at applying PBPK models in scenarios relevant to human health risk assessment was performed by Schroeter and colleagues [19]. These investigators used their PBPK model to predict brain manganese concentrations in monkeys and people following subchronic manganese inhalation (Figure 3). The predicted globus pallidus manganese concentrations for monkeys (Figure 3(a)) compared favorably with those observed by Dorman et al. [21] in monkeys subchronically exposed to manganese sulfate ($MnSO_4$), giving added confidence that the PBPK models were designed and parameterized appropriately. The human simulations performed by Schroeter mimicked an 8 hr/day 5 day/week occupational exposure. The larger magnitude changes predicted in monkeys compared with humans at higher inhalation exposure concentrations may be due to saturation of manganese binding sites in the monkey at the higher manganese concentrations in the diet. Human diets are typically low in manganese content compared to diets in laboratory animal chows, which are often supplemented to much higher (~100 ppm) levels. At the lowest human exposure concentration used in our simulations (0.001 mg Mn/m^3), the model predicted no appreciable increase (<1% change from basal concentrations) in human globus pallidus manganese concentrations above the background levels associated with normal dietary exposure (Figure 3(b)). At an exposure concentration of 0.01 mg Mn/m^3, slight increases

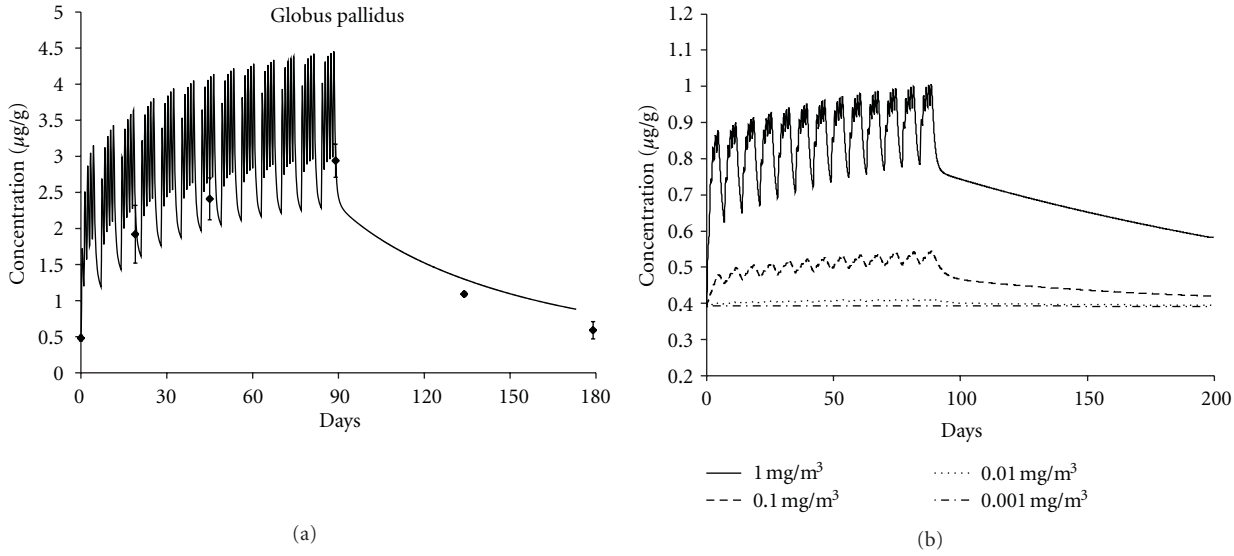

Figure 3: Curves showing simulated end-of-exposure brain tissue manganese concentrations in monkeys (a) and people (b) as a function of inhalation exposure concentration (mg Mn/m^3). Simulated exposures are for 90 days (5 days/week) for either 6 h/day (monkeys) or 8 h/day (human beings). The monkey simulation results at 1.5 mg/m^3 (a) are compared with data from Dorman et al. [21] depicted with symbols showing means and standard errors (SEs) from four to six monkeys per time-point. The larger magnitude changes predicted in monkeys compared with humans at higher inhalation exposure concentrations could be due to the saturation of manganese binding sites in the monkey coming from higher manganese concentrations in the diet of the monkeys. Modified from [19].

(~5%) in globus pallidus manganese concentration above background levels were predicted during the inhalation exposure period. More significant (>30%) increases in globus pallidus manganese concentrations were predicted at the higher exposure concentrations (>0.1 mg Mn/m^3). These data are consistent with derivations of benchmark concentrations for subclinical neurological effects from occupational studies at concentrations of 0.2 mg Mn/m^3 [25] and indicate that significant increases in tissue manganese concentration above normal background variability are required for subclinical effects to be manifested.

In light of our success in describing the rat and monkey tissue data and concordance with human responses and specific exposures, we conducted additional simulations using the available PBPK manganese models identified in Tables 2 and 3 to address other exposure scenarios of concern to toxicologists and risk assessors. Our goal was to predict tissue concentrations in individuals with altered physiology due to developmental life stage (Scenario 1) or disease (Scenario 2). A second goal was to use the PBPK models to predict brain manganese concentrations with prolonged inhalation exposure and variable dietary manganese intake (Scenario 3). The results of these simulations could help guide risk assessors in the application of intra- or interspecies uncertainty factors (UFs) as they establish exposure guidelines for the general public (e.g., an inhalation reference concentration or RfC) or workers (e.g., threshold limit value or TLV). In most risk assessments, UFs are applied to lower the acceptable air concentration to protect potentially susceptible subpopulations or account for species differences in response. For example, the current US EPA manganese RfC derivation incorporates a composite UF of 1000 that included UFs of 10 to protect sensitive individuals, 10 for use of a LOAEL, and 10 for database limitations, such as less than chronic periods of exposure, inadequate information regarding developmental and reproductive toxicity, and uncertainty about the toxicity of various forms of manganese [26].

The alternative PBPK model-based approach we present in this manuscript results in the development of pharmacokinetic chemical-specific adjustment factors (CSAFs) (or data-derived extrapolation factors (DDEFs)) that could be used in lieu of default UFs used in most risk assessments [27, 28]. A pharmacokinetic CSAF is a ratio in humans or animals of a measurable metric for internal exposure to the active compound such as area under the curve (AUC) (AUC is a surrogate for the daily and/or cumulative manganese dose received by an individual), C_{max}, or clearance between a baseline and potentially susceptible subpopulation [27]. While serving the same purpose as UFs, these extrapolation factors are based on data directly pertinent to the chemical of interest, rather than having their basis on default assumptions about inter- and intraspecies variability [28]. This approach leads to a higher confidence in the calculated adjustment factor and contributes to consistency in regulatory processes and decisions [28]. Unless otherwise noted, all simulations in these scenarios provide results for total tissue manganese concentration.

Scenario 1. Consideration of Potentially Susceptible Subpopulations Based on Lifestage and Pregnancy Status. Age-related changes in physiology can influence the pharmacokinetics of xenobiotics, and some experimental data suggest that that the aged nervous system may be at increased risk following

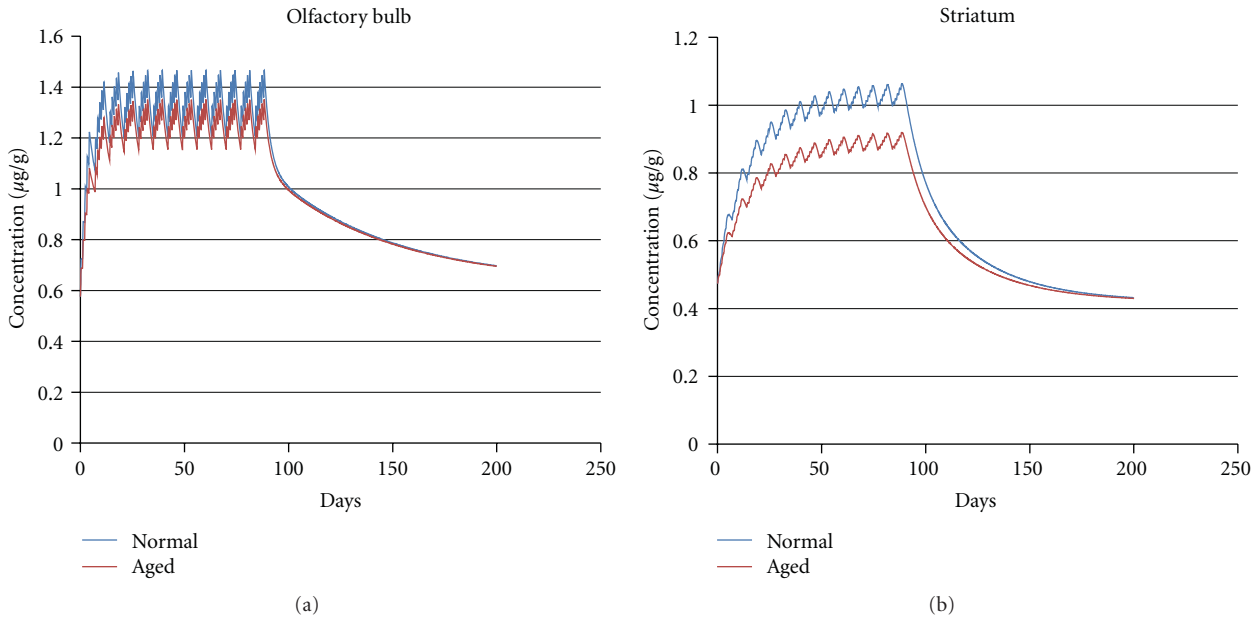

Figure 4: Simulated olfactory bulb (L) and striatum (R) manganese concentrations in adult and aged (16 month old) male rats following 6 hr/d inhalation $MnSO_4$ exposure at 0.5 mg Mn/m^3 for 90 days. Model simulations for aged rats had a 25% decrease in minute volume consistent with reported reduction in pulmonary function [22, 23].

exposure to manganese. For example, manganese-induced depletion of striatal glutathione is more severe in aged (20 months old) rats than in young (3-month-old) rats following repeated (7 day) high-dose (15–100 mg Mn/kg/day) oral exposure to manganese chloride [29]. Occupational and environmental exposure studies indicate that increased age may be a risk factor for manganese-induced neurobehavioral deficits [30]. To explore this question more quantitatively, we used the rodent PBPK model, as data were available in the literature regarding the degree to which pulmonary function declines with age.

Model simulations for aged rats (Figure 4) used a 25% decrease in minute volume consistent with reported reduction in pulmonary function in aged rats [22, 23]. Aged rats had lower target brain tissue manganese concentrations than middle-aged animals at the same exposures. This difference is likely due to the decreased breathing rates and pulmonary capacity of aged animals [31]. Since the manganese tissue concentration in the potentially susceptible subpopulation was less than in adult males, a pharmacokinetic CSAF for the aged life stage should be <1. Extending this simulation from rats to humans will require some changes to the physiological parameters used in the current models. For example, changes in liver volume and hepatic blood flow that significantly impact xenobiotic metabolism and clearance occur in geriatric human patients [32]. Likewise, aged humans have altered biliary [33], pulmonary [34], and gastrointestinal [35] function that may alter manganese pharmacokinetics. These complexities require a human model simulation of this scenario that lies outside of the focus of the present manuscript. However, we have provided the template for generating a pharmacokinetic CSAF for aged individuals. This preliminary analysis indicates that large adjustment factors may not be necessary to extrapolate from adult males, which typically are the subject of the occupational epidemiological studies that determine the point of departure in manganese risk assessments, to aged life stages.

Evaluation of other life stages is also important since they are also covered in the extrapolations from occupational studies by UFs. Epidemiological studies in children have reported an association between elevated dietary manganese exposure and neurobehavioral and neurocognitive deficits [36]. Concerns for potential vulnerability to manganese neurotoxicity during fetal and neonatal development have been raised by regulatory agencies [37]. PBPK models developed for this program can be used to quantitatively estimate the role that higher intestinal absorption of ingested manganese and a lower basal biliary excretion rate seen in children (see [1] for review) affect dose-to-target-tissue during manganese inhalation. To this end, Yoon and coworkers [20] used their human PBPK model to estimate average expected daily AUCs for the globus pallidus among different life stages (nonpregnant, pregnant, and lactating women, fetuses, nursing infants, and 3-year-old children) for three different exposure conditions, namely, 0, 0.001, and 0.01 mg Mn/m^3 for 24 hr/day 7 day/week (see [20], Figure 7). Exposure durations in the different simulations varied with life stage (~9 month pregnancy for women and their fetuses; 4 months for nursing infants and their mother, and 3 years after birth for children). The average daily AUC to the globus pallidus was calculated at the end of each simulation after running the model for appropriate durations for the selected life stages. Pregnancy and lactation did not greatly affect the simulated internal dose of Mn in the brain.

Table 3: Overview of human PBPK models developed for manganese.

Model goal(s)	Brief model description	Route(s) of exposure‡ and species	Mn pharmacokinetic data set(s) used in model development	Reference
Refine the multi-route Mn PBPK model for monkeys and extend to human beings.	Blood, brain (globus pallidus, pituitary gland, olfactory bulb, and cerebellum), respiratory tract (olfactory mucosa and lung epithelium), liver, kidneys, bone, and "rest of body" compartments. More extensive description of gastrointestinal tract (gut lumen and epithelium) and peritoneal cavity. Saturable Mn binding in all tissues. Preferential accumulation of Mn in several brain regions. Deposition of Mn within the respiratory tract and olfactory uptake and "nose-to-brain" Mn transport were based in part on additional models describing regional particle deposition within the respiratory tract.	Mn: O, INH ^{54}Mn: IV, IP, O, SC Rhesus monkey Human	Monkey inhalation study used previously [6]. Whole-body elimination or fecal excretion data available from ^{54}Mn tracer kinetic studies in monkeys and people	[19]
Develop a PBPK model that could predict fetal Mn dose and Mn disposition in women and fetus following maternal Mn exposure.	Lactation and gestation models similar to those developed for rodents [15, 16]. Same compartments for women as above [9] except for excluding the pituitary gland and including the placenta and mammary gland. Fetal model included blood, brain, lung, bone, liver, and "rest of body" compartments. Saturable binding and other model features similar to above [9]. Key model features included: placental Mn transfer via active transport, lactational transfer of Mn used diffusion-mediated secretion, higher gut absorption in nursing neonates, low but inducible biliary excretion of Mn in neonates, transition of neonatal features of gut absorption and biliary excretion to those of adults, and enhanced brain uptake of Mn during fetal and postnatal development.	Mn: O, INH Human	Variety of data obtained in people including: reported brain Mn concentration at birth and children, Mn concentrations in the umbilical cord, milk, newborn blood, bone, and other tissues. Age appropriate tissue weights and blood flows.	[20]

‡O: oral; IP: intraperitoneal; IV: intravenous; INH: inhalation; SC: subcutaneous. Where applicable, Mn tracer form and route of exposure have also been provided.

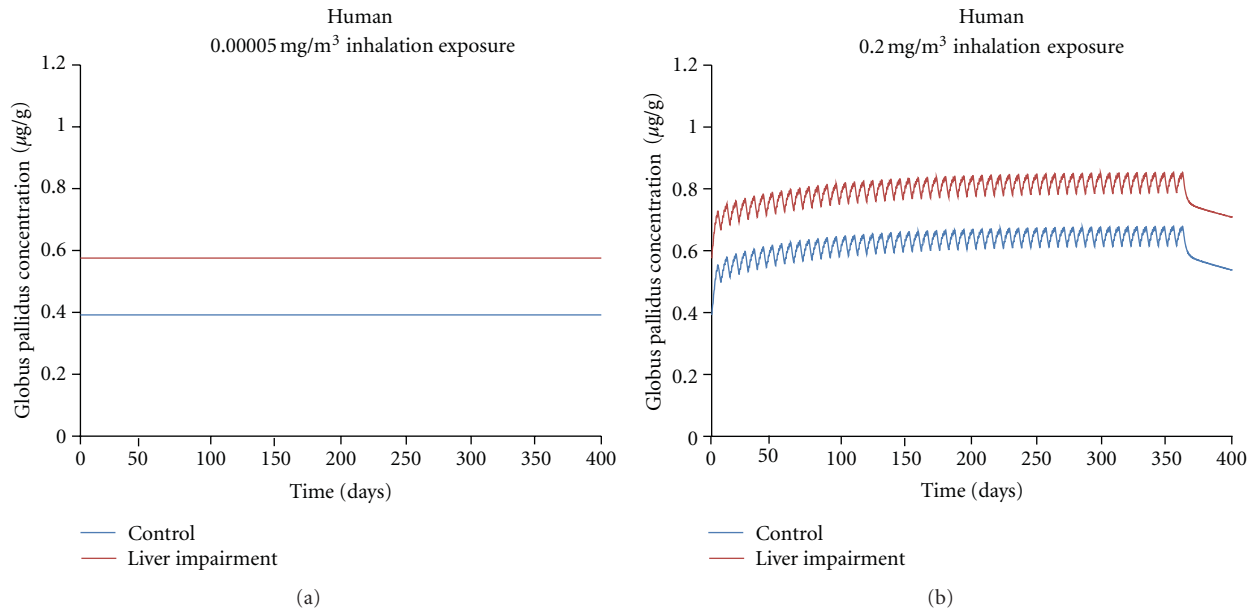

Figure 5: Simulated globus pallidus manganese concentrations in humans following inhalation exposure to $MnSO_4$ at 0.00005 (a) or 0.2 mg (b) Mn/m^3 for 8 hr/d, 5 d/wk, for one year. Simulations were performed using the human model developed by Schroeter et al. [19] with the following exceptions: model simulations for humans with hepatobiliary impairment had a 50% decrease in liver blood flow and a 50% decrease in biliary excretion (K_{bileC}) to simulate moderate hepatobiliary disease (see text for more details).

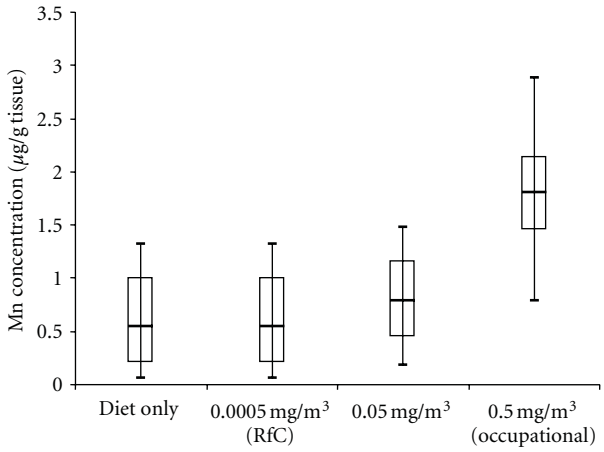

Figure 6: Distributions (min, 5th, med, 95th and max) of globus pallidus concentrations simulated for a human population with the input distributions described in Scenario 3 (see text for more details). Comparison of steady-state brain manganese concentration following 365 days of continuous exposure (24 hr/7 days). There is an overlap of tissue Mn levels between inhaled exposure and dietary variability. Changes in globus pallidal manganese concentrations from exposures <0.05 mg Mn/m^3 are small when compared to the impact of normal dietary variation.

The average daily AUCs were greater in men than in women at high-dose environmental exposure of Mn, that is, exposures where brain Mn concentration started to rise from the basal level. The change in the average daily globus pallidus AUC resulting from high-dose manganese inhalation was greater in nursing infants compared to other life stages due to the lower (marginally deficient) basal levels of tissue manganese at this age [20]. For example, the estimated average AUC in the highly exposed infants was approximately 11.5 μg Mn·hr/g/day compared to approximately 7.9 μg Mn·hr/g/day in unexposed infants, while the AUC in the adult males increased from 9.3 μg Mn·hr/g/day to 11.5 μg Mn·hr/g/day. This apparent increase in sensitivity toward increasing tissue concentration is due to the lower basal tissue levels in neonates and likely represents the enhanced demand for manganese during this life stage [20, 38]. Both in adults and children after weaning, the relative contribution of inhalation (0.01 mg/m^3) was smaller than their normal dietary intake at these inhalation exposures. Because no life-stage achieved a higher AUC than adult males, the PK simulations support a pharmacokinetic CSAF of 1 for fetal, neonatal, pregnant, and nonpregnant female life-stages.

Scenario 2. Consideration of Individuals with Moderate-to-Severe Hepatobiliary Dysfunction. Individuals with severe hepatobiliary disease often develop elevated brain manganese concentrations when compared with normal individuals [39]. For example, Rose and coworkers [39] reported brain manganese concentrations in autopsy samples taken from patients with liver cirrhosis. When compared to age-matched controls, cirrhotic patients had significantly elevated brain manganese concentrations. These increases were most marked in the globus pallidus, where patients with severe cirrhosis had mean (±SEM) pallidal manganese concentrations of 4.04 ± 1.54 μg/g versus 1.41 ± 0.91 μg/g in controls. Rose and coworkers [39] also examined whether rat models using an end-to-side portacaval anastomosis or

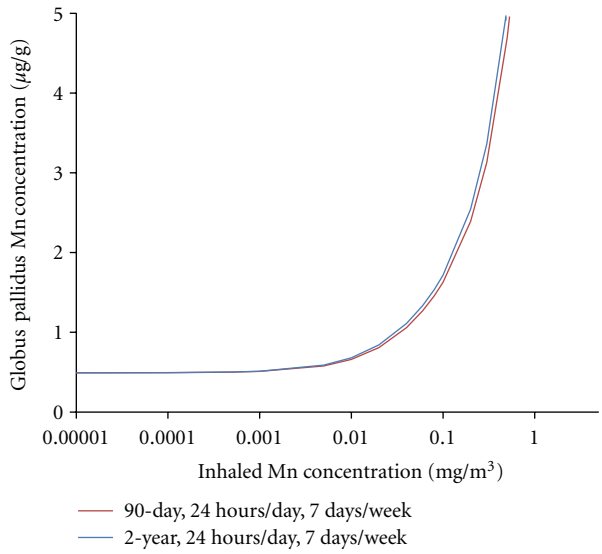

Figure 7: Simulated end-of-exposure nonhuman primate globus pallidus manganese concentrations following a 24 h/d, 7 d/wk inhalation for either 90 days (subchronic) or 2 yr (chronic) exposure to $MnSO_4$. These simulations indicate that globus pallidus manganese concentrations are expected to rapidly reach pseudosteady-state levels during high dose manganese exposure, and that duration of exposure has a minimal effect. Its contribution only occurs once exposures reach the threshold to cause tissue accumulation.

an intracholedochal injection of formalin and concomitant ligation of the bile duct to create an experimental model of biliary cirrhosis could mimic these findings. As expected, rats with biliary cirrhosis or a portacaval-shunt had increased pallidal (increased by 27% to 57%) and caudate/putamen (increased by 57 to 67%) manganese concentrations when compared with sham operated or normal control groups. It is important to note that the humans and animals studied by Rose had significant clinical liver disease. For example, the cirrhotic patients studied by Rose et al. [39] died of an extreme form of hepatic encephalopathy (i.e., hepatic coma).

Individuals with liver or biliary cirrhosis can also develop significant changes in hepatic blood flow that may affect manganese pharmacokinetics. Annet and coworkers [40] reported that patients with chronic liver disease of various grades (i.e., Child-Pugh classes A, B, and C) had mean (±SD) apparent liver perfusion rates of 36.29 ± 17.96 mL/min/100 mL liver volume versus 65.22 ± 24.73 mL/min/100 mL liver volume in patients without liver cirrhosis (as measured using magnetic resonance imaging). An approximately 50% reduction in total hepatic blood flow has been seen in dogs with side-to-side or end-to-side portacaval anastomoses [41]. Other investigators have reported significant (~50%) reductions in hepatic blood flow in rats with common bile duct ligation [42]. A similar observation is also seen in people with hepatic cirrhosis [43]. These studies indicate that there should be a 50% reduction in hepatic blood flow in the PBPK model parameters for consistency with the observations of experimentally induced hepatobiliary dysfunction.

Impaired secretion of bile acids, bilirubin, and other organic anions, consistent with reduced biliary function, is also observed in liver disease [44]. For example, rats with mild hepatic stenosis have an approximate 15% reduction in basal bile flow when compared with control animals [45]. One animal model in which biliary function has been quantitatively examined is liver dysfunction induced by the subchronic to chronic administration of TPN, an intravenous diet given in severe cases of GI disorders. Das et al. [46] reported that rabbits receiving TPN will develop qualitatively similar decreases in bile flow (reduced by 60%), bile acid secretion (52%), and sulfobromophthalein (BSP) excretion (38%) when compared with control animals. These animals also developed hepatocellular degeneration and portal tract inflammation. Thus, the available data support using a 50% reduction in bile flow in the PBPK model simulation.

In this study, we used the Schroeter et al. [19] model to simulate globus pallidus manganese concentrations in humans following a one year inhalation $MnSO_4$ exposure to either 0.00005 (the USEPA RfC) or 0.2 mg (the current ACGIH TLV) Mn/m^3 for 8 hr/d, 5 d/wk. Model simulations for people with hepatobiliary impairment had a 50% decrease in liver blood flow and a concomitant 50% decrease in biliary excretion (K_{bileC}) consistent with changes reported in people and/or animals with liver disease as discussed above. The simulations show that, regardless of inhalation concentration, the model predicted higher pallidal brain manganese concentrations due to hepatic dysfunction alone (Figure 5), which was expected based on available data. Inhalation at the RfC had no significant effect on pallidal concentrations, regardless of hepatobiliary function (Figure 5(a)). Inhalation concentrations at the TLV produced an increase in end-of-exposure pallidal manganese concentrations that were in addition to the increase from hepatobiliary disease (approx. 0.85 μg/g versus 0.68 μg/g in controls, Figure 5(b)). A CSAF of ~1.25 (0.85/0.68) is supported by the PBPK modeling for this extremely sensitive subgroup. Since this CSAF value was determined at occupational exposure levels, and no changes were observed at the RfC, this disease-related CSAF is likely conservative for environmental exposures which do not cause tissue accumulation.

Scenario 3. Consideration of Dietary Mn Variability and Chronic Manganese Inhalation. The strengths of using PBPK models in risk assessment include the ability to use the models to examine both dietary and inhaled intakes and support extrapolations from high to low doses, across routes, for different animal species, and for durations of exposure longer than those used in the studies that the models were based on [47]. To date, the most complete pharmacokinetic datasets for inhaled manganese available for PBPK model development and validation were developed for rats and monkeys using exposure durations of up to 90 exposure days (typically 6 hr/day, 5 days/week, reviewed in [5]). The manganese PBPK models described in this manuscript can be used to extrapolate beyond these exposure conditions.

This scenario demonstrates this ability by predicting globus pallidus manganese concentrations in people following a continuous (24 hr/day) chronic (1 year) manganese exposure (Figure 6).

The monkey PBPK model developed by Nong et al. [14] scaled to humans was used to simulate globus pallidus manganese concentrations in people while varying the dietary intake. Normal variation of manganese concentration in globus pallidus due to the fluctuation in daily dietary exposure was simulated in an adult human population of 10,000 using Monte Carlo techniques. These simulations varied the daily dietary intake of manganese using published data (mean [±SD]: 2.43 ± 1.8 mg/day; range 0.07–6.2 mg/day) [48]. Published distribution values (mean) were used for body weight (70 kg), tissue volumes (as % body weight) for blood (8%), bone (12%), brain (2%), liver (3%), lung (1%), and the remainder of the body (0.74%) [49, 50]. Distribution values (mean) for tissue blood flow (as % cardiac output) for bone (4%), brain (11%), liver (23%), and nose (1%) were also used [49, 50]. The coefficient of variation used for body weight, tissue volume, and blood flow parameters was 0.30. Mean values for cardiac output and pulmonary ventilation were set at 13 L/hr/kg and 20 L/hr/kg, respectively. A coefficient of variation used for these parameters was 0.50. All parameter distributions were truncated by two standard deviations and statistical correlations of parameters were not included in our analysis. Air manganese concentrations ranged from current USEPA RfC (0.00005 mg Mn/m^3) to 0.5 mg Mn/m^3, a concentration that represents potential occupational exposure levels, although with continuous exposure in this case.

A second question that we wanted to explore is the effect of exposure duration on the rate at which globus pallidus manganese concentrations change following manganese inhalation. Here, we compared the end-of-exposure tissue concentrations of a subchronic (90-day) versus 2-year exposure duration with the nonhuman primate model (Figure 7). Globus pallidus manganese concentrations rapidly reach pseudosteady state levels during high dose manganese exposure. These simulations are in accord with observations reported by Dorman and coworkers [21] who reported that rhesus monkeys exposed (5 d/week) for 15, 33, or 65 exposure days to $MnSO_4$ at 1.5 mg Mn/m^3 developed mean (±SEM) globus pallidus manganese concentrations of 1.92 ± 0.40, 2.41 ± 0.29, and 2.94 ± 0.23 μg Mn/g tissue wet weight, respectively, all of which were significantly different ($P < 0.05$) than background tissue levels of 0.48 ± 0.04 μg Mn/g tissue wet weight. Extending the simulation to 2 years produced a very slight leftward shift of the exposure-accumulation curve, but it did not change the threshold for tissue accumulation. For example, at 0.2 mg $MnSO_4/m^3$ (the current ACGIH TLV), a pharmacokinetic CSAF for subchronic to chronic duration is 1.06. Once exposure passes the threshold for tissue accumulation, a PK CSAF for duration of exposure is maximally 1.1.

Results of these simulations show several important findings. Brain manganese concentrations are controlled over a wide range of low-to-moderate exposure conditions at and above typical environmental exposures. Due to homeostatic controls, changes in globus pallidal manganese concentrations from exposures that exceed the current RfC even by several orders of magnitude (0.05 mg Mn/m^3) are small when compared to those seen as a result of normal variation in the dietary intake of manganese as demonstrated by the Monte Carlo analysis of dietary variation (Figure 6). However, once these homeostatic mechanism(s) are overwhelmed, pallidal manganese concentrations rise rapidly. The threshold for this response appears to occur at approximately 0.001–0.01 mg Mn/m^3 (Figure 7).

5. Future Applications of PBPK Models

The scenarios that we have explored here can easily be broadened to address other concerns raised in relation to the human health risk assessment of manganese. Another scenario that may prove useful to risk assessors is a consideration of the effect of altered iron homeostasis on manganese pharmacokinetics, since iron deficiency and iron-deficient anemia exist worldwide [51]. Inadequate tissue iron status resulting from dietary iron deficiency or anemia can lead to altered brain manganese deposition in animals [52–54]. It is unknown whether interactions between iron and manganese for divalent metal transporter 1 (DMT1) and other shared cellular membrane metal transporters account for this effect [55, 56]. Once these pathways and interactions are more fully elucidated, especially with quantitative measurements, these features can be incorporated into the existing PBPK models.

Although the PBPK models were originally created to support the risk assessment of combustion products of the fuel additive MMT (see [5]), they have much broader application to toxicologists and risk assessors. PBPK models can consider the impact of particle size and solubility on manganese dosimetry, especially as it relates to nanomaterials. Manganese nanoparticle exposure may occur during occupational exposure scenarios, potentially including welding. Nanoparticles display several curious inhalation pharmacokinetic behaviors that may be independent of chemical form [57]. For example, inhaled nanomaterials are deposited extensively in the nasal cavity [58]; in addition, a large percentage (~75%) of the nanomaterials that reach the alveolar region remain at that site, with less than 5% of inhaled nanoparticles translocating out of the lungs [59]; charged nanoparticles are more likely to travel to the brain via axonal transport within the olfactory nerve than are neutral nanoparticles [60]; and nanoparticle size also influences organ distribution and renal excretion [61, 62]. Several PBPK models have been developed for nanoparticles [11, 62–64]. These models were parameterized and validated using experimental pharmacokinetic data collected for different nanomaterials (e.g., iridium, silver, or technetium-labeled carbon nanoparticles) using data obtained from rats or humans. There is only sparse data on the pharmacokinetics of manganese-based nanoparticles. Some work examined translocation of manganese oxide (MnO_2) nanoparticles from the nasal cavity to the brain [65]; however, these investigators relied on the use of nasal instillation rather than inhalation. Elder and coworkers [66] exposed rats to

MnO_2 nanoparticles with individual aerodynamic diameters of 3–8 nm (note these particles form ~30 nm agglomerates in the exposure system) for 6 hr/day, 5 days/wk, for a total of 12 inhalation exposure days. In this study, the olfactory bulb showed the greatest changes in proinflammatory gene expression when compared to the midbrain, striatum, and other brain regions. This finding supports the conclusion that inhaled manganese nanoparticles, like larger particles, can undergo olfactory transport from the nasal cavity to the olfactory bulb. However, PBPK modeling in rodents and MRI analysis in primates have demonstrated that the olfactory pathway does not appear to significantly impact manganese delivery to tissues outside of the olfactory pathway [67, 68]. While research on manganese nanoparticles is still limited, there is some evidence that soluble manganese may be more bioavailable and cause more effects relative to equivalent amounts of nanoparticle manganese. Whereas most of the deposited nanomaterial appears to stay in the lung, soluble manganese is readily bioavailable [14, 59, 69]. Furthermore, manganese nanoparticles appear to be less toxic than an equivalent dose of soluble Mn^{2+}. Daily intratracheal instillation of soluble $MnCl_2$ in rats for 3–6 weeks led to increased brain manganese levels, a reduction in body weight gain, and a decrease of open field motility when compared to controls, whereas the equivalent dose of MnO_2 nanoparticles had no significant effects [65]. Also, MnO_2 nanoparticles were less toxic to PC-12 cells *in vitro* by the MTT assay than an equivalent dose (in ug/mL) of soluble Mn acetate [70]. Thus, the current PBPK modeling, based on soluble manganese ($MnSO_4$), may represent a worst-case scenario relative to nano-manganese after accounting for differences in pulmonary deposition. This expectation will be further clarified as more data become available comparing the pharmacokinetics and pharmacodynamics of nano- and soluble manganese.

Another potential application of the manganese PBPK models for risk assessment is the evaluation of the literature on the neurological outcomes of manganese exposure in primates, potentially identifying tissue concentrations that lead to adverse effects. This assessment would allow the models to explore the pharmacodynamic aspects of Mn exposure. The models could then be used to select the most appropriate dose metric for establishing a point of departure in future risk assessments. A previous attempt to evaluate dose response for the effects of Mn in experimental animals [71] relied on estimated cumulative intake of Mn as the only measure for comparison across studies with different doses, durations, and exposure routes. Alternative toxicologically relevant dose metrics, including estimated peak concentration, average concentration, and cumulative dose (i.e., AUC) during the Mn exposure period could be estimated using a PBPK model known to accurately account for dose dependencies of Mn distribution in the monkey for combined inhalation and dietary exposures. A large nonhuman primate response literature exists for analysis, including exposures by inhalation, oral, intraperitoneal, and subcutaneous dose routes, and spanned durations up to 2 years [71]. This type of analysis using PBPK models is currently underway and will make it possible to provide a consistent description of the dose response relationship for the effects of Mn independent of exposure route.

Finally, PBPK models may be used in an alternative dosimetric-based risk assessment strategy for essential elements considering dietary intake, natural tissue background levels, and dietary and population variability. An upper safe exposure value could be based on an air concentration that changes brain tissue levels by no more than some fraction of the normal variability within a healthy population [7, 72]. The relationship between exposure levels and target-tissue levels would be determined by the use of PBPK models, which would account for the existence of the dose-dependent transition (i.e., threshold level) for accumulation. This methodology is inherently conservative with respect to neurological outcome, as the air guideline would be set to prevent only tissue accumulation. Potentially sensitive subpopulations as described in the scenarios here can be quantitatively taken into account with PBPK modeling instead of the application of UFs as described in the scenarios here. Another key advantage of a pharmacokinetic approach for risk assessment is that it is not reliant upon existing occupational studies, which have limitations with respect to exposure assessment, evaluation of adverse effects, and establishing causation (reviewed in [30]), to establish a point of departure [72]. Similar PBPK model-based dosimetry approaches should also be considered for risk assessments with other essential metals, such as copper and zinc. However, the development of a comprehensive PBPK model for any essential element depends on the availability of a sufficiently diverse and robust data set to enable model construction and validation. These data now exist for Mn, due in large part to the Alternative Tier 2 testing program for MMT [5].

6. Conclusions

The development of PBPK models facilitates more rigorous quantitative analyses of the available pharmacokinetic data and allows the comparison and consideration of dose to target tissue in risk assessment decisions. While PBPK modeling for many exogenous compounds has become routine, there are significantly more challenges in understanding the full set of biological factors that control uptake, distribution, and clearance of manganese and other essential nutrients that exert toxicity at high doses. An overarching goal of our modeling efforts was to evaluate situations that may lead to increased brain accumulation due to altered manganese regulation in healthy and potentially susceptible human populations. These subpopulations, identified as part of the Alternative Tier 2 testing program for MMT, include adult males, females, the aged, fetuses, neonates, and pregnant women, as well as those with high or low dietary manganese intake. Pharmacokinetic CSAFs were calculated to extrapolate from adult males, which are the typical subjects evaluated in occupational manganese studies, to these other life stages. These values were all ≤ 1, indicating that no pharmacokinetic adjustment is needed

to account for these populations. Regarding duration of exposure, a CSAF of 1 to 1.1 is calculated depending on the inhalation concentration once exposure levels increase above the threshold for tissue accumulation (i.e., 0.001–0.01 ug/m^3). In addition, while diseased individuals are not typically included in the extrapolations done in typical health risk assessments of environmental exposure, we have now extended the simulations to include those with moderate to severe hepatobiliary insufficiency to represent a population at a higher risk of manganese effects. The simulations suggest that an impaired individual may have elevated brain manganese concentrations regardless of manganese inhalation levels, and typical environmental levels do not increase this burden. At higher exposure levels, a CSAF of 1.25 is derived for the extremely sensitive subgroup. In total, the pharmacokinetic CSAFs developed here are less than the pharmacokinetic portion of the typical UF of 10 for human variability incorporated in current risk assessments of ambient manganese exposure. Future efforts can refine the scenarios presented here in humans, examine the effect of iron homeostasis, and evaluate the effects of particle size and solubility, including manganese nanoparticles.

A second outcome of these efforts is the increased confidence in the quantitative predictions of elevated manganese levels that might serve as a basis for a dosimetry-based risk assessment. An underlying assumption to this risk assessment approach is that elevated brain manganese concentration is a prerequisite for the development of manganese neurotoxicity. From a risk assessor's perspective, an upper safe exposure value could be based on an air concentration that changes brain tissue levels by no more than some fraction of the normal variability within a population [7, 72]. While some data gaps still exist regarding the biology of manganese transport and storage, the models described in this manuscript capture the main dose-dependent characteristics of manganese disposition. Using a Monte Carlo analysis to simulate population variability on target tissue manganese levels, modeling simulations indicate that air manganese concentrations of 0.001–0.01 mg/m^3 are required to begin to influence natural background tissue concentrations in adult males, which are the most sensitive subgroup regarding manganese tissue accumulation currently examined. With the forthcoming evaluation of monkey studies of Mn toxicity using the model to assess dosimetry and with applications to human datasets, the current PBPK model should be an important component of future tissue-dose-based approaches for Mn risk assessment.

In summary, data collection efforts associated with the Alternative Tier 2 testing program for MMT over the past 10 to 15 years on tissue Mn after inhalation exposures at different dietary levels and associated PBPK modeling have greatly improved understanding of the integration of multiple processes that collectively control Mn concentrations in various tissues. These efforts produced a multidose route, multispecies PBPK model that recapitulates dose-dependent brain accumulation on excessive exposures. The key biological characteristics required in fitting the model to the rat and monkey tissue time course data were finite capacities for tissue binding, slow dissociation of bound Mn, dose-dependent elimination from liver and dose-dependent uptake from the diet. As expected with control process for an essential metal with high-exposure toxicity, the physiological processes preserve body stores of Mn at low intakes accelerate excretion and reduce oral absorption at higher intakes. These dose-dependent processes are well known in a general manner, but not in terms of every biochemical detail. Biological determinants for tissue binding, membrane transport, Mn retention in enterocyte and sloughing of these cells into the intestinal lumen are under investigation. Further detail regarding these steps will refine specific parameters in the current PBPK model. One area ripe for inclusion in the next-generation PBPK model is increased knowledge of metal transporters [73–75]. More detailed dose-dependencies for these transporters would elaborate the asymmetric, dose-dependent uptake processes into brain in the present model [76]. However, the relative rate constants cannot vary significantly from the current ones since the simulations with the current model show very good correspondence with all available tissue time-course data. Thus, despite some gaps in understanding the underlying biology, the PBPK modeling with Mn shows clearly how similar processes work to control basal Mn levels to a remarkably common concentration across species and how they accomplish control of tissue Mn in the face of widely different dietary intake. Controls for Mn after inhalation include enhanced elimination but lack the ability to restrict absorption through the lung epithelium afforded by the gut epithelium for oral ingestion of the metal. Clearly, the current human PBPK model stands poised to assist in further integration of emerging knowledge into a more quantitative and biologically complete description of regulation of Mn in the body. Future work, potentially including uncertainty and sensitivity analyses, will examine the inherent limitations of modeling and scaling to help determine the precise level of confidence that can be ascribed to the current predictions of human globus pallidus manganese concentrations. However, in its present form, the human PBPK model for Mn already provides a solid foundation for improving risk assessment for this essential metal that also causes neurotoxicity in humans with higher dose exposures.

Acknowledgments

The invaluable contributions of Dr. Andy Nong in the development of the manganese PBPK models and the generation of Figure 6 are gratefully acknowledged. The authors would like to thank the members of the modeling Technical Advisory Panel, including Drs. Daniel Krewski (chair), Jeff Fisher, and Michele Medinsky for their helpful contributions and review of the manganese PBPK models. This publication and work are based on studies sponsored and funded by Afton Chemical Corporation in satisfaction of registration requirements arising under Section 211(a) and (b) of the Clean Air Act and corresponding regulations at 40 CFR Substance 79.50 et seq.

References

[1] M. Aschner, K. M. Erikson, and D. C. Dorman, "Manganese dosimetry: species differences and implications for neurotoxicity," *Critical Reviews in Toxicology*, vol. 35, no. 1, pp. 1–32, 2005.

[2] T. R. Guilarte, "Manganese and Parkinson's disease: a critical review and new findings," *Environmental Health Perspectives*, vol. 118, no. 8, pp. 1071–1080, 2010.

[3] Agency for Toxic Substances and Disease Registry (ATSDR), "Toxicological Profile for Manganese," U.S. Department of Health and Human Services, Atlanta, Ga, USA, 2008, http://www.atsdr.cdc.gov/toxprofiles/tp.asp?id=102&tid=23.

[4] U.S. Environmental Protection Agency, "Reevaluation of inhalation risks associated with methylcyclopentadienyl manganese tricarbonyl (MMT) in gasoline," EPA Office of Research and Development. EPA Air Docket A-93-26 No. II-A-12, 1994.

[5] D. C. Dorman, M. E. Andersen, and M. D. Taylor, "Update on a pharmacokinetic-centric Alternative Tier II Program for MMT. Part I. Program implementation and lessons learned," *Journal of Toxicology*, vol. 2012, Article ID 946742, 10 pages, 2012.

[6] W. K. Boyes, "Essentiality, toxicity, and uncertainty in the risk assessment of manganese," *Journal of Toxicology and Environmental Health A*, vol. 73, no. 2-3, pp. 159–165, 2010.

[7] M. E. Andersen, J. M. Gearhart, and H. J. Clewell, "Pharmacokinetic data needs to support risk assessments for inhaled and ingested manganese," *NeuroToxicology*, vol. 20, no. 2-3, pp. 161–172, 1999.

[8] D. C. Dorman, M. F. Struve, H. J. Clewell, and M. E. Andersen, "Application of pharmacokinetic data to the risk assessment of inhaled manganese," *NeuroToxicology*, vol. 27, no. 5, pp. 752–764, 2006.

[9] J. G. Teeguarden, D. C. Dorman, T. R. Covington, H. J. Clewell, and M. E. Andersen, "Pharmacokinetic modeling of manganese. I. Dose dependencies of uptake and elimination," *Journal of Toxicology and Environmental Health A*, vol. 70, no. 18, pp. 1493–1504, 2007.

[10] J. G. Teeguarden, D. C. Dorman, A. Nong, T. R. Covington, H. J. Clewell, and M. E. Andersen, "Pharmacokinetic modeling of manganese. II. Hepatic processing after ingestion and inhalation," *Journal of Toxicology and Environmental Health A*, vol. 70, no. 18, pp. 1505–1514, 2007.

[11] L. MacCalman, C. L. Tran, and E. Kuempel, "Development of a bio-mathematical model in rats to describe clearance, retention and translocation of inhaled nano particles throughout the body," *Journal of Physics: Conference Series*, vol. 151, Article ID 012028, 2009.

[12] J. G. Teeguarden, J. Gearhart, H. J. Clewell, T. R. Covington, A. Nong, and M. E. Andersen, "Pharmacokinetic modeling of manganese. III. Physiological approaches accounting for background and tracer kinetics," *Journal of Toxicology and Environmental Health A*, vol. 70, no. 18, pp. 1515–1526, 2007.

[13] A. Nong, J. G. Teeguarden, H. J. Clewell, D. C. Dorman, and M. E. Andersen, "Pharmacokinetic modeling of manganese in the rat IV: assessing factors that contribute to brain accumulation during inhalation exposure," *Journal of Toxicology and Environmental Health A*, vol. 71, no. 7, pp. 413–426, 2008.

[14] A. Nong, M. D. Taylor, H. J. Clewell, D. C. Dorman, and M. E. Andersen, "Manganese tissue dosimetry in rats and monkeys: accounting for dietary and inhaled Mn with physiologically based pharmacokinetic modeling," *Toxicological Sciences*, vol. 108, no. 1, pp. 22–34, 2009.

[15] M. Yoon, A. Nong, H. J. Clewell, M. D. Taylor, D. C. Dorman, and M. E. Andersen, "Lactational transfer of manganese in rats: predicting manganese tissue concentration in the dam and pups from inhalation exposure with a pharmacokinetic model," *Toxicological Sciences*, vol. 112, no. 1, pp. 23–43, 2009.

[16] M. Yoon, A. Nong, H. J. Clewell, M. D. Taylor, D. C. Dorman, and M. E. Andersen, "Evaluating placental transfer and tissue concentrations of manganese in the pregnant rat and fetuses after inhalation exposures with a PBPK model," *Toxicological Sciences*, vol. 112, no. 1, pp. 44–58, 2009.

[17] S. Anjilvel and B. Asgharian, "A multiple-path model of particle deposition in the rat lung," *Fundamental and Applied Toxicology*, vol. 28, no. 1, pp. 41–50, 1995.

[18] J. D. Schroeter, J. S. Kimbell, E. A. Gross et al., "Application of physiological computational fluid dynamics models to predict interspecies nasal dosimetry of inhaled acrolein," *Inhalation Toxicology*, vol. 20, no. 3, pp. 227–243, 2008.

[19] J. D. Schroeter, A. Nong, M. Yoon et al., "Analysis of manganese tracer kinetics and target tissue dosimetry in monkeys and humans with multi-route physiologically based pharmacokinetic models," *Toxicological Sciences*, vol. 120, no. 2, pp. 481–498, 2011.

[20] M. Yoon, J. D. Schroeter, A. Nong et al., "Physiologically based pharmacokinetic modeling of fetal and neonatal manganese exposure in humans: describing manganese homeostasis during development," *Toxicological Sciences*, vol. 122, no. 2, pp. 297–316, 2011.

[21] D. C. Dorman, M. F. Struve, M. W. Marshall, C. U. Parkinson, R. A. James, and B. A. Wong, "Tissue manganese concentrations in young male rhesus monkeys following subchronic manganese sulfate inhalation," *Toxicological Sciences*, vol. 92, no. 1, pp. 201–210, 2006.

[22] T. Nagase, Y. Fukuchi, S. Teramoto, T. Matsuse, and H. Orimo, "Mechanical interdependence in relation to age: effects of lung volume on airway resistance in rats," *Journal of Applied Physiology*, vol. 77, no. 3, pp. 1172–1177, 1994.

[23] P. H. Saldiva, M. P. Caldeira, and W. A. Zin, "Respiratory mechanics in the aging rat," *Brazilian Journal of Medical and Biological Research*, vol. 21, no. 4, pp. 863–868, 1988.

[24] J. L. Aschner and M. Aschner, "Nutritional aspects of manganese homeostasis," *Molecular Aspects of Medicine*, vol. 26, no. 4-5, pp. 353–362, 2005.

[25] H. J. Clewell III, G. A. Lawrence, D. B. Calne, and K. S. Crump, "Determination of an occupational exposure guideline for manganese using the benchmark method," *Risk Analysis*, vol. 23, no. 5, pp. 1031–1046, 2003.

[26] U.S. Environmental Protection Agency (USEPA), "Integrated Risk Information System (IRIS) Manganese (CASRN 7439-96-5) Reference Concentration for Chronic Inhalation Exposure (RfC)," 1993, http://www.epa.gov/iris/subst/0373.htm.

[27] M. E. Meek, A. Renwick, E. Ohanian et al., "Guidelines for application of chemical-specific adjustment factors in dose/concentration-response assessment," *Toxicology*, vol. 181-182, pp. 115–120, 2002.

[28] U.S. Environmental Protection Agency Office of the Science Advisor, "Guidance for Applying Quantitative Data to Develop Data-Derived Extrapolation Factors for Interspecies and Intraspecies Extrapolation," 2011, http://www.epa.gov/raf/DDEF/index.htm.

[29] M. S. Desole, G. Esposito, R. Migheli et al., "Cellular defence mechanisms in the striatum of young and aged rats subchronically exposed to manganese," *Neuropharmacology*, vol. 34, no. 3, pp. 289–295, 1995.

[30] A. B. Santamaria, C. A. Cushing, J. M. Antonini, B. L. Finley, and F. S. Mowat, "State-of-the-science review: does manganese exposure during welding pose a neurological risk?" *Journal of Toxicology and Environmental Health B*, vol. 10, no. 6, pp. 417–465, 2007.

[31] D. C. Dorman, B. E. McManus, M. W. Marshall, R. A. James, and M. F. Struve, "Old age and gender influence the pharmacokinetics of inhaled manganese sulfate and manganese phosphate in rats," *Toxicology and Applied Pharmacology*, vol. 197, no. 2, pp. 113–124, 2004.

[32] D. L. Schmucker, "Aging and the liver: an update," *Journals of Gerontology A*, vol. 53, no. 5, pp. B315–B320, 1998.

[33] S. O. Ross and C. E. Forsmark, "Pancreatic and biliary disorders in the elderly," *Gastroenterology Clinics of North America*, vol. 30, no. 2, pp. 531–545, 2001.

[34] L. Wang, F. H. Y. Green, S. M. Smiley-Jewell, and K. E. Pinkerton, "Susceptibility of the aging lung to environmental injury," *Seminars in Respiratory and Critical Care Medicine*, vol. 31, no. 5, pp. 539–553, 2010.

[35] A. Bhutto and J. E. Morley, "The clinical significance of gastrointestinal changes with aging," *Current Opinion in Clinical Nutrition and Metabolic Care*, vol. 11, no. 5, pp. 651–660, 2008.

[36] J. A. Menezes-Filho, M. Bouchard, P. De, and J. C. Moreira, "Manganese exposure and the neuropsychological effect on children and adolescents: a review," *Revista Panamericana de Salud Publica*, vol. 26, no. 6, pp. 541–548, 2009.

[37] B. S. Winder, A. G. Salmon, and M. A. Marty, "Inhalation of an essential metal: development of reference exposure levels for manganese," *Regulatory Toxicology and Pharmacology*, vol. 57, no. 2-3, pp. 195–199, 2010.

[38] M. Aschner, "Manganese: Brain transport and emerging research needs," *Environmental Health Perspectives*, vol. 108, no. 3, pp. 429–432, 2000.

[39] C. Rose, R. F. Butterworth, J. Zayed et al., "Manganese deposition in basal ganglia structures results from both portal-systemic shunting and liver dysfunction," *Gastroenterology*, vol. 117, no. 3, pp. 640–644, 1999.

[40] L. Annet, R. Materne, E. Danse, J. Jamart, Y. Horsmans, and B. E. Van Beers, "Hepatic flow parameters measured with MR imaging and Doppler US: correlations with degree of cirrhosis and portal hypertension," *Radiology*, vol. 229, no. 2, pp. 409–414, 2003.

[41] J. E. Restrepo and W. D. Warren, "Total liver blood flow after portacaval shunts, hepatic artery ligation and 70 per cent hepatectomy," *Annals of surgery*, vol. 156, pp. 719–726, 1962.

[42] D. R. Hunt, "Changes in liver flow with development of biliary obstruction in the rat," *Australian and New Zealand Journal of Surgery*, vol. 49, no. 6, pp. 733–737, 1979.

[43] M. H. F. El-Shabrawi, M. El-Raziky, M. Sheiba et al., "Value of duplex doppler ultrasonography in non-invasive assessment of children with chronic liver disease," *World Journal of Gastroenterology*, vol. 16, no. 48, pp. 6139–6144, 2010.

[44] M. Trauner, P. J. Meier, and J. L. Boyer, "Molecular regulation of hepatocellular transport systems in cholestasis," *Journal of Hepatology*, vol. 31, no. 1, pp. 165–178, 1999.

[45] E. A. Rodriguez-Garay, C. Larocca, G. Pisani, M. Del Luján Alvarez, and G. P. Rodriguez, "Adaptive hepatic changes in mild stenosis of the common bile duct in the rat," *Research in Experimental Medicine*, vol. 198, no. 6, pp. 307–323, 1999.

[46] J. B. Das, I. L. Uzoaru, and G. G. Ansari, "Biliary lithocholate and cholestasis during and after total parenteral nutrition: an experimental study," *Proceedings of the Society for Experimental Biology and Medicine*, vol. 210, no. 3, pp. 253–259, 1995.

[47] M. B. Reddy, R. S. H. Yang, M. E. Andersen, and H. J. Clewell III, *Physiologically Based Pharmacokinetic Modeling: Science and Applications*, Wiley, Hoboken, NJ, USA, 2005.

[48] Institute of Medicine (IOM) The National Academy of Sciences, *Dietary Reference Intakes for Vitamin A, Vitamin K, Arsenic, Boron, Chromium, Copper, Iodine, Iron, Manganese, Molybdenum, Nickel, Silicon, Vanadium, and Zinc*, National Academy Press, Washington, DC, USA, 2001.

[49] C. E. Hack, T. R. Covington, G. Lawrence et al., "A pharmacokinetic model of the intracellular dosimetry of inhaled nickel," *Journal of Toxicology and Environmental Health A*, vol. 70, no. 5, pp. 445–464, 2007.

[50] P. S. Price, R. B. Conolly, C. F. Chaisson et al., "Modeling interindividual variation in physiological factors used in PBPK models of humans," *Critical Reviews in Toxicology*, vol. 33, no. 5, pp. 469–503, 2003.

[51] S. F. Clark, "Iron deficiency anemia," *Nutrition in Clinical Practice*, vol. 23, no. 2, pp. 128–141, 2008.

[52] K. M. Erikson, T. Syversen, E. Steinnes, and M. Aschner, "Globus pallidus: a target brain region for divalent metal accumulation associated with dietary iron deficiency," *Journal of Nutritional Biochemistry*, vol. 15, no. 6, pp. 335–341, 2004.

[53] V. A. Fitsanakis, N. Zhang, M. J. Avison, K. M. Erikson, J. C. Gore, and M. Aschner, "Changes in dietary iron exacerbate regional brain manganese accumulation as determined by magnetic resonance imaging," *Toxicological Sciences*, vol. 120, no. 1, pp. 146–153, 2011.

[54] J. D. Park, K. Y. Kim, D. W. Kim et al., "Tissue distribution of manganese in iron-sufficient or iron-deficient rats after stainless steel welding-fume exposure," *Inhalation Toxicology*, vol. 19, no. 6-7, pp. 563–572, 2007.

[55] K. M. Erikson and M. Aschner, "Increased manganese uptake by primary astrocyte cultures with altered iron status is mediated primarily by divalent metal transporter," *NeuroToxicology*, vol. 27, no. 1, pp. 125–130, 2006.

[56] B. B. Williams, G. F. Kwakye, M. Wegrzynowicz et al., "Altered manganese homeostasis and manganese toxicity in a huntington's disease striatal cell model are not explained by defects in the iron transport system," *Toxicological Sciences*, vol. 117, no. 1, pp. 169–179, 2010.

[57] R. S. H. Yang, L. W. Chang, C. S. Yang, and P. Lin, "Pharmacokinetics and physiologically-based pharmacokinetic modeling of nanoparticles," *Journal of Nanoscience and Nanotechnology*, vol. 10, no. 12, pp. 8482–8490, 2010.

[58] Y. S. Cheng, H. C. Yeh, R. A. Guilmette, S. Q. Simpson, K. H. Cheng, and D. L. Swift, "Nasal deposition of ultrafine particles in human volunteers and its relationship to airway geometry," *Aerosol Science and Technology*, vol. 25, no. 3, pp. 274–291, 1996.

[59] M. Simkó and M. O. Mattsson, "Risks from accidental exposures to engineered nanoparticles and neurological health effects: a critical review," *Particle and Fibre Toxicology*, vol. 7, article no. 42, 2010.

[60] W. Yang, J. I. Peters, and R. O. Williams, "Inhaled nanoparticles—a current review," *International Journal of Pharmaceutics*, vol. 356, no. 1-2, pp. 239–247, 2008.

[61] W. I. Hagens, A. G. Oomen, W. H. de Jong, F. R. Cassee, and A. J. A. M. Sips, "What do we (need to) know about the kinetic properties of nanoparticles in the body?" *Regulatory Toxicology and Pharmacology*, vol. 49, no. 3, pp. 217–229, 2007.

[62] M. Li, K. T. Al-Jamal, K. Kostarelos, and J. Reineke, "Physiologically based pharmacokinetic modeling of nanoparticles," *ACS Nano*, vol. 4, no. 11, pp. 6303–6317, 2010.

[63] A. R. R. Péry, C. Brochot, P. H. M. Hoet, A. Nemmar, and F. Y. Bois, "Development of a physiologically based kinetic model for 99m-Technetium-labelled carbon nanoparticles inhaled by humans Human PBPK model for carbon nanoparticles," *Inhalation Toxicology*, vol. 21, no. 13, pp. 1099–1107, 2009.

[64] D. P. K. Lankveld, A. G. Oomen, P. Krystek et al., "The kinetics of the tissue distribution of silver nanoparticles of different sizes," *Biomaterials*, vol. 31, no. 32, pp. 8350–8361, 2010.

[65] G. Oszlánczi, T. Vezér, L. Sárközi, E. Horváth, Z. Kónya, and A. Papp, "Functional neurotoxicity of Mn-containing nanoparticles in rats," *Ecotoxicology and Environmental Safety*, vol. 73, no. 8, pp. 2004–2009, 2010.

[66] A. Elder, R. Gelein, V. Silva et al., "Translocation of inhaled ultrafine manganese oxide particles to the central nervous system," *Environmental Health Perspectives*, vol. 114, no. 8, pp. 1172–1178, 2006.

[67] T. L. Leavens, D. Rao, M. E. Andersen, and D. C. Dorman, "Evaluating transport of manganese from olfactory mucosa to striatum by pharmacokinetic modeling," *Toxicological Sciences*, vol. 97, no. 2, pp. 265–278, 2007.

[68] D. C. Dorman, M. F. Struve, B. A. Wong, J. A. Dye, and I. D. Robertson, "Correlation of brain magnetic resonance imaging changes with pallidal manganese concentrations in rhesus monkeys following subchronic manganese inhalation," *Toxicological Sciences*, vol. 92, no. 1, pp. 219–227, 2006.

[69] D. Vitarella, O. Moss, and D. C. Dorman, "Pulmonary clearance of manganese phosphate, manganese sulfate, and manganese tetraoxide by CD rats following intratracheal instillation," *Inhalation Toxicology*, vol. 12, no. 10, pp. 941–957, 2000.

[70] S. M. Hussain, A. K. Javorina, A. M. Schrand, H. M. H. M. Duhart, S. F. Ali, and J. J. Schlager, "The interaction of manganese nanoparticles with PC-12 cells induces dopamine depletion," *Toxicological Sciences*, vol. 92, no. 2, pp. 456–463, 2006.

[71] R. Gwiazda, R. Lucchini, and D. Smith, "Adequacy and consistency of animal studies to evaluate the neurotoxicity of chronic low-level manganese exposure in humans," *Journal of Toxicology and Environmental Health A*, vol. 70, no. 7, pp. 594–605, 2007.

[72] M. E. Andersen, D. C. Dorman, H. J. Clewell III, M. D. Taylor, and A. Nong, "Multi-dose-route, Multi-Species pharmacokinetic models for manganese and their use in risk assessment," *Journal of Toxicology and Environmental Health A*, vol. 73, no. 2-3, pp. 217–234, 2010.

[73] M. Lu and D. Fu, "Structure of the zinc transporter YiiP," *Science*, vol. 317, no. 5845, pp. 1746–1748, 2007.

[74] B. R. Chandra, M. Yogavel, and A. Sharma, "Structural analysis of ABC-family periplasmic zinc binding protein provides new insights into mechanism of ligand uptake and release," *Journal of Molecular Biology*, vol. 367, no. 4, pp. 970–982, 2007.

[75] R. J. McMahon and R. J. Cousins, "Mammalian zinc transporters," *Journal of Nutrition*, vol. 128, no. 4, pp. 667–670, 1998.

[76] D. H. Nies, "How cells control zinc homeostasis," *Science*, vol. 317, no. 5845, pp. 1695–1696, 2007.

Hindawi Publishing Corporation
Journal of Toxicology
Volume 2012, Article ID 959070, 7 pages
doi:10.1155/2012/959070

Research Article

Short Communication: Is Ethanol-Based Hand Sanitizer Involved in Acute Pancreatitis after Excessive Disinfection?—An Evaluation with the Use of PBPK Model

Céline Huynh-Delerme,[1] Catherine Artigou,[1] Laurent Bodin,[2] Robert Tardif,[3] Ginette Charest-Tardif,[3] Cécile Verdier,[1] Nessryne Sater,[1] Mostafa Ould-Elhkim,[1] and Catherine Desmares[1]

[1] *Department of Cosmetic, Biocide, and Tatoo Products, French Health Products Safety Agency (Afssaps), 143-147 Boulevard Anatole France, 93285 Saint-Denis Cedex, France*
[2] *Department of Risk Assessment, French Agency for Food, Environmental and Occupational Health Safety (Anses), 24-31 Avenue du Général Leclerc, 94701 Maisons-Alfort Cedex, France*
[3] *Département de Santé Environnementale et Santé au Travail, Faculté de Médecine, Université de Montréal, Montréal, QC, Canada 3J7 H3C*

Correspondence should be addressed to Mostafa Ould-Elhkim, mostafa.ouldelhkim@afssaps.sante.fr

Received 20 October 2011; Accepted 6 February 2012

Academic Editor: Marina V. Evans

An occupational physician reported to the French Health Products Safety Agency (Afssaps) a case of adverse effect of acute pancreatitis (AP) in a teaching nurse, after multiple demonstrations with ethanol-based hand sanitizers (EBHSs) used in a classroom with defective mechanical ventilation. It was suggested by the occupational physician that the exposure to ethanol may have produced a significant blood ethanol concentration and subsequently the AP. In order to verify if the confinement situation due to defective mechanical ventilation could increase the systemic exposure to ethanol *via* inhalation route, a physiologically based pharmacokinetic (PBPK) modeling was used to predict ethanol blood levels. Under the worst case scenario, the simulation by PBPK modeling showed that the maximum blood ethanol concentration which can be predicted of 5.9 mg/l is of the same order of magnitude to endogenous ethanol concentration (mean = 1.1 mg/L; median = 0.4 mg/L; range = 0–35 mg/L) in nondrinker humans (Al-Awadhi et al., 2004). The present study does not support the likelihood that EBHS leads to an increase in systemic ethanol concentration high enough to provoke an acute pancreatitis.

1. Introduction

Ethanol in hand sanitizing gel is widely used not only in health care settings but also in other areas that involve hand hygiene. Ethanol is considered an effective substance against a large spectrum of microorganisms which can linger on the skin. Health care systems and infection control organizations have begun advocating the routine use of hand sanitizing gel, as health care professionals may apply alcohol-based hand sanitizers more than 50 times a day, if using these products prior to and just following each patient.

However, as alcohol drinking is associated with an increased risk of a number of cancers, birth defects, or other health disease disorders like pancreatitis, there is no common consensus on the safety of ethanol-based hand sanitizers (EBHSs) in the literature. In its recent opinion, the French Health Products Safety Agency (Afssaps) considered that the use of ethanol as hand disinfectant is safe, taking into consideration the low dermal absorption even after excessive disinfection [1]. Although this absence of risk is established, the Afssaps recommended to consumers to privilege the washing hands with soap and water due to its sufficient microbiological efficacy. Ethanol hand sanitizers should rather be used when soap and water hand washing is not available [2].

In this context, an occupational physician reported to the French Health Products Safety Agency a case of acute pancreatitis (AP) in a 46-year-old teaching nurse. She has been

working in a nursing school for seven years. This adverse effect appeared after demonstrations using ethanol-based hand sanitizers for two successive days in a classroom under conditions of defective mechanical ventilation. Knowing the relationship between excessive alcohol consumption and risk factor associated with either acute or chronic pancreatitis, the occupational physician suggested that the exposure to ethanol by hand skin and also mainly *via* inhalation route may have led to a significant systemic ethanol concentration increase and consequently to the AP symptom.

The reconstitution of the events showed the following.

(i) A two successive-day demonstration (TSDD) with EBHS was carried out in mid-September (2009) without any complaint.

(ii) However, three days after this TSDD, the trainer complained of headaches after having stayed 30 minutes in the office opened on the classroom, in which the demonstration has been carried out.

(iii) Six days after the TSDD, the trainer, seven students, and the manager of local "committee for health, safety and working conditions" suffered from malaise and headache in the same office. The intervention of the firemen excluded possible carbon monoxide intoxication but they noted a strong smell of alcohol. The technical agent who was called in highlighted the ventilation defect.

(iv) Seven days after the TSDD, the trainer had headaches and dizziness again after having stayed two hours in the same premises without any ethanol handling.

(v) She did not work the ten following days.

(vi) Seventeen days after the TSDD, while at home, she felt severe epigastric pain radiating to the low dorsal after having drunk a glass of red wine.

(vii) Eighteen days after the TSDD, based on the clinical symptoms observed the day before and the biochemical analysis (lipase at 1174 IU/L (range 23–300 IU/L) and an amylase at 142 IU/L (range 25–125 IU/L)), it was suggested an acute pancreatitis diagnosis.

(viii) Thirty days after the TSDD, the biochemical analysis performed again was normal (lipase 187 IU/L and amylase 50 IU/L). Transaminase, aspartate aminotransferase, and alanine aminotransferase were also normal. In the end, the abdominal scan performed was normal.

On the other hand, the medical history shows that the teaching nurse presented a hyperthyroidism treated in early 2009 by NeoMercazole and Levothyrox for 3 months. At that time, lipase and amylase were normal. This treatment was stopped at least one month before the onset of the AP. She has been treated for hypertension with a chlorothiazidic diuretic, Esidrex, for 3 or 4 years. The diuretic was stopped about two months after the first event.

The patient did not take oral contraceptives and she drank alcohol without abuse.

This lead to the question as whether or not EBHS use could have resulted in significant blood ethanol concentration increase. This study was carried out firstly, to predict, by theoretical approach, ethanol concentration in the classroom air following EBHS use under defective ventilation; secondly, to estimate, using a physiologically based pharmacokinetic (PBPK) model, the blood ethanol concentration likely to be reached after ethanol inhalation in the classroom air.

2. Materials and Methods

2.1. Exposure Conditions

EBHS Used. The hand disinfectant contained ethanol at 700 mg/g (755 mL/L) in the presence of thickening, moisturizing and emollient agents, and water. It contained neither perfumes nor dyes. The potential implication of each product ingredient in the manifestation of pancreatitis was also checked.

Exposure. Training for auxiliary nurses was conducted for two successive days in the same classroom, 28 students and two trainers were in the classroom. The amount of product used for each friction was 3 mL; with a daily number of frictions per day equal to 3 per person. Thus, the total was 180 frictions (540 mL EBHS, i.e., 378 mL of ethanol) for two days.

Class Volume. The classroom volume alone was 116 m^3. It is opened to another handling room and office; thus, the total volume was 310 m^3. However, in order to simulate worst case conditions, the total exposure to EBHS of 540 mL for two days was considered only in 116 m^3.

2.2. Exposure Assessment. The air ethanol concentration was estimated using an American Industrial Hygiene Association (AIHA) software [4]. Assessments of exposure to indoor air pollutants usually employ spatially well-mixed models which assume homogeneous concentrations throughout a building or room. The theoretical approach used with AIHA software is based on the description of the spray and the substance behavior but also on the modeling of the ethanol concentrations occurring in homogenous, mixed rooms.

As mechanical ventilation was defective, 0.08 m^3/min considered as the worst scenario was retained.

Considering the number of frictions, the following scenario was considered: total rubbing hands equal to 180 frictions (3 times/30 persons/2 days) with EBHS, over a period of 48 hours interrupted by a night.

The ethanol atmospheric emission was calculated as follows: 30 rubbing hands (RH) at time 0 h, 30 RH at 3 h, and 30 RH at 6 h (for the first day), and 30 RH at 24 h, 30 RH at 27 h, and 30 RH at 30 h (for the second day), with 3 mL EBHS at 70% ethanol and a density mass of 0.8.

2.3. Blood Ethanol Calculation. Blood ethanol concentrations were predicted using a physiologically based pharmacokinetic (PBPK) model, the ACSLX software (Version

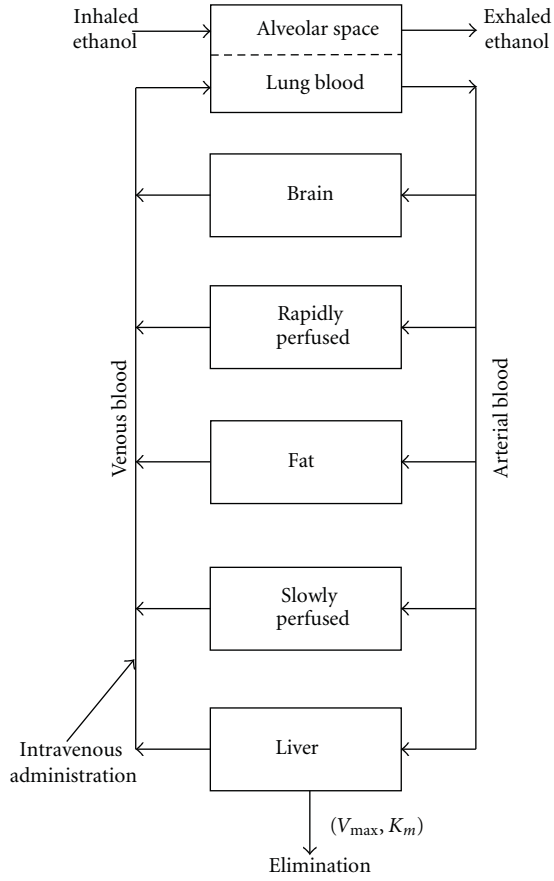

Figure 1: Schematic representation of the ethanol physiologically based pharmacokinetic model (PBPK) proposed by Pastino et al. [3].

3.0.1.6; AEgis Technologies Group, Inc.), which allows simulation of inhalation exposure to various air ethanol concentrations and prediction of its toxicokinetic behaviour [5].

The blood flow limited PBPK model for ethanol was previously developed for human by Schlouch and Tardif [6] and for rodent by Pastino et al. [3]. Compartments for the present model include liver, brain, fat, rapidly perfused tissue, slowly perfused tissue and blood. A schematic diagram of the PBPK model for ethanol inhalation is represented in Figure 1. Mass-balance equations were written describing the rate of change in ethanol concentration for each compartment.

The blood flows and tissue volumes for each compartment (Table 1) were obtained from the report prepared by the United States Environmental Protection Agency (US EPA) on "Physiological Parameter Values for PBPK Models" [7]. The ethanol partition coefficients for rats were determined by Pastino et al. [3].

The fractional uptake in the airways is reported to be mostly between 55 and 62% [3].

3. Results

3.1. Air Ethanol Concentrations Estimation. The air ethanol concentration was estimated using the AIHA software [4]. As mechanical ventilation was defective, several maximizing scenarios were used considering a low air change rate of 0.08 m^3/min (Figures 2(a) and 2(b)). In addition, it was also considered that for each simultaneous 30 frictions, an atmospheric ethanol emission of 50.4 g of ethanol was calculated, resulting in an atmospheric concentration of 0.43 g/m^3.

Changes over time for worst case scenario make it possible to predict the following peaks of exposure.

3.1.1. During the First Day. At time 0 (T_0), the atmospheric concentration after the first frictions was 0.43 g/m^3.

At T_{3h}, it was 0.81 g/m^3, coming from both the second frictions (0.43 g/m^3) and the residual concentration of 0.38 g/m^3 from the first frictions at T_0.

At T_{6h}, the atmospheric concentration was 1.15 g/m^3 corresponding to the sum of the atmospheric concentration resulting from the frictions at T_{6h} (0.43 g/m^3) and the residual concentration of 0.72 g/m^3 present in the atmosphere after the preceding frictions.

3.1.2. During the Second Day. At T_{0h}, the atmospheric concentration was 0.97 g/m^3 (sum of the frictions at T_{0h} (0.43 g/m^3) and the remaining residual concentration from all the night of 0.54 g/m^3). At T_{3h}, the atmospheric concentration was 1.23 g/m^3 (sum of frictions at T_{3h} (0.43 g/m^3) and

Table 1: Model parameters for the ethanol PBPK.

Physiological parameters of the model PBPK for ethanol	
Body weight	70
Cardiac output (L/h/kg)$^{0.75}$	18
Alveolar ventilation (L/h/kg)$^{0.75}$	18
Absorbed fraction	0.62
Fraction of cardiac output to each compartment	
Fat	0.05
Liver	0.25
Rapidly perfused	0.39
Slowly perfused	0.19
Brain	0.12
Total	1.00
Fraction of body volume compartments	
Fat	0.213
Liver	0.0257
Rapidly perfused	0.0443
Slowly perfused	0.607
Brain	0.02
Total	0.91
Physicochemical and metabolic parameters	
Partition coefficients	
Blood: air	2280
Fat: air	226
Liver: air	1730
Rapidly perfused: air	2030
Slowly perfused: air	1710
Brain: air	1870
Liver metabolic parameter	
Metabolism rate (mg/h/kg)$^{0.75}$	359.5
Affinity constant (mg/L)	82.1

the residual concentration of 0.8 g/m^3). At T_{6h}, the atmospheric concentration was 1.58 g/m^3 (sum of 0.43 g/m^3 and 1.15 g/m^3, as residual atmospheric concentration).

In conclusion, these results made possible to predict the atmospheric ethanol mean concentration after two successive days: 408 mg/m^3 (time 0–3 h), 768 mg/m^3 (time 3–6 h), 1108 mg/m^3 (time 6–8 h) for the first day and 924 mg/m^3 (time 0–3 h), 1224 mg/m^3 (time 3–6 h), and 1518 mg/m^3 (time 6–8 h) for the second day (Figures 2(a) and 2(b)). It was considered a total of 378 mL of ethanol (i.e., 180 frictions of 3 mL or 540 mL EBHS at 70% ethanol) in a classroom volume of 116 m^3, under the worst case scenario of a defective ventilation giving a low air change rate of 0.08 m^3/min.

3.2. Blood Ethanol Concentration Calculation. Blood ethanol concentration induced by these exposures is predicted using a physiologically based toxicokinetic model to simulate inhalation route exposure to various airborne concentrations of ethanol and to predict its toxicokinetic behaviour [5].

PBPK modeling of ethanol takes into account physicochemical and biochemical parameters to predict blood ethanol over time following exposure. This model was developed by Schlouch and Tardif [6].

In our study, the maximum blood ethanol concentration was estimated to reach a plateau at 5.9 mg/L when breathing air with an ethanol mean concentration of 924 mg/m^3 (time 0–3 h), 1224 mg/m^3 (time 3–6 h), and 1518 mg/m^3 (time 6–8 h) (the maximal occupational exposure concentration) (Table 2).

4. Discussion

The absorbed ethanol is found in the blood in variable proportions, depending on the route of exposure. Several epidemiological studies show that alcoholic beverages consumption increases the cancer risk in human [8]. Harmful effects on reproduction and development in the liver and in the central and peripheral nervous system have also been observed. These effects can be observed after ingestion of 12 g of ethanol per day (i.e., the equivalent of one glass of wine) and leading to a peak blood from 150 to 250 mg/L, which represents relatively high levels of blood ethanol concentration (ethanolaemia peak). In our study, the low elevation of blood ethanol concentration (5.9 mg/L) obtained by simulation in the patient, which remains within the limit values of endogenous blood ethanol concentration in nondrinker humans [9], does not seem to be a trigger of AP, on the basis of the current knowledge.

Several AP's cases reported in the literature are in relation with consumption of alcoholic beverages by oral route. High blood concentrations are more likely after drinking alcoholic beverages. The elimination rate is dependent on whether person is an alcoholic with an induced metabolism or not. The metabolite acetaldehyde is very reactive and may be responsible for some of the harmful effects of ethanol.

The AP causes are multiple and remain undetermined in 15 to 25% of cases [10]. In western countries, migration of gall stones in the biliary tract is the main cause (38%). In our study, the negativity of exploration by radiological scan does not confirm the role of gall stones. Alcohol abuse is the second leading cause (36%). The results of a meta-analysis published in 2009 [11] highlighted an exponential dose-response relationship between average volume of alcohol consumption and pancreatitis. Overall, the results indicate a nonlinear association between alcohol consumption and the relative risk of pancreatitis [11]. The risk curve between alcohol consumption and pancreatitis was relatively flat at low levels of alcohol consumption, and it markedly increased with increasing levels of consumption. It is nonexistent among low alcohol consumers (up to 2 drinks per day or 24 g of alcohol), occurring in individuals consuming 36 g alcohol per day and only becoming statistically significant for a daily consumption of 48 g of alcohol. Alcohol causes an AP in 10% of very excessive drinkers (more than 80 g alcohol per day). The drugs come in third place and are involved in about 5% of AP. There is no semiological criterion specific of a drug AP even if hydrochlorothiazide can cause acute pancreatitis, as it has been reported in the literature for this drug. In addition, many other causes have been described, of low frequency and some still discussed [12]: genetic predisposition,

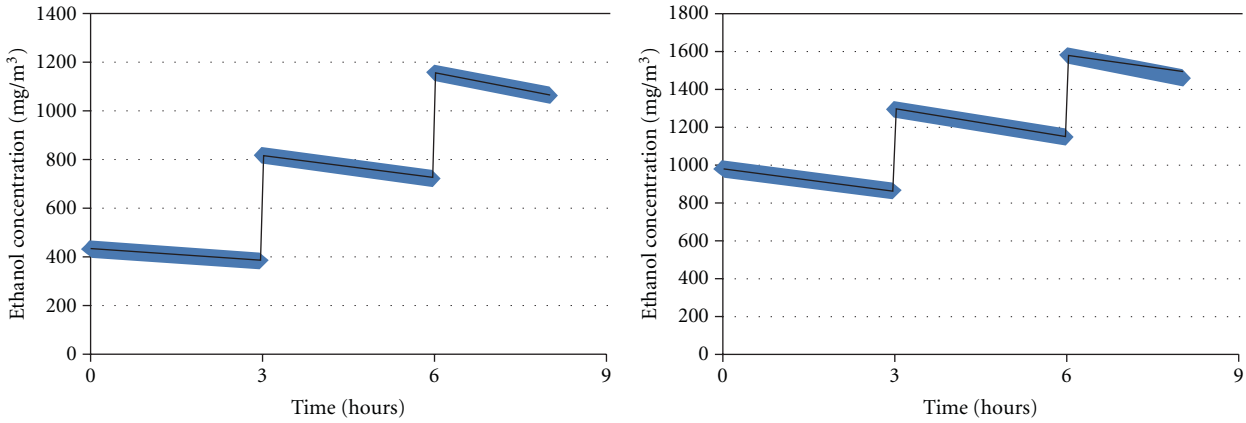

Figure 2: (a) Atmospheric ethanol concentration (day 1). By using the AIHA software, the ethanol atmospheric emission was calculated as follows: 30 rubbing hands (RH) at time 0 h, 30 RH at 3 h and 30 RH at 6 h resulting in a mean ethanol atmospheric concentration of 408 mg/m^3 (time 0–3 h), 768 mg/m^3 (time 3–6 h), and 1108 mg/m^3 (time 6–8 h). (b) Atmospheric ethanol concentration (day 2). By using the AIHA software, the ethanol atmospheric emission was calculated as follows: 30 rubbing hands (RH) at time 0 h, 30 RH at 3 h, and 30 RH at 6 h resulting in a mean ethanol atmospheric concentration of 924 mg/m^3 (time 0–3 h), 1224 mg/m^3 (time 3–6 h), and 1518 mg/m^3 (time 6–8 h).

Table 2: Blood ethanol concentration predictions (BECPs) based on 8 h exposure average (mg/L). The BECP was calculated by using the PBPK model of ethanol with the following exposure condition previously estimated. *For the day 1*, the atmospheric ethanol concentration was 408 mg/m^3 (time 0–3 h), 768 mg/m^3 (time 3–6 h), and 1108 mg/m^3 (time 6–8 h). *For the day 2*, the atmospheric ethanol concentration was 924 mg/m^3 (time 0–3 h), 1224 mg/m^3 (time 3–6 h), and 1518 mg/m^3 (time 6–8 h).

		T (h)	BECP
Blood ethanol concentration (mg/L)	Day 1	0	0.00
		8	4.21
	Day 2	24	0.00
		32	5.9

congenital malformation of the pancreas, tumours, infection, hypertriglyceridemia, hypercalcemia, pregnancy, and so on.

In the current state of knowledge, the side effects of ethanol, related to chronic exposure by dermal absorption or inhalation route, have not sufficiently been documented in humans. A retrospective study in connection with the dermal use of alcohol-based hand sanitizers conducted by the French Poison Control Centers in 2009 reported that side effects listed are mostly related to misuse [13]. In addition, apart from this case, no other AP has been reported in link with the use of ethanol as EBHS.

The likelihood that dermal exposure increases plasmatic concentration was excluded right away for the reason that our earlier risk assessment and other several studies showed a very low to negligible dermal absorption, even after intensive use of EBHS. It is generally allowed that, on nondamaged skin, about 1% of the dose of ethanol initially placed on the surface actually penetrates the skin barrier. The amount is thus negligible when compared to pulmonary absorption, which is estimated at 60% [14, 15].

Indeed, in the literature, several studies have been conducted to explore the dermal absorption issue [16–19] and concluded that ethanol skin absorption does not increase blood ethanol concentration significantly. In the Afssaps's risk assessment opinion published in 2009 [1], all these data relative to the exposure by dermal route was analyzed and the conclusion retained put forward that the low or negligible absorption allows to conclude for an absence of the risk for the consumer even after an excessive use.

Inhalation of ethanol vapors at normal atmospheric concentrations will thus not result in any significant blood concentration [20]. The metabolic elimination of ethanol from the blood will in most cases exceed the uptake.

Lester and Greenberg [21] showed that inhalation of ethanol vapor does not seem to cause any severe acute effects at ethanol concentrations below 10,000 mg/m^3. However, headache and cough have been reported after about 30 minutes of inhaling ethanol vapor at concentrations of 2600 and 3400 mg/m^3, respectively. When the concentration increases, the airways become irritated with resulting cough, lachrymation, and breathing difficulties [22].

In case ethanol vapor exposure, the manifestation of undesirable effects require that the ethanol reaches in one hand plasma and in the other hand target organ. The concentration in the plasma depends on the concentration in air, the exposure duration, the breathing rate, the absorption of ethanol across the lung, the basal metabolism, and also the elimination rate of ethanol.

In this study, the situation of confinement and exposure to ethanol by inhalation route showed that maximum blood ethanol amounted to 5.9 mg/L. The results are consistent with studies in the literature. Indeed, Campbell and Wilson [23] found after exposure to ethanol vapor concentration

of 1900 mg/m^3 in the air for 3 h a slight elevation of blood ethanol by repeated measurements at 0, 35, 60, 120, and 180 minutes limited to less than 2 mg/L. Miller et al. [19] conducted a study on five volunteers working at the hospital emergency department rubbing their hands 50 times in four hours using a EBHS containing 62% ethanol. Blood ethanol remains below 0.5 mg/L. In addition, an estimation of blood ethanol by modeling in the Afsset's risk assessment report [20] showed that, after 42 frictions with a EBHS containing 80% ethanol, repeated 8 hours, it was estimated at 1.28 mg/L, within the range of endogenous blood ethanol concentration. Pendlington et al. [24] conducted three studies whose aim was to determine the rate of evaporation and absorption of ethanol and to estimate the dermal penetration of ethanol *in vitro* on pig skin and *in vivo* in humans in 16 volunteers using an aerosol spray. The results of these studies indicate a short half-life of evaporation (about 11 seconds) and skin absorption strongly increased by the occlusion. The *in vitro* study does not determine a dermal absorption rate. Thus, the results in humans have shown no detectable blood ethanol at the limit of detection of 9 mg/L and this after evaporation of a quantity of up to 17.28 g of an aerosol constituted of 44% ethanol.

In other hand, malaise and headache recorded of 9 persons at day six after the two successive-day demonstration remained unclear, one of the possible explanations is probably due to the symptoms collective type of discomfort related to the syndrome of chemical smell intolerance [25]. This concerns subjects exposed to low concentrations of aerial contaminants, with various symptoms suggesting the entanglement of objective reasons not well understood with psychological subjective factors. Based on low exposure (atmospheric and/or systemic) concentration to ethanol predicted, it is not possible to relate rationally the effect observed with EBHS uses.

Using a physiologically based toxicokinetic model to simulate inhalation route in this study, the systemic concentration of 5.9 mg/mL predicted is not easily related to the acute pancreatitis reported. A study conducted in 1557 nondrinkers volunteers showed that the endogenous blood ethanol is related to the synthesis of ethanol by microorganisms in the digestive tract which is between 0 and 35.2 mg/L, with a mean of 1.1 mg/L and median of 0.4 mg/L. The endogenous ethanol seems produced by yeast fermentation and other intestinal microorganisms and/or restored by food. Indeed, for example, certain fruit juices can contain up to 3 g ethanol/L [26] and an apple juice 2 g/L. Recall that a glass of alcohol (10–12 g of ethanol) leads to a peak blood from 150 to 250 mg/L and drunkenness can appear only from 1.5 g/L of ethanol [27, 28].

Finally, in general family and personal history, clinical symptoms, biochemical analysis, and/or radiological tests as scan identify the majority of aetiologies of AP. In our study, the Afssaps suggested further investigations in the absence of track on the origin of the AP. Thus, the etiological investigation is worth pursuing in order to properly rule out a tumour origin.

5. Conclusion

Our study shows the ethanol exposure under the conditions of defective mechanical ventilation in the classroom resulted in a maximum blood ethanol concentration of 5.9 mg/L determined by PBPK modeling, which is considered in the same order of magnitude as the endogenous serum ethanol. According to Al-Awadhi et al. [9], the endogenous ethanol level could be reaching an average of 1.1 mg/L (0 to 35 mg/L) after absorption of ethanol synthesized by digestive tract microorganisms. As example, each glass of alcoholic beverage contains about 12 g of ethanol [28] and leads after oral absorption to a pick plasma ethanol concentration at about 250 mg/L.

Under the conditions of this study no relationship can be made between the exposure to EBHS and the increase of blood ethanol concentration being able to lead to the occurrence of the reported acute pancreatitis.

Acknowledgments

The authors gratefully acknowledge Dr. Cyril Vadrot for the reading of the disinfection part and Pr. Philippe Ruszniewski for suggestions on the pancreatitis aetiology.

References

[1] Afssaps, "Rapport de l'Agence française de sécurité sanitaire des produits de santé relatif à l'innocuité des produits hydro-alcooliques (PHA) à base d'éthanol utilisés pour la désinfection des mains à peau saine par le grand public dans le cadre de l'épidémie de la grippe A (H1N1)," 2009, http://www.afssaps.fr/Dossiers-thematiques/Pandemie-grippale/Les-produits-hydroalcooliques/(offset)/8.

[2] Afssaps, "Avis de l'agence française de sécurité sanitaire des produits de santé relatif à l'utilisation de désinfectants pour les mains à peau saine (produits hydroalcooliques; PHA) par le grand public, dans le cadre de l'épidémie de la grippe A (H1N1) v," 2009, http://www.afssaps.fr/var/afssaps_site/storage/original/application/61e214a666eb691596a04b75393bcb29.pdf.

[3] G. M. Pastino, B. Asgharian, K. Roberts, M. A. Medinsky, and J. A. Bond, "A comparison of physiologically based pharmacokinetic model predictions and experimental data for inhaled ethanol in male and female B6C3F1 mice, F344 rats, and humans," *Toxicology and Applied Pharmacology*, vol. 145, no. 1, pp. 147–157, 1997.

[4] American Industrial Hygiene Association software, http://www.aiha.org/insideaiha/volunteergroups/EASC/Pages/EASC-Topics.aspx.

[5] acsLX software, "Prediction of Physiogically-based pharmacokinetic model," http://www.aegistg.com/.

[6] E. Schlouch and R. Tardif, "Modélisation toxicocinétique de l'exposition à l'éthanol," *Université de Montréal. Présenté à Santé Canada*, pp. 1–35, 1999.

[7] US EPA, "Approaches for the Application of Physiologically Based Pharmacokinetic (PBPK) Models and Supporting Data in Risk Assessment," 2006.

[8] International Agency for Research on Cancer (IARC), "Attributable Causes of Cancer in France in the year 2000," pp. 1–177, 2007, http://www.iarc.fr/en/publications/pdfs-online/wrk/wrk3/CausesofCancerFrance2000.pdf.

[9] A. Al-Awadhi, I. A. Wasfi, F. Al Reyami, and Z. Al-Hatali, "Autobrewing revisited: endogenous concentrations of blood ethanol in residents of the United Arab Emirates," *Science and Justice*, vol. 44, no. 3, pp. 149–152, 2004.

[10] J. L. Frossard, M. L. Steer, and C. M. Pastor, "Acute pancreatitis," *The Lancet*, vol. 371, no. 9607, pp. 143–152, 2008.

[11] H. M. Irving, A. V. Samokhvalov, and J. Rehm, "Alcohol as a risk factor for pancreatitis. A systematic review and meta-analysis," *Journal of the Pancreas*, vol. 10, no. 4, pp. 387–392, 2009.

[12] A. S. Khan, S. U. Latif, and M. A. Eloubeidi, "Controversies in the etiologies of acute pancreatitis," *Journal of the Pancreas*, vol. 11, no. 6, pp. 545–552, 2010.

[13] CAPV and Centres Antipoison et de Toxicovigilance, "Produits hydroalcooliques destinés à l'usage cutané : étude rétrospective des cas d'intoxications recensés dans les CAPV en 2009," pp. 1–31, 2010, http://www.centres-antipoison.net/CCTV/Rapport_CCTV_PHA_VF_2010.

[14] Dutch Expert Committee on Occupational Standards, *Ethanol: Evaluation of the Health Effects from Occupational Exposure*, Gezondheidsraad, 2006.

[15] P. W. Kruhoffer, "Handling of inspired vaporized ethanol in the airways and lungs (with comments on forensic aspects)," *Forensic Science International*, vol. 21, no. 1, pp. 1–17, 1983.

[16] T. L. Brown, S. Gamon, P. Tester et al., "Can alcohol-based hand-rub solutions cause you to lose your driver's license? Comparative cutaneous absorption of various alcohols," *Antimicrobial Agents and Chemotherapy*, vol. 51, no. 3, pp. 1107–1108, 2007.

[17] S. Kinnula, T. Tapiainen, M. Renko, and M. Uhari, "Safety of alcohol hand gel use among children and personnel at a child day care center," *American Journal of Infection Control*, vol. 37, no. 4, pp. 318–321, 2009.

[18] A. Kramer, H. Below, N. Bieber et al., "Quantity of ethanol absorption after excessive hand disinfection using three commercially available hand rubs is minimal and below toxic levels for humans," *BMC Infectious Diseases*, vol. 7, article 117, 2007.

[19] M. A. Miller, A. Rosin, M. E. Levsky, M. M. Patel, T. J. D. Gregory, and C. S. Crystal, "Does the clinical use of ethanol-based hand sanitizer elevate blood alcohol levels? A prospective study," *American Journal of Emergency Medicine*, vol. 24, no. 7, pp. 815–817, 2006.

[20] Afsset, "L'éthanol en population professionnelle—evaluation des risques de l'éthanol en population professionnelle," pp. 1–336, 2010, http://www.afssa.fr/Documents/CHIM-Ra-Ethanol.

[21] D. Lester and L. A. Greenberg, "The inhalation of ethyl alcohol by man. I. Industrial hygiene and medicolegal aspects. II. Individuals treated with tetraethylthiuram disulfide," *Quarterly Journal of Studies on Alcohol*, vol. 12, no. 2, pp. 168–178, 1951.

[22] P. Andersson and K. Victorin, *Inhalation of Ethanol: Literature Survey and Risk Assessment*, Karolinska Institute, Stockholm, Sweden, 1996, IMM-rapport 3/96. Institutet for Miljomedicin (Institute of Environmental Medicine).

[23] L. Campbell and H. K. Wilson, "Blood alcohol concentrations following the inhalation of ethanol vapour under controlled conditions," *Journal of the Forensic Science Society*, vol. 26, no. 2, pp. 129–135, 1986.

[24] R. U. Pendlington, E. Whittle, J. A. Robinson, and D. Howes, "Fate of ethanol topically applied to skin," *Food and Chemical Toxicology*, vol. 39, no. 2, pp. 169–174, 2001.

[25] M. R. Cullen, "The worker with multiple chemical sensitivities: an overview," *Occupational Medicine*, vol. 2, no. 4, pp. 655–661, 1987.

[26] B. Windirsch, B. Brinkmann, and H. Taschan, "Alkoholgehalte ausgewählter Lebensmittel," *Lebensmittelchemie*, vol. 59, pp. 149–150, 2005.

[27] D. Lamiable, G. Hoizey, H. Marty, and R. Vistelle, "Intoxication aigue à l'éthanol," *Revue Francaise des Laboratoires*, vol. 2000, no. 323, pp. 27–30, 2000.

[28] International Agency for Research on Cancer (IARC), *Monographs on the Evaluation of Carcinogenic Risks to Humans*, vol. 44, World Health Organization, Lyon, France, 1988.

Hindawi Publishing Corporation
Journal of Toxicology
Volume 2012, Article ID 760281, 18 pages
doi:10.1155/2012/760281

Research Article

Reconstruction of Exposure to *m*-Xylene from Human Biomonitoring Data Using PBPK Modelling, Bayesian Inference, and Markov Chain Monte Carlo Simulation

Kevin McNally,[1] Richard Cotton,[1] John Cocker,[1] Kate Jones,[1] Mike Bartels,[2] David Rick,[2] Paul Price,[2] and George Loizou[1,3]

[1] *Health and Safety Laboratory, Harpur Hill, Buxton, Derbyshire SK17 9JN, UK*
[2] *Toxicology & Environmental Research and Consulting, The Dow Chemical Company, Midland, MI 48674, USA*
[3] *Mathematical Sciences Unit, Health and Safety Laboratory, Harpur Hill, Buxton, Derbyshire SK17 9JN, UK*

Correspondence should be addressed to George Loizou, george.loizou@hsl.gov.uk

Received 22 September 2011; Revised 8 December 2011; Accepted 14 December 2011

Academic Editor: Kannan Krishnan

There are numerous biomonitoring programs, both recent and ongoing, to evaluate environmental exposure of humans to chemicals. Due to the lack of exposure and kinetic data, the correlation of biomarker levels with exposure concentrations leads to difficulty in utilizing biomonitoring data for biological guidance values. Exposure reconstruction or reverse dosimetry is the retrospective interpretation of external exposure consistent with biomonitoring data. We investigated the integration of physiologically based pharmacokinetic modelling, global sensitivity analysis, Bayesian inference, and Markov chain Monte Carlo simulation to obtain a population estimate of inhalation exposure to *m*-xylene. We used exhaled breath and venous blood *m*-xylene and urinary 3-methylhippuric acid measurements from a controlled human volunteer study in order to evaluate the ability of our computational framework to predict known inhalation exposures. We also investigated the importance of model structure and dimensionality with respect to its ability to reconstruct exposure.

1. Introduction

There are numerous programs, recent and ongoing, to evaluate environmental exposure of humans to chemicals, for example, EU ESBIO, COPHES, US CDC NHANES, Canadian Health Measures Survey [1–4]. Exposure assessment is relatively simple for occupational situations but more complex for the general public where exposure occurs via poorly defined exposure scenarios and multiple pathways. Under such circumstances human biological monitoring (BM or biomonitoring) can be the most reliable exposure assessment methodology as it provides an estimate of internal or absorbed dose of chemical by integrating exposure from all routes [5]. BM is the repeated controlled measurement of a chemical, its metabolites, or biochemical markers in accessible samples such as bodily fluids (e.g., urine, blood, saliva), exhaled air, and hair [6]. In risk characterisation, BM is often superior to other methods of exposure assessment, such as personal air measurements or dermal deposition assessments, because actual estimated body burden or biologically effective dose is a composite measure of the differences in individual behaviour (e.g., personal hygiene), work rate (characterised by different respiration rates), physiology, metabolism, and hence susceptibility [5]. Uncertainty in external exposure assessment due to inter- and intraindividual variability can also be reduced by using BM if the measured biomarker, either parent chemical or metabolite, is proportionately related to the ultimate toxic entity [5].

It has been proposed that the effects on public health from exposure to environmental chemicals may be better understood when the relationships between key events along the exposure-health evaluation-risk assessment continuum are established [7]. BM is one such tool that can link external exposure and biologically effective dose. Unfortunately, it is more often the case that BM data are reported without

the corresponding external exposure data, which then requires definition of the relationship with biologically effective dose. "Exposure reconstruction" or "reverse dosimetry" are terms used to describe procedures for determining estimates of external exposure consistent with BM data.

There have been a number of studies in which physiologically based pharmacokinetic (PBPK) modelling and statistical techniques were used to "reconstruct exposure or dose" consistent with human BM data at both the individual and population levels [8–15]. Population-based estimates of exposure that account for human interindividual variability, both in the modelling of chemical disposition in the body and in the description of plausible exposure conditions, can be achieved using the Bayesian inference [10]. Gelman et al. [16] used a Bayesian approach as a general method of parameter estimation in PBPK models. This method was originally applied to PBPK model calibration [17–20]. Lyons et al. [10] extended PBPK model calibration to include the unique exposure for each individual as another parameter to be estimated, alongside two additional "hyperparameters", the mean and standard deviation of exposures at the population level, to model variability in exposure. In this way the model could be applied to interpret population-based BM data.

The use of a PBPK model is significant because all the parameters represent anatomical, physiological, and biochemical characteristics which constrain variability to within biologically plausible limits. The limits on variability bestowed by biological structure suggest that the "ill-posed" problem of reverse dosimetry can be addressed to a certain extent. The ill-posed problem refers to the situation where any number of reverse dosimetry outcomes (reconstructed exposures) are possible, for example, an unstable model where a small change in the data may lead to a large change in output of the inverse function or no unique solution, and therefore a myriad of possible solutions or no solution at all ([21] cited by Lyons et al. [10]). Instead, knowledge regarding ranges, central values, and measures of dispersion are ascribed to model parameters, which are combined with specific data from separate studies to define informative prior distributions. Therefore, the linking of a PBPK model with Bayesian inference has a number of advantages with regard to exposure reconstruction. Firstly, it is an appropriate approach for systems where tissue dose is not necessarily linearly related to external exposure [10, 22, 23]. Secondly, defining informative prior distributions around parameters converts a deterministic model to a population model. Thirdly, this combination can extract population variability and multiple routes of exposure information integrated within BM data.

The use of a PBPK model to link BM to external exposures has already been described as significant. However, an aspect of exposure reconstruction that has not yet been adequately explored is whether any particular model is an adequate representation of the biological system it is built to emulate. If there are inadequacies in the PBPK model, then the exposure estimates will be wrong. By using data generated from a laboratory study where both the BM outputs and the exposure are known, exposure can be treated as an unknown variable to be estimated from the data, which allows the PBPK model to be evaluated and any inadequacies to be addressed. Whilst comparable data from laboratory-based studies are not a prerequisite for population-based modelling, indeed for chemicals with adverse health effects such data will not be available, human volunteer studies provide much richer data than will be available for population-based modelling. Within this environment it is possible to study how contextual information about individuals, in addition to samples, improves the results of dose reconstruction, the effect of interindividual variability on biomarker profiles can be studied, and the use of a PBPK model alongside new data streams, such as the exhaled-breath measurements used in this study, can be validated. The results from controlled laboratory-based studies for a variety of chemicals and exposure scenarios could inform improvements in population-based modelling.

In this study we used a PBPK model to evaluate the reconstruction of inhalation exposure to *m*-xylene from experimental BM data obtained in a controlled human volunteer study. Biomonitoring data comprised of timed measurements of venous blood and exhaled *m*-xylene and urinary 3-methylhippuric acid (MHA). In addition, we investigated the reconstruction of inhalation exposure when using the individual volunteer anthropometric measurements of body mass, body fat mass, resting alveolar ventilation rate, urine flow, urine creatinine concentration, and blood:air partition coefficient in addition to BM data. We also investigated the use of global sensitivity analysis [24] to reduce the computational cost of reverse dosimetry which, depending on the selected model output, is achieved by setting unimportant parameters of the PBPK model to central estimates.

2. Materials and Methods

2.1. Volunteers. The UK Health and Safety Executive Research Ethics Committee approved the study. Volunteers, who all were Health and Safety Laboratory staff, provided written informed consent before participating. Eight volunteers, 7 male and 1 female (aged 29 to 54) (Table 1), took part, were in good health at the time of the study, did not suffer from respiratory disease, and were not on any medications. Medical assessments were made immediately before the start and at the end of each experiment, to ensure that each volunteer was fit to participate and then to be discharged, respectively. The medical supervisor was present throughout the exposure period. All volunteers were asked to refrain from alcohol consumption for at least 72 h before entering the study. Body mass, height, body mass index (BMI), mass of body fat, resting minute volume, mean urine flow, urinary creatinine concentration, and *m*-xylene blood : air partition coefficient for each volunteer were measured (Table 1). Body fat was estimated using a bioelectrical impedance analyser (Bodystat 1500 Ltd., Isle of Man, UK) and by skinfold thickness measurements (Holtain callipers, Holtain Ltd, Crymych, UK). The value for mass of body fat used was the mean of the two techniques. Resting minute volume was measured using a Morgan Medical Pulmolab TF 501 apparatus at the Respiratory Function

Table 1: Individual volunteer parameters.

Volunteer	Age	Body weight (BW) (kg)	Height (m)	BMI (kg/m^2)	Mass of body fat (VfaC) (% (BW))	Resting alveolar ventilation rate (QPC) (l/hr)	Urine flow (R_{urine}) (l/hr)	Urinary creatinine (CRE) (mmol/l)	*m*-Xylene blood : air partition coefficient (Pba)
A	54	79	1.68	28.00	0.218	383.3	0.070	14.8	15.1
B	51	61.5	1.78	19.32	0.192	409.3	0.125	7.30	16.8
C	47	89	1.91	24.40	0.169	477.5	0.090	14.9	11.4
D	48	85	1.75	27.80	0.263	362.7	0.091	13.0	18.0
E	29	76	1.85	22.20	0.130	327.2	0.088	12.5	26.5
F	25	76	1.83	22.70	0.162	352.6	0.055	14.8	20.2
G	41	75	1.70	26.00	0.179	462.2	0.076	12.8	—
H	29	68	1.70	23.50	0.299	348.6	0.074	10.2	21.6
Mean		76.2	1.78	24.24	0.202	390.4	0.083	12.5	18.5
SD		8.73	0.08	2.95	0.056	54.89	0.021	2.70	4.90
CV		0.115	0.05	0.122	0.277	0.141	0.247	0.212	0.26

Unit of the Royal Hallamshire Hospital, Sheffield. Alveolar ventilation rate was assumed to be 70% of minute volume.

2.2. Chemicals. *m*-xylene (99%) and 3-methylhippuric acid (MHA) (98%) were obtained from Aldrich Chemical Co. (Dorset, UK). All other chemicals used were reagent grade or higher.

2.3. Exposure Protocol. Exposures were performed in the Health and Safety Laboratory Controlled Atmosphere Facility (CAF), a purpose built room 8 m^3 in volume. Purging *m*-xylene-filled bubblers with compressed air into the CAF generated atmospheres of *m*-xylene vapour. The atmospheric concentration within the CAF was monitored continuously with a Miran infrared spectrophotometer (calibrated by an internal, closed-loop system) and by gas chromatography (Varian 6000, with a 0.05 m %0.5 mm i.d., with 5% OV10, 100–120 mesh Chrom CHP packing; injector temperature 120°C, N_2 carrier gas flow rate 40 mL min^{-1}, oven temperature 60°C) with flame ionisation detection (detector temperature 200°C, H_2 flow rate 25 mL min^{-1}, air flow rate 300 mL min^{-1}, calibration using a gas sampling valve against a standard atmosphere). The CAF temperature was maintained at 25°C and 30% humidity for all experiments.

Groups of 4 volunteers were exposed for 4 h on two separate occasions to a target concentration of 40 ppm *m*-xylene vapour. The actual exposure concentrations for the duration of the experiments were measured at 39.0 ± 3 and 37.0 ± 2 ppm, respectively.

2.4. Biomonitoring Data (BM). Blood (CV) and exhaled alveolar (CXPPM) *m*-xylene and urinary MHA (C_{urine}) concentrations were measured. Volunteers provided blood samples from the antecubital vein via an indwelling soft cannula. Blood samples were stored (48 hours maximum) at 4°C as whole blood until analysed. Blood samples were assayed in duplicate as follows. A 250 μL sample was added to 750 μL of H_2O in a 10 mL headspace vial, which was capped with a PTFE-lined rubber septum. The sample was then incubated and continually stirred at 65°C for 10 minutes. A one mL headspace aliquot was taken using a warmed (75°C) gas-tight syringe (Fisons HS800 headspace sampler) and analysed by gas chromatography (Carlo Erba GC8000; column BP-5, 25 m % 0.32 mm i.d., 5 μm film) and mass spectrometry (Fisons MD800 MS) operating in selected ion monitoring mode using positive electron ionisation (*m/z* [M^+] 106). The limit of detection of the assay was 0.1 μmol/l with intra- and interassay coefficients of variation of 5 and 10%, respectively.

End tidal breath samples (alveolar air) were taken and analysed according to the method of Dyne et al. [25] described previously [26].

Urine volume was recorded and samples were stored at −20°C until analysed. The major metabolite, MHA, was measured in the urine to assess the rate of biotransformation and elimination of *m*-xylene. A 0.5 mL sample of urine was mixed with 0.5 mL methanol and analysed by HPLC (Hewlett Packard 1050 Series, with autosampler, pump, degasser; column 3 μm ODS, 100 % 4.6 mm) with a mobile phase of 0.1% acetic acid:methanol (85 : 15 with gradient elution), using diode array detection at a detection wavelength of 230 nm. The limit of detection of the assay was 40 μmol l^{-1} with intra- and interassay coefficients of variation of 2 and 5%, respectively. Creatinine concentration was measured by using a Cobas Mira (ABX France) and an automated alkaline picrate method [27]. The coefficient of variation for intraday analysis was 1.5% and for interday analysis was 3% at 6 mM.

Venous blood samples were taken at 0, 1, 2, 3, 4, 4.33, 4.67, 5, 6, 7, 8, and 23 hours. The blood data were separated into two sets corresponding to measurements made on different occasions to investigate the importance of data quality in reverse dosimetry (Figures 1(a) and 1(b)). The analysts explain that blood data deemed unreliable may be due to imperfect sealing of sample vials leading to losses. This explanation is plausible when compared to the appearance of the exhaled breath and urine data for all volunteers, which are qualitatively similar. Also, the peak CV concentrations of the reliable data are quantitatively and qualitatively comparable with data from similar human volunteer studies [28, 29].

Exhaled air samples were taken at 0, 4.017, 4.33, 4.67, 5, 6, 7, 8, and 24 hours (Figure 2). Urine samples were taken at 0, 4, 6, 8, 10, 12, 14, 24, 27, and 31 hours (Figure 3).

Anthropometric measurements for each volunteer are listed in Table 1.

2.5. The PBPK Model. A human PBPK model that includes a bladder compartment to simulate fluctuations in metabolite concentration in urine caused by micturition [30] was adapted to study the inhalation pharmacokinetics of *m*-xylene. Liver, adipose, richly and slowly perfused tissues, and the bladder represent the body (Figure 4). The model parameter abbreviations and point values, which are similar to previous models, are listed in Table 2 along with the distributions used in the sensitivity analysis (SA) [26, 31]. Exhalation, metabolism, and renal excretion were the routes of elimination. The concentration of unbound MHA, the main metabolite of *m*-xylene in the blood, assumed to be equivalent to the concentration of compound flowing through the kidney was described by the following equations:

$$\begin{aligned}
\frac{d(\mathrm{MHA}_B)}{dt} &= \left(\mathrm{MRL}i \times \frac{\mathrm{MW}_{\mathrm{MHA}}}{\mathrm{MW}_{xyl}}\right) - (\mathrm{MHA}_B \times K_1),\\
\frac{d(\mathrm{MHA}_U)}{dt} &= \mathrm{MHA}_B \times K_1,\\
\mathrm{MRL}i &= \frac{V_{\max} \times \mathrm{CVL}i}{K_M + \mathrm{CVL}i},\\
\mathrm{C}_{\mathrm{urine}} &= \frac{\mathrm{MHA}_U}{\mathrm{Vol}_U \times \mathrm{CRE}},
\end{aligned} \tag{1}$$

where MRL*i* is the rate of metabolism of *m*-xylene to MHA in the liver, MW_{MHA} and MW_{xyl} are the molecular weights of MHA and *m*-xylene, respectively, MHA_B is the amount of MHA in the blood, K_1 is a first-order elimination rate constant describing removal of MHA_B from the blood to the urine, V_{max} is the limiting rate and K_M is the Michaelis-Menten constant for hepatic metabolism of *m*-xylene, CVL*i* is the hepatic venous effluent concentration of *m*-xylene,

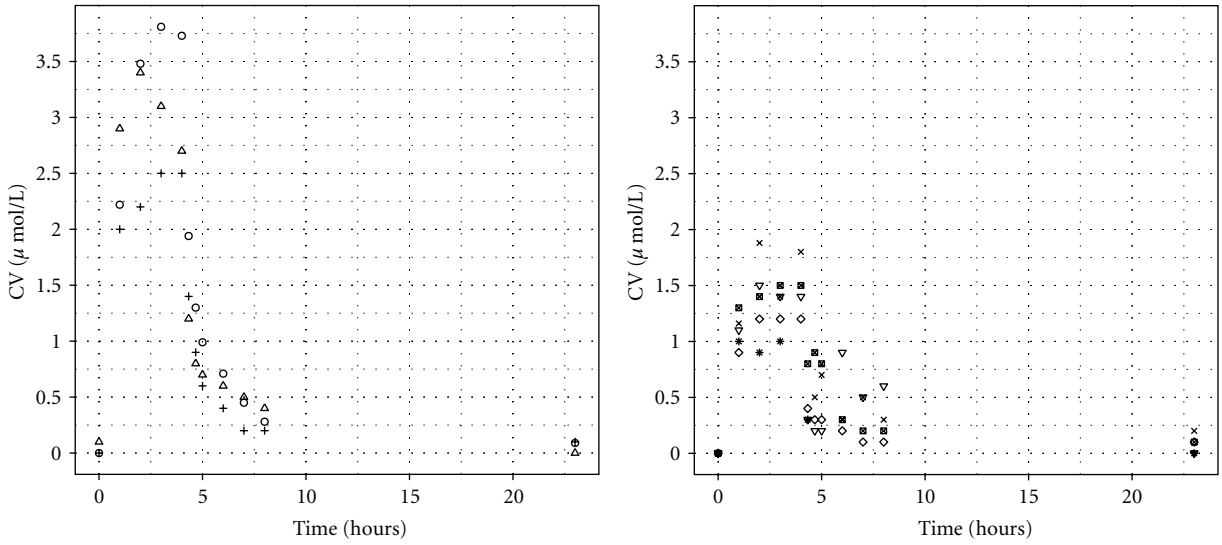

(a) Good-quality data (b) Poor-quality data

Figure 1: (a) Venous blood concentrations of *m*-xylene. Data from three volunteers were prepared and measured on a different day than other four. This set of data has the expected appearance and was considered acceptable for use in reverse dosimetry. (b) Venous blood concentrations of *m*-xylene. Data from four volunteers were prepared and measured on a different day than other three. This set of data does not have the expected appearance and was considered unacceptable for use in reverse dosimetry.

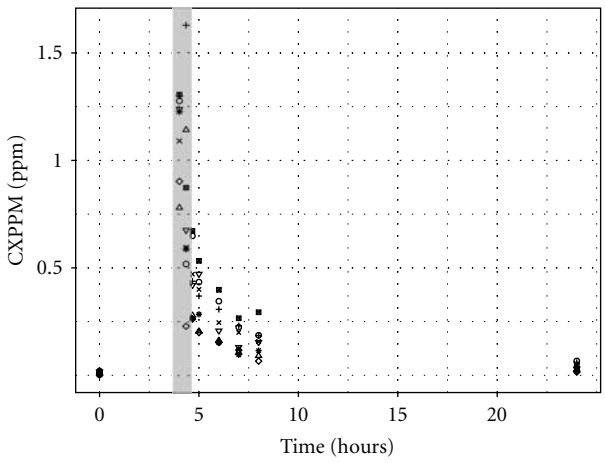

Figure 2: Exhaled *m*-xylene. Data from eight volunteers used in reverse dosimetry. The data points enclosed within the grey bar were excluded from the final exposure reconstruction simulations.

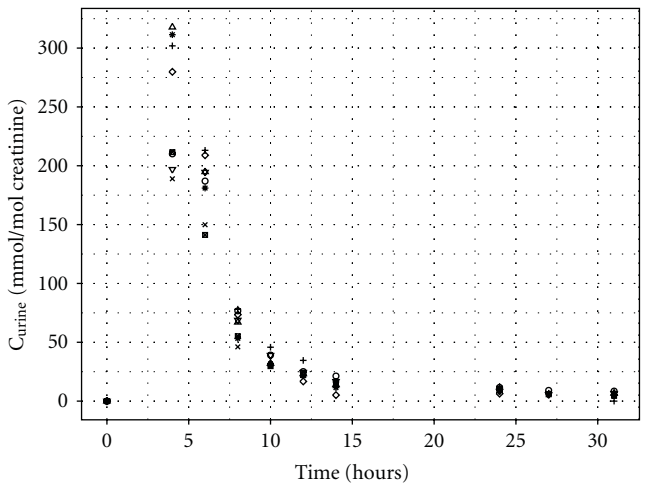

Figure 3: Urinary 3-methylhippuric acid (MHA). Urinary excretion of MHA expressed against creatinine for eight volunteers used in reverse dosimetry.

MHA_U is the amount of MHA in the urine, Vol_U is the volume of urine in the bladder, and CRE is the concentration of creatinine. The concentration of MHA in the urine was expressed in mmol/mol creatinine. To imitate micturition, the bladder is assumed to fill with urine at a constant (but adjustable) rate and empty at discrete time intervals (when the volume of urine reduces to zero). This enables comparison to be made between model predictions and experimental observations with timed sampling in human volunteer studies [30].

The Michaelis-Menten constant K_M and the *in vitro* V_{max} for hepatic metabolism of *m*-xylene were obtained from the literature [32]. *In vitro-in vivo* extrapolation of V_{max} was obtained by multiplying the *in vitro* value by a human hepatic microsomal protein yield (MPY) of 32 mg g^{-1} wet weight liver and the mass of liver (M_{Li}) (g) [33, 34]:

$$in\ vivo\ V_{max} = in\ vitro\ V_{max} \times \mathrm{MPY} \times M_{Li}. \quad (2)$$

2.6. Parameter Distributions. Anatomical and physiological parameter distributions used for SA and MCMC simulations listed in Table 2 were obtained from the freely

Table 2: Anatomical, physiological, and kinetic constants and parameters used in the PBPK model.

Parameter	Abbreviation	Value	Distribution
Molecular mass *m*-xylene (g/mol)	MW_{xyl}	106.17	—
Molecular mass MHA (g/mol)	MW_{MHA}	193.2	—
Body mass (kg)	BW		Normal BW~N(76.2, $(8.73)^2$)
Vascularised tissue (proportion of body mass)	VT	0.91	—
Cardiac output (L h^{-1} $BW^{-0.75}$)	QCC		Normal QCC~N(13.8, $(2.5)^2$)
Metabolism (Liver)			
In vitro Michaelis constant (mMol L^{-1})	K_M		Normal K_M ~N(11.8, $(1.4)^2$)
In vitro maximum rate of metabolism (pmol min^{-1} mg^{-1} microsomal protein)	V_{max}		Normal V_{max} ~ N(895, $(68)^2$)
Microsomal protein yield per gram wet weight liver (mg g^{-1})	MPY		Lognormal ln (MPY)~N(3.7, $(2.9)^2$)
Gas exchange			
Respiratory rate (L h^{-1})	QPC		Normal QPC~N(390.4, $(54.9)^2$)
Respiratory dead space (proportion respiratory rate)	DS	0.3	—
Partition coefficient			
Blood : air partition coefficient	Pba		Normal Pba~N(18.5, $(4.9)^2$)
Rapidly perfused	Prpda		Uniform Prpda~U(50–150)
Slowly perfused	Pspda		Uniform Pspda~U(40–80)
Adipose	Pfaa		Uniform Pfaa~U(1400–2200)
Liver	Plia		Uniform Plia~U(150–350)
Tissue blood flow as a fraction of cardiac output			
Rapidly perfused	QrpdC	0.48	—
Slowly perfused	QspdC	0.22	Uniform QspdC~U(0.2–0.35)
Adipose	QfaC	0.05	Normal QfaC~N(0.053,$(0.003)^2$)
Liver	QliC	0.25	Normal QliC~N(0.271,$(0.01)^2$)
Tissue mass as a fraction of body mass			
Rapidly perfused	VrpdC	0.09	—
Slowly perfused	VspdC	0.604	—
Adipose	VfaC	0.19	Lognormal ln(VfaC)~N(−1.59,$(-2.88)^2$)
Liver	VliC	0.0257	Normal VliC~N(0.036,$(0.01)^2$)
Bladder compartment			
Rate of urine production (L h^{-1})	R_{urine}	0.07	Normal R_{urine} ~ N(0.083,$(0.021)^2$)
Urinary creatinine concentration (mmol L^{-1})	CRE	12.5	Normal CRE~N(12.5,$(2.7)^2$)
First-order elimination rate constant (h^{-1})	K_1		Uniform K_1 ~U(5–20)

available web-based application PopGen, which is a virtual (healthy) human population generator (http://xnet.hsl.gov.uk/popgen/). A human population, comprising 50% male and 50% female, white Caucasians, age range 16–65, height range 140–200 cm, body mass indices 18.5–30, was generated to encompass the characteristics of the volunteers that took part in the study described below. In PopGen, organ masses and blood flows are determined for virtual individuals from both *a priori* distributions of anthropometric parameters such as body mass, height, and body mass index and measured data from existing studies. The algorithms were derived and evaluated by Willmann et al. [35].

No distributions were available for the partition coefficients (PCs) *Prpda*, *Pspda*, *Pfaa*, and *Plia*. Therefore, uniform distributions were assigned and the ranges set were considered reasonable assumptions. *VspdC* and *VrpdC*, the masses of the slowly and rapidly perfused tissues respectively, were not included in the SA because they are aggregated compartments from which organs and tissues are subtracted when discretely defined during model building. The model was re-parameterised as proposed by Gelman et al. [16] to ensure that mass balance and blood blow constraints were not violated.

The mean value for K_1, the first-order elimination rate constant describing removal of MHA_B from the blood to the urine, was estimated by simulating the postexposure urinary excretion of methylhippuric acid following exposures at 1–10, 11–20, 21–30, and 31–40 ppm [36]. The four datasets were digitised and K_1 estimated using the quasi-Newton

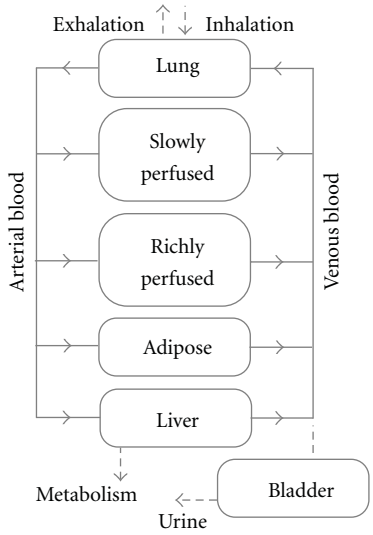

Figure 4: Schematic of the PBPK model for *m*-xylene with a bladder compartment, to simulate fluctuations in the concentration of the main metabolite, methylhippuric acid.

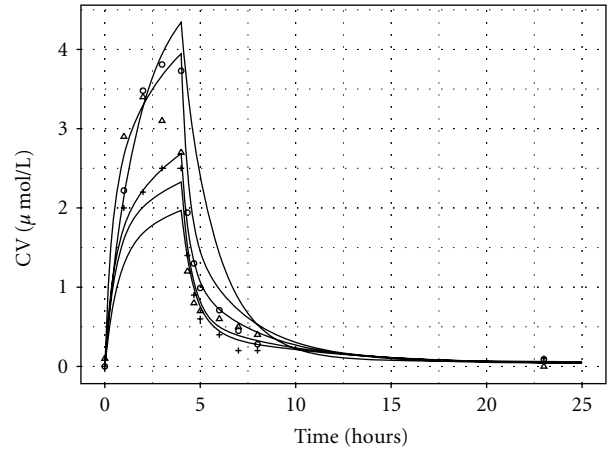

Figure 5: A comparison of 5 CV biomarker profiles corresponding to parameter sets sampled from the priors and reliable CV measurements.

algorithm within acslX Libero. The mean value for K_1 was used in all simulations as sensitivity analysis demonstrated the model output; in this case urinary excretion of methylhippuric acid was relatively insensitive to this parameter.

2.7. Sensitivity Analysis. The extended Fourier amplitude sensitivity test (eFAST) for the quantitative sensitivity analysis (SA) of model parameters and the presentation of SA results as Lowry plots have been described previously [24]. The sensitivities of CV and CXPPM at the 3- and 5-hour time points within the distribution and elimination phases, respectively, and at 5 and 8 hours for C_{urine} in the early and latter urinary elimination phases are reported. Sensitivity analysis results were computed on a much finer timescale. However, the two time points selected for reporting were broadly representative of the SA results: from 0 to 4 hours absorption into the body and the period after 4 hours elimination from the body for CV and CXPPM, 4 to 8 hours "rapid elimination," and after 8 hours "return to baseline" for C_{urine}.

2.8. Calibration. A distribution of plausible exposures was achieved through calibration of the sensitive parameters of the PBPK model using the human volunteer data, a process referred to as reverse dosimetry. Specifically, this required a comparison of the time-varying model predictions of concentrations of substance in blood (CV), breath (CXPPM), and urine (C_{urine}) with measurements in these media.

The output from the PBPK model was represented by

$$\mu_{ij} = \eta\left(\mathbf{x}_j, \theta_j, \lambda, \mathbf{t}_i\right), \tag{3}$$

where μ_{ij} is the corresponding model prediction for subject j at time t_i, $\mathbf{x}_j$ represents the vector of anthropometric measurements, and θ_j represents the vector of unknown variables for subject j. Vectors $\mathbf{x}$ and θ represent the vectors of anthropometric measurements and unknown parameters for all subjects, respectively. Parameter λ represents the (presumed) unknown exposure concentration and t_i indexes a specific time. SA was used to simplify the PBPK model prior to attempting calibration. Individualised parameters were only ascribed to the most important (sensitive) parameters in the model, whereas parameters that the model was relatively insensitive to were assumed to be common to all subjects and fixed at central values within their plausible ranges (Table 2). As the data were obtained in a laboratory-based study, a common exposure to all participants was assumed. More intricate hierarchical models of exposure are required to account for the heterogeneity of exposure for population studies [10].

An infinite family of parameter sets, which are inputs to the PBPK model, are defined by the (prior) probability distributions on model parameters. Each parameter set is used to overwrite the initial (default) parameters, thereby constituting a different PBPK model. In Figure 5 the reliable CV measurements and the biomarker profiles corresponding to 5 parameter sets drawn from the prior distributions of the model parameters are shown. Each PBPK model specified by a particular parameter set is unique; however, very different sets of parameters may define similar PBPK models (with respect to specific model outputs). The objective of the reverse dosimetry is to calibrate or tune the unknown parameters of the model θ and the exposure concentration λ such that the observational data and model predictions are in close agreement. Convergence to a unique solution was not possible (due to both measurement error and model inadequacy); however, calibration should result in a substantial reduction in the domain of the family of models that are consistent with measurements. Formally, inference was achieved through application of the *Bayes theorem*. The posterior distribution results in a narrower range of biomarker profiles than that depicted in Figure 5.

A model that linked model predictions to observations was required. The considerations in choosing an appropriate

form were that the model predictions and observations in subjects are strictly nonnegative; the magnitude of prediction errors was proportional to the magnitude of the substance; prediction errors were asymmetric, with observations much greater than predicted by the model more likely than observations far below the model predictions. These features all suggest that a model on the log scale was appropriate. Here, as in other works [10, 15, 16] a lognormal distribution was assumed for modelling the probabilistic relationship between model predictions and observations.

Letting y_{ij} denote a measurement made on the jth subject at time i, where μ_{ij} is the corresponding model prediction, the *likelihood* based on all individuals at all measurement times is written as

$$f(\mathbf{y} \mid \theta,\ \lambda,\ \sigma) = \prod_{j=1}^{J}\prod_{i=1}^{T} \frac{1}{\sqrt{2\pi\sigma^2}}\ \exp\left[-0.5\left(\frac{\ln\left(y_{ij}\right) - \ln\left(\mu_{ij}\right)}{\sigma}\right)^2\right]. \quad (4)$$

The likelihood is a function of both parameters and data. This introduces a final unknown parameter σ, which is a statistical measure of the goodness of fit.

The Bayes theorem was applied. This states that the *posterior distribution* of the model parameters (θ, λ, and σ) is proportional to the product of the likelihood and the prior (which is itself the product of the priors for θ, λ, and σ). The posterior distribution is a representation of prior beliefs (and constraints on parameters) updated by data:

$$f(\theta,\ \lambda,\ \sigma \mid \mathbf{y}) \propto\ f(\mathbf{y} \mid \theta,\ \lambda,\ \sigma) \times\ f(\theta) \times\ f(\lambda) \times\ f(\sigma). \quad (5)$$

Prior distributions for the θ_j are given in Table 2. Whilst each individual has a unique physiology, the same set of prior distributions modelled the uncertainty in each individual physiological parameters. However, whilst common prior distributions were assumed, the subjects had unique posterior distributions (informed by their personal BM data). A uniform prior on the (presumed unknown) exposure concentration between 0 and 200 ppm was assumed; the upper limit of this distribution was chosen such that the prior distribution should have no influence on the posterior distribution of λ. A noninformative prior (a uniform prior on the positive real line for $\ln \sigma$) was assumed for σ.

2.9. Inference. The form of the posterior distribution (5) is complex because the PBPK model requires a numerical solution, and this could not be obtained in closed form. Inference about the parameters of the model was made using a Markov chain Monte Carlo (MCMC) sampling algorithm [37]. A single-component Metropolis-Hastings algorithm was used to draw samples.

The samples from (5) index an updated family of PBPK models that are consistent with prior beliefs and laboratory-based observations on subjects.

2.10. The Simulations. The simulations were designed to investigate the precision of reconstructed exposures whilst minimising computational cost and reducing the number of influential unknown model parameters. A reduction in computational burden was achieved primarily through SA, with distributions ascribed only to those parameters with a significant contribution to model output variance. The use of the anthropometric measurements (**x**) listed in Table 1 allowed a reduction in the number of unknown and important parameters. The simulations analysed were therefore as follows.

(1) Computational cost and the reliability of SA analysis were investigated by comparing the precision of two simulations where exposure was reconstructed from C_{urine}. The first updated 17 parameters and the second updated the 11 most important parameters.

(2) Exposure reconstruction from CV by updating the 11 most important parameters.

(3) Exposure reconstruction from CV using the 11 most important parameters where eight were updated and three were individual anthropometric measurements.

(4) Exposure reconstruction from suspect CV data using the 11 most important parameters where eight were updated and three were individual anthropometric measurements.

(5) Exposure reconstruction from CXPPM using the 11 most important parameters.

(6) Exposure reconstruction from CXPPM using the 11 most important parameters where seven were updated and four were individual anthropometric measurements.

(7) Exposure reconstruction from C_{urine} by using the 11 most important parameters where six were updated and five were individual anthropometric measurements (including individual R_{urine} and CRE measured at each sampling time).

The simulations and specific anthropometric measurements used are listed in Table 3.

Table 3: Summary of simulations.

Simulations	Number of updated parameters		
	CV	CXPPM	C_{urine}
Full set (mean values)	0	—	17
Most influential	11	11	11
Most influential-(**x**)	8	7	6
	Parameters not updated		
Measured parameters (**x**)	QPC	QPC	QPC
	PBA	PBA	PBA
	BW	BW	BW
		VfaC	R_{urine}
			CRE

2.11. Software. The numerical solutions to the model equations were obtained using acslX Libero version 3.0.1.6 (AEgis

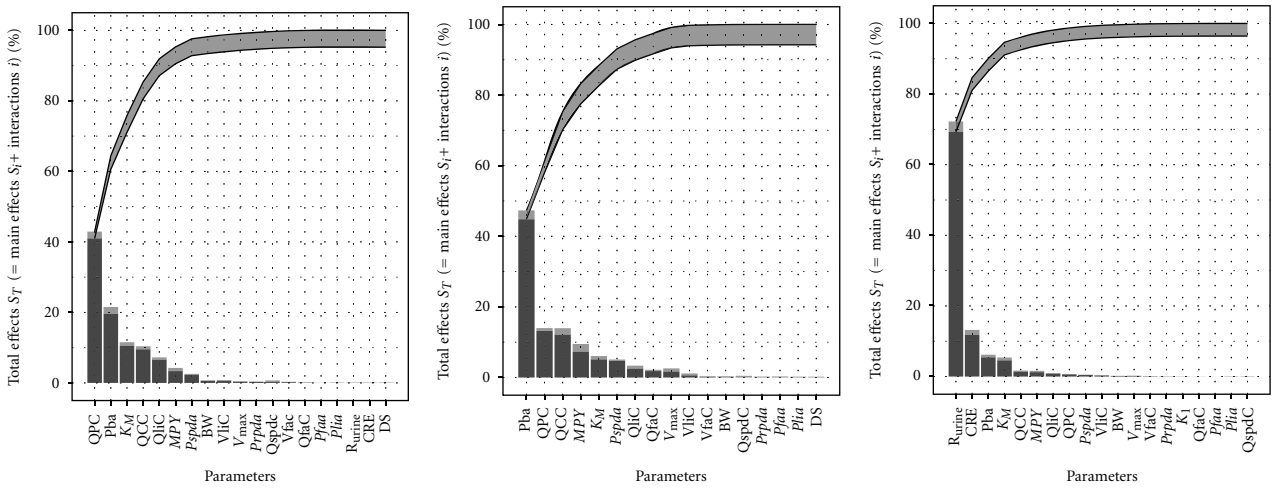

(a) CV, 3 hours (b) CXPPM, 3 hours (c) C_{urine}, 5 hours

Figure 6: Lowry plot of the eFAST quantitative measure. The total effect of a parameter S_{T_i} comprised the main effect S_i (black bar) and any interactions with other parameters (grey bar) given as a proportion of variance. The ribbon, representing variance due to parameter interactions, is bounded by the cumulative sum of main effects (lower bold line) and the minimum of the cumulative sum of the total effects (upper bold line), (a) CV at 3 hours, (b) CXPPM at 3 hours, (c) C_{urine} at 5 hours.

Technologies; http://www.acslx.com/). The M functions for eFAST and MCMC modelling included with the acslX optimum suite of tools were adapted for use in this study. Lowry plots and histograms were created using R and ggplot2 [38, 39] with additional code by Takahashi [40]. Data were digitised using Grab It! Graph Digitizer (DataTrend Software, Inc.; http://www.datatrendsoftware.com/). The computer used in this study was a Dell Optiplex 755 Intel Core 2 Duo CPU 3.00 GHz 2.00 GB RAM.

3. Results

3.1. Sensitivity Analysis. Figures 6(a), 6(b), and 6(c) are typical Lowry plots for CV and CXPPM at 3 hours and C_{urine} at 5 hours used to select the most influential parameters. The total effect of a parameter S_{T_i} comprised the main effect S_i (black bar) and any interactions with other parameters (grey bar) given as a proportion of variance. The ribbon, representing variance due to parameter interactions, is bounded below by the cumulative sum of main effects (lower bold line) and above by the minimum of the cumulative sum of the total effects and one minus the sum of the main effects that were not included (upper bold line). The most influential parameters were selected by reading across from the 95% variance point on the y-axis to the upper bold line and then down to the x-axis. All parameters to the left of this point were selected and used in the dose reconstruction. The most influential parameters at the latter time points of five hours for CV and CXPPM and eight hours C_{urine} were selected in the same way (Lowry plots not shown). In Table 4 the most influential parameters at the latter time points are listed alongside those from the earlier time points. The parameters in bold are those that only become influential at the latter time points. These were added to the parameters that were influential at the earlier time points in order to ensure that prior distributions were assigned to all influential parameters across the entire time period of interest. The measured parameters listed in Table 1 are also listed in Table 3 to indicate when they were used in each simulation and are italicised in Table 4 to indicate when they contributed to variance of dose metric.

Table 4: Model parameters accounting for 100% variance at different time points.

CV		CXPPM		C_{urine}	
3 h	5 h	3 h	5 h	5 h	8 h
QPC[a]	*QPC*	*Pba*	*Pba*	R_{urine}	R_{urine}
Pba	**QspdC**	*QPC*	*QPC*	*CRE*	*BW*
KM	KM	QCC	QspdC	*BW*	*QPC*
QCC	QCC	KM	KM	*Pba*	*CRE*
QliC	*Pba*	QliC	QCC	KM	***VfaC***
MPY	QliC	MPY	**Prpda**	QCC	**Qspdc**
Pspda	Prpda	Pspda	QliC	MPY	**Pspda**
BW	MPY	VliC	MPY	QliC	*Pba*
VliC	Pspda	*BW*	Pspda	*QPC*	QCC
		QspdC	VliC		**Pfaa**

[a] Italicised abbreviations correspond to parameters measured for each volunteer listed in Table 1.

3.2. Computational Cost and Reliability of SA (Simulation 1). Initially, two simulations calibrating to the observed urine measurements (C_{urine}) from the volunteers were run. Both simulations employed the distributions listed in Table 2. The subset of anthropometric parameters listed in Table 1, where measurements were available for each individual, was not used in this first stage; that is, $\mathbf{x}_j$ was an empty set. The two initial simulations differed only in terms of the numbers

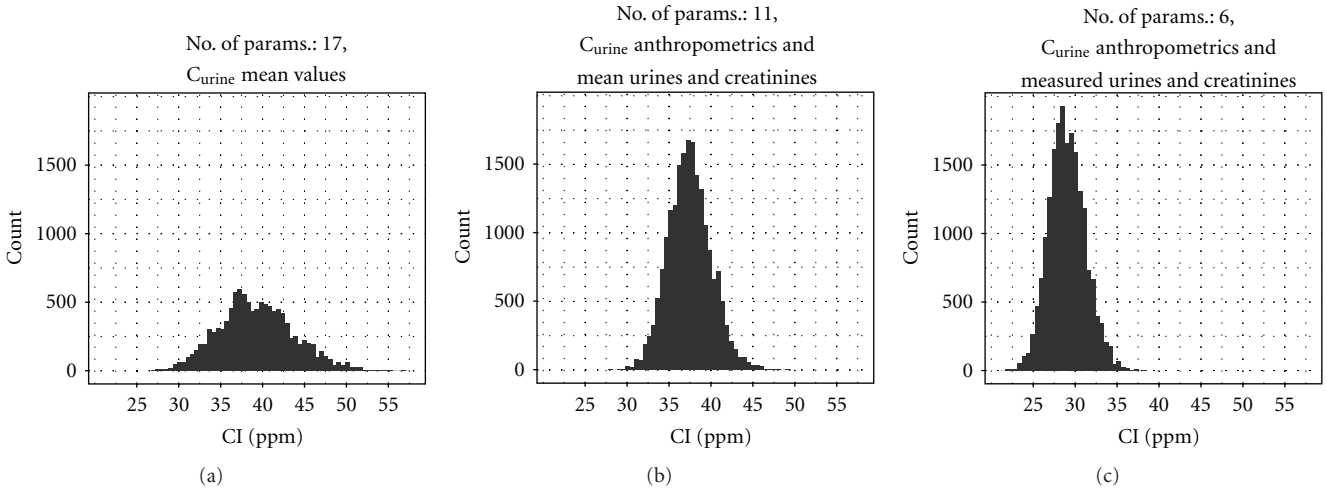

Figure 7: Comparison of estimated posterior distributions for 4-hour inhalation exposure to *m*-xylene. Posterior distributions were estimated by updating the entire set of parameters, most influential parameters, or by fixing the measured parameters and updating the remaining most influential: (a) C_{urine}, full parameter set, (b) C_{urine}, most influential, (c) C_{urine}, most influential and measured spot urine production rates and creatinine concentrations.

of updated parameters for each individual; in the first case $\boldsymbol{\theta}_j$ contained 17 unique parameters for each individual; in the latter case $\boldsymbol{\theta}_j$ contained the 11 most sensitive parameters for each individual with the remaining parameters fixed at central values and common to all individuals (Table 3). In addition, both models also contained the unknown exposure, λ, and the statistical measure of fit, σ. In total, the models contained 138 $((17 * 8) + \lambda + \sigma)$ and $((11 * 8) + \lambda + \sigma)$ parameters, respectively. The objective of the comparison was to demonstrate that SA techniques could be utilized before attempting a calibration in order to reduce the dimensionality of the calculation, with only a small loss of precision. The prior distributions for each of the model parameters were common to all individuals in both simulations. Prior distributions are given in Table 2 for physiological parameters. Prior distributions for the rate of urine production and creatinine concentrations were estimated from experimental data generated in the human volunteer study (Table 1). The urine samples from the individuals allowed their unique physiological parameters to be updated, and posterior distributions were obtained for all varying parameters for each individual. Typical posterior distributions for λ estimated from C_{urine} are shown in Figures 7(a), 7(b), and 7(c). The mean, median, and a 95% interval for λ and the posterior median for σ are listed in Table 5. The posterior distributions for λ and σ were similar for the models that contained 138 (Figure 7(a)) and 90 (Figure 7(b)) unknown parameters respectively; however, there was a small difference in the central estimates for λ. This is entirely consistent with the results of the SA and demonstrates the value of appropriate SA techniques to the modeling process. Therefore, further simulations were conducted using models with prior distributions on only the most sensitive parameters.

Due to the relatively small number of volunteers in the study, it was computationally feasible to calibrate to large numbers of individualized parameters for each subject. In a population-based study, it is likely that a balance between precision (number of individualized parameters) and computational cost would have to be achieved. For a calibration using the urine data, Figure 6(c) indicates that a calibration model using individualized parameters for the six most sensitive parameters would be adequate for capturing the majority of variance during the rapid elimination phase; however, additional parameters would be required in order to capture a large proportion of the variance in the return to baseline (slower elimination phase) period (Table 4). It is important that contributions to the variance over the full range of the measurements are considered.

3.3. Exposure Reconstruction from Venous Blood Biomarker (Simulations 2–4). Two calibration models were fitted to each of the reliable CV, CXPPM, and C_{urine} datasets. The initial model did not include the measurements of the anthropometric parameters listed in Table 1 ($\mathbf{x}_j$ was an empty set), whilst the second calibration model made use of these data; therefore, there was a reduction in the vector of uncertain parameters $\boldsymbol{\theta}_j$ for each individual (Table 3). Calibration models making use of the unreliable CV data were also run to allow a comparison with the reliable CV data.

The best estimates of exposure λ were obtained using the reliable CV data from three volunteers (Data from the fourth volunteer were not used due to problems with taking blood samples.) although the 95% interval for λ was widest using the reliable CV data, which can be explained by the smaller number of volunteers and measurements (compared with data from CXPPM and C_{urine}). The central estimate of λ was close to the target exposure of 37–39 ppm (Figure 8(a) and Table 5, reliable data, most influential), and model predictions were consistent with the observed biomarker profile (discussed later on in results). There was a small

Table 5: Posterior distributions of inhalation exposure to *m*-xylene.

Biomonitoring data	Parameters updated		*m*-xylene inhalation exposure posterior distribution				Statistical measure of fit
			Mean	Median	2.5%	97.5%	Median
CV	Reliable data	All parameters fixed at central values ("mean human")	24.0	23.8	21.0	29.0	0.55
		Most influential (Figure 8(a))	33.8	33.5	26.6	41.5	0.35
		Most influential including measured parameters (x) (Figure 8(b))	36.2	35.9	29.5	44.5	0.38
	Unreliable data	Most influential including measured parameters (x) (Figure 8(c))	19.5	19.1	15.3	25.0	0.71
CXPPM	Most influential (Figure 9(a))		16.0	15.8	11.4	21.4	0.58
	Most influential including measured parameters (x) (Figure 9(b))		15.9	15.8	13.0	19.6	0.59
C_{urine}	All parameters (mean R_{urine} and CRE) (Figure 7(a))		39.3	39.1	31.2	48.7	0.356
	Most influential (mean R_{urine} and CRE)		38.7	38.4	30.7	48.2	0.349
	Most influential including measured parameters (x) (mean R_{urine} and CRE) (Figure 7(b))		37.5	37.4	32.7	42.7	0.37
	Most influential including measured parameters (x) (individual timed R_{urine} and CRE) (Figure 7(c))		29.0	28.9	25.1	33.6	0.4

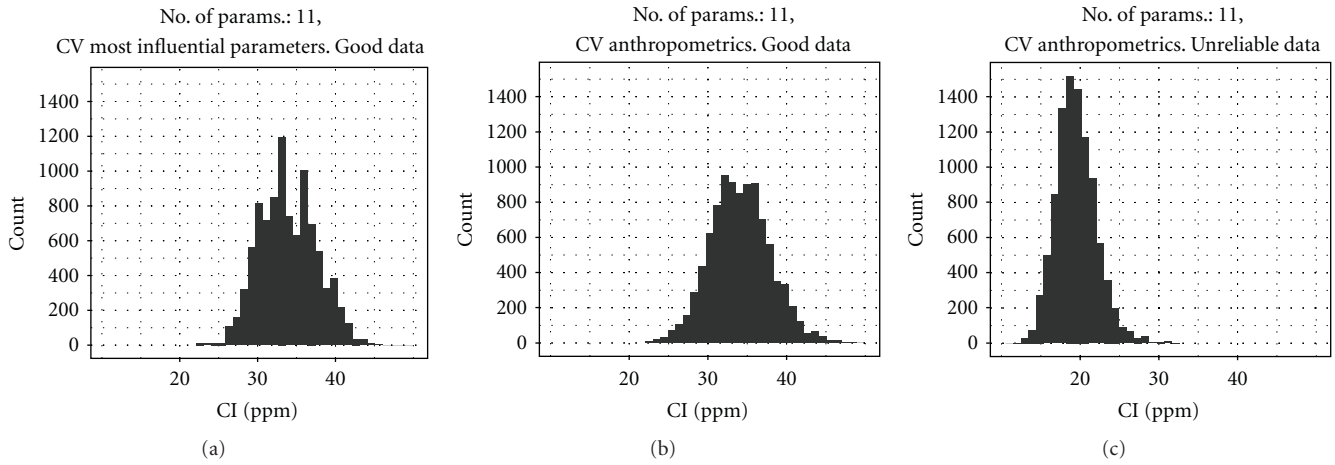

Figure 8: Comparison of estimated posterior distributions for 4-hour inhalation exposure to *m*-xylene. Posterior distributions were estimated by updating the most influential parameters or by fixing the measured parameters and updating the remaining most influential: (a) CV, most influential, (b) CV, fixed, measured, and remaining most influential, (c) CV, most influential, using unreliable data.

improvement in the central estimate of λ after making use of measured parameters $\mathbf{x}$ (comprising of QPC, Pba, and body weight) for each subject; the 95% interval for λ (Figure 8(b) and Table 5, reliable data, most influential including measured parameters) was shifted upward although the width of the interval was unchanged.

The change in the posterior distribution of λ that resulted from using anthropometric measurements can be attributed to the correlations between λ and the measured parameters $\mathbf{x}$. Whilst the exposure concentration is *a priori* independent of physical parameters, it is correlated with these parameters through the statistical model. In particular both QPC and Pba were negatively correlated (correlations between both QPC and Pba and λ were approximately -0.2 for each individual) with the exposure concentration in the model that treated these measured parameters as unknown. The calibration model is ill posed and cannot distinguish between the case of a low exposure and efficient transfer to the blood (larger values of QPC and Pba), the case of a high exposure and inefficient transfer to the blood (smaller values of QPC and Pba), or the continuum that exists between these two extreme cases; all are consistent with the observed data. Including measured values and thereby reducing the number of uncertain parameters in the model reduced the domain of models that were consistent with the venous blood data. There was a small increase in σ when including measured parameters $\mathbf{x}$, a result of 9 less "free" parameters to describe the measurements.

Exposure reconstruction was also attempted using unreliable CV data from four volunteers (Figure 8(c) and Table 5, unreliable data, most influential including measured parameters). The mean and median (17.4 and 17.3 ppm) of the exposure λ estimated from these data were approximately half of the known exposure. The 95% interval for λ was also very narrow. This is not a surprising finding as the CV measurements (Figure 1(b)) were much lower and more erratic compared with the reliable data (Figure 1(a)). It is clear from visual inspection of Figures 1(a) and 1(b) that the data in Figure 1(b) reach a peak at below 2 μmol/l and qualitatively have an unusual profile. As mentioned previously, the analysts explain that this may be due to imperfect sealing of sample vials leading to losses.

3.4. Exposure Reconstruction from Exhaled Breath Biomarker (Simulations 5-6). Exposure reconstruction using the entire CXPPM dataset resulted in a posterior distribution for λ that was concentrated on a range well below the "true" value (16.0, 15.8, 11.4, 21.4, mean and median, 2.5% and 97.5%, resp.). The simulation was repeated after excluding the measurements made at 4 hours 1 minute (i.e., one minute after exiting the exposure facility). Exclusion of these measurements is justified because, during exposure and immediately after leaving the source of exposure, the concentration of solvent in breath reflects the portion of the inhaled concentration that has not been absorbed, therefore, is not representative of circulating blood solvent levels. However, the posterior distribution for λ was not much improved after excluding the first measurement (Figure 9(a)) and Table 5, most influential) although still well below the target exposure. The model that included measured anthropometric parameters had an almost identical central estimate of exposure (Figure 9(b) and Table 5, most influential, including measured parameters, $\mathbf{x}$). The error σ was similarly large for both of these models indicating that, even at the estimated exposures, the fit to the measurements (discussed in Section 3.6) was poor.

3.5. Exposure Reconstruction from Urinary Biomarker (Simulation 7). The first three exposure reconstructions that were attempted using the urine samples resulted in a posterior distribution for λ that had similar central estimates of exposure to those obtained from the reliable CV data. This is not surprising because the rate of appearance of metabolite in the urine was simulated using an empirical rate constant, K_1, which in effect simply imposes a delay in the appearance of metabolite in the urine from the blood.

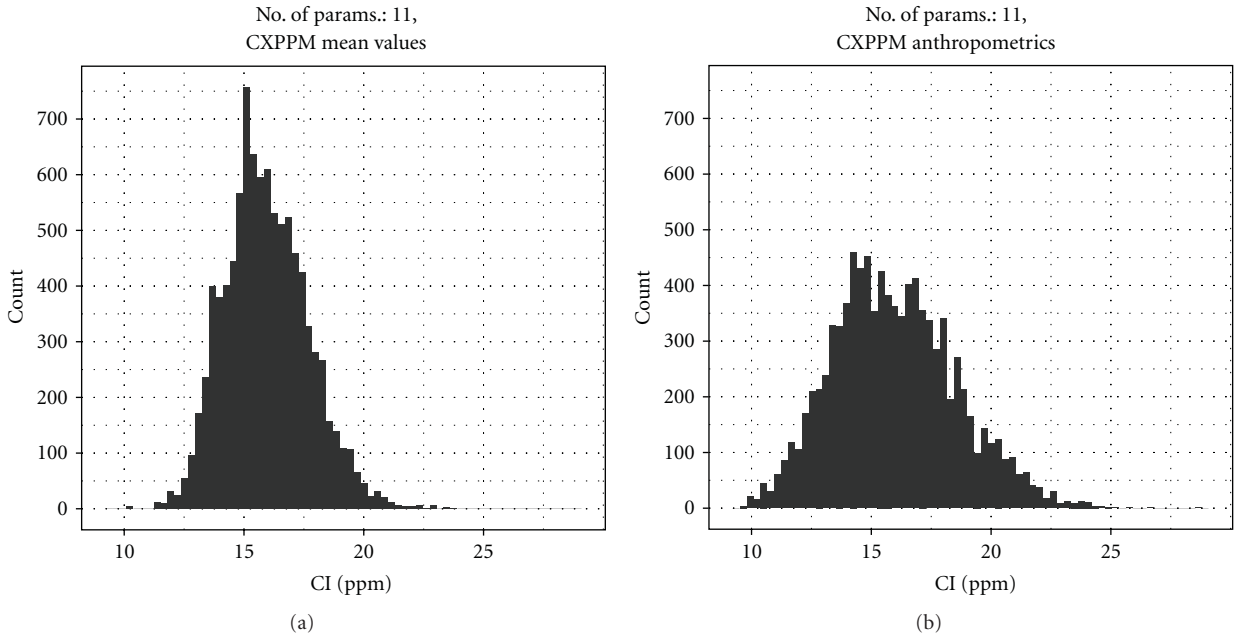

Figure 9: Comparison of estimated posterior distributions for 4-hour inhalation exposure to *m*-xylene. Posterior distributions were estimated by updating the most influential parameters or by fixing the measured parameters and updating the remaining most influential: (a) CXPPM, full parameter set, (b) CXPPM, most influential.

The model including measured parameters, **x**, but with mean values for R_{urine} and CRE had a narrower confidence interval for λ compared with the initial models; this reduction in uncertainty can be largely attributed to R_{urine} and CRE, which sensitivity analysis showed were the most influential parameters.

A modified PBPK model that allowed a time varying rate of urine production was fit to the data (Figure 7(c) and Table 5, most influential, including measured parameters, **x**, individual timed R_{urine}, and CRE). This model had a lower central estimate for the exposure λ (mean and median; 29.0 and 28.9 ppm, resp.), and the narrowest 95% interval for λ (25.1 to 33.6). The target exposure was outside the 95% interval using the most appropriate model (that reflects real BM data, assuming that urine volumes would be recorded during sample collection). The reasons for this finding are discussed in the following section.

3.6. Validation and Model Criticism. A key assumption of the calibration model was of independent, normally distributed residuals (the differences between log model predictions and log (CV, CXPPM, C_{urine}) measurements. Model validation was conducted to assess whether this assumption was satisfied.

Calibration using data from (reliable) CV measurements satisfied this assumption. Model predictions, from one iteration of parameters from the MCMC algorithm and corresponding measurements for three volunteers (A, C and D), are shown in Figure 10(a). Given that the PBPK model could predict the observed biomarker profile suggests that the model adequately describes the inhalation and subsequent excretion of *m*-xylene from the blood.

For CXPPM the model assumption of normally distributed residuals was not satisfied.

Predictions from the PBPK model from one iteration of parameters from the MCMC algorithm and corresponding measurements for three (representative) volunteers are shown in Figure 10(b). The figure demonstrates that the model was unable to replicate the very rapid decay of *m*-xylene in breath samples; the PBPK model proved to be inconsistent with measurements for any combination of model parameters. When using the data from CXPPM, the MCMC algorithm converged to a stationary distribution that minimized the overpredictions from the model and clearly the posterior distribution for λ is an unreliable estimate of exposure. The biomarker profiles from the eight volunteers were consistent and indicated that the measurements were reliable; therefore, the issue is with the PBPK model. The information from CV measurements gives some context to interpret this result as these data highlight that the model can adequately describe the uptake, and indeed the elimination of *m*-xylene, from the blood. Therefore, the PBPK model currently lacks some biological detail for describing the mechanism of exhalation of *m*-xylene. This is an area of ongoing research.

Whilst the estimates of exposure using the C_{urine} measurements and the PBPK model with individualised urine volume and creatinine measurements were close to the target exposure, the assumptions of the calibration model were not satisfied. Model predictions, from one iteration of parameters from the MCMC algorithm and corresponding measurements for three volunteers, are shown in Figure 10(c). The model proved a reasonable fit to measurements taken between 8 and 14 hours but overpredicted the initial elimination (4 and 6 hours) and

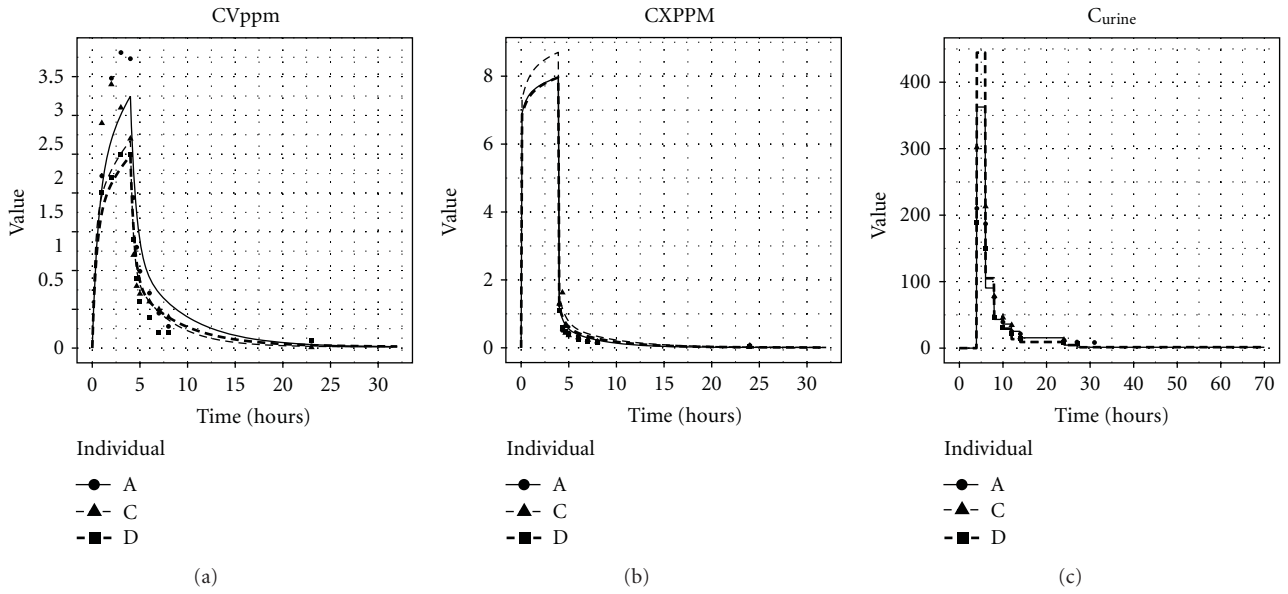

Figure 10: Model predictions for three volunteers from one iteration of the Markov chain and the associated measurements: (a) urine predictions and data, (b) CV predictions and data, (c) CX predictions and data.

under-predicted the concentrations the following day (at 24, 27, and 30 hours). The large difference in results from the model using the individualised urine volume and creatinine measurements compared with the other PBPK models based upon the urine measurements resulted from the former model providing a better fit to the measurements at 6 and 8 hours, whereas the latter models were a better fit to measurements at 24, 27, and 30. Given that the uptake of *m*-xylene to the blood is adequately described, this suggests the model lacks biological detail in the elimination of substance in urine.

Elimination of *m*-xylene in urine has been studied over a 60-hour period [36]. The data from this study are consistent with our own laboratory based study in showing that there is an initial decay to a nonzero value (the first 10 hours or so after exposure has ceased) and a much slower elimination of substance (taking in excess of 2 days) that follows. The model may require a "deep tissue" compartment to simulate the slower redistribution from fat and other tissue storage compartments [41].

3.7. Additional Results. A model using the reliable CV data with just the exposure concentration varying and all parameters fixed at central values was run for comparison (Table 5, all parameters fixed at central values). Such a model does not take human variability into account; the measurements are all, in effect, on the "mean human" with parameters set at the central values listed in Table 2. The result was a much lower central estimate of λ (24 and 23.8 ppm, mean and median, resp.), a narrower 95% confidence interval for the exposure (21–29 ppm), and a larger median for ρ (0.55). These latter two results are consistent with expectations. The lower range of exposures resulted from the 3 volunteers not being representative of the "mean human" (in particular with respect to PBA and QPC).

This admittedly unusual result demonstrates that it is important to recognise and model all known sources of uncertainty. However, the large difference in the 95% confidence intervals between this and our fitted models does suggest that the prior distributions for the model parameters were too wide; the subjects in our study were more homogeneous than the general population. More precise results would have been obtained if prior distributions based upon the study population had been adopted. In future work a greater emphasis will be placed on understanding and properly defining the study population.

4. Discussion

In this paper it was demonstrated that SA techniques could be used to reduce the dimensionality of the calibration problem with a relatively small loss of precision. The use of SA in this context is consistent with good modelling practice, with SA used as an integral part of the modelling process [42–45]. SA demonstrated that exposure reconstruction using urine data requires a greater number of individualised parameters in the PBPK model than either exhaled breath or blood. This is not surprising as the PBPK model needs to describe uptake, distribution, metabolism, and excretion in order to reconstruct exposure using urine measurements, and excretion from the body (in urine) takes in excess of 30 hours. More parameters are required to describe this process, with some parameters only becoming important at later periods (Table 4). In comparison the SA results for blood and breath models were more consistent, the same parameters were important throughout the full time-scale, although the relative importance of parameters did change, parameters governing uptake dominated during exposure, and these became less important after exposure ceased. It is important that the SA of the PBPK model covers the

full period where measurements (for comparison with the model) are available, so that the important parameters for model calibration using the available data are identified.

The results from SA did inform one substantial improvement in the description of urination in the PBPK model. It was noted that the model was especially sensitive to R_{urine}, the rate of urine production, and to a lesser extent CRE. The initial PBPK model represented these as constants (either unknown constants represented by probability distributions or as constants estimated from measurements, depending upon the model) for each individual. However, the experimental data revealed that there were substantial variations for each individual in both the rate of urine production and CRE over the 31-hour period of the study. The PBPK model was modified to allow time varying rates of R_{urine} and CRE. Here it can be seen that SA techniques can be used to inform model development as well as to reduce complexity. Also, the results of SA can help inform the prioritisation of resources and effort in the generation of good-quality data.

The aim of this work was not to estimate the most precise exposure for the subjects using all available measurements; rather the aim was to reconstruct exposure using a single measurement series and account for all significant uncertainties. This work can be viewed as an intermediate step between laboratory- and population-based studies. Models have been independently fit to breath, blood, and urine measurements, as these are a closer approximation to the data from a population-based study. However, whilst the models were independently fit, a more complete picture of the inadequacies of the PBPK model is obtained by interpreting the results collectively.

Looking into the future, the greatest challenge is to obtain estimates of a variable exposure concentration from biological monitoring data available from individual "spot samples," typically at the end of a shift for workplace exposures or at random times for environmental exposures. The appropriate extension to the calibration model compared with that used for data from our controlled laboratory study is straightforward. Each individual will have a unique exposure; a hierarchical model of exposure (Lyons et al., [10]) can be used to obtain a central estimate and an estimate of the variability in personal exposures. A greater challenge is that in general a single sample per individual may be available, *and* the time between the completion of exposure and the production of a urine sample will vary. As this study has shown, there is a strong correlation between the length of time after exposure and the sample concentration for nonpersistent and semipersistent chemicals (Figures 1, 2, and 3). Based upon the data available from biological monitoring, it will be very difficult to isolate personal exposures, after accounting for both biological variability *and* time after exposure. An intricate calibration model will be required. This is a major challenge for future work, although empirical statistical models may prove a useful tool. One option might be a two-phased approach: in the initial phase, a nonlinear mixed-effect model could be used, with a mean corresponding to a PBPK model containing the unknown exposure concentration as the sole unknown parameter and systematic differences between humans modelled by random effects. The posterior distribution for the exposure concentration from this first phase could provide an informative prior for the exposure concentration in more detailed PBPK models. The precision of exposure reconstruction would undoubtedly be improved if some contextual information (relating to the time since the last "significant" exposure) accompanied each sample.

Although this work has focussed on the calibration problem with respect to the exposure concentration, the data allow all the model parameters to be updated in light of the data. This includes updating the parameters for each (experimental) subject for quantities where population variability is well characterised (such as organ sizes and blood flows) and quantities about which there is considerable uncertainty in the general population. Some of the partition coefficients fell into this latter category; uniform distributions with wide support were used as the prior distributions for the partition coefficients *Pspda*, *Prpda,* and *Pfaa*. In principle the data would allow individualised partition coefficients to be estimated for each of the subjects. However, when there is uncertainty about variability in the general population, it is appealing to structure a model in order to learn about population variability; this can be achieved using a hierarchical model that incorporates a population mean and standard deviation into the calibration model. However, in this work the SA indicated that the model was insensitive to these uncertain partition coefficients, and these were therefore fixed at central values in the model.

Initial models using CV, CXPPM, and C_{urine} data ignored the subset of anthropometric parameters (listed in Table 1) that were available for each individual, and it was possible to compare the posterior distributions for these parameters with the known values. The posterior distributions for these parameters were similar to the priors: the data from subjects did result in some small changes; however, due to the large number of uncertain parameters for each individual, coupled with an unknown exposure, the changes were modest. For body weight (BW), the fat mass (VfaC), the blood : air partition (Pba) coefficient, and alveolar ventilation (QPC), in general the posteriors moved toward the known values (compared with the priors), although there was only a modest reduction in uncertainty compared with the prior. This is consistent with expectations; as the PBPK model is ill posed, a strong convergence to the known values for these parameters could not be achieved.

Given that the priors were similar to the posteriors, it is important to question the value of a fully Bayesian analysis using an MCMC algorithm that updates the parameters for each individual compared with a Monte-Carlo (MC) algorithm that accounts for interindividual differences by sampling from the priors. In this case a comparison of prior and posterior distributions for individual parameters is overly simplistic. A priori all parameters are independent, whereas parameters are correlated in the posterior distribution. This means that the multidimensional posterior is a very different shape to the multidimensional prior, even though the marginal distributions are similar. Specifically, a smaller domain of PBPK models is consistent with the observed data after calibration. In cases where fewer data

are available for calibration, MCMC will not offer the same improvements over MC sampling.

Throughout the paper we have used the terms *uncertainty* and *variability*, which are important and related concepts. There are numerous and wide ranging uncertainties in many modelling scenarios. O'Hagan and Oakley [46] identify the main components of uncertainty for computer models as parameter uncertainty, model inadequacy, residual variability, and code uncertainty. The various uncertainties in a model can be described as aleatory uncertainties, which arise from inherent variability or randomness in systems, and epistemic uncertainties, which arise due to imperfect knowledge. Oberkampf et al. [47] noted that a variety of terms in the literature have been used to describe these two classes of uncertainty; the terms irreducible (aleatory) and reducible (epistemic) uncertainty have perhaps the greatest clarity. Model inadequacy is a reducible source of uncertainty, residual variability may contain both reducible and irreducible uncertainties, and parameter value uncertainty is generally irreducible [46]. Probability can represent both reducible and irreducible sources of uncertainty.

Other authors use the term variability in place of alleatory uncertainty; however, we feel that this lacks clarity [48]. Variability is certainly closely related to alleatory uncertainty and can be both a cause of *and* a result of alleatory uncertainty. This can be seen in parameter value uncertainty, where interindividual differences (variability) between humans (partition coefficients, blood flows, organ masses, etc.) are represented by probability. There is parameter value (alleatory) uncertainty in a PBPK model for any given human due to interindividual differences; the unique parameters for any individual are *unknown*; only variation across the population is known. The net result is an increased variability in the outputs of that model, which arise from the parameter value uncertainty. Epistemic uncertainty also results in increased variability in model outputs.

In conclusion, the integration of PBPK modelling, global SA, Bayesian inference, and Markov chain Monte Carlo simulation is a powerful approach for exposure reconstruction from BM data. The use of global SA techniques could be used to reduce the dimensionality of PBPK models with a minimal loss of precision and with consequent savings in computational cost. Also, the use of SA in the model building and calibration phases is consistent with good modelling practice. However, the precision of posterior estimates of exposure is exquisitely dependent upon the ability of the PBPK model to characterise the chosen biomarker, which in turn is also exquisitely dependent upon the extent of biological detail captured in a PBPK model. Further work, on the level of detail required to satisfactorily describe renal elimination and exhalation of volatile biomarkers of exposure, is required.

Funding

This work was supported by the European Chemical Industry Council (CEFIC) (Grant number CEFIC-LRI-HBM2-DOW-0806) and the UK Department of Health (Grant number LOIZOU/CHEM/98/1).

Conflict of Interests

The authors declare that there are no conflict of interests.

Acknowledgments

The authors thank Professor David Fishwick, Judith Waterhouse, Lisa Bradshaw, and the staff of the Respiratory Function Unit of the Royal Hallamshire Hospital. They thank Dr. Hora Soltani for measuring the body composition of the volunteers using the bioimpedance apparatus. The authors thank Conrad Housand (AEgis Technologies) for assistance with writing the time varying rate of urine production model, time-dependent M functions for SA, and MCMC analyses. Finally, they thank Dr. Cecilia Tan for her insightful comments on an earlier draft of this paper.

References

[1] Consortium to Perform Human Biomonitoring on a European Scale (COPHES), Human Biomonitoring For Europe: A Harmonised Approach: http://www.eu-hbm.info/cophes.

[2] ESBIO, Expert Team to Support Biomonitoring in Europe: http://www.eu-humanbiomonitoring.org/sub/esbio.htm .

[3] Centers for Disease Control and Prevention (CDC), National Biomonitoring Program: http://www.cdc.gov/biomonitoring/environmental_chemicals.html.

[4] Canadian Health Measures Survey (CHMS), Canadian Health Measures Survey: http://www.statcan.gc.ca/cgi-bin/imdb/p2SV.pl?Function=getSurvey&SDDS=5071&lang=en&db=imdb&adm=8&dis=2

[5] P. J. Boogaard, S. M. Hays, and L. L. Aylward, "Human biomonitoring as a pragmatic tool to support health risk management of chemicals—examples under the EU REACH programme," *Regulatory Toxicology and Pharmacology*, vol. 59, no. 1, pp. 125–132, 2011.

[6] M. Manno, C. Viau, J. Cocker et al., "Biomonitoring for occupational health risk assessment (BOHRA)," *Toxicology Letters*, vol. 192, no. 1, pp. 3–16, 2010.

[7] National Research Council, *Human Biomonitoring for Environmental Chemicals*, National Academies Press, Washington, DC, USA, 2006.

[8] H. J. Clewell, Y. M. Tan, J. L. Campbell, and M. E. Andersen, "Quantitative Interpretation of Human Biomonitoring Data," *Toxicology and Applied Pharmacology*, vol. 231, no. 1, pp. 122–133, 2008.

[9] K. H. Liao, Y. M. Tan, and H. J. Clewell, "Development of a screening approach to interpret human biomonitoring data on volatile organic compounds: reverse dosimetry on biomonitoring data for trichloroethylene," *Risk Analysis*, vol. 27, no. 5, pp. 1223–1236, 2007.

[10] M. A. Lyons, R. S. H. Yang, A. N. Mayeno, and B. Reisfeld, "Computational toxicology of chloroform: reverse dosimetry using Bayesian inference, Markov chain Monte Carlo simulation, and human biomonitoring data," *Environmental Health Perspectives*, vol. 116, no. 8, pp. 1040–1046, 2008.

[11] Y. M. Tan, K. H. Liao, and H. J. Clewell, "Reverse dosimetry: interpreting trihalomethanes biomonitoring data using physiologically based pharmacokinetic modeling," *Journal of Exposure Science and Environmental Epidemiology*, vol. 17, no. 7, pp. 591–603, 2007.

[12] Y. M. Tan, K. Liao, R. Conolly, B. Blount, A. Mason, and H. Clewell, "Use of a physiologically based pharmacokinetic model to identify exposures consistent with human biomonitoring data for chloroform," *Journal of Toxicology and Environmental Health A*, vol. 69, no. 18, pp. 1727–1756, 2006.

[13] P. G. Georgopoulos, A. Roy, and M. A. Gallo, "Reconstruction of short-term multi-route exposure to volatile organic compounds using physiologically based pharmacokinetic models," *Journal of Exposure Analysis and Environmental Epidemiology*, vol. 4, no. 3, pp. 309–328, 1994.

[14] A. Roy and P. G. Georgopoulos, "Reconstructing week-long exposures to volatile organic compounds using physiologically based pharmacokinetic models," *Journal of Exposure Analysis and Environmental Epidemiology*, vol. 8, no. 3, pp. 407–422, 1998.

[15] P. L. Mosquin, A. C. Licata, B. Liu, S. C. J. Sumner, and M. S. Okino, "Reconstructing exposures from small samples using physiologically based pharmacokinetic models and multiple biomarkers," *Journal of Exposure Science and Environmental Epidemiology*, vol. 19, no. 3, pp. 284–297, 2009.

[16] A. Gelman, F. Bois, and J. Jiang, "Physiological pharmacokinetic analysis using population modeling and informative prior distributions," *Journal of the American Statistical Association*, vol. 91, no. 436, pp. 1400–1412, 1996.

[17] P. Bernillon and F. Y. Bois, "Statistical issues in toxicokinetic modeling: a Bayesian perspective," *Environmental Health Perspectives*, vol. 108, no. 5, pp. 883–893, 2000.

[18] C. E. Hack, "Bayesian analysis of physiologically based toxicokinetic and toxicodynamic models," *Toxicology*, vol. 221, no. 2-3, pp. 241–248, 2006.

[19] F. Jonsson and G. Johanson, "Bayesian estimation of variability in adipose tissue blood flow in man by physiologically based pharmacokinetic modeling of inhalation exposure to toluene," *Toxicology*, vol. 157, no. 3, pp. 177–193, 2001.

[20] T. R. Covington, P. Robinan Gentry, C. B. van Landingham, M. E. Andersen, J. E. Kester, and H. J. Clewell, "The use of Markov chain Monte Carlo uncertainty analysis to support a public health goal for perchloroethylene," *Regulatory Toxicology and Pharmacology*, vol. 47, no. 1, pp. 1–18, 2007.

[21] J. Hadamard, "Sur les problemes aux derivees partielles et leur signification physique," *Bulletin of the University of Princeton*, vol. 13, pp. 49–52, 1902.

[22] M. D. Sohn, T. E. McKone, and J. N. Blancato, "Reconstructing population exposures from dose biomarkers: inhalation of trichloroethylene (TCE) as a case study," *Journal of Exposure Analysis and Environmental Epidemiology*, vol. 14, no. 3, pp. 204–213, 2004.

[23] B. C. Allen, C. E. Hack, and H. J. Clewell, "Use of Markov chain Monte Carlo analysis with a physiologically-based pharmacokinetic model of methylmercury to estimate exposures in U.S. women of childbearing age," *Risk Analysis*, vol. 27, no. 4, pp. 947–959, 2007.

[24] K. McNally, R. Cotton, and G. Loizou, "A workflow for global sensitivity analysis of PBPK models, Frontiers in Pharmacology," *Predictive Toxicity*, vol. 2, article 31, pp. 1–21, 2011.

[25] D. Dyne, J. Cocker, and H. K. Wilson, "A novel device for capturing breath samples for solvent analysis," *Science of the Total Environment*, vol. 199, no. 1-2, pp. 83–89, 1997.

[26] G. D. Loizou, K. Jones, P. Akrill, D. Dyne, and J. Cocker, "Estimation of the dermal absorption of m-xylene vapor in humans using breath sampling and physiologically based pharmacokinetic analysis," *Toxicological Sciences*, vol. 48, no. 2, pp. 170–179, 1999.

[27] R. W. Bonsnes and H. H. Taussky, "On the colorimetric determination of creatinine by the Jaffe reaction," *Journal of Biological Chemistry*, vol. 158, pp. 581–591, 1945.

[28] R. Tardif, A. Sato, S. Lapare, and J. Brodeur, "Ethanol induced modification of m-xylene toxicokinetics in humans," *Occupational and Environmental Medicine*, vol. 51, no. 3, pp. 187–191, 1994.

[29] L. Campbell, H. K. Wilson, A. M. Samuel, and D. Gompertz, "Interactions of m-xylene and aspirin metabolism in man," *British Journal of Industrial Medicine*, vol. 45, no. 2, pp. 127–132, 1988.

[30] S. J. Franks, M. K. Spendiff, J. Cocker, and G. D. Loizou, "Physiologically based pharmacokinetic modelling of human exposure to 2-butoxyethanol," *Toxicology Letters*, vol. 162, no. 2-3, pp. 164–173, 2006.

[31] A. J. MacDonald, A. Rostami-Hodjegan, G. T. Tucker, and D. A. Linkens, "Analysis of solvent central nervous system toxicity and ethanol interactions using a human population physiologically based kinetic and dynamic model," *Regulatory Toxicology and Pharmacology*, vol. 35, no. 2, pp. 165–176, 2002.

[32] W. Tassaneeyakul, D. J. Birkett, J. W. Edwards et al., "Human cytochrome P450 isoform specificity in the regioselective metabolism of toluene and o-, m- and p-xylene 1," *Journal of Pharmacology and Experimental Therapeutics*, vol. 276, no. 1, pp. 101–108, 1996.

[33] E. M. Howgate, K. Rowland Yeo, N. J. Proctor, G. T. Tucker, and A. Rostami-Hodjegan, "Prediction of in vivo drug clearance from in vitro data. I: impact of inter-individual variability," *Xenobiotica*, vol. 36, no. 6, pp. 473–497, 2006.

[34] Z. E. Barter, M. K. Bayliss, P. H. Beaune et al., "Scaling factors for the extrapolation of in vivo metabolic drug clearance from in vitro data: reaching a consensus on values of human microsomal protein and hepatocellularity per gram of liver," *Current Drug Metabolism*, vol. 8, no. 1, pp. 33–45, 2007.

[35] S. Willmann, K. Höhn, A. Edginton et al., "Development of a physiology-based whole-body population model for assessing the influence of individual variability on the pharmacokinetics of drugs," *Journal of Pharmacokinetics and Pharmacodynamics*, vol. 34, no. 3, pp. 401–431, 2007.

[36] K. Engström, K. Husman, P. Pfäffli, and V. Riihimaki, "Evaluation of occupational exposure to xylene by blood, exhaled air and urine analysis," *Scandinavian Journal of Work, Environment and Health*, vol. 4, no. 2, pp. 114–121, 1978.

[37] S. P. Brooks, "Markov chain Monte Carlo method and its application," *Journal of the Royal Statistical Society Series D*, vol. 47, no. 1, pp. 69–100, 1998.

[38] R Development Core Team, *R: A Language and Environment for Statistical Computing*, R Foundation for Statistical Computing, Vienna, Austria, 2010.

[39] H. Wickham, *Ggplot2: Elegant Graphics for Data Analysis*, Springer, New York, NY, USA, 2009.

[40] K. Takahashi, build_legend, http://tiny.cc/lkl06, 2010.

[41] M. E. Andersen, R. Sarangapani, R. H. Reitz, R. H. Gallavan, I. D. Dobrev, and K. P. Plotzke, "Physiological modeling reveals novel pharmacokinetic behavior for inhaled octamethylcyclotetrasiloxane in rats," *Toxicological Sciences*, vol. 60, no. 2, pp. 214–231, 2001.

[42] A. Saltelli, S. Tarantola, F. Campolongo, and M. Ratto, *Sensitivity Analysis in Practice: A Guide to Assessing Scientific Models*, John Wiley & Sons, Chichester, UK, 2004.

[43] F. Campolongo and A. Saltelli, "Sensitivity analysis of an environmental model: an application of different analysis methods," *Reliability Engineering and System Safety*, vol. 57, no. 1, pp. 49–69, 1997.

[44] G. Loizou, M. Spendiff, H. A. Barton et al., "Development of good modelling practice for physiologically based pharmacokinetic models for use in risk assessment: the first steps," *Regulatory Toxicology and Pharmacology*, vol. 50, no. 3, pp. 400–411, 2008.

[45] World Health Organization (WHO), "Characterization and application of physiologically based pharmacokinetic models in risk assessment," Harmonization Project Document 9, World Health Organization, Geneva, Switzerland, 2010.

[46] A. O'Hagan and J. E. Oakley, "Probability is perfect, but we can't elicit it perfectly," *Reliability Engineering and System Safety*, vol. 85, no. 1–3, pp. 239–248, 2004.

[47] W. L. Oberkampf, J. C. Helton, C. A. Joslyn, S. F. Wojtkiewicz, and S. Ferson, "Challenge problems: uncertainty in system response given uncertain parameters," *Reliability Engineering and System Safety*, vol. 85, no. 1–3, pp. 11–19, 2004.

[48] F. Y. Bois, M. Jamei, and H. J. Clewell, "PBPK modelling of inter-individual variability in the pharmacokinetics of environmental chemicals," *Toxicology*, vol. 278, no. 3, pp. 256–267, 2010.

Hindawi Publishing Corporation
Journal of Toxicology
Volume 2012, Article ID 946742, 10 pages
doi:10.1155/2012/946742

Review Article

Update on a Pharmacokinetic-Centric Alternative Tier II Program for MMT—Part I: Program Implementation and Lessons Learned

David C. Dorman,[1] Melvin E. Andersen,[2] Jerry M. Roper,[3] and Michael D. Taylor[3]

[1] *College of Veterinary Medicine, North Carolina State University, Raleigh, NC 27607, USA*
[2] *Institute for Chemical Safety Sciences, The Hamner Institutes for Health Sciences, Research Triangle Park, NC 27709, USA*
[3] *Health, Safety, Environment, and Security, Afton Chemical Corp., Richmond, VA 23219, USA*

Correspondence should be addressed to Michael D. Taylor, mike.taylor@aftonchemical.com

Received 30 September 2011; Accepted 18 January 2012

Academic Editor: Kannan Krishnan

Concerns have been raised regarding environmental manganese exposure since high exposures have been associated with neurological disorders. The USA Environmental Protection Agency most recent human health risk assessment of inhaled manganese conducted in 1993 identified specific areas of uncertainty regarding manganese pharmacokinetics. This led to the development of a test rule under the USA Clean Air Act that required the generation of pharmacokinetic information on the inorganic manganese combustion products of the organometallic fuel additive methylcyclopentadienyl manganese tricarbonyl (MMT). The Alternative Tier 2 testing program for MMT, described in this paper, has yielded substantial pharmacokinetic data and has enabled the generation of physiologically based pharmacokinetic (PBPK) models for manganese. These models are capable of predicting tissue manganese concentrations across a variety of dose routes, levels, and durations while accounting for factors such as age, gender, and reproductive status, enabling the consideration of tissue dosimetry in future risk assessments.

1. Introduction

Methylcyclopentadienyl manganese tricarbonyl (MMT®, a registered trademark of Afton Chemical Corporation) is an organometallic fuel additive that was developed by the Ethyl Corporation in the 1950s. MMT is currently marketed globally by Afton Chemical Corporation among others. MMT has been used in a variety of fuels, including leaded and unleaded gasoline, diesel and turbine fuel, and fuel oil to raise octane and improve combustion [1]. Manganese concentrations in unleaded gasoline typically range from 5 to 20 ppm when MMT is used. In the United States, MMT is approved for use up to 8.3 ppm in conventional unleaded gasoline.

As a fuel additive, MMT falls under the regulatory domain of the United States Environmental Protection Agency (USEPA), and MMT manufacturers and/or importers are subject to relevant provisions of the USA Clean Air Act (CAA). This paper provides an overview of the novel CAA Alternative Tier 2 test program for MMT designed to collect critical manganese pharmacokinetic data in animals (all test reports and correspondence related to the Alternative Tier 2 Testing for MMT can be found in the Federal Docket Management System (FDMS) at http://www.regulations.gov identified by docket number EPA-HQ-OAR-2004-0074.). Follow-up efforts led to the development of a series of physiologically based pharmacokinetic (PBPK) models for manganese. This paper will briefly examine the toxicology of manganese, the regulatory history of MMT, the design and conduct of the Alternative Tier 2 program for MMT, key research findings derived from the health effects research program, and critical lessons learned that can be applied to other chemicals. The second paper in this two-part series [2] describes the PBPK models in greater detail and provides a framework for their application to the risk assessment of manganese.

2. Manganese Toxicology: Public Health Concerns about MMT

Manganese is an essential trace metal that is required for normal amino acid, lipid, protein, and carbohydrate metabolism. Under certain high-dose exposure conditions or disease states (e.g., hepatobiliary dysfunction), however, manganese can induce adverse neurological, reproductive, and respiratory effects in humans [3]. Manganese toxicity is dependent on the dose to target tissue and develops after inhalation, oral, and parenteral exposure; however, this paper will focus predominantly on inhalation. Atmospheric sources of manganese include manmade and natural sources including wind erosion of dusts and soils. Industries associated with manganese emissions include ferroalloy production, iron and steel foundries, and power plant and coke oven combustion emissions. Ambient (background) levels of manganese in rural and urban air range from 0.005 to 0.07 μg Mn/m^3 [4].

Neurological effects occur at lower dose levels than other adverse effects, so consideration of these effects drives the human health risk assessment of inhaled manganese [4–6]. The earliest manifestations of manganese neurotoxicity (manganism) include fatigue, headache, muscle cramps, loss of appetite, apathy, insomnia, and diminished libido. As manganese exposure continues and the disease progresses, patients may develop dystonia, bradykinesia, rigidity, gait disorders, postural instability, micrographia, and muscle tremors (for review see [7]). These signs are associated with primary involvement of the globus pallidus. Individuals with chronic manganese neurotoxicity resemble patients with Parkinson's disease; however, these syndromes can be distinguished both clinically and with neuroimaging studies [7]. Although these syndromes are clinically distinct, some studies suggest that manganese overexposure may pose a risk factor for Parkinson's disease [7, 8].

A variety of inhalation exposure scenarios exist for manganese from occupational settings with mid- to high-dose exposures to much lower exposures found in the general environment. Forms of manganese include but are not limited to manganese dioxide (MnO_2) and other oxides, manganese sulfate ($MnSO_4$), manganese phosphates ($MnPO_4$), and organometallic manganese compounds. Absent underlying hepatobiliary disease, frank manganese neurotoxicity has been observed in workers that have been chronically exposed to dusts or fumes that contain high levels (>1 mg Mn/m^3) of manganese [4]. More subtle neurobehavioral effects have been reported in welders and other workers at lower (~0.2 mg Mn/m^3) exposure concentrations [9]. One of the more influential occupational studies was performed by Roels and coworkers [10]. This cross-sectional study of male workers was used by the USEPA as their critical study for deriving their chronic inhalation reference concentration for manganese (RfC) of 0.05 μg/m^3 that was last updated in 1993 [6]. According to USEPA, an RfC is an estimate (with uncertainty spanning perhaps an order of magnitude) of a continuous inhalation exposure to the human population (including sensitive subgroups) that is likely to be without an appreciable risk of deleterious effects during a lifetime. Roels et al. [10] assessed employees from a Belgian alkaline battery production plant and controls from a polymer processing plant. Personal air samplers in the battery plant indicated an 8 hr time weighted average (TWA) exposure of 0.215 mg/m^3 for respirable manganese. An average cumulative exposure of 1.2 mg/m^3·years of respirable manganese was associated with decrements in some neurofunctional performances (e.g., mean reaction times, eye-hand coordination and muscles tremor scores) between the exposed group and the control group. Health Canada current risk assessment relied on a study of Italian ferroalloy workers performed by Lucchini and coworkers [11] for the derivation of their RfC for manganese [5]. Lucchini examined several cohorts of workers (furnace, casting, and welding job functions) between 1981 and 1997. Manganese exposures for all classes of workers dropped appreciably during this time. For example, the geometric mean manganese concentrations (in total dust) went from 167 to 54.7 μg/m^3 in the maintenance area where welding was performed. An exposure concentration of approximately 71 μg Mn/m^3 was derived from an estimated cumulative exposure index. Lucchini reported an association between occupational manganese exposure and some neurological effects including higher symptom reporting, increased tremor frequency, altered motor function, and impaired memory. Bailey and colleagues [12] published an alternative RfC value of 2–7 μg Mn/m^3 that was based upon their use of epidemiological studies published after 1992. The American Conference of Industrial Hygienists (ACGIH) threshold limit value (TLV) for elemental manganese and related inorganic compounds is 0.2 mg Mn/m^3 [13]. This standard is set as a time-weighted average for an 8 hr shift 5 days per week designed to protect workers in occupational settings.

Ambient manganese exposure data are needed to assess the potential public health impacts of MMT in fuel. Several of the most significant studies were performed in Canadian cities when MMT was widely used in the local fuel supply. For example, an extremely large effort using probabilistic sampling techniques measured manganese exposure levels in Toronto residents when all fuel contained MMT [14]. The results of this study and related analyses of data from personal samplers [15, 16] suggest that the median annualized nonoccupational exposure concentration was 0.008 μg/m^3 with the highest long-term exposures at or near 0.022 μg/m^3. as a respirable fraction ($PM_{2.5}$). Roadway measurement of soil manganese concentrations did not reveal a measurable increase in manganese levels along urban Toronto highways [17]. Studies from Australia have shed additional light on the impact of MMT on atmospheric manganese concentrations [18, 19]. Gulson and coworkers reported no significant changes in environmental samples or blood manganese concentrations in children following the introduction of MMT in Sydney.

Concerns regarding the use of MMT as a gasoline fuel additive have also been influenced by the USA experience of tetraethyl lead in gasoline. Concerns about automotive emissions of lead prompted the USEPA in 1973 to phase out the use of lead in gasoline [20]. The experience with tetraethyl lead created an environment of distrust between

public health officials, environmental legislators, advocacy groups, and fuel manufacturers. USEPA health effects testing program for MMT emerged from this challenging climate.

3. Overview of the Regulatory History of MMT

Manganese is listed as an air toxic by the USEPA. When the USEPA ordered the phasing out of leaded gasoline, MMT and other alternative octane enhancers were used in unleaded gasoline. In 1977, a Congressional amendment to the CAA banned the use of all fuel additives not "substantially similar" to gasoline, including MMT, unless the USEPA granted a waiver [21]. The prohibition on the use of MMT in gasoline was largely based on concerns that MMT use could affect the first generation of automotive emissions-control systems. Ethyl Corporation first applied for this waiver in 1978. This and several subsequent waiver petitions submitted by Ethyl Corporation were denied because of USEPA concerns regarding potential increases in exhaust hydrocarbon emissions resulting from MMT use [21].

As part of a later waiver application for MMT, the USEPA conducted a risk assessment of exposure to inhaled manganese in 1993, with the publication of an inhalation RfC of 0.05 μg/m^3 [6]. The USEPA used standard RfC development methodologies for a noncancer endpoint and based the RfC on the Roels et al. study [10] that evaluated neurobehavioral and motor movement impairments observed in workers exposed to manganese dioxide (MnO_2). The exposure concentration reported by Roels was considered by the USEPA to be a lowest-observable-adverse-effect level (LOAEL). The LOAEL value was adjusted for continuous exposure durations, and several uncertainty factors were applied. These uncertainty factors included use of a LOAEL instead of a no-observable-adverse-effect level (NOAEL), extrapolation from subchronic to chronic, protection of potential sensitive members of the human population, and a factor reflecting other uncertainties in the database, such as less-than chronic periods of exposure, inadequate information regarding developmental and reproductive toxicity, and uncertainty about the toxicity of various forms of manganese [22]. Although the nutritional essentiality of manganese in the diet was discussed in the documentation of the RfC, it played no practical role in the calculation of an RfC [21].

The USEPA also published a risk characterization that included exposure and dose-response assessments for MMT in gasoline [23, 24]. After completing this evaluation, EPA determined that use of MMT would not "cause or contribute" to the failure of vehicle emission control systems. EPA was unable to determine, however, whether a risk to the public health occurred from use in gasoline [25]. The agency stated "[a]lthough it is not possible based on the present information to conclude whether specific adverse health effects will be associated with manganese exposures in the vicinity of or exceeding the (estimated safe level over a lifetime of exposure), neither is it possible to conclude that adverse health effects will not be associated with such exposures. . .Given the information that is available at present and the uncertainties discussed here, a reasonable basis exists for concern regarding potential public health risks, especially for sensitive subpopulations, if MMT were to be widely used in unleaded gasoline [25]." The USEPA also concluded that long-term animal testing and exposure research were needed to more accurately define the risk. Coincidental to these activities, in July 1994, the USEPA Administrator denied Ethyl Corporation newest waiver petition specifically because of concerns about potential risks to public health [24] and refused to register MMT for use in the USA In 1995, the Ethyl Corporation successfully challenged the denial of its petition based on public health concerns (*Ethyl Corporation v. Browner,* 51 F.3d 1053 (D.C. Cir. 1995)), as well as USEPA decision not to register MMT (*Ethyl Corporation v. Browner,* 67 F.3d 941 (D.C. Cir. 1995)). As a result, the USEPA formally approved the use of MMT in conventional unleaded gasoline and registered it as a fuel additive under the CAA, allowing for its domestic sale.

Provisions of the CAA provide the USEPA with the authority to require testing of fuels and fuel additives used in motor vehicles, including MMT, to help fill data gaps and provide information that potentially would result in a more definitive risk evaluation. These health testing requirements are addressed in Sections 211(b)(2) and 211(e) of the CAA. Section 211(b)(2) states "For the purpose of registration of fuels and fuel additives, the Administrator shall, on a regular basis, require the manufacturer of any fuel or fuel additive" to conduct "Tier 2" tests to determine potential public health and environmental effects of the fuel or additive (including carcinogenic, teratogenic, or mutagenic effects). These studies would be conducted using test procedures and protocols established by the USEPA. Moreover, the CAA also provides USEPA with the discretion to modify the standard Tier 2 health effects testing requirements for a fuel or fuel additive by substituting, adding, or deleting testing requirements or changing the underlying vehicle/engine specifications (40 CFR 79.58(c)). Health effects testing for MMT fell under this so-called "Alternative Tier 2" requirement, as the concern and subsequent testing was focused around the inorganic exhaust products of MMT and not MMT itself.

4. Establishment of the Alternative Tier 2 Testing Program for MMT

In 2001, the Ethyl Corporation was notified by the USEPA of the Alternative Tier 2 provisions for MMT which fell within two general categories: pharmacokinetic testing of manganese compounds and characterization of manganese emissions from vehicles utilizing fuels containing MMT. A central objective of the MMT Alternative Tier 2 program was to generate data to support development of physiologically based pharmacokinetic (PBPK) models for manganese. As a result, PBPK model development became the subject of a series of studies funded by Afton Chemical Corp. and handled in a way similar to other facets of the Alternative Tier 2 program.

Multiple pharmacokinetic studies were performed in response to the USEPA mandate (Table 1). Studies that were required by the USEPA were performed in accordance with

Table 1: Overview of the pharmacokinetic studies conducted in response to the Alternative Tier 2 test program for MMT. The following forms of manganese (Mn) were used in these studies: Mn tetroxide, Mn sulfate, and Mn phosphate. Some studies also involved intravenous administration of radiolabeled Mn chloride ($^{54}MnCl_2$) to assess whole-body (WB) clearance.

Pharmacokinetic endpoint of interest	Regulatory Status	Animal Species	Manganese species and exposure conditions	Primary publication(s)
Particle solubility and dissolution kinetics	Voluntary	Rat	Phosphate, sulfate, and tetraoxide—intratracheal instillation 0, 0.04, 0.08, or 0.16 μg Mn/g Rats killed at 0, 1, 3, or 14 d	[42]
Exposure-response and WB clearance	Voluntary	Rat	Phosphate inhalation 6 h/d for either 5 d/wk or 7 d/wk at 0, 0.03, 0.3, or 3 mg Mn/m^3 for up to 14 d	[43]
Particle solubility and WB clearance	Voluntary	Rat	Sulfate and tetroxide inhalation 6 h/d for 7 d/wk at 0, 0.03, 0.3, or 3 mg Mn/m^3 for 14 d	[44]
Diet-inhalation interaction and WB clearance	Voluntary	Rat	Sulfate or tetroxide inhalation 6 h/d for 7 d/wk at 0, 0.03, or 0.3 mg Mn/m^3 for 14 d Low (2 ppm), sufficient (10 ppm), or high (100 ppm) Mn diets	[45, 46]
Olfactory transport of Mn	Voluntary	Rat	Chloride and phosphate inhalation ~0.5 mg Mn/m^3 for 90 min Occluded nostril model	[47, 48]
Individual susceptibility WB clearance Nasal pathology	Required	Rat	Inhalation Exposed 6 h/d for 5 d/wk to sulfate at 0.01, 0.1, or 0.5 mg Mn/m^3 or phosphate at 0.1 mg Mn/m^3 for up to 90 d Adult male, adult female, and senescent male	[49, 50]
Individual susceptibility	Required	Rat	Sulfate inhalation Exposed 6 h/d for 7 d/wk at 0, 0.05, 0.5, or 1 mg Mn/m^3 throughout the majority of pregnancy or lactation.	[41, 51]
Species differences Brain imaging Respiratory tract pathology and neurochemistry	Required	Rhesus monkey	Sulfate inhalation Exposed 6 h/d for 5 d/wk at 0, 0.06, 0.3, or 1.5 mg Mn/m^3 for up to 90 d.	[34–38]

the USEPA Good Laboratory Practice (GLP) Standards for Inhalation Exposure Health Effects Testing (40 CFR Part 79.60). All studies were performed at The Hamner Institutes for Health Sciences (Hamner) (formerly the Chemical Industry Institute of Toxicology (CIIT)). All required study protocols, protocol amendments, and draft final reports underwent independent scientific review by project specific "technical advisory panels" (TAPs) composed of individuals with expertise in inhalation toxicology, pharmacokinetics, and neurotoxicology (Figure 1). Members of the TAPs, which changed for the different facets of the test program, were chosen by the study sponsor with input from the testing laboratory and approved by the USEPA. All study results underwent additional independent peer review during subsequent publication of the work in scientific journals.

Several critical decisions were reached early in the MMT test program. These concerned the form of manganese to be examined, animal species used, and endpoints of interest. The main focus of the test program was to evaluate combustion products of MMT. This decision was influenced in part by the observation that MMT undergoes rapid photolysis when exposed to light, forming methylcyclopentadiene, cyclopentadiene, carbon monoxide, and a manganese carbonyl that is readily oxidized to trimanganese tetroxide [26]. One early dilemma facing study toxicologists was determination of these combustion products. Early studies performed by Ter Haar and coworkers [27] showed that the primary combustion product from MMT was Mn_3O_4. This study used fuel spiked with large concentrations of MMT, an automobile without a catalytic converter, and X-ray diffraction methods for chemical speciation, resulting in an artifactual apparent enrichment of Mn_3O_4 in the exhaust. Zayed et al. [28], using scanning electron microscopy coupled with energy dispersive X-ray spectrometry, also suggested that the chemical form of emitted manganese was as an oxide but could not rule out sulfates and other manganese species. Other studies, using lower treat rates representative of actual use patterns and more advanced analytical methods, including X-ray absorption near-edge structure (XANES) spectra and K-edge X-ray absorption

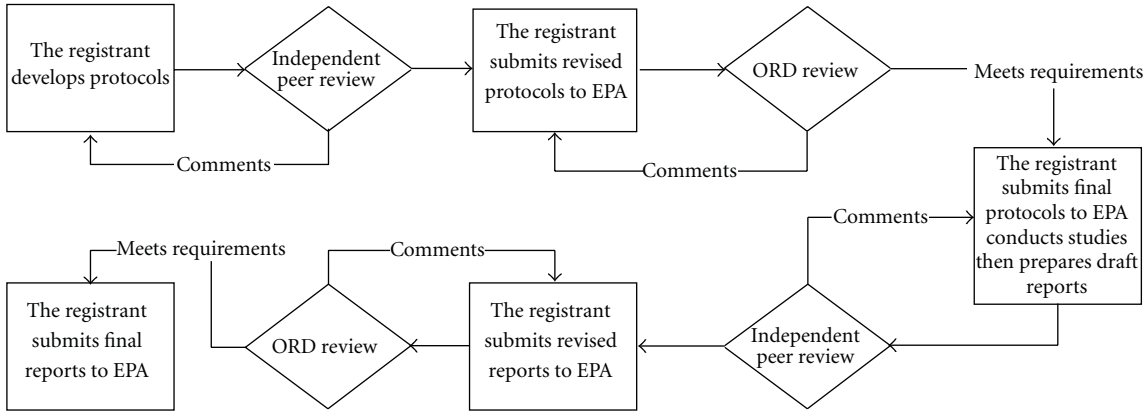

Figure 1: Schematic overview of steps used to develop and review study protocols and produce final reports. Independent peer review was carried out by the appropriate TAP. Completed final reports for all of the manganese studies can be found in the Federal Docket Management System (FDMS) at http://www.regulations.gov identified by docket number EPA-HQ-OAR-2004-0074. EPA: Environmental Protection Agency; ORD: EPA Office of Research and Development.

fine structure (XAFS) spectroscopy, showed the presence of three major manganese-containing components in tailpipe emissions: a divalent manganese phosphate, sulfate, and oxides (most likely as Mn_3O_4) [29–31]. The percentage of each component varied somewhat depending on the driving cycle and vehicle but remained relatively constant with the sulfate and the phosphate forms being the major (~80%) components [1].

The USEPA subsequently agreed to the use of commercially available manganese phosphate (as hureaulite), $MnSO_4$, and Mn_3O_4 for the inhalation studies rather than rely on the use of a dynamometer system that used MMT in the fuel source to generate exhaust particulates. This decision also allowed the Hamner research team to achieve the high exposure concentrations (mg/m^3) required to conduct the study. Such high concentrations were necessary to ensure tissue accumulation so the data could be used to inform the subsequent PBPK models. Similar aerosol concentrations and particle sizes were used in the Hamner inhalation studies to facilitate direct comparison of tissue manganese burdens among these experiments. Early studies used all three forms of manganese while later experiments relied upon the form of manganese ($MnSO_4$) that produced the greatest increase in brain manganese concentrations, representing a "worse-case scenario" with regards to potential brain delivery.

Another unique feature of the MMT alternative Tier 2 test program was the use of rhesus monkeys for certain studies. A substantial literature base describing species differences in neurological responses following high-dose manganese exposure existed at the time the Alternative Tier 2 program was launched. Unlike rats, manganese-exposed monkeys develop distribution patterns for this metal within the brain that mimic those seen in heavily exposed people and develop similar neuropathology and behavioral responses [32–34]. Despite these pharmacodynamic differences in response between rats and humans, pharmacokinetic data obtained from rats remained valuable because rats and primates show similar overall pharmacokinetic responses to manganese exposure, including the induction of homeostatic control mechanisms. The rat data provided critical insights into the dose-response relationship for inhaled manganese, especially during different life stages.

Once the decision to use rhesus monkeys was reached, there was a concerted effort to maximize the data that could be obtained from this study. Study endpoints included tissue manganese concentrations following $MnSO_4$ exposure [35], brain magnetic resonance imaging (MRI) studies [36], respiratory tract pathology [37], catecholamine neurochemistry [38], biomarkers of neurotoxicity and oxidative stress [39], and metabolomic biomarkers of exposure [40]. The USEPA waived the GLP requirements for certain study endpoints, including the MRI study, neurochemistry measurements, and the assessment of biomarker endpoints.

Another challenge that faced the research team was conduct of the required gestational and lactational inhalational studies. These studies required the coexposure of lactating rat dams and their pups. Inhalation developmental neurotoxicity and pharmacokinetic studies generally rely on maternal separation during exposure, resulting in pup stress that may alter development, thereby confounding study results. To overcome this potential confounding variable, Vitarella and coworkers [41] developed a unique single-animal exposure cylinder designed to house a rat dam and her litter. These investigators first tested concentrations of manganese phosphate within the exposure cylinder to verify that particle concentrations within this system were equivalent to those achieved within a stainless steel 1-m^3 inhalation chamber. Once developed, this system was then used to support the rat lactational exposure study required by the USEPA [42].

5. Key Research Findings

A number of significant discoveries emerged from this testing program (Table 2). While these studies are described in detail

Table 2: Notable scientific contributions derived from the MMT Alternative Tier 2 test program.

Pharmacokinetic endpoint	Key Finding(s)
Chemical form of manganese	Lung uptake and brain (tissue) delivery is highly influenced by solubility (sulfate ≫ phosphate > tetroxide)
Dose and duration dependences	Manganese uptake and elimination rates depend on exposure dose and exposure duration Delivery to the brain and development of pseudosteady manganese concentrations develop rapidly Biliary excretion shows similar time and concentration dependencies.
Homeostatic control	Manganese concentration in brain remains controlled at low levels of exposure and accumulates at air concentrations >10–50 $\mu g/m^3$
Dose metrics	Dose rate rather than cumulative dose appears to be the appropriate dose metric at low levels of exposure
Route of exposure	The observed pharmacokinetic differences between dietary and inhaled manganese can be attributed to rates of uptake and elimination required to achieve the same target tissue doses
Olfactory transport	Inhaled manganese is taken up by the nasal olfactory epithelium and transported directly via the olfactory nerve to the olfactory bulb
Species differences	Despite specific pharmacokinetic differences between rats and nonhuman primates, similar overall pharmacokinetic responses to and homeostatic controls of manganese were observed across species

in their individual publications, several significant findings are summarized here.

Solubility. The Hamner particle solubility studies showed that hureaulite and Mn_3O_4 are relatively insoluble in simulated lung lining fluids, while $MnSO_4$ is considerably more soluble in biological fluids [52]. These studies also showed that soluble manganese forms like the sulfate are more rapidly cleared from the rat lung and delivered to the rat brain following inhalation than are insoluble manganese oxide and phosphate particles.

Direct Olfactory to Deep Brain Transport. One project goal was to determine whether inhaled manganese could be transported to the brain directly via the olfactory nerve. Interest in this topic was sparked by the knowledge that the olfactory system forms a direct interface between the air and the brain. The Hamner conducted studies in rats using short-term (90 min) inhalation exposure to radiolabeled (^{54}Mn) aerosols in rats with one occluded nostril, thus restricting olfactory transport of manganese to only one side of the rat brain. These novel studies dramatically demonstrated that the olfactory route contributes the vast majority (>90%) of the ^{54}Mn found in the olfactory pathway of the rat brain up to 8 days following acute inhalation exposure. To our knowledge, this was the first study to demonstrate that an inhaled metal could be delivered to the olfactory brain regions directly via the olfactory nerve. Although olfactory transport rapidly delivers manganese to brain structures in the olfactory pathway, it appears to be relatively slow (and inefficient) in delivering inhaled manganese to the rat striatum and other more distant brain structures [53].

Addition of Inhaled Manganese to Existing Oral Exposures. Individuals with either deficient or excessive manganese tissue burdens have been postulated to be at increased risk for manganese toxicity following inhalation exposure [45]. Two related 14-day inhalation studies conducted by the Hamner demonstrated that manganese body burden does not influence brain manganese concentrations following inhalation [44, 54]. These studies placed postnatal day (PND) 10 rats on specially formulated diets that contained 2, 10, or 100 ppm manganese. The lowest and highest diets were chosen in order to provide the animals with a marginally deficient or high-normal level of manganese. The 10 ppm manganese diet used in the studies met rodent dietary guidelines. Once tissue manganese concentrations stabilized (i.e., after 2 months on the special diets), rats were exposed by whole-body inhalation for 6 hr/day on 14 consecutive days to $MnSO_4$ or Mn_3O_4 at concentrations equivalent to 0, 0.03, or 0.3 mg Mn/m^3. Feeding the 2 ppm manganese diet was associated with a number of effects, including reduced body weight gain, decreased liver manganese concentrations, and reduced whole-body manganese clearance rates. Although rats kept on this diet and then exposed to 0.3 mg Mn/m^3 developed increased manganese concentrations in some tissues, the studies did not demonstrate any statistically significant diet and inhalation interactions on brain manganese concentrations.

Neonatal Exposures. Concerns have been raised regarding increased risk of neonates for manganese-induced neurotoxicity [32]. The increased sensitivity of neonatal animals to manganese appears to be due in part to their ability to develop higher brain manganese levels than adults when faced with equivalent or lesser manganese exposures by high-dose oral gavage [51]. Factors influencing this increased susceptibility of neonatal animals may include enhanced manganese absorption from the gastrointestinal tract, an incompletely formed blood-brain barrier, and a greatly reduced basal biliary manganese excretory rate until weaning. However, information was more limited regarding the potential risks in neonates exposed to airborne manganese. To further assess this concern, the Hamner exposed rat

dams and their offspring to air or $MnSO_4$ (0.05, 0.5, or 1 mg Mn/m^3) for 6 hr/day, 7 days/week starting 28 days prior to breeding and from PND 1 through 18. The experimentally determined manganese concentration in neonatal striatum and the model-predicted AUC for this brain region did not imply significantly higher exposures in the pups when compared to those in adults up to the inhaled dose of 1 mg/m^3 [55, 56]. Despite the virtual absence of basal biliary excretion in neonatal rats, they appear to induce their biliary excretion when challenged with excess manganese through the oral route [57]. This inducible excretion in neonates was shown to be applicable to inhaled manganese as well to a level comparable to adults [56]. Because neonates have an increased requirement for manganese for optimal brain development, further elaboration of the dose-response relationship between brain manganese levels and neurotoxicity may further elucidate the potential vulnerability of neonatal brain to manganese.

Studies in Rhesus Monkeys. The Hamner inhalation study that exposed juvenile rhesus monkeys to $MnSO_4$ is amongst the most critical completed to date with manganese. In this study, one group of monkeys was exposed to either air or $MnSO_4$ (0.06, 0.3, or 1.5 mg Mn/m^3) for 65 exposure days (6 hr/day, 5 days/week) before tissue analysis. Additional monkeys were exposed to $MnSO_4$ at 1.5 mg Mn/m^3 for 15 or 33 exposure days and evaluated immediately thereafter or for 65 exposure days followed by a 45- or 90-day delay before evaluation. Monkeys exposed to $MnSO_4$ at $\geq$0.06 mg Mn/m^3 developed increased manganese concentrations in the globus pallidus, putamen, olfactory epithelium, olfactory bulb, and cerebellum. Absolute manganese concentrations in the $MnSO_4$-exposed monkeys demonstrated a decreasing peripheral-central concentration gradient within the olfactory system (i.e., olfactory epithelium $\gg$ olfactory bulb > olfactory tract > olfactory cortex). These data are consistent with direct olfactory transport of inhaled manganese. Increased pallidal manganese concentrations were evident by brain MRI and further confirmed by atomic absorption spectrometry analysis of the tissues [36]. MRI changes seen in this monkey study were similar to those reported in welders that have had high manganese exposure and subsequently developed bilateral hyperintensity on T1-weighted images in the globus pallidus and other brain regions [7]. Signal hyperintensities could not be visualized by MRI between the olfactory bulb and more distal sites, suggesting that direct translocation of manganese from the olfactory bulb to the globus pallidus did not occur in the manganese-exposed monkeys. Metabolomic analysis of serum and chemical analysis of brain tissues from the $MnSO_4$-exposed monkeys revealed changes indicative of oxidative stress at higher exposure concentrations [39, 40]. Dorman and coworkers [37] also reported that exposure of monkeys to $MnSO_4$ at 1.5 mg Mn/m^3 for $\geq$15 exposure days resulted in increased lung manganese concentrations, mild subacute bronchiolitis, alveolar duct inflammation, and proliferation of bronchus-associated lymphoid tissue. Bronchiolitis and alveolar duct inflammatory changes were absent 45 days after exposure, suggesting that these lesions are reversible upon cessation of subchronic high-dose manganese exposure.

6. Lessons Learned

The work described herein represents the most extensive set of pharmacokinetic studies performed to date under the USEPA Alternative Tier 2 requirements. The pharmacokinetic data that was collected through this testing program has dramatically improved our understanding of the health risks posed by manganese. These studies have led to an improved understanding of the exposure conditions that lead to increased concentrations of the metal within the adult and developing brain and other tissues. This work has also led to the development of predictive, PBPK models for inhaled manganese that relate lung, brain, and other tissue manganese concentrations to exposure concentrations [2]. These PBPK models should lead to the development of human health risk assessments for inhaled manganese that will consider both its essentiality and neurotoxicity.

This testing program also represents an example of productive industry/government cooperation despite the challenging regulatory climate under which it commenced [22]. Evidence of cooperation was manifested by the sponsor's willingness to conduct additional studies that were outside of the scope of the required testing program. Some examples included work to evaluate olfactory transport of manganese following inhalation, short-term (2 weeks) pharmacokinetic studies, and experiments designed to examine the elimination kinetics of inhaled manganese (see Table 1). Many of these studies were needed to develop the framework for subsequent development of the PBPK models. In addition, the sponsor also voluntarily developed the human PBPK models, as only the animal models were required by USEPA. All parties involved in this program shared a common desire to develop the most robust set of experiments possible. Figure 1 shows the extensive review and oversight by EPA and others that contributed to the development of robust experimental protocols. In addition, all parties involved recognized the value of the development and use of novel technologies (e.g., inhalation exposure systems for lactating rats) and incorporation of a wide array of endpoints, including MRI. There was also great value in conducting the work at a multidisciplinary independent research institute that could help facilitate discussions between the USEPA and the research sponsor. Incorporation of additional manganese TAPs composed of external experts also built on the Hamner's rich history of independent external peer review of their research programs. This testing program also benefited from multiple postdoctoral fellows and undergraduate researchers; thus, this program also played a key role in training new scientists.

Finally, the MMT testing program is aligned with the National Research Council vision described in their report entitled "*Toxicity Testing in the 21st Century: A Vision and a Strategy*" [58]. The three main components of the NRC vision for the future of toxicity testing are chemical characterization, toxicity testing, and dose-response and

extrapolation modeling. The NCR vision also describes a paradigm shift away from a focus on identifying adverse effects observed in experimental animals at high doses toward identifying and avoiding biologically significant perturbations of key toxicity pathways [59]. The identification of transition points between normal function and exposures that lead to accumulation and effects of an agent, as well as a consideration of the adaptive changes that respond to initial perturbations and function to maintain homeostasis, is a key to the NRC vision (see [58, Figure 2.2]). In our opinion, significant changes in tissue manganese concentrations represent a critical early step in the development of manganese neurotoxicity. Importantly, this work has identified a dose-dependent transition in manganese kinetics, which is a point where there is a change in the relationship of tissue accumulation as a function of dose [60, 61]. The pharmacokinetic data and PBPK modeling have shown that background tissue manganese levels are well maintained at low to moderate exposure levels, due to the existence of homeostatic control mechanisms, such as increased biliary manganese excretion, that serve to regulate tissue levels. Only once those mechanisms are overwhelmed do tissue levels start to increase significantly. Due to the existence of this dose-dependent transition, only roughly one order of magnitude separates the point of departures on which previous manganese risk assessments are based and a level of exposure at which no significant changes in Mn tissue concentration is predicted to occur in target tissues. This may indicate that large uncertainty factors are not necessary when extrapolating high-dose occupational exposure levels to low environmental exposure levels for the general population for an essential element such as Mn. The human PBPK models for Mn that emerged from this program can be used to further analyze the relationship between exposure and target tissue concentration and provide a consistent dose-response relationship for the effects of Mn regardless of exposure route and duration [43]. The models can be used to extrapolate to lower exposures to determine a concentration at which no significant effect on brain concentrations would be expected compared to normal variation. The human PBPK model can consider all life stages (fetuses, neonates, adults, and old age), both genders, pregnancy, and form of Mn. This model will be a critical tool for the quantitative risk assessment of environmental and occupational exposures to Mn. The model and these applications are discussed in more detail in Part 2 of this series [2].

Acknowledgments

The authors would like to thank Dr. William K. Boyes for generously providing Figure 1 and contributing to helpful discussions regarding this paper. Members of the in-life Technical Advisory Panel, including Drs. Gunter Oberdorster (Chair), Fred Hochberg, Joseph Rodricks, Karl Keene, and Michael Aschner, and the modeling Technical Advisory Panel, including Drs. Daniel Krewski (Chair), Jeff Fisher, and Michele Medinsky, are gratefully acknowledged. This publication and work is based on studies sponsored and funded by Afton Chemical Corporation in satisfaction of registration requirements arising under Section 211(a) and (b) of the Clean Air Act and corresponding regulations at 40 CFR Substance 79.50 et seq.

References

[1] G. D. Pfeifer, J. M. Roper, D. Dorman, and D. R. Lynam, "Health and environmental testing of manganese exhaust products from use of methylcyclopentadienyl manganese tricarbonyl in gasoline," *Science of the Total Environment*, vol. 334-335, pp. 397–408, 2004.

[2] M. D. Taylor, M. E. Andersen, J. D. Schroeter, M. Yoon, A. M. Keene, and D. C. Dorman, "Update on a pharmacokinetic-centricalternative Tier II program for MMT. Part II. physiologically-based pharmacokinetic modeling and manganese risk assessment," *Journal of Toxicology*. In press.

[3] J. L. Aschner and M. Aschner, "Nutritional aspects of manganese homeostasis," *Molecular Aspects of Medicine*, vol. 26, no. 4-5, pp. 353–362, 2005.

[4] Agency for Toxic Substances and Disease Registry (ATSDR), *Toxicological Profile for Manganese*, U.S. Department of Health and Human Services, Atlanta, Ga, USA, 2008, http://www.atsdr.cdc.gov/toxprofiles/tp.asp?id=102&tid=23.

[5] Health Canada, "Human Health Risk Assessment for Inhaled Manganese," ISBN: 978-1-100-15221-9, 2010, http://www.hc-sc.gc.ca/ewh-semt/pubs/air/manganese-eng.php.

[6] U.S. Environmental Protection Agency (USEPA), "Integrated Risk Information System (IRIS) Manganese (CASRN 7439-96-5) Reference Concentration for Chronic Inhalation Exposure (RfC)," 1993, http://www.epa.gov/iris/subst/0373.htm.

[7] T. R. Guilarte, "Manganese and Parkinson's disease: a critical review and new findings," *Environmental Health Perspectives*, vol. 118, no. 8, pp. 1071–1080, 2010.

[8] M. Aschner, K. M. Erikson, E. H. Hernández, and R. Tjalkens, "Manganese and its role in Parkinson's disease: from transport to neuropathology," *NeuroMolecular Medicine*, vol. 11, no. 4, pp. 252–266, 2009.

[9] A. B. Santamaria and S. I. Sulsky, "Risk assessment of an essential element: manganese," *Journal of Toxicology and Environmental Health A*, vol. 73, no. 2-3, pp. 128–155, 2010.

[10] H. A. Roels, P. Ghyselen, J. P. Buchet, E. Ceulemans, and R. R. Lauwerys, "Assessment of the permissible exposure level to manganese in workers exposed to manganese dioxide dust," *British Journal of Industrial Medicine*, vol. 49, no. 1, pp. 25–34, 1992.

[11] R. Lucchini, P. Apostoli, C. Perrone et al., "Long term exposure to "low levels" of manganese oxides and neurofunctional changes in ferroalloy workers," *NeuroToxicology*, vol. 20, no. 2-3, pp. 287–298, 1999.

[12] L. A. Bailey, J. E. Goodman, and B. D. Beck, "Proposal for a revised Reference Concentration (RfC) for manganese based on recent epidemiological studies," *Regulatory Toxicology and Pharmacology*, vol. 55, no. 3, pp. 330–339, 2009.

[13] American Conference of Governmental Industrial Hygienists (ACGIH) 2011 TLVs and BEIs, Publication #0111.

[14] E. D. Pellizzari, C. A. Clayton, C. E. Rodes et al., "Particulate matter and manganese exposures in Toronto, Canada," *Atmospheric Environment*, vol. 33, no. 5, pp. 721–734, 1999.

[15] C. A. Clayton, E. D. Pellizzari, C. E. Rodes, R. E. Mason, and L. L. Piper, "Estimating distributions of long-term particulate matter and manganese exposures for residents of Toronto,

Canada," *Atmospheric Environment*, vol. 33, no. 16, pp. 2515–2526, 1999.

[16] K. S. Crump, "Manganese exposures in Toronto during use of the gasoline additive, methylcyclopentadienyl manganese tricarbonyl," *Journal of Exposure Analysis and Environmental Epidemiology*, vol. 10, no. 3, pp. 227–239, 2000.

[17] A. K. Bhuie and D. N. Roy, "Deposition of Mn from automotive combustion of methylcyclopentadienyl manganese tricarbonyl beside the major highways in the greater Toronto area, Canada," *Journal of the Air and Waste Management Association*, vol. 51, no. 9, pp. 1288–1301, 2001.

[18] B. Gulson, K. Mizon, A. Taylor et al., "Changes in manganese and lead in the environment and young children associated with the introduction of methylcyclopentadienyl manganese tricarbonyl in gasoline—Preliminary results," *Environmental Research*, vol. 100, no. 1, pp. 100–114, 2006.

[19] B. Gulson, K. Mizon, A. Taylor et al., "Longitudinal monitoring of selected elements in blood of healthy young children," *Journal of Trace Elements in Medicine and Biology*, vol. 22, no. 3, pp. 206–214, 2008.

[20] K. Bridbord and D. Hanson, "A personal perspective on the initial federal health-based regulation to remove lead from gasoline," *Environmental Health Perspectives*, vol. 117, no. 8, pp. 1195–1201, 2009.

[21] J. M. Davis, "Methylcyclopentadienyl manganese tricarbonyl: health risk uncertainties and research directions," *Environmental Health Perspectives*, vol. 106, supplement 1, pp. 191–201, 1998.

[22] W. K. Boyes, "Essentiality, toxicity, and uncertainty in the risk assessment of manganese," *Journal of Toxicology and Environmental Health A*, vol. 73, no. 2-3, pp. 159–165, 2010.

[23] J. M. Davis, "Inhalation health risks of manganese: an EPA perspective," *NeuroToxicology*, vol. 20, no. 2-3, pp. 511–518, 1999.

[24] U.S. Environmental Protection Agency (USEPA), Fuels and fuel additives; waiver decision/circuit court remand. Fed Reg 59:42227-42247, 1994.

[25] U.S. Environmental Protection Agency (USEPA) (2011), Comments on the Gasoline Additive MMT (methylcyclopentadienyl manganese tricarbonyl), 2011, http://www.epa.gov/otaq/regs/fuels/additive/mmt_cmts.htm.

[26] A. W. Garrison, M. G. Cipollone, N. L. Wolfe, and R. R. Swank, "Environmental fate of methylcyclopentadienyl manganese tricarbonyl," *Environmental Toxicology and Chemistry*, vol. 14, no. 11, pp. 1859–1864, 1995.

[27] G. L. Ter Haar, M. E. Griffing, and M. Brandt, "Methylcyclopentadienyl manganese tricarbonyl as an antiknock: composition and fate of manganese exhaust products," *Journal of the Air Pollution Control Association*, vol. 25, no. 8, pp. 858–860, 1975.

[28] J. Zayed, B. Hong, and G. L'Espérance, "Characterization of manganese-containing particles collected from the exhaust emissions of automobiles running with MMT additive," *Environmental Science and Technology*, vol. 33, no. 19, pp. 3341–3346, 1999.

[29] C. Colmenares, S. Deutsch, C. Evans et al., "Analysis of manganese particulates from automotive decomposition of methylcyclopentadienyl manganese tricarbonyl," *Applied Surface Science*, vol. 151, no. 3, pp. 189–202, 1999.

[30] N. Mölders, P. J. Schilling, J. Wong, J. W. Rods, and I. L. Smith, "X-ray fluorescence mapping and micro-XANES spectroscopic characterization of exhaust particulates emitted from auto engines burning MMT-added gasoline," *Environmental Science and Technology*, vol. 35, no. 15, pp. 3122–3129, 2001.

[31] T. Ressler, J. Wong, J. Roos, and I. L. Smith, "Quantitative speciation of mn-bearing particulates emitted from autos burning (methylcyclopentadienyl) manganese tricarbonyl-added gasolines using XANES spectroscopy," *Environmental Science and Technology*, vol. 34, no. 6, pp. 950–958, 2000.

[32] M. Aschner, K. M. Erikson, and D. C. Dorman, "Manganese dosimetry: species differences and implications for neurotoxicity," *Critical Reviews in Toxicology*, vol. 35, no. 1, pp. 1–32, 2005.

[33] W. K. Boyes and D. B. Miller, "A review of rodent models of manganese neurotoxicity," *Neurotoxicology*, abstract 468, 1998.

[34] C. W. Olanow, P. F. Good, H. Shinotoh et al., "Manganese intoxication in the rhesus monkey: a clinical, imaging, pathologic, and biochemical study," *Neurology*, vol. 46, no. 2, pp. 492–498, 1996.

[35] D. C. Dorman, M. F. Struve, M. W. Marshall, C. U. Parkinson, R. A. James, and B. A. Wong, "Tissue manganese concentrations in young male rhesus monkeys following subchronic manganese sulfate inhalation," *Toxicological Sciences*, vol. 92, no. 1, pp. 201–210, 2006.

[36] D. C. Dorman, M. F. Struve, B. A. Wong, J. A. Dye, and I. D. Robertson, "Correlation of brain magnetic resonance imaging changes with pallidal manganese concentrations in rhesus monkeys following subchronic manganese inhalation," *Toxicological Sciences*, vol. 92, no. 1, pp. 219–227, 2006.

[37] D. C. Dorman, M. F. Struve, E. A. Gross, B. A. Wong, and P. C. Howroyd, "Sub-chronic inhalation of high concentrations of manganese sulfate induces lower airway pathology in rhesus monkeys," *Respiratory Research*, vol. 6, article 121, 2005.

[38] M. F. Struve, B. E. McManus, B. A. Wong, and D. C. Dorman, "Basal ganglia neurotransmitter concentrations in rhesus monkeys following subchronic manganese sulfate inhalation," *American Journal of Industrial Medicine*, vol. 50, no. 10, pp. 772–778, 2007.

[39] K. M. Erikson, D. C. Dorman, L. H. Lash, and M. Aschner, "Manganese inhalation by rhesus monkeys is associated with brain regional changes in biomarkers of neurotoxicity," *Toxicological Sciences*, vol. 97, no. 2, pp. 459–466, 2007.

[40] D. C. Dorman, M. F. Struve, A. Norris, and A. J. Higgins, "Metabolomic analyses of body fluids after subchronic manganese inhalation in Rhesus monkeys," *Toxicological Sciences*, vol. 106, no. 1, pp. 46–54, 2008.

[41] D. Vitarella, R. A. James, K. L. Miller, M. F. Struve, B. A. Wong, and D. C. Dorman, "Development of an inhalation system for the simultaneous exposure of rat dams and pups during developmental neurotoxicity studies," *Inhalation Toxicology*, vol. 10, no. 12, pp. 1095–1117, 1998.

[42] D. C. Dorman, A. M. McElveen, M. W. Marshall et al., "Maternal-fetal distribution of manganese in the rat following inhalation exposure to manganese sulfate," *NeuroToxicology*, vol. 26, no. 4, pp. 625–632, 2005.

[43] J. D. Schroeter, A. Nong, M. Yoon et al., "Analysis of manganese tracer kinetics and target tissue dosimetry in monkeys and humans with multi-route physiologically based pharmacokinetic models," *Toxicological Sciences*, vol. 120, no. 2, pp. 481–498, 2011.

[44] D. C. Dorman, M. F. Struve, R. A. James, M. W. Marshall, C. U. Parkinson, and B. A. Wong, "Influence of particle solubility on the delivery of inhaled manganese to the rat brain:

manganese sulfate and manganese tetroxide pharmacokinetics following repeated (14-day) exposure," *Toxicology and Applied Pharmacology*, vol. 170, no. 2, pp. 79–87, 2001.

[45] B. Weiss, "Manganese in the context of an integrated risk and decision process," *NeuroToxicology*, vol. 20, no. 2-3, pp. 519–526, 1999.

[46] D. Vitarella, B. A. Wong, O. R. Moss, and D. C. Dorman, "Pharmacokinetics of inhaled manganese phosphate in male Sprague-Dawley rats following subacute (14-day) exposure," *Toxicology and Applied Pharmacology*, vol. 163, no. 3, pp. 279–285, 2000.

[47] D. C. Dorman, M. F. Struve, and B. A. Wong, "Brain manganese concentrations in rats following manganese tetroxide inhalation are unaffected by dietary manganese intake," *NeuroToxicology*, vol. 23, no. 2, pp. 185–195, 2002.

[48] K. A. Brenneman, B. A. Wong, M. A. Buccellato, E. R. Costa, E. A. Gross, and D. C. Dorman, "Direct olfactory transport of inhaled manganese ($^{54}MnCl_2$) to the rat brain: toxicokinetic investigations in a unilateral nasal occlusion model," *Toxicology and Applied Pharmacology*, vol. 169, no. 3, pp. 238–248, 2000.

[49] D. C. Dorman, K. A. Brenneman, A. M. McElveen, S. E. Lynch, K. C. Roberts, and B. A. Wong, "Olfactory transport: a direct route of delivery of inhaled manganese phosphate to the rat brain," *Journal of Toxicology and Environmental Health A*, vol. 65, no. 20, pp. 1493–1511, 2002.

[50] D. C. Dorman, B. E. McManus, M. W. Marshall, R. A. James, and M. F. Struve, "Old age and gender influence the pharmacokinetics of inhaled manganese sulfate and manganese phosphate in rats," *Toxicology and Applied Pharmacology*, vol. 197, no. 2, pp. 113–124, 2004.

[51] D. C. Dorman, M. F. Struve, D. Vitarella, F. L. Byerly, J. Goetz, and R. Miller, "Neurotoxicity of manganese chloride in neonatal and adult CD rats following subchronic (21-day) high-dose oral exposure," *Journal of Applied Toxicology*, vol. 20, no. 3, pp. 179–187, 2000.

[52] D. Vitarella, O. Moss, and D. C. Dorman, "Pulmonary clearance of manganese phosphate, manganese sulfate, and manganese tetraoxide by CD rats following intratracheal instillation," *Inhalation Toxicology*, vol. 12, no. 10, pp. 941–957, 2000.

[53] T. L. Leavens, D. Rao, M. E. Andersen, and D. C. Dorman, "Evaluating transport of manganese from olfactory mucosa to striatum by pharmacokinetic modeling," *Toxicological Sciences*, vol. 97, no. 2, pp. 265–278, 2007.

[54] D. C. Dorman, M. F. Struve, A. James, B. E. McManus, M. W. Marshall, and B. A. Wong, "Influence of dietary manganese on the pharmacokinetics of inhaled manganese sulfate in male CD rats," *Toxicological Sciences*, vol. 60, no. 2, pp. 242–251, 2001.

[55] D. C. Dorman, A. M. McElveen, M. W. Marshall et al., "Tissue manganese concentrations in lactating rats and their offspring following combined in utero and lactation exposure to inhaled manganese sulfate," *Toxicological Sciences*, vol. 84, no. 1, pp. 12–21, 2005.

[56] M. Yoon, A. Nong, H. J. Clewell, M. D. Taylor, D. C. Dorman, and M. E. Andersen, "Lactational transfer of manganese in rats: predicting manganese tissue concentration in the dam and pups from inhalation exposure with a pharmacokinetic model," *Toxicological Sciences*, vol. 112, no. 1, pp. 23–43, 2009.

[57] N. Ballatori, E. Miles, and T. W. Clarkson, "Homeostatic control of manganese excretion in the neonatal rat," *American Journal of Physiology—Regulatory Integrative and Comparative Physiology*, vol. 252, no. 5, part 2, pp. R842–R847, 1987.

[58] National Research Council (NRC), *Toxicity Testing in the 21st Century: A Vision and a Strategy*, National Academy Press, Washington, DC, USA, 2007.

[59] D. Krewski, M. E. Andersen, E. Mantus, and L. Zeise, "Toxicity testing in the 21st century: implications for human health risk assessment," *Risk Analysis*, vol. 29, no. 4, pp. 474–479, 2009.

[60] W. Slikker Jr., M. E. Andersen, M. S. Bogdanffy et al., "Dose-dependent transitions in mechanisms of toxicity," *Toxicology and Applied Pharmacology*, vol. 201, no. 3, pp. 203–225, 2004.

[61] W. Slikker Jr., M. E. Andersen, M. S. Bogdanffy et al., "Dose-dependent transitions in mechanisms of toxicity: case studies," *Toxicology and Applied Pharmacology*, vol. 201, no. 3, pp. 226–294, 2004.

Hindawi Publishing Corporation
Journal of Toxicology
Volume 2012, Article ID 904603, 11 pages
doi:10.1155/2012/904603

Review Article

Application of Physiologically Based Pharmacokinetic Models in Chemical Risk Assessment

Moiz Mumtaz,[1] Jeffrey Fisher,[2] Benjamin Blount,[3] and Patricia Ruiz[1]

[1] *Computational Toxicology and Methods Development Laboratory, Division of Toxicology and Environmental Medicine (DTEM), Agency for Toxic Substances and Disease Registry (ATSDR), Atlanta, GA 30333, USA*
[2] *National Center for Toxicological Research, USFDA, Jefferson, AR 72079, USA*
[3] *Division of Laboratory Studies, National Center for Environmental Health, Centers for Disease Control and Prevention (CDC), Atlanta, GA 30341, USA*

Correspondence should be addressed to Moiz Mumtaz, mgm4@cdc.gov

Received 20 October 2011; Accepted 21 December 2011

Academic Editor: Kannan Krishnan

Post-exposure risk assessment of chemical and environmental stressors is a public health challenge. Linking exposure to health outcomes is a 4-step process: exposure assessment, hazard identification, dose response assessment, and risk characterization. This process is increasingly adopting "in silico" tools such as physiologically based pharmacokinetic (PBPK) models to fine-tune exposure assessments and determine internal doses in target organs/tissues. Many excellent PBPK models have been developed. But most, because of their scientific sophistication, have found limited field application—health assessors rarely use them. Over the years, government agencies, stakeholders/partners, and the scientific community have attempted to use these models or their underlying principles in combination with other practical procedures. During the past two decades, through cooperative agreements and contracts at several research and higher education institutions, ATSDR funded translational research has encouraged the use of various types of models. Such collaborative efforts have led to the development and use of transparent and user-friendly models. The "human PBPK model toolkit" is one such project. While not necessarily state of the art, this toolkit is sufficiently accurate for screening purposes. Highlighted in this paper are some selected examples of environmental and occupational exposure assessments of chemicals and their mixtures.

1. Background

As industrial society inhabitants, we are exposed to hundreds of chemicals and to an increasing number of chemical combinations, as mixtures. Exposure to multiple chemicals simultaneously or sequentially is the rule rather than the exception [1]. Chemical risk assessments estimate public health consequences from exposure—specifically, exposure to environmental, occupational, or therapeutic chemicals. Most often, estimates of unintentional exposures are based on imprecise metrics of external (air, water, and soil) concentrations and default exposure factors. Chemical exposure assessment thus continues to challenge public health and environmental protection.

Evaluation of human exposure data in the context of public health (i.e., the linking of exposures to health outcome through the establishment of the cause-effect relationship) is a complex process. To establish this relationship, several traditional programs have been used, including health surveillance and disease registries. Through these programs, researchers closely monitor chemical releases in the environment and conduct health studies. When exposed cohorts of human populations are identified, disease registries are established. The cause-effect relationship brings together several biochemical and molecular processes such as nature of the exposures, pharmacokinetics/pharmacodynamics of the chemical(s), and interactions of the biologically effective moiety with the target tissue macromolecules [2]. Critical data gaps exist in these cause-effect relationships. In the absence of a complete set of data, in silico/computational tools can help fill the data gaps [3–8] (Figure 1). In silico modeling employs the mathematical know-how and

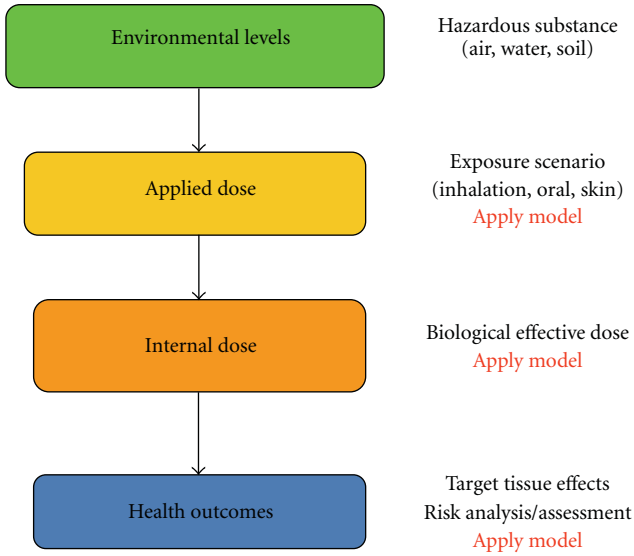

Figure 1: Application of in silico models in establishing the cause and effect relationship.

the computer science advances to evaluate exposures and sometimes to predict risk posed by chemicals.

Several in silico models are used to track the movement of chemicals through the environment and through the human body. Physiologically based pharmacokinetic (PBPK) models are a family of such tools; their potential applications in human health risk assessment have stirred considerable interest. The salient feature of PBPK models is that through simulation they can approximate the kinetic behavior of chemical(s). The models are actually designed to integrate the physical and biological characteristics of a chemical with the physiological happenings in the body to estimate internal dose in target tissues/organs.

In 1995, a group of experts were brought together by ATSDR to advice on the application of computational tools for human risk assessment of toxic substances [9]. Since then, in silico modeling has been applied, where possible, for hazard identification and to determine internal dose through quantitative structure-activity relationship (QSAR), PBPK, PBPK/pharmacodynamic, and biologically based dose-response (BBDR) modeling [10–15].

Engaged academics, stakeholders, and other interested parties have supported modeling projects, advancement of model development, and model applications. We have highlighted in this paper selected PBPK model applications at the Agency for Toxic Substances and Disease Registry (ATSDR) and National Center for Environmental Health (NCEH), Centers for Disease Control and Prevention (CDC), that led to derivation of minimal risk levels (MRLs); risk assessment of mixtures; assessment of occupational exposures; site specific assessment; interpretation of human biomonitoring data.

2. PBPK Modeling and Minimal Risk Levels (MRLs)

Minimal risk levels (MRLs) are estimates of daily human exposure to a hazardous substance at or below which that substance is unlikely to pose a measurable risk of harmful (adverse), noncancerous effects. MRLs are calculated for an exposure route (inhalation or oral) over a specified period (acute, intermediate, or chronic). MRL calculations are typically based on toxicity studies conducted with specific routes of administration. From such data no observed adverse effect levels (NOAELs) or lowest observed adverse effect levels (LOAELs) are identified and adjusted for associated uncertainties. Sometimes data might be appropriate for MRL derivation from one route but not from another. Database gaps or lack of suitable experimental studies prevent using this empirical approach to derive MRLs for all priority pollutants and for all routes of potential exposure. To circumvent this problem, we examined the potential use of PBPK modeling by studying methylene chloride (MC) and trichloroethylene (TCE). PBPK models were available, and MRLs were derived for both these chemicals of interest [16–19]. We used PBPK models to derive each MRL using the study that had provided the basis for the then-current MRL.

In general, the MRLs derived using PBPK models were somewhat higher compared with those derived using the traditional approach. For MC, PBPK-derived MRLs tended to be higher (ratio of 2 to 15) for both inhalation and oral exposure. For TCE, PBPK-derived MRLs tended to be slightly higher (ratio of 1 to 4) for inhalation exposure but yielded much lower MRLs (ratio of 0.03 to 0.20) for oral exposure. These differences were chemical, exposure route-dependent, and varied as a function of dose metric used. The general conclusion of this exercise was that a full PBPK model may not be necessary to derive an MRL—a good understanding and application of basic pharmacokinetic principles might suffice [16].

3. PBPK/PD Modeling of Mixtures

Exposure to multiple chemical or nonchemical stressors is a fact of life. Recently, more attention has been paid to the risk assessment of such exposures [1]. Because PBPK models can incorporate pharmacodynamic characteristics of a chemical, they can be employed in cumulative risk assessment for exposure to multiple chemicals [20]. As methods of chemical mixture risk assessment have evolved during the past two decades, they have undergone drastic changes. Initially, single chemical methods, with slight modifications, were used to evaluate simple mixture toxicities. Then, specific methods were developed to advance these methods further. These, in turn, were followed by the first generation of PBPK modeling approaches. Now, they are being replaced by the more advanced second-generation PBPK/PD models. From the first generation's evaluation of simple mixtures to the second generation's evaluation of more complex mixtures, the development process has gone through different phases. Today's sophisticated models allow integration of concurrent

exposure to multiple chemicals through integrating cellular and molecular biology information of the component chemicals and available mechanistic data [21].

If more than one chemical enters the body, a potential arises for interactions among chemicals, their metabolites, and the biological molecules/systems. Interaction threshold (IT) is defined as combined total dose of chemicals at which interactions become significant in terms of joint toxicity of a mixture. In most cases, experimental determination of low-dose interaction thresholds is economically infeasible—it needs a large number of laboratory animals. Instead, researchers have used an empirical weight-of-evidence methodology to evaluate binary interactions [22]. This methodology incorporates a "bottom-up" approach to evaluate multicomponent mixtures [22, 23].

If, however, appropriate data are available, PBPK/PD modeling actually is better than any other method to simulate various exposure scenarios and to study interactions. These models can also address episodic or pulse exposures. We studied interactions between two organophosphates: chlorpyrifos and parathion [24, 25]. They are both potent pesticides found together in the environment, have similar metabolic pathways, and the parent chemicals, and their respective metabolites cause toxicity by inhibition of acetylcholinesterase (AchE). Chlorpyrifos is rapidly desulfurated by CYP450 3A4 and 2D6 to chlorpyrifos-oxon. Chlorpyrifos-oxon is 300 to 400 times more potent at inhibiting rat brain AChE than is chlorpyrifos. Parathion is desulfurated in the liver by CYP450 3A4, 3A5, 1A2, and 2D6 to paraoxon. Paraoxon is also a much more active inhibitor of AChE than is its parent. The same isoenzymes—P450, 3A4, and 2D6—are involved in the metabolism of both chemicals to the oxon that inhibits AChE.

Thus, to evaluate the PK and PD interactions between chlorpyrifos and parathion, we developed a mixture PBPK/PD model that comprised four individual submodels (chlorpyrifos, chlorpyrifos-oxon, parathion, paraoxon) [25]. The two parent models were linked to their metabolite models through the liver compartments (Figure 2). The predicted metabolite concentrations in blood were linked to a PD model for AChE kinetics, where the competition for cholinesterase occurs. Model simulations indicated that for each chemical, additivity takes place at oral dose levels below 0.08 mg/kg. At higher doses, antagonism by enzymatic competitive inhibition occurs. We determined the interaction threshold by comparing the levels of simulated mixture response with levels anticipated from the individual response addition. In this modeling exercise, we showed that PBPK/PD modeling can improve experimental study design and can help risk assessors to quantify mixture risks for low-dose exposures.

Still, for a mixture that contains a large number of chemicals, a "bottom-up" approach could be tedious and impractical. Petroleum hydrocarbon mixtures such as gasoline, diesel fuel, aviation fuel, and asphalt liquids typically contain hundreds of compounds. These compounds include aliphatic and aromatic hydrocarbons within a specific molecular weight range and sometimes lesser amounts of additives. And they often exhibit qualitatively similar pharmacokinetic (PK) and pharmacodynamic (PD) properties. Nevertheless, some components do exhibit specific biological effects, such as methyl *t*-butyl ether and benzene in gasoline. One of the potential pharmacokinetic interactions of many components in such mixtures is inhibition of the metabolism of some components. Due to the mixtures' complexity, a quantitative description of the pharmacokinetics of each component has not been available, particularly in the context of differing blends of these mixtures.

Consequently, we developed a PBPK modeling approach to describe the kinetics of whole gasoline [26]. The approach simplifies the problem by isolating specific components for which a description is helpful and by treating the remaining components as a single, lumped chemical. In this manner, the effect of the nonisolated components (i.e., inhibition) is taken into account. As previously shown for simple mixtures, this gasoline model was developed by linking at the binary level individual PBPK models through the liver compartment—where competitive inhibition of hepatic metabolism occurs. During gas-uptake kinetics experiments in rats exposed to whole gasoline, kinetics data were used for the single chemicals, for simple mixtures of the isolated chemicals, and for the isolated and lumped chemicals. While some sacrifice in model accuracy occurs with a chemical-lumping approach, such a model still affords a good representation of the kinetics of five isolated chemicals (*n*-hexane, benzene, toluene, ethylbenzene, and *o*-xylene) during exposure to various levels of two different gasoline blends. When appropriate kinetics data are available for model development, the approach could be applicable to other hydrocarbon mixtures.

4. A Biologically Based Dose-Response (BBDR) Model of Hypothalamic-Pituitary-Thyroid Axis

Some environmental chemicals affect endocrine function. Even at very low levels, these chemicals could alter hormone systems. The hypothalamic-pituitary-thyroid (HPT) axis controls many physiologic functions, including metabolism, development, and reproduction. A biologically based dose-response (BBDR) model for adult rats includes submodels for dietary iodide, thyroid-stimulating hormone (TSH), and the thyroid hormones thyroxine (T4) and 3,5,3′- triiodothyronine (T3) [27, 28]. The independently developed individual submodels were linked together to form the endogeneous BBDR-HPT axis model. The resultant model incorporates key biological processes, including

(1) the influence of T4 on TSH production (the HPT axis negative feedback loop),

(2) stimulation of thyroidal T4 and T3 production by TSH,

(3) TSH upregulation of the thyroid sodium (Na(+))/iodide symporter,

(4) recycling of iodide from metabolism of thyroid hormones.

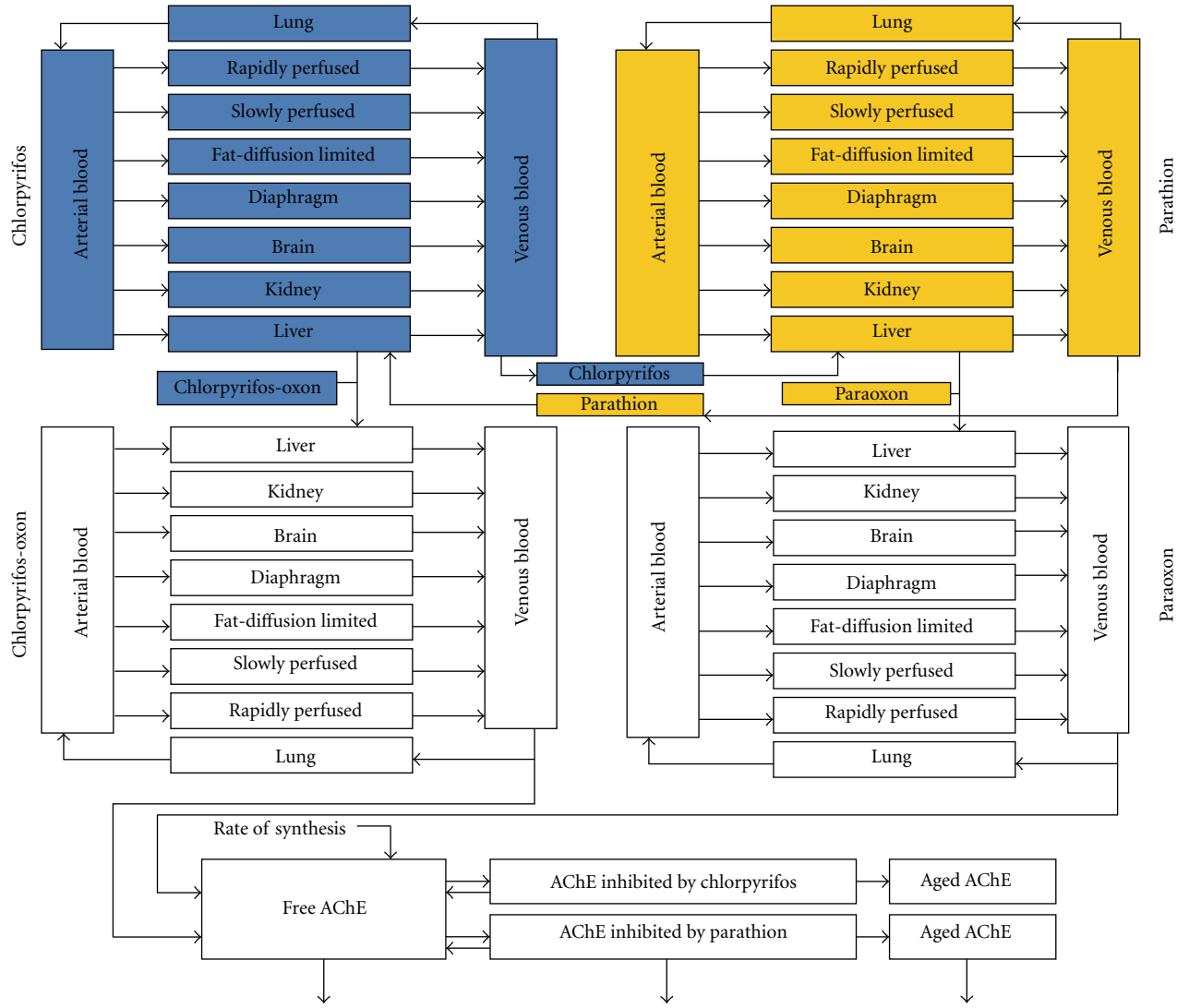

Figure 2: A schematic diagram of the physiologically based pharmacokinetic/pharmacodynamic (PBPK/PD) model of acetylcholinesterase (AchE) inhibition by binary mixtures of chlorpyrifos, parathion, and their metabolites: chlorpyrifos-oxon and paraoxon.

The model was calibrated to predict steady-state concentrations of iodide, T4, T3, and TSH for the euthyroid rat, whose dietary intake of iodide was 20 μg/day. Then, the model was used to predict perturbations in the HPT axis caused by insufficient dietary iodide intake. Simulation results were compared with experimental findings. The BBDR-HPT axis model was successful in simulating perturbations in serum T4, TSH, and thyroid iodide stores for low-iodide diets. When dietary iodide intake becomes insufficient to sustain the HPT axis, the model simulations show a steep dose-response relationship between dietary iodide intake and serum T4 and TSH. This BBDR-HPT axis model might link with PBPK models for thyroid-active chemicals to evaluate and predict dose-dependent HPT axis alterations based on hypothesized modes of action.

5. PBPK Modeling in Occupational Exposures Studies

In another study, we examined the potential toxicity from coexposure to three CNS depressants: toluene, ethylbenzene, and xylene were evaluated under resting and working conditions [29]. Under OSHA and American Conference of Governmental Industrial Hygienists (ACGIH) guidelines, the mixture formula (unity calculation) provides a method for evaluating exposures to mixtures of chemicals that cause similar toxicities [30]. According to the formula, if exposures are reduced in proportion to the number of chemicals and their respective exposure limits, the overall exposure is acceptable. Most of the occupational exposure limits are derived from studies of resting humans or animals. But this

approach assumes that responses are additive. To determine the additivity assumption's validity, unity calculations were performed for a variety of exposures to toluene, to ethylbenzene, to xylene, or to all three. In the calculation, the concentration of each chemical in blood was used rather than the inhaled concentration. The blood concentrations were predicted using a validated PBPK model to allow exploration of a variety of exposure scenarios. At rest, a modest overexposure—2.9 to 4.6 times—occurs due to pharmacokinetic interactions. But the study showed that workers with higher activity might experience a significantly higher absorbed dose that could result in 87% higher internal doses. This study showed the importance of work load's effect on internal chemical doses.

6. Site-Specific Assessment Integrating PBPK/QSAR Modeling

In a highly contaminated residential area, total polychlorinated biphenyls (PCBs) soil levels ranged from 17.4 to 840 mg/kg—much higher than the maximum soil level of 1.5 mg/kg reported nationally [31]. The national average range of PCBs in serum is 4–7 μg/L, but the serum levels of some of its residents ranged between 76.3 and 187.5 μg/L [10]. The major human exposure to PCBs is through ingestion of contaminated food. We wanted to determine whether soil ingestion contributed to these higher levels in the serum of area residents. PBPK models of the 25 most common PCB congeners were developed based on a published method [32]. Partition coefficients and metabolic constants for the models were determined using published QSAR procedures [33, 34].

The models were then used to estimate the contribution of these 25 PCB congeners through soil ingestion to the levels of serum PCBs. PBPK simulations were run using a soil ingestion default rate of 50 mg/day for a lifetime exposure scenario. Simulations using average national soil levels showed that only 0.6% of the total PCBs levels are from soil. Thus, nationwide soil ingestion was not a major contributor to serum blood levels. To confirm this in the contaminated area residents, a probabilistic distribution for PCB blood levels was derived based on the actual PCB soil measurements of the area. The distribution was then applied to the 25 PBPK models to derive a distribution of predicted total PCBs in blood for lifetime exposure scenarios. The derived distribution of blood levels was superimposed on the actual distribution of measured serum levels. The distribution of actual blood levels for 9 out of 10 persons fell within the modeled exposure range, while the mean of the actual blood levels distribution fell within the 2-percentile, lower end of the simulated curve (Figure 3).

Thus, in this community, soil did not appear to contribute significantly to serum levels. Because of lack of actual exposure data of the community, however, the simulations were run on default exposure assumptions. Dietary intake (e.g., fish) or inhalation could be the alternative source of PCBs serum levels. These types of PBPK modeling studies help us determine relative contribution of environmental media to the overall internal doses of chemicals.

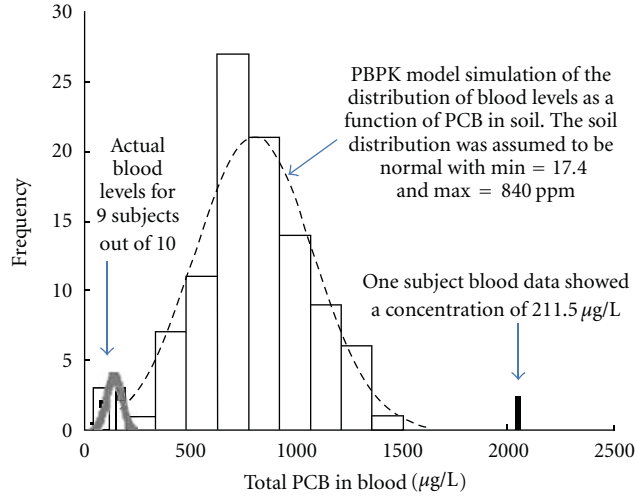

Figure 3: The distribution of actual levels of total PCBs in blood near a waste site.

7. Human PBPK Tool Kit Development: The General Approach

To better serve health assessors and increase their use, we are developing a "human PBPK model toolkit" to assist with site-specific health assessments [35–37]. This toolkit will comprise a series of published models coded in Berkeley Madonna—a common simulation language [36]. Ultimately a Web linkage to a PBPK database will be available where health assessors and other related health workers can access easily many different models for use in assessment activities.

At the outset, we conducted literature review to identify available human PBPK models for the chemicals of interest. Following literature searches of human health-related databases such as Medline, Toxline, and PubMed, we identified hundreds of PBPK models. These models varied in their complexity based on the scientific understanding of the chemistry, biological behavior, and insights gained into the mechanism(s) or mode of action of a given chemical's toxicity. Thus, the models contained different numbers of compartments (e.g., liver, kidney, and other organs). Often the compartments were designed for parent chemicals, but some included metabolite(s). The criteria we used for model selection included critical scientific issues such as the number of datasets used to calibrate and evaluate the model, the model's maturity (number of predecessor models from which the model was derived), and the author's experience. Currently, the toolkit includes models that are at various stages of development for environmental contaminants, including volatile organic compounds (VOCs) and metals [12, 13, 37].

We also developed a generic 7-compartment VOC model; it consists of blood, fat, skin, kidney, and liver, rapidly and slowly perfused tissue compartments, and a gas exchange

compartment [37]. We included these compartments in the model based on their use in previously published PBPK models [38–43]. The generic VOC PBPK model can be used for six VOCs:

(i) benzene (BEN),

(ii) carbon tetrachloride (CCl_4),

(iii) dichloromethane (DCM),

(iv) perchloroethylene (PCE),

(v) trichloroethylene (TCE),

(vi) vinyl chloride (VC).

All compartments were described as well mixed and flow limited. We obtained chemical-specific and biochemical parameters for the model from published literature [41–48]. The model code allowed simulation of three routes of exposure, either individually or simultaneously: inhalation, oral ingestion, and dermal absorption. Due to the lack of available published human datasets, we did not conduct a comparison of the generic model predictions for dermal route. In the current model version, we also did not include original-model simulations for metabolites and metabolite data. Nevertheless, a critical future improvement for this model's postscreening use is incorporation of metabolite information, particularly when metabolite(s) mediate toxicity.

Our first test of the model's applicability was to compare the published human kinetic data for each VOC with the corresponding published model predictions. To test further the model's reliability, we calculated the area under the concentration curve (AUC) for blood or exhaled breath for each VOC using both our generic and original model. For each kinetic time course dataset, we also calculated the mean of the sum of the squared differences (MSSDs) between model prediction and observation. MSSD was computed by squaring the difference between a measured data point and the value of the simulation at the corresponding time. Then, the summed squares were divided by the number of data points. The MSSD was thus determined for both the published model and for our generic VOCs model [37].

For each of the specific VOCs, we used the VOC PBPK model to estimate the blood concentrations for the available minimal risk levels (MRLs) values [49–54]. We repeated this process for each VOC for which biomonitoring data on human blood levels were available from the National Health and Nutrition Examination Survey (NHANES) [55]. Steady-state VOC concentrations in venous blood were then compared with NHANES data using these simplified assumptions about exposure frequency and duration. If the measured NHANES blood levels were below those estimated from the simulations, the exposures would be regarded as "safe" [37].

We also reviewed published human metals PBPK models for arsenic, mercury, and cadmium [56–61]. We selected the best model available based on performance, accuracy, and reproducibility and recoded them using Berkeley Madonna [36]. We took from the literature human physiological and chemical-specific parameters describing the absorption, distribution, and blood and tissue partitioning of As, Hg, and Cd. The PBPK models allow simulation of different routes of exposure, either individually or simultaneously.

A published Cd toxicokinetic model [59–61] describes aggregated lung, liver, kidney, blood, and other tissues. Intake by oral and inhalation routes are transferred to an uptake pool that distributes to three blood compartments [61]. The model predicted the urinary concentrations of Cd considered a surrogate for body burden in assessing health risk from exposure**,** including the sex- and age-stratified geometric urinary mean. This model was used to predict the creatinine-corrected urinary Cd concentrations among females and males from the *Fourth National Report on Human Exposure to Environmental Chemicals* [55].

We recoded a human PBPK model for arsenic. It consists of interconnected submodels for inorganic arsenic and its metabolites, monomethyl arsenic (MMA), and dimethylarsenic (DMA) [56]. It includes compartments for lung, liver, GI tract, kidney, muscle, brain, skin, and the heart. Single or continuous oral exposures to inorganic arsenic in the +3 or +5 valence state or exposures via drinking water were simulated. The recoded model adequately simulated experimental human data found in the published literature [56]. Using a visual comparison, the model performance was in good agreement with the original model. We evaluated performance by calculating values for percent median absolute performance error (MAPE %), median performance error (MPE %), and root median square performance error (RMSPE %) based on estimates of performance error (PE) [12].

We recoded a human toxicokinetic model for methylmercury based on the Carrier et al. model [12, 57, 58]. The model consists of a total body compartment. By a first-order process, methylmercury enters this compartment from the GI tract. The amount of methylmercury in blood is proportional to that in the total body compartment. The recoded model reproduced all the simulations of the original model [57, 58]. By visual comparison, the model performance was in good agreement with the original model. We evaluated the model performance by calculating a value for percent median absolute performance error (MAPE %), median performance error (MPE %), and root median square performance error (RMSPE %) based on estimates-of-performance error (PE). The model could simulate and could accurately predict the available total body burden of mercury experimental data. The model predictions were similar to those observed experimentally and found in published literature. Overall, the current model could integrate those various experimental data that are critical determinants of methylmercury kinetics. The current model duplicates the time courses of various tissue burdens for different dose regimens and exposure scenarios.

8. PBPK: Biomonitoring Data and Its Interpretation

Several population-representative biomonitoring programs are underway in Canada, California, Asia, and Europe.

These biomonitoring programs are similar to CDC's National Health and Nutrition Examination Survey (NHANES) that provides representative data for the United States. For risk managers, the growing availability of such data for hundreds of chemicals provides an opportunity as well as a challenge. To address the interpretation of such data, several alternative methods have been proposed, such as reverse dosimetry [62] and biomonitoring equivalents (BEs) [63].

The reverse dosimetry approach employs PBPK models as a tool; this tool interprets NHANES data to estimate the intake dose or external environmental concentration based on a measured tissue concentration [64–68]. We used the chloroform PBPK model [48] in combination with a mass transfer model [69] that describes the transfer of volatile organic chemicals (VOCs) from water to air during showering—an event that contributes significantly to VOC inhalation exposure. We incorporated exposure contributions from multiroutes and -sources into the published PBPK model [48]. This integrated model was used to predict chloroform concentrations in blood and exhaled breath from multiroute exposure to chloroform in the general population. MATLAB Simulink, the graphical simulation tool (The Math-Works, Inc., Natick, MA) was used for time-course and dose-response simulations, with a Monte Carlo sensitivity analysis. The predictive ability of this combined model was evaluated with three published studies that provided exhaled breath or blood chloroform concentrations. The studies also gave the most complete descriptions of how the volunteers were exposed and when the exhaled breath or blood samples were collected. To make it as close to reality as possible, we varied—together with other parameters in the model—the time of blood and exhaled breath samples collection and starting time of showering and water drinking. We ran the model for 10,000 iterations.

Reverse dosimetry was carried out by performing Monte Carlo analysis using appropriate varied timing of sampling and exposure. A reference chloroform concentration in water (1 μg/L) was then used to predict the distribution of chloroform concentrations in blood (pg/mL). The values thus obtained were then inverted to obtain a distribution of an "exposure conversion factor" (ECF) in (μg/L in water)/(pg/mL in blood). The distribution of the ECF can be multiplied by any observed chloroform concentrations in blood to estimate a distribution of chloroform concentrations in water to which a person might have been exposed. Our original assumption was that a simple structured PBPK model was adequate—a complex model increased the number of parameters and associated uncertainties. On the contrary, we found that a comprehensive exposure regimen was needed to aggregate all major contributing factors, including spatial and temporal profiles of chloroform in water, chloroform in ambient air, human activities, and water consumption patterns.

Showering was shown to yield much higher chloroform concentrations in blood than did water drinking—a conclusion consistent with previous experimental study. Still, that chloroform *metabolites* induce cytolethality in target tissues but not the parent compound is well known. Despite chloroform's higher concentration in blood after showering than after water-drinking exposure, that more chloroform is metabolized (first-pass) after water drinking exposure is possible and may exert more toxicity compared with showering exposure. This experience shows that only by integrating biomonitoring and PBPK/PD modeling techniques into both exposure and risk assessments can we obtain a more scientific basis for regulatory decisions that protect the public health.

Biomonitoring equivalents (BEs) are also used to interpret exposures [63, 70–72]. BEs estimate the concentration of a chemical or its metabolite in a biological medium consistent with an existing exposure guidance value such as a tolerable daily intake, minimal risk levels, or reference dose. The BE approach integrates available pharmacokinetic data necessary to convert, in a biological medium, a current exposure guidance value into an equivalent concentration. A range of pharmacokinetic data and approaches not limited to PBPK modeling is used to derive BE values. If human pharmacokinetic information is available, a target external dose is converted into the corresponding expected internal dose (concentration of parent compound or metabolite in blood or urine or both) in humans. Alternatively, if pharmacokinetic data are available in the animal species used in the study, those data provide the point of departure (POD) on which the exposure guidance value is based. The internal dose is then estimated in the animal at the POD. The appropriate uncertainty factors (UFs) then correspond to those used in the derivation of the exposure guidance value and are applied to derive a BE.

We also collected risk assessment-based chronic exposure reference values such as reference doses (RfDs), reference concentrations (RfCs), tolerable daily intakes (TDIs), cancer slope factors, and key pharmacokinetic model parameters for 47 VOCs [71]. Using steady-state solutions to a generic PBPK model structure, chemical-specific, steady-state venous blood concentrations were estimated across chemicals associated with unit oral and inhalation exposure rates and with chronic exposure at the identified exposure reference values. The thus-derived screening values—estimates of average blood concentrations—were then consistent with what would be expected in a typical adult human exposed at steady-state to the identified reference values. These screening values might be rough. But they do allow comparison of measured blood VOC concentrations to a benchmark consistent with existing risk assessments for these compounds rather than bright lines separating safe from unsafe exposure levels. Such a comparison can assist in the integration of these biomonitoring data into risk assessment, management, and prioritization decisions. Thus, in this instance, fully developed PBPK models, while useful, are not required [63, 71]. The BE values can be used as screening levels and can also be used to classify chemicals into low, medium, and high-priority categories for risk assessment followup.

9. Conclusions

After decades of toxicity testing, the emerging reality is that routine toxicity testing cannot fill the large data gaps that

daily confront data generators (experimental scientists) and data users (assessors/regulators). And recent years have seen a shift away from studying health effects in whole animals. This shift also serves to refine, reduce, and replace animal use as the basis of ICCVAM legislation. In fact, more recently, this shift has spurred the use of human *in vitro* systems and high-throughput data generation.

As new chemicals and contaminants enter the environment, reliance on in silico modeling will increase. PBPK, PBPK/PD, BBDR models are tools that will help establish the cause-effect relationship—the basic tenant of risk assessment. The chief advantage of these tools, particularly the PBPK models, is their predictive power. It is this power that fills database gaps through simulations based on meticulously articulated scientific facts.

Many scientifically accurate and advanced PBPK models have been developed to evaluate carcinogenic and noncarcinogenic health effects. They are capable of route-to-route, exposure duration, interspecies, and other extrapolations commonly used in risk assessment. But health risk assessors—most of whom have limited experience with simulation software—are uncomfortable with the multiple simulation languages such as MatLab, Simusolve, and AcslX used to code those simulations. This limitation also restricts field application of the models in public health practice. Even experienced PBPK modelers, due to the lack of key information or equations, sometimes face problems when reconstructing published PBPK models for application. For these reasons, risk managers, decision makers, and the risk assessment community have been hesitant to adopt them. Having the models in easier-to-use form capable of solving real life problems will greatly increase their value and will help integrate technological and scientific advances into decision making.

PBPK models can also be useful in targeted research. They can estimate target organ concentrations of chemicals and integrate such information to predict whole-animal exposures. Because they are designed to determine the internal tissue concentration of a chemical from multiple exposure routes, they can help to determine the appropriate dose in target organs that could be used in *in vitro* toxicity testing systems. Combining *in vitro* pharmacokinetics and pharmacodynamics information could produce a concentration suitable for risk assessment [73, 74]. Once identified, the *in vivo* exposure corresponding to the *in vitro* concentration could be estimated through *in vitro-in vivo* extrapolation [75, 76]. Developing appropriate dose metrics, incorporating mode of action, and other chemical specific information could predict *in vivo* dose response curves from *in vitro* data [66, 76, 77]. But such extrapolations as determination of human external exposures to VOCs based on measured blood levels need careful assessment of the interval between exposure and sampling time since the latter only represent the concentration at the sample time and are a product of complex exposures from multiple routes and multiple sources [66, 78–80].

Hypothetically, reverse dosimetry shows the opposite could also be true [62, 64, 66]. That is, if we know the *in vitro* concentration that causes adverse effect(s) at a cellular or organ level, we could use these models to extrapolate to *in vivo* tissue level and ultimately to a human-allowable external dose. Some advances are being made towards this goal by integrating human dosimetry insights gained through *in vitro* studies and high throughput screening [81, 82]. Employing computational techniques and new simulation platforms, it has been shown that estimated oral equivalents could then be compared with allowable human exposures through environmental media.

In summary, though these models have not yet realized their potential, in silico toxicology is a growing field that will produce new and innovative computational tools. High-throughput screening and *in vitro* testing are changing toxicology testing strategies. In fact, such tests are helping to create the next generation of computational tools. But development of in silico tools should continually consider the two critical qualities necessary for the end-user—ease of use and accessibility. Training, increased transparency, and enhanced application could also help in-silico tools' acceptance as a real-life decision making tool. Finally, translational research, such as the development of the human PBPK toolkit, could further contribute to in-silico tools' accessibility and ease of use.

Disclosure

The findings and conclusions in this paper are those of the author(s) and do not necessarily represent the official position of the Centers for Disease Control and Prevention/the Agency for Toxic Substances and Disease Registry or the US Food and drug Administration. Mention of trade names is not an endorsement of any commercial product.

Acknowledgment

The authors acknowledge the editorial review and suggestions of Wallace Sagendorph, Office of Communications, Centers for Disease Control and Prevention (CDC).

References

[1] Y.-M. Tan, H. Clewell, J. Campbell, and M. Andersen, "Evaluating pharmacokinetic and pharmacodynamic interactions with computational models in supporting cumulative risk assessment," *International Journal of Environmental Research and Public Health*, vol. 8, no. 5, pp. 1613–1630, 2011.

[2] K. S. Pang and M. R. Durk, "Physiologically-based pharmacokinetic modeling for absorption, transport, metabolism and excretion," *Journal of Pharmacokinetics and Pharmacodynamics*, vol. 37, no. 6, pp. 591–615, 2010.

[3] R. S. DeWoskin, "PBPK models in risk assessment-A focus on chloroprene," *Chemico-Biological Interactions*, vol. 166, no. 1–3, pp. 352–359, 2007.

[4] M. Reddy, R. S. H. Yang, H. J. Clewell, and M. E. Andersen, Eds., *Physiologically Based Pharmacokinetic Modeling*, John Wiley & Sons, Hoboken, NJ, USA, 2005.

[5] R. Dixit, J. Riviere, K. Krishnan, and M. E. Andersen, "Toxicokinetics and physiologically based toxicokinetics in toxicology and risk assessment," *Journal of Toxicology and Environmental Health—Part B*, vol. 6, no. 1, pp. 1–40, 2003.

[6] R. S. DeWoskin, S. Barone, H. J. Clewell, and R. W. Setzer, "Improving the development and use of biologically based dose response models (BBDR) in risk assessment," *Human and Ecological Risk Assessment*, vol. 7, no. 5, pp. 1091–1120, 2001.

[7] U.S. Environmental Protection Agency, Approaches for the Application of Physiologically Based Pharmacokinetic (PBPK) Models and Supporting Data in Risk Assessment, EPA/600/R-05/043F, U.S. Environmental Protection Agency, Washington, DC, USA, 2006.

[8] L. H. Clark, R. W. Setzer, and H. A. Barton, "Framework for evaluation of physiologically-based pharmacokinetic models for use in safety or risk assessment," *Risk Analysis*, vol. 24, no. 6, pp. 1697–1717, 2004.

[9] M. E. Andersen, "Development of physiologically based pharmacokinetic and physiologically based pharmacodynamic models for applications in toxicology and risk assessment," *Toxicology Letters*, vol. 79, no. 1–3, pp. 35–44, 1995.

[10] H. A. El-Masri, M. M. Mumtaz, G. Choudhary, W. Cibulas, and C. T. De Rosa, "Applications of computational toxicology methods at the Agency for Toxic Substances and Disease Registry," *International Journal of Hygiene and Environmental Health*, vol. 205, no. 1-2, pp. 63–69, 2002.

[11] M. M. Mumtaz, L. A. Knauf, D. J. Reisman et al., "Assessment of effect levels of chemicals from quantitative structure- activity relationship (QSAR) models. I. Chronic lowest-observed-adverse- effect level (LOAEL)," *Toxicology Letters*, vol. 79, no. 1–3, pp. 131–143, 1995.

[12] P. Ruiz, B. A. Fowler, J. D. Osterloh, J. Fisher, and M. Mumtaz, "Physiologically based pharmacokinetic (PBPK) tool kit for environmental pollutants—metals," *SAR and QSAR in Environmental Research*, vol. 21, no. 7, pp. 603–618, 2010.

[13] P. Ruiz, M. Mumtaz, J. Osterloh, J. Fisher, and B. A. Fowler, "Interpreting NHANES biomonitoring data, cadmium," *Toxicology Letters*, vol. 198, no. 1, pp. 44–48, 2010.

[14] P. Ruiz, M. Mumtaz, and V. Gombar, "Assessing the toxic effects of ethylene glycol ethers using Quantitative Structure Toxicity Relationship models," *Toxicology and Applied Pharmacology*, vol. 254, no. 2, pp. 198–205, 2011.

[15] E. Demchuk, P. Ruiz, J. D. Wilson et al., "Computational toxicology methods in public health practice," *Toxicology Mechanisms and Methods*, vol. 18, no. 2-3, pp. 119–135, 2008.

[16] H. J. Clewell, P. R. Gentry, and J. M. Gearhart, "Investigation of the potential impact of benchmark dose and pharmacokinetic modeling in noncancer risk assessment," *Journal of Toxicology and Environmental Health—Part A*, vol. 52, no. 6, pp. 475–515, 1997.

[17] Agency for Toxic Substances and Disease Registry (ATSDR), "Minimal risk levels for priority substances and guidance for derivation," *Federal Register*, vol. 61, no. 125, pp. 33511–33520, 1996.

[18] Agency for Toxic Substances and Disease Registry (ATSDR), *Toxicological Profile for Mercury Compounds, Update*, ATSDR, Atlanta, Ga, USA, 1997.

[19] Agency for Toxic Substances and Disease Registry (ATSDR), *Toxicological Profile for Mercury Compounds, Update*, ATSDR, Atlanta, Ga, USA, 1995.

[20] J. L. Campbell, K. Krishnan, H. J. Clewell, and M.E. Andersen, "Kinetic interactions of chemical mixtures," in *Principles and Practice of Mixtures Toxicology*, M. Mumtaz, Ed., Wiley, Weinheim, Germany, 2010.

[21] K. Kannan, A. Sasso, and P. Georgopoulos, "Phramocokinetic mechanisms of interactions in chemical mixtures," in *Principles and Practice of Mixtures Toxicology*, M. Mumtaz, Ed., Wiley, Weinheim, Germany, 2010.

[22] M. M. Mumtaz and P. R. Durkin, "A weight-of-evidence approach for assessing interactions in chemical mixtures," *Toxicology and Industrial Health*, vol. 8, no. 6, pp. 377–406, 1992.

[23] M. M. Mumtaz, C. T. De Rosa, J. Groten, V. J. Feron, H. Hansen, and P. R. Durkin, "Estimation of toxicity of chemical mixtures through modeling of chemical interactions," *Environmental Health Perspectives*, vol. 106, no. 6, pp. 1353–1360, 1998.

[24] Agency for Toxic Substances and Disease Registry (ATSDR), *Toxicological Profile of Chlorpyrifos*, U.S. Department of Health and Human Services, Agency for Toxic Substances and Disease Registry, Atlanta, GA, USA, 1997.

[25] H. A. El-Masri, M. M. Mumtaz, and M. L. Yushak, "Application of physiologically-based pharmacokinetic modeling to investigate the toxicological interaction between chlorpyrifos and parathion in the rat," *Environmental Toxicology and Pharmacology*, vol. 16, no. 1-2, pp. 57–71, 2004.

[26] J. E. Dennison, M. E. Andersen, I. D. Dobrev, M. M. Mumtaz, and R. S.H. Yang, "PBPK modeling of complex hydrocarbon mixtures: gasoline," *Environmental Toxicology and Pharmacology*, vol. 16, no. 1-2, pp. 107–119, 2004.

[27] E. D. McLanahan, M. E. Andersen, M. Mumtaz, and J. W. Fisher, "BBPK model of the hypothalamic-pituitary-thyroid axis in the adult rat," *The Toxicologist*, vol. 96, no. 1, article 394, 2007.

[28] E. D. Mclanahan, M. E. Andersen, and J. W. Fisher, "A biologically based dose-response model for dietary iodide and the hypothalamic-pituitary-thyroid axis in the adult Rat: evaluation of iodide deficiency," *Toxicological Sciences*, vol. 102, no. 2, pp. 241–253, 2008.

[29] J. E. Dennison, P. L. Bigelow, M. M. Mumtaz, M. E. Andersen, I. D. Dobrev, and R. S. H. Yang, "Evaluation of potential toxicity from co-exposure to three CNS depressants (toluene, ethylbenzene, and xylene) under resting and working conditions using PBPK modeling," *Journal of Occupational and Environmental Hygiene*, vol. 2, no. 3, pp. 127–135, 2005.

[30] Occupational Safety and Health Administration (OSHA), "Air Contaminants," Code of Federal Regulations, Title 29, Part 1910.1000, 2004.

[31] Agency for Toxic Substances and Disease Registry (ATSDR), *Toxicological Profile of Polychlorinated Biphenyls*, U.S. Department of Health and Human Services, Agency for Toxic Substances and Disease Registry, Atlanta, Ga, USA, 2000.

[32] R. J. Lutz, R. L. Dedrick, and H. B. Matthews, "A preliminary pharmacokinetic model for several chlorinated biphenyls in the rat," *Drug Metabolism and Disposition*, vol. 5, no. 4, pp. 386–396, 1977.

[33] F. M. Parham, M. C. Kohn, H. B. Matthews, C. DeRosa, and C. J. Portier, "Using structural information to create physiologically based pharmacokinetic models for all polychlorinated biphenyls I. Tissue:Blood partition coefficients," *Toxicology and Applied Pharmacology*, vol. 144, no. 2, pp. 340–347, 1997.

[34] F. M. Parham and C. J. Portier, "Using structural information to create physiologically based pharmacokinetic models for all polychlorinated biphenyls. II: rates of metabolism," *Toxicology and Applied Pharmacology*, vol. 151, no. 1, pp. 110–116, 1998.

[35] A. N. Edginton and G. Joshi, "Have physiologically-based pharmacokinetic models delivered?" *Expert Opinion on Drug Metabolism and Toxicology*, vol. 7, no. 8, pp. 929–934, 2011.

[36] R. I. Macey and G. F. Oster, *Berkeley Madonna. Version 8.3.9*, Berkeley Madonna, 1996–2006.

[37] M. M. Mumtaz, M. Ray, S. R. Crowell, D. Keys, J. Fisher, and P. Ruiz, "Translational research to develop a human pbpk

models tool kit-volatile organic compounds (VOCS)," *Journal of Toxicology and Environmental Health—Part A*, vol. 75, no. 1, pp. 6–24, 2012.

[38] K. Yokley, H. T. Tran, K. Pekari et al., "Physiologically-based pharmacokinetic modeling of benzene in humans: a Bayesian approach," *Risk Analysis*, vol. 26, no. 4, pp. 925–943, 2006.

[39] K. D. Thrall, M. E. Vucelick, R. A. Gies et al., "Comparative metabolism of carbon tetrachloride in rats, mice, and hamsters using gas uptake and PBPK modeling," *Journal of Toxicology and Environmental Health—Part A*, vol. 60, no. 8, pp. 531–548, 2000.

[40] R. M. David, H. J. Clewell, P. R. Gentry, T. R. Covington, D. A. Morgott, and D. J. Marino, "Revised assessment of cancer risk to dichloromethane II. Application of probabilistic methods to cancer risk determinations," *Regulatory Toxicology and Pharmacology*, vol. 45, no. 1, pp. 55–65, 2006.

[41] T. R. Covington, P. Robinan Gentry, C. B. Van Landingham, M. E. Andersen, J. E. Kester, and H. J. Clewell, "The use of Markov chain Monte Carlo uncertainty analysis to support a Public Health Goal for perchloroethylene," *Regulatory Toxicology and Pharmacology*, vol. 47, no. 1, pp. 1–18, 2007.

[42] J. W. Fisher, D. Mahle, and R. Abbas, "A human physiologically based pharmacokinetic model for trichloroethylene and its metabolites, trichloroacetic acid and free trichloroethanol," *Toxicology and Applied Pharmacology*, vol. 152, no. 2, pp. 339–359, 1998.

[43] H. J. Clewell, P. R. Gentry, J. M. Gearhart, B. C. Allen, and M. E. Andersen, "Comparison of cancer risk estimates for vinyl chloride using animal and human data with a PBPK model," *Science of the Total Environment*, vol. 274, no. 1–3, pp. 37–66, 2001.

[44] H. J. Clewell, P. R. Gentry, T. R. Covington, and J. M. Gearhart, "Development of a physiologically based pharmacokinetic model of trichloroethylene and its metabolites for use in risk assessment," *Environmental Health Perspectives*, vol. 108, no. 2, pp. 283–305, 2000.

[45] H. J. Clewell, P. R. Gentry, J. E. Kester, and M. E. Andersen, "Evaluation of physiologically based pharmacokinetic models in risk assessment: an example with perchloroethylene," *Critical Reviews in Toxicology*, vol. 35, no. 5, pp. 413–433, 2005.

[46] R. P. Brown, M. D. Delp, S. L. Lindstedt, L. R. Rhomberg, and R. P. Beliles, "Physiological parameter values for physiologically based pharmacokinetic models," *Toxicology and Industrial Health*, vol. 13, no. 4, pp. 407–484, 1997.

[47] A. L. Cowles, H. H. Borgstedt, and A. J. Gillies, "Tissue weights and rates of blood flow in man for the prediction of anesthetic uptake and distribution," *Anesthesiology*, vol. 35, no. 5, pp. 523–526, 1971.

[48] R. A. Corley, S. M. Gordon, and L. A. Wallace, "Physiologically based pharmacokinetic modeling of the temperature- dependent dermal absorption of chloroform by humans following bath water exposures," *Toxicological Sciences*, vol. 53, no. 1, pp. 13–23, 2000.

[49] Agency for Toxic Substances and Disease Registry (ATSDR), *Toxicological Profile for Perchloroethylene*, U.S. Department of Health and Human Services, Public Health Service, Atlanta, Ga, USA, 1997.

[50] Agency for Toxic Substances and Disease Registry (ATSDR), *Toxicological Profile for Trichloroethylene*, U.S. Department of Health and Human Services, Public Health Service, Atlanta, Ga, USA, 1997.

[51] Agency for Toxic Substances and Disease Registry (ATSDR), *Toxicological Profile for Dichloromethane*, U.S. Department of Health and Human Services, Public Health Service, Atlanta, Ga, USA, 2000.

[52] Agency for Toxic Substances and Disease Registry (ATSDR), *Toxicological Profile for Carbon Tetrachloride*, U.S. Department of Health and Human Services, Public Health Service, Atlanta, Ga, USA, 2005.

[53] Agency for Toxic Substances and Disease Registry (ATSDR), *Toxicological Profile for Vinyl Chloride*, U.S. Department of Health and Human Services, Public Health Service, Atlanta, Ga, USA, 2006.

[54] Agency for Toxic Substances and Disease Registry (ATSDR), *Toxicological Profile for Benzene*, U.S. Department of Health and Human Services, Public Health Service, Atlanta, Ga, USA, 2007.

[55] Centers for Disease Control and Prevention (CDC), *Fourth National Report on Human Exposure to Environmental Chemicals*, Division of Laboratory Sciences, National Center for Environmental Health, Atlanta, Ga, USA, 2009.

[56] H. A. El-Masri and E. M. Kenyon, "Development of a human physiologically based pharmacokinetic (PBPK) model for inorganic arsenic and its mono- and di-methylated metabolites," *Journal of Pharmacokinetics and Pharmacodynamics*, vol. 35, no. 1, pp. 31–68, 2008.

[57] G. Carrier, R. C. Brunet, M. Caza, and M. Bouchard, "A toxicokinetic model for predicting the tissue distribution and elimination of organic and inorganic mercury following exposure to methyl mercury in animals and humans. I. Development and validation of the model using experimental data in rats," *Toxicology and Applied Pharmacology*, vol. 171, no. 1, pp. 38–49, 2001.

[58] G. Carrier, M. Bouchard, R. C. Brunet, and M. Caza, "A toxicokinetic model for predicting the tissue distribution and elimination of organic and inorganic mercury following exposure to methyl mercury in animals and humans. II. Application and validation of the model in humans," *Toxicology and Applied Pharmacology*, vol. 171, no. 1, pp. 50–60, 2001.

[59] H. Choudhury, T. Harvey, W. C. Thayer et al., "Urinary cadmium elimination as a biomarker of exposure for evaluating a cadmium dietary exposure—biokinetics model," *Journal of Toxicology and Environmental Health—Part A*, vol. 63, no. 5, pp. 321–350, 2001.

[60] G. L. Diamond, W. C. Thayer, and H. Choudhury, "Pharmacokinetics/pharmacodynamics (PK/PD) modeling of risks of kidney toxicity from exposure to cadmium: estimates of dietary risks in the U.S. population," *Journal of Toxicology and Environmental Health—Part A*, vol. 66, no. 22, pp. 2141–2164, 2003.

[61] T. Kjellström and G. F. Nordberg, "A kinetic model of cadmium metabolism in the human being," *Environmental Research*, vol. 16, no. 1–3, pp. 248–269, 1978.

[62] Y.-M. Tan, K. H. Liao, and H. J. Clewell, "Reverse dosimetry: interpreting trihalomethanes biomonitoring data using physiologically based pharmacokinetic modeling," *Journal of Exposure Science and Environmental Epidemiology*, vol. 17, no. 7, pp. 591–603, 2007.

[63] S. M. Hays, R. A. Becker, H. W. Leung, L. L. Aylward, and D. W. Pyatt, "Biomonitoring equivalents: a screening approach for interpreting biomonitoring results from a public health risk perspective," *Regulatory Toxicology and Pharmacology*, vol. 47, no. 1, pp. 96–109, 2007.

[64] Y. M. Tan, K. Liao, R. Conolly, B. Blount, A. Mason, and H. Clewell, "Use of a physiologically based pharmacokinetic model to identify exposures consistent with human

biomonitoring data for chloroform," *Journal of Toxicology and Environmental Health—Part A*, vol. 69, no. 18, pp. 1727–1756, 2006.

[65] K. H. Liao, Y. M. Tan, and H. J. Clewell, "Development of a screening approach to interpret human biomonitoring data on volatile organic compounds: reverse dosimetry on biomonitoring data for trichloroethylene," *Risk Analysis*, vol. 27, no. 5, pp. 1223–1236, 2007.

[66] H. J. Clewell, Y. M. Tan, J. L. Campbell, and M. E. Andersen, "Quantitative interpretation of human biomonitoring data," *Toxicology and Applied Pharmacology*, vol. 231, no. 1, pp. 122–133, 2008.

[67] M. A. Lyons, R. S. H. Yang, A. N. Mayeno, and B. Reisfeld, "Computational toxicology of chloroform: reverse dosimetry using Bayesian inference, Markov chain Monte Carlo simulation, and human biomonitoring data," *Environmental Health Perspectives*, vol. 116, no. 8, pp. 1040–1046, 2008.

[68] P. G. Georgopoulos, A. Roy, and M. A. Gallo, "Reconstruction of short-term multi-route exposure to volatile organic compounds using physiologically based pharmacokinetic models," *Journal of Exposure Analysis and Environmental Epidemiology*, vol. 4, no. 3, pp. 309–328, 1994.

[69] C. P. Weisel, H. Kim, P. Haltmeier, and J. B. Klotz, "Exposure estimates to disinfection by-products of chlorinated drinking water," *Environmental Health Perspectives*, vol. 107, no. 2, pp. 103–110, 1999.

[70] C. R. Kirman, L. L. Aylward, B. C. Blount, D. W. Pyatt, and S. M. Hays, "Evaluation of NHANES biomonitoring data for volatile organic chemicals in blood: application of chemical-specific screening criteria," *Journal of Exposure Science and Environmental Epidemiology*, vol. 22, no. 1, pp. 24–34, 2012.

[71] L. L. Aylward, C. R. Kirman, B. C. Blount, and S. M. Hays, "Chemical-specific screening criteria for interpretation of biomonitoring data for volatile organic compounds (VOCs)—application of steady-state PBPK model solutions," *Regulatory Toxicology and Pharmacology*, vol. 58, no. 1, pp. 33–44, 2010.

[72] S. M. Hays, L. L. Aylward, J. S. LaKind et al., "Guidelines for the derivation of biomonitoring equivalents: report from the biomonitoring equivalents expert workshop," *Regulatory Toxicology and Pharmacology*, vol. 51, no. 3, supplement, pp. S4–S15, 2008.

[73] A. Forsby and B. Blaauboer, "Integration of *in vitro* neurotoxicity data with biokinetic modelling for the estimation of *in vivo* neurotoxicity," *Human and Experimental Toxicology*, vol. 26, no. 4, pp. 333–338, 2007.

[74] B. J. Blaauboer, "The integration of data on physico-chemical properties, *in vitro*-derived toxicity data and physiologically based kinetic and dynamic as modelling a tool in hazard and risk assessment. A commentary," *Toxicology Letters*, vol. 138, no. 1-2, pp. 161–171, 2003.

[75] S. S. De Buck and C. E. Mackie, "Physiologically based approaches towards the prediction of pharmacokinetics: *in vitro-in vivo* extrapolation," *Expert Opinion on Drug Metabolism and Toxicology*, vol. 3, no. 6, pp. 865–878, 2007.

[76] B. J. Blaauboer, "Biokinetic modeling and *in vitro-in vivo* extrapolations," *Journal of Toxicology and Environmental Health—Part B*, vol. 13, no. 2–4, pp. 242–252, 2010.

[77] J. Louisse, E. de Jong, J. J. M. van de Sandt et al., "The use of *in vitro* toxicity data and physiologically based kinetic modeling to predict dose-response curves for *in vivo* developmental toxicity of glycol ethers in rat and man," *Toxicological Sciences*, vol. 118, no. 2, pp. 470–484, 2010.

[78] M. D. Sohn, T. E. McKone, and J. N. Blancato, "Reconstructing population exposures from dose biomarkers: inhalation of trichloroethylene (TCE) as a case study," *Journal of Exposure Analysis and Environmental Epidemiology*, vol. 14, no. 3, pp. 204–213, 2004.

[79] T. E. McKone, "Linking a PBPK model for chloroform with measured breath concentrations in showers: implications for dermal exposure models," *Journal of Exposure Analysis and Environmental Epidemiology*, vol. 3, no. 3, pp. 339–365, 1993.

[80] K. T. Bogen and T. E. McKone, "Linking indoor air and pharmacokinetic models to assess tetrachloroethylene risk," *Risk Analysis*, vol. 8, no. 4, pp. 509–520, 1988.

[81] D. M. Rotroff, B. A. Wetmore, D. J. Dix et al., "Incorporating human dosimetry and exposure into high-throughput *in vitro* toxicity screening," *Toxicological Sciences*, vol. 117, no. 2, pp. 348–358, 2010.

[82] B. A. Wetmore, J. F. Wambaugh, S. S. Ferguson et al., "Integration of dosimetry, exposure, and high-throughput screening data in chemical toxicity assessment," *Toxicological Sciences*, vol. 125, no. 1, pp. 157–174, 2012.

Hindawi Publishing Corporation
Journal of Toxicology
Volume 2012, Article ID 404329, 14 pages
doi:10.1155/2012/404329

Research Article

Modeling the Human Kinetic Adjustment Factor for Inhaled Volatile Organic Chemicals: Whole Population Approach versus Distinct Subpopulation Approach

M. Valcke,[1,2] A. Nong,[1] and K. Krishnan[1]

[1] *Département de Santé Environnementale et de Santé au Travail, Université de Montréal, Montreal, QC, Canada H3T 1A8*
[2] *Institut National de Santé Publique du Québec, Montréal, QC, Canada H2P 1E2*

Correspondence should be addressed to K. Krishnan, kannan.krishnan@umontreal.ca

Received 21 September 2011; Accepted 21 October 2011

Academic Editor: Marina V. Evans

The objective of this study was to evaluate the impact of whole- and sub-population-related variabilities on the determination of the human kinetic adjustment factor (HKAF) used in risk assessment of inhaled volatile organic chemicals (VOCs). Monte Carlo simulations were applied to a steady-state algorithm to generate population distributions for blood concentrations (CAss) and rates of metabolism (RAMs) for inhalation exposures to benzene (BZ) and 1,4-dioxane (1,4-D). The simulated population consisted of various proportions of adults, elderly, children, neonates and pregnant women as per the Canadian demography. Subgroup-specific input parameters were obtained from the literature and P3M software. Under the "whole population" approach, the HKAF was computed as the ratio of the entire population's upper percentile value (99th, 95th) of dose metrics to the median value in either the entire population or the adult population. Under the "distinct subpopulation" approach, the upper percentile values in each subpopulation were considered, and the greatest resulting HKAF was retained. CAss-based HKAFs that considered the Canadian demography varied between 1.2 (BZ) and 2.8 (1,4-D). The "distinct subpopulation" CAss-based HKAF varied between 1.6 (BZ) and 8.5 (1,4-D). RAM-based HKAFs always remained below 1.6. Overall, this study evaluated for the first time the impact of underlying assumptions with respect to the interindividual variability considered (whole population or each subpopulation taken separately) when determining the HKAF.

1. Introduction

An interindividual variability (or uncertainty) factor (IVF) of a default value of 10 is usually applied to the point of departure (POD) for deriving reference doses (RfDs) or reference concentrations (RfCs) for use in noncancer risk assessment [1–3]. As reviewed by Price et al. [4], the IVF has historically been defined as a factor required to protect the sensitive members of the population since the POD is generally determined for average healthy individuals. Actually, two models have been proposed to describe the IVF. Under the "sensitive population" model, the IVF is applied to correct for the possible failure of a critical study to include a sufficient number of members pertaining to distinct subpopulation exhibiting an increased sensitivity. Conversely, under the "finite sample size" model, the application of the IVF relates to the possibility that the retained POD may fail to identify the toxicity threshold in the overall population simply because of the finite size of the sample in which it was determined [4]. Thus, the IVF accounts for the overall biological variability in the human population.

In the last 20 years, the IVF has been divided into two constitutive components (toxicokinetic and toxicodynamic factors), equal to 3.16 each based on pharmaceutical data [5–7]. This subdivision can be used in the evaluation of the magnitude and adequacy of the IVF for specific chemicals, and its replacement when appropriate data are available, by quantifying chemical-specific adjustment factors (CSAFs) [8, 9]. Under this method, the CSAF for interindividual variability in toxicokinetics, also referred to as the human kinetic adjustment factor (HKAF), can be determined based on the population distributions of relevant pharmacokinetic parameters (e.g., half-life, maximal concentration). The HKAF is calculated as the ratio between the upper percentile

Table 1: Chemical-specific parameters used in the steady-state algorithm.

Parameter	Chemical	
	Benzene[a]	1,4-Dioxane[b]
$V\max_c$ (mg/h-kg$^{0.75}$)	2.11	0.27
Km (mg/L)	0.1	3.0
Blood : air partition coefficient (P_b)	7.4	3650
Exposure concentration (mg/m^3, UF × RfC)[c]	0.3	3

[a][22]. [b][23]. [c][10].

BW: body weight; Km: Michaëlis-Menten constant, P_b: blood : air partition coefficient, RfC: reference concentration; UF: interindividual uncertainty factor; $V\max_c$: constant maximum rate of metabolism.

value of a parameter (i.e., 95th) and its central tendency value (i.e., median) in the whole population or between an upper percentile value in a presumed susceptible subpopulation and the central tendency value in the general healthy population [8, 9].

Neither the historical definitions of IVF [4] nor the IPCS guidance document on CSAFs [8] clearly defines the "average healthy individual," forming the point of comparison for the presumed sensitive subpopulations. Particularly, it is unclear as to whether this individual is the average healthy adult or the average healthy individual from the whole population (which includes both healthy adults and sensitive subpopulations). But presumably because the POD used to derive the RfD or RfC is generally determined in healthy adults (animal or human) [10], HKAF evaluations conducted using experimental data for drugs [11–13] or PBPK model simulation data for environmental toxicants [14–16] have relied on what can be called a "distinct subpopulation" approach. Thus, the experimental or simulated data in the presumed susceptible individuals (e.g., neonates, pregnant women, elderly, polymorphic individuals) have often been compared with the corresponding data in healthy adults.

Alternatively, HKAF can be quantified using a "whole population" approach as done recently by Mörk and Johanson [17]. In this study, HKAFs were calculated for inhaled acetone based on a simulated distribution of steady-state blood concentration in an entire population, including adults and various age-defined groups of children. The PBPK modeling results in the different subgroups were weighted according to demographic representation in Sweden. Excluding the endogenous production of acetone, an HKAF of 1.9 was obtained by dividing the 95th percentile value of the entire population by the median. In comparison, using the 95th percentile value of that same dose metric in 3-month-old babies as well as 10 and 15 yr old children resulted in HKAFs of 2, 2.4, and 1.7, respectively.

The hypothesis that the HKAF determined upon the "whole population" approach is quite different from the one determined based on the "distinct subpopulation" approach stems from the results of Mörk and Johanson [17]. This potential difference could be significant from a regulatory standpoint because it may not lead to comparable levels of protection for the different subgroups that compose the whole population. It is also not known whether the population composition and the chemical considered may impact this potential difference. Thus, the objective of the current study was to evaluate the magnitude and adequacy of the HKAFs determined by the "whole population" approach as compared to the "distinct subpopulation" approach. In effect, population distributions of internal dose metrics following chronic exposure to two chemicals exhibiting different clearance characteristics were used to compute the HKAF as

(i) the ratio of the upper percentile value in the entire population including adults and nonadults over the median in adults and in this entire population;

(ii) the ratio of the upper percentile value in presumed susceptible subpopulation over the median in adults and in the entire population including adults and non-adults.

2. Methods

A physiologically based steady-state algorithm combined with Monte Carlo simulation software was used to generate population distributions of blood concentration (CAss) and rate of metabolism (RAM) for chronic inhalation exposure to two chemicals with contrasting systemic clearance characteristics. The population distributions were reconstructed based on different proportions of randomly selected adults, elderly, children, neonates, and PW, and they were used to compute HKAFs based on "whole population" and "distinct subpopulation" approaches.

2.1. Selection of Surrogate Chemicals and Their Specific Parameters. Two VOCs were chosen as surrogate chemicals because they exhibit contrasting systemic clearances based on their pulmonary clearance potential (different blood : air partition coefficient (P_b)) and their hepatic clearance (different hepatic extraction ratios). Benzene was chosen as an extensively cleared chemical because of its high pulmonary clearance (low P_b, 7.4) and high hepatic extraction ratio. Conversely, 1,4-dioxane was chosen as a poorly cleared chemical due to its low pulmonary clearance (P_b = 3650) and low hepatic extraction ratio. While benzene is a known substrate of CYP2E1 [18], for which extensive data on interindividual variability are available [19, 20], 1,4-dioxane was included in this study to facilitate the coverage of a range of physico/biochemical properties of potential substrates of CYP2E1 [21]. Chemical-specific parameters are indicated in Table 1 and were taken from the literature [10, 22, 23]. The choice of these two surrogate VOCs and associated kinetic parameters was undertaken to reflect the range of kinetic characteristics of hypothetical substances for evaluating the HKAF. As such, the present modeling study did not focus on any aspect of the risk assessment relating to these specific chemicals.

2.2. Use of a Biologically Based Steady-State Model for the Simulation of Continuous Inhalation Exposure in Different Subpopulations. The current study relies on the use of

a steady-state model for inhalation exposures (e.g., [24–27]), because the current study aimed at reconstructing population distributions of internal dose metrics for continuous lifetime exposures. Briefly, the algorithm computes the arterial blood concentration at steady-state (CAss) from the alveolar ventilation rate (Qp), the concentration in air (Ci), and the hepatic ($Ql \times E_{hep}$) and pulmonary (Qp/P_b) clearances [27]:

$$CAss = \frac{Qp \times Ci}{Ql \times E_{hep} + Qp/P_b}, \quad (1)$$

where Ql is the liver blood flow, P_b is the blood : air partition coefficient, and E_{hep} is the hepatic extraction ratio of the chemical and is calculated from its intrinsic clearance (Clint) as follows:

$$E_{hep} = \frac{Clint}{Clint + Ql}. \quad (2)$$

Also, the rate of metabolised parent compound per unit volume of liver (RAM) is calculated as

$$RAM = \frac{CA_{ss} \times Ql \times E_{hep}}{Vl}. \quad (3)$$

As indicated in Table 2, Qp, Ql, and Vl were calculated for a given individual by applying equations derived from Price et al. [28] to the individual's body weight [16]. The input data are listed in Table 2 for each subpopulation considered [15, 16, 19, 20, 28, 29]. These include six age groups covering the lifespan (neonates (0–30 d), infants (1–12 mo), toddlers (1–3 yr), children/adolescents (4–17 yr), adults (18–64 yr), and elderly (65–90 yr)), as well as pregnant women (15–44 yr). Ql and Vl for pregnant women were actually calculated on the basis of the body weight for nonpregnant women, whereas the appropriate increase in alveolar ventilation rate at any time during pregnancy was accounted for when computing Qp [16].

2.3. Generation of Distributions of Internal Dose Metrics by Means of Monte Carlo Simulations. Constant inhalation exposure to a benzene concentration corresponding to 10× the RfC (Table 1) was simulated in each subpopulation. Given the lack of an RfC for 1,4-dioxane, and its approximately tenfold greater RfD compared to benzene [10], a concentration that was ten times greater than the benzene concentration was specified. Monte Carlo simulations were performed using the Crystal Ball software (Oracle, Redwood Shores, CA) to generate distributions of the various internal dose metrics (see below). The intrinsic clearance in (2) was corrected for a given individual in any subpopulation by adjusting the maximum rate of metabolism ($V\max_{ind}$) using enzyme-specific catalytic turnover [14–16]. This was determined based on the $V\max$ in an adult of average body weight (BW_{avg_ad}), as well as the (individual (ind)/average adult (avg_ad)) ratios of the liver volumes and CYP2E1 hepatic content (in pmol/mg of microsomal protein):

$$V\max_{ind} = \frac{V_{max_c} \times BW_{avg\_ad}^{0.75}}{[CYP2E1]_{avg\_ad} \times Vl_{avg\_ad}} \times [CYP2E1]_{ind} \times Vl_{ind}. \quad (4)$$

A constant hepatic microsomal protein concentration was assumed across the subpopulations as discussed in Valcke and Krishnan [16].

2.3.1. Distributions in the "Whole Population" and Corresponding HKAFs. Distributions of the internal dose metrics were generated for a theoretical population of 100,000 people with the demographic characteristics of Canada [30]. Therefore, the number of iterations used in the Monte Carlo simulations for each subpopulation corresponded to the targeted number of individuals. This number was based on the demographic proportions of each subpopulation (Table 3). Because the number of individuals appeared relatively constant across census' age ranges of same duration, the number of individuals pertaining to an age range different than those defined in the census could easily be estimated. For example, the number of toddlers aged 1–3 was considered as 60% of the total individuals 0–4 yr old. Finally, the number of pregnant women was calculated based on the pregnancy rate of 104/1,000 from Ventura et al. [31] and on the number of women aged 15–44 yr from the census data. The dose metric values "generated" by the Monte Carlo simulations for each subpopulation were then merged into a single "Canadian population dataset" of 100,000 values. To calculate the HKAFs based on the "whole population" approach, the ratio of the upper percentile value of the dose metric in the entire Canadian population to its median value was computed. The percentage of each subpopulation that was protected by a "whole population" HKAF was determined by identifying the number of individuals in each subpopulation exhibiting an internal dose metric that was lower than the entire population's upper percentile value underlying the HKAF, that is, 95th or 99th.

2.3.2. Distributions in Each "Distinct Subpopulation" and Corresponding HKAFs. Distributions of the internal dose metrics for 100,000 individuals of each subpopulation were generated and the chemical- and dose-metric-specific HKAFs were calculated based on the "distinct subpopulation" approach, that is, as the ratio of the upper percentile value (i.e., 95th or 99th) in each subpopulation to the median value in adults or the whole Canadian population (see above). Also, for a given dose metric, the greatest "distinct subpopulation-" based HKAF was multiplied by the median in the whole Canadian population (see above) to obtain a threshold dose metric value. This threshold corresponded to the percentile that was referred to for determining the proportion of individuals from the entire population that was covered by the greatest "distinct subpopulation" HKAF.

Table 2: Physiological parameters distributions used in the Monte Carlo simulations of the internal dose metrics with the steady-state algorithm.

Parameter[a]	Subpopulation Median age (range)						
	Adults 41 (18–64)	Neonate 14 d (0–30 d)	Infants 6.5 m (1–12 mo)	Toddlers 2 (1–3)	Children and adolescents 12 (4–17)	Elderly 78 (65–90)	Pregnant women 29 (15–44)
Sampled parameters							
Body weight (BW) (Kg: m ± SD, range)	76 ± 17, 37–152[b]	4 ± 1, 2–7[c]	9 ± 2, 3–15[b]	13 ± 2, 7–32[b]	36 ± 16, 9–113[b]	72 ± 16, 33–155[b]	70 ± 18, 36–152[d]
[CYP2E1] (pmol/mg MSP: m ± SD, range)	49 ± 2, 11–130[e]	18 ± 14, 1–56[c]	36 ± 21, 10–86[c]	42 ± 18, 18–74[c]	53 ± 23, 22–95[c]	[f]	[f]
Calculated parameters[b],[g]							
Alveolar ventilation rate (Qp)	$= [((0.2519 \times BW^{0.7609}) + (0.2508 \times BW^{0.7815}))/2)] \times$ "variability term" (i.e., 1 ± 0.1 (0.8–1.2))						
Liver volume (Vl)	$= 0.05012 \times BW^{0.78} \times$ "variability term" (i.e., 1 ± 0.14(0.66–1.34))						
Liver blood flow (Ql)	$= 0.92 \times Vl \times$ "variability term" (i.e., 1 ± 0.13 (0.67–1.33))						

[a] Log normal distributions for sampled parameters and normal distributions for "variability terms." All indicated means are arithmetic, except note [e](see below). [b] P^3M database [28]. [c] [19]. [d] Distribution for non-pregnant women taken from P^3M database [28], and, to each of these values, the mean body weight increase at any week during pregnancy (normal distribution of 5 ± 4.4 kg (0–14.1)) based on data from ICRP was added [16, 29]. [e] (Geometric mean ± geometric standard deviation) [20]. [f] Same as for adults. [g] [16].
CYP2E1: cytochrome p-450 2E1; MSP: microsomal protein; SD: standard deviation.

Table 3: Reconstruction of the hypothetical populations of 100,000 people with the Canadian demographic profile.

Subpopulation (age range)	Canadian population in 2009[a] Median age = 39.7 yr	
	Population size (%)	Corresponding reconstructed population size and number (n) of Monte Carlo iterations
Adults (18–64)	21,685,253 (63.92)	63,923
Neonates (0–30 d)	31,303 (0.09)	93
Infants (1–12 mo)	344,329 (1.02)	1,015
Toddlers (1–3)	1,126,896 (3.32)	3,322
Children and adolescents (4–17)	5,382,420 (15.87)	15,866
Elderly (65–90)	4,634,673 (13.66)	13,662
Pregnant women[b] (15–44)	718,950 (2.12)	2,119
TOTAL	33,923,824 (100)	100,000

[a] [30]. [b] Based on a pregnancy rate of 104/1,000 in U.S. women aged 15–44 yr [31].

2.4. Evaluation of the Impact of Demography on the Computed HKAFs. Given that the HKAF values as computed herein rely on the distribution of internal dose metrics in a general population composed of various proportions of each subpopulation, it was hypothesized that the demographic characteristics of a given general population may impact this calculation. To test this hypothesis, HKAFs were evaluated on the basis of dose metric distributions generated for a theoretical "younger population." These distributions were reconstructed by multiplying by 3 the number of individuals of each subpopulation <18 yr, as well as pregnant women, as compared to the numbers that were previously used to reconstruct the Canadian population distributions (Table 3). The number of adults was also adjusted to maintain a total of 100,000 dose metric values. Thus, more than 60% of the resulting "younger population" was aged <18 y, as compared to approximately 20% for the Canadian population.

3. Results

3.1. Distributions of Internal Dose Metrics in Each Subpopulation and the Entire Canadian Population. Figures 1 and 2 show the simulation of internal dose metric distributions in each subpopulation (making up the entire Canadian population) exposed to benzene and 1,4-dioxane, respectively. The shapes of the Canadian population distributions appeared normal for CAss of benzene and lognormal in the other cases. The ranges (1st–99th percentile) and median dose metrics that were obtained when simulating 100,000 individuals in each subpopulation are indicated in Table 4. Based on the median and 99th percentile dose metrics, neonates and pregnant women were the most susceptible subpopulations (i.e., they exhibited the highest dose metric) based on CAss and RAM, respectively. The median dose metric in the most susceptible subpopulation was always greater than the median dose metric in the Canadian population, but it was lower than the 99th percentile value, except for the CAss value for 1,4-dioxane. In this case, the median value in neonates (2.3 mg/L) was greater than the 99th percentile value in the whole population (2.14 mg/L). The internal variability of internal dose metrics in the Canadian population can be appraised by the ratio of the 99th to the 1st percentile values. The greatest variability was obtained for 1,4-dioxane based on simulations of CAss exhibiting an approximately sevenfold difference. The population variability was lower in every other case ((99th/1st percentile) ratios lower than 3). Similar trends were obtained for each specific subpopulation, although the magnitude of the differences varied. In particular, neonates exhibited a tenfold (99th/1st percentile) ratio of CAss for 1,4-dioxane. This dose metric exhibits a variability leading to such ratio that is always greater than 5 regardless of the subpopulation. In every other subpopulation and dose metric, the ratio was at most equal to 3 (neonates' RAM for 1,4-dioxane).

3.2. HKAF Values

3.2.1. "Whole Population" Approach. HKAFs determined based on the "whole population" approach, which used both the median adult ($HKAF_{ad}$) and the median individual in the entire Canadian population ($HKAF_{pop}$) as referents, are indicated in Table 5. CAss-based HKAFs varied between 1.2 and 1.3 for benzene and between 2.1 and 2.8 for 1,4-dioxane. These values were slightly lower than the highest "distinct subpopulation-" based HKAFs for benzene but were significantly lower than the 1,4-dioxane values (see below). Considering the RAM, all the HKAF values were between 1.2 and 1.6 regardless of the chemical. These values were slightly lower than the highest RAM-based HKAFs obtained with the "distinct subpopulation" approach in pregnant women (1.5–2.1, see below).

3.2.2. "Distinct Subpopulation" Approach. Table 5 shows that the 95th and the 99th percentile-based HKAFs that were computed using the "distinct subpopulation" approach were comparable whether the median adult ($HKAF_{ad}$) or the median individual in the whole population ($HKAF_{pop}$) was used as a referent. In addition to the referent adults, results for neonates and pregnant women are presented because

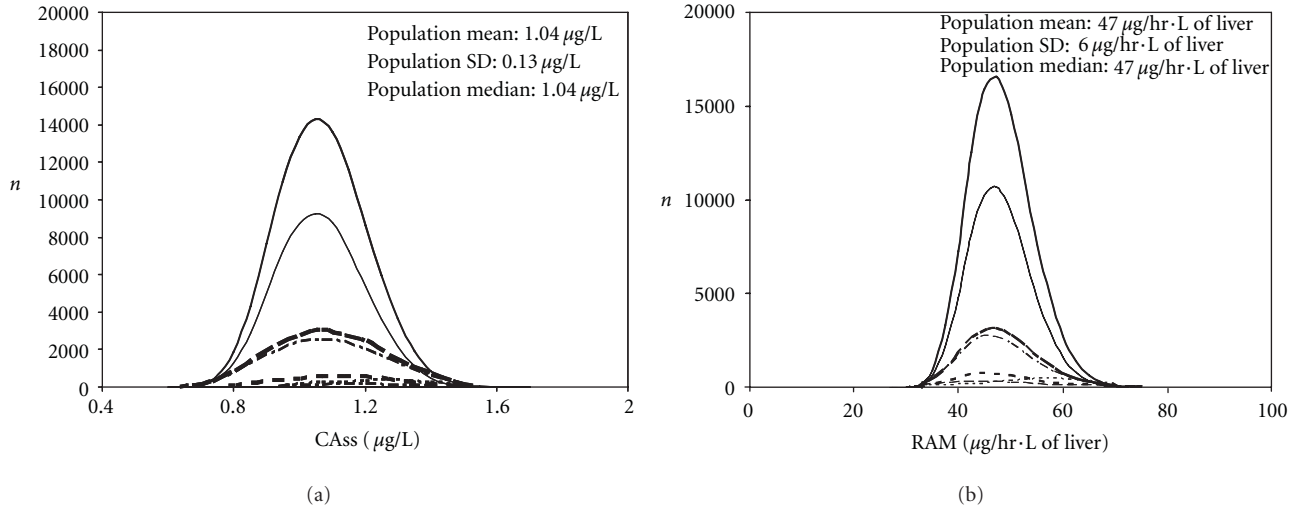

(a) (b)

Figure 1: Distributions of individual values obtained for CAss (a) and RAM (b) in each subpopulation within the whole Canadian population for constant inhalation exposure to benzene. From top to bottom, the distributions are shown for the entire Canadian population (thick —), adults (—), children and adolescents (— –), elderly (–·–·–), toddlers (– – -), pregnant women (-------), infants (-··-··-), and neonates (indistinguishable).

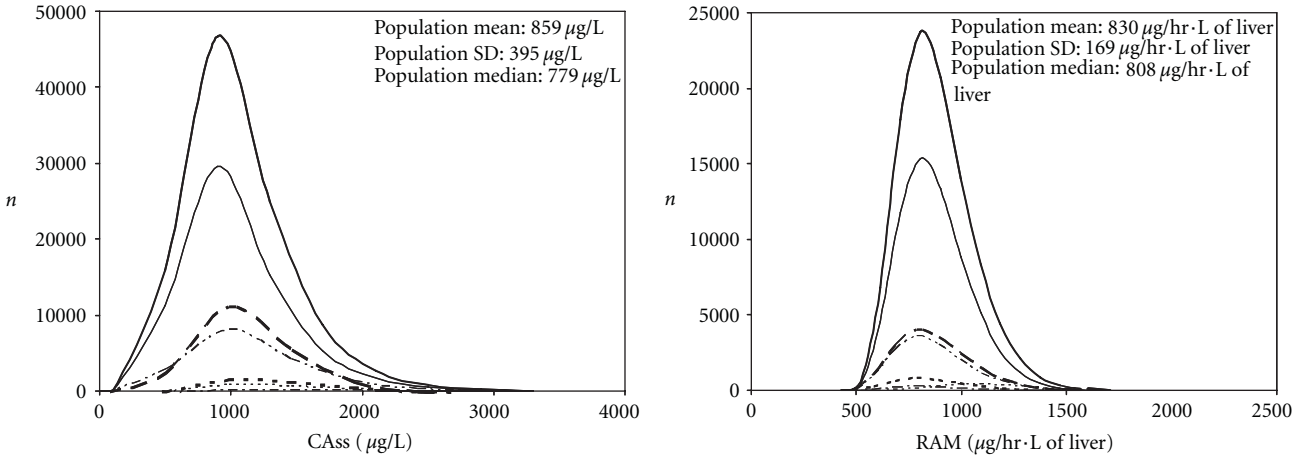

(a) (b)

Figure 2: Distributions of individual values obtained for CAss (a) and RAM (b) in each subpopulation within the whole Canadian population for constant inhalation exposure to 1,4-dioxane. From top to bottom, the distributions are shown for the entire Canadian population (thick —), adults (—), children and adolescents (— –), elderly (–·–·–), toddlers (– – -), pregnant women (-------), infants (-··-··-), and neonates (indistinguishable).

they were, toxicokinetically, the most susceptible based on their respective CAss and RAM (Table 4). HKAFs for infants were also shown because they exceeded the default 3.16 value when CAss of 1,4-dioxane was considered, on the basis of the 99th percentile value (3.8). The default value was also exceeded based only on CAss of 1,4-dioxane in neonates (range: 6.5–8.5) and the 99th percentile value in pregnant women (3.5). Neonates exhibited the greatest CAss-based HKAFs for inhaled benzene (1.6–1.7). Otherwise, pregnant women showed the greatest RAM-based HKAFs for benzene (1.5–1.6) and 1,4-dioxane (1.8–2.1). HKAFs in other subpopulations remained in the range of the HKAFs presented in Table 5 for any given dose metric (data not shown).

3.3. Proportions of the Whole Population or the Distinct Subpopulations Covered by the Different HKAFs. Table 6 shows the proportion of each subpopulation that was covered by the various HKAFs defined using the "whole population" approach. The 95th or 99th percentile-based "whole population" HKAFs generally protect at least, or very close to, 95% and 99%, respectively, of the individuals of each subpopulation. However, only 57% of the neonates, 78% of the pregnant women, and 89% of the infants were covered by the 95th percentile-based "whole population," CAss-based HKAF for benzene. Corresponding values for the 99th percentile-based HKAF values were 73%, 92%, and 97%, respectively. In the case of 1,4-dioxane, 27%, 76%, and 86% of the neonates, infants, and pregnant women were

Table 4: Distribution statistics of various dose metrics in each subpopulation based on 100,000 Monte Carlo iterations and the entire Canadian populations for constant inhalation exposure.

Subpopulation Statistics	Dose metrics			
	Benzene		1,4-Dioxane	
	CAss	RAM	CAss	RAM
Adults				
1st percentile	0.76	35	285	531
Median	1.04	46	763	806
99th percentile	1.36	62	2119	1291
Neonates				
1st percentile	0.88	20	682	371
Median	1.26	39	2299	686
99th percentile	1.76	55	6486	1149
Infants				
1st percentile	0.8	33	420	526
Median	1.11	45	1150	787
99th percentile	1.44	60	2928	1246
Toddlers				
1st percentile	0.79	35	382	534
Median	1.08	47	968	804
99th percentile	1.38	60	2099	1271
Children and adolescents				
1st percentile	0.77	35	352	538
Median	1.04	47	774	814
99th percentile	1.35	61	1744	1293
Elderly				
1st percentile	0.76	35	286	530
Median	1.04	46	766	807
99th percentile	1.37	62	2144	1291
Pregnant Women				
1st percentile	0.85	41	372	673
Median	1.16	55	995	1050
99th percentile	1.49	73	2698	1686
Canadian population				
1st percentile	0.76	35	299	533
Median	1.04	47	779	808
99th percentile	1.36	63	2139	1306

CAss: blood concentration of parent compound (μg/L); RAM: rate of metabolism (μg/h-L of liver).

covered by the 95th percentile-based HKAF, respectively. Corresponding values for the 99th percentile HKAFs were 48%, 92%, and 96%, respectively, and the default 3.16 factor appears to cover only 60% of the neonates. Considering the RAM, the lack of coverage by the "whole population-" based HKAF concerns pregnant women, as only 63% and 85% of them are covered by, respectively, the 95th and 99th percentile-based HKAF for benzene. These numbers are 66% and 86% in the case of 1,4-dioxane. Finally, when the HKAF was computed with the "distinct subpopulation" approach and the greatest value was retained, more than 99% of the entire Canadian population was covered for every dose metric considered (Table 6).

3.4. Impact of the Demography on the Computed HKAFs. The impact of the demographic characteristics on the HKAF values as computed herein can be appreciated from the results shown in Figure 3 for CAss and Figure 4 for RAM. The distributions for 100,000 referents (adult) and the most susceptible individuals (neonates for CAss, pregnant women for RAM) are also shown in these figures for comparison purposes. For benzene (Figure 3(a)), the change in demographics did not impact the overall population distribution of CAss (indistinguishable from adults) and thus, not the HKAF. The change of demographics shifts minimally to the right the population distribution of CAss for 1,4-dioxane (Figure 3(b)). The impact on the various

Table 5: HKAFs obtained by the "distinct subpopulation" approach on the basis of 100,000 Monte Carlo iterations in adults, neonates, infants, and pregnant women and by the "whole population" approach for the Canadian population.

HKAF assumption	Dose metrics			
	Benzene		1,4-Dioxane	
	CAss	RAM	CAss	RAM
"Whole population" approach				
$HKAF_{ad}$ [(a)]				
Based on 95th percentile	1.2	1.3	2.1	1.4
Based on 99th percentile	1.3	1.4	2.8	1.6
$HKAF_{pop}$ [(b)]				
Based on 95th percentile	1.2	1.2	2.1	1.4
Based on 99th percentile	1.3	1.4	2.8	1.6
"Distinct subpopulation" approach				
In adults				
$HKAF_{ad}$ [(c)]				
Based on 95th percentile	1.2	1.2	2.1	1.4
Based on 99th percentile	1.3	1.3	2.8	1.6
$HKAF_{pop}$ [(d)]				
Based on 95th percentile	1.2	1.2	2.0	1.4
Based on 99th percentile	1.3	1.3	2.7	1.6
In neonates				
$HKAF_{ad}$ [(c)]				
Based on 95th percentile	*1.6*	1.1	*6.6*	1.2
Based on 99th percentile	*1.7*	1.2	*8.5*	1.4
$HKAF_{pop}$ [(d)]				
Based on 95th percentile	*1.6*	1.1	*6.5*	1.2
Based on 99th percentile	*1.7*	1.2	*8.3*	1.4
In infants				
$HKAF_{ad}$ [(c)]				
Based on 95th percentile	1.3	1.2	3.1	1.4
Based on 99th percentile	1.4	1.3	3.8	1.6
$HKAF_{pop}$ [(d)]				
Based on 95th percentile	1.3	1.2	3.0	1.4
Based on 99th percentile	1.4	1.3	3.8	1.5
In pregnant women				
$HKAF_{ad}$ [(c)]				
Based on 95th percentile	1.4	*1.5*	2.7	*1.8*
Based on 99th percentile	1.5	*1.6*	3.5	*2.1*
$HKAF_{pop}$ [(d)]				
Based on 95th percentile	1.4	*1.5*	2.6	*1.8*
Based on 99th percentile	1.5	*1.6*	3.5	*2.1*

Italicized values indicate the highest HKAF among each subpopulation for a given dose metric.
[(a)]Computed as the ratio of the upper percentile value in the Canadian population (95th or 99th) to the median in 100,000 adults. [(b)]Computed as the ratio of the upper percentile value in the Canadian population (95th or 99th) to its median. [(c)]Computed as the ratio of the upper percentile value in the subpopulation (95th or 99th) to the median in adults. [(d)]Computed as the ratio of the upper percentile value in the subpopulation (95th or 99th) to the median in the Canadian population.
CAss: blood concentration of parent compound; $HKAF_{(ad/pop)}$: human kinetic adjustment factor using either the median in adult ("ad") or whole population ("pop") as referent; RAM: rate of metabolism.

Table 6: Percentage of individuals in the diverse Canadian subpopulations that are covered by the HKAF and the default factor for various dose metrics and chemicals.

Subpopulation	Variability descriptor	Dose metrics			
		Benzene		1,4-Dioxane	
		CAss (%)	RAM (%)	CAss (%)	RAM (%)
Adults					
	"whole population"[a] $HKAF_{95th}$	96	96	95	97
	"whole population"[a] $HKAF_{99th}$	99	>99	>99	>99
	Default 3.16 factor	100	100	>99	100
Neonates					
	"whole population"[a] $HKAF_{95th}$	57	100	27	100
	"whole population"[a] $HKAF_{99th}$	73	100	48	100
	Default 3.16 factor	100	100	60	100
Infants					
	"whole population"[a] $HKAF_{95th}$	89	97	76	97
	"whole population"[a] $HKAF_{99th}$	97	>99	92	>99
	Default 3.16 factor	100	100	97	100
Toddlers					
	"whole population"[a] $HKAF_{95th}$	93	97	92	96
	"whole population"[a] $HKAF_{99th}$	99	>99	99	99
	Default 3.16 factor	100	100	>99	100
Children and adolescents					
	"whole population"[a] $HKAF_{95th}$	96	96	98	95
	"whole population"[a] $HKAF_{99th}$	>99	>99	>99	>99
	Default 3.16 factor	100	100	100	100
Elderly					
	"whole population"[a] $HKAF_{95th}$	95	96	95	96
	"whole population"[a] $HKAF_{99th}$	>99	99	99	>99
	Default 3.16 factor	100	100	>99	100
Pregnant Women					
	"whole population"[a] $HKAF_{95th}$	78	63	86	66
	"whole population"[a] $HKAF_{99th}$	92	85	96	86
	Default 3.16 factor	100	100	98	100
Canadian population					
	Greatest[b] "distinct subpopulation" $HKAF_{95th}$	>99	>99	>99	>99
	Greatest[b] "distinct subpopulation" $HKAF_{99th}$	>99	>99	>99	>99
	Default 3.16 factor	100	100	>99	100

[a]Based on the median value in the whole Canadian population. [b]Based on the median value in adults in Table 5.
CAss: blood concentration of parent compound (μg/L); RAM: rate of metabolism (μg/h-L of liver).

HKAFs was low ("whole population" HKAF = 2.69 versus 2.75) with differences of 3% or less for the relevant statistical descriptors. Considering RAM, when the number of significantly less susceptible neonates, and infants, and more susceptible pregnant women, was increased at the expense of adults, the entire population distribution of the dose metric for both chemicals was widened slightly and particularly for 1,4-dioxane (Figure 4). The impact of pregnant women was apparent with a slight burst in the "younger" population distribution, which was observed near the pregnant women's approximate median value. On the basis of the 99th percentile values, this resulted in virtually unchanged HKAFs for benzene (Figure 4(a)), but marginal changes were observed for 1,4-dioxane (Figure 4(b)). The "whole population" HKAFs that were calculated from the indicated statistical descriptors are 1.67 (1342/806) and 1.75 (1342/765), which were based on median values in adults or population distributions, respectively, for the "younger" population. In comparison, the "whole population" HKAF for the Canadian population was 1.62. The "distinct subpopulation" HKAF for pregnant women was also slightly increased, from 2.09 for the Canadian and adult populations to 2.2 for the "younger" population due to lower median values (765 μg/h-L of liver versus 808 or 806 μg/h-L of liver).

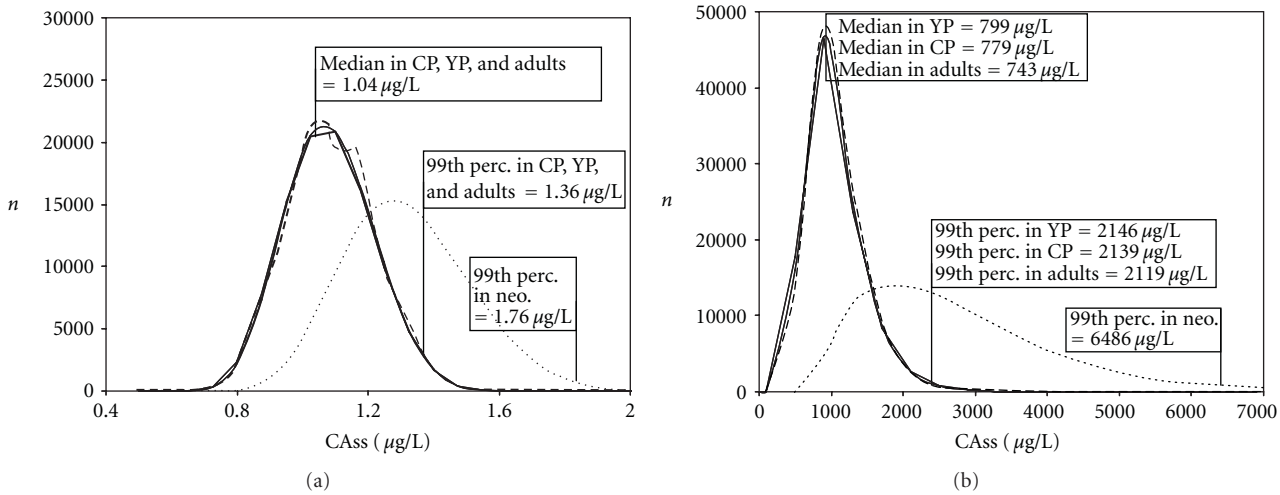

Figure 3: Distribution of individual values obtained for CAss for constant inhalation exposure to benzene (a) and 1,4-dioxane (b) in the entire Canadian (CP, thick —) and "younger" (YP, – –) populations of 100,000 people, in 100,000 adults (—) and in 100,000 of the most susceptible neonates (neo, . . .). Median and 99th percentile values only (for clarity reasons) are indicated.

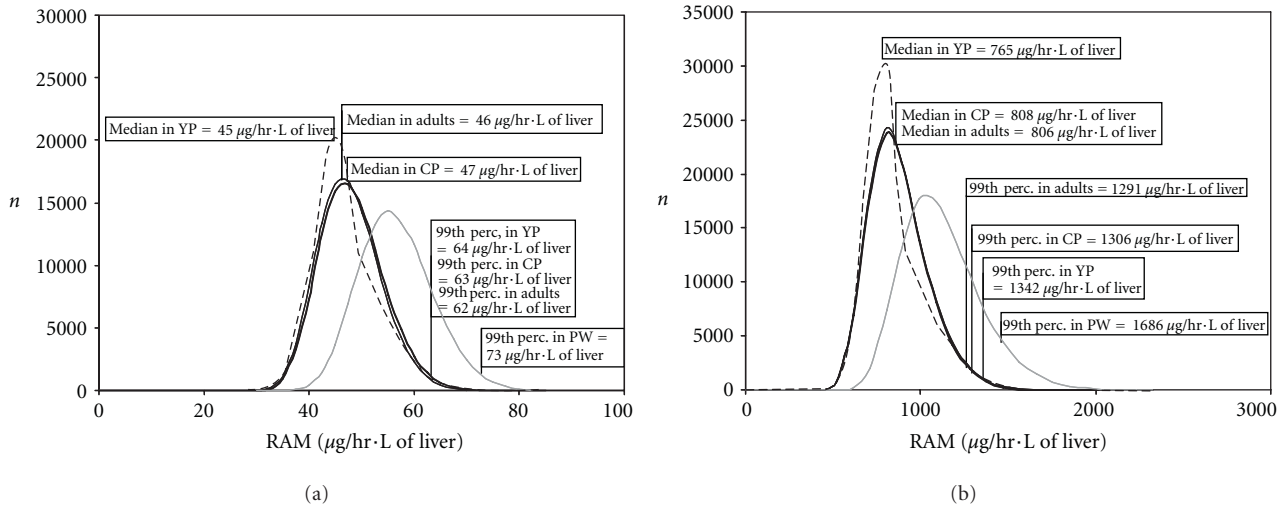

Figure 4: Distribution of individual values obtained for RAM for constant inhalation exposure to benzene (a) and 1,4-dioxane (b) in the entire Canadian (CP, thick —), and "younger" (YP, – –) populations of 100,000 people, in 100,000 adults (—) and in 100,000 of the most susceptible pregnant women (PW, grey —).

4. Discussion

This study performed Monte Carlo simulations on a steady-state algorithm to reconstruct representative subpopulation and whole population distributions of internal dose metrics for continuous inhalation exposure to a highly (benzene) and poorly (1,4-dioxane) cleared chemical. This allowed evaluating the impact of various assumptions on the resulting HKAF.

Virtual populations have been reconstructed to evaluate the population variability of the pharmacokinetic of drugs (e.g., [32, 33]), but to date, the same approach had not been realized for environmental contaminants. This procedure realized in the context of the present study allowed obtaining results showing that the impact of the approach chosen to compute the HKAF depends on the chemical and dose metric considered. The "whole population" approach used here can be related to the "Finite Sample Size" model of IVF from Price et al. [4], whereas the "distinct subpopulation-" based HKAF can be associated to these authors' "sensitive population" model. When the most sensitive individuals, based on dosimetric considerations, constitute a very small fraction of the entire population, a "whole population-" based HKAF might not be sufficient to cover them adequately. For instance, less than 60% of the neonates, constituting less than 0.1% of the whole Canadian population in this study, were covered by the "whole population" HKAF based on their 95th percentile CAss value. This was also the case of infants, who constituted a mere 1% of the entire population, for whom less than 90% of the individuals

simulated were covered by that same HKAF (Table 6). The reasons for these results can be determined from Figures 1 and 2. Because toxicokinetically sensitive neonates and infants make up a small proportion of the population, their CAss values do not stand out at the right end of the whole population distributions (Figures 1(a) and 2(a)). Thus, the "distinct subpopulation-" based HKAF would appear to be more adequate in these cases because the focus is then put on the most sensitive subpopulations, regardless of whether the data follow unimodal or bimodal distributions. Conversely, when the more sparse individuals (neonates and infants) are rather less sensitive than the vast majority of the individuals composing the entire population, as for RAM, the approach taken to compute the HKAF does not impact its value (Table 5).

The results obtained in Figures 3 and 4 can be viewed as a "sensitivity analysis" of the impact of demography on the HKAF. Replacing a significant number of adults from the Canadian population with individuals who are generally equally susceptible as adults (Table 4) resulted in a "younger" population distribution of CAss for benzene that remained virtually unchanged (Figure 3(a)). In the case of 1,4-dioxane (Figure 3(b)), every replacing individual pertained to subpopulations that were more susceptible than adults (Table 4), and, as a result, the population distribution of CAss slightly shifted to the right towards the most susceptible neonates. In the case of RAM, the individuals replacing the adults were either more susceptible (pregnant women) or less susceptible (children), leading to population distributions that were wider for both chemicals (Figure 4). As mentioned in Section 3, the sensitivity of the HKAF to the population demography (i.e., the impact of the population distribution shift on the estimated HKAF) was marginal because the differences in the susceptibilities were not very pronounced between the subpopulations, with the exceptions of neonates and infants based on CAss (particularly for 1,4-dioxane), and pregnant women based on the RAM. However, the impact of these subpopulations' dose metric on the entire population distribution always remained minimal because of their small percentage in the entire population.

While in our study, demography appears to have, at the most, a very marginal effect on HKAF, the population distributions of CAss are conversely significantly influenced by the determining physiological parameters. Indeed, intake and pulmonary clearance of both benzene and 1,4-dioxane are driven by alveolar ventilation rate, which is rather log normally distributed when adjusted to the body weight (Figure 5(a)). However, blood-flow limited metabolism results in hepatic blood flow being the determining parameter for the clearance of benzene whereas for 1,4-dioxane, hepatic enzyme concentration and thus Vmax (see (4)) is determinant of its enzyme-limited clearance. As a result, the distribution of body-weight-adjusted liver blood flow (Figure 5(b)), which is more skewed than the distributions of Vmax (Figure 5(c)) or Clint (central tendency, range: ≈400 L/h, 0–1600 L/h), yields a population distribution of CAss that is more skewed for benzene (Figure 1(a)) than for 1,4-dioxane (Figure 2(a)). Indeed, the hepatic clearance of the latter is rather driven by the Vmax (Figure 5(d)) and the corresponding Clint (central tendency, range: ≈1.7 L/h, 0–7 L/h). Correspondingly, "whole population-" based HKAFs are smaller for benzene than 1,4-dioxane (Table 5).

The toxicokinetic determinants, including physiological parameters, of the susceptibility of each subpopulation to a given chemical based on any dose metric have been thoroughly discussed elsewhere [16]. Briefly, neonates are the most susceptible population based on CAss (Table 5) because they are exposed to a greater-than-adult body-weight-adjusted dose by inhalation, or to a poorly metabolized chemical (1,4-dioxane) for which hepatic metabolism is enzyme-limited, thus reduced in neonates. For pregnant women, their greater susceptibility on the basis of RAM is due to their increased intake on a body weight basis (due to high Qp) combined with their efficient hepatic clearance, a combination that yields a high rate of conversion of inhaled parent compound into metabolites. Greater inhalation uptake on a body weight basis and corresponding blood concentration of inhaled VOCs, for young children and pregnant women as compared to adults, have been consistently documented and discussed in the literature [14–16, 29, 34–39]. The systemic clearance of high P_b, poorly metabolized 1,4-dioxane is Qp-dependent (for pulmonary clearance) and enzyme-dependent (for hepatic clearance), and the greater intrasubpopulation variability of CAss that was observed for this chemical was expected. This greater variability results in neonates and infants constituting the only subpopulation for which the consideration of the 99th percentile value rather than the 95th significantly changes their HKAF value (Table 5). Else, the intra-subpopulation variability was rather low for every dose metric.

The "distinct subpopulation-" based $HKAF_{ad}$ that was obtained for benzene exposure in infants (1.3–1.4, Table 5) and toddlers (1.25–1.33, not shown) was very similar to the values obtained for other inhaled VOCs by Pelekis et al. [40] for a 10 kg child. Using a deterministic steady-state approach, these authors obtained an average factor of 1.1 ± 0.6 for eight chemicals highly cleared by either pulmonary or hepatic clearance or both. Also, a ratio of the neonate's 95th percentile value to the adult's median value of blood concentrations for dichloromethane was slightly above 2 in the study by Pelekis et al. [41] for continuous inhalation exposure, as compared to 1.6 for benzene in the current study. Besides, the "distinct subpopulation-" based $HKAF_{pop}$ that was obtained in neonates for 1,4-dioxane (6.5, Table 5) was markedly greater than the value (2) obtained by Mörk and Johanson [17] for acetone, a chemical that is similar to 1,4-dioxane (poorly metabolized and highly water soluble with a P_b of 260). The HKAF obtained for 1,4-dioxane in children and adolescents (1.8, not shown) is comparable to those obtained by these authors for 10 and 15 yr old children for acetone (1.7–2.4). The discrepancy for neonates might be explained by the difference in the mean age considered (14 days versus 3 months) and related hepatic enzyme content. The "whole population-" based $HKAF_{pop}$ obtained here based on the 95th percentile (2.1) compares well to Mörk and Johanson's results (i.e., 1.9). Finally, Renwick and Lazarus [7] determined that more than 99% of individuals in

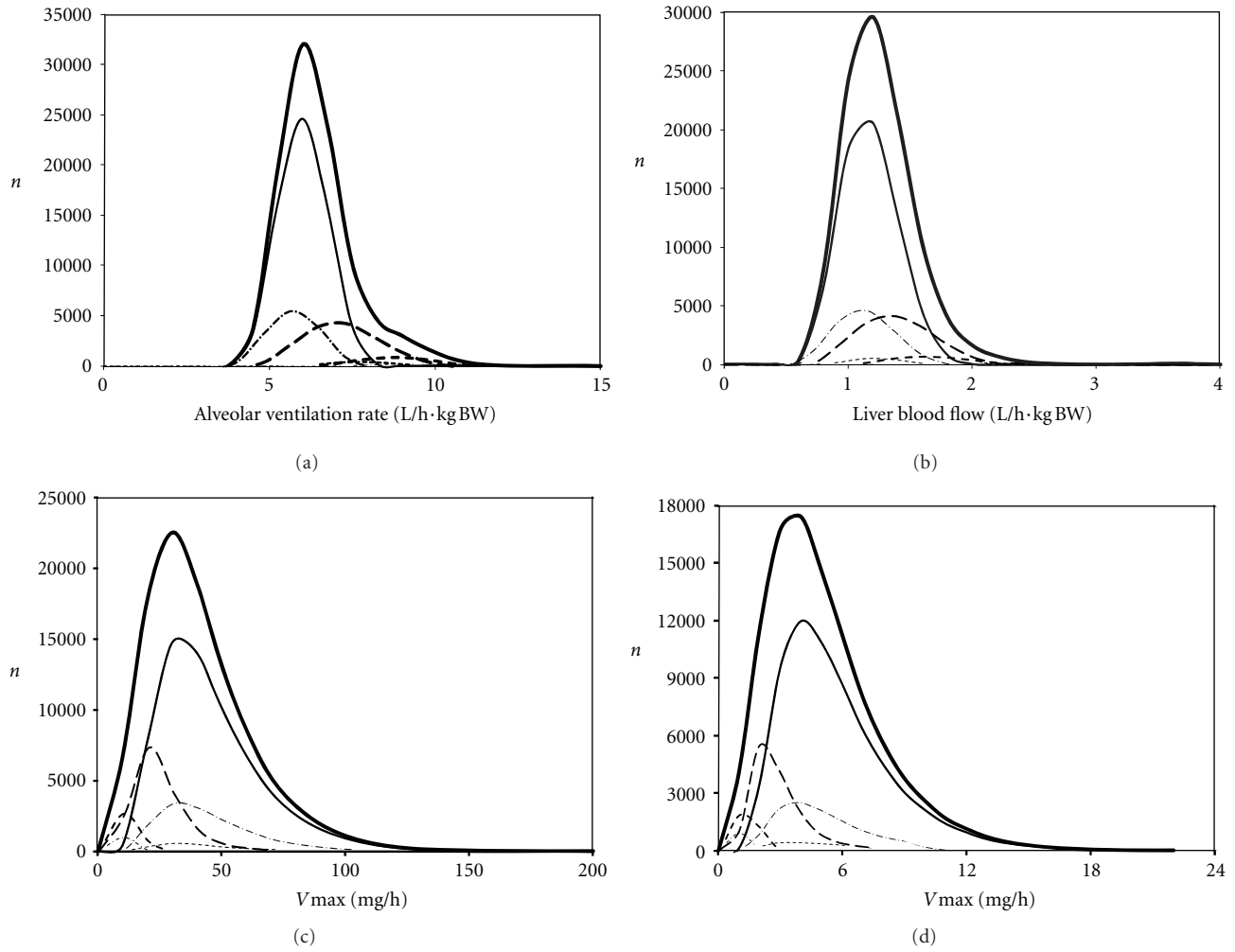

Figure 5: Distributions of individual values obtained for several physiological parameters in each subpopulation within the whole virtual Canadian population. From top to bottom, distributions for body weight-adjusted alveolar ventilation rate (a), body weight-adjusted liver blood flow (b) and maximal rate of metabolism of benzene (c) and 1,4-dioxane (d) are shown for the entire Canadian population (thick —), adults (—), children and adolescents (— –), elderly (–·–·–), toddlers (– – -), pregnant women (-------), infants (-··-··-), and neonates (indistinguishable).

a theoretical population of 1 million would be covered by the default factor, a proportion also obtained in this study.

Among the limitations of this study are other demographic characteristics, including gender differentiation, that could have been considered when generating the population distributions. In particular, ethnicity can be a critical determinant of population variability in toxicokinetics [7] because it is often linked to polymorphic metabolism [42]. However, multiplying subpopulation categories would increase the uncertainty linked to analyzing the distribution of the dose metric in very rare individuals like those with genetic polymorphisms. Besides, gender-related differences in the blood toxicokinetics of several VOCs have been considered insignificant [38, 43]. Furthermore, ethnicity is likely not a primary factor determining CYP2E1 activity because the population variability in the enzyme expression caused by factors other than polymorphism, such as ethanol consumption and xenobiotic coexposure [44] is considerable. Another limitation relates to the use of only healthy individuals in this study; the HKAFs calculated thus do not account for diseased people with altered hepatic or extrahepatic clearance.

In conclusion, this study has, for the first time, systematically compared different approaches for computing the HKAF under various assumptions related to the population/subpopulation variability in internal dose metric for continuous inhalation exposure. This was determined for two environmental chemicals exhibiting different patterns of systemic clearance, to encompass a range of other potential chemicals with such characteristics. This study contributes to clarify the implications of the different underlying assumptions that relate to the interindividual variability considered when determining the HKAF for any risk management consideration, including adequate coverage or not of the most susceptible, but sparse, individuals of a given population. In this regard, relying on the "distinct subpopulation" approach appears more conservative (protective) as it better covers the most susceptible individuals, in particular if they compose a small proportion of the general population.

Fundamentally, the difference in the extent of coverage afforded by these two approaches would appear to depend upon the proportion of the most sensitive individuals in the target population for a risk assessment. Moreover, the present work has illustrated the feasibility of a novel approach for characterizing demography-based population variability of internal dose metrics for environmental contaminants.

Abbreviations

CSAF:	Chemical-specific adjustment factor
CAss:	Arterial blood concentration at steady-state
CYP:	Cytochrome P-450
HKAF:	Human kinetic adjustment factor
$HKAF_{(ad/pop)}$:	Human kinetic adjustment factor using as referent the median in either the adults (ad) or in the population (pop)
IVF:	Interindividual variability uncertainty factor
Km:	Michaelis-Menten constant
P_b:	Blood : air partition coefficient
PBPK:	Physiologically based pharmacokinetic
POD:	Point of departure
Ql:	Liver blood flow
Qp:	Alveolar ventilation rate
RAM:	Rate of metabolism
RfC:	Reference concentration
RfD:	Reference dose
Vmax:	Maximum rate of metabolism
Vl:	Volume of liver
VOC:	Volatile organic compound.

Acknowledgment

Financial support from the Programme stratégique de formation des IRSC et du RRSPQ en recherche transdisciplinaire sur les interventions de santé publique: Promotion, Prévention et Politiques Publiques (4P) is acknowledged (M. Valcke). Dr. A. Nong's current address is Environmental Health Science and Research Bureau, Health Canada, Ottawa, ON, Canada K1A 0K9.

References

[1] M. L. Dourson, S. P. Felter, and D. Robinson, "Evolution of science-based uncertainty factors in noncancer risk assessment," *Regulatory Toxicology and Pharmacology*, vol. 24, no. 2, pp. 108–120, 1996.

[2] M. L. Dourson and J. F. Stara, "Regulatory history and experimental support of uncertainty (safety) factors," *Regulatory Toxicology and Pharmacology*, vol. 3, no. 3, pp. 224–238, 1983.

[3] U.S.EPA., A review of the reference dose and reference concentration process. Risk Assessment Forum. EPA/630/P-02/00F. Washington, DC, USA, 2002.

[4] P. S. Price, R. E. Keenan, and B. Schwab, "Defining the interindividual (intraspecies) uncertainty factor," *Human and Ecological Risk Assessment*, vol. 5, no. 5, pp. 1023–1033, 1999.

[5] J. L. C. M. Dorne and A. G. Renwick, "The refinement of uncertainty/safety factors in risk assessment by the incorporation of data on toxicokinetic variability in humans," *Toxicological Sciences*, vol. 86, no. 1, pp. 20–26, 2005.

[6] IPCS, *Assessing Human Health Risks of Chemicals: Derivation of Guidance Values for Health Based Exposure Limits*, World Health Organization, International Panel on Chemical Safety. Environmental Health Criteria, Geneva, Switzerland, 1994.

[7] A. G. Renwick and N. R. Lazarus, "Human variability and noncancer risk assessment—an analysis of the default uncertainty factor," *Regulatory Toxicology and Pharmacology*, vol. 27, no. 1 I, pp. 3–20, 1998.

[8] IPCS, *Chemical-Specific Adjustment Factors (CSAFs) for Interspecies Differences and Human Variability: Guidance Document for the Use of Data in Dose/Concentration-Response Assessment*, WHO, Geneva, Switzerland, 2005.

[9] M. E. Meek, A. Renwick, E. Ohanian et al., "Guidelines for application of chemical-specific adjustment factors in dose/concentration-response assessment," *Toxicology*, vol. 181-182, pp. 115–120, 2002.

[10] U.S.EPA., Integrated Risk Information System. U.S. Environmental Protection Agency, Washington, DC, USA, 2010.

[11] G. Ginsberg, D. Hattis, B. Sonawane et al., "Evaluation of child/adult pharmacokinetic differences from a database derived from the therapeutic drug literature," *Toxicological Sciences*, vol. 66, no. 2, pp. 185–200, 2002.

[12] J. L. C. M. Dorne, K. Walton, and A. G. Renwick, "Human variability in xenobiotic metabolism and pathway-related uncertainty factors for chemical risk assessment: a review," *Food and Chemical Toxicology*, vol. 43, no. 2, pp. 203–216, 2005.

[13] J. L. C. M. Dorne, "Human variability in hepatic and renal elimination: implications for risk assessment," *Journal of Applied Toxicology*, vol. 27, no. 5, pp. 411–420, 2007.

[14] A. Nong, D. G. McCarver, R. N. Hines, and K. Krishnan, "Modeling interchild differences in pharmacokinetics on the basis of subject-specific data on physiology and hepatic CYP2E1 levels: a case study with toluene," *Toxicology and Applied Pharmacology*, vol. 214, no. 1, pp. 78–87, 2006.

[15] M. Valcke and K. Krishnan, "Evaluation of the impact of the exposure route on the human kinetic adjustment factor," *Regulatory Toxicology and Pharmacology*, vol. 59, no. 2, pp. 258–269, 2011.

[16] M. Valcke and K. Krishnan, "An assessment of the impact of physico-chemical and biochemical characteristics on the human kinetic adjustment factor for systemic toxicants," *Toxicology*, vol. 286, no. 1–3, pp. 36–47, 2011.

[17] A. K. Mörk and G. Johanson, "Chemical-specific adjustment factors for intraspecies variability of acetone toxicokinetics using a probabilistic approach," *Toxicological Sciences*, vol. 116, no. 1, pp. 336–348, 2010.

[18] M. J. J. Ronis, K. O. Lindros, and M. Ingelman-Sundberg, "The CYP2E family," in *Cytochrome P450 Metabolic and Toxicological Aspects*, C. Ioannides, Ed., pp. 211–240, CRC Press, Boca Raton, Fla, USA, 1996.

[19] E. K. Johnsrud, S. B. Koukouritaki, K. Divakaran, L. L. Brunengraber, R. N. Hines, and D. G. McCarver, "Human hepatic CYP2E1 expression during development," *Journal of Pharmacology and Experimental Therapeutics*, vol. 307, no. 1, pp. 402–407, 2003.

[20] J. C. Lipscomb, L. K. Teuschler, J. C. Swartout, C. A. F. Striley, and J. E. Snawder, "Variance of microsomal protein and cytochrome P450 2E1 and 3A forms in adult human liver," *Toxicology Mechanisms and Methods*, vol. 13, no. 1, pp. 45–51, 2003.

[21] A. Nannelli, A. De Rubertis, V. Longo, and P. G. Gervasi, "Effects of dioxane on cytochrome P450 enzymes in liver, kidney, lung and nasal mucosa of rat," *Archives of Toxicology*, vol. 79, no. 2, pp. 74–82, 2005.

[22] S. Haddad, M. Béliveau, R. Tardif, and K. Krishnan, "A PBPK modeling-based approach to account for interactions in the health risk assessment of chemical mixtures," *Toxicological Sciences*, vol. 63, no. 1, pp. 125–131, 2001.

[23] R. H. Reitz, P. S. McCroskey, C. N. Park, M. E. Andersen, and M. I. Gargas, "Development of a physiologically based pharmacokinetic model for risk assessment with 1,4-dioxane," *Toxicology and Applied Pharmacology*, vol. 105, no. 1, pp. 37–54, 1990.

[24] M. E. Andersen, "Pharmacokinetics of inhaled gases and vapors," *Neurobehavioral Toxicology and Teratology*, vol. 3, no. 4, pp. 383–389, 1981.

[25] W. A. Chiu and P. White, "Steady-state solutions to PBPK models and their applications to risk assessment I: route-to-route extrapolation of volatile chemicals," *Risk Analysis*, vol. 26, no. 3, pp. 769–780, 2006.

[26] G. A. Csanády and J. G. Filser, "The relevance of physical activity for the kinetics of inhaled gaseous substances," *Archives of Toxicology*, vol. 74, no. 11, pp. 663–672, 2001.

[27] M. Pelekis, D. Krewski, and K. Krishnan, "Physiologically based algebraic expressions for predicting steady-state toxicokinetics of inhaled vapors," *Toxicology Methods*, vol. 7, no. 3, pp. 205–225, 1997.

[28] P. S. Price, R. B. Conolly, C. F. Chaisson et al., "Modeling interindividual variation in physiological factors used in PBPK models of humans," *Critical Reviews in Toxicology*, vol. 33, no. 5, pp. 469–503, 2003.

[29] ICRP, "Basic anatomical and physiological data for use in radiological protection: reference values. A report of age- and gender-related differences in the anatomical and physiological characteristics of reference individuals. ICRP Publication 89," *Annals of the ICRP*, vol. 32, no. 3-4, pp. 5–265, 2002.

[30] Statistiques Canada, Estimations de la population selon le sexe et le groupe d'âge au 1er juillet 2010, Canada http://www.statcan.gc.ca/daily-quotidien/100929/t100929b4-fra.htm.

[31] S. J. Ventura, J. C. Abma, W. D. Mosher, and S. K. Henshaw, "Estimated pregnancy rates by outcome for the United States, 1990–2004," *National Vital Statistics Reports*, vol. 56, no. 15, pp. 1–28, 2008.

[32] M. Jamei, G. L. Dickinson, and A. Rostami-Hodjegan, "A framework for assessing inter-individual variability in pharmacokinetics using virtual human populations and integrating general knowledge of physical chemistry, biology, anatomy, physiology and genetics: a tale of 'bottom-up' vs 'top-down' recognition of covariates," *Drug Metabolism and Pharmacokinetics*, vol. 24, no. 1, pp. 53–75, 2009.

[33] S. F. Hudachek and D. L. Gustafson, "Customized in silico population mimics actual population in docetaxel population pharmacokinetic analysis," *Journal of Pharmaceutical Sciences*, vol. 100, no. 3, pp. 1156–1166, 2011.

[34] P. Brochu, J. F. Ducré-Robitaille, and J. Brodeur, "Physiological daily inhalation rates for free-living pregnant and lactating adolescents and women aged 11 to 55 years, using data from doubly labeled water measurements for use in health risk assessment," *Human and Ecological Risk Assessment*, vol. 12, no. 4, pp. 702–735, 2006.

[35] P. Brochu, J. Brodeur, and K. Krishnan, "Derivation of physiological inhalation rates in children, adults, and elderly based on nighttime and daytime respiratory parameters," *Inhalation Toxicology*, vol. 23, no. 2, pp. 74–94, 2011.

[36] E. M. Faustman and P. Ribeiro, "Pharmacokinetic consideration in developmental toxicity," in *Developmental Toxicology: Risk Assessment and the Future*, R. D. Hood, Ed., pp. 109–136, D. Van Nostrand Reinhold Company, New York, NY, USA, 1990.

[37] K. Price, S. Haddad, and K. Krishnan, "Physiological modeling of age-specific changes in the pharmacokinetics of organic chemicals in children," *Journal of Toxicology and Environmental Health—Part A*, vol. 66, no. 5, pp. 417–433, 2003.

[38] R. Sarangapani, P. Robinan Gentry, T. R. Covington, J. G. Teeguarden, and H. J. Clewell, "Evaluation of the potential impact of age- and gender-specific lung morphology and ventilation rate on the dosimetry of vapors," *Inhalation Toxicology*, vol. 15, no. 10, pp. 987–1016, 2003.

[39] WHO, *Principles for Evaluating Health Risks in Children Associated with Exposure to Chemicals*, Environmental Health Criteria 237, World Health Organization, Geneva, Switzerland, 2006.

[40] M. Pelekis, L. A. Gephart, and S. E. Lerman, "Physiological-model-based derivation of the adult and child pharmacokinetic intraspecies uncertainty factors for volatile organic compounds," *Regulatory Toxicology and Pharmacology*, vol. 33, no. 1, pp. 12–20, 2001.

[41] M. Pelekis, M. J. Nicolich, and J. S. Gauthier, "Probabilistic framework for the estimation of the adult and child toxicokinetic intraspecies uncertainty factors," *Risk Analysis*, vol. 23, no. 6, pp. 1239–1255, 2003.

[42] L. T. Haber, A. Maier, P. R. Gentry, H. J. Clewell, and M. L. Dourson, "Genetic polymorphisms in assessing interindividual variability in delivered dose," *Regulatory Toxicology and Pharmacology*, vol. 35, no. 2 I, pp. 177–197, 2002.

[43] H. J. Clewell, P. R. Gentry, T. R. Covington, R. Sarangapani, and J. G. Teeguarden, "Evaluation of the potential impact of age- and gender-specific pharmacokinetic differences on tissue dosimetry," *Toxicological Sciences*, vol. 79, no. 2, pp. 381–393, 2004.

[44] P. Neafsey, G. Ginsberg, D. Hattis, D. O. Johns, K. Z. Guyton, and B. Sonawane, "Genetic polymorphism in CYP2E1: population distribution of CYP2E1 activity," *Journal of Toxicology and Environmental Health—Part B*, vol. 12, no. 5-6, pp. 362–388, 2009.

Hindawi Publishing Corporation
Journal of Toxicology
Volume 2012, Article ID 941082, 10 pages
doi:10.1155/2012/941082

Review Article

Development of Screening Tools for the Interpretation of Chemical Biomonitoring Data

Richard A. Becker,[1] Sean M. Hays,[2] Steven Robison,[3] and Lesa L. Aylward[4]

[1] *Regulatory and Technical Affairs Department, American Chemistry Council, Washington, DC 20002, USA*
[2] *Summit Toxicology, LLP, Lyons, CO 80540, USA*
[3] *Central Product Safety, Procter & Gamble, Cincinnati, OH 45253, USA*
[4] *Summit Toxicology, LLP, Falls Church, VA 22044, USA*

Correspondence should be addressed to Lesa L. Aylward, laylward@summittoxicology.com

Received 26 August 2011; Accepted 5 December 2011

Academic Editor: Jane C. Caldwell

Evaluation of a larger number of chemicals in commerce from the perspective of potential human health risk has become a focus of attention in North America and Europe. Screening-level chemical risk assessment evaluations consider both exposure and hazard. Exposures are increasingly being evaluated through biomonitoring studies in humans. Interpreting human biomonitoring results requires comparison to toxicity guidance values. However, conventional chemical-specific risk assessments result in identification of toxicity-based exposure guidance values such as tolerable daily intakes (TDIs) as applied doses that cannot directly be used to evaluate exposure information provided by biomonitoring data in a health risk context. This paper describes a variety of approaches for development of screening-level exposure guidance values with translation from an external dose to a biomarker concentration framework for interpreting biomonitoring data in a risk context. Applications of tools and concepts including biomonitoring equivalents (BEs), the threshold of toxicologic concern (TTC), and generic toxicokinetic and physiologically based toxicokinetic models are described. These approaches employ varying levels of existing chemical-specific data, chemical class-specific assessments, and generic modeling tools in response to varying levels of available data in order to allow assessment and prioritization of chemical exposures for refined assessment in a risk management context.

1. Introduction

Recognition of the large numbers of chemicals in commerce and increased focus on evaluation of these chemicals from the perspective of potential human health risk has become a focus of attention in North America and Europe. These efforts are devoted not only to evaluation of "new" chemicals but also to an examination of existing chemical substances. These efforts include those under the Health Canada Chemicals Management Plan, the European Registration, Evaluation, Authorisation and Restriction of Chemicals (REACh), the High Production Volume (HPV) Challenge Program, and the US Environmental Protection Agency's (US EPA) Chemical Assessment and Management Program (ChAMP) initiatives. Chemical evaluation is also being discussed as part of potential improvements to the US Toxic Substances Control Act. Because of the large number of chemicals involved and the need for efficient processes that assure focus on substances which could pose the greatest health concerns, tiered approaches that begin with conservative risk-based screening-level assumptions and proceed to more refined data-intensive approaches have been recommended for these types of efforts [1, 2].

Chemical risk assessment evaluations consider both exposure and hazard, and a tiered set of approaches employing various levels of data for screening-level assessments is often recommended [1, 3, 4]. Exposure screening considers chemical uses, identifies potential exposure media or pathways, and invokes conservative assumptions in the estimation of potential daily exposure rates. Hazard evaluation includes the identification of established tolerable exposure levels (e.g., reference doses or tolerable daily intakes [RfDs or

TDIs]). In the absence of such established guidance values, robust no observed adverse effect levels (NOAELs) or benchmark doses (BMDs) can be used as a point of departure (POD) and adjustment factors for extrapolation applied (as necessary), and margins of safety (MOS) can then be calculated for risk-based screening. Finally, in the absence of robust toxicological data, a generic screening approach such as that developed under the threshold of toxicological concern (TTC) framework [5–7] for setting conservative tolerable intake rates has been widely used.

In this paper, we explore approaches for using chemical biomonitoring data in risk assessment evaluation of chemicals. As with external exposure-based assessments, exposure assessments based on biomonitoring data require health- or risk-based benchmarks for evaluation of biomarker data. However, because biomarker data is typically expressed in units of biomarker concentration (e.g., μg/L urine) and risk-based benchmarks are typically expressed in units of applied dose (mg/kg-day), direct comparison cannot be made. Two approaches are possible: (1) the biomarker can be back calculated to an applied dose (reverse dosimetry; see, e.g., [8]), or (2) the benchmark can be forward calculated to a corresponding biomarker concentration for use as a screening value (forward dosimetry; see Hays et al. [9]).

Dosimetry calculations, whether forward or reverse, require the use of pharmacokinetic data and modeling and assumptions regarding exposure patterns. This paper describes methods for interpreting human biomonitoring data in a risk context, illustrating the use of the forward dosimetry biomonitoring equivalents approach for five scenarios. The first three are applicable to substances for which toxicokinetics are well understood but that have different levels of toxicity data: (1) substances with established government risk assessments, (2) substances with sufficient toxicity datasets but as of yet no government-generated (or -vetted) risk assessment, and (3) substances amenable to the generic screening TTC approach for setting conservative tolerable intake rates. These latter two approaches are needed because, for many chemicals in common use today, there may not be authoritative, government-conducted, or "approved" chemical-specific risk assessment-based exposure guidance values available. The additional scenarios addressed in this paper include (4) the absence of chemical-specific toxicokinetic data or models, and (5) the absence of both toxicity-based guidance values and toxicokinetic data. The framework of the cases and approaches described here is summarized in Figure 1 and discussed in detail below.

2. Using Risk Assessment Methods to Interpret Human Biomonitoring Results

Human biomonitoring, in which chemicals or their metabolites, are measured in biological media such as blood or urine, has become a powerful tool in the assessment of chemical exposures in the general population and in studies of targeted populations [10, 11]. Human biomonitoring data provide a reflection of integrated exposure from multiple pathways and routes in terms of internal, biologically relevant dose. In situations in which exposures to a chemical potentially occur through multiple or ill-defined exposure routes or pathways, well-designed and conducted human biomonitoring studies can provide robust and reliable exposure data that can complement and refine or replace external exposure estimation based on more indirect approaches and generic assumptions. Biomonitoring can be particularly useful in cases where widespread population exposure is possible (e.g., residues of agricultural chemicals, food packaging constituents, consumer product ingredients, etc.). Biomonitoring can also be used as an accessory tool in evaluation of exposure to chemical ingredients in consumer products in targeted, controlled exposure studies (see below for example with triclosan).

2.1. Biomonitoring Equivalents Based on Substances with Established Government Risk Assessments and Established Toxicokinetics. Screening criteria for determining the health significance of human biomonitoring results would ideally be based on robust datasets relating potential adverse effects to biomarker concentrations in human populations (see, e.g., the US Centers for Disease Control and Prevention (CDC) blood lead level of concern; see http://www.cdc.gov/nceh/lead/). However, data to support such assessments exist for only a few environmental chemicals because this approach requires establishment of causality in epidemiological studies and a robust understanding of human dose response. Thus, in an alternative approach, the concept of biomonitoring equivalents (BEs) has been developed, and guidelines for the derivation and communication of these values have been published [9, 12, 13].

In conventional risk assessment, concentrations in environmental media are used with specific contact scenarios to derive an estimate of external dose (mg/kg-day), and this is then compared to an external dose health-based guidance value, such as an ADI, RfD or TDI (mg/kg-day). In the initial screening-level evaluation, estimated exposure rates are compared to hazard- or risk-based benchmarks to assess whether more refined evaluations are required. When an RfD, or TDI or analogous screening value such as a TTC is available, the screening-level exposure estimate is compared directly to that value to assess whether exposure rates above that value are anticipated. If a NOAEL or other POD is used as the benchmark, then adjustment factors (AFs) (synonymous with uncertainty factors or safety factors) are generally used to extrapolate from animal toxicity to humans (default 10x) and to account for human variability (default 10x). Depending upon the database and quality of studies, additional AFs may be used [14]. If a toxicity database is not robust, use of an additional database uncertainty factor should be considered. Once the screening level health-based exposure guidance value has been determined, then a margin of safety (MOS) can be calculated by comparing this to the estimated daily dose rate (D):

$$\text{MOS} = \frac{(\text{POD}/\text{AFs})}{D}. \quad (1)$$

MOS values below 1 indicate that exposures exceed the screening level health-based exposure guidance value. If

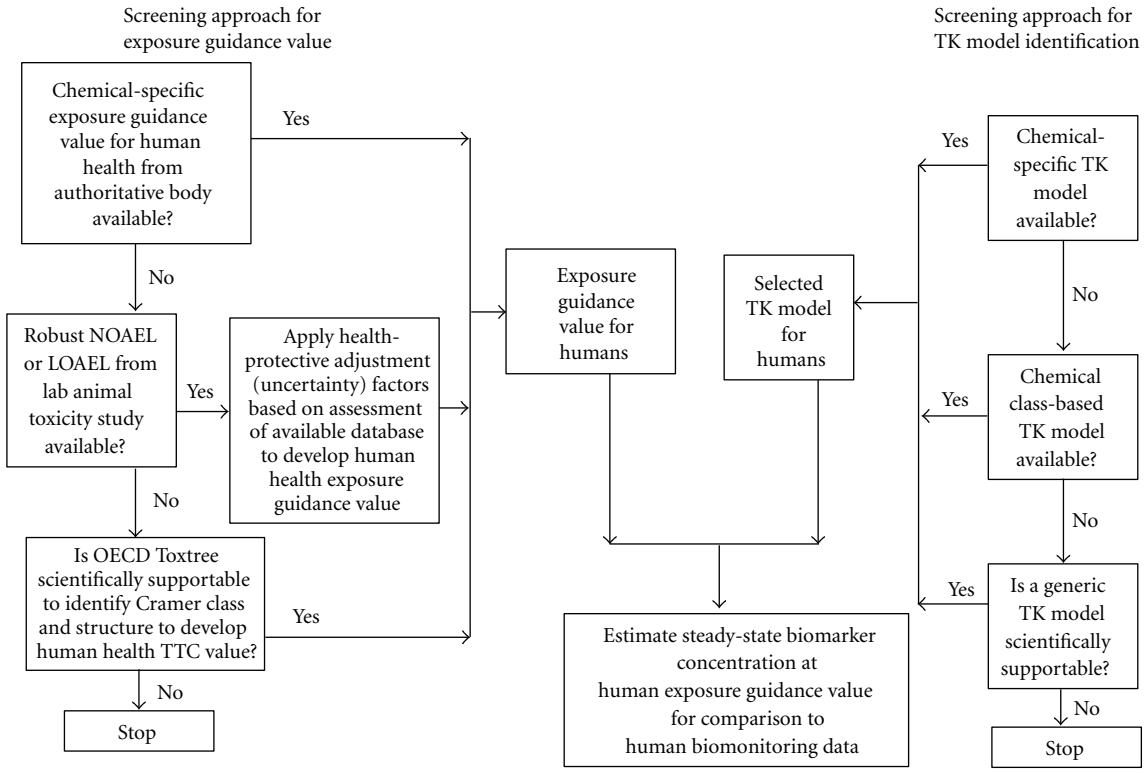

Figure 1: Flowchart showing approaches for development of screening values for assessment of biomonitoring data for chemicals with varying levels of available data on both hazard and toxicokinetics.

screening approaches have been used in the exposure or hazard assessment process, further refinement in those assessments may be warranted. Such refinements to provide greater certainty of potential hazards and exposures may include generation of product-specific exposure data for chemical uses with higher estimated exposure rates, conducting specific toxicity studies to address database deficiencies, or other exposure or hazard characterization refinements. Results of refined assessments can be used to identify the need for, and useful focus of, potential risk management strategies.

In the biomonitoring equivalent approach for interpreting biomonitoring exposure data (internal dose concentrations) in a risk assessment context, external dose health-based guidance values are translated to estimates of corresponding steady-state biomarker concentrations. A biomonitoring equivalent (BE) is defined as the concentration or range of concentrations of a chemical or its metabolites in a biological medium (blood, urine, or other medium) that is consistent with an existing health-based exposure guidance value such as a reference dose (RfD) or tolerable or acceptable daily intake (TDI or ADI) [12]. BEs are intended to be used as screening tools to provide an assessment of which chemical biomarkers are present at levels well below, near, or at or above concentrations that are consistent with existing risk assessments and exposure guidance values, and thus can provide an evaluation of relative priority for risk assessment followup. BEs provide a translational tool allowing application of the foundational risk assessment paradigm to the evaluation of exposure information provided by biomonitoring data. Development of BE values requires an underlying exposure guidance value (such as an RfD or TDI) as well as sufficient understanding of pharmacokinetics of the chemical in humans or key laboratory species. BEs are similar in concept to the HBM-I assessment values derived by the German human biomonitoring council (reviewed in Angerer et al. [15]). For interpreting human biomonitoring data in a risk context, the margin of safety (MOS) approach is used

$$\text{MOS} = \frac{\text{BE}}{[\text{Biomarker}]}. \quad (2)$$

When the MOS value is 1 or greater, then the exposure to the substance is not likely to be of concern.

BE values have been derived for approximately 80 chemicals in a variety of chemical classes (see Angerer et al. [15] for review). BE derivations have been published for persistent organic compounds including dioxins, hexachlorobenzene, and DDT and metabolites, for approximately 40 volatile organic compounds, for several phthalates and phenols including di-2(ethylhexyl)phthalate, bisphenol A, and triclosan, for selected pyrethroid pesticides, and for selected brominated flame retardant compounds. For many of these chemicals, multiple BE values have been derived corresponding to different available risk assessment exposure guidance value (e.g., EPA RfDs versus TDI values derived by the European Food Safety Authority [EFSA]). For these chemicals, screening level assessments of population biomonitoring data can be made by comparison of the data to the BE value

corresponding to the risk assessment exposure guidance value deemed most appropriate.

2.2. Risk-Based Interpretation of Biomonitoring Based on Substances with Sufficient Toxicity Datasets but No Government-Generated (or Approved) Risk Assessment. Establishing comprehensive, risk assessment-based exposure guidance values such as RfDs or TDIs is a resource-intensive effort that may take several years to complete for substances with extensive datasets. In many cases, substantial toxicological data exist for chemicals, but no formal risk assessment-based exposure guidance values such as an RfD or TDI have yet been established by a government agency. Further, some existing risk-assessment based values may now be outdated, based on the availability of newer, more relevant hazard or exposure data. Thus, for many chemicals in common use today, there may not be authoritative, government-conducted or -approved chemical-specific risk assessment-based exposure guidance values available. In the absence of such established guidance values, robust no observed adverse effect levels or benchmark doses based on a review of available datasets can be used as a point of departure, and by use of appropriate AFs, screening level health-based exposure guidance values can be derived. If appropriate pharmacokinetic data are available, these screening level health-based exposure guidance values can be translated to corresponding internal biomarker concentrations and used to assess human biomonitoring data in a parallel fashion. A MOS based on comparison of the biomonitoring data to the biomarker concentration level consistent with the screening level health-based exposure guidance value can then be calculated.

An example of this approach has been presented by Aylward and Hays [16] for the flame retardant hexabromocyclododecane (HBCD). Although a substantial database of toxicity data for both standard and endocrine-sensitive endpoints is available, no exposure guidance values have been established. Both Health Canada and the European Union have conducted provisional or draft risk assessments in which sensitive PODs were identified [17, 18]. Data were available on measured or estimated lipid-adjusted HBCD concentrations in experimental animals at the identified POD dose levels. Substantial data on lipid-adjusted HBCD concentrations in human serum and milk were available and tabulated. Comparison of those data to the biomarker concentrations in the animal studies at the PODs showed margins of exposure (MOEs) in excess of 5,000 for general population exposures to HBCD [16]. In this case, a MOE comparison was made, which is analogous to the MOS approach, except with the MOE, AFs are not used, and comparison is made directly to the POD.

A similar MOE approach was incorporated as part of a risk assessment for triclosan conducted by the European Commission Scientific Committee on Consumer Products (ECSCCP) [19]. In this case, serum concentrations of triclosan were measured throughout the course of a chronic animal bioassay selected by the ECSCCP as the basis for establishment of a TDI. Thus, serum concentrations in rats corresponding to the NOAEL dosing regimen were directly available from the toxicological database. In contrast to HBCD, in which general population exposures are incidental and due to trace levels of HBCD released into the environment, triclosan is added intentionally as an antibacterial agent to a variety of directly applied and used personal care products such as toothpaste or soap. Thus, direct consumer exposure is anticipated. The conventional risk assessment approach entails estimation of exposure levels using generic assumptions about each use scenario, contact rates, absorption, and so forth. However, because consumers may experience exposures to multiple products containing triclosan, with potential exposure via more than one route (dermal, ingestion), the conventional exposure assessment process can be cumbersome, requiring assessment of many exposure scenarios and reliance on multiple conservative, potentially compounding, exposure assumptions.

In the ECSCCP evaluation, in addition to a conventional MOE assessment based on estimated external doses from use of multiple products compared to an animal NOAEL, a biomarker-based assessment was also conducted. Peak serum levels were measured in volunteers using multiple triclosan-containing products (toothpaste, deodorant stick, and hand soap) and compared to the serum levels at the NOAEL in rats in the chronic bioassay. The conventional assessment based on estimated external doses resulted in an MOE of approximately 380 compared to the administered dose rates in rats at the NOAEL. The corresponding assessment based on comparison of human serum levels to serum levels measured in the animal bioassay at the NOAEL resulted in an MOE of approximately 940. This result confirms (1) that the approach based on estimated external exposures incorporates conservative assumptions and (2) the practical utility of risk-based screening using biomonitoring data.

The triclosan example illustrates the value of including measurements of blood biomarker concentrations in toxicological assays, as recommended by Barton et al. [20] and Saghir et al. [21]. Biomarker concentrations, and in particular blood or serum concentrations of chemicals, provide a reflection of biologically relevant absorbed dose and tissue concentrations. Comparison of biomarker concentrations in humans under real-world product use scenarios to the corresponding biomarker concentrations in laboratory animals under bioassay conditions at the POD potentially reduces uncertainties associated with reliance on estimated external exposure doses in the process of safety assessment of products.

Interpreting human biomonitoring data in a risk context for substances that lack comprehensive, health-based exposure guidance values is challenging.

Programs such as Health Canada's Chemicals Management Plan, the European Union (EU) Registration, Evaluation, Authorisation, and Restriction of Chemical (REACh), and the US Toxic Substances Control Act (HPV Challenge Program and ChAMP), while they may be lacking health-based exposure guidance values, can often provide sufficient data to support this screening-level approach.

For example, under the High Production Volume (HPV) Challenge Program (http://www.epa.gov/chemrtk/index.htm) which is now substantially complete, toxicity

data and other relevant information on approximately 2,200 chemicals produced or imported into the US, in quantities >1,000,000 lbs./year, has been submitted to EPA to enable screening based on the OECD's SIDS paradigm. This data, which covers about 90–95% by volume of chemicals in commerce in the US, is publicly available and was evaluated by EPA, under the Chemical Assessment and Management Program (ChAMP) initiative, to derive screening-level hazard characterizations, and then, for a subset of these, a screening-level risk-based prioritization. From its initiation in 2007 to 2009, when it was superseded, EPA's ChAMP developed 786 hazard characterizations and 220 risk-based prioritizations [22, 23].

For each of these substances, the hazard characterizations generated by EPA provide a concise assessment of the toxicity data and include delineation of LOAELs and NOAELs for effects on (1) major organ systems (from both acute and repeated exposures), (2) the developing organism in utero, (3) reproduction, and (4) the fidelity of DNA (http://www.epa.gov/champ/). The LOAELS or NOAELs (as appropriate) for these substances can be readily accessed from EPA's HPVIS online database (http://www.epa.gov/hpv/hpvis/index.html) and used for deriving a POD. These values are typically expressed as applied doses in mg/kg-day. AFs for toxicodynamics can then be applied to derive a screening level health-based exposure guidance value, which is also in units of applied dose (mg/kg-bw/day). Then, by using chemical-specific toxicokinetic data or models (CSTK), a biomarker concentration level typically in units of concentration in blood or urine consistent with this screening level health-based exposure guidance values can be developed. Biomonitoring results can then be interpreted in a risk context using the MOS procedure.

When using this approach, it is important to recognize that the typical AFs of 10x for extrapolating to animals to humans and 10x to account for human variability each contain both dynamic and kinetic components [24]. Thus, to use this method to interpret human biomonitoring data, when deriving the screening level health-based exposure guidance value from a NOAEL or POD based on an oral toxicity lab animal study, it is important to use in the first step only the dynamic components of the AFs (typically 2.5x or 3.16x to extrapolate from animals to humans and 3.16x to account for human variability) should be used [24, 25]. Then, in a second step, the CSTK data or model needs to be used to convert the applied dose into a concentration and in doing so, the CSTK may allow replacement of the kinetic components of the typical AFs. If both the typical 10x for extrapolating from animals to humans and the 10x to account for human variability are applied to the lab animal toxicity NOAEL and the CSTK is also applied, "double counting" for toxicokinetics would occur.

2.3. Risk-Based Interpretation of Biomonitoring Based on the Thresholds of Toxicological Concern (TTC) Method. In some cases, no robust toxicological data on which to base selection of a POD are available for a chemical. In this case, the TTC approach can provide a method for selection of a provisional, conservative tolerable daily dose level based on historical data and distributions of NOAEL values (or cancer potency values) along with an appropriate uncertainty factor (or low dose linear extrapolation factor) for a wide range of compounds [5–7, 26, 27]. The threshold of toxicological concern (TTC) evolved from concepts initially developed by Frawley [28] and further refined by the US FDA as the threshold of regulation [29, 30] and was initially developed based on extrapolated risk data for carcinogens with the assumption that if the carcinogenicity endpoint was protected, all other toxicological endpoints would also be protected. These concepts were considerably expanded to include consideration of chemical structure in conjunction with toxicity data for other toxicological endpoints [5, 27]. One of the most important enhancements to the original work was the consideration of chemical structure and the addition of a decision tree linked to exposures that pose little or no health risk. The acceptable exposure levels were derived by an extensive analysis of the existing toxicology data for 730 chemicals tested for carcinogenicity (low dose risk based) and more than 600 chemicals tested for repeat dose toxicity (NOAEL based) [31].

The TTC approach provides a decision tree linking chemical structure with toxicity. Chemical characteristics are used to identify a generic, conservative tolerable daily intake rate, the TTC. The TTC approach is based on an analysis of two comprehensive databases of toxicity data: one that is relevant to genotoxic carcinogens and one that is relevant to repeat dose endpoints not predicted on an assumption of potential genotoxic carcinogenicity. These tools are used by first assessing conservatively whether or not the chemical has structural features (alerts) suggestive of the potential for carcinogenicity via a genotoxic mode of action. Chemicals with alerts for potential genotoxic carcinogenicity are subject to an exposure limit based on the distribution of potencies of historically tested carcinogens. Chemicals without alerts for genotoxicity may move further along the decision tree, and, based on their structures, be categorized into one of three classes that are associated with three different conservative tolerable intake rates, or TTCs [27]. The category-specific recommended TTC levels are considered to be conservative estimates of chronic daily intake rates that are unlikely to result in adverse effects. This is based on the analysis of the distribution of no observed adverse effect levels (NOAELS) for compounds in the three categories. These values are based on the 5th percentile NOAELS along with the application of default uncertainty factors [5–7]. Applying the TTC approach permits rapid evaluation of exposure levels to chemicals with little or no chemical-specific toxicology data to determine if exposures are sufficient to trigger concern for a potential for health risk. Exposures below the TTCs are judged to pose a very low probability of an appreciable risk to human health.

Although the approach was originally developed to support exposures to indirect food additives and later to dietary exposures, the underlying datasets are broad and, consequently, application of the TTC concept to a broader range of exposure scenarios has been considered [32–37]. Initial development and application of the TTC approach was

focused on systemic exposure resulting from oral administration or exposure to compounds. More recently, the TTC approach was extended to consider systemic exposure following topical application of cosmetic products [32, 35]. There has also been the suggestion that TTC can be applied to inhalation exposure and risk assessment [33, 35–37]. It also has been proposed that the TTC can be applied to intentionally added materials found at low concentrations in food [7, 34]. Although there are broad categories of chemicals that can be evaluated using the TTC, there are certain materials that have insufficient data in the underlying toxicity datasets, have been identified as carcinogens with potencies that fall outside of the distribution, or have concerns related to bioaccumulation for the TTC to be applied. These include metals, organometals, and the polyhalogenated dioxins, furans and biphenyl derivatives [27].

Application of the TTC requires a careful evaluation of the chemical(s) under consideration and application of the decision tree to assign the chemical to the appropriate tier of the decision tree. This decision tree is outlined in several publications [27] and has been implemented as part of the OECD QSAR Toolbox (available at http://www.oecd.org/document/54/0,3746,en_2649_34379_42923638_1_1_1_1,00.html). An additional module is also available for identifying alerts for carcinogenicity that may be used as part of the weight of the evidence on whether or not to consider the chemical as a potential genotoxic carcinogen. Use of the decision tree approach offers a way to prioritize which materials need more in-depth evaluation.

The TTC methodology was developed to evaluate the potential for risk to low-level exposure to chemicals in the diet and has subsequently been applied to ingredients or contaminants in pharmaceutical and consumer products. Since biomonitoring represents a "real-world" measurement of such low-level exposure application of the TTC principles offers an approach to evaluating the measured exposures in a risk-based context. TTC values are typically expressed as applied doses, as either mg/kg-day or mg/day (for a defined population). To use a TTC value to interpret human biomonitoring data thus requires conversion to an internal dose concentration. If sufficient chemical-specific toxicokinetic data are available, the TTC could be translated into a corresponding biomarker concentration under the assumption of chronic steady-state exposure at the TTC level. As discussed above, in converting to an internal dose concentration, attention must be paid to proper application of AFs for dynamics and kinetics to avoid "double counting." This typically will entail review of the derivation of TTC, removal of the default AF used for toxicokinetics, then applying chemical-specific toxicokinetic data or models to obtain an internal biomarker concentration level equivalent to the TTC. Biomonitoring results can then be interpreted in a risk context using the MOS procedure. This would also provide a way to identify chemicals where additional biomonitoring would add little value. For example, if a chemical was in Cramer Class 3, which has an assigned TTC of 90 μg/day, and the biomonitoring data such as those from national biomonitoring programs such as the US National Health and Nutrition Examination Survey (NHANES) or the Canadian Health Measures Survey (CHMS) indicated, through reverse dosimetry estimations, that exposure levels at the 95th percentile were likely orders of magnitude less than 90 μg/day, that chemical could be a candidate for removal from the biomonitoring program.

In a practical sense, for a chemical with little or no toxicological data for which the TTC approach is used to identify a screening intake level, the chemical-specific toxicokinetic data or measurements required to estimate corresponding biomarker values may not be available. In such cases, generic toxicokinetic approaches may be considered; these are discussed further below.

2.4. Risk-Based Interpretation of Biomonitoring in the Absence of Chemical-Specific Toxicokinetic Data or Models. For many chemicals, risk assessment-based exposure guidance values or robust POD values are available. However, little or no chemical-specific toxicokinetic data may exist because such data have not necessarily been considered to be part of the core toxicological test batteries used to assess chemical safety. For such chemicals, provisional estimates of biomarker concentrations corresponding to key benchmarks may still be possible, albeit with greater uncertainty or built-in conservatism.

One approach relies upon a read-across from other chemicals that are structurally similar or that have similar chemical and physical properties. If chemicals are closely related, data for a well-studied chemical may be used and serve as a surrogate for a structurally similar compound with fewer data. Recently criteria have been established for structural analog identification and selection [38], and this process has been validated with a set of case studies [39].

More broadly, chemicals that exhibit similar physical and chemical properties may be evaluated using a generic model applicable to that class. For example, Chiu and White [40] demonstrated the derivation and application of steady-state solutions to a generic physiologically based toxicokinetic (PBTK) model for volatile organic compounds (VOCs) in route-to-route extrapolation. The steady-state solutions require very limited chemical-specific data to implement, and such data can often be generated in vitro [41]. Aylward et al. [42] collected the required chemical-specific data from the literature as well as current risk assessment-based exposure guidance values for approximately 40 VOC compounds. They implemented the steady-state solutions to the generic PBTK model to estimate steady-state blood concentrations predicted to arise from steady-state exposures.

The resulting estimated chemical-specific blood concentrations corresponding to exposure guidance values were proposed for use as screening values for evaluation of biomonitoring data for these VOCs [42]. Across this class of compounds, variation in physical/chemical and metabolic properties resulted in estimated steady-state blood concentrations for a unit inhalation exposure (e.g., 1 mg/m^3) that varied by approximately one order of magnitude, while those arising from a unit of oral exposure (1 mg/kg-day) varied over approximately 2 orders of magnitude [42]. Therefore, if an exposure guidance value is available for a chemical expected to have similar physical, chemical, and metabolic

behavior to those included here, a range of likely steady-state blood concentrations potentially consistent with the exposure guidance value could be estimated.

Other PBTK model structures potentially applicable to a wider range of compounds have been proposed and used in a variety of contexts. Rotroff et al. [43] used in vitro methods to develop estimates of the metabolic clearance and protein binding for a series of chemicals included in the US EPA Phase I ToxCast program. These parameters were used in a generic PBTK model to relate blood or serum concentrations to corresponding steady-state external dose rates using commercially available software. Bartels et al. [44] presented initial results of a comprehensive effort to develop a generic PBTK model structure that accommodates varying levels of chemical-specific information and allows prediction of biomarker concentrations (both urinary and blood) associated with a specified exposure guidance value. On the toxicity assessment front, Louisse et al. [45] demonstrated the integration of in vitro toxicity data with toxicokinetic models to assess glycol ethers. These efforts highlight the potential utility of targeted data development including in vitro assessments of metabolism and measured or estimated chemical and physical properties in allowing development of provisional biomarker screening or assessment values based on current risk assessments. If human biomonitoring data approach or exceed these screening values, allocation of resources to development of more detailed, data-driven evaluations of toxicokinetic characteristics may be appropriate.

2.5. Risk-Based Interpretation of Biomonitoring in the Absence of Both Guidance Values and Toxicokinetic Data. Most of the chemicals currently being assessed in the US NHANES and the Canadian Health Measures Surveys are well-studied substances. However, even among this group of compounds, there is sometimes a lack of derived toxicity guidance values, and, more commonly, a lack of detailed chemical-specific toxicokinetic data needed to translate external exposure levels into expected corresponding biomarker concentrations as required to support development of BEs. As biomonitoring programs are expanded to include less well-studied substances, compounds that lack both comprehensive toxicity datasets, and toxicokinetic data needed for development of full BE values are likely to be included. In such cases, provisional screening assessment values may still be derived using combinations of the approaches outlined above.

For example, the Aylward et al. [42] evaluation of screening BE values for assessment of VOCs could be applied to chemicals lacking both exposure guidance values and toxicokinetic data. The screening values estimated by Chiu and White [40] incorporate both the toxicokinetic behavior of the chemicals as well as the risk assessment-based tolerable exposure levels based on noncancer endpoints. The cumulative distribution of estimated screening blood concentrations for these VOCs is presented in Figure 2. The values span more than five orders of magnitude in blood concentration. If a chemical is judged to be similar in general physical, chemical, and toxicological characteristics to those included in the group evaluated by Aylward et al. [42] but lacks the information necessary for a chemical specific BE, a lower percentile of blood concentration from the distribution represented here might be selected as an initial screening value for evaluation of blood concentrations of that chemical measured in humans. This approach is conceptually similar to the TTC approach, but conducted on a biomarker concentration basis rather than an intake dose basis.

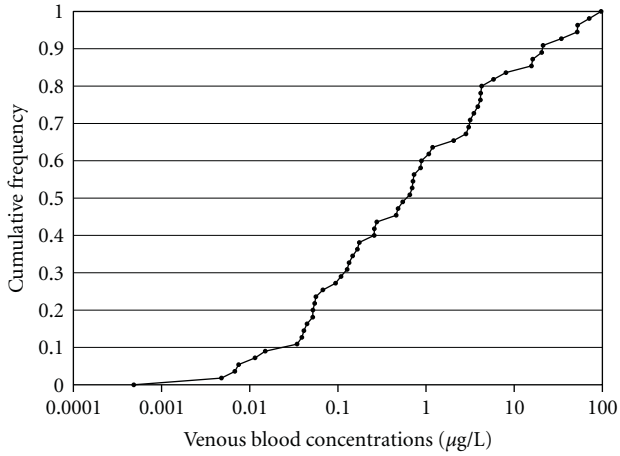

Figure 2: Estimated steady-state venous blood concentrations corresponding to oral and inhalation exposure guidance values (56 values) for 38 VOCs from Aylward et al. [42]. Some chemicals had both oral and inhalation exposure guidance values, while others had only one.

Similarly, the TTC approach could be applied to a chemical to estimate a conservative level of tolerable external exposure, and a generic PBTK model such as that developed by Bartels et al. [44] could be used to estimate a corresponding biomarker concentration for use as a screening value.

2.6. Decision Tree for Screening Level, Risk-Based Interpretation of Biomonitoring Data. Figure 1 provides a general flowchart of the various approaches described here. The flowchart is conceptually similar to the tiered screening process described in a 2001 review by the Health Council of the Netherlands [46], with the added component of extension of the tiered approach to evaluation of biomonitoring data. These approaches should be applied in an iterative framework, with increasing refinement indicated when MOS values are judged to be insufficient. Use of all-generic approaches to derive provisional screening values clearly results in values that are highly uncertain, requiring the use of health-protective assumptions in the screening process. If chemicals being detected in biomonitoring surveys fall into this category of lacking both toxicological and toxicokinetic data, these chemicals may be candidates for early research to fill selected data gaps in order to refine the assessments for those chemicals.

3. Discussion and Conclusions

The collection and reporting of human biomonitoring data continues to grow, and the advanced analytical chemistry

techniques employed can now accurately quantify substances in reasonable sample volumes of blood or urine from individuals. And while authoritative organizations have cautioned that detection does not equate to illness or injury, the absence of methods to interpret human biomonitoring in a health risk context reduces the value of these data because of the inability to prioritize among the detected chemicals on the basis of potential risk posed by the detected levels. Employing tools to interpret biomonitoring data which results in a risk assessment-based context can assist risk managers in addressing concerns about chemical exposures. It also provides a framework for determining whether additional product stewardship and/or regulatory risk management actions may be warranted.

The BE approach has proven to be useful as a screening tool to provide an assessment of which chemical biomarkers are present at levels well below, near, or at or above concentrations that are consistent with exposure guidance values derived in existing authoritative government risk assessments. As discussed here, the underlying approach developed for the BEs can also be used in cases where such authoritative risk assessments are not yet available or where robust toxicokinetic models aren't at hand. Both the NOAEL approach and the TTC method discussed here can be used to establish benchmarks that will allow screening-level evaluation of biomonitoring data. Although there are uncertainties when using such methods, by employing health protective assumptions, such as additional uncertainty factors to account for database shortcomings, the derived Points of Departure from the NOAEL and TTC approaches can be used with a reasonable degree of confidence that they are health protective.

As with any method used for chemical exposure assessment, the quality and representativeness of the biomonitoring data must be considered in the process of interpreting the data. While a complete discussion of the factors relevant to evaluation of biomonitoring data is outside the scope of this paper, some of these factors include the stability and specificity of the biomarker and the representativeness of the sampling frame used to generate the data. Similarly, the robustness and reliability of the toxicokinetic models and data used to translate affect the confidence in the derived Biomonitoring Equivalents (discussed in Hays et al. [9]).

The methods described here represent a range of approaches that can be applied depending on the level of chemical-specific information available. Obviously, as the level of chemical-specific data decreases and reliance on generic assumptions increases, the uncertainty associated with the derived screening values increases. If human biomonitoring data approach or exceed these screening values, allocation of resources to development of more detailed, data-driven evaluations may be appropriate in order to inform risk managers. In such cases, an iterative approach to development and application of human biomonitoring assessment values is appropriate. Such an approach allows for and takes advantage of targeted data development. Such data may include in vitro assessments of metabolism, measured or estimated chemical and physical properties, or in vivo toxicokinetics and metabolism studies to refine provisional toxicokinetic estimates.

Abbreviations

ADI:	Acceptable daily intake
AF:	Adjustment factor
BE:	Biomonitoring equivalent
BMD:	Benchmark dose
CDC:	Centers for Disease Control and Prevention
ChAMP:	Chemical Assessment and Management Program
CHMS:	Canadian Health Measures Survey
CSTK:	Chemical-specific toxicokinetic
ECSCCP:	European Commission Scientific Committee on Consumer Products
EFSA:	European Food Safety Authority
EPA:	Environmental Protection Agency
HBCD:	Hexabromocyclododecane
HBM-I:	Human biomonitoring value-I
HPV:	High production volume
MOE:	Margin of exposure
MOS:	Margin of safety
NHANES:	National Health and Nutrition Examination Survey
NOAEL:	No observed adverse effect level
PBTK:	Physiologically based toxicokinetic
POD:	Point of departure
REACh:	Registration, evaluation, authorisation and restriction of chemicals
RfD:	Reference dose
TDI:	Tolerable daily intake
TTC:	Threshold of toxicological concern
VOC:	Volatile organic chemical.

References

[1] M. Meek, A. Boobis, K. Crofton, G. Heinemeyer, M. vanRaaij, and C. Vickers, "Risk assessment of combined exposure to multiple chemicals: a WHO/IPCS framework," *Regulatory Toxicology and Pharmacology*, vol. 60, supplement 1, no. 2, pp. S1–S14, 2011.

[2] L. M. Plunkett, A. M. Kaplan, and R. A. Becker, "An enhanced tiered toxicity testing framework with triggers for assessing hazards and risks of commodity chemicals," *Regulatory Toxicology and Pharmacology*, vol. 58, no. 3, pp. 382–394, 2010.

[3] M. Meek and V. Armstrong, "The assessment and management of industrial chemicals in Canada," in *Risk Assessment of Chemicals*, K. van Leeuwen and T. Vermeire, Eds., Kluwer Academic Publishers, Dordrecht, The Netherlands, 2007.

[4] H. Sanderson, J. L. Counts, K. L. Stanton, and R. I. Sedlak, "Exposure and prioritization—human screening data and methods for high production volume chemicals in consumer products: amine oxides a case study," *Risk Analysis*, vol. 26, no. 6, pp. 1637–1657, 2006.

[5] I. C. Munro, R. A. Ford, E. Kennepohl, and J. G. Sprenger, "Correlation of structural class with no-observed-effect levels: a proposal for establishing a threshold of concern," *Food and Chemical Toxicology*, vol. 34, no. 9, pp. 829–867, 1996.

[6] I. C. Munro, R. A. Ford, E. Kennepohl, and J. G. Sprenger, "Thresholds of toxicological concern based on

structure-activity relationships," *Drug Metabolism Reviews*, vol. 28, no. 1-2, pp. 209–217, 1996.

[7] I. C. Munro, A. G. Renwick, and B. Danielewska-Nikiel, "The Threshold of Toxicological Concern (TTC) in risk assessment," *Toxicology Letters*, vol. 180, no. 2, pp. 151–156, 2008.

[8] Y. M. Tan, K. H. Liao, and H. J. Clewell, "Reverse dosimetry: interpreting trihalomethanes biomonitoring data using physiologically based pharmacokinetic modeling," *Journal of Exposure Science and Environmental Epidemiology*, vol. 17, no. 7, pp. 591–603, 2007.

[9] S. M. Hays, R. A. Becker, H. W. Leung, L. L. Aylward, and D. W. Pyatt, "Biomonitoring equivalents: a screening approach for interpreting biomonitoring results from a public health risk perspective," *Regulatory Toxicology and Pharmacology*, vol. 47, no. 1, pp. 96–109, 2007.

[10] J. Angerer, U. Ewers, and M. Wilhelm, "Human biomonitoring: state of the art," *International Journal of Hygiene and Environmental Health*, vol. 210, no. 3-4, pp. 201–228, 2007.

[11] Centers for Disease Control and Prevention, "Fourth National Report on Human Exposures to Environmental Chemicals," 2009, http://www.cdc.gov/ExposureReport/.

[12] S. M. Hays, L. L. Aylward, J. S. LaKind et al., "Guidelines for the derivation of biomonitoring equivalents: report from the Biomonitoring Equivalents Expert Workshop," *Regulatory Toxicology and Pharmacology*, vol. 51, no. 3, pp. S4–S15, 2008.

[13] J. S. LaKind, L. L. Aylward, C. Brunk et al., "Guidelines for the communication of biomonitoring equivalents: report from the Biomonitoring Equivalents Expert Workshop," *Regulatory Toxicology and Pharmacology*, vol. 51, no. 3, pp. S16–S26, 2008.

[14] M. Dourson and C. DeRosa, "The use of uncertainty factors in establishing safe levels of exposure," in *Statistics in Toxicology*, D. Krewski and C. Franklin, Eds., Gordon and Breach Science, New York, NY, USA, 1991.

[15] J. Angerer, L. L. Aylward, S. M. Hays, B. Heinzow, and M. Wilhelm, "Human biomonitoring assessment values: approaches and data requirements," *International Journal of Hygiene and Environmental Health*, vol. 214, no. 5, pp. 348–360, 2011.

[16] L. L. Aylward and S. M. Hays, "Biomonitoring-based risk assessment for hexabromocyclododecane (HBCD)," *International Journal of Hygiene and Environmental Health*, vol. 214, no. 3, pp. 179–187, 2011.

[17] Canada Health, "Draft Screening Assessment Cyclododecane, 1,2,5,6,9,10- Hexabromo-Chemical Abstracts Service," Registry Number 3194-55-6. August 2010.

[18] European Union, "Risk Assessment Hexabromocyclododecane.CAS-No.: ," 25637-99-4. EINECS-No.:247-148-4, 2008.

[19] European Commission Scientific Committee on Consumer Products (ECSCCP). Scientific Committee on Consumer Products (SCCP) Opinion on Triclosan COLIPA No. P32, 2009.

[20] H. A. Barton, T. P. Pastoor, K. Baetcke et al., "The acquisition and application of absorption, distribution, metabolism, and excretion (ADME) data in agricultural chemical safety assessments," *Critical Reviews in Toxicology*, vol. 36, no. 1, pp. 9–35, 2006.

[21] S. A. Saghir, A. L. Mendrala, M. J. Bartels et al., "Strategies to assess systemic exposure of chemicals in subchronic/chronic diet and drinking water studies," *Toxicology and Applied Pharmacology*, vol. 211, no. 3, pp. 245–260, 2006.

[22] U.S. Environmental Protection Agency, "HPV Chemical Hazard Characterizations," 2011.

[23] U.S. Environmental Protection Agency, "Risk-Based Prioritization (RBP) Decisions Summary," 3/31/2009, 2011.

[24] WHO/IPCS, "Chemical-specific Adjustment Factors for Interspecies Differences and Human Variability: Guidance Document for Use in Dose/Concentration-Response Assessment," 2005, http://www.inchem.org/documents/harmproj/harmproj/harmproj2.pdf.

[25] L. L. Aylward, R. A. Becker, C. R. Kirman, and S. M. Hays, "Assessment of margin of exposure based on biomarkers in blood: an exploratory analysis," *Regulatory Toxicology and Pharmacology*, vol. 61, no. 1, pp. 44–52, 2011.

[26] R. Kroes, J. Kleiner, and A. Renwick, "The threshold of toxicological concern concept in risk assessment," *Toxicological Sciences*, vol. 86, no. 2, pp. 226–230, 2005.

[27] R. Kroes, A. G. Renwick, M. Cheeseman et al., "Structure-based thresholds of toxicological concern (TTC): guidance for application to substances present at low levels in the diet," *Food and Chemical Toxicology*, vol. 42, no. 1, pp. 65–83, 2004.

[28] J. P. Frawley, "Scientific evidence and common sense as a basis for food-packaging regulations," *Food and Cosmetics Toxicology*, vol. 5, pp. 293–308, 1967.

[29] U.S. Food and Drug Administration, "Food Additives; Threshold of regulation for substances used in food-contact articles," 21 CFR Parts 5, 25, 170, 171, and 174. Docket Nos. 77P-0122 and 92N-0181, 1995.

[30] A.M. Rulis, "De Minimus and the threshold of regulation. Food Protection Technology. Current and Projected Technologies for Food Protection—recommendations and implementation," in *Proceedings of the Conference for Food Protection*, 1986.

[31] R. Kroes, C. Galli, I. Munro et al., "Threshold of toxicological concern for chemical substances present in the diet: a practical tool for assessing the need for toxicity testing," *Food and Chemical Toxicology*, vol. 38, no. 2-3, pp. 255–312, 2000.

[32] K. Blackburn, J. A. Stickney, H. L. Carlson-Lynch, P. M. McGinnis, L. Chappell, and S. P. Felter, "Application of the threshold of toxicological concern approach to ingredients in personal and household care products," *Regulatory Toxicology and Pharmacology*, vol. 43, no. 3, pp. 249–259, 2005.

[33] P. Carthew, C. Clapp, and S. Gutsell, "Exposure based waiving: the application of the toxicological threshold of concern (TTC) to inhalation exposure for aerosol ingredients in consumer products," *Food and Chemical Toxicology*, vol. 47, no. 6, pp. 1287–1295, 2009.

[34] S. Felter, R. W. Lane, M. E. Latulippe et al., "Refining the threshold of toxicological concern (TTC) for risk prioritization of trace chemicals in food," *Food and Chemical Toxicology*, vol. 47, no. 9, pp. 2236–2245, 2009.

[35] R. Kroes, A. G. Renwick, V. Feron et al., "Application of the threshold of toxicological concern (TTC) to the safety evaluation of cosmetic ingredients," *Food and Chemical Toxicology*, vol. 45, no. 12, pp. 2533–2562, 2007.

[36] R. Drew and J. Frangos, "The concentration of no toxicological concern (CoNTC): a risk assessment screening tool for air toxics," *Journal of Toxicology and Environmental Health A*, vol. 70, no. 19, pp. 1584–1593, 2007.

[37] S. E. Escher, I. Tluczkiewicz, M. Batke et al., "Evaluation of inhalation TTC values with the database RepDose," *Regulatory Toxicology and Pharmacology*, vol. 58, no. 2, pp. 259–274, 2010.

[38] S. Wu, K. Blackburn, J. Amburgey, J. Jaworska, and T. Federle, "A framework for using structural, reactivity, metabolic and physicochemical similarity to evaluate the suitability of analogs for SAR-based toxicological assessments," *Regulatory Toxicology and Pharmacology*, vol. 56, no. 1, pp. 67–81, 2010.

[39] K. Blackburn, D. Bjerke, G. Daston et al., "Case studies to test: a framework for using structural, reactivity, metabolic and physicochemical similarity to evaluate the suitability of analogs for SAR-based toxicological assessments," *Regulatory Toxicology and Pharmacology*, vol. 60, no. 1, pp. 120–135, 2011.

[40] W. A. Chiu and P. White, "Steady-state solutions to PBPK models and their applications to risk assessment I: route-to-route extrapolation of volatile chemicals," *Risk Analysis*, vol. 26, no. 3, pp. 769–780, 2006.

[41] J. C. Lipscomb and T. S. Poet, "In vitro measurements of metabolism for application in pharmacokinetic modeling," *Pharmacology and Therapeutics*, vol. 118, no. 1, pp. 82–103, 2008.

[42] L. L. Aylward, C. R. Kirman, B. C. Blount, and S. M. Hays, "Chemical-specific screening criteria for interpretation of biomonitoring data for volatile organic compounds (VOCs)—application of steady-state PBPK model solutions," *Regulatory Toxicology and Pharmacology*, vol. 58, no. 1, pp. 33–44, 2010.

[43] D. M. Rotroff, B. A. Wetmore, D. J. Dix et al., "Incorporating human dosimetry and exposure into high-throughput in vitro toxicity screening," *Toxicological Sciences*, vol. 117, no. 2, pp. 348–358, 2010.

[44] M. Bartels, D. Rick, P. Price et al., "Development of PK- and PBPK-based modeling tools for derivation of biomonitoring guidance," in *Proceedings of the 12th International Congress of Toxicology (IUTOX '10)*, July 2010.

[45] J. Louisse, E. de Jong, J. J. M. van de Sandt et al., "The use of in vitro toxicity data and physiologically based kinetic modeling to predict dose-response curves for in vivo developmental toxicity of glycol ethers in rat and man," *Toxicological Sciences*, vol. 118, no. 2, Article ID kfq270, pp. 470–484, 2010.

[46] Health Council of the Netherlands, "Toxicity Testing: A more efficient approach," http://www.gezondheidsraad.nl/sites/default/files/01@24E_0.pdf.

Hindawi Publishing Corporation
Journal of Toxicology
Volume 2012, Article ID 410143, 8 pages
doi:10.1155/2012/410143

Research Article

An *In Silico* Approach for Evaluating a Fraction-Based, Risk Assessment Method for Total Petroleum Hydrocarbon Mixtures

Nina Ching Y. Wang,[1] Glenn E. Rice,[1] Linda K. Teuschler,[1] Joan Colman,[2] and Raymond S. H. Yang[3]

[1] *National Center for Environmental Assessment, Office of Research and Development, U.S. Environmental Protection Agency, Cincinnati, OH 45268, USA*
[2] *Chemical, Biological and Environmental Center, SRC, Inc., Syracuse, NY 13212, USA*
[3] *Quantitative and Computational Toxicology Group, Department of Environmental and Radiological Health Sciences, College of Veterinary Medicine & Biomedical Sciences, Colorado State University, Fort Collins, CO 80523, USA*

Correspondence should be addressed to Nina Ching Y. Wang, wang.nina@epa.gov

Received 25 August 2011; Accepted 1 November 2011

Academic Editor: Marina V. Evans

Both the Massachusetts Department of Environmental Protection (MADEP) and the Total Petroleum Hydrocarbon Criteria Working Group (TPHCWG) developed fraction-based approaches for assessing human health risks posed by total petroleum hydrocarbon (TPH) mixtures in the environment. Both organizations defined TPH fractions based on their expected environmental fate and by analytical chemical methods. They derived toxicity values for selected compounds within each fraction and used these as surrogates to assess hazard or risk of exposure to the whole fractions. Membership in a TPH fraction is generally defined by the number of carbon atoms in a compound and by a compound's equivalent carbon (EC) number index, which can predict its environmental fate. Here, we systematically and objectively re-evaluate the assignment of TPH to specific fractions using comparative molecular field analysis and hierarchical clustering. The approach is transparent and reproducible, reducing inherent reliance on judgment when toxicity information is limited. Our evaluation of membership in these fractions is highly consistent (~80% on average across various fractions) with the empirical approach of MADEP and TPHCWG. Furthermore, the results support the general methodology of mixture risk assessment to assess both cancer and noncancer risk values after the application of fractionation.

1. Introduction

Contamination of the environment by petroleum products including crude oil, lubricating oils, and a wide variety of fuels is widespread. Typically, these petroleum products are complex mixtures containing hundreds to thousands of different hydrocarbon compounds, including aliphatic compounds (e.g., straight-chain, branched-chain, and cyclic alkanes and alkenes) as well as aromatic compounds (e.g., benzene and alkyl benzenes, polycyclic aromatic hydrocarbons). Once released into the environment, the composition of a petroleum hydrocarbon mixture can change due to weathering (http://facstaff.gpc.edu/~pgore/geology/geo101/weather.htm). During chemical weathering, components of petroleum mixtures can degrade and partition, such that the more soluble or volatile compounds can be readily transported to other environmental media and locations, while the relatively nonmobile and recalcitrant components (i.e., the weathered products) remain near the point of release. Thus, the actual petroleum hydrocarbon mixtures to which a population might be exposed will vary with the petroleum product released, environmental conditions, elapsed time following release, and exposure medium.

Table 1: MADEP toxicity values for TPH fractions [3].

Hydrocarbon fraction	Oral (mg/kg/day)	Inhalation (mg/m^3)
Aliphatic		
No.1: C5–C8	0.04	0.2
No.2: C9–C18	0.1	0.2
No.3: C19–C32	2.0	NV[a]
Aromatic		
No.1: C6–C8	SC[b]	SC[b]
No.2: C9–C18	0.03[c]	0.05
No.3: C19–C32	0.03[c]	NV[a]

[a]NV: not volatile. [b]SC: used single chemical values (fraction includes benzene, toluene, xylene, and ethyl benzene). [c]MADEP grouped the entire range of aromatics from C9–C32 into a single fraction for oral noncancer toxicity.

Assessment of human health risks associated with petroleum-hydrocarbon-contaminated sites routinely begins with an analysis of "total petroleum hydrocarbons" (TPHs). TPHs are loosely defined hydrocarbon mixtures. While the components included in a mixture of TPHs depend on the method of analysis and chemical nature of the TPH contaminating material (e.g., jet fuels, gasoline, etc.), TPHs typically represent the total mass of hydrocarbons without identifying specific individual compounds. As TPHs is not a consistent entity, the assessment of health effects and development of toxicity criteria such as reference doses (RfDs) and cancer slope factors for such complex mixtures as a whole are problematic (the RfD is an estimate of the dose of daily exposure to a substance (with uncertainty spanning perhaps an order of magnitude) for a human population (including sensitive subgroups) that is likely to be without an appreciable risk of deleterious effects during a lifetime [1]).

As previously mentioned, both the Massachusetts Department of Environmental Protection (MADEP) and the Total Petroleum Hydrocarbons Criteria Working Group (TPHsCWG) recommended a "fraction-based approach" for assessing human health risks associated with TPH exposures [2–8]. Both MADEP and TPHCWG divide the aliphatic TPHs into three aliphatic fractions designated as aliph1–3 (Table 1). MADEP grouped the entire range of aromatics from C9–C32 into a single fraction for the assessment of oral noncancer toxicity and divided the fraction into C9–C18 and C19–C32 fractions for the assessment of inhalation noncancer toxicity. In contrast, TPHCWG divided the aromatic compounds into three individual aromatic fractions designated as arom1–3. Following measurements to determine the concentrations of the six fractions present at a given site, human exposure to the individual fractions can be estimated (Figure 1).

The noncancer health risk associated with each fraction is then predicted based on the dose-response function of a fraction-specific surrogate chemical(s). The underlying assumption is that each member of a fraction is toxicologically similar and shares a common mode of action (MOA). USA EPA [9] defines "similar components" as single chemicals that cause the same biologic activity or are expected to cause the same type of biologic activity based on chemical structure. These components also may be expected to have comparable kinetic characteristics and toxicity. A Hazard Index based on an assumption of dose addition is then calculated to assess potential noncancer health risks using both chronic and subchronic surrogate toxicity values [9].

The cancer health risks associated with each fraction can be estimated assuming either response addition for all fractions but arom3 or dose addition for a subset of TPHs in the arom3 fraction. For individual TPHs that have cancer slope factors, the products of the TPH exposures and the cancer slope factors are summed to estimate cancer risks posed by those compounds under an assumption of response addition. For groups of carcinogenic TPHs assumed to act through a common toxic mode of action, the relative potency factor approach is used. This approach requires both the existence of toxicological dose-response data for at least one component of the mixture, (i.e., the index chemical), and scientific judgment that the toxicity of the other individual compounds in the mixture are toxicologically similar [9]. Using this approach, some polycyclic aromatic hydrocarbons assigned to the arom3 fraction are assumed to be dose-additive. These hydrocarbons have been assigned a relative potency factor. The relative potency factors for each compound are combined with the compound-specific-intake estimates to calculate an index chemical equivalent dose. These equivalent doses are summed, and the total equivalent dose is compared to a cancer slope factor for the index chemical (i.e., benzo[a]pyrene); cancer risk for the fraction is estimated based on this comparison [10].

As discussed by Teuschler [11], this approach to risk assessment of TPHs "illustrates a flexible method for characterizing TPH exposures that reflects differences in chemical composition across various sites and provides a reasonable method for calculating potential health risks." We summarized the conceptual basis of the MADEP/TPHCWG approach in Figure 1 principally based on the natural and logical course of chemical extraction, separation, and analysis. Such chemical analyses are intimately associated with the physicochemical properties of the component chemicals present in the TPH mixture (see http://hhpprtv.ornl.gov/issue_papers/ComplexMixturesofAliphaticandAromaticHydrocarbons.pdf for full analysis).

For this chemical mixtures risk assessment approach, the accurate assignment of the individual TPHs into specific fractions is critical. Fraction or membership assignments have been based on physicochemical properties (including molecular structure such as aromatic versus aliphatic), analytical data, prevalence in the environment (e.g., fate and transport), and toxicological properties. The analytical data are based on the number of carbon atoms (C) in the compounds comprising the fraction or equivalent carbon (EC) number index. Inaccurate assignments of TPHs into fractions could lead to erroneous evaluations of the overall noncancer and cancer risks. Table 1 summarizes noncancer toxicity values for various TPH fractions derived by MADEP.

Because *in silico* molecular modeling or computational modeling is often employed for analysis, interpretation, and visualization of heterogeneous datasets from various sources

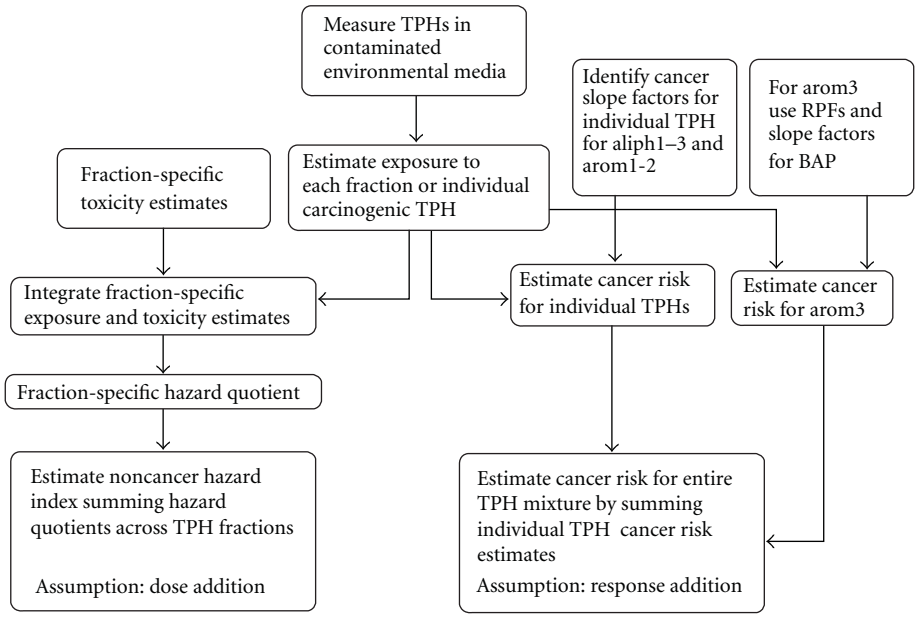

Figure 1: Approach to estimate TPH cancer risks and noncancer Hazard Indices using component and mixture fraction methods. Whole mixture toxicity data are not available for the many, highly variable TPH mixtures of concern that are found at different sites, and as a result, both MADEP and TPHWG have proposed a fractional and subsequent surrogate/component-based approach for the risk assessment of TPHs. This figure shows that following the measurement of TPHs in either soil or water, both MADEP and TPHWG recommend that exposure estimates be developed for each fraction. Relying on surrogates for each fraction, Figure 1 shows that whole mixture risk assessments can be done using data directly on the mixture of concern, on a sufficiently similar mixture, on a mixture's fractions, or on a subset of its components.

(e.g., fractions) [12–15], we used an *in silico* approach in this paper to systematically examine the assignment of 111 selected TPH components into specific fractions. These examinations are based on a molecular modeling approach achieved through the application of comparative molecular field analysis (CoMFA[2]), which is based on three-dimensional (3D) shape, electrostatic and hydrogen bonding characteristics (assuming similar MOAs and molecular targets) and then evaluated by hierarchical clustering. CoMFA was specifically selected for capturing molecular interactions between TPHs and their potential common molecular targets. TPHs with common molecular targets will likely be clustered together based on their CoMFA descriptors, and these clustered TPHs are expected to be assigned to a specific fraction (e.g., arom3 TPHs bind to aryl hydrocarbon receptor). Additional analysis by structure-activity relationship can also be utilized to evaluate membership consistency within a fraction. This approach was applied to examine the underlying association of chemicals within each fraction, thereby providing information relevant to the assumed common toxicity of individual TPHs in each fraction. We compared the assignments predicted using this method to those developed by MADEP.

2. Materials and Methods

2.1. Selection of Individual TPHs. The selection of aliphatic and aromatic TPHs was based on their abundance in contaminated sites (e.g., composition and type of fuels) and/or known qualitative significant toxicity (e.g., endpoints or critical effects). Overall, 51 aliphatics and 60 aromatics were chosen based on the available toxicity information as the two main datasets for subsequent analysis and validation. All selected aliphatic and aromatic TPHs are listed in Figures 2 and 3, respectively.

2.2. Carbon Atoms (C) and Equivalent Carbon (EC). The EC number is measured by comparing a compound's retention time in gas chromatography to that of various *n*-alkanes [3, 8]. This index is equivalent to the retention time of the compounds on a boiling-point gas chromatography (GC) column (nonpolar capillary column) normalized to the *n*-alkanes. For example, benzene, a C6 aromatic compound, has an EC of 6.5 because its boiling-point and GC retention time are approximately halfway between those of *n*-hexane (C6, EC6) and *n*-heptane (C7, EC7). Physical and chemical properties of hydrocarbons that are useful in predicting fate and transport including vapor pressure, solubility, partition coefficient, and Henry's Law constants are predictably related to the EC and can be estimated using algorithms. Both MADEP and TPHCWG have adopted this method for the fractionation of TPHs.

2.3. In Silico Approach. Following the selection of the TPHs, the analysis was conducted in three steps as follows: (1) molecular modeling; (2) CoMFA analysis; (3) hierarchical clustering analysis. Each step illustrates the characteristics

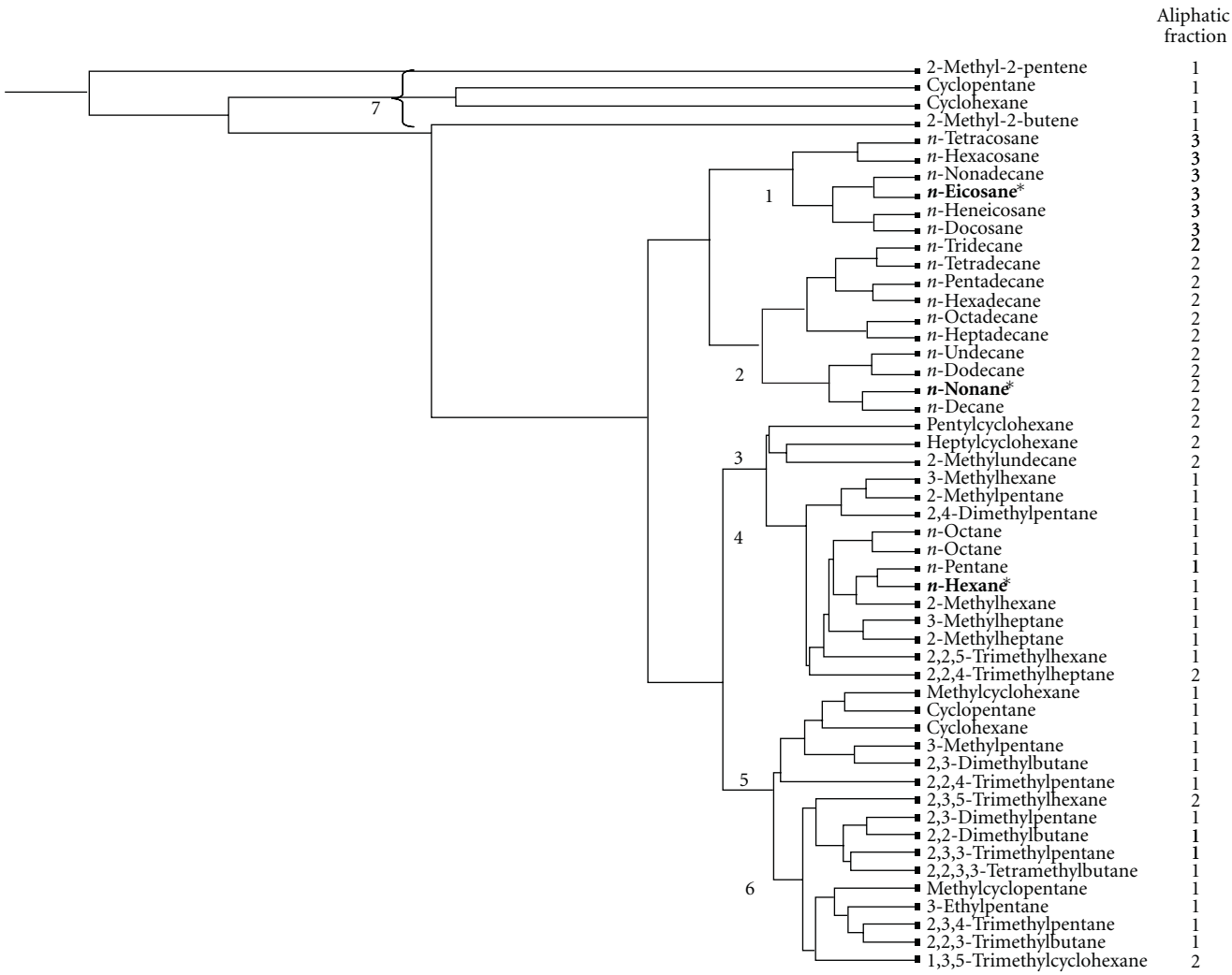

Figure 2: Hierarchical cluster analysis based on CoMFA for all aliphatic fractions. Surrogate chemicals proposed by MADEP [3] are shown in bold and with asterisks.

and physicochemical properties of hydrocarbons within each fraction.

Step 1. Molecular Modeling. Initial structures of the 111 TPHs were built using the Sketch Molecule module in Sybyl 8.0 (Tripos, Inc., St. Louis, MO, USA), and energy was subsequently minimized to yield a stable conformation using the MMFF94 force field and electrostatic charges [16]. The 51 aliphatics and 60 aromatics were processed and used as two separate datasets for further analyses. Each dataset was aligned using its common core structure (i.e., pentane for aliphatics; and benzene for aromatics) prior to COMFA analysis.

Step 2. Comparative Molecular Field Analysis (CoMFA). Because most TPHs are postulated to have similar toxic effects or modes of action (e.g., toxicity, binding affinity, etc.), a CoMFA [17] was conducted based on the current understanding of mixtures risk assessment [9, 10]. CoMFA is a commonly used 3D quantitative structure-activity relationship technique from which inferences can be made about chemicals of interest based on data from known active molecules. In general, to apply CoMFA to a group of chemicals, all that is required for the analysis is the biological activity (e.g., IC_{50}) and the 3D structures of the molecules assuming common molecular target(s). However, for this paper, only the CoMFA descriptors were needed for further hierarchical clustering; no biological activity data were used. It was not our intent to develop quantitive structure-activity relationship models. The 3D structures of the molecules were constructed as described in *Step 1.* Briefly, TPHs were placed in a 3D grid with 2-Å spacing encompassing all of the chemicals. At each grid point, both steric energy and electrostatic energy were measured for each chemical by a probe atom (sp^3-hybridized carbon with +1 charge). All steric and electrostatic energies were set to the default cutoff value of 30 kcal/mol. All other parameters for CoMFA were set to the default values in Sybyl 8.0. CoMFA values for each compound were computed according to procedures in the software manual (Sybyl 8.0, Tripos, Inc.).

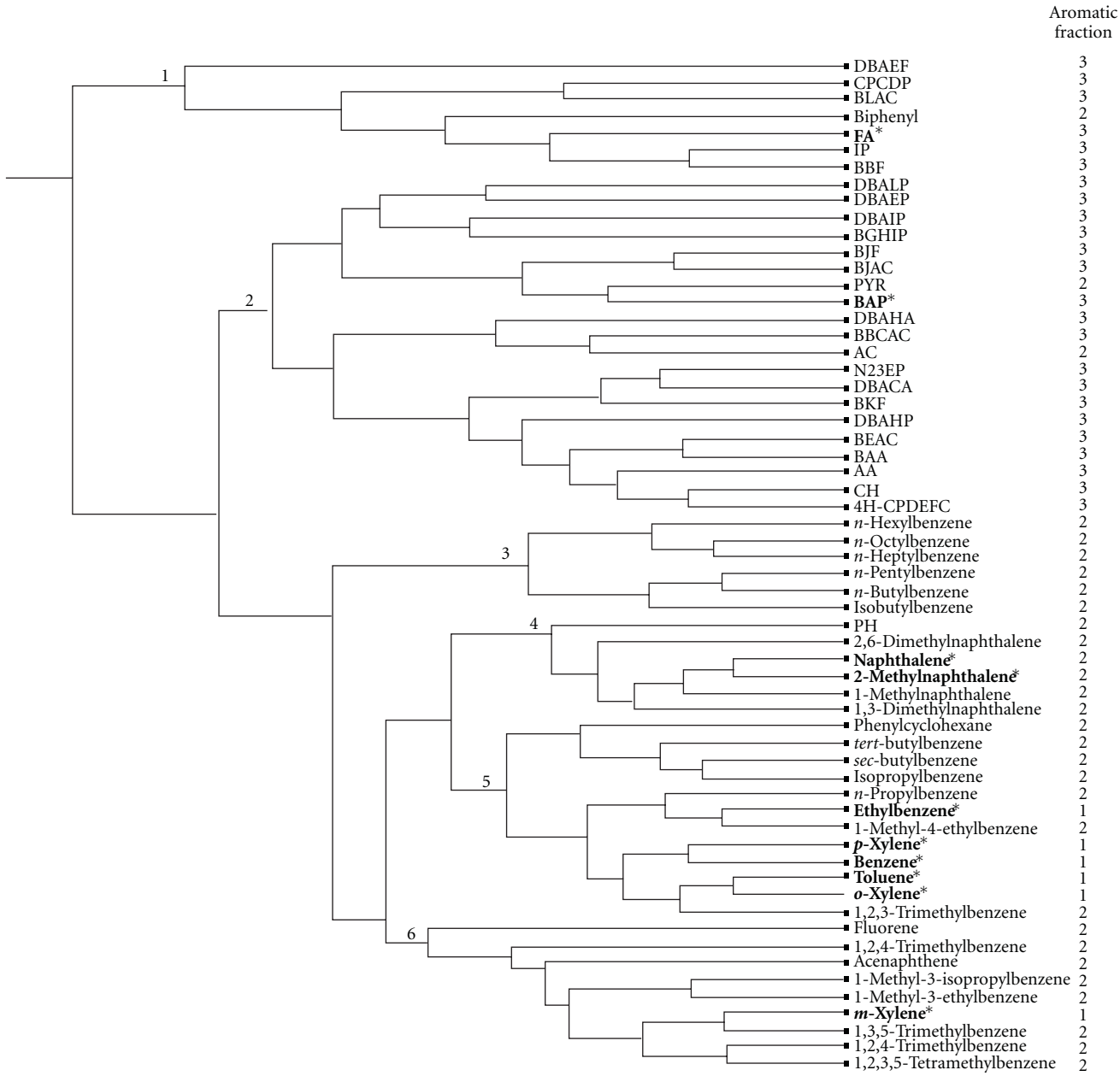

Figure 3: Hierarchical cluster analysis based on CoMFA for all aromatic fractions. Proposed surrogate or component chemicals are shown in bold and with asterisks. DBalP: Dibenzo[a,l]pyrene, BlAC: Benzo[l]aceanthrylene, IP: Indeno[1,2,3-c,d]pyrene, FA: Fluoranthene, CPcdP: Clclopenta[c,d]pyrene, DBacA: Dibenzo[a,c]anthracene, BbcAC: 11H-Benzo[b,c]aceanthrylene, AA: Anthanthrene, DBahA: Dibenzo[a,h]anthracene, BjAC: Benzo[j]aceanthrylene, BeAC: Benzo[e]aceanthrylene, BjF: Benzo[j]fluoranthene, BaA: Benzo[a]anthracene, N23eP: Naphtho[2,3-e]pyrene, BghiP: Benzo[g,h,i]perylene, Pyr: Pyrene, PH: Phenanthrene, AC: Anthracene, DBaiP: Dibenzo[a,i]pyrene, DBahP: Dibenzo[a,h]pyrene, DBaeF: Dibenzo[a,e]fluoranthene, DBaeP: Dibenzo[a,e]pyrene, BkF: Benzo[k]fluoranthene, BbF: Benzo[b]fluoranthene, BaP: Benzo[a]pyrene, CH: Chrysene, 4H-CPdefC: 4H-Cyclopenta[d,e,f]chrysene.

Step 3. Hierarchical Clustering Analysis. Once the CoMFA values of all selected TPHs were calculated, two heuristic hierarchical clustering analyses were separately conducted for aliphatic and aromatic groups (Figures 2 and 3). In general, a hierarchical clustering analysis attempts to find groupings within a set of data. Based on the Euclidean distance between points, a dendrogram showing the similarity/dissimilarity of clusters at increasing levels of detail is displayed (Sybyl 8.0, Tripos, Inc.). A hierarchical clustering analysis is performed based on the CoMFA results from Step 2 above. Initially, each dot (i.e., chemical) on the rightmost column of the dataset of TPHs can be considered as a basic cluster. The next nearest pair of clusters is merged (indicating similarity in chemical structure and potential biological interactions), then the next nearest (to the left), and so forth until there is only one cluster containing all the dots (chemicals) and branches.

The overall hierarchical clustering process is captured as a dendrogram or inverted tree (note: for this paper, Figures 2 and 3 have been rotated 90° counterclockwise to facilitate viewing). The rotated dendrogram should be read from the right to the left, where each node at the rightmost end represents a chemical, and the central branch at the next merging point represents the entire dataset for one cluster. The lengths of the horizontal lines in the dendrogram provide relative qualitative information about the linkage distance (e.g., similarity) between various clusters. For instance, clusters represented by long unbranched strands are strongly separated from other clusters (Figures 2 and 3).

The main property used to determine the distances on which clustering operates is CoMFA descriptors. Once the CoMFA column (an array of 3D descriptors) is generated, the linkage method for hierarchical clustering is *Complete* as recommended by the software manual (Sybyl 8.0, Tripos, Inc.). In general, the *Complete* linkage yields the fewest singletons and the most balanced distribution of points among clusters (Sybyl 8.0, Tripos, Inc.). Because clusters based on the *Complete* linkage method are comprised of only similar components, this represents a significant advantage over the other three linkage methods. Thus, we presented results from the *Complete* linkage method only (other linkage methods were attempted but no major difference in overall pattern of clustering was found; data not shown). The full details of algorithms can be found in the software manual (Sybyl 8.0, Tripos, Inc.).

3. Results and Discussion

The dendrogram results are displayed in Figures 2 and 3 of aliphatics and aromatics, respectively. The fraction assignment developed by MADEP is in the first column of Table 1 and is also indicated in the rightmost column in Figures 2 and 3. The clusters are labeled by numbers in Figures 2 and 3. Based on intrinsic chemical structures (e.g., cyclic versus single chain, and branched versus unbranched hydrocarbons) and the final hierarchical clustering, seven clusters were manually assigned for the aliphatic fractions (aliph1–3; numbers 1–7 in Figure 2) based on the separation of clusters and degree of branching, and six clusters were manually assigned for the aromatic fractions (arom1–3; numbers 1–6 in Figure 3). Consistency of the fraction assignments for the TPHs was assessed based on the assignment of the global clusters.

3.1. Clustering Results of Aliphatic TPHs. For the aliphatic group containing 51 component chemicals, it is apparent that alkenes (Cluster number 7) are strongly separate and are most dissimilar to the rest of TPHs that are mostly straight and branched alkanes (Figure 2). If considering all alkenes as a global cluster on its own, the rest of dendrogram can be grouped into six clusters based on the comparable length of horizontal lines (i.e., CoMFA similarity) as labeled in Figure 2. Based on this classification or grouping, we compared membership of each TPH component within each cluster to its actual fraction assignment by MADEP as indicated in the aliphatic fraction column. In general, Cluster number 1 represents aliph3, Cluster number 2 represents aliph2, and the remaining clusters represent aliph1. Consistency of fraction assignment is summarized in Table 2. The overall consistency with the MADEP fraction assignment is the highest (100%) for aliph3, followed by aliph1 (86.2%) and aliph2 (62.5%). The overall consistency for the three aliphatic fractions is 80.4%. The aliphatic dendrogram suggests that some TPHs assigned by MADEP to aliph2 may be more similar to compounds in aliph1 based on their 2D and 3D physicochemical properties. To determine whether this hypothesis is valid, further hierarchical analysis based on both toxicity values and CoMFA will be necessary. This hierarchical clustering is heuristic in the sense that it depends on physiochemical properties (CoMFA) only. Future work may include a 2-way hierarchical clustering using both CoMFA and a common toxicity endpoint and data which could facilitate direct comparison of underlying toxicity and further evaluation of the proposed surrogate chemical within each fraction.

Table 2: Consistency of fraction assignment.

Hydrocarbon fraction	Consistency	Percent consistency
Aliphatic		
No.1: C5–C8	25/29	86.2%
No.2: C9–C18	10/16	62.5%
No.3: C19–C32	16/16	100%
Total	41/51	80.4%
Aromatic		
No.1: C6–C8	5/6	83.3%
No.2: C9–C18	24/30	66.7%
No.3: C19–C32	24/24	100%
Total	53/60	88.3%

3.2. Clustering Results of Aromatic TPHs. For the aromatic group containing 60 component chemicals, six clusters can be identified based on the leftmost level (Figure 3). Clusters numbers 3–6 can be considered as a global cluster based on the comparable length of horizontal lines (Figure 3). This global cluster consists of arom1 and arom2 TPHs only. Cluster number 1 is the furthest separated from the rest of the clusters, but it is closer to Cluster number 2. Clusters numbers 1 and 2 can be considered as another global cluster, which consists of all arom3 TPHs.

The percent consistency is the highest for arom3 (100%), followed by arom1 (83.3%), and arom2 (66.7%). The overall consistency for the three aromatic fractions is 88.3%. The low consistency percentage within the arom2 fraction can be explained by two noticeable discrepancies for some TPHs as follows. (1) Three TPHs (pyrene, anthracene, and biphenyl) were shown to be strongly clustered with the arom3 fraction Clusters numbers 1 and 2 instead of arom2 Clusters numbers 3, 4, and 6 (Figure 3), and (2) seven TPHs with lower EC indices within the arom2 fraction clustered closely with the arom1 TPHs (e.g., *n*-propylbenzene). Based on the clustering

results, we would recommend further analyses for pyrene, anthracene, and biphenyl for this mixtures risk assessment approach, as they may be considered as part of arom3 rather than arom2. As for the low EC TPHs within the arom2 fraction (e.g., *n*-propylbenzne, isopropylbenzene, etc.), there is some suggestive evidence that the cutoff for the arom2 may be changed to EC11 instead of EC9 by including straight and branched propylbenzene and butylbenzene in certain circumstances. This is based on available oral toxicity values for ethylbenzene (EC8.5) and isopropylbenzene (EC9.13), as both have similar lowest-observed-adverse-effect levels (LOAELs) of 291 and 331 mg/kg-day, no-observed-adverse-effect levels (NOAELs) of 97.1 and 110 mg/kg-day, respectively, as well as identical RfDs of 0.1 mg/kg-day. Further details can be found in the U.S. Environmental Protection Agency's Integrated Risk Information System database [1]. A recent two-generation reproductive study with repeated exposure to *n*-butylbenzene suggests that a LOAEL may be identified at 300 mg/kg-day based on hepatotoxicity (e.g., increase liver weight and associated hepatocellular hypertrophy; [18]), which is close to the LOAEL for ethylbenzene based on similar liver toxicity endpoints. Additional toxicity testing and/or risk assessment for the low EC TPHs will be needed to support the deviation from the criteria for the arom2 fraction for these specific TPHs.

As for components that are not typically considered as surrogate chemicals for a specific fraction, components with different and more potent toxicities such as naphthalene and other substituted naphthalenes in arom2 fraction should be assessed separately based on the recommendation of MADEP. We found that all naphthalenes clustered closely (Cluster number 4 in Figure 3), and our results supports the MADEP recommendation. The only inconsistently classified arom1 TPH was *m*-xylene, as it is shown to cluster closely with branched alkylbenzenes (Cluster number 6 in Figure 3). It is uncertain why *m*-xylene did not cluster with either *p* or *o*-xylene. We tentatively hypothesize that there may be different metabolizing enzymes that are position-specific, because the overall shape and volume of *m*-xylene are significantly different from that of *p*- and *o*-xylenes.

3.3. Comparison of Fraction Assignments. In general, the assignment of membership in a fraction using our integrated CoMFA/hierarchical clustering approach was consistent with the MADEP assignments based on analytical chemistry for environmental fate and transport. We found that the rate of consistency with the MADEP assignments is >80% on average for the three fractions in the aliphatic and aromatic groups. We believe that CoMFA/hierarchical clustering approach for assigning components or individual TPHs to specific fractions is complementary to the established fraction-based approach for TPH mixture assessment.

4. Conclusions

The *in silico* molecular modeling approach presented in this paper is an important contribution to the assessment of risks posed by TPH mixtures and represents the first known case study that applies computational tools to augment a mixtures risk assessment approach. This integrated CoMFA/hierarchical clustering approach allows systematic and objective evaluation of TPH fractions and fractional membership through a repeatable process. The approach is capable of clustering or grouping members within a fraction and assigning membership in a fraction (i.e., a local cluster). This approach can also identify TPHs that belong in other fractions (i.e., global clusters). Finally, the approach is transparent and reproducible, reducing inherent uncertainty in judgments when chemistry and toxicity information is limited or not available.

We used the approach to independently evaluate membership assignments in the TPH fractions that were developed by MADEP. In general, we found the composition of the MADEP fractions to be consistent with results from the CoMFA/hierarchical clustering approach. Concordance between these approaches reduces the uncertainty associated with applications of this mixtures method. However, we also observed some discrepancies between our results and those of MADEP. For instance, MADEP includes the C5–C8 TPHs in the arom1 fraction, but our analysis suggests that some C9-C10 TPHs (e.g., *n*-propylbenzene, isopropylbenzene, and *n*-butylbenzene) in MADEP's arom2 fraction have physicochemical and toxicological properties similar to TPHs in the arom1 fraction, and may therefore be more appropriately assigned to arom1. The application of our approach suggests that additional toxicological evaluations of some "borderline" TPHs may provide useful insight into their assignment to a specific fraction.

Overall, our approach has some limitations in distinguishing one fraction from another (e.g., arom1 from arom2) and in defining a cutoff in terms of carbon or EC number. It is also highly dependent on the available toxicity information, because the clustering results could change with consideration of compound-specific toxicity values. We believe that in the future, development of a two-way hierarchical clustering (i.e., CoMFA and toxicity information) would perform better than the CoMFA-based approach alone using a subset of TPHs within a fraction. Further studies could include hierarchical clustering using both CoMFA descriptors and repeated dose toxicity information (e.g., NOAELs, LOAELs, reference values, and cancer slope factors) as an extra level of filtering for the hierarchical clustering analysis. A refined clustering using both CoMFA and a common toxicity endpoint would facilitate a direct comparison of underlying toxicity and potentially validate the proposed surrogate chemical within each fraction. By taking the information and knowledge gained from both the toxicology and chemistry fields, an empirical approach is available to define similarity and ultimately the grouping for a specified fraction for future risk assessments of TPH mixtures.

A significant future application of this approach involves assigning toxicologically unknown TPHs to fractions prior to analytical chemistry measurements. Without the actual measurement of EC number or an expert's judgment, one cannot assign a TPH to a specific fraction with confidence. Using this *in silico* approach, toxicologically unknown TPHs

can be considered with the rest of the toxicologically known TPHs in all fractions based on CoMFA descriptors, and the cluster/fraction which it most closely associates with can be subsequently identified (i.e., a range of toxicity can be inferred). Based on clustering, one may assign membership in an appropriate fraction based on proximity to the surrogate chemical or the overall clustering/grouping of TPHs in a fraction (i.e., similar components or chemicals within a fraction tend to cluster together). In addition, toxicity of the surrogate chemical within the assigned fraction could serve as the surrogate toxicity for the unknown TPHs. While this transparent and empirical approach can address uncertainty for toxicologically unknown TPHs in a mixture, it cannot predict an actual toxicity value for the TPHs with unknown toxicity.

Abbreviations

C:	Carbon
CoMFA:	Comparative molecular field analysis
EC:	Equivalent carbon
GC:	Gas chromatography
NOAEL:	No-observed-adverse-effect level
LOAEL:	Lowest-observed-adverse-effect level
MADEP:	Massachusetts Department of Environmental Protection
MOA:	Mode of action
RfD:	Reference dose
TPH:	Total petroleum hydrocarbon
TPHCWG:	Total petroleum hydrocarbon criteria working group.

Acknowledgments/Disclaimers

The authors acknowledge Drs. Scott Wesselkamper and Belinda Hawkins for their critical **Disclaimer** review and editorial suggestions. The views expressed in this paper are those of the authors and do not necessarily reflect the views and policies of the U.S. Environmental Protection Agency. Mention of trade names or commercial products does not constitute endorsement or recommendation for use.

References

[1] U.S. Environmental Protection Agency, *Integrated Risk Information System (IRIS)*, Office of Research and Development, Washington, DC, USA, 2010.

[2] MADEP (Massachusettes Department of Environmental Protection), *Characterizing Risks Posed by Petroleum Contaminated Sites: Implementation of the MADEP VPH/EPH Approach*, Cleanup, Boston, Mass, USA, 2002.

[3] MADEP (Massachusettes Department of Environmental Protection), *Updated Petroleum Hydrocarbon Fraction Toxicity Values for the VPH/EPH/APH Methodology*, Office of Research and Standards, Boston, Mass, USA, 2003.

[4] TPHCWG (Total Petroleum Hydrocarbon Criteria Working Group), *Selection of Representative TPH Fractions Based on Fate and Transport Considerations*, vol. 3, Amherst Scientific Publishers, Amherst, Mass, USA, 1997.

[5] TPHCWG (Total Petroleum Hydrocarbon Criteria Working Group), *Development of Fraction Specific Reference Doses (RfDs) and Reference Concentrations (RfCs) for Total Petroleum Hydrocarbons (TPH)*, vol. 4, Amherst Scientific Publishers, Amherst, Mass, USA, 1997.

[6] TPHCWG (Total Petroleum Hydrocarbon Criteria Working Group), *Petroleum Hydrocarbon Analysis of Soil andWater in the Environment*, vol. 1, Amherst Scientific Publishers, Amherst, Mass, USA, 1998.

[7] TPHCWG (Total Petroleum Hydrocarbon Criteria Working Group), *Composition of Petroleum Mixtures*, vol. 2, Amherst Scientific Publishers, Amherst, Mass, USA, 1998.

[8] TPHCWG (Total Petroleum Hydrocarbon Criteria Working Group), *Human Health Risk-Based Evaluation of Petroleum Release Sites: Implementing the Working Group Approach*, vol. 5, Amherst Scientific Publishers, Amherst, Mass, USA, 1999.

[9] U.S. Environmental Protection Agency, *Supplementary Guidance for Conducting Health Risk Assessment of Chemical Mixtures*, EPA/630/R-00/002, U.S. Environmental Protection Agency, Washington, DC, USA, 2000.

[10] U.S. Environmental Protection Agency, *Provisional Guidance for Quantitative Risk Assessment of Polycyclic Aromatic Hydrocarbons*, EPA/600/R-93/089, U.S. Environmental Protection Agency, Cincinnati, OH, USA, 1993.

[11] L. K. Teuschler, "Deciding which chemical mixtures risk assessment methods work best for what mixtures," *Toxicology and Applied Pharmacology*, vol. 223, no. 2, pp. 139–147, 2007.

[12] M. Béliveau and K. Krishnan, "A spreadsheet program for modeling quantitative structure-pharmacokinetic relationships for inhaled volatile organics in humans," *SAR and QSAR in Environmental Research*, vol. 16, no. 1-2, pp. 63–77, 2005.

[13] M. Béliveau, R. Tardif, and K. Krishnan, "Quantitative structure-property relationships for physiologically based pharmacokinetic modeling of volatile organic chemicals in rats," *Toxicology and Applied Pharmacology*, vol. 189, no. 3, pp. 221–232, 2003.

[14] J. B. Knaak, C. C. Dary, F. Power, C. B. Thompson, and J. N. Blancato, "Physicochemical and biological data for the development of predictive organophosphorus pesticide QSARs and PBPK/PD models for human risk assessment," *Critical Reviews in Toxicology*, vol. 34, no. 2, pp. 143–207, 2004.

[15] R. Venkatapathy, C. Y. Wang, R. M. Bruce, and C. Moudgal, "Development of quantitative structure-activity relationship (QSAR) models to predict the carcinogenic potency of chemicals. I. Alternative toxicity measures as an estimator of carcinogenic potency," *Toxicology and Applied Pharmacology*, vol. 234, no. 2, pp. 209–221, 2009.

[16] T. A. Halgren, "MMFF VI. MMFF94s option for energy minimization studies," *Journal of Computational Chemistry*, vol. 20, no. 7, pp. 720–729, 1999.

[17] R. D. Cramer, D. E. Patterson, and J. D. Bunce, "Comparative molecular field analysis (CoMFA). 1. Effect of shape on binding of steroids to carrier proteins," *Journal of the American Chemical Society*, vol. 110, no. 18, pp. 5959–5967, 1988.

[18] H. Izumi, E. Kimura, T. Ota, and S. Shimazu, "A two-generation reproductive toxicity study of n-butylbenzene in rats," *Journal of Toxicological Sciences*, vol. 30, pp. 21–38, 2005.

Hindawi Publishing Corporation
Journal of Toxicology
Volume 2012, Article ID 131854, 8 pages
doi:10.1155/2012/131854

Research Article

Reconstructing Organophosphorus Pesticide Doses Using the Reversed Dosimetry Approach in a Simple Physiologically-Based Pharmacokinetic Model

Chensheng Lu[1] and Leo Andres[2]

[1] *Department of Environmental Health, Harvard School of Public Health, 401 Park Drive, Boston, MA 02215, USA*
[2] *Atlanta Clinical and Translational Science Institute, School of Medicine, Emory University, 1440 Clifton Road, Atlanta, GA 30322, USA*

Correspondence should be addressed to Chensheng Lu, cslu@hsph.harvard.edu

Received 6 September 2011; Revised 21 October 2011; Accepted 24 October 2011

Academic Editor: Marina V. Evans

We illustrated the development of a simple pharmacokinetic (SPK) model aiming to estimate the absorbed chlorpyrifos doses using urinary biomarker data, 3,5,6-trichlorpyridinol as the model input. The effectiveness of the SPK model in the pesticide risk assessment was evaluated by comparing dose estimates using different urinary composite data. The dose estimates resulting from the first morning voids appeared to be lower than but not significantly different to those using before bedtime, lunch or dinner voids. We found similar trend for dose estimates using three different urinary composite data. However, the dose estimates using the SPK model for individual children were significantly higher than those from the conventional physiologically based pharmacokinetic (PBPK) modeling using aggregate environmental measurements of chlorpyrifos as the model inputs. The use of urinary data in the SPK model intuitively provided a plausible alternative to the conventional PBPK model in reconstructing the absorbed chlorpyrifos dose.

1. Introduction

A physiologically based pharmacokinetic (PBPK) model would allow for simulating the dynamics of pesticide absorption, distribution, metabolism, and elimination (ADME) from different routes of exposures and, in theory, could be used as a tool for evaluating biomarker measurements (e.g. blood or urine levels) associated with the exposures [1–4]. The mechanistic representation of biological processes embedded in the PBPK model allows systematic route, dose, and species extrapolation, and for these reasons, PBPK models have been applied in pesticide risk assessments that are relevant for the interpretation of biomarker data [5–12].

Although the interpretation of PBPK model outputs could provide a link to the regulatory metrics in the form of reference dose, its application remains problematic due to the fundamental limitations resulting from the potential measurement errors associated with the aggregate exposure measurements [11, 13]. Although those aggregate exposure data are needed in order to simulate the dynamics of ADME for a specific pesticide, the uncertainties, mainly the temporal and spatial variations, associated with the measurements may inadvertently be carried over to the model outcomes. Those uncertainties, however, are merely explicit statements of underlying assumption applied in the analysis of urinary biomarker data.

A simple pharmacokinetic (SPK) model incorporating reverse dosimetry and PBPK modeling approach, on the other hand, only requires urinary biomarker data as inputs and the a-priori knowledge of the exposure pathways for individuals [14, 15]. The use of urinary biomarker data in the SPK simulation might be advantageous over the traditional PBPK model because urinary excretion is a primary route of elimination for many compounds, and urine samples are relatively easy to collect from individuals comparing to the aggregate environmental samples. The SPK model allows for the estimation of absorbed dose from a dominated route of exposure while reducing the number of inputs into the model

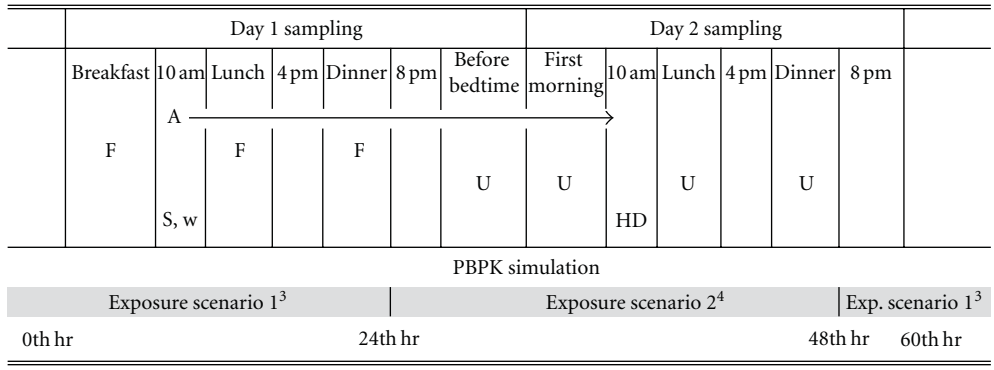

Figure 1: Sampling schedule for the 1998 study[1] and the corresponding PBPK model simulation[2].

and could potentially minimize the uncertainties. Therefore, the development of SPK model may be important in the field of PBPK model by reducing the resources needed to model the dose metrics of certain chemicals.

In this paper, we illustrated the development of an SPK model adapted from a previously published PBPK model and the performance of the exploratory analysis using urinary biomarker data as inputs to the SPK model. The effectiveness of the SPK model in the pesticide risk assessment was evaluated by comparing the dose estimates among three different composites of biomarker data.

2. Methods

The development of the SPK model began with the pharmacokinetic equations that are used in previously developed PBPK models for animal and human data [2, 11, 16, 17]. While the solution of a conventional PBPK model results in a uniquely determined excretion profile of urinary biomarker, the "reverse" dosimetry analysis in this SPK model development, which uses urinary biomarker concentrations as input, does not lead to a unique solution. It is, therefore, necessary to constrain the dose profile with additional information to reach an optimum dosing profile. We assumed that the predominant exposure pathway for organophosphorus (OP) pesticides is via foods and, therefore, constructed the SPK model focusing on oral ingestion. Such assumption was based on the results of aggregate exposure assessment, and the previous PBPK model outputs which shows very little OP residues in the environment [18] and suggests dietary intakes of OP pesticides constitute the majority of urinary metabolite concentrations [11], respectively.

2.1. Urinary Biomarker Data. Data employed in this SPK model simulation were collected from a cross-sectional study with repeated biological and environmental sampling conducted in Washington State in 1998. Results for the environmental measurements of several OP pesticides and their respective urinary metabolites, as well as for absorbed dose reconstruction using a conventional PBPK model, were published previously [11, 18–20]. In brief, the study was conducted in the homes of 13 children ages 3–6, who either lived in an urban/suburban (nonagricultural) area or in the agricultural region in which OPs have been used in the nearby fruit tree orchards. Each home was sampled for two 24-hour periods (over 3 days) in summer and fall of 1998. Environmental and biological sample collections included 24-hour indoor air, drinking water; outdoors soil, house dust, toy wipes, 24-hour duplicate diets, and 4 spot urine samples over a 24-hour period (Figure 1). The 1998 study was designed to capture the aggregate OP exposures in the subsequent 4 spot urines over the course of a 24-hour period. These were the before bedtime voids on the first day and the first morning lunch, and dinner voids on the second day. Chlorpyrifos (CPF) was selected as the modeled pesticide in this study because it was commonly detected in the environmental matrices, and its specific metabolite, 3,5,6-trichlorpyridinol (TCPY), was frequently measured in the urine samples, as compared to other OP pesticides.

Urinary data from the 1998 study, including TCPY concentrations, urine void volumes, and urine sample collection times, were used as inputs into the SPK model to estimate the absorbed dose of CPF. The study protocol and procedures to obtain the assent of the children and informed consent of their parents or guardians were reviewed and approved by the University of Washington Institutional Review Board (IRB). The use of those data in the PBPK model analysis was reviewed and approved by Emory University IRB.

2.2. Model Development and Validation

2.2.1. Input File Construction. A database was created in Microsoft Access 2002 to hold study variables and data. Tables in the database were structured in the same form as the raw study data to allow for easier manipulation of the data later in the analysis. There were missing values (not collected), including the void and exposure times, values for void volumes, and values for the weight of the study subjects that were necessary to create the data file. Values for the default void and exposure times were chosen based on a previous data file for the Matlab PK model script. Values for the default void volume were taken from a study by Voorhess [21] which examined urinary catecholamine excretion by healthy children. Lastly, values for the default weights of children were taken from table 7-3 of the Exposure Factors Handbook [22]. Tables were created to hold these values specific to sample, age, or sex depending on the measure.

Queries were written in SQL to create the data files for input into the SPK model. SQL was used to join data from separate data tables into one query output, to make logic and arithmetic transformations to the data for input into the model, and to allow for dynamic creation of data files simplifying modification of data input file creation. Since some of the data that are necessary to create the input file were missing, default values had to be calculated. This was done according to the type of data that was available and which data would provide values that would best represent the inputs. The script would first try to determine values based on data that would yield the most representative values. If this data was not available, then it would try other data that would yield less representative values successively based on availability of the relevant data until it reached the least representative values.

The main query that produced the data file was qry_createdata. This query pulled data from database tables and other queries. These queries were qry_calcttime and qry_urinesampcalc. The qry_calcttime query was used to calculate the previous and current void times using available data and default values depending on the data that was available. The qry_urinesampcalc query was used to calculate the urinary excretion rate from metabolite concentrations, sample void volumes, and times from qry_calcttime. Once these queries produced the correct data for input into the model, the main query was used to export the data from Access into Excel 97–2002 format.

Once constructed, each of the input file for the Matlab SPK model script (see supplementary material available online at doi:10.1155/2012/131854) had nine variables. The first variable held the subject ID and study period. The subject ID was the part before the separator, and the study period was the part after the separator. For the study period, 1 signified the summer period, and 2 signified the fall period. For example, the identifier 114.1 denoted subject ID 114 in the summer study period. The second variable reflected whether the subject resided in an agricultural area. The third variable held the average metabolite urinary excretion rate that was calculated using the urinary metabolite concentration, the volume of the void, and the times for the previous and current void

$$\mathrm{UER_{avg}\ (mmoL/hr)} = \frac{C_u V_u}{\left(t_c - t_p\right)}. \quad (1)$$

In this formula, $\mathrm{UER_{avg}}$ is the average urinary excretion rate between the current void and the previous void, C_u is the measured metabolite concentration in the urine, V_u is the volume of the void, t_c is the time of the current void, and t_p is the time of the previous void [1]. The fourth variable held the body weight of the child in kilograms. The fifth variable denoted the route of the exposure and scenario, where 1 is an inhalation exposure, 2 is a dermal exposure, and 3 through 7 are bolus events. In this analysis, 3 was the first morning void on the second day, 4 was the lunchtime void, 5 was the before bedtime void on the first day, and 6 was the dinnertime void on the second day. The sixth variable held the start time of the exposure event on a 24-hour clock with 0 at midnight before the exposure event. The seventh variable held the end time of the exposure event. However, for the current analysis, this variable was not used since the exposures that were analyzed were bolus events. The eighth variable held the time of the previous urine void before the exposure event on a 24-hour clock. The ninth variable held the time of the current urine void sample before the exposure event on a 24-hour clock.

2.2.2. Data Processing. Once input files were created, the SPK model was run using Matlab version 7.0.1. Each input into the simple SPK model was able to calculate an estimated absorbed dose for CPF by fitting the input variables to a generalized dose absorption curve. It then calculated the absorbed dose by finding the area under the curve over the course of a day. Due to the construction of the script, the model was only able to compute one dose estimate from one exposure rather than from a collection of exposures. Using the output from the SPK model script, we composited four spot urine samples in three different ways in order to estimate the daily absorbed doses of CPF in three different scenarios.

For the first composite (SPK I) scenario, only TCPY concentrations from the first morning void were used to calculate the dose estimate. This void was suggested to be an accurate measure of TCPY metabolite because it was assumed that TCPY concentrations in the urine were 0 after the before bedtime void [20]. Urine would then be formed and held during the night and voided in the morning, which would give the sample greater accuracy in determining metabolite concentrations since a long period of time had elapsed before the void.

For the second composite (SPK II) scenario, dose estimates from the before bedtime void and the first morning void were averaged normalized by the volume of each void. This was done because the SPK model was only able to analyze one sample at a time rather than taking a collection of samples and computing a dose from them. In this calculation, it was assumed that metabolite concentrations from the before bedtime void and the first morning void were both due to exposure from dinner on the first day. Since metabolite concentrations were assumed to be caused by the same exposure event (dinner event), they should compute to the same absorbed dose. Therefore, the two dose estimates were averaged to provide a fair measure based on both outputs.

In order to determine the times used to calculate the urinary excretion rate for the before bedtime sample of SPK II, we used the volume of the void sample to estimate the time that the urine was allowed to collect in the bladder. This estimate was based on the average daily void volume of children of the same age and gender over a 24-hour period [21]. By dividing the sample void volume by the average daily void volume, the time that the urine was allowed to collect in the bladder was estimated using (2), in which $(t_c - t_p)$ is the difference in hours from the time of the current void (t_c) to the time of the previous void (t_p), V_u is the volume of the urine sample, and $\mathrm{V_{avg24}}$ is the volume of the average daily void over the span of 24 hours:

$$\left(t_c - t_p\right) \approx \left(\frac{V_u}{\mathrm{V_{avg24}}}\right) * 24 \quad (2)$$

For the third composite (SPK III) scenario, dose estimates from the before bedtime void on the first day, and the first morning void, the lunchtime void, and the dinner void on the second day were averaged to reach a single absorbed dose estimate. For this calculation, the beginning exposure time for the lunch and dinner voids on the second day was set at dinner time on the first day. We assumed that part of the urinary metabolite measurements from the lunchtime and dinner voids on the second day may come from dinnertime exposure on the first day. Since absorbed dose estimates could not be calculated using more than one exposure, a composite meal exposure was created using urinary metabolite measurements from the before bedtime void on the first day, the first morning void, the lunchtime void, and the dinnertime void on the second day. The time of the composite meal exposure was set at dinnertime on the first day. The results from the four estimates were then averaged to get an overall absorbed dose estimate. Again, the times used to calculate the urinary excretion rate were estimated from dividing the sample void volume by the average daily void volume using (2).

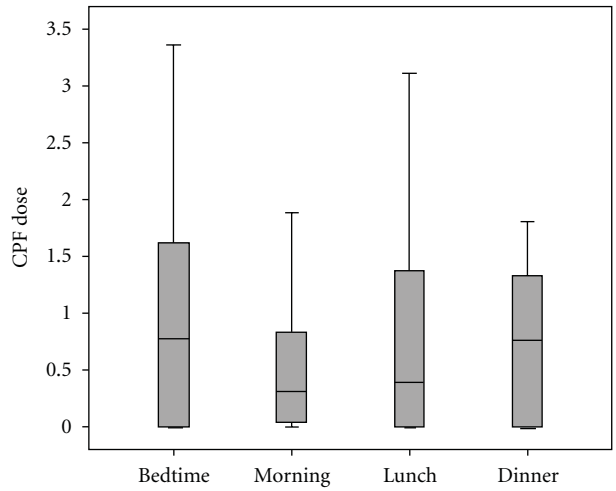

Figure 2: The dose estimates (CPF_DOSE, μg/kg/day) for chlorpyrifos using 3,5,6-trichlorpyridinol concentrations in the spot urine samples collected at before bedtime in Day 1 and the first morning, lunch, and dinner voids in Day 2 as the SPK model inputs.

3. Results and Discussion

The PBPK model was developed to quantitatively integrate the physiological, metabolic, and biochemical factors associated with ADME. Although the initial model validation has proven the accuracy of predicting CPF exposures, it was found later that the effectiveness of the PBPK model was highly dependent on the model parameters and the limitation of the input exposure data [2]. This limitation has been highlighted in a recent study in which the PBPK model failed to predict TCPY excretion as compared to TCPY levels measured in urine collected from study subjects [11]. Such failure exposes the vulnerability of employing PBPK models in risk assessment without sufficient knowledge or assurance of the quality of exposure data that are used as PBPK model inputs. Therefore, we were prompted to develop this simple pharmacokinetic model in order to improve the ability for estimating absorbed dose using urinary metabolite data as the model inputs. Should TCPY levels measured in urine be considered the gold standard in reflecting the exposure to CPF (by subtracting the preformed portion of TCPY), the use of urinary TCPY data in the pharmacokinetic analysis would provide more reliable dose estimates of CPF than using aggregate exposure data.

The SPK model simulation yielded to a total of 88 CPF dose estimates, separated by summer and fall seasons. The dose estimates resulted from the first morning void measurements appeared to be lower than but not significantly different to those using before bedtime, lunch, or dinner voids (Figure 2). Those estimates were modeled assuming that the exposure to CPF occurred during dinner meal (at 7 pm) on the first day. Knowing that the biological half-life for orally ingested CPF is approximately 16 hours [23], the estimated absorption curve for the first morning void may mostly reflect the intake of CPF from dinner last night. Dose estimates for spot urine samples collected later in the 2nd day were increasingly larger, suggesting additional CPF exposures from earlier in the day (breakfast and lunch). Dose estimates from before bedtime void samples were likely to be representative of CPF exposures that occurred throughout the first day rather than intakes from dinner, as was modeled.

The disparity among the dose estimates using spot urinary TCPY measurements in different time points raises the concern of the validity of using single spot urinary measurement as the basis of dose estimation in risk assessment. The magnitude of such uncertainty would be considerably larger under the circumstance in which spot urine samples are collected at different time points within a predetermined time period (e.g., 24 hours) from individuals. For instance, the National Health and Nutrition Examination Survey (NHANES) conducted by the Center for Disease Control and Prevention (CDC) collected single spot urine samples from subjects based on their appointments. If TCPY data from NHANES were used in the SPK model simulation, the interpretation and the conclusions of the estimated doses for CPF in NHANES subjects should therefore be cautiously made. Georgopoulos et al. [13] also raised this issue in their case study involving the use of a physiologically based toxicokinetic modeling in conjunction with numerical "inversion" techniques for reconstructing CPF exposure using TCPY data measured in the National Human Exposure Assessment Survey (NHEXAS). As authors stated "Although the NHEXAS data set provides a significant amount of supporting exposure-related information, especially when compared to national studies such as the NHANES, this information is still not adequate for detailed reconstruction of exposures under several conditions," as demonstrated in the paper.

We estimated the daily absorbed CPF doses for individual children using three different composites of the 4 spot urine biomarker measurements (Table 1). Dose estimates for SPK I, II and III were not significantly different (one-way ANOVA); however, the box plot in Figure 3 showed that

Table 1: Descriptive statistics for the estimated daily dose (μg/kg/day) of chlorpyrifos in thirteen children ages 2–5 using the simple pharmacokinetic model.

Overall	SPK I	SPK II	SPK III
Mean (St. Dev.)	0.98 (1.95)	0.97 (1.19)	0.87 (0.81)
Median	0.37	0.82	0.92
N	21	23	26
95% confidence interval (lower, upper)	(0.09, 1.86)	(0.43, 1.51)	(0.51, 1.24)
Min–max	(0, 9.13)	(0, 5.5)	(0, 3.65)
Summer season			
Mean (St. Dev.)	0.55 (0.58)	0.8 (1.0)	0.73 (0.68)
Median	0.34	0.27	0.52
N	10	11	13
95% confidence interval (lower, upper)	(0.19, 0.91)	(0.24, 1.37)	(0.37, 1.09)
Min–max	(0, 1.89)	(0, 3.36)	(0, 2.5)
Fall season			
Mean (St. Dev.)	1.3 (2.53)	1.32 (1.42)	1.13 (0.9)
Median	0.42	0.97	0.94
N	11	12	13
95% confidence interval (lower, upper)	(0, 2.67)	(0.55, 2.09)	(0.66, 1.6)
Min–max	(0.05, 9.13)	(0.2, 5.5)	(0.23, 3.65)
Urban/suburban children			
Mean (St. Dev.)	0.48 (0.52)	0.67 (0.64)	0.63 (0.55)[1]
Median	0.35	0.48	0.45
N	11	12	12
95% confidence interval (lower, upper)	(0.19, 0.77)	(0.31, 1.03)	(0.32, 0.94)
Min–max	(0.04, 1.88)	(0.02, 2.27)	(0.01, 1.97)
Agricultural children			
Mean (St. Dev.)	1.53 (2.73)	1.51 (1.58)	1.19 (0.92)[1]
Median	0.88	1.06	1.04
N	10	11	14
95% confidence interval (lower, upper)	(0.1, 2.96)	(0.91, 2.11)	(0.68, 1.7)
Min–max	(0, 9.12)	(0, 5.5)	(0, 3.65)

[1] Marginally significantly different (one-way ANOVA, $P = 0.077$).

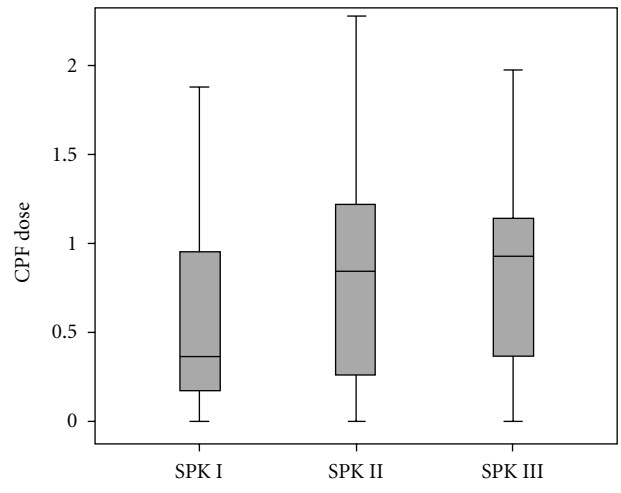

Figure 3: The dose estimates (CPF_DOSE, μg/kg/day) for chlorpyrifos using urinary 3,5,6-trichlorpyridinol concentrations in three different spot urine sample composite methods; SPK_I, SPK_II, and SPK_III.

the median dose estimate from SPK I model simulation are lower than those of SPK II and III, consistent to the trend for the individual void simulations. While this may suggest that dose estimates between models reflect similar CPF exposure among subjects, it is also possible that the similarity among dose estimates is merely the result of the dose estimation being based on shared data. For instance, SPK II was based on the average between SPK I and the dose estimates using the before bedtime voids, and SPK III was based on the estimates that comprised the SPK II estimate and estimates from the lunch and dinner samples. The SPK II dose estimates seemed to be more accurately representative of the daily exposure to CPF simply because it takes into account the excretion of TCPY in before bedtime voids in day 1 and the first morning voids in day 2. The additional CPF exposure between lunch and dinner, if any, captured in the SPK III dose estimates did not significantly increase the overall daily dose estimates would support the validity of using SPK II as the benchmark for daily CPF absorbed dose. Comparing the dose estimates by seasonality and the

Table 2: The dose estimates (μg/kg/day) for chlorpyrifos using PBPK, SPK I, SPK II and SPK III model simulations.

Subject ID[1]	Season	Body wt. (kg)	PBPK	SPK I[2]	SPK II[3]	SPK III[4]
R1	Summer	15.5	0.004	0.546	0.273	1.140
R2	Summer	21.4	0.003	0.281	0.246	0.380
R3	Summer	14.5	0.004	0.043	0.022	0.014
R4	Summer	16.8	0.003	0.831	1.439	0.987
R5	Summer	13.4	0.004	0.338	0.213	0.158
R6	Summer	19.6	0.003	n.a.[5]	0.840	0.520
S1	Summer	17.3	0.003	0	0	0
S2	Summer	18.2	0	0.224	0.112	0.488
S3	Summer	15	0	n.a.[5]	3.357	2.497
S4	Summer	15.5	0	1.881	1.450	1.282
S5	Summer	16.8	0.004	n.a.[5]	n.a.[5]	0.326
S6	Summer	22.7	0.440	0.808	0.820	0.672
S7	Summer	14.5	0	n.a.[5]	n.a.[5]	1.056
R1	Fall	15.5	0.004	1.881	2.274	1.973
R2	Fall	21.4	0.003	0.051	0.204	0.229
R3	Fall	14.5	0.012	0.347	0.980	0.944
R4	Fall	16.8	0.003	0.366	0.541	0.603
R5	Fall	13.4	0.018	0.082	0.483	0.368
R6	Fall	19.6	0.005	0.476	0.476	0.250
S1	Fall	17.3	2.302	9.125	5.496	3.647
S2	Fall	18.2	0.003	0.172	0.949	1.110
S3	Fall	15	0.004	1.060	1.060	1.219
S4	Fall	15.5	0	0.956	1.260	1.017
S5	Fall	16.8	0	1.028	1.184	0.922
S6	Fall	22.7	0.001	0.041	0.969	0.934
S7	Fall	14.5	0.006	n.a.[5]	n.a.[5]	1.513

[1]"R" for children living in agricultural community and "S" for children living in urban/suburban community.
[2]Significantly different to PBPK dose estimates (paired t-test, $P < 0.001$).
[3]Significantly different to PBPK dose estimates (paired t-test, $P = 0.02$).
[4]Significantly different to PBPK dose estimates (paired t-test, $P < 0.001$).
[5]Missing data due to missing spot urine samples.

community where children lived in 1998, we found that children living in urban/suburban have higher CPF exposure than those lived in agricultural community, and their CPF exposure was higher in fall than in summer season.

The SPK dose estimates for individual children participating in the 1998 study were significantly higher than those using the conventional PBPK model approaching, as published earlier [11]. The highest PBPK predicted CPY dose of 2.3 μg/kg/day resulted from the consumption of a food item containing 350 ng/g of CPF remained as the highest in the SPK I, II, and III simulations with the estimated CPF doses of 9.1, 5.5, and 3.7 μg/kg/day, respectively (Table 2). The striking difference of dose estimates between these two pharmacokinetic models may be primarily due to the differences of input data. The use of aggregate exposure assessment as the input variables in the PBPK models targeted at chemicals with short biological half-lives, such as CPF, is prone to significant spatial and temporal variations associated with exposures that would lead to inaccurate outcome measurements. This is evident by the fact that the majority of the data collected from the environment (Figure 1) where the children lived were nondetectable for CPF residue, while spot urine samples collected from those same children frequently contained TCPY. By taking into account the degradation of CPF in the environment (or in foods) in the PBPK model simulation as described in previous studies [11, 24, 25], the PBPK model predicted that TCPY excretion was still not within a reasonable range of accuracy to the measured TCPY levels which are used in the SPK model simulation. It is apparent that the 24-hr aggregate exposure assessment is not capable of capturing CPF exposure in those children. This leads to the serious doubt of the validity of applying aggregate exposure measurements to the PBPK model simulation and subsequently in the risk assessment. The use of urinary TCPY data in the SPK model simulation intuitively provided a plausible alternative to PBPK model in reconstructing the absorbed CPF dose. In theory, the dose estimates resulting from either PBPK or SPK approach should yield to numerical values that are not significantly different to each other, particularly in this case in which both models were constructed using identical parameters, and the input data were collected from

a study that is designed specifically for validating the PBPK model simulation. However, the problem of significant under estimation of CPY doses using the traditional PBPK, as identified in this paper, would be even more prevalent and dramatic under other circumstances in which less-structured environmental exposure data are collected and used as the PBPK model inputs.

4. Study Limitations

Similar to other PBPK model applications, assumptions are needed in the SPK models in order to facilitate the model simulation. The unique assumptions for SPK model simulation include the prior knowledge of the predominant exposure pathway (such as dietary intake in this project) and the default time of exposure (dinner in Day 1). Without detail information of the exposure, those assumptions have to be made either arbitrarily (time of exposure) or by interpretation of study observations (dietary ingestion). A mischaracterization of the predominant exposure pathway (such as dietary intake versus inhalation) will lead to completely different SPK simulation and outcomes.

Due to the limitation in constructing the script files, the SPK model is only able to compute one dose estimate from one urinary biomarker data input, instead of from a series of urinary biomarker data input within 24 hours. In order to overcome this limitation, we used the average dose estimates in SPK II and SPK III to incorporate more urinary biomarker data that is related to the interest of a specific exposure event in the simulation. It is likely that we would introduce unknown uncertainties to the overall simulation because urinary TCPY levels measured in the dinner time may include CPF exposure in Day 2 which is not the interest of the analysis. Although the magnitude of such uncertainty is relatively minimal in this study, by further examining the data for SPK II and SPK III, we acknowledge the existence of such uncertainty.

Acknowledgment

This work was supported by the U.S. Environmental Protection Agency under the Science to Achieve Results research assistance program (R-832244 and R-829364). The authors would like to thank Dr. Miles S. Okino and Christina Holbrook for their assistance with the PBPK model development. Authors declare no competing financial interests in this work.

References

[1] M. L. Rigas, M. S. Okino, and J. J. Quackenboss, "Use of a pharmacokinetic model to assess chlorpyrifos exposure and dose in children, based on urinary biomarker measurements," *Toxicological Sciences*, vol. 61, no. 2, pp. 374–381, 2001.

[2] C. Timchalk, R. J. Nolan, A. L. Mendrala, D. A. Dittenber, K. A. Brzak, and J. L. Mattsson, "A physiologically based pharmacokinetic and pharmacodynamic (PBPK/PD) model for the organophosphate insecticide chlorpyrifos in rats and humans," *Toxicological Sciences*, vol. 66, no. 1, pp. 34–53, 2002.

[3] X. Zhang, A. M. Tsang, M. S. Okino et al., "A physiologically based pharmacokinetic/pharmacodynamic model for carbofuran in sprague-dawley rats using the exposure-related dose estimating model," *Toxicological Sciences*, vol. 100, no. 2, pp. 345–359, 2007.

[4] C. A. Ellison, J. N. Smith, P. J. Lein, and J. R. Olson, "Pharmacokinetics and pharmacodynamics of chlorpyrifos in adult male Long-Evans rats following repeated subcutaneous exposure to chlorpyrifos," *Toxicology*, vol. 287, no. 1–3, pp. 137–144, 2011.

[5] J. N. Blancato, "Pharmacokinetics, chemical interactions, and toxicological risk assessment in perspective," *Environmental Health Perspectives*, vol. 102, supplement 9, pp. 133–137, 1994.

[6] H. J. Clewell, P. R. Gentry, J. M. Gearhart, B. C. Allen, and M. E. Andersen, "Comparison of cancer risk estimates for vinyl chloride using animal and human data with a PBPK model," *Science of the Total Environment*, vol. 274, no. 1–3, pp. 37–66, 2001.

[7] J. B. Knaak, C. C. Dary, M. S. Okino et al., "Parameters for carbamate pesticide QSAR and PBPK/PD models for human risk assessment," *Reviews of Environmental Contamination and Toxicology*, vol. 193, pp. 53–212, 2008.

[8] A. Campbell, "Development of PBPK model of molinate and molinate sulfoxide in rats and humans," *Regulatory Toxicology and Pharmacology*, vol. 53, no. 3, pp. 195–204, 2009.

[9] P. L. Mosquin, A. C. Licata, B. Liu, S. C. Sumner, and M. S. Okino, "Reconstructing exposures from small samples using physiologically based pharmacokinetic models and multiple biomarkers," *Journal of Exposure Science & Environmental Epidemiology*, vol. 19, no. 3, pp. 284–297, 2009.

[10] S. J. Godin, M. J. DeVito, M. F. Hughes et al., "Physiologically based pharmacokinetic modeling of deltamethrin: development of a rat and human diffusion-limited model," *Toxicological Sciences*, vol. 115, no. 2, pp. 330–343, 2010.

[11] C. Lu, C. M. Holbrook, and L. M. Andres, "The implications of using a physiologically based pharmacokinetic (PBPK) model for pesticide risk assessment," *Environmental Health Perspectives*, vol. 118, no. 1, pp. 125–130, 2010.

[12] R. Tornero-Velez, A. Mirfazaelian, K. B. Kim et al., "Evaluation of deltamethrin kinetics and dosimetry in the maturing rat using a PBPK model," *Toxicology and Applied Pharmacology*, vol. 244, no. 2, pp. 208–217, 2010.

[13] P. G. Georgopoulos, A. F. Sasso, S. S. Isukapalli et al., "Reconstructing population exposures to environmental chemicals from biomarkers: challenges and opportunities," *Journal of Exposure Science & Environmental Epidemiology*, vol. 19, no. 2, pp. 149–171, 2009.

[14] Y. M. Tan, K. Liao, R. Conolly, B. Blount, A. Mason, and H. Clewell, "Use of a physiologically based pharmacokinetic model to identify exposures consistent with human biomonitoring data for chloroform," *Journal of Toxicology and Environmental Health A*, vol. 69, no. 18, pp. 1727–1756, 2006.

[15] H. J. Clewell, Y. M. Tan, J. L. Campbell, and M. E. Andersen, "Quantitative interpretation of human biomonitoring data," *Toxicology and Applied Pharmacology*, vol. 231, no. 1, pp. 122–133, 2008.

[16] C. Timchalk, T. S. Poet, M. N. Hinman, A. L. Busby, and A. A. Kousba, "Pharmacokinetic and pharmacodynamic interaction for a binary mixture of chlorpyrifos and diazinon in the rat," *Toxicology and Applied Pharmacology*, vol. 205, no. 1, pp. 31–42, 2005.

[17] J. N. Blancato, F. W. Power, R. N. Brown, and C. C. Dary, ") Exposure Related Dose Estimating Model (ERDEM)

a Physiologically-Based Pharmacokinetic and Pharmacodynamic (PBPK/PD) model for assessing human exposure and risk," Tech. Rep. EPA/600/R-06/061, U.S. Environmental Protection Agency, Washington, DC, USA, 2006, (NTIS PB2006-114712).

[18] C. Lu, G. Kedan, J. Fisker-Andersen, J. C. Kissel, and R. A. Fenske, "Multipathway organophosphorus pesticide exposures of preschool children living in agricultural and nonagricultural communities," *Environmental Research*, vol. 96, no. 3, pp. 283–289, 2004.

[19] R. A. Fenske, C. Lu, G. Kedan, J. Fisker-Andersen, and C. Curl, "Assessment of organophosphorous pesticide exposures in the diets of preschool children in Washington State," *Journal of Exposure Analysis and Environmental Epidemiology*, vol. 12, no. 1, pp. 21–28, 2002.

[20] J. C. Kissel, C. L. Curl, G. Kedan et al., "Comparison of organophosphorus pesticide metabolite levels in single and multiple daily urine samples collected from preschool children in Washington State," *Journal of Exposure Analysis and Environmental Epidemiology*, vol. 15, no. 2, pp. 164–171, 2005.

[21] M. L. Voorhess, "Urinary catecholamine excretion by healthy children. I. Daily excretion of dopamine, norepinephrine, epinephrine, and 3-methoxy-4-hydroxymandelic acid," *Pediatrics*, vol. 39, no. 2, pp. 252–257, 1967.

[22] United States Environmental Protection Agency (USEPA). Exposure Factor Handbook, 1997, http://rais.ornl.gov/documents/EFH_Final_1997_EPA600P95002Fa.pdf.

[23] P. Griffin, H. Mason, K. Heywood, and J. Cocker, "Oral and dermal absorption of chlorpyrifos: a human volunteer study," *Occupational and Environmental Medicine*, vol. 56, no. 1, pp. 10–13, 1999.

[24] M. K. Morgan, L. S. Sheldon, C. W. Croghan et al., "Exposures of preschool children to chlorpyrifos and its degradation product 3,5,6-trichloro-2-pyridinol in their everyday environments," *Journal of Exposure Analysis and Environmental Epidemiology*, vol. 15, no. 4, pp. 297–309, 2005.

[25] C. Lu, R. Bravo, L. M. Caltabiano, R. M. Irish, G. Weerasekera, and D. B. Barr, "The presence of dialkylphosphates in fresh fruit juices: implication for organophosphorus pesticide exposure and risk assessments," *Journal of Toxicology and Environmental Health A*, vol. 68, no. 3, pp. 209–227, 2005.

Hindawi Publishing Corporation
Journal of Toxicology
Volume 2012, Article ID 895391, 10 pages
doi:10.1155/2012/895391

Research Article

Bayesian Analysis of a Lipid-Based Physiologically Based Toxicokinetic Model for a Mixture of PCBs in Rats

Alan F. Sasso,[1,2] Panos G. Georgopoulos,[1] Sastry S. Isukapalli,[1] and Kannan Krishnan[3]

[1] *Environmental and Occupational Health Sciences Institute, UMDNJ-RW Johnson Medical School, Rutgers University, 170 Frelinghuysen Road, Piscataway, NJ 08854, USA*
[2] *Department of Chemical and Biochemical Engineering, Rutgers University, 98 Brett Road, Piscataway, NJ 08854, USA*
[3] *Département de Santé Environnementale et Santé au Travail, 2375 Cote-Sainte-Catherine, Université de Montréal, Montreal, Road QC, Canada, H3C 3J7*

Correspondence should be addressed to Sastry S. Isukapalli, sastry@ccl.rutgers.edu

Received 12 August 2011; Revised 5 October 2011; Accepted 6 October 2011

Academic Editor: Jane C. Caldwell

A lipid-based physiologically based toxicokinetic (PBTK) model has been developed for a mixture of six polychlorinated biphenyls (PCBs) in rats. The aim of this study was to apply population Bayesian analysis to a lipid PBTK model, while incorporating an internal exposure-response model linking enzyme induction and metabolic rate. Lipid-based physiologically based toxicokinetic models are a subset of PBTK models that can simulate concentrations of highly lipophilic compounds in tissue lipids, without the need for partition coefficients. A hierarchical treatment of population metabolic parameters and a CYP450 induction model were incorporated into the lipid-based PBTK framework, and Markov-Chain Monte Carlo was applied to *in vivo* data. A mass balance of CYP1A and CYP2B in the liver was necessary to model PCB metabolism at high doses. The linked PBTK/induction model remained on a lipid basis and was capable of modeling PCB concentrations in multiple tissues for all dose levels and dose profiles.

1. Introduction

Polychlorinated biphenyls (PCBs) are industrial chemicals that have persisted in the environment despite widespread international bans beginning in the 1970s [1]. There are a total of 209 possible PCB congeners, and many of these co-occur in the environment based on the composition of commercially produced PCB mixtures [2]. Mixtures of PCBs are commonly detected in blood samples of the human population, with estimated elimination half-lives of up to 10–15 years [3]. Assessing risks from these mixtures is complicated by the significant variability of toxicological properties of individual PCBs, the time-varying changes in the composition of PCB mixtures in the environment [4], and the metabolic interactions among individual PCBs in the body [5–7].

Physiologically based toxicokinetic (PBTK) models are well-established tools for simulating internal doses and biomarkers of environmental contaminants [8]. PBTK modeling for mixtures of chemicals has gained prominence for risk assessment applications and provides a means for capturing the various types of metabolic interactions among individual constituents [9, 10]. However, for complex mixtures, PBTK models typically need a large number of parameters and often require significant time and data for model development and evaluation. Approaches that minimize the number of parameters in mixture PBTK models while still capturing the major interactions can help reduce such data burdens.

For the class of highly lipophilic compounds such as PCBs and dioxins, one approach for PBTK model reduction is the use of lipid-based models, which assume contaminants only accumulate in the lipids of tissues and blood [11, 12]. Lipid-based PBTK models do not require tissue/blood partition coefficients, which significantly reduces the number of chemical-specific parameters needed for modeling the toxicokinetics of complex mixtures. In these models, residence times in each compartment are assumed to be dependent on tissue lipid volumes and lipid flow rates, which are chemical-independent. Under such scenarios, chemical-specific parameters are limited to absorption, metabolism,

Table 1: Lipid content of rat tissues [11, 14].

Tissue	NLE†	NLE/total lipid
Blood	0.0019	0.576
Plasma	0.0009	0.748
Fat	0.8536	0.998
Liver	0.0425	0.710
Rapidly perfused	0.0425	0.710
Poorly perfused	0.0120	0.632

†Neutral lipid equivalent ratio (mL NLE/mL tissue).

elimination, and metabolic interactions. Lipid-based PBTK modeling provides a generalized treatment of highly lipophilic chemicals, leading to more efficient modeling of complex mixtures (e.g., Emond et al. [11]).

However, parameterization and optimization of lipid-based PBTK models present challenges due to the reduced degrees of freedom, since partition coefficients for each tissue-chemical combination are not considered. This decreased flexibility requires the use of sophisticated parameter estimation techniques for reducing model errors, especially when experimental data include substantial population variability. Bayesian parameter estimation techniques are highly useful in handling such complex population parameter estimation and optimization problems [13]. To date, lipid-based PBTK models for mixtures of chemicals have not been widely used. This study involves the development of a lipid-based PBTK model for a mixture of PCBs, and subsequent model parameterization, refinement, and optimization using Bayesian parameter estimation techniques.

2. Methods

2.1. Data. The data published by Emond et al. [11] consisted of rats receiving oral doses of a mixture of 6 PCB congeners: 118 (2,3′,4,4′,5-pentachlorobiphenyl), 138 (2,2′,3′,4,4′,5-hexachlorobiphenyl), 153 (2,2′,4,4′,5,5′-hexachlorobiphenyl), 170 (2,2′,3,3′,4,4′,5-heptachlorobiphenyl), 180 (2,2′,3,4,4′,5,5′-heptachlorobiphenyl), and 187 (2,2′,3,4,5,5′,6-heptachlorobiphenyl). The dosing regimen consisted of 3 dose levels (5, 50, and 500 μg/kg body weight of each PCB), and 4 dose protocols (one dose per day, one dose per week, consecutive daily doses for 13 days followed by no exposure, and 13 irregularly timed doses). Rats were either sacrificed at 41 days or 90 days for data collection. PCB concentrations in total lipids of plasma, liver, and adipose tissue were measured (adipose tissue concentrations were measured for only those rats sacrificed at 90 days). Body weight and liver weight at time of sacrifice were measured. The final data consisted of approximately six rats for each dose level/dose protocol/sacrifice day combination (142 rats in total) [11].

2.2. Toxicokinetic Model. The new PBTK model developed here is an extension of the lipid-based PCB mixture model by Emond et al. [11]. The original model formulation required alternative clearance parameters at different dose levels and dose protocols, thus increasing the number of parameters and creating model discontinuity. The updated model provides an alternative formulation that incorporates CYP450 induction, thus facilitating the use of a single set of parameters for wider applicability of the model.

The model consists of five compartments (blood, adipose tissue, liver, slowly and rapidly perfused), with mean physiology defined in Table 1. The overall clearance of PCBs is empirically described in the liver and represented as a function of CYP450 metabolism (metabolites are subsequently excreted in urine or feces [18]), which is modeled as a first-order process [11]. It is assumed that PCBs accumulate only in the neutral lipid spaces of blood and tissues. Any accumulation outside of the lipid fraction is assumed to be negligible and is not incorporated into the mass balance. Compartment volumes correspond to the lipid volumes in each tissue, and the total cardiac output is corrected for the fractional lipid content of blood. The PBTK model is based on chemical concentration in neutral lipid equivalent (NLE) components of blood and tissues, which can be converted to concentration in total lipids (the measurable quantity [14]). The lipid-based mass balances for tissues in the PBTK model are defined in the same manner as the original model [11]:

$$\begin{aligned} \frac{dA_{\text{nlt}}}{dt} &= Q_{\text{nlt}}(C_{\text{nla}} - C_{\text{nlt}}), \\ C_{\text{nlt}} &= \frac{A_{\text{nlt}}}{V_{\text{nlt}}}, \\ C_{\text{tlt}} &= C_{\text{nlt}} \frac{V_{\text{nlt}}}{V_{\text{tlt}}}, \end{aligned} \tag{1}$$

where A_{nlt} is the mass of chemical in the tissue NLEs (μg), Q_{nlt} is the flow rate of blood NLEs through the tissue (mL NLE/h), C_{nla} is the chemical concentration in the NLE fraction of arterial blood (μg/mL NLE), C_{nlt} is the chemical concentration in the tissue NLEs (μg/mL NLE), C_{tlt} is the chemical concentration expressed in terms of total lipids in tissue (μg/mL of total lipid), V_{nlt} is the volume of neutral lipid equivalents in tissue (mL NLE), and V_{tlt} is the volume of total lipids in tissue (mL total lipid). Volumes of total lipids in tissues are measurable quantities, while neutral lipid equivalents are quantities that are derived by assuming NLEs are composed of all the neutral lipids and 30% of the phospholipids in tissue [11, 14].

NLE-based volumes in Table 2 are obtained by multiplying conventional values with NLE ratios in Table 1. Flows are obtained by multiplying conventional values with the blood NLE ratio. The ratio of NLE/total lipid in Table 2 ($V_{\text{nlt}}/V_{\text{tlt}}$) is used to convert concentrations from NLE basis to total lipid basis. To convert liver, fat, and plasma NLE concentrations to a total lipid basis, the corresponding values in Table 1 (column 3) are used.

2.3. Induction Model. High chronic doses of the PCB mixture caused an increased elimination rate for all PCBs, which was attributed to CYP450 induction [11]. PBTK models predicting changes in metabolic rate due to CYP450 induction have been previously implemented for other chemicals [17, 20–23]. A CYP450 balance in the liver can be defined as

$$\frac{dA^{\text{CYP}}}{dt} = k_0 - k_e \times A^{\text{CYP}} + S(t), \tag{2}$$

Table 2: Physiological values for a standard 225 g rat (adapted from [11]).

Tissue	Conventional model†	NLE-based model
	Blood flow rates	
Fat	448 mL/h	0.85 mL lipid/h
Liver	1245 mL/h	2.36 mL lipid/h
Rapidly perfused	2540 mL/h	4.82 mL lipid/h
Poorly perfused	747 mL/h	1.42 mL lipid/h
Cardiac output	4980 mL/h	9.45 mL lipid/h
	Volumes	
Blood	20.0 mL	0.038 mL lipid
Fat	17.5 mL	14.938 mL lipid
Liver	10.0 mL	0.425 mL lipid
Rapidly perfused	12.5 mL	0.531 mL lipid
Poorly perfused	167.5 mL	2.010 mL lipid

†Physiological parameter values obtained from [15, 16].

where A^{CYP} is the mass (per gram protein) of CYP450 in the liver, k_0 is the basal CYP450 production rate (mass/time), k_e is the CYP450 degradation rate (time^{-1}), and $S(t)$ is the stimulation function for induction exposure response (mass/time). The initial condition for A^{CYP} is the baseline level A_0^{CYP}. In the presence of zero inducer, $S(t)$ is zero and (2) is at steady state, and, therefore, k_0 is equivalent to $k_e A_0^{\mathrm{CYP}}$.

For simplicity, a linear function was adopted for $S(t)$. While a Hill equation could have been implemented, it was determined that optimizing Hill parameters with weak prior information was impractical. The internal exposure-response parameters of this particular mixture are highly uncertain. Furthermore, lipid-based model formulations assume that contaminant concentration outside of the lipid space is negligible. If only unbound chemical outside of the lipid space can initiate a toxicological response (i.e., by binding to a receptor), a lipid model will assume that this external/unbound concentration remains low and does not approach saturation. The initiation of CYP450 induction was modeled as proportional to the inducing PCB concentration:

$$S(t) = k_0 F C_{\mathrm{IND}}, \tag{3}$$

where C_{IND} is a relative metric for inducer concentration, and F (≥ 0) is the induction slope factor defining the increase in CYP450 enzyme production caused by C_{IND}. The induction slope is defined as a factor of the basal production rate.

In previous PBTK models for lipophilic contaminants, the inducer concentration C_{IND} was defined to be the chemical concentration bound to the Ah-receptor [17]. The Ah-receptor has consistently been demonstrated to be crucial for CYP450 induction by PCBs [24]. Since only unbound chemical outside of the lipid space can bind to the Ah-receptor [23], assumptions from the prior PBPK models do not apply. To maintain the parsimony of the model and maintain lipid-based concentrations throughout, C_{IND} was defined as the concentration of the inducing PCB congener(s) in the neutral-lipid space of the liver. Any additional steps in the induction process (i.e., concentration gradients between free and lipid-space PCB, and Ah-receptor binding) were essentially lumped into the dose response parameter F. During the model development phase, it was observed that introducing a time-lag into the stimulation function to account for unspecified processes had a negligible impact on predicted lipid concentrations. This was likely due to the larger timescales of dose protocols and simulated data collection times.

The following relationship between CYP450 levels and metabolic clearance was determined to be flexible enough to model the data over a wide range of doses:

$$v_{\mathrm{cl}} = v_0 \frac{A^{\mathrm{CYP}}}{A_0^{\mathrm{CYP}}}, \tag{4}$$

where v_{cl} is metabolic clearance as a function of CYP450 concentration (mL/h) and v_0 is the basal metabolic clearance under low exposure and negligible induction conditions (mL/h).

The rate of metabolism of each PCB is the product of the PCB concentration in the neutral lipid space of the liver $C_{\mathrm{nlL}}(A_{\mathrm{nlL}}/V_{\mathrm{nlL}})$ and the v_{cl} for the particular PCB:

$$\frac{dA_{\mathrm{n1L}}}{dt} = Q_{\mathrm{n1L}}(C_{\mathrm{n1a}} - C_{\mathrm{n1L}}) - v_0 \cdot \frac{A^{\mathrm{CYP}}}{A_0^{\mathrm{CYP}}} \cdot C_{\mathrm{n1L}}, \tag{5}$$

$$\frac{dA^{\mathrm{CYP}}}{dt} = k_0 - k_{\mathrm{e}} \times A^{\mathrm{CYP}} + k_0 F C_{\mathrm{IND}}. \tag{6}$$

PCB induction and metabolism are congener specific and are functions of structure and classification [2]. Non-ortho PCBs ("dioxin-like" PCBs with no ortho-substituted chlorines) assume a coplanar position and are strong inducers of CYP1A. Multi-ortho-substituted PCBs cannot become coplanar and interact primarily with CYP2B. Mono-ortho PCBs can assume both planar and coplanar positions and are considered "mixed-type" inducers [2, 25, 26]. PCB congeners 138, 153, 170, and 180 are di-ortho; 187 is tri-ortho; and 118 is mono-ortho. In the current dataset, PCB 118 shows significantly higher clearance than other congeners at the high-dose level [11].

To model the difference in PCB 118 metabolism at the high doses, the PBTK model assumes the multi-ortho PCBs are metabolized through the CYP2B pathway, while PCB 118 is metabolized via CYP1A. It was also assumed that both types of PCBs induce CYP2B, but induction of CYP1A by multi-ortho PCBs was negligible. These assumptions were based on *in vitro* studies of different classes of PCBs. A study in rat hepatocytes found that mono-ortho PCBs are primarily metabolized by CYP1A and primarily induce CYP1A (with CYP2B being induced to a lesser extent) [27]. CYP1A induction by PCB 118 has also been shown to be orders of magnitude greater than induction by multi-ortho PCBs [28]. Meanwhile, CYP2B induction from both PCB 118 and multi-ortho PCBs was the same order of magnitude [25].

Equations (2) through (6) were applied with parameters to describe both CYP1A and CYP2B kinetics. For each PCB, (5) was applied using a basal metabolic clearance (v_0) specific to that PCB, with the induction scaling factor dependent on the PCB classification (mono-ortho or multi-ortho). Induced clearance of PCB 118 was dependent on the CYP1A

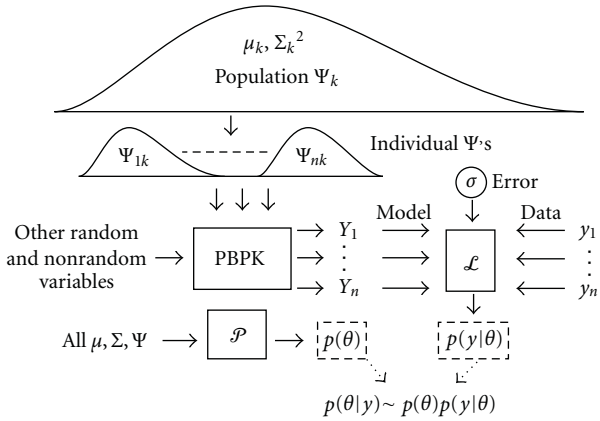

Figure 1: Schematic of a hierarchical Bayesian framework (adapted from [19]).

Table 3: Basal CYP1A/2B parameters [17].

Parameter	Symbol	Units	Value
Initial steady-state CYP1A/2B	A_0	nmol/g protein	0.1†
CYP1A/2B degradation	k_e	h^{-1}	0.04
Basal CYP1A/2B production	k_0	nmol/h/g protein	0.004

†Computed from the steady-state mass balance.

ratio, while induction of the others was dependent on CYP2B ratio. For the induction of CYP1A, C_{IND} in (6) was assumed to be the concentration of PCB 118 in the neutral lipid space of the liver. For CYP2B induction, C_{IND} was assumed to be the total PCB concentration (sum of all 6 PCBs) in the neutral lipid space of the liver. This assumes an additive effect on CYP2B induction, with each PCB having equal weight. Separate values for the induction factor F were used to describe CYP1A and CYP2B induction.

Parameters for baseline CYP450 dynamics were obtained from literature and are summarized in Table 3. For simplicity, the same parameters were used for both CYP1A and CYP2B enzymes and were obtained from a model for CYP1A [17]. Alternatively, CYP2B-specific parameters from a similar PBTK-induction model can be used [22]. A recent study in female rats estimated CYP1A content to be a factor of two greater than CYP2B in the liver [29], which could also be used to inform the model. It was found that optimizing the model using separate 1A/2B parameters produced nearly identical final results, due to the fact that the synthesis and degradation parameters were proportionally the same. Additionally, the initial amounts and the synthesis/degradation rates are not entirely identifiable and are related via the steady-state mass balance. Since the induction in this model will only be affected by the increase of CYP450 relative to the baseline, the actual baseline values are less important, and some adjustments can be made to those assumptions without reoptimization of induction factor F.

2.4. Hierarchical Bayesian Model. Interanimal variation existed in the data which could not be attributed to differences in physiology or tissue lipid content alone. It was assumed that this inter-rat variation can be attributed to basal metabolic clearance v_0. A hierarchical model for basal clearance was constructed to optimize the population distribution of v_0 to the observed data (Figure 1).

A generalized population model assumes random variable Ψ_{ik} (where i denotes an individual within the population, and k denotes the particular variable) is derived from a distribution of mean μ_k and standard deviation Σ_k. Both random and nonrandom variables are used as inputs to the PBTK model to predict Y_i. The likelihood function L calculates the probability that Y_i is an adequate prediction of data y_i given the set of random variables. The prior function P calculates the probability of all random variable values conditional on their population assumptions. The posterior probability is proportional to the product of the likelihood and prior.

A lognormal error function was implemented as the likelihood, which assumes the log of data measurements y_i are scattered in a normal distribution from the log of their corresponding model predictions Y_i:

$$\log y_i = \log Y_i + N_{\text{rnd}}(\mu = 0, \sigma). \tag{7}$$

The population and error parameters to be estimated are summarized in Table 4. It was assumed that metabolic clearances at the individual level (v_0) were derived from a lognormal population distribution defined by μv_0 and Σv_0. Priors on μv_0 for each PCB were set as wide and noninformative. The priors for population variances Σv_0 for each PCB were assumed to be inverse-gamma with a shape parameter of 1 (indicating large uncertainty), and a scale parameter of 0.8 (the initial assumption on the lognormal Σ). The prior probabilities of individual-level parameters were calculated using the values of population μ and Σ for each parameter at the current iteration. Upper and lower limits for the uniform priors on mean population basal clearances (μv_0) were set by observing model behavior at extreme values. It was determined that scaling the basal rate by body-weight$^{0.75}$ slightly improved convergence and model fit, due to the increasing body weight over the 90-day period, and variation in body weight of the studied population. Noninformative distributions were used for the priors on σ. Since three tissues were measured (plasma, liver, and fat), three separate values for σ were optimized.

Table 4: Population-level parameters to be estimated by Bayesian analysis.

Parameter	Unknowns	Prior
Basal metabolic rate†	μv_0	Wide uniform
	Σv_0	Inverse gamma
Induction factor	F^{2B}	Wide uniform
	F^{1A}	Wide uniform
Model/data error‡	σ	Wide uniform

†One each for PCBs 118, 138, 153, 170, 180, 187, in (mL/h/kg$^{0.75}$).
‡One each for plasma, liver, and fat.

During the testing phase of the optimization, interindividual variation in cardiac output, fractional organ volumes, and blood flow rates were incorporated by using informative

population priors based on standard literature values for Sprague-Dawley rats. This involved optimizing individual-level physiology while holding population-level distributions constant. It was found that nearly identical final results were obtained regardless of whether variation in physiology was incorporated into the model. In order to improve convergence, mean values for organ physiology were used. Individual-level data of measured liver weight ratios and the change in body weights over the course of the study were still incorporated into the PBTK model during the optimization.

2.5. Computational Implementation. The PBTK model was developed in the MATLAB software environment [30], while implementing an open-source Metropolis-Hastings toolbox [31]. The PBTK model is available from the institute website (http://www.ccl.rutgers.edu/onlineCodes/PCBmixturePBPK) and is also provided as a supplemental file. Markov-Chain Monte Carlo (MCMC) with Metropolis sampling was used to iteratively converge to the posterior distribution. The number of PBTK model parameters for each of the 142 rats, added with population and error parameters, leads to over 1000 parameters in total. Convergence issues arise with such high dimensions and noninformative priors. Additionally, each Metropolis step requires the solution of over 800 systems of differential equations, and multiple independent Markov chains are required to assess convergence. Since the system might not converge for 100,000 iterations, it was necessary to apply simplifying assumptions to reduce model evaluations and improve convergence.

Because a minimal induction effect was observed at the lowest dose [11], the parameter optimization was decomposed into two steps. For the first step, induction was neglected and the model was optimized using only the low-dose data in order to obtain the basal metabolic rate (v_0) for each PCB. The resulting population distributions were then used as informative priors in the second step. For step 2, induction was incorporated in the model, and parameters were optimized using only data for the two high doses. While MCMC was still performed on the individual-level values for v_0 in step 2, they were defined by stronger population priors than in step 1. The population mean and variance for v_0 were not updated in step 2, since the final distribution of all individual-level clearances from step 2 remained consistent with the population priors. Had any anomalies been identified (i.e., many individual-level parameters being optimized at the upper or lower limits), the population parameters would have been reoptimized in the second step. The model/data error parameters (σ) were optimized in both steps, since it was observed that allowing these parameters to freely explore the space improved convergence.

Splitting the problem into two steps helped to reduce convergence problems, since basal and induced metabolic clearances are inherently nonidentifiable. Interindividual variation of the induction factor F was neglected in step 2 (i.e., the prior probability on ΣF was assumed to be extremely small). Assuming negligible variation on F eliminates the need to estimate individual-level values for each rat and can prevent poor mixing of the Markov chains. Interindividual variation in metabolism would be accounted for by variations in basal clearance. Two induction factors (one each for 1B and 2A induction) would be optimized to fit the entire population.

For both step 1 and step 2 of the parameter optimization, three sets of independent Markov chains were initiated using over dispersed initial guesses. After adjustments in the random-walk parameters to optimize the acceptance rate (it was determined that the optimal acceptance rate for this system was approximately 10% [32]), the chains were run for 50,000 iterations. The chains were considered converged if the Gelman-Rubin convergence statistic was close to 1 for the parameters from all three independent sets of chains [33]. The PBTK models and Metropolis sampler were implemented in MATLAB on a cluster of multi core processors. Convergence of the Markov chains typically occurred after 80,000 iterations and three days computational time.

3. Results and Discussion

3.1. Posterior Distributions. Results are summarized in Table 4. Mean basal clearances ranged between 0.017 and 0.038 mL/h/kg$^{0.75}$. The population lognormal standard deviations for basal clearances (Σv_0) were reduced by over half for most of the PCBs, and metabolic clearance was predicted to deviate from the mean by a factor of 2 in the population. Congener 187 was the only PCB to have a lognormal standard deviation greater than 0.5 for basal clearance. PCB 153 clearance had exhibited poor convergence, as indicated by the Gelman-Rubin statistic, despite repeated optimization attempts. The mono-ortho congener 118 had the highest basal clearance, which may be due to a slight induction effect at the lowest dose. Since distributions for basal metabolic rate of all 6 PCBs were relatively similar, an additional MCMC analysis was performed for step 1 assuming a single population distribution for all PCB clearances v_0^{all}. The population distribution of v_0^{all} was in agreement with those determined for the individual PCBs and represents a condensed posterior distribution for all six PCBs. Additionally, better convergence was achieved for the lumped standard deviation. Step 2 of the MCMC analysis (determination of induction parameters) was performed using the 6 separate PCB distributions.

3.2. Model Evaluation. Monte Carlo simulations consisting of 1000 model runs using parameters randomly sampled from the posterior distributions (Table 5) were performed to assess the behavior of the population model. For these simulations, median population μ and Σ were used to randomly generate individual-level clearance parameters so that the effect of parameter variability could be observed. Figure 2 illustrates the variation of the population model and experimental data at the 5 μg/kg dose level. At this low dose level, data and model predictions for both classes of PCBs (multi-ortho and mono-ortho) are similar across dose protocols and tissue type. The variation in model outputs as a function of parameter variability was in agreement with the amount of scatter observed in the data. At the highest dose level, metabolic clearance differs between PCB 118 and the multi-ortho PCBs (Figure 3). The magnitude of this

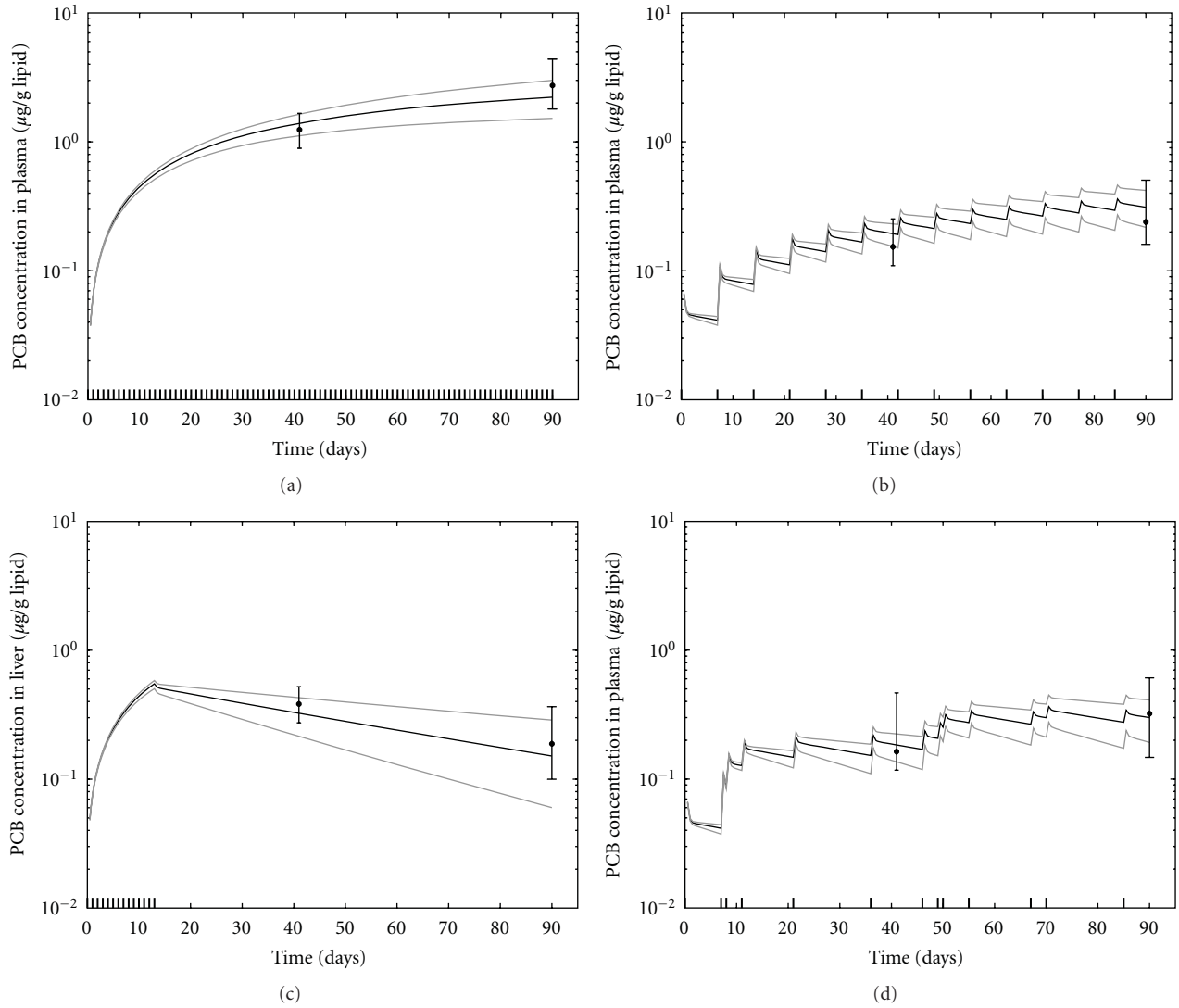

Figure 2: Model predictions and data for all PCB concentrations in tissue lipids at the 5 μg/kg dose level, and the four dose protocols ((a) Daily, (b) weekly, (c) daily to day 13, (d) nonperiodic). Data points represent the median of all PCBs for all rats at time of sacrifice, and error bars represent the minimum and maximum measured values. Modeled results represent the median and 95% confidence interval of 1000 model runs using parameters randomly sampled from the posterior distributions.

difference was also a function of dose protocol. The model was also able to capture differences in the time profiles between tissues that were due to lipid content (Figure 4).

The performance of the induction model remained consistent with previous observations by Emond et al. [11]. At the highest continuous dose level, metabolic clearance of the multi-ortho PCBs may increase by a factor of 3, while clearance of PCB 118 may increase by a factor of 5. Increases in metabolic rate varied by dose protocol, due to the dynamic behavior of the CYP450 balance. The induction effect is the greatest, and the difference between PCB 118 and multi-ortho PCB concentrations is the largest, when doses occur daily as opposed to sporadically (Figure 3). At the lowest dose, the induction model predicts negligible increase in metabolic clearance for both PCB groups. The model was able to simulate induction as a consistent and continuous function across all dose levels and protocols, while reproducing observed data. A scatter plot comparing all data with model results (using the individual-level posterior values sampled from the converged Markov chains) is presented in Figure 5, along with the condensed posterior distribution of basal metabolic clearance of all PCBs.

The lipid-based toxicokinetic model does have inherent limitations. Because these models do not include partition coefficients for each PCB/tissue combination, they cannot capture differences in the ordering of PCB concentrations that are observed between different tissues of the same rat. While PCB 118 is observed as having the lowest concentration in all tissue lipids for most of the rats, there is a slight tissue dependency among the ordering of multi-ortho PCBs. For example, PCB 180 was usually observed to have the second-highest PCB concentration in fat lipid but had either the lowest or second-lowest concentration in plasma and liver lipids. PCB 187 usually had the highest concentrations

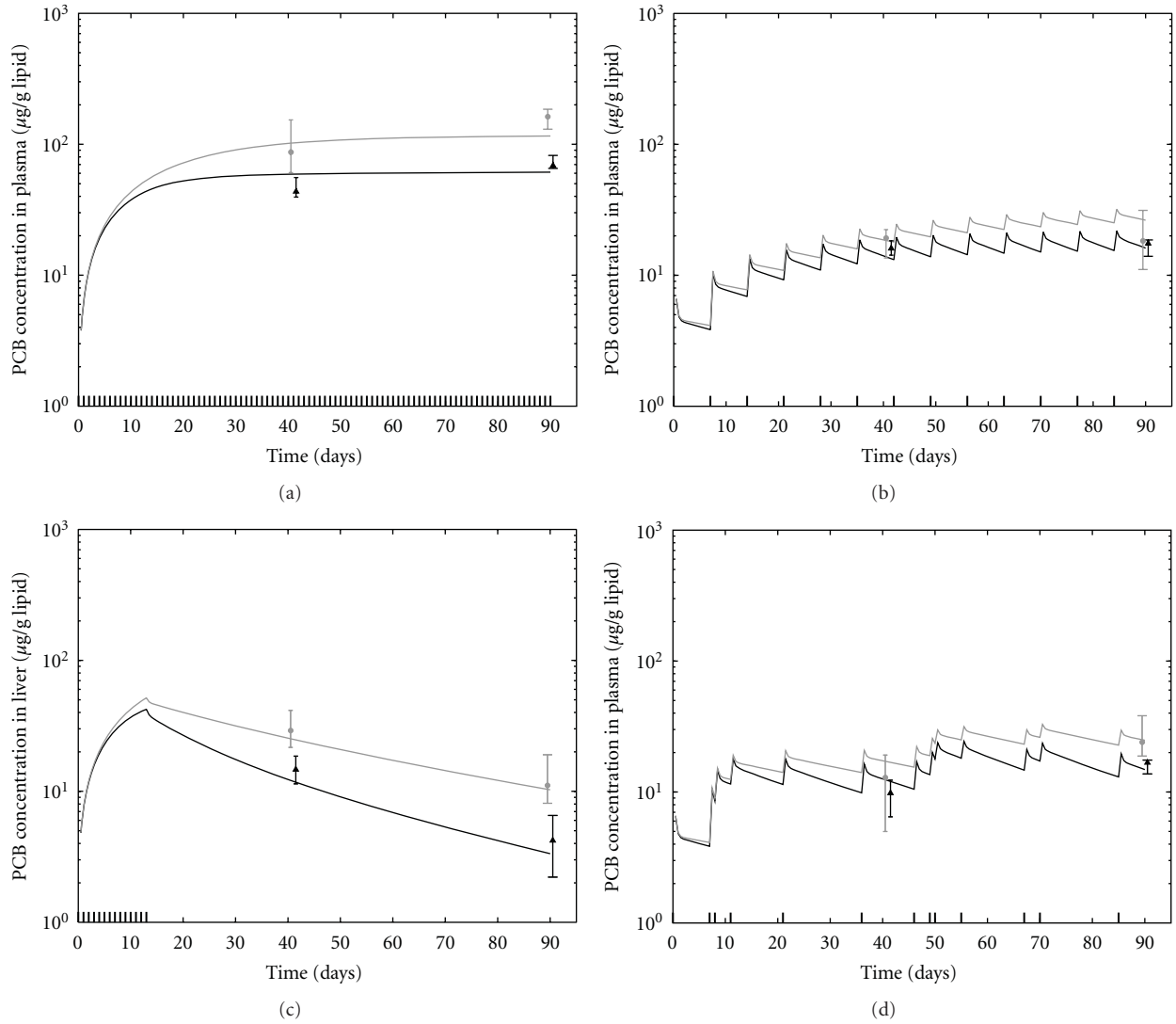

Figure 3: Model predictions and data for all PCBs at the 500 μg/kg dose level and the four dose protocols. Data represents the median measurements across rats at time of sacrifice (grey circle: all multi-ortho PCBs, black triangle: PCB 118). Modeled results are for the median over all multi-ortho PCBs (grey line), and the median results for PCB 118 (black line), resulting from 1000 model runs using parameters randomly sampled from the posterior distributions.

in plasma and fat, but not liver. The magnitude of the differences between multi-ortho PCB concentrations was relatively small. However, the effect is somewhat visible in the model/data scatter plot (Figure 5(b)), where trends exist in each cluster due to a consistent over- or underprediction of specific PCB-tissue combinations. Slight correlations between the clearance parameters are also inherent in the model, and an attempt was made to use the multivariate prior distribution from step 1 in the step 2 optimization. However, convergence issues and the lack of congener-specific tissue affinity parameters ultimately made an accurate characterization of these correlations infeasible.

The other modeling simplification involves the estimation of a basal metabolic rate based on the low-dose data. If the metabolic rate is significantly increased at low exposures due to induction, optimizations at the higher doses will be biased. For low doses of PCB 126 (a potent dioxin-like PCB) in rats, *in vivo* studies have shown significant increases in EROD (7-ethoxyresorufin-O-deethylase) activity (which is indicative of CYP1A). A 10-fold increase in EROD activity has been observed after a single 7.5 μg/kg dose [7], and a 95-fold increase was observed for 1 μg/kg/day exposure [34]. Low-dose induction of CYP2B, indicated by PROD (7-pentoxyresorufin-O-dealkylase) activity, has been observed due to mixtures of mono-ortho and multi-ortho PCBs [25]. Rats orally exposed to PCB 153 (one of the congeners in the current study) showed a 4-fold induction of CYP1A and a 20-fold induction of CYP2B at 3 mg/kg [35]. Since the current work concerns doses at the μg/kg level of the relatively low potent PCBs, the CYP induction implemented here (maximum of about 5-fold) does not contradict earlier studies. Additionally, since the increase in metabolic rate between the 5 and 50 μg/kg dose levels was very small in this study, the assumption of negligible rate increase between the

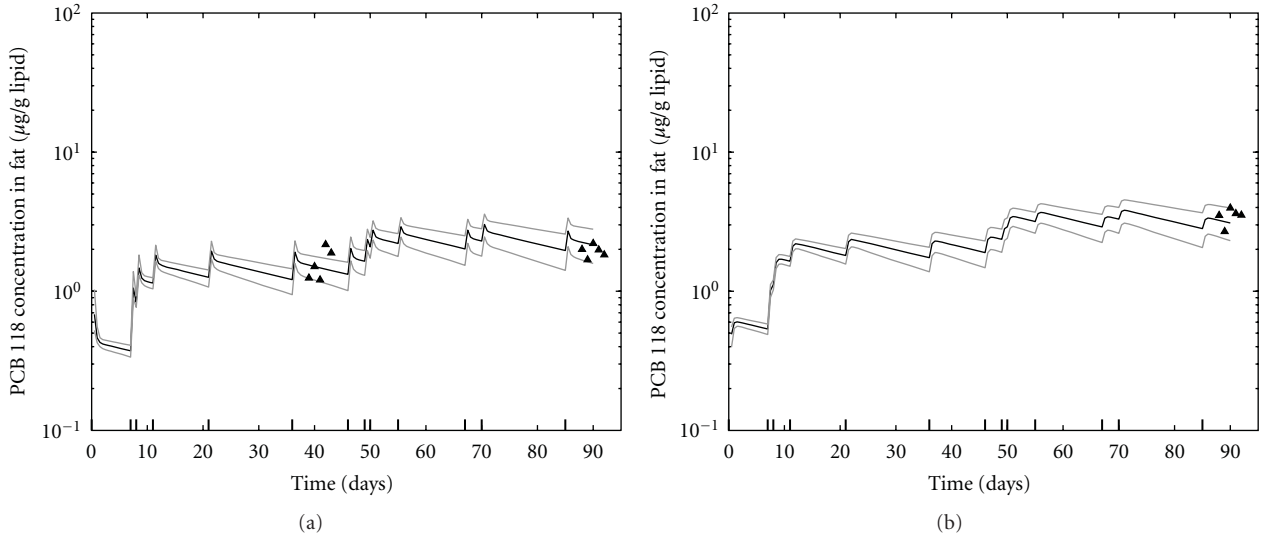

Figure 4: Model predictions for PCB 118 in liver (a) and fat lipids (b) for the nonperiodic dose scenario at the 50 μg/kg dose level. Data for all rats are shown (black triangles), and measurements for each rat at time of sacrifice have been shifted slightly on the x-axis. Modeled results are the median and 95% confidence interval of 1000 model runs using parameters randomly sampled from the posterior distribution.

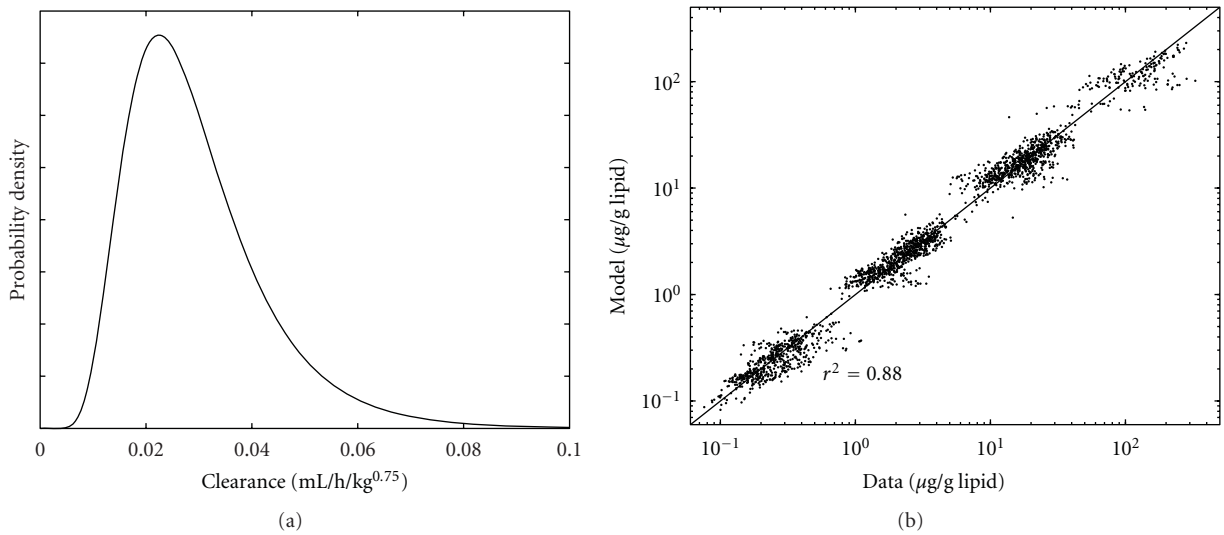

Figure 5: Population distribution of consolidated basal metabolic clearance v_0^{all} (a), and scatter plot of PBTK model predictions versus measured data using the optimized individual-level values of the Markov chains (b).

"true" basal rate and the rate estimated at low-dose appears to be rational.

Other simplifying assumptions include linearization of the biological exposure response, neglecting Ah-receptor binding, and discretizing the induction model into 2 PCB groups (multi-ortho and non-ortho) and 2 enzyme groups (CYP1A and CYP2B). Competitive inhibition for P450s [5], regional hepatic CYP450 induction [6], and induction of Phase-II metabolic enzymes [7] were also neglected. Such model complexities lie outside the scope of this work and would have made MCMC analysis infeasible due to weak prior information and nonidentifiable parameters. While the Bayesian framework implicitly incorporated these and other discrepancies into the model/data error for each tissue, the actual model/data error can never be truly known. It is typically assumed that the collection of additional replicates will reduce the uncertainties. However, there is a point where additional replication will not yield model improvements. An observation to this effect occurred during an initial testing phase of the Bayesian framework. The model optimization results were originally evaluated by a "data-splitting" technique, where one rat from each dose-level/dose-protocol/sacrifice-time was omitted from the optimization dataset. The optimized model was then tested against this omitted data to assess performance. It was later found that optimizing the model to the full data set produced nearly identical posterior values (including model/data error) as optimizing to the dataset containing approximately 17%

Table 5: Population posterior distributions.

Parameter*	μ (CV/R)†	Σ (CV/R)
v_0^{118}	0.038 (0.02/1.0)	0.24 (0.13/1.2)
v_0^{138}	0.026 (0.02/1.2)	0.35 (0.17/1.1)
v_0^{153}	0.025 (0.02/1.3)	0.35 (0.16/1.5)
v_0^{170}	0.029 (0.02/1.0)	0.38 (0.16/1.0)
v_0^{180}	0.035 (0.02/1.1)	0.31 (0.15/1.0)
v_0^{187}	0.017 (0.02/1.1)	0.55 (0.25/1.0)
v_0^{all}	0.027 (0.03/1.0)	0.43 (0.08/1.1)
F^{2B}	0.0025 (0.01/1.0)	
F^{1A}	0.045 (0.02/1.2)	
σ_{fat}	0.30 (0.06/1.0)‡ 0.23 (0.04/1.0)	
σ_{plasma}	0.19 (0.04/1.2) 0.23 (0.03/1.3)	
σ_{liver}	0.40 (0.05/1.1) 0.36 (0.03/1.0)	

*Units for v_0 are (mL/h/kg$^{0.75}$); F is unitless.
†CV: coefficient of variance of chain, R: Gelman-Rubin.
‡One value each for step 1 (top) and step 2 (bottom).

fewer rodents. Future studies involving mixtures of contaminants having very similar toxicokinetic properties would benefit from a value-of-information analysis at the experimental design phase, in order to reduce the number of test rodents needed to develop a mixture model.

4. Conclusions

This is the first application of a large-scale population Bayesian analysis to a mixture PBTK model. Despite the lack of partition coefficients and reduced degrees of freedom, the optimized model was capable of reproducing experimental data in multiple tissue lipids for a wide range of PCB dose levels and protocols. The application of a linear induction dose-response model, and the use of lipid-based concentrations, illustrated parsimonious alternatives to highly complex nonlinear models containing large numbers of parameters. While the current modeling effort sought to avoid the issue of nonidentifiability or overparameterization, further improvement could be made by incorporation of a fully mechanistic model for CYP450 induction. However, such a model would likely require predictions of PCB concentrations outside of the lipid space, and the type of additional data needed would depend on the aims and scope of the proposed mechanistic model.

Acknowledgments

This work was supported through the USEPA-funded Environmental Bioinformatics and Computational Toxicology Center (GAD R 832721-010), USEPA-funded Center for Exposure and Risk Modeling (CERM—EPAR827033), and the NIEHS-sponsored UMDNJ Center for Environmental Exposures and Disease (Grant no. NIEHS P30ES005022).

References

[1] WHO, *Polychlorinated Biphenyls: Human Health Aspects, Concise International Chemical Assessment Document 55*, World Health Organization, Geneva, Switzerland, 2003.

[2] S. H. Safe, "Polychlorinated biphenyls (PCBs): environmental impact, biochemical and toxic responses, and implications for risk assessment," *Critical Reviews in Toxicology*, vol. 24, no. 2, pp. 87–149, 1994.

[3] R. Ritter, M. Scheringer, M. MacLeod, C. Moeckel, K. C. Jones, and K. Hungerbuhler, "Intrinsic human elimination half-lives of polychlorinated biphenyls derived from the temporal evolution of cross-sectional biomonitoring data from the United Kingdom," *Environmental Health Perspectives*, vol. 119, no. 2, pp. 225–231, 2011.

[4] K. Hornbuckle and L. Robertson, "Polychlorinated biphenyls (PCBs): sources, exposures, toxicities," *Environmental Science and Technology*, vol. 44, no. 8, pp. 2749–2751, 2010.

[5] J. J. Chen, G. S. Chen, and N. J. Bunce, "Inhibition of CYP 1A2-dependent MROD activity in rat liver microsomes: an explanation of the hepatic sequestration of a limited subset of halogenated aromatic hydrocarbons," *Environmental Toxicology*, vol. 18, no. 2, pp. 115–119, 2003.

[6] L. S. Chubb, M. E. Andersen, C. J. Broccardo et al., "Regional induction of CYP1A1 in rat liver following treatment with mixtures of PCB 126 and PCB 153," *Toxicologic Pathology*, vol. 32, no. 4, pp. 467–473, 2004.

[7] J. W. Fisher, J. Campbell, S. Muralidhara et al., "Effect of PCB 126 on hepatic metabolism of thyroxine and perturbations in the hypothalamic-pituitary-thyroid axis in the rat," *Toxicological Sciences*, vol. 90, no. 1, pp. 87–95, 2006.

[8] M. B. Reddy, R. S. H. Yang, H. J. Clewell, and M. E. Andersen, *Physiologically Based Pharmacokinetic Modeling: Science and Applications*, Wiley-Interscience, Hoboken, NJ, USA, 2005.

[9] K. Price and K. Krishnan, "An integrated QSAR-PBPK modelling approach for predicting the inhalation toxicokinetics of mixtures of volatile organic chemicals in the rat," *SAR and QSAR in Environmental Research*, vol. 22, no. 1, pp. 107–28, 2011.

[10] K. Krishnan, S. Haddad, M. Beliveau, and R. Tardif, "Physiological modeling and extrapolation of pharmacokinetic interactions from binary to more complex chemical mixtures," *Environmental Health Perspectives*, vol. 110, supplement 6, pp. 989–994, 2002.

[11] C. Emond, M. Charbonneau, and K. Krishnan, "Physiologically based modeling of the accumulation in plasma and tissue lipids of a mixture of PCB congeners in female sprague-dawley rats," *Journal of Toxicology and Environmental Health A*, vol. 68, no. 16, pp. 1393–1412, 2005.

[12] S. Trapp, L. Ma Bomholtz, and C. N. Legind, "Coupled mother-child model for bioaccumulation of POPs in nursing infants," *Environmental Pollution*, vol. 156, no. 1, pp. 90–98, 2008.

[13] F. Y. Bois, M. Jamei, and H. J. Clewell, "PBPK modelling of inter-individual variability in the pharmacokinetics of environmental chemicals," *Toxicology*, vol. 278, no. 3, pp. 256–267, 2010.

[14] P. Poulin and K. Krishnan, "Molecular structure-based prediction of the partition coefficients of organic chemicals for physiological pharmacokinetic models," *Toxicology Methods*, vol. 6, no. 3, pp. 117–137, 1996.

[15] L. B. Kedderis, J. J. Mills, M. E. Andersen, and L. S. Birnbaum, "A physiologically based pharmacokinetic model for 2,3,7,8-tetrabromodibenzo-p-dioxin (TBDD) in the rat:

tissue distribution and CYP1A induction," *Toxicology and Applied Pharmacology*, vol. 121, no. 1, pp. 87–98, 1993.

[16] K. Krishnan and M. E. Andersen, "Physiologically based pharmacokinetic modeling in toxicology," in *Principles and Methods of Toxicology*, A. W. Hayes, Ed., pp. 1931–1241, Raven Press, New York, NY, USA, 2001.

[17] M. E. Andersen, L. S. Birnbaum, H. A. Barton, and C. R. Eklund, "Regional hepatic CYP1A1 and CYP1A2 induction with 2,3,7,8-tetrachlorodibenzo-p-dioxin evaluated with a multicompartment geometric model of hepatic zonation," *Toxicology and Applied Pharmacology*, vol. 144, no. 1, pp. 145–155, 1997.

[18] H. B. Matthews and R. L. Dedrick, "Pharmacokinetics of PCBs," *Annual Review of Pharmacology and Toxicology*, vol. 24, pp. 85–103, 1984.

[19] C. E. Hack, W. A. Chiu, Q. Jay Zhao, and H. J. Clewell, "Bayesian population analysis of a harmonized physiologically based pharmacokinetic model of trichloroethylene and its metabolites," *Regulatory Toxicology and Pharmacology*, vol. 46, no. 1, pp. 63–83, 2006.

[20] C. Emond, L. S. Birnbaum, and M. J. DeVito, "Physiologically based pharmacokinetic model for developmental exposures to TCDD in the rat," *Toxicological Sciences*, vol. 80, no. 1, pp. 115–133, 2004.

[21] C. Emond, L. S. Birnbaum, and M. J. DeVito, "Use of a physiologically based pharmacokinetic model for rats to study the influence of body fat mass and induction of CYP1A2 on the pharmacokinetics of TCDD," *Environmental Health Perspectives*, vol. 114, no. 9, pp. 1394–1400, 2006.

[22] R. Sarangapani, J. Teeguarden, K. P. Plotzke, J. M. McKim Jr., and M. E. Andersen, "Dose-response modeling of cytochrome P450 induction in rats by octamethylcyclotetrasiloxane," *Toxicological Sciences*, vol. 67, no. 2, pp. 159–172, 2002.

[23] X. Wang, M. J. Santostefano, M. V. Evans, V. M. Richardson, J. J. Diliberto, and L. S. Birnbaum, "Determination of parameters responsible for pharmacokinetic behavior of TCDD in female Sprague-Dawley rats," *Toxicology and Applied Pharmacology*, vol. 147, no. 1, pp. 151–168, 1997.

[24] C. P. Curran, C. V. Vorhees, M. T. Williams, M. B. Genter, M. L. Miller, and D. W. Nebert, "In utero and lactational exposure to a complex mixture of polychlorinated biphenyls: toxicity in pups dependent on the Cyp1a2 and Ahr genotypes," *Toxicological Sciences*, vol. 119, no. 1, pp. 189–208, 2011.

[25] K. Connor, S. Safe, C. R. Jefcoate, and M. Larsen, "Structure-dependent induction of CYP2B by polychlorinated biphenyl congeners in female Sprague-Dawley rats," *Biochemical Pharmacology*, vol. 50, no. 11, pp. 1913–1920, 1995.

[26] K. Hu and N. J. Bunce, "Metabolism of polychlorinated dibenzo-p-dioxins and related dioxin-like compounds," *Journal of Toxicology and Environmental Health B*, vol. 2, no. 2, pp. 183–210, 1999.

[27] F. Yang, Y. Xu, H. Pan, and D. Wu, "Induction of hepatic cytochrome P4501A1/2B activity and disruption of thyroglobulin synthesis/secretion by mono-ortho polychlorinated biphenyl and its hydroxylated metabolites in rat cell lines," *Environmental Toxicology and Chemistry*, vol. 27, no. 1, pp. 220–225, 2008.

[28] A. S. A. M. Van Der Burght, P. J. Clijsters, G. J. Horbach, P. L. Andersson, M. Tysklind, and M. Van Den Berg, "Structure-dependent induction of CYP1A by polychlorinated biphenyls in hepatocytes of cynomolgus monkeys (Macaca fascicularis)," *Toxicology and Applied Pharmacology*, vol. 155, no. 1, pp. 13–23, 1999.

[29] S. Y. Lee, S. J. Oh, K. U. Yun et al., "Expression of hepatic and ovarian cytochrome P450 during estrous cycle in rats," *Arch Toxicol*, vol. 86, no. 1, pp. 75–85, 2012.

[30] MATLAB, The MathWorks Inc., Natick, Mass, USA, http://www.mathworks.com/products/matlab/.

[31] H. Haario, M. Laine, A. Mira, and E. Saksman, "DRAM: efficient adaptive MCMC," *Statistics and Computing*, vol. 16, no. 4, pp. 339–354, 2006.

[32] M. Bédard, "Optimal acceptance rates for Metropolis algorithms: moving beyond 0.234," *Stochastic Processes and Their Applications*, vol. 118, no. 12, pp. 2198–2222, 2008.

[33] A. Gelman, *Bayesian Data Analysis*, Chapman & Hall/CRC, Boca Raton, Fla, USA, 2004.

[34] H. Toyoshiba, N. J. Walker, A. J. Bailer, and C. J. Portier, "Evaluation of toxic equivalency factors for induction of cytochromes P450 CYP1A1 and CYP1A2 enzyme activity by dioxin-like compounds," *Toxicology and Applied Pharmacology*, vol. 194, no. 2, pp. 156–168, 2004.

[35] J. M. Sanders, L. T. Burka, C. S. Smith, W. Black, R. James, and M. L. Cunningham, "Differential expression of CYP1A, 2B, and 3A genes in the F344 rat following exposure to a polybrominated diphenyl ether mixture or individual components," *Toxicological Sciences*, vol. 88, no. 1, pp. 127–133, 2005.